NONLINEAR GUIDED-WAVE PHENOMENA

Sponsored by
Optical Society of America

1991 TECHNICAL DIGEST SERIES VOLUME 15

SEPTEMBER 2–4, 1991 CAMBRIDGE, ENGLAND UNITED KINGDOM

REPORT DOCUMENTATION PAGE

Form Approved
OMB No. 0704-0188

1. AGENCY USE ONLY (Leave blank)	2. REPORT DATE	3. REPORT TYPE AND DATES COVERED
	May 22, 1992	Final 1/1/91-12/31/91

4. TITLE AND SUBTITLE
Organization of the 1991 Optical Society of America Photonic Science Topical Meeting Series (OSA 115)

5. FUNDING NUMBERS
G - AFOSR-91-0176

6. AUTHOR(S)
Jarus W. Quinn

7. PERFORMING ORGANIZATION NAME(S) AND ADDRESS(ES)
Optical Society of America
2010 Massachusetts Ave. NW
Washington, DC 20036

8. PERFORMING ORGANIZATION REPORT NUMBER
AFOSR-TR- 92 0510

9. SPONSORING/MONITORING AGENCY NAME(S) AND ADDRESS(ES)
US Air Force Office of Scientific Research
Department of the Air Force
Bolling Air Force Base
Washington, DC 20332-6448
NE
Schlossberg

10. SPONSORING/MONITORING AGENCY REPORT NUMBER
2305/A1

11. SUPPLEMENTARY NOTES

12a. DISTRIBUTION/AVAILABILITY STATEMENT
Approved for public release
Distribution unlimited

12b. DISTRIBUTION CODE

13. ABSTRACT (Maximum 200 words)

Attach list of reports supported by Optical Society of America
Photorefractive Materials, Effects, and Devices
Integrated Photonics Research
Nonlinear Guided Wave Phenomena
Optical Amplifiers and Their Applications
Optical computing
Picosecond Electronics and Optoelectronics
Quantum Optoelectronics
Photonic Switching
Microphysics of Surfaces: Beam Induced Processes
Soft X-ray Projection Lithography
Short Wavelength Coherent Radiation, Generation & Applications
Presistent Spectral Hole-Buring: Science & Applications

14. SUBJECT TERMS	15. NUMBER OF PAGES
	16. PRICE CODE

17. SECURITY CLASSIFICATION OF REPORT	18. SECURITY CLASSIFICATION OF THIS PAGE	19. SECURITY CLASSIFICATION OF ABSTRACT	20. LIMITATION OF ABSTRACT
[redacted]	[redacted]	[redacted]	[redacted]

Nonlinear Guided-Wave Phenomena

Summaries of papers presented at the Nonlinear Guided-Wave Phenomena Topical Meeting

September 2–4, 1991
Cambridge, England, United Kingdom

1991 Technical Digest Series
Volume 15

CONFERENCE EDITION

Sponsored by
Optical Society of America

In Cooperation with
IEEE/Lasers and Electro-Optics Society
The Institute of Physics, United Kingdom
The Institution of Electrical Engineers, United Kingdom

Optical Society of America
2010 Massachusetts Avenue, NW
Washington, DC 20036

Articles in this publication may be cited in other publications. In order to facilitate access to the original publication source, the following form for the citation is suggested:

> Name of Author(s), "Title of Paper," in Technical Digest on Nonlinear Guided-Wave Phenomena, 1991 (Optical Society of America, Washington, D.C., 1991), Vol. 15, pp. xx-xx.

ISBN Number

Conference Edition	1-55752-202-2 (softcover)
Postconference Edition	1-55752-203-0 (hardcover)
(Note: Postconference Edition includes postdeadline papers.)	
1991 Technical Digest Series	1-55752-192-1 (hardcover)

Library of Congress Catalog Card Number

Conference Edition	90-64484
Postconference Edition	90-64483

CONTENTS

TECHNICAL PROGRAM COMMITTEE

Allan D. Boardman, Cochair
University of Salford, UK

Nick J. Doran, Cochair
British Telecom Research Laboratories, UK

William J. Stewart, Cochair
Plessey, UK

Fatkhulla Abdulaev
Uzbek Academy of Sciences, USSR

Gunnar Arvidsson
Royal Institute of Technology, Sweden

Keith J. Blow
British Telecom Research Laboratories, UK

E. M. Dianov
USSR Academy of Sciences, USSR

Brian Henderson
University of Strathclyde, UK

A. Hadjifotiou
S. T. L., UK

Erich P. Ippen
Massachusetts Institute of Technology, USA

Mohammad Islam
AT&T Bell Laboratories, USA

Alexander E. Kaplan
The Johns Hopkins University, USA

Falk Lederer
Friedrich-Schiller-Universitat Jena, Germany

Guus Mohlmann
AKZO, The Netherlands

T. Morioka
NTT Transmission Systems Laboratories, Japan

Masataka Nakazawa
NTT Transmission Systems Laboratories, Japan

Hiroshi Nishihara
Osaka University, Japan

Daniel B. Ostrowsky
University of Nice, France

Colin Pask
Australian Defense Force Academy, Australia

Frank P. Payne
University of Cambridge, UK

Raymond Reinisch
LEMO, France

Philip Russell
University of Kent, UK

Yaron Silberberg
Bellcore, USA

John Sipe
University of Toronto, Canada

Allan W. Snyder
The Australian National University, Australia

W. Sohler
Universitat of Paderborn,
Federal Republic of Germany

George Stegeman
University of Central Florida, USA

Roger H. Stolen
AT&T Bell Laboratories, USA

Roy Taylor
Imperial College, UK

W. Jack Tomlinson
Bellcore, USA

Stefano Trillo
Fondazione Ugo Bordoni, Italy

Andrew C. Walker
Heriot-Watt University, Scotland, UK

Eva Weinert-Raczka
Technical University of Szczecin, Poland

Herbert G. Winful
University of Michigan, USA

SUNDAY, SEPTEMBER 1, 1991

PALMERSTON FOYER/BAR—Fisher Building

6:00 pm–8:00 pm **REGISTRATION**

CHAPEL COURTYARD (next to Second Court)

6:00 pm–8:00 pm **OUTDOOR INFORMAL RECEPTION (for Meeting attendees)**

THE GREAT HALL (between First & Second Court)

7:30 pm–9:00 pm **DINNER (for St. John's residents only)**

MONDAY, SEPTEMBER 2, 1991

BUTTERY DINING ROOM—Second Court

8:00 am–9:00 am **BREAKFAST (for St. John's residents only)**

PALMERSTON FOYER/BAR—Fisher Building

8:00 am–5:30 pm **REGISTRATION. SPEAKER AND PRESIDER CHECKIN**

PALMERSTON ROOM—Fisher Building

8:50 am–9:00 am **OPENING REMARKS**
N. J. Doran, *British Telecom Laboratories, U.K.*

9:00 am–10:45 am
MA, SOLITON TRANSMISSION
N. J. Doran, *British Telecom Laboratories, U.K., Presider*

9:00 am
MA1 Ultralong distance soliton transmission using erbium fiber amplifiers, L. F. Mollenauer, *AT&T Bell Laboratories, USA.* We report soliton transmission through a chain of dispersion shifted fiber segments and low gain erbium amplifiers, with measured bit error rate $< 10^{-9}$ over transoceanic paths at 2.5 Gbits/sec. **(p. 2)**

9:45 am
MA2 Constraints on the design of long-haul soliton systems, J. V. Wright, S. F. Carter, *British Telecom Laboratories, U.K.* Constraints on the operation of single- and two-channel soliton systems are considered with reference to a 6000-km system operating at 5 Gbit/sec. **(p. 6)**

MONDAY, SEPTEMBER 2, 1991—*Continued*

10:00 am
MA3 Qualitative dynamics of modulated soliton pulse trains, J. M. Arnold, *U. Glasgow, U.K.* The stability and long-distance evolution of modulated soliton pulse trains are analysed by linearization about an equilibrium. The stable linearized soliton channel exhibits a greatly enhanced range. **(p. 10)**

10:15 am
MA4 4 × 5 Gbit/sec optical time division multiplexed nonlinear transmission over 205 km, D. M. Spirit, G. E. Wickens, L. C. Blank, *British Telecom Laboratories, U.K.* Full BER characterization is presented of a 4 × 5 Gbit/sec optical time division multiplexed system over a 205-km transmission link in the presence of optical fiber nonlinearities. **(p. 14)**

10:30 am
MA5 Ultralong nonlinear fiber optics data transmission using dual-frequency laser sources, P. V. Mamyshev, S. V. Chernikov, A. M. Prokhorov, *General Physics Institute of the Academy of Sciences of the U.S.S.R.* We suggest a new method for high-bit-rate ultralong nonlinear data transmission. The system uses a dual-frequency cw laser source and has all the advantages of soliton transmission. **(p. 18)**

PALMERSTON FOYER/BAR—Fisher Building

10:45 am–11:15 am **COFFEE AND BISCUITS**

PALMERSTON ROOM—Fisher Building

11:15 am–12:45 pm
MB, RAMAN EFFECTS IN FIBERS
K. Blow, *British Telecom Laboratories, U.K., Presider*

11:15 am (Invited)
MB1 Modulational instability and Raman scattering in optical fibers, Ekaterina A. Golovchenko, *General Physics Institute, U.S.S.R.* We have investigated gain coefficients and output spectra shapes resulting from combined action of modulational instability and Raman scattering in single-mode fibers, including high birefringent fibers. **(p. 24)**

11:45 am
MB2 Stimulated Raman scattering in optical fibers: spontaneous initiation and spatial propagation, Raymond J. Hawkins, *Lawrence Livermore National Laboratory;* R. H. Stolen, *AT&T Bell Laboratories, USA.* We show that the Raman response function is related directly to the strength of the polarization fluctuations in optical fibers and, thus, provides a way of calculating the seed for stimulated Raman scattering. **(p. 28)**

12:00 m
MB3 Negative contribution to n_2 in silica fibers, R. H. Stolen, *AT&T Bell Laboratories;* W. J. Tomlinson, *Bellcore, USA.* The Raman part of the nonlinear index of silica is negative for pulse widths less than 30 fsec. This negative n_2 comes from the time delay in the Raman response. **(p. 32)**

12:15 pm
MB4 Soliton self-frequency shift in telecommunications fiber, J. K. Lucek, K. J. Blow, *British Telecom Laboratories, U.K.* The effects of fiber length and launched power on the soliton self-frequency shift are investigated and compared with results obtained from exact computer calculations. **(p. 36)**

12:30 pm
MB5 Generation of spatiotemporal patterns and all-optical switching based on coherently induced modulational instability in fibers, S. Trillo, S. Wabnitz, *Fondazione Ugo Bordoni, Rome, Italy.* We investigate the characteristics of the spatiotemporal patterns generated by coherently induced modulational instability in either isotropic or birefringent fibers. Novel applications to all-optical signal processing are discussed. **(p. 40)**

THE GREAT HALL (between First & Second Court)

12:45 pm-2:00 pm LUNCH BUFFET (for St. John's residents only)

PALMERSTON ROOM—Fisher Building

2:00 pm-3:30 pm
MC, ERBIUM LASERS
Roy Taylor, *Imperial College, U.K., Presider*

2:00 pm
MC1 Pulse repetition rates in a passive self-starting femtosecond soliton fiber laser, D. J. Richardson, R. I. Laming, D. N. Payne, V. J. Matsas, M. W. Phillips, *Southampton U., U.K.* Several unusual pulsing modes are observed in a self-starting passively mode-locked erbium fiber soliton laser capable of generating pulses with durations as short as 320 fsec. **(p. 46)**

2:15 pm
MC2 Interacting solitons in an erbium fiber laser, R. P. Davey, N. Langford, A. I. Ferguson, *U. Strathclyde, U.K.* We report novel behavior from a mode-locked erbium fiber laser. Self-sustaining 2.5 psec duration solitons have been generated, which seem to experience soliton interactions, causing complex pulse trains. **(p. 50)**

2:30 pm
MC3 Noise in a passively mode-locked fiber laser, M. H. Ober, M. Hofer, F. Haberl, M. E. Fermann, *Technische U. Vienna, Austria.* The noise performance of a passively mode-locked fiber laser is characterized. In a 300 Hz-10 kHz frequency band rms amplitude fluctuations of 0.07% and a timing jitter of 200 fsec are measured. **(p. 52)**

MONDAY, SEPTEMBER 2, 1991—*Continued*

2:45 pm
MC4 Pulse amplification and shaping using a nonlinear amplifying loop mirror, E. J. Greer, *Imperial College, U.K.*; K. Smith, N. J. Doran, D. M. Bird, K. H. Cameron, *British Telecom Laboratories, U.K.* We describe a nonlinear amplifying loop mirror comprising an 8.8-km length of dispersion shifted fiber and a lumped erbium fiber amplifier. The low switching powers (< 1 mW peak) afforded by the high gain (≈ 30 dB) and long loop length permit the efficient amplification (≈ 20 dB) and filtering of mode-locked semiconductor laser pulses. **(p. 56)**

3:00 pm
MC5 Soliton formation and propagation in a high gain fiber laser, S. M. J. Kelly, *Imperial College, U.K.*; K. Smith, K. J. Blow, N. J. Doran, *British Telecom Laboratories, U.K.* The stability of solitons propagating in the presence of a large periodic energy variation is considered. The results are applied to mode-locked erbium fiber lasers. **(p. 60)**

3:15 pm
MC6 Quantum propagation in optical fibers, K. J. Blow, S. J. D. Phoenix, *British Telecom Laboratories, U.K.*; R. Loudon, *U. Essex, U.K.* Self-phase modulation is shown to give quadrature squeezing at low power. At high power this is destroyed indicating number state generation. **(p. 64)**

PALMERSTON FOYER/BAR—Fisher Building

3:30 PM-4:00 PM TEA AND BISCUITS

PALMERSTON ROOM—Fisher Building

4:00 PM-5:30 pm
MD, NONLINEAR OPTICAL POLYMERS
George Stegeman, *U. Central Florida, Presider*

4:00 pm
MD1 Nonlinear optical polymers: waveguide devices based on second-order effects, Winfried H. G. Horsthuis, Gustaaf R. Mohlmann, Hans W. Mertens, *AKZO Research Laboratories Arnhem, The Netherlands.* Progress in second-order polymeric integrated-optic devices is reviewed. Realization issues, device performance, and the stability of the devices are discussed. **(p. 70)**

4:30 pm
MD2 Large nonlinear phase shifts in a nitrobenzene-cored single-mode fiber, Raman Kashyap, Neil Finlayson, *British Telecom Laboratories, U.K.* Nonlinear polarization effects are demonstrated in a 10-cm length of single-mode nitrobenzene-cored optical fiber. An optically induced phase shift of at least 12π has been measured at a peak power level of 14 W. **(p. 74)**

4:45 pm
MD3 Electrooptic waveguide grating using the new nonlinear-optic polymer *p*-NAn-PVA, S. Ura, R. Ohyama, T. Suhara, H. Nishihara, *Osaka U., Japan.* Electrooptic switching was demonstrated by using new nonlinear-optic polymer waveguide and interdigital electrodes. The electrooptic coefficient induced by electric-field poling was 14 pm/V. **(p. 78)**

5:00 pm
MD4 New polymers for nonlinear optics, Manabu Kishimoto, Dechun Zou, Iwao Seo, *Mitsubishi Petrochemical Co. Ltd., Japan.* Vinylidene cyanide copolymers bearing NLO-active dyes on side chains were synthesized. Poled films of the copolymers have exhibited large and stable second-order optical nonlinearities. **(p. 82)**

5:15 pm
MD5 Second harmonic generation from a polyurethane waveguide on a silver grating coupler, M. Kull, J.-L. Coutaz, G. Vitrant, R. Reinisch, *ENSERG, France;* R. Meyrueix, *Flamel Technologies, France.* Experimental results of second-harmonic generation by excitation of guided modes and the surface plasmon in a polyurethane coated silver grating are presented. **(p. 86)**

DIRAC ROOM—Fisher Building (First Level)

5:30 pm–7:00 pm
ME, POSTER SESSION: 1

ME1 Poster Paper
Efficient finite element scheme for highly nonlinear waveguides, H. E. Hernandez-Figueroa, *Imperial College, U.K.* A novel numerical approach is presented—the split-step finite element method—and compared with the split-step finite difference method. As an example, multisoliton emission from a highly nonlinear slab is adopted. **(p. 92)**

ME2 Poster Paper
Finite element analysis of two-transverse-dimensional bistable nonlinear integrated-optical waveguides, B. M. A. Rahman, *City U., U.K.;* F. A. Fernandez, R. D. Ettinger, J. B. Davies, *University College London, U.K.* A rigorous two-transverse-dimensional finite element solution of nonlinear strip-loaded optical waveguides confirms the existence of two stable states with the same total power. **(p. 96)**

ME3 Poster Paper
Analysis of TM-polarized nonlinear guided waves based on conservation laws, K. Gniadek, M. Rusek, *Warsaw U. Technology, Poland.* We investigate the properties and the relationship between two electric field components of TM-polarized guided waves in the linear thin film sandwiched between two nonlinear Kerr type media. **(p. 100)**

ME4 Poster Paper
TE waves propagating in a nonlinear planar asymmetric converging waveguide Y-junction, Sien Chi, Tian-Tsorng Shi, *National Chiao Tung U., China.* It is found that the nonlinear TE wave injected into the thinner branch with appropriate power will evolve into the fundamental mode of the stem. **(p. 104)**

ME5 Poster Paper
Spatial soliton propagation through a periodically modulated layer in a nonlinear medium, F. Kh. Abdullaev, A. A. Abdumalikov, *Uzbek Academy of Sciences, U.S.S.R.* Propagation of self-focused channel incident to a periodically modulated thin film in a nonlinear medium is investigated. Nonlinear resonances and chaotic behavior appearing at beam propagation along the film are found. **(p. 108)**

ME6 Poster Paper
Amplification of nonlinear waves in a symmetric planar waveguide, Nail N. Akhmediev, N. V. Mitskevich, *F. V. Lukin Research & Development Institute of Physical Problems, U.S.S.R.;* N. N. Nabiev, *P. N. Lebedev Physical Institute of the Academy of Sciences of the U.S.S.R.* The gain process of modes of a nonlinear symmetric planar waveguide is investigated. It is shown using numerical simulations that the gain process is adiabatic at low values of gain. **(p. 112)**

ME7 Poster Paper
Four-wave mixing limitation in multichannel coherent optical communication, Johan Nilsson, *Royal Institute of Technology, Sweden;* Milan Dado, *U. Transport & Communication, Czechoslovakia;* Bozena Jaskorzynska, *Institute of Optical Research, Sweden.* We simulate multichannel coherent transmission influenced by four-wave mixing and the resulting degradation of signal detectability dependent on system parameters. Our model accurately reproduces available experimental results. **(p. 115)**

CASTLEREAGH ROOM—Fisher Building (Second Level)

5:30 pm–7:00 pm
MF, POSTER SESSION: 2

MF1 Poster Paper
Mixed states of optical solitons on different carrying frequencies, L. M. Kovachev, *Bulgarian Academy of Sciences.* Self-confinement of wave packets on different carrying frequencies in single-mode optical fiber is investigated. Spectral bandwidths for experimental observation of this phenomenon are determined. **(p. 120)**

MF2 Poster Paper
Pulse propagation in nonlinear optical fibers with spatial inhomogeneities, E. Ryder, D. F. Parker, A. P. Mayer, *U. Edinburgh, U.K.* The propagation of envelope pulses in nonlinear optical fibers with carrier wave frequency in the monomode regime is described by a pair of nonlinearly coupled nonlinear Schrodinger equations. **(p. 124)**

MF3 Poster Paper
Interactions between solitons in a single-mode fiber, Boris A. Malomed, *P. P. Shirshov Institute for Oceanology of the Academy of Sciences of the U.S.S.R.* Interactions between well separated solitons and a collision between solitons with a large frequency difference are studied by perturbation theory. Stable bound states are discovered, and the collision-induced energy exchange is calculated. **(p. 128)**

MF4 Poster Paper
Cross-phase-modulation-induced nonelastic collisions of optical solitons, A. Hook, M. Lisak, D. Anderson, *Chalmers U. Technology, Sweden;* V. N. Serkin, *Institute for General Physics of the Academy of Sciences of the U.S.S.R.* Conditions for nonelastic, incoherent collisions of solitons at different wavelengths and the generation of symbiotic soliton pairs are investigated. A new nonlinear effect is also predicted. **(p. 132)**

MF5 Poster Paper
Erbium fiber soliton laser pumped by a laser diode, K. Smith, R. Wyatt, N. J. Doran, *British Telecom Laboratories, U.K.;* E. J. Greer, *Imperial College, U.K.;* R. Davey, *U. Strathclyde, U.K.* We describe the generation of picosecond pulses around 1.55 μm from a totally integrated mode-locked erbium-doped fiber laser. Temporal, spectral, and power characteristics of the laser output are consistent with fundamental soliton pulses. **(p. 136)**

MF6 Poster Paper
Ultrashort pulse amplification in erbium-doped fiber amplifiers, D. V. Korobkin, Jr., I. Yu Khrushchev, A. B. Grudinin, E. M. Dianov, *General Physics Institute of the Academy of Sciences of the U.S.S.R.* Pulses of 34-fsec duration have been obtained from an erbium-doped fiber amplifier by injecting pulses of 80-fsec duration. It has been found that the erbium ions influence the Raman gain. **(p. 140)**

BOYS SMITH ROOM—Fisher Building (Lower Level)

5:30 pm-7:00 pm
MG, POSTER SESSION: 3

MG1 Poster Paper
Proposal of high capacity all-optical TDMA networks, F. Matera, M. Romagnoli, M. Settembre, M. Tamrurrini, *Fondazione Ugo Bordoni, Italy.* Two scheme of all opticalTDMA networks are proposed with the demultiplexed processing obtained by means of an optical gate based on the second harmonic generation process. The maximum throughput is obtained when solitons are used and is equal to 125 Gbits/s. **(p. 146)**

MG2 Poster Paper
Optical fiber transmission scheme with ultrahigh bit rate capability, G. R. Boyer, M. A. Franco, M. K. Jackson, A. Mysyrowicz, *Ecole Polytechnique-Ecole Nationale Superieure de Techniques Avancees, France.* An optical fiber transmission scheme with 500 Gbit/sec rate is demonstrated experimentally. Limitations of the system due to optical nonlinearities are observed and discussed. **(p. 150)**

MONDAY, SEPTEMBER 2, 1991—*Continued*

MG3 Poster Paper
Distortion of a broadband-intensity signal during its transmission through a chain of lumped amplifiers due to their saturation, A. V. Luchnikov, A. N. Pilipetskii, *General Physics Institute of the Academy of Sciences of the U.S.S.R.* The SNR decrease of a broadband-intensity signal from saturation in lumped erbium-doped fiber amplifiers applying to soliton communication systems is theoretically analyzed. **(p. 153)**

MG4 Poster Paper
Gain saturation by the random pulse train and noise characteristics of a long-distance soliton-based system, A. N. Starodumov, *General Physics Institute of the Academy of Sciences of the U.S.S.R.* The effect of random gain saturation in optical amplifiers caused by information bearing solitons is investigated. The degradation of the SNR at the output of the communication line is evaluated. **(p. 157)**

MG5 Poster Paper
Influence of self-phase modulation on ultralong-span optical transmission at zero dispersion, S. F. Carter, E. G. Bryant, J. V. Wright, *British Telecom Laboratories, U.K.* Computer modeling is used to evaluate a long-span optically amplified transmission system. The combined effects of dispersion, Kerr effect, and amplifier noise are considered. **(p. 161)**

MG6 Poster Paper
Electrostrictional interaction of optical pulses in long-distance soliton communication systems, E. M. Dianov, A. V. Luchnikov, A. N. Pilipetskii, A. M. Prokhorov, *General Physics Institute of the Academy of Sciences of the U.S.S.R.* We consider the influence of the optical soliton electrostrictional long-range interaction on the bit error rate in long distance communication systems. **(p. 165)**

THE GREAT HALL (between First & Second Court)

7:00 pm-9:00 pm **RECEPTION & BANQUET DINNER (for Meeting attendees and guests with tickets)**

TUESDAY, SEPTEMBER 3, 1991

BUTTERY DINING ROOM—Second Court

8:00 am-9:00 am **BREAKFAST (for St. John's residents only)**

PALMERSTON FOYER/BAR—Fisher Building

8:00 am-5:30 pm **REGISTRATION, SPEAKER AND PRESIDER CHECKIN**

PALMERSTON ROOM—Fisher Building

9:00 am-10:30 am
TuA, ERBIUM-DOPED FIBERS AND AMPLIFIERS
Roger Stolen, *AT&T Bell Laboratories, Presider*

9:00 am (Invited Paper)
TuA1 Coherent effects in Er-doped fibers: photon echo with femtosecond pulses, Y. Silberberg, V. L. da Silva, J. P. Heritage, E. W. Chase, M. A. Saifi, M. J. Andrejco, *Bellcore, USA*. We report the observation of photon-echo in Er-doped fibers. We demonstrate time-reversal and autoconvolution of femtoseond pulses, suggesting that Er-doped fibers are a promising medium for femtosecond time-domain optical signal processing. **(p. 170)**

9:30 am
TuA2 Soliton frequency stabilization and Raman self-frequency shift suppression in fibers doped with Er and Tm ions, E. M. Dianov, K. K. Konstantinov, A. N. Pilipetskii, A. N. Starodumov, *General Physics Institute of the Academy of Sciences of the U.S.S.R.* Soliton frequency stabilization occurs only for determined input soliton energy and wavelength. When parameters differ from the optimum an unusual effect takes place: soliton energy and wavelength oscillations along the fiber. **(p. 174)**

9:45 am
TuA3 Soliton self-frequency shift in the amplification of femtosecond fundamental solitons using Er-doped fibers, W. Hodel, J. Schutz, H. P. Weber, *U. Bern, Switzerland*. Numerical calculations demonstrate that amplification of ultrashort fundamental solitons leads to a gain enhanced soliton self-frequency shift that severely limits the amplification efficiency. **(p. 178)**

10:00 am
TuA4 Theory of ultrashort soliton amplification in erbium-doped fibers, I. R. Gabitov, *L. D. Landau Institute for Theoretical Physics, U.S.S.R.*; M. Romagnoli, S. Wabnitz, *Fondazione Ugo Bordoni, Italy*. Coherent effects and self-Raman scattering in erbium-doped fiber amplifiers lead to ultrashort soliton collapse, pulse train generation, and soliton collisions. **(p. 182)**

TUESDAY, SEPTEMBER 3, 1991—*Continued*

10:15 am
TuA5 Theory of femtosecond soliton amplification in rare-earth-doped fibers, V. V. Afanasjev, V. N. Serkin, *General Physics Institute of the Academy of Sciences of the U.S.S.R.*; V. A. Vysloukh, *Moscow State U., U.S.S.R.* The influence of dispersion, nonlinearity effects, and Raman self-frequency shift on dynamics of soliton amplification and compression in rare-earth-doped fibers are investigated. Utmost degrees of femtosecond soliton amplification and compression are discussed. **(p. 186)**

PALMERSTON FOYER/BAR—Fisher Building

10:30 am-11:00 am **COFFEE AND BISCUITS**

PALMERSTON ROOM—Fisher Building

TuB, SEMICONDUCTORS
Allan D. Boardman, *U. Salford, U.K., Presider*

11:00 am (Invited Paper)
TuB1 Nonlinear guided waves in semiconductors: induced focusing and directional coupling, H. M. Gibbs, G. Khitrova, R. Jin, C. L. Chuang, Jiajin Xu, *U. Arizona*. Two-transverse-dimension plasma-theory computations are in good agreement with observations in GaAs/AlGaAs waveguides of nonlinear directional coupling and the recently predicted induced focusing in a self-defocusing medium. **(p. 192)**

11:30 am
TuB2 Ultrafast optical Kerr effect in active semiconductor waveguides, C. T. Hultgren, E. P. Ippen, *Massachusetts Institute of Technology, USA*. Studies of index dynamics in active AlGaAs waveguides reveal a large, apparently instantaneous optical Kerr effect in addition to changes related to carrier temperature and number. **(p. 196)**

11:45 am
TuB3 All-optical modulation by interaction between interband and intraband light in an *n*-doped quantum well structure, Susumu Noda, Tetsuro Okuda, Takao Yamashita, Akio Sasaki, *Kyoto U., Japan*. All-optical modulation using *n*-doped quantum wells is demonstrated. The modulation is made by the nonlinear third-order interaction between interband and intraband light through a guided-wave structure. **(p. 200)**

12:00 m
TuB4 Nonlinear refraction and absorption of an InGaAs single quantum well in an InGaAsP waveguide, J. E. Ehrlich, D. J. Goodwill, D. T. Neilson, A. C. Walker, *Heriot-Watt U., U.K.*; C. I. Johnston, W. Sibbett, *U. St. Andrews, U.K.* We report absorptive and refractive-index changes from optically induced electronic excitation of a single quantum well of InGaAs within a linear InGaAsP waveguide under quasi-cw excitation. **(p. 204)**

12:15 pm
TuB5 Nonlinear optical properties of a single quantum well waveguide and a nonlinear asymmetric interferometer, K. Al Hemyari, C. N. Ironside, *U. Glasgow, U.K.*; B. S. Bhumbra, *STC Technology, Ltd., U.K.* The nonlinear optical properties of a single quantum well waveguide are investigated to gain an understanding of the operation of an integrated nonlinear interferometer. **(p. 208)**

12:30 pm
TuB6 Nonlinear directional coupler based on Rb:KTP waveguides, K. S. Buritskii, E. M. Dianov, V. A. Maslov, V. A. Chernykh, E. O. Shcherbakov, *General Physics Institute of the Academy of Sciences of the U.S.S.R.* The passing of subnanosecond light pulses through a nonlinear directional coupler, fabricated in KTP crystal, was investigated. Nonlinear switching of 40% of light power from one channel to another was observed at 5-kW input power. **(p. 212)**

THE GREAT HALL (between First & Second Court)

12:45 pm–2:00 pm **LUNCH BUFFET (for St. John's residents only)**

PALMERSTON ROOM—Fisher Building

2:00 pm–3:30 pm
TuC, MULTIPHOTON EFFECTS
G. Arviddson, *Royal Institute of Technology, Sweden, Presider*

2:00 pm **(Invited Paper)**
TuC1 Prospects for nonlinear organics in guided wave optics, George I. Stegeman, *U. Central Florida, USA.* We discuss the use of organic materials with second and third order nonlinearities in guided wave geometries. **(p. 218)**

2:30 pm
TuC2 Nonlinear absorption processes at half the band gap in GaAs-based semiconductors, A. Villeneuve, G. I. Stegeman, *U. Central Florida, USA*; G. Scelsi, *Columbia U., USA*; C. N. Ironside, J. S. Aitchison, *U. of Glasgow, U.K.*; J. T. Boyd, *U. Cincinnati, USA.* We have measured the two-photon absorption coefficient versus wavelength in GaAs waveguides near one half the band gap using both single beam and pump-probe techniques. **(p. 222)**

2:45 pm
TuC3 Measurement of high frequency electrooptic coefficients in ferroelectric liquid crystal materials, J. Y. Liu, *Sharp Laboratories of Europe, U.K.*; M. G. Robinson, K. M. Johnson, D. Doroski, *U. Colorado.* The high frequency electrooptic effect in ferroelectric liquid crystal is presented by using prism coupling and Fabry-Perot techniques. Results indicate $r_{42} \approx 0.3$ pm/V for SCE9. **(p. 226)**

TUESDAY, SEPTEMBER 3, 1991—*Continued*

3:00 pm
TuC4 Quasi-phase-matched second-harmonic generation in lithium tantalate waveguides: experiments and simulations, Henrik Ahlfeldt, Gunnar Arvidsson, Bozena Jaskorzynska, *Institute of Optical Research, Sweden.* We report generation of blue light by quasi-phase-matched SHG in $LiTaO_3$ waveguides, and calculations on the design of such waveguides in $LiTaO_3$ compared with $LiNbO_3$. **(p. 230)**

3:15 pm
TuC5 Grating couplers for Kerr-type nonlinear waveguides: a simplified theory, R. Reinisch, G. Vitrant, *LEMO—ENSERG, France*; P. Vincent, M. Neviere, *U. Marseille-St. Jerome, France.* We present a simplified theory of nonlinear grating couplers, whose accuracy can be easily checked, which gives the guided wave and the radiated diffracted order intensities. **(p. 234)**

PALMERSTON FOYER/BAR—Fisher Building

3:30 pm–4:00 pm **TEA AND BISCUITS**

PALMERSTON ROOM—Fisher Building

4:00 pm–5:00 pm
TuD, NOVEL EFFECTS
Yaron Silberberg, *Bellcore, Presider*

4:00 pm **(Invited Paper)**
TuD1 Remote nonlinear switching and large nonlinear effects in resonant optical waveguides, Falk Lederer, U. Trutschel, M. Mann, C. Wachter, *Jena Friedrich-Schiller U., Germany.* We investigate nonlinear effects in resonant waveguides, where the guiding mechanism relies on Fabry-Perot action or Bragg reflection. We discuss the action of nonlinear cut-off modulators as well as a remote nonlinear directional coupler. **(p. 240)**

4:30 pm
TuD2 Photonic Bloch waves and field microstructure in nonlinear gratings: an intuitive approach, P. St. J. Russell, *U. Southampton, U.K.* The field microstructure of photonic Bloch waves is used to explain the physical origins of bistable, oscillatory, and unstable Bragg reflections from a nonlinear grating half-space. **(p. 244)**

4:45 pm
TuD3 Experimental observation of picosecond dark soliton propagation over 1 km fiber in the near infrared, P. Emplit, J.-P. Hamaide, M. Haelterman, *Universite Libre de Bruxelles, Belgium.* We investigate nonlinear propagation of picosecond dark pulses over 1-km single-mode fiber in the near infrared. Odd-symmetry dark pulses are shown to propagate without distortion at the power corresponding to the NLSE fundamental dark soliton. Our results constitute a first evidence of dark soliton propagation over fiber length compatible with optical telecommunication systems. **(p. 248)**

5:00 pm
TuD4 HE_{1m} self-guided modes: vector solutions and stability, J.-L. Archambault, S. Lacroix, *Ecole Polytechnique de Montreal, Canada;* A. W. Snyder, *Australian National U.* HE_{1m} self-guided modes in a Kerr-law medium are shown to be stable solutions of the vector equation. Accurate analytical expressions are derived using a first-order Gaussian approximation. **(p. 252)**

5:15 pm
TuD5 Limitation for transmission capacity in soliton-based optical fiber communications due to stimulated Brillouin scattering, Carlos Montes, *U. Nice-Sophia Antipolis, France;* Alexander M. Rubshchik, *Institute of Automation & Electrometry, U.S.S.R.* We show that for nonshifted-dispersion single-mode fibers the soliton information may be perturbed above some power threshold for currently high bit rates (f_{bit} = 20 GHz). **(p. 256)**

DIRAC ROOM—Fisher Building (First Level)

5:30 pm–7:00 pm
TuE, POSTER SESSION: 4

TuE1 Poster Paper
Nonlinearity enhancement in a four-layer GaAs/GaAlAs waveguide, Shaomei Chen, Changjun Liao, Huaichen Jin, Zhaohong Huang, *South China Normal U., China.* Ionization of deep level defects at a twin-layer core offers fixed positive charged centers and free electrons diffused to one side, resulting in enhanced nonlinearity. **(p. 262)**

TuE2 Poster Paper
Large nonresonant nonlinearities in DANS-based polymer waveguides: role of microscopic cascading, G. Assanto, G. I. Stegeman, *U. Central Florida;* M. B. Marques, *U. Porto, Portugal;* W. E. Torruellas, *Raytheon Research Division;* W. H. G. Horsthuis, G. R. Mohlmann, E. W. P. Erdhuisen, *AKZO Research Laboratories, The Netherlands.* Nonlinear grating coupling and third-harmonic generation measurements of DANS groups on side-chain polymers show large nonresonant nonlinearities dominated by cascading of the local second-order nonlinearity. **(p. 266)**

TuE3 Poster Paper
Characteristics of annealed proton exchanged waveguides for quasi-phase-matched frequency conversion in periodically poled $LiNbO_3$ waveguides, M. M. Fejer, M. L. Bortz, E. J. Lim, *Stanford U., USA.* We discuss the dependence of $\chi^{(2)}$, index of refraction, diffusion coefficients, and ferroelectric domains on proton concentration, and their effect on visible and infrared frequency conversion in proton exchanged $LiNbO_3$. **(p. 270)**

TuE4 Poster Paper
Flowing afterglow synthesis of polythiophene films, Peter Haaland, James Targove, *U.S. Air Force Institute of Technology, USA.* Dense uniform films of polythiophene have been synthesized in a flowing afterglow reactor and characterized by spectroscopic ellipsometry, atomic force microscopy, and optical waveguiding. **(p. 274)**

TuE5 Poster Paper
Instabilities of a dispersive nonlinear all-fiber ring cavity, Real Vallee, Michel Piche, *U. Laval, Canada.* The dynamical instabilities at the output of an all-fiber ring cavity synchronously pumped by a train of 1-psec pulses at 858 nm are considered. The combination of the intrinsic instabilities and the group velocity dispersion is analyzed via a numerical simulation of the nonlinear Schrodinger equation. **(p. 278)**

TuE6 Poster Paper
Doubly nonlinear fiber loop lasers, P. E. Langridge, W. J. Firth, *U. Strathclyde, U.K.* We consider a novel-passively mode-locked fiber laser in the form of a loop resonator with NL coupling to and from the active medium. **(p. 281)**

TuE7 Poster Paper
Fiber optical element for ultrashort pulse control and switching, D. V. Khaidarov, *Uzbek Academy of Sciences, U.S.S.R.* A fiber-optical loop is investigated as an element for femtosecond fundamental soliton self-switching and conversion. Interaction between soliton and cw radiation in the loop leads to formation of ultrashort pulses with a linear chirp. **(p. 283)**

CASTLEREAGH ROOM—Fisher Building (Second Level)

5:30 pm–7:00 pm
TuF POSTER SESSION: 5

TuF1 Poster Paper
Spatio-temporal dynamics of light pulses in nonlinear weak-guiding optical waveguides, L. A. Melnikov, R. G. Bauer, *Chernyshevsky State U., U.S.S.R.* We have investigated the pulse-envelope evolution in parabolic graded-index optical fiber including self-focusing, group velocity dispersion, and self-phase modulation simultaneously. **(p. 288)**

TuF2 Poster Paper
Soliton propagation in media with noncentral symmetry, Qi Guo, Chang-Jun Liao, Shong-Hao Liu, *South China Normal U., China.* It is theoretically demonstrated, we believe for the first time, that solitons described by the nonlinear Schrodinger equation can exist in waveguides made of media with noncentral symmetry. **(p. 292)**

TuF3 Poster Paper
Mechanisms of the coherent photovoltaic effect for second-harmonic generation in glass fibers, V. O. Sokolov, V. B. Sulimov, *Institute of General Physics of the Academy of Sciences of the U.S.S.R.* Mechanisms of the direct current creation under coherent pump and second-harmonic waves due to electron excitation from defects in the conduction band are discussed. Defect models and current estimates are presented. **(p. 296)**

TuF4 Poster Paper
Correlation of UV radiation with the process of second harmonic generation in Ge-doped optical fibers, F. B. Baikabulov, P. V. Chernov, S. K. Isaev, L. S. Kornienko, A. O. Ribaltovsky, Yu. P. Yatsenko, *Moscow State U., U.S.S.R.* We have found that the seeding process is accompanied by parametric third- and fourth-harmonic generation and 400-nm fluorescence. Correlation is revealed between UV radiation and seeding time. **(p. 300)**

TuF5 Poster Paper
Theory of photoinduced second-harmonic generation caused by phase transition in defects in silica glass, E. M. Dianov, V. O. Sokolov, V. B. Sulimov, *General Physics Institute of the Academy of Sciences of the U.S.S.R.* A theory of photoinduced second-harmonic generation in doped silica is proposed. The collective pseudo-Jahn Teller phase transition in a system of defects results in nonzero second-order macroscopic susceptibility. **(p. 304)**

TuF6 Poster Paper
Distributed out-coupling of second harmonic generation in a waveguide, *Z. Weissman, A. Hardy, E. Marom, Tel Aviv U., Israel.* We show that the conversion efficiency of waveguide with strong dispersion and second-harmonic absorption can be significantly increased by distributed out-coupling through a nonresonant first-order corrugation. **(p. 308)**

BOYS SMITH ROOM—Fisher Building (Lower Level)

5:30 pm–7:00 pm
TuG POSTER SESSION: 6

TuG1 Poster Paper
Nonlinear CdS grating coupler: cw and pulsed operation, M. Bertolotti, F. Michelotti, C. Nisio, E. Fazio, *U. Rome, Italy;* G. Assanto, *U. Central Florida, USA;* C. Cali, *U. Palermo, Italy.* The nonlinear coupling properties of a CdS grating realized a 200-Å thin layer on a glass waveguide buried between a linear guide and the substrate are experimentally investigated. Input grating efficiency vs incident power is studied in both cw and pulsed regimes. **(p. 312)**

TuG2 Poster Paper
Polarization-induced switching and bistability in a nonlinear prism coupler, Jan Danckaert, *Brussels Free U., Belgium;* Guy Vitrant, Raymond Reinisch, *LEMO-ENSBERG, France.* Using a modal theory for nonlinear planar resonators, we study polarization-induced irradiance switching and polarization bistability in waveguides with a diffusive third-order nonlinearity. **(p. 313)**

TUESDAY, SEPTEMBER 3, 1991—*Continued*

TuG3 Poster Paper
Ideal switching in an active coupler, A. W. Snyder, Y. Chen, *Australian National U.;* D. N. Payne, *U. Southampton, U.K.* An unconventional use of material gain is advanced for fast switching at low power in short twin-core couplers, creating a resonance mismatch. **(p. 317)**

TuG4 Poster Paper
Nonlinear bent directional couplers with asymmetrical distribution of nonlinearity, Miroslaw A. Karpierz, *Warsaw U. Technology, Poland.* The nonlinear directional coupler with bending waveguides is analyzed in the presence of asymmetrical distribution of nonlinearity. It is shown that the asymmetrical configuration requires lower critical power than the symmetrical configuration. **(p. 321)**

TuG5 Poster Paper
Directional couplers with varying placement of nonlinearity in quaternary semiconductors, C. P. Hussell, R. Srivastava, R. V. Ramaswamy, *U. Florida;* M. Bloemer, P. Ashley, *U.S. Army Missile Command, USA.* We demonstrate that the performance of nonlinear directional couplers in compound semiconductors can be optimized by placing the multiple quantum well nonlinearity in the coupling region only. **(p. 325)**

TuG6 Poster Paper
Nonlinear directional coupler switched by the external wave, Ewa Weinert-Raczka, *Technical U. Szczecin, Poland;* Jan Petykiewicz, *Warsaw U. Technology, Poland.* A new mode of operation for traditional nonlinear directional couplers is proposed that relies on a power exchange between weak modes controlled by a strong external wave. **(p. 329)**

TuG7 Poster Paper
Nonlinear switching characteristic of an ARROW-based directional coupler, U. Trutschel, M. Mann, C. Wachter, F. Lederer, L. Leine, *Jena Friedrich-Schiller U., Germany.* A nonlinear directional coupler consisting of two coupled ARROWs is presented. The coupling and switching characteristic between the far removed ARROWs is investigated in detail. **(p. 333)**

THE GREAT HALL (between First & Second Court)

7:30 pm–9:00 pm DINNER (for St. John's residents only)

PALMERSTON ROOM —Fisher Building

9:00 pm–10:30 pm
POSTDEADLINE PAPER SESSION
William J. Stewart, *Plessey, U.K., Presider*

WEDNESDAY, SEPTEMBER 4, 1991

BUTTERY DINING ROOM—Second Court

8:00 am–9:00 am **BREAKFAST (for St. John's residents only)**

CASTLEREAGH ROOM—Fisher Building (Second Level)

8:00 am–9:00 am **LUGGAGE ROOM (Residents of St. Johns's College *must* vacate sleeping rooms by 9:00 am)**

PALMERSTON FOYER/BAR—Fisher Building

8:00 am–4:00 pm **REGISTRATION, SPEAKER AND PRESIDER CHECKIN**

PALMERSTON ROOM—Fisher Building

9:00 am–10:45 am
WA, FIBER SWITCHES: 1
Philip Russell, *U. Southampton, U.K., Presider*

9:00 am (Invited Paper)
WA1 All-optical switching in optical fiber devices, K. J. Blow, *British Telecom Laboratories, U.K.* In the last few years a number of fiber based devices have demonstrated all-optical switching and are reviewed briefly. Recent results on long Mach-Zehnder and fiber loop devices are discussed. **(p. 338)**

9:30 am
WA2 All-optical gigabit switching in a nonlinear loop mirror using semiconductor lasers, B. P. Nelson, K. J. Blow, P. D. Constantine, N. J. Doran, J. K. Lucek, I. W. Marshall, K. Smith, *British Telecom Laboratories, U.K.* We have demonstrated switching of a 20-Gbit pulse train at 2.5 Gbit in an all-fiber NOLM. An entirely semiconductor powered configuration was used with a long loop (6.4 km) ensuring low power (10 mW) for the switching pulses. **(p. 342)**

9:45 am
WA3 All-optical logic gates based on cross-phase modulation in a nonlinear fiber interferometer, J.-M. Jeong, M. E. Marhic, *Northwestern U., USA.* Eight two-input Boolean functions are demonstrated in a versatile nonlinear interferometer with a 400-m long single-mode fiber loop using cross-phase modulation. **(p. 345)**

10:00 am
WA4 Ultrafast multibeatlength all-optical fiber switch, N. Finlayson, B. K. Nayar, N. J. Doran, *British Telecom Laboratories, U.K.* We have fabricated a simple and stable all-optical polarization switch from a 1.1-km length of fiber. To our knowledge this is the first all-optical switch to operate successfully in the multibeatlength regime. Low switching power occurs as a result. **(p. 349)**

WEDNESDAY, SEPTEMBER 4, 1991—*Continued*

10:15 am
WA5 Observation of polarization switching and pulse break-up in spun fiber, P. Ferro, M. Haelterman, S. Trillo, S. Wabnitz, B. Daino, *Fondazione Ugo Bordoni, Italy.* We have observed the complete self-switching of the polarization state along the profile of picosecond pulses in a 200-m long spun birefringent fiber. **(p. 353)**

10:30 am
WA6 Nonlinear polarization effects in self-switching nonlinear fiber loop mirror devices, B. K. Nayar, N. Finlayson, N. J. Doran, *British Telecom Laboratories, U.K.* The polarization sensitivity of a nonlinear fiber loop mirror fabricated using standard telecommunication fiber and operating in reflection, transmission, and intermediate modes is presented. **(p. 357)**

PALMERSTON FOYER/BAR—Fisher Building

10:45 am–11:15 am **COFFEE AND BISCUITS**

PALMERSTON ROOM—Fisher Building

11:15 am–12:30 pm
WB, FIBER SWITCHES: 2
Andrew C. Walker, *Heriot-Watt U., U.K., Presider*

11:15 am (Invited Paper)
WB1 Billiard ball soliton interaction gates, M. N. Islam, C. E. Soccolich, *AT&T Bell Laboratories, USA.* We demonstrate a cascadable, phase-independent, conservative-logic interaction gate that has two identical frequency inputs and that is based on elastic collisions between temporal solitons in optical fibers. **(p. 362)**

11:45 am
WB2 Application of ultrafast gates to a soliton ring network, C. E. Soccolich, M. N. Islam, B. J. Hong, M. Chbat, J. R. Sauer, *AT&T Bell Laboratories, USA.* We describe the system architecture for a 100-Gbit/sec self-routing, soliton ring network that uses ultrafast soliton dragging and trapping logic gates to select and decode packet headers. **(p. 366)**

12:00 m
WB3 All-optical routing switch with tolerance to timing jitter at 2.5 Gbit/sec, P. M. W. French, M. C. Gabriel, H. Avramopoulos, D. J. Di Giovanni, R. E. LaMarche, H. M. Presby, N. A. Whitaker, Jr., *AT&T Bell Laboratories, USA.* All-optical routing/demultiplexing has been demonstrated at 2.5 Gbit/sec. Complete switching of arbitrary pulse patterns has been achieved in spite of timing errors as large as 380 psec. **(p. 370)**

12:15 pm
WB4 Ultrafast, dual-path optical Kerr demultiplexer utilizing a polarization rotating mirror, T. Morioka, H. Takara, M. Saruwatari, *NTT Transmission Systems Laboratories, Japan.* All-optical Kerr switching in a reflective, dual-path configuration is proposed and its stable 50 Gbit/sec operation has been demonstrated. The scheme utilizes polarization rotation upon reflection that compensates for birefringence and phase turbulence in the Kerr media. **(p. 374)**

THE GREAT HALL (between First & Second Court)

12:30 pm–2:00 pm LUNCH BUFFET (for St. John's residents only)

PALMERSTON ROOM—Fisher Building

2:00 pm–4:00 pm
WC, SPATIAL SOLITONS
Frank P. Payne, *U. Cambridge, U.K., Presider*

2:00 pm (Invited Paper)
WC1 *Soliton self-trapping of light beams,* A. Barthelemy, C. Froehly, O. Guy, M. Shalaby, D. F. Reynaud, U. Limoges, France; R. de la Fuente, *U. Santiago de Compostela, Spain.* Spatial solitons are monochromatic patterns exhibiting stable self-trapping above their self-focusing threshold. Self-trapping stability requires the two-dimensionality of the propagating fields. We describe the generation and properties of such beams in two and three dimensions. **(p. 380)**

2:30 pm
WC2 *Spatial dark solitons,* G. A. Swartzlander, Jr., A. E. Kaplan, *Johns Hopkins U.*; D. R. Andersen, *U. Iowa, USA.* Spatial dark solitons are experimentally found (and verified by numerical simulations and anlytical solutions) in a laser beam propagating in various self-defocusing nonlinear materials. **(p. 384)**

2:45 pm
WC3 Spatial solitons: mutual interactions and magneto-optic surfaces, A. D. Boardman, Xie Kang, *U. Salford, U.K.* Critical interactions between differently polarized spatial solitons are calculated analytically. Numerical investigations, including diffusion and saturation, are reported. Magnetooptic reflection of solitons is analyzed. **(p. 288)**

3:00 pm
WC4 Transverse solitary waves: observation and computation. G. Khitrova, J. W. Grantham, Jiajin Xu, H. M. Gibbs, *U. Arizona;* J. F. Valley, *Lockheed Palo Alto Research Laboratories, USA.* The cell-exit transverse profile for cavityless propagation through sodium vapor forms a stationary pattern of spots that bifurcates with input power or detuning in agreement with computations. **(p. 391)**

WEDNESDAY, SEPTEMBER 4, 1991—
Continued

3:15 pm
WC5 Steering one spatial solitary beam by another, A. W. Snyder, L. Poladian, D. J. Mitchell, *Australian National U.* We report on the curious interaction of bright and dark spatial solitary waves of both planar and circular symmetry in both Kerr and threshold nonlinearities. **((p. 395)**

3:30 pm
WC6 Spatial solitons in planar waveguides, R. A. Sammut, C. Pask, Q. Y. Li, *U. New South Wales, Australia.* We develop methods for interpreting beam propagation in planar waveguides in terms of 2-D spatial solitons and we examine transitions to 3-D self-trapping. **(p. 399)**

3:45 pm
WC7 Dynamic effects of Kerr nonlinearity and spatial diffraction on self-phase modulation of optical pulses, M. Karlsson, D. Anderson, M. Desaix, M. Lisak, *Chalmers U. Technology, Sweden.* The nonlinear self-phase modulation characteristics of optical pulses are shown to be qualitatively unaffected by diffraction effects, contrary to recent claims. **(p. 403)**

Soliton Transmission

MA 9:00am–10:45am
Palmerston Room

N. J. Doran, *Presider*
British Telecom Laboratories, United Kingdom

ULTRALONG DISTANCE SOLITON TRANSMISSION USING ERBIUM FIBER AMPLIFIERS

L. F. Mollenauer
Rm 4C-306
AT&T Bell Laboratories
Holmdel, NJ 07733

Summary

Long distance transmission using a chain of optical amplifiers is potentially much cheaper and faster than with conventional electronic regenerators. Erbium doped fiber amplifiers, with their low pump-power requirements, lack of pulse chirping, independence of gain on polarization, built in automatic gain control, and perfect compatibility with transmission fibers, have done much to make this "all-optical" approach truly practical. It can be shown, however, that the full capacity of such a system can be realized only by using solitons.

Solitons can be transmitted perfectly well through a chain of low gain amplifiers and dispersion shifted fiber segments, as long as the characteristic dispersion distance, $(2/\pi)z_0$, is great enough with respect to the amplifier spacing [1]. For such transmission, it is necessary only to make the path-average power over each amplification period equal to the usual soliton power in lossless fiber. We have verified this point experimentally [2,3] over paths as great as 12,000 km and at pulse rates to 2.5 Gbits/s by using the recirculating loop shown in Fig. 1. In all cases, broadening of the ~50 ps pulse train can be explained almost entirely by a modest jitter in pulse arrival times from the Gordon-Haus effect [4]; furthermore, at about 5000 or 6000 km, the pulse shapes look more nearly text book perfect than they do at the beginning. Thus there is no significant broadening or other distortion of the individual pulses. Our experiments [2] have also shown no significant interaction between soliton pairs spaced 5 or more pulse widths apart, and a complete absence of the long distance interaction discovered earlier in experiments using high dispersion fiber [5].

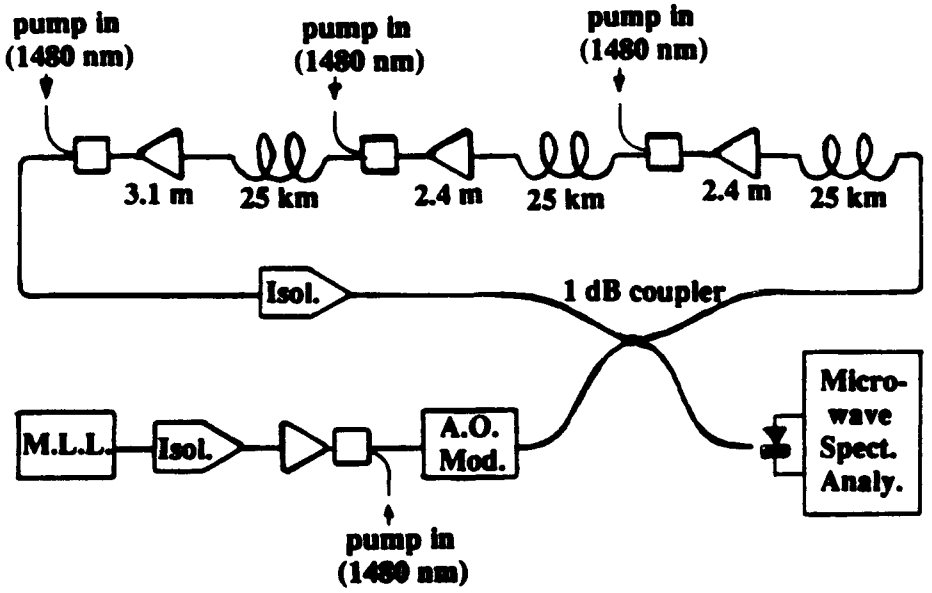

Fig. 1: Schematic of the recirculating loop. The 25 km lengths of AT&T dispersion shifted fiber had $\bar{D}$ = 1.38 ps/nm/km, A_{eff} = 35 μm^2, 0.25 dB/km loss at $\lambda_{sig.}$ = 1532 nm, and a polarization dispersion parameter less than 0.2 ps/$km^{1/2}$. The acousto-optic modulator is used for its ability to reject the signal pulse stream >80 dB once the loop has been filled.

The ultimate test, however, lies in direct bit error rate measurements. Recently, we have devised a novel technique to facilitate such measurements in a recirculating loop. First, with an electro-optic modulator, we impose a 2^{12} bit pseudo random word, followed by its logical complement, onto the stream of pulses emerging from a mode-locked external cavity diode laser, and fill the loop with that repeated pattern. We then split the loop output into two parts, delay one part by exactly one word length, and then detect and regenerate each part. The two sets of complementary, regenerated data are then compared in an ultrafast *exclusive nor* gate, whose output goes high only when an error is present. Finally, those errors corresponding to the final round trip are gated out with an *and* gate and sent to a counter. Figure 2 shows the best results we have obtained to date at 2.5 Gbits/s. Note that we have achieved essentially "error-free" transmission (error rate $\leq 10^{-10}$) over 7500 km, the undersea distance between New Jersey and England.

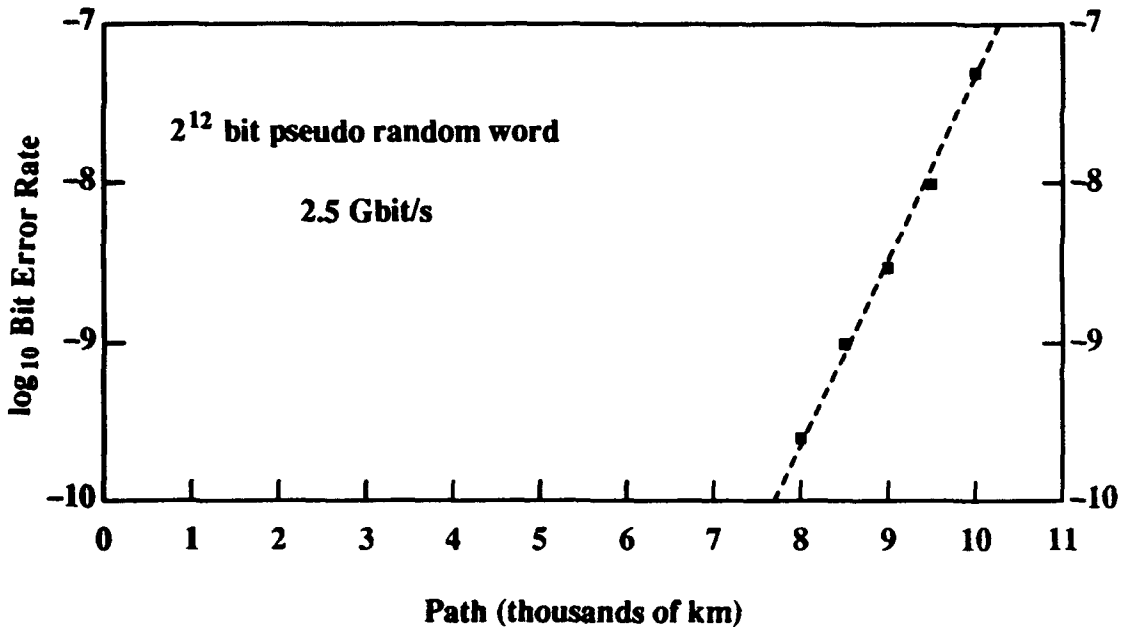

Fig. 2: Measured bit error rate for soliton transmission at 2.5 Gbits/s as a function of the total path traversed.

While that error free distance is a good beginning, it is considerably less than predicted by the simplest theory [6]. We speculate that the difference can be explained in terms of a less than 100% amplitude margin of the regenerators, and in terms of excess noise at the signal frequency created by dispersive wave radiation shed by the initially imperfect pulses fed into the transmission line. Nevertheless, with improved fiber (A_{eff} = 50μm^2, loss rate 0.21 dB/km, as opposed to the parameters cited above in the caption to Fig. 1), and with the lower n_{sp} possible with operation at 1550 nm rather than at 1532 nm, we expect soon to be able to extend error free transmission to well beyond the trans-Pacific undersea distance of 9000-10000 km.

Finally, we believe that the 2.5 Gbit/s rate can be at least doubled through a novel technique [7] involving combined polarization and time division multiplexing, as we have shown, both theoretically and experimentally, that solitons maintain a nearly complete degree of polarization over trans- oceanic distances. Furthermore, the interaction between adjacent, orthogonally polarized pulses is greatly reduced. That single channel rate can then be further multiplied by wavelength division multiplexing. That is, we have shown [8] that the well-known transparency of solitons to each other in collisions can be maintained, as long as the collision length (the distance solitons of different channels must travel down the fiber in order to pass through each other) is greater than two or more times the amplifier spacing.

REFERENCES

[1] L. F. Mollenauer, S. G. Evangelides, and H. A. Haus, "Long distance soliton propagation using lumped amplifiers and dispersion shifted fiber," *J. Lightwave Technol.* **9**, pp. 194-197 (Feb. 1991).

[2] L. F. Mollenauer, M. J. Neubelt, S. G. Evangelides, J. P. Gordon, J. R. Simpson, and L. G. Cohen, "Experimental study of soliton transmission over more than 10,000 km in dispersion-shifted fiber," *Opt. Lett.* **15**, pp. 1203-1205 (1990).

[3] L. F. Mollenauer, B. M. Nyman, M. J. Neubelt, G. Raybon, and S. G. Evangelides, "Demonstration of soliton transmission at 2.4 Gbits/s over 12,000 km," *Electron. Lett.* **27**, pp. 178-179 (Jan. 1991).

[4] J. P. Gordon and H. A. Haus, "Random walk of coherently amplified solitons in optical fiber transmission," *Opt. Lett.* **11**, pp. 665-667 (1986).

[5] K. Smith and L. F. Mollenauer, "Experimental observation of soliton interaction over long fiber paths: discovery of a long-range interaction," *Opt. Lett.* **14**, pp. 1284-1286 (1989).

[6] J. P. Gordon and L. F. Mollenauer, "Effects of fiber nonlinearities and amplifier spacing on ultra long distance transmission," to be pub. in the *J. Lightwave Technol.* **9**, pp. 170-173 (Feb. 1991).

[7] S. G. Evangelides, L. F. Mollenauer, J. P. Gordon, and N. S. Bergano, "Polarization division multiplexing with solitons," submitted to *J. Lightwave Technol.*.

[8] L. F. Mollenauer, S. G. Evangelides, and J. P. Gordon, "Wavelength Division Multiplexing with Solitons in Ultra Long Distance Transmission Using Lumped Amplifiers," *J. Lightwave Technol.* **9**, pp. 362-367 (March 1991).

Constraints on the Design of Long-Haul Soliton Systems

J V Wright and S F Carter
BT Laboratories
Martlesham Heath, IP5 7RE, UK.
Tel: +44 473 643555

1. Introduction

Erbium doped fibre amplifiers now allow the possibility of deploying optically transparent systems over trans-oceanic and trans-continental distances. However it is now well established that fibre non-linearities cannot be ignored in such systems. For example, when a single channel system is operated in the anomalous dispersion régime, ie. with $\lambda > \lambda_0$ where λ_0 is the wavelength of zero chromatic dispersion, self phase modulation (SPM) may lead to pulse compression or pulse break up. When operated with $\lambda < \lambda_0$, SPM leads to increased dispersion and pulse broadening. A choice may be made to avoid the non-linearities as far as possible; for example by minimising the amplifier spacing, by using the minimum optical power consistent with the required electrical signal-to-noise ratio (SNR) and by careful choice of the operating wavelength with respect to λ_0. Alternatively, one may choose to use actively the fibre non-linearity to design a soliton based system operating in the anomalous dispersion régime. This paper attempts to consider some of the design constraints for such a system. In particular it considers a system operating at 5Gbit/s over a total distance L_{sys} of 6000km.

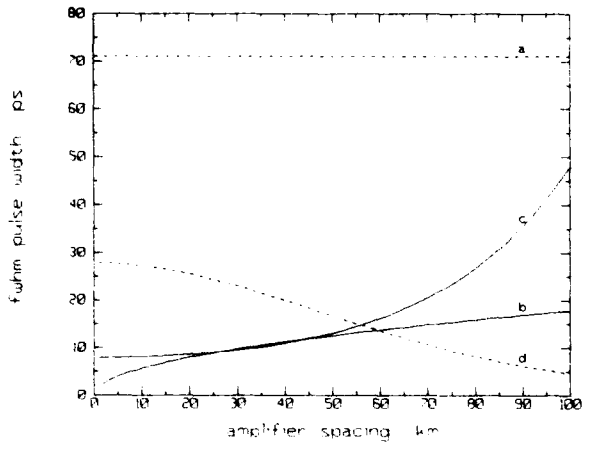

Figure 1. Soliton design diagram for a 6000km system operating at 5Gbit/s, D = 1ps/(km nm).

2. Soliton Design Diagram

The basic problems can be discussed with respect to Figure 1 which shows a typical operating window [1] for a soliton based system using fibre whose mean chromatic dispersion D is 1ps/(km nm) and with amplifiers whose gains are set to exactly compensate for the fibre loss of 0.22dB/km. The two axes show the amplifier spacing L_{amp} and the soliton FWHM pulse width. This is equal to 1.763τ where τ is the characteristic width of a soliton described by the amplitude function $\mathrm{sech}(t/\tau)$. The Figure shows four curves labelled a - d which delimit the borders between safe and unsafe operating regions. These will be discussed further in the following sections. The useful operating region lies below the dashed curves and above the solid curves. The operating window therefore consists of the half-eye which is centred around 20ps on the vertical axis and extending out to 50km on the horizontal axis.

2.1 Soliton-soliton interactions

A pair of adjacent solitons must be kept sufficiently far apart to prevent mutual interaction, otherwise they will undergo a periodic collapse with a period given approximately by

$$z_p = z_0 \exp(T/2\tau) \qquad (1)$$

where z_0 is the soliton period and T is the bit interval [2]. The collapse occurs fairly suddenly so it is sufficient to ensure that L_{sys} is less than $z_p/4$, hence the maximum bit rate is determined by

$$T \geq 2\tau \ln(4L_{sys}/z_0) \qquad (2)$$

This inequality is shown as curve (a) in Figure 1, the safe region lying below the curve.

2.2 Fibre perturbations

The fibre attenuation will cause the power of the soliton to decay between each amplifier. However this does not unduly affect the soliton provided that the period of the perturbation, ie. the amplifier spacing L_{amp} is short compared to the full soliton period $8z_0$ [3]. That is when

$$L_{amp} \leq 8z_0/10 \qquad (3)$$

where a factor of ten has been included for safety. This inequality is shown as curve (b) in Figure 1, the

safe region lying above the curve. We have examined the accuracy of this by using numerical simulation. A 63 bit pseudo random sequence of 20ps FWHM solitons was propagated over a total distance of 6000km using lumped amplifiers positioned every 40km to exactly compensate for the fibre loss of 0.22dB/km, but without introducing any noise at this stage. This combination of width and amplifier spacing lies just on the boundary of the operating window.

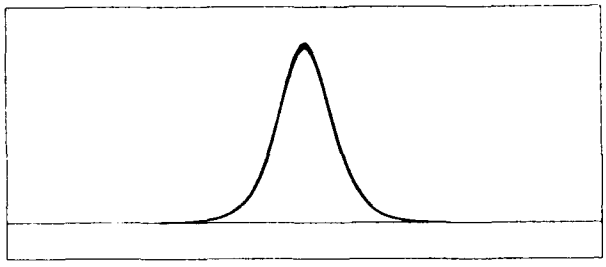

Figure 2. Eye diagram without noise: L_{sys} = 6000km, L_{amp} = 40km, D = 1ps/(km nm), τ_{fwhm} = 20ps.

Figure 2 shows the resultant eye diagram which has been generated by superimposing every bit within one bit interval of 200ps. The fluctuations in peak intensity between each bit are only just discernible, amounting to less than ±2%, even before applying a post detector filter.

2.3 Amplifier noise and Gordon-Haus jitter

Each amplifier in the chain generates amplified spontaneous emission (ASE) noise whose optical power per polarisation mode within a bandwidth B centred on the optical frequency ν is given by

$$(G - 1)\mu h \nu B \qquad (4)$$

where G is the power gain and μ is the inversion factor of the amplifier (μ = 1 in an ideal amplifier). The ASE induces a random shift in the carrier frequency of the soliton which interacts with the fibre dispersion to produce a random timing jitter (Gordon-Haus jitter [4]) whose variance is given by

$$\langle \delta t^2 \rangle = \frac{(G - 1)\mu h n_2 D L_{sys}^3}{9\tau A_{eff} L_{amp}} \qquad (5)$$

where $n_2 = 3.2\times10^{-20}$ m^2/W is the non-linear coefficient and $A_{eff} = 40\mu$m^2 is the effective area of the fibre. In order to maintain an acceptable bit error ratio (BER), the rms jitter must be kept small compared to the bit interval. Figure 3 shows the expected error floor as a function of the normalised jitter $\langle \delta t^2 \rangle^{1/2}/T$. This has been derived by assuming that the convolution of the soliton with the receiver response gives a raised cosine of FWHM equal to one bit period. The error floor degrades

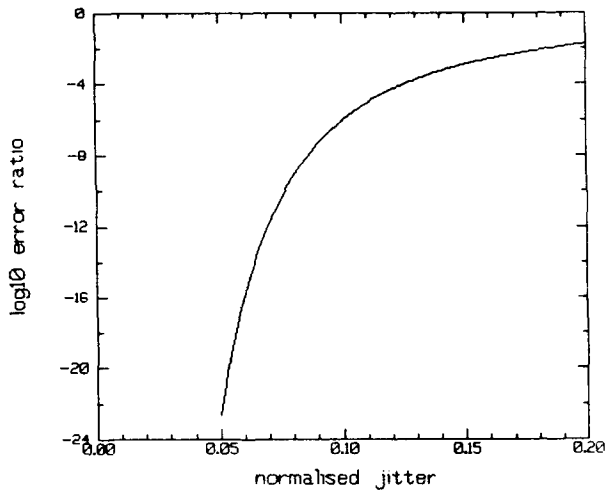

Figure 3. Error floor as a function of normalised jitter $\langle \delta t^2 \rangle^{1/2}/T$.

very rapidly with increased jitter and we have used the criterion that the normalised jitter should be less than 0.06 to provide a BER floor at an acceptable level. Using this criterion and assuming an ideal amplifier with μ = 1, (5) is shown in Figure 1 as curve (c). The safe region lies above this curve.

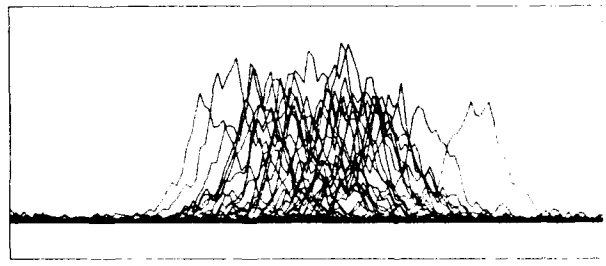

Figure 4. Eye diagram with ASE: L_{sys} = 6000km, L_{amp} = 40km, D = 1ps/(km nm), τ_{fwhm} = 20ps.

Figure 4 is an eye diagram showing the effect of Gordon-Haus jitter. This is the result of a numerical simulation that is identical with that used for Figure 2 but with the addition of random noise at each amplifier corresponding to a noise figure of 7dB (μ = 2.5). In addition the gain of the amplifier was increased by an extra 6dB to allow for extra losses immediately before and after each amplifier that would be required in a practical system to allow for optical isolators, optical filters, pump redundancy and wdm couplers etc. We can see that the solitons are now severely distorted from their sech profiles, there is a large variation in their amplitudes and significant jitter has been introduced, in this case amounting to an rms value of 18ps, ie. a normalised jitter of 0.09. With a 200ps bit interval, this would give rise to a BER floor at

about 4×10^{-8}. Note that the error is larger than that expected from Figure 1 because of the increased ASE in the simulation resulting from the higher noise figure and the excess loss. This underlines the importance of minimising excess loss particularly at the input of the amplifier.

However the derivation of (5) assumes linear propagation once the ASE has perturbed the soliton frequency at each amplifier. We should therefore ask what effect does the fibre non-linearity have on the propagation of the ASE and its interaction with the soliton? For example, Marcuse has shown that ASE has a very significant effect on the propagation of NRZ format pulses when operating close to λ_0 [5]. To investigate this, we have examined the accumulation of jitter as a function of system length using the same parameters as for Figure 4.

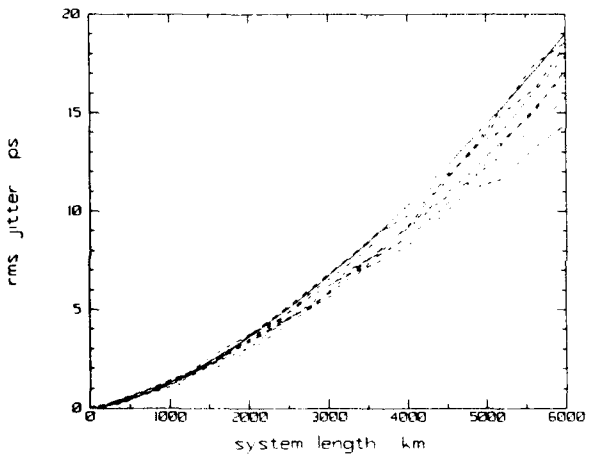

Figure 5. Jitter accumulation at 5Gbit/s: dashed curves show numerical simulations with different noise seeds, solid curve shows theoretical value from (5). L_{amp} = 40km, D = 1ps/(km nm), τ_{fwhm} = 20ps.

This is shown in Figure 5 as a series of dashed lines for seven different noise distributions (differing only in the seed value for the random variable generator). The theoretical curve derived from (5) but with suitable modification to account for the excess loss before and after the amplifier is also shown as a solid line. The agreement between the numerical simulations and the theoretical curve is very good, both show an $L_{sys}^{3/2}$ length dependence with the numerical values on average showing slightly smaller jitter. This shows that the non-linearity has had a minimal effect on the propagation of the ASE when using soliton parameters close to those required by the operating window. Hence curve (c) in Figure 1 should represent a good estimate of the limitations imposed by Gordon-Haus jitter.

2.4 Resultant SNR

The system must be designed to achieve an acceptable SNR at the detector where the dominant noise effect is likely to be the beating between the optical signal frequencies and the ASE frequencies (sig-spon beat noise). The SNR is then given by [6]

$$\frac{\langle i_{sig}^2 \rangle}{\langle i_{sig\text{-}spon}^2 \rangle} = \frac{(e\,P_{out}/h\,\nu)^2}{(2e/h\,\nu)^2\,P_{out}\,F_{out}} \qquad (6)$$

where $F_{out} = N(G-1)\mu h\,\nu B$ is the total ASE power at the output of the $N'th$ amplifier in a bandwidth B ($N \approx L_{sys}/L_{amp}$) and where P_{out} is the average optical signal power at the output of the amplifier. This may be expressed in terms of the peak power P_0 required to support a first order soliton using the path averaged soliton prescription [1,3]

$$P_{out} = \frac{P_0\,\tau\,G\ln(G)}{T(G-1)} \qquad (7)$$

The SNR requirements are shown on Figure 1 as curve (d), the safe region lying below the curve. This has used (6) with $B = 0.8/T$ to set a 23dB SNR which will provide a 7.4dB margin above the 10^{-9} error ratio level.

2.5 Discussion

The design diagram shown in Figure 1 is ideal in the sense that it has been based on an ideal amplifier that only compensates for the fibre loss. A more realistic diagram would have to accommodate additional ASE which would produce increased jitter and also reduce the SNR. Hence curves (c) and (d) would close up and severely limit the maximum amplifier separation. Perhaps the biggest problem is curve (d) which represents the SNR. This could be opened up by a number of techniques; for example by using multiple solitons per bit interval [1], by using higher dispersion fibre which gives a higher soliton peak power or by sacrificing some of the margin on the BER requirements.

3. Wavelength Division Multiplexing

Solitons at one wavelength are transparent to those at a different wavelength and will pass through each other (collide) with their shapes preserved. This is an attractive feature which allows the possibility of wavelength division multiplexing (WDM). However, following a soliton collision, the slower soliton will be retarded and the faster one will be advanced by an amount $\delta t = 1/(\tau(\pi\Delta f)^2)$ where Δf is the difference in optical frequencies [7]. Since the maximum number of collisions that can occur is

$D\,\Delta\lambda\,L_{sys}/T$, the maximum jitter that a soliton may experience is given by

$$\frac{D\,\Delta\lambda\,L_{sys}}{\tau(\pi\Delta f)^2\,T} = \frac{\lambda^2\,D\,L_{sys}}{\pi^2\,c\,\tau\,T\,\Delta f} \qquad (8)$$

In order to maximise the number of channels, Δf should be made as small as possible but this will maximise the collision jitter. As an example, consider a two channel system with Δf = 60GHz and keeping the other parameters as before, then the spread in bit arrival times could be up to 37ps. This maximum can only occur with an unbounded data sequence since this makes it possible for one data bit to pass through a complete string of 0's in the other channel whilst another bit could collide with a complete string of 1's. However this problem can be minimised by using suitable coding schemes.

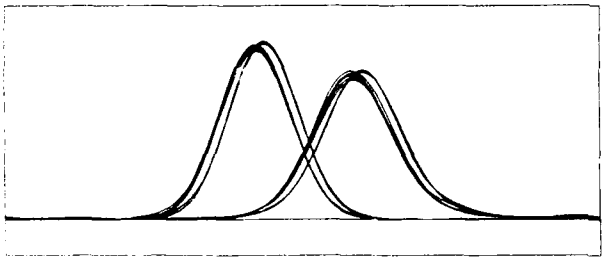

Figure 6. *Eye diagram for one channel from a two channel* system after 800km without noise: Δf = 60GHz, L_{amp} = 40km, D = 1ps/(km nm), τ_{fwhm} = 20ps, channels initially superimposed.

Figure 6 shows an eye diagram for one channel selected after 800km from a two channel system where Δf = 60GHz. Each channel contains 63 bit sequences of uncorrelated data. It can be seen that the data is bunched with two distinct arrival times. The data continues to separate beyond 800km and eventually overspills into adjacent bit intervals rendering the system inoperable. This problem is caused by having the data in the two channels initially superimposed. This is understandable because the frequencies of the two solitons involved in a collision change as they approach each other. The maximum change occurs when they overlap and the frequencies then return to their original values as they separate. So here some bits are initially in the middle of a collision (when both channels have data 1's in that bit interval) but others are not (when either channel has a data 0 in that bit interval). Therefore those bits that were initially in collision will now suffer an unbalanced frequency shift as they separate. This is converted by the product of fibre dispersion and distance into the temporal shift observed in Figure 6. It therefore is important to avoid an initial overlap of data.

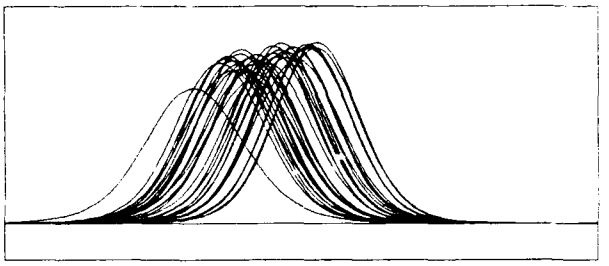

Figure 7. Eye diagram for one channel from a two channel system after 6000km without noise: Δf = 60GHz, L_{amp} = 40km, D = 1ps/(km nm), τ_{fwhm} = 20ps, channels initially separated by $T/2$.

Figure 7 shows the resultant eye diagram, now after 6000km, when the data was initially separated by half a bit interval. The normalised jitter is about 0.052 and would not cause any problems following the post detector filter. The majority of the jitter arises from the collision shifts described by (8) and caused by unbalanced data in the two channels.

4. Conclusions

This paper has looked at some constraints on the operation of a soliton system at 5Gbit/s over 6000km and identified Gordon-Haus jitter and provision of an adequate SNR as the limiting factors, particularly when there is excess loss before the amplifiers. With repeater spacings in the range from 30-40km, the system should also be capable of supporting WDM with at least two channels separated by as little as 60GHz, provided that the data in each channel is initially interleaved. Coding to provide a balanced sequence of 1's and 0's may also be desirable.

5. References

[1] K J Blow and N Doran, OFC 91, San Diego.

[2] J P Gordon, Opt Lett, vol 8, p596, 1983.

[3] L F Mollenauer, J P Gordon and M N Islam, IEEE J Quantum Electron, QJE 22, p157, 1986.

[4] J P Gordon and H A Haus, Opt Lett, vol 11, p665, 1986.

[5] D Marcuse, J Lightwave Tech, vol 9, p356, 1991.

[6] A Yariv, Opt Lett, vol 15, p1064, 1990.

[7] L F Mollenauer, S G Evangelides and J P Gordon, J Lightwave Tech, vol 9, p362, 1991.

QUALITATIVE DYNAMICS OF MODULATED SOLITON PULSE TRAINS

J. M. Arnold
Department of Electronics & Electrical Engineering
University of Glasgow, Glasgow G12 8QQ,
Scotland
Tel: 041-339 8855

1. Introduction

The recent advances in the technology of passive optical amplification have brought closer the realisation of optical fibre communication systems using soliton pulses which are not limited by dispersion. This in turn creates a new generation of theoretical problems concerned with the evolution of information-bearing pulse trains along a nonlinear channel. Previously, these theoretical models have been constructed primarily on the basis of the behaviour of isolated 1- or 2-soliton phenomena, as deduced by perturbation theory carried out on the Inverse Scattering Theory (IST) for the exactly-integrable Nonlinear Schrodinger Equation (NLSE) [1-4] or by direct numerical solution of the NLSE [5,6]. However, there are many circumstances in which the behaviour of a small number of isolated solitons may not properly represent the behaviour of a very long pulse train with neighbouring pulses coupled by a weak nonlinear intersoliton interaction; for example, two isolated solitons in the repulsive phase of the intersoliton interaction will diverge apart indefinitely, but this cannot happen when those two pulses form part of a long train of pulses, since the diverging pulses must eventually meet and interact with other pulses in the same train. Although the IST method is extremely useful for predicting the evolution of initial conditions consisting of a small number of solitons in the absence of an IST continuum, the presence of a large number of solitons or IST continuum in the initial conditions renders the method intractable. Even the simplest case of an infinitely long pulse train of periodically repeated identical solitons involves much more difficult analytical techniques than the conventional IST method and the true physical case of a modulated pulse train containing an infinite number of solitons is not tractable by any known analytical method, despite preserving the integrability of the NLSE.

It is therefore clear that the new applications in communications theory of soliton-bearing channels will require the development of new mathematical tools for their understanding. In this paper we describe methods which view the modulated soliton pulse train as a dynamical system, following a reduction of the number of variables required to describe the field. The new variables are 'quasiparticle' parameters, such as the position, energy or momentum of each soliton, which

are subjected to interactions through various types of potential. Using this description it is relatively easy to show that infinitely long periodic soliton pulse trains can be classified according to their stability under modulation of the parameters in the initial conditions; here we show that position and phase modulations are stable for solitons in the repulsive phase, and unstable in the attractive phase. These predictions, obtained from a qualitative reduced quasiparticle description, can be checked against rigorous results from a full linearised perturbation theory of the NLSE, with exact agreement [7]. Furthermore, it transpires that the equations for positional modulation are those of the Toda lattice [8], which is an integrable system with its own solitonic solutions.

2. Qualitative theory of soliton interactions

The behaviour of the wave envelope ϕ for a single mode optical fibre is described by the NLSE

$$i\partial_x\phi + \tfrac{1}{2}\partial_t^2\phi + |\phi|^2\phi = 0 \qquad (1)$$

where x and t are the fibre length and time in a coordinate moving at the linear group velocity, both in normalised units [9]. This equation has normalised 1-soliton solutions

$$\phi = e^{ix/2}\,\mathrm{sech}(t) \qquad (2)$$

from which other solutions are derivable by scaling operations such as $\phi \to \eta\phi$, $t \to \eta t$., $x \to \eta^2 x$ with an arbitrary scale factor η. Using the IST method, Gordon [1] has shown that the 2-soliton state with degenerate velocities can be approximated by

$$\phi = e^{ix/2}\left\{a_1 e^{i\alpha_1}\,\mathrm{sech}(t - t_1) + a_2 e^{i\alpha_2}\,\mathrm{sech}(t - t_2)\right\} \qquad (3)$$

where the soliton phases α_n and positions t_n evolve with x according to

$$\begin{aligned} d_x^2 t_n &= -(-1)^n 4e^{-\tau}\cos\alpha \\ d_x^2 \alpha_n &= (-1)^n 4e^{-\tau}\sin\alpha \end{aligned} \qquad (4)$$

and $\tau = t_2 - t_1 > 0$, $\alpha = \alpha_2 - \alpha_1 > 0$, with initial conditions $\partial_x\alpha = 0$, $\partial_x\tau = 0$, $a_1 = a_2 = 1$ at $x = 0$. When $\alpha = 0$ or π it can be shown that α is a constant of the motion, in which case (4) reduces to

$$d_x^2 t_n = \pm(-1)^n 4e^{-\tau} \qquad (5)$$

where the upper sign represents the repulsive phase $\alpha = \pi$ and the lower sign represents the attractive phase $\alpha = 0$. These equations were also derived in a wider context without the IST method by Anderson and Lisak [2]. Equation (5) represents Newton's Law for a 'force' between two 'particles' of unit mass placed at 'positions' t_1 and t_2 as 'time' x evolves.

Suppose now that the initial conditions consist of an infinite number of solitons placed at points $t_n = nT + q_n$, and the exponentially decreasing force on the right-hand-side of (5) is assumed to act linearly between nearest neighbours only; then (5) is modified heuristically to

$$d_x^2 q_n = \pm 4e^{-T}\left\{e^{(q_n - q_{n-1})} - e^{(q_{n+1} - q_n)}\right\} \qquad (6)$$

Equation (6) with the upper sign is the standard expression of the Toda lattice equation [8], and as such (6) is completely integrable by the IST method.

3. Stability of the soliton lattice

When all the q_n are zero, the intersoliton forces all balance and there is no net force; the soliton train is then periodic with period T ($\alpha=0$) or quasiperiodic with quasiperiod T and full period 2T ($\alpha=\pi$). Equation (6) may be linearised about $q_n=0$, with the result

$$d_x^2 q_n = \pm 4e^{-T}\{q_{n-1} + q_{n+1} - 2q_n\} \tag{7}$$

Equation (7) has solutions which are real-valued superpositions of the separated Fourier components

$$q_n = e^{in\beta} e^{i\lambda x} \tag{8}$$

with

$$\lambda^2 = \pm 8e^{-T}(1-\cos\beta). \tag{9}$$

The soliton lattice is stable if λ^2 is positve or zero; if λ^2 is negative the lattice is unstable. These classifications apply (for all $\beta\neq 0$) to the upper and lower signs respectively in (9), corresponding to stable repulsive and unstable attractive interactions, respectively. The length scale L over which these effects become manifest is $|\lambda|^{-1}$, which for the worst case $\beta=\pi$ is $L=(1/4)e^{T/2}$ in normalised soliton units. This is comparable with the length $(\pi/4)e^{T/2}$ for the collapse of an isolated 2-soliton pair, initially T units apart at x=0, in the attractive phase [1].

The results obtained above are exactly verified by a rigorous linearised perturbation theory applied to the quasiperiodic stationary solutions of the NLSE, which is too complicated to reproduce here [7]. They are interpreted as follows. In the unstable (attractive) phase small perturbations of soliton position grow exponentially with propagation distance x, with largest growth in the frequency component $\beta=\pi$. In the stable (repulsive) case small perturbations of position disperse due to the β-dependence of λ. Thus in either case if the soliton position is the carrier of information (PPM) the intersoliton interaction modifies the spectral distribution of the information, leading to intersymbol interference in the stable case and preferential dominance of the $\beta=\pi$ component in the unstable case. On the other hand, if additive noise is present at x=0 this is gradually worked into the positions of the pulses through the nonlinear interaction as x increases. The intersoliton interaction effect must be added to the Gordon-Haus effect [10] in assessing the limitations due to noise, and it is clear that these will be qualitatively and quantitatively different for the two cases of stable or unstable pulse trains.

4. Information dispersion in the stable case

We consider now the case of a stable periodic soliton train ($\alpha=\pi$) subjected to small perturbations of the soliton positions, given by the quantities $\{q_n\}$. These may be regarded as samples taken at periodic intervals of a bandlimited function with spectrum $Q(\beta)$:

$$q_n = \frac{1}{2\pi}\int_{-\pi}^{\pi} Q(\beta)e^{in\beta}d\beta \qquad (10)$$

The behaviour of small perturbations is essentially linear. Each Fourier component of frequency β evolves with propagation distance according to (8), so that after propagation a distance x the displacements change to

$$q_n(x) = \frac{1}{2\pi}\int_{-\pi}^{\pi} Q(\beta)e^{i\lambda x}e^{in\beta}d\beta \qquad (11)$$

where we recall that λ is a function of β. For example, when $Q=1$, corresponding to $q_n(0)=\delta_{n0}$, then as x increases $q_n(x)$ acquires nonzero values on the lattice points $n\neq 0$. This phenomenon is essentially intersymbol interference; information initially placed on the node $n=0$ disperses onto other nodes as propagation distance increases, However, this dispersion takes place on much longer distance scales than the ordinary linear dispersion of the fibre (on the order $e^{T/2}$ times as far). Therefore an effective linear channel can be produced using solitons which achieves greatly enhanced propagation lengths before dispersion limits channel capacity. The example treated here is that of PPM (pulse position modulation), but an identical treatment of soliton phase modulation produces the same stability exponents and the same enhancement of the linear channel capacity; the case of amplitude modulation is rather more complicated, but has the same qualitative features.

5. References

1. Gordon, J.P.: Optics Lett., 8, 596, 1983.
2. Anderson, D. and Lisak, M.: Optics Lett., 11, 174, 1986.
3. Karpmann, V. I. and Solov'ev, V. V.: Physica D, 3, 487, 1981.
4. Kodama, Y. and Nozaki, K.: Optics Lett., 12, 1038, 1987.
5. Blow, K. J. and Doran, N. J.: Elect. Lett., 19, 429, 1983.
6. Hermansson, B. and Yevick, D.: Elect. Lett., 19, 570, 1983.
7. Arnold, J. M.: in preparation, 1991.
8. Toda, M.: Chap. 4 in *'Solitons'*, ed. R. Bullough and P. Caudrey, Springer-Verlag, 1980
9. Butcher, P. and Cotter, D.: *'The elements of nonlinear optics'*, CUP, 1990.
10. Gordon, J. P. and Haus, H. A.: Optics Lett., 11,665, 1986.

4x5Gbit/s optical time division multiplexed nonlinear transmission over 205km

D M Spirit, G E Wickens and L C Blank

BT Laboratories, Martlesham Heath, Ipswich IP5 7RE, United Kingdom

Tel: +44 473 646949, Fax: +44 473 644886

Introduction

In order to fulfil the demand for increasingly sophisticated and bandwidth intensive services, telecommunications operators will require flexible optical transmission networks which will operate at higher data rates than those installed to date. At present, the maximum data capacity of installed optical systems is limited by the bandwidth of the electronics in the terminal and repeater equipment (currently around 2.5Gbit/s). Optical wavelength [1] or time [2] division multiplexing techniques may be used to access data rates substantially over 10Gbit/s, offering a substantial increase in capacity. Both multiplexing techniques could be used in conjunction with switching in either the wavelength or time domains to allow increased network flexibility through, for example, the drop-and-insert function. Discrete erbium-doped fibre amplification is an excellent method of compensating for the loss of the transmission link, providing bit-rate independent amplification. However, the regenerative function of conventional opto-electronic repeaters is no longer available in fibre amplifiers: linear dispersion of the optical pulses now becomes a major system constraint. The availability of fibre amplifiers with excellent performance in the 1550nm window restricts the signal wavelength of optically multiplexed systems to this wavelength range, implying the use of dispersion-shifted transmission fibre. The operation of wavelength division multiplexed transmission with more than a few channels over fibre with low dispersion can lead to significant system penalties due to four wave mixing, even over fibre spans of less than 100km [3]. An alternative approach to ultra-high speed transmission is to use time division multiplexing, requiring a transmitter configuration based on short (≈ps) optical pulses. In this instance, nonlinear optical pulse compression in the transmission fibre may be used to advantage to significantly reduce (or even balance completely [4]) the linear dispersion of the optical pulses, permitting transmission well beyond the usual dispersion limit.

In this paper, we present the results of optical time division multiplexed transmission with the signal wavelength 1nm and 6nm above the fibre dispersion zero. Close to the wavelength of zero dispersion, signal power levels were maintained at a relatively low level in order to avoid detrimental optical nonlinearities. In this case, full BER measurements indicate error-free transmission over 205km with a receiver penalty due to noise accumulation of only 0.8dB. At wavelengths significantly above the dispersion zero, signal power levels were increased in order to provide suitable nonlinear pulse compression to compensate for linear fibre dispersion. The system is based on four 5Gbit/s electrical channels, providing a total optical data rate of 20Gbit/s. All the electronic components in the transmitter and receiver have no more bandwidth than would be required for a 5Gbit/s system.

System description

The system has been described in detail elsewhere [5] and so only a brief summary will be given here. The optical source is a mode-locked semiconductor laser which produces a continuous pulse train at a repetition rate of 5GHz. The pulses have a full width half maximum (FWHM) of 14ps, and are close to transform limited (time-bandwidth product ≈ 0.4). The output from the laser is split into 4 channels by a passive 1x4 fused fibre device and each of the 5GHz repetition rate optical pulse trains is externally modulated by NRZ data from a 5Gbit/s pseudorandom generator to produce four distinct 5Gbit/s optical RZ data streams. Each modulator is followed by a variable fibre delay line to allow interleaving of the four channels in a 4x1 passive coupler to produce a single 20Gbit/s RZ data stream. The mean output power from the interleaver is -14dBm, which can be boosted as high as +13dBm in an erbium-doped fibre power amplifier.

The receiver consists of an erbium-doped fibre pre-amplifier, an optical demultiplexer to retrieve a single optical 5Gbit/s data stream, and a wideband receiver. The receiver electronics convert the RZ optical data into 5Gbit/s NRZ electrical data which is used as the input to an error detector and a 5GHz clock recovery circuit. The output from the clock recovery circuit drives both the optical demultiplexer and the error detector. The demultiplexer consists of two lithium niobate Mach-Zehnder modulators in tandem, both driven with 5GHz sine waves [6]. Hence both the transmitter and receiver in the 20Gbit/s system operate using electronic components appropriate for operation at only 5Gbit/s.

The transmission link comprises of four 51.2km lengths of dispersion-shifted fibre with three intermediate erbium-doped fibre amplifiers. The mean wavelength of zero dispersion of the 205km of fibre is 1554.2nm. The mean loss of each fibre span is 11dB and the anomalous group delay dispersion at the two signal wavelengths is 0.085ps/nm/km at 1555.4nm and 0.4ps/nm/km at 1560.5nm. However, in order to reduce detrimental nonlinear optical effects (observed as pulse breakup and spectral spreading), the mean power launched into each fibre span was limited to a maximum of +7dBm.

System results

Operating 1.2nm above the wavelength of zero dispersion of the optical fibre, optical nonlinearity led to a broadening of the optical signal spectrum from 0.28nm at the transmitter to 0.36nm after transmission through 205km. In the time domain, this corresponds to a measured pulsewidth of 14ps directly after the transmitter and 11ps at the receiver input. Figure 1 shows the bit error ratio curves for a single demultiplexed 5Gbit/s data streams for the transmitter and receiver running back-to-back and also after transmission through 205km of fibre. Operating back-to-back, the receiver sensitivity for 20Gbit/s data was -20.5dBm as measured at the input to the pre-amplifier. After transmission through 205km of fibre, the sensitivity was degraded by only 0.8dB. To separate fibre effects (linear dispersion and optical nonlinearity) from amplifier effects (noise accumulation) the system was operated using optical attenuators of appropriate values to replace each fibre span. In this instance, a system penalty of 0.7dB was obtained, which is within 0.1dB of that of the fibre system. The discrepancy is within the accuracy of the power measurements and implies that the measured system penalty was almost entirely due to the spontaneous emssion of the fibre amplifiers.

At the higher signal wavelength of 1560.5nm, the linear fibre group delay dispersion of

0.4ps/nm/km is sufficient to broaden the transmitter pulses to approximately 30ps FWHM after transmission through 205km of fibre. This is illustrated in figure 2a, which shows part (...110101110101...) of a 20Gbit/s data pattern after propagation through the fibre link. In this case, the launch power into each 51.2km fibre span is less than +3dBm. It is clear that whilst isolated pulses (...010...) are still distinct, pulse broadening causes a lack of contrast between adjacent pulses which are not separated by zeros (...01110...). This would introduce a dispersion penalty into a system operated under these conditions. Increasing the signal launch power into each 51.2km fibre span to ≈ +7dBm causes nonlinear pulse compression which restores the contrast between adjacent pulses (figure 2b). Further increase of the signal power over-compensates for linear dispersion, causing pulses to interact with each other and become severely distorted (see figure 2c for launch powers of ≈ +10dBm).

Conclusions

We have demonstrated a 4x5Gbit/s time division multiplexed transmission system over 205km based on a mode-locked laser transmitter. Full BER measurements on a system operated 1nm above the wavelength of zero dispersion indicate negligible penalty associated with fibre nonlinearities. At longer wavelengths, fibre nonlinearities can be used to advantage to significantly reduce pulse broadening and should permit the operation at wavelengths where linear dispersion would normally be sufficient to prevent this system from operating at all. Full BER measurements on the nonlinear system operating under the conditions of figure 2b (and others) will be presented at the conference.

References

1 Taga, H., Yoshida, Y., Edagawa, N., Yamamoto, S. and Wakabayashi, H.: "459km, 2.4Gbit/s four wavelength multiplexing optical fibre transmission experiment using six Er-doped fibre amplifiers", Electron. Lett., 1990, 26, pp. 500-501

2 Tucker, R. S. et al: "16Gbit/s optical time-division multiplexed transmission system experiment", in Technical Digest of Optical Communication Conference OFC'88 (Washington, Optical Society of America), 1988, paper THB4

3 Chraplyvy, A. R.: "Limitations on lightwave communications imposed by optical fiber nonlinearities", J. Lightwave Technol., 1990, 8, pp. 1548-1557

4 Iwatsuki, K., Suzuki, S., Nishi, S., Saruwatari, M. and Nakagawa, K.: "20Gb/s optical soliton data transmission over 70km using distributed fiber amplifiers", IEEE Photonics Technol. Lett., 1990, 2, pp. 905-907

5 Wickens, G. E., Spirit, D. M. and Blank, L. C.,: "20Gbit/s, 205km optical time division multiplexed transmission system", accepted for publication in Electron. Lett., 1991

6 Blank, L. C.: "Multi-Gbit/s optical time division multiplexing employing $LiNbO_3$ switches with low frequency sinewave drive", Electron. Lett., 1988, 24, pp. 1543-1544

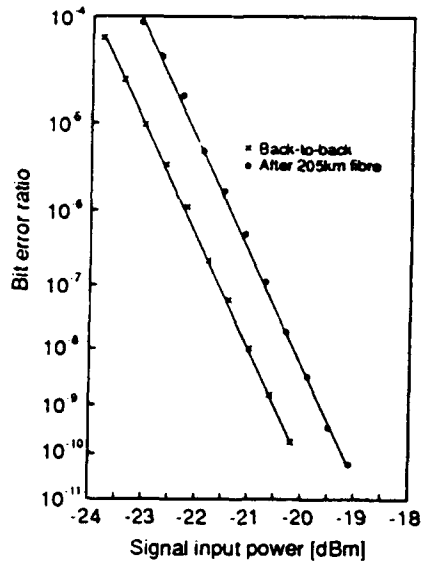

Figure 1: Bit error rate curve for 20Gbit/s system and received eye after 205km transmission

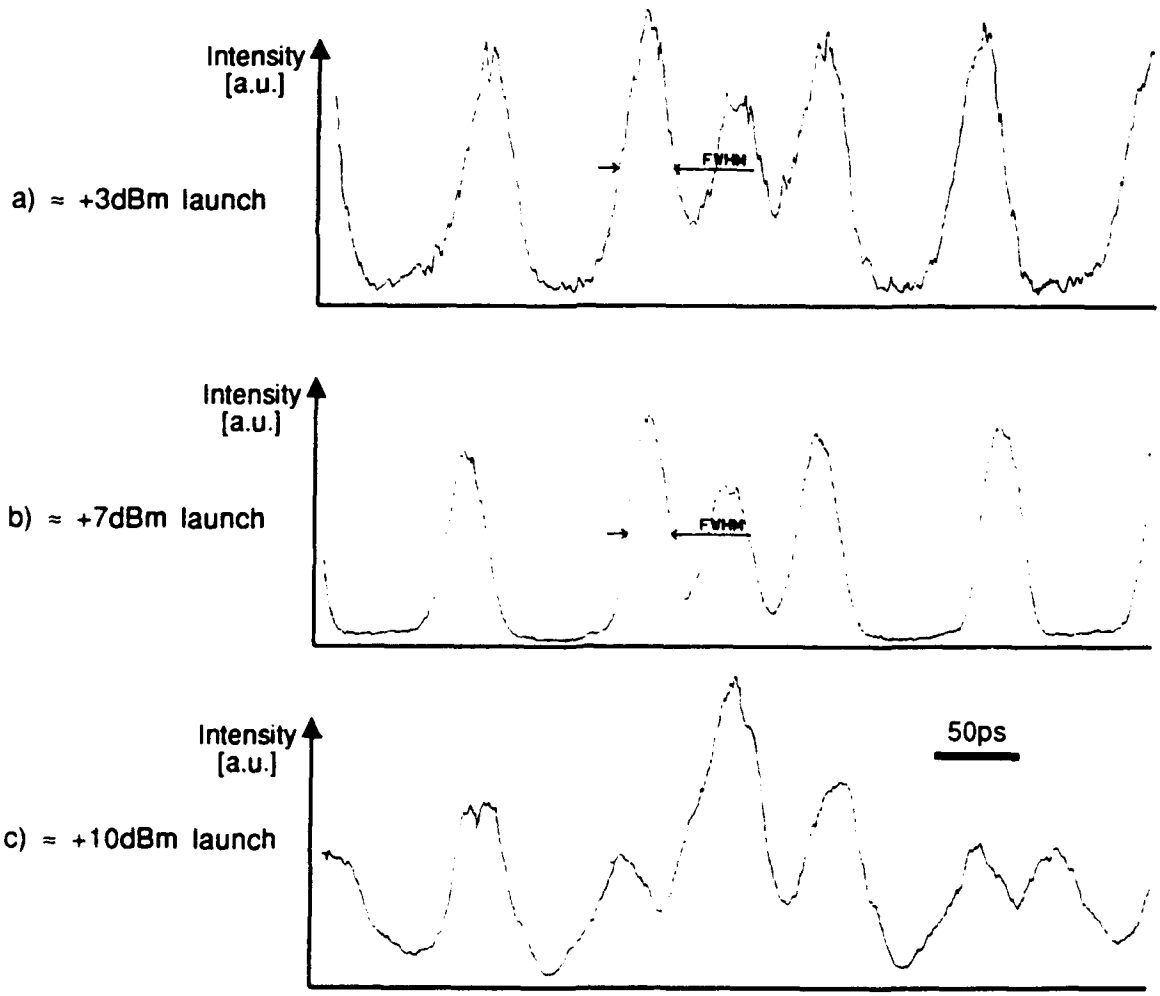

Figure 2: 4x5Gbit/s interleaved output from 205km fibre, 6nm above dispersion zero, ...110101110101... part of 20Gbit/s pattern, for different launch powers into each 51.2km fibre span

Ultra long nonlinear fiber optics data transmission using dual-frequency laser sources.

P.V. Mamyshev, S.V. Chernikov, A.M.Prokhorov.

General Physics Institute, Academy of Sciences of the USSR
38 Vavilov Street, Moscow 117942, USSR

In previous papers [1-3] we have shown that it is possible to generate high-repetition-rate (GHz-THz) trains of uninteracting solitons from a dual-frequency signal by using a weak amplifica tion of the signal in fibers. The length of the fiber necessary for the soliton train generation grows quadratically with increase of the generated solitons pulse width. The fiber length varies from 10-300 m for the soliton pulsewidth of about 100 fsec to thousands of km for the case of relatively long (about 50 psec) solitons [3]. At the present state of fiber optics technology there are reasons that relatively long solitons are required for ultra long distance transmission [4.5]. But the discussed method requires too long fibers for generation of such solitons.

We suggest here a modification of such a method for high-bit-rate ultra long data transmission. Our analysis is based on a well- -known nonlinear Schrodinger equation for the electric field envelope:

$$i\frac{\partial \Psi(\xi,\tau)}{\partial \xi} + \frac{1}{2}\frac{\partial^2 \Psi(\xi,\tau)}{\partial \tau^2} + |\Psi(\xi,\tau)|^2 \Psi(\xi,\tau) - i\alpha\Psi(\xi,\tau) = 0$$

Here the electric field $E(t,z)=A(t,z)\exp(ik_0 z - i\omega_0 t)$; z is the axial fiber coordinate; k_0 is the propagation constant; t is time; ω_0 is the light frequency; $\Psi(\xi,\tau)=A(z,t)/A_0$; $A_0^2=2c|k_2(0)|/(t_0^2\,\omega_0 N_2)$; N_2 is the nonlinear refractive index; $\xi=z/z_0$; $z_0 = t_0^2/|k_2(0)|$; $\tau=(t - k_1 z)/t_0$; $k_1 = \partial^1 k/\partial\omega^1\big|_{\omega=\omega_0}$.

Now the dual-frequency radiation $\Psi(\tau,0)=a\sin(\pi\tau/T)$ (see Fig.1a) is coded before coupling into the fiber (Fig.1b). The fiber, where the signal is reshaped into a stream of soliton-like pulses, plays also a role of a transmission fiber (Fig.1c). One can see that practically all the signal energy contains in the solitons at the fiber output.

Note that adjacent pulses in the input signal have opposite signs

of electric field, and so the adjacent pules repulse from each other during the propagation. This feature is very important for the formation of soliton pulses [3]. On the other hand the repulsion is rather weak and does not lead to temporal shifts of the pulses on more than 5-7% of T, despite the fact that ratio of the period to soliton duration is rather low at the fiber output $T/(\tau_{sol}(FWHM))\approx 4$. Note also that the system can work as in the case of the fiber with a weak net amplification ($\alpha>0$) as well as in the case of the fiber without amplification ($\alpha=0$, this situation is considered in Figs.1, 2).

We show that this nonlinear communication line has all the advantages of the soliton transmission:

- dispersive compensation of nonlinear effects;
- stability against perturbations of the fiber parameters (dispersion, mode area, etc.) along the fiber length;
- stability of data streams in a chain of lumped amplifiers;
- potential for multi-channel wavelength division multiplexing (see Fig.2).

The long distance transmission system should incorporate linear optical amplifiers which offset the signal loss in the fiber. These emit amplified spontaneous emission (ASE) noise. ASE noise is the source of error, because it leads to the energy fluctuations and to the expected Gaussian distribution of pulse arrival times [6]. Our estimations show that error caused by these effects in the proposed data transmission system should be not higher than that for the case of soliton transmission system discussed earlier [5].

References.

1. E. M. Dianov, P. V. Mamyshev, A. M. Prokhorov, and S. V. Chernikov, Optics Letters, 14, 1008-1010 (1989).
2. V. A. Bogatyrev et.al, Topical Meeting on Nonlinear Guided--Wave Phenomena, 1989.Technical digest Series, vol.2, postdeadline paper PD-9. Washington D.C.: OSA.
3. P. V. Mamyshev, S. V. Chernikov, and E. M. Dianov, "Generation of fundamental soliton trains for high-bit-rate optical fiber communication lines", to be published in IEEE J. of Quantum Electron.
4. L.F.Mollenauer, S.G.Evangelides, and H.A.Haus, "Long distance soliton propagation using lurped amplifiers and dispersion shifted fibers", joint issue of IEEE J.Quantum Electron and IEEE J.Lightwave Technol.(to be published).
5. J.P.Gordon and L.F.Mollenauer, "Effect of fiber nonlinearities and amplifier spacing on ultra long distance transmission", *ibid.*
6. J.P.Gordon, and H.Haus, Opt. Lett. 11, 665 (1986).

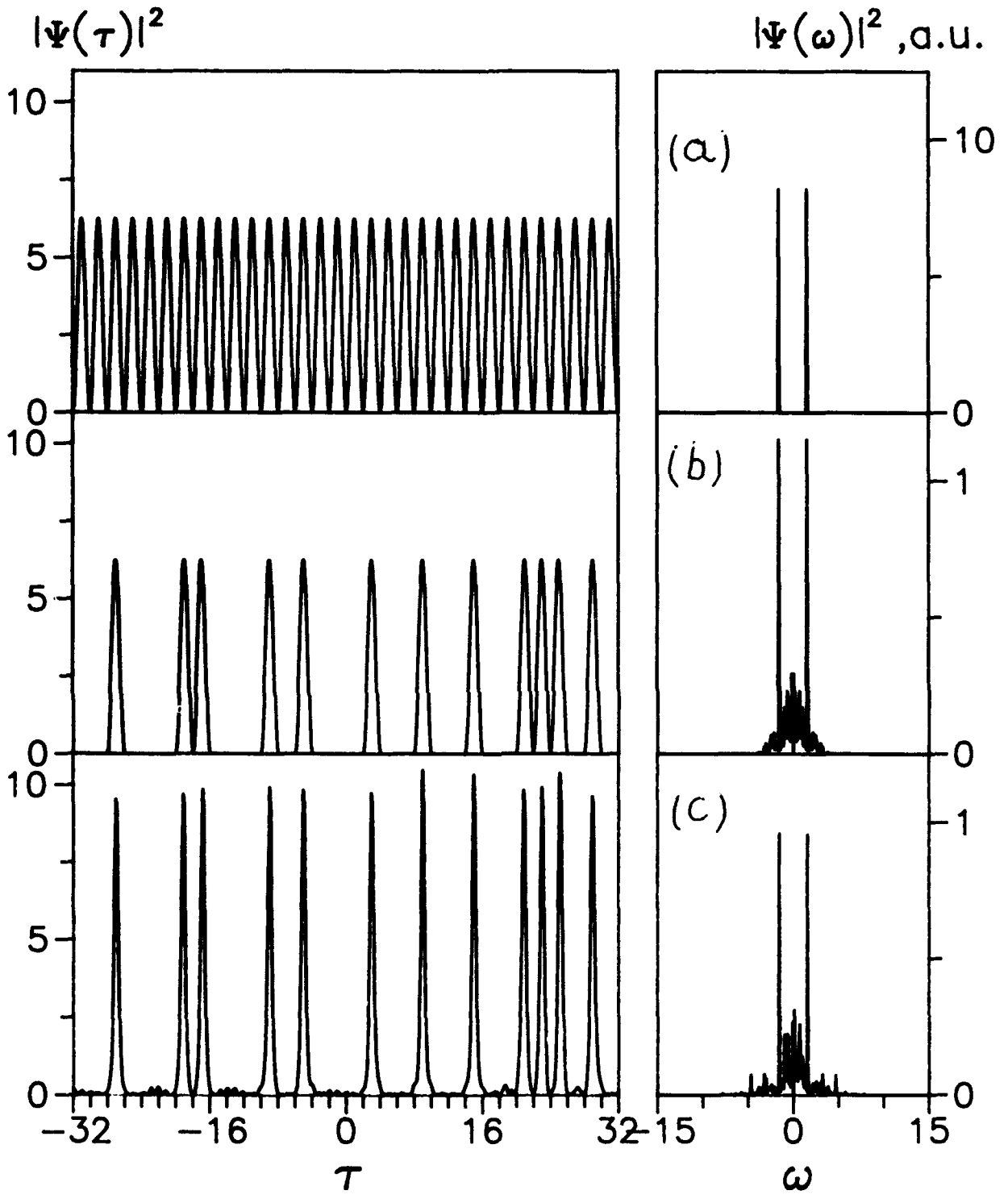

Figure 1.(a) The dual-frequency signal before data coding. Temporal and spectral intensities are shown. The dimensionless parameters are: a=2.5; T=2.
(b). The signal (a) coded by data.
(c) The signal (b) after transmission through the fiber, α=0; ξ=1.15. The dimensional parameters can be as follows: 4 GBits/sec data transmission, fiber dispersion D=1.38 ps/nm/km, λ=1.55 μm, fiber length L=10,000 km, T=250 psec.

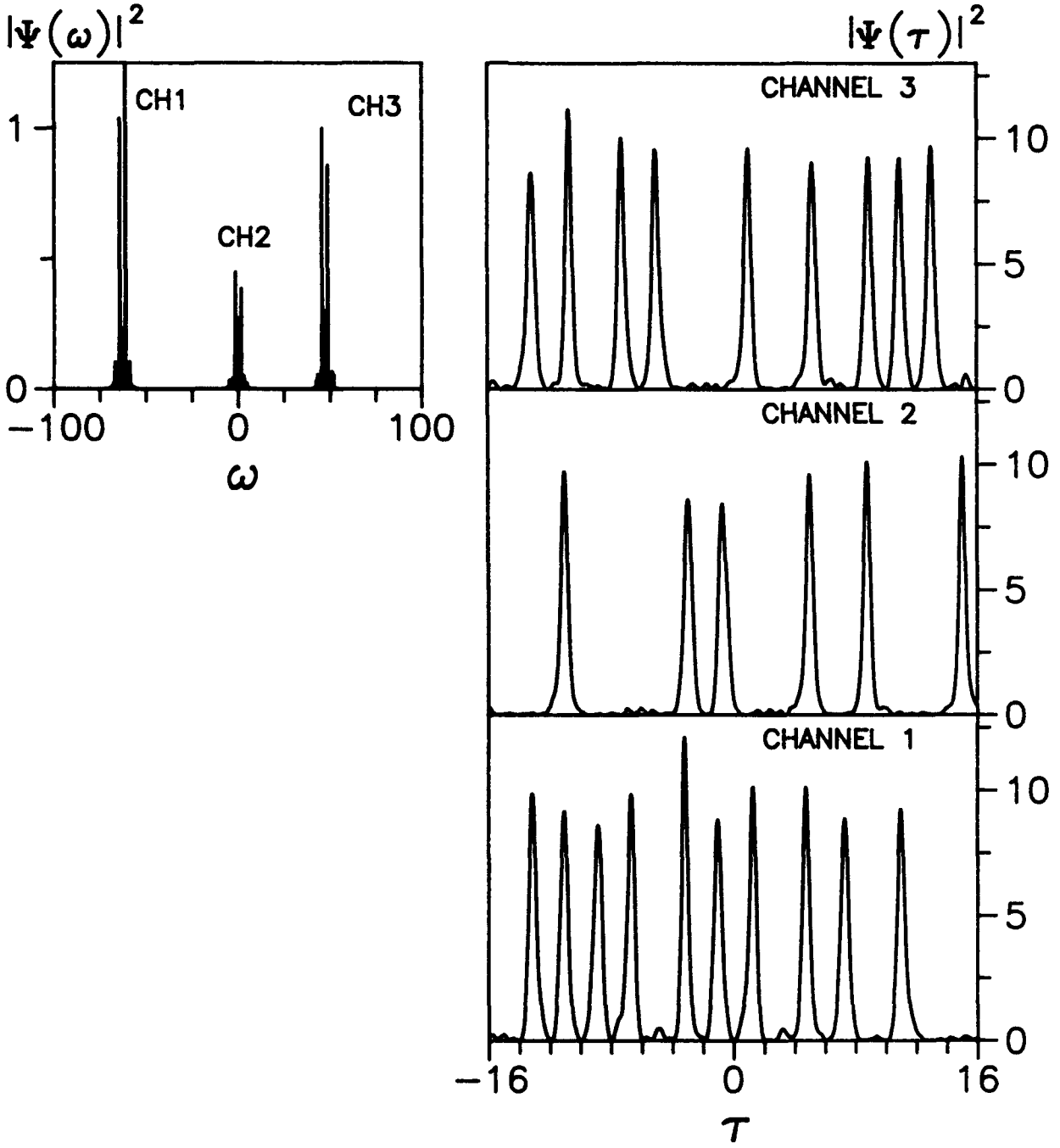

Figure 2. Numerical simulations of wavelength division multiplexing 10,000 km long system employing three channels of 4 GBits/sec each. Parameters of each channel are the same as in Fig.1, spectral separation between the channels are 2.7 cm^{-1} and 2 cm^{-1}.
Left side - total spectrum of three channels at the fiber output.
Right side - data streams in the channels after spectral filtering at the fiber output.

Monday, September 2, 1991

Raman Effects in Fibers

MB 11:15am–12:45pm
Palmerston Room

K. Blow, *Presider*
British Telecom Laboratories, United Kingdom

Modulational Instability and Raman Scattering in Optical Fibers

Ekaterina A. Golovchenko

General Physics Institute, Academy of Sciences of the USSR
Vavilov Str. 38, 11733 Moscow, USSR
Tel. 132-81-21

Modulational Instability (MI) is one of the most beautiful nonlinear effects in optical fibers. MI causes the exponential amplification of small temporal perturbations of the cw pump radiation . In spectral domain Stokes and anti-Stokes components are exponentially amplified at the frequency shifts determined by pump intensity [1]. Depending on the polarization properties of optical fibers various types of MI can be observed both in the regions of positive and negative fiber group velocity dispersion (GVD) [2].

The effect of MI is developing side by side with another nonlinear process - that is the process of stimulated Raman scattering (SRS). SRS also results in exponential amplification of spectral components. But in the case of SRS only Stokes spectral components experience exponential amplification at the frequency shift of about 440 cm^{-1}. SRS in optical fibers is characterized by a broad gain line which covers the spectral band of more than 1000 cm^{-1} [3]. The maximum value of the resonant (nuclear) nonlinear Raman susceptibility is only 4 times smaller than that of electronic nonlinear susceptibility. Thus Raman nonlinearity can considerably affect the MI gain parameters and on the other hand the parametric effects (MI) can result in change of Raman gain coefficient at Raman frequency shift (440 cm^{-1}).

However till lately the parametric effects and SRS in fibers were discussed as the processes independent of each other. We report now the results of theoretical investigations of the interplay between the parametric effects (for various types of MI) and SRS.

1. To begin with we shall discuss the scalar case, i. e. when the pump wave is polarized along one of the fiber principle axes and the Stokes-anti-Stokes sidebands are amplified in the same polarization. We have derived the relation for the Stokes and anti-Stokes components exponential amplification coefficient which is describing both the effect of MI and SRS [4]. The analysis showed that in the region of positive GVD Raman gain coefficient for the small values of phase mismatch is decreasing through the parametric coupling between Stokes and anti-Stokes waves. Simultaneous generation of the first

Raman Stokes and anti-Stokes occurs in such a regime of Raman gain parametric suppression [4,6].The significance of a single-mode fiber as a nonlinear medium is that phase-matching can be achieved through increasing of the input pump power and that it also depends on the value of fiber GVD [4,6]. Thus the phase-matching regime can be easily obtained in an experiment. The effect of Raman gain parametric suppression can be used to increase the range of the ultrashort laser pulse frequency chirping with corresponding increase of the degree of pulse compression in fiber-grating compressors.

In the region of negative GVD of fibers Raman nonlinearity influence on the MI gain line causes the decrease of the maximum MI gain and of the frequency shift that corresponds to the maximum of amplification. In addition Raman effect results in the discontinuities in the dependence of the MI frequency shift on pump intensity [5].

We also present a detail analysis of Raman and MI spectra evolution in the field of cw pump which is based on numerical simulation of the nonlinear Schrodinger equation (NSE) with an additional term describing Raman scattering. We discuss the features of Raman spectrum dynamics in the regime of phase-matching (i. e. in the regime of Raman gain parametric suppression) for the region of positive GVD. When pump is in the region of negative GVD the MI spectrum at the frequency shift determined by input pump intensity is originating before SRS as the MI gain coefficient is 4 times greater than that of SRS. In time domain MI spectrum represents a sequence of solitons with the average durations of about the inverse MI frequency shift. These solitons generated in the MI spectral band are then experiencing the effect of Raman self-frequency shift [6]. We discuss how the type of the output spectrum depends on the initial pump intensity. For small initial pump intensity the rate of MI soliton self-frequency shift is small too. Thus the first Raman Stokes at the frequency shift 440 cm^{-1} reaches saturation regime much earlier than any considerable self-frequency shift of MI solitons takes place. As a result a cascade generation of the discrete Raman Stokes components is observed. For larger pump intensities Raman continuum spectrum is formed from the MI band [7]. We also demonstrate various regimes of the spectral continuum generation and analyze their temporal structure.

2. The discussed above scalar description of nonlinear light propagation through fiber is involving a single NSE. For this case negative GVD is a necessary condition of MI. On the other hand it was proved both theoretically [2,8-10] and experimentally [9-11] that MI in birefringent fibers is developing even in the region of positive GVD of fibers. We present here a theoretical analysis of the Stokes-anti-Stokes perturbations amplification based on the interplay between MI and Raman effects in high-birefringent fibers. Light propagation in fiber is described now by two uncoherently coupled NSEs for the two principle polarization axes of fiber.

The case under consideration is when the pump wave intensity is split between the principle fiber axes. We have found the relation for the exponential gain coefficient of the Stokes u_s and anti-Stokes u_a spectral components:

$$((i\lambda+p)^2 - B_1)((i\lambda+p)^2 - B_2) = C^2 \qquad (1)$$

where λ is the gain coefficient $u_{s,a} \propto \exp(\lambda z)$, $p=\Omega\Delta/2$, $\Delta=(1/v_y-1/v_x)$ is the fiber group velocity mismatch. Note that functional form of Eq. (1) coincides with the dispersion relation obtained in [9,10], but in our case the coefficients B_1, B_2, C are the complicated functions of nonlinear Raman susceptibilities $\chi_{xxxx}(\Omega)$ and $\chi_{xyxy}(\Omega)$ [3]. The coefficients B_1, B_2, C also depend on the values of pump intensities in the principle axes and fiber GVD. Thus Eq.(1) describes both the effect of MI and Raman scattering. It should be underlined that the main difference from the scalar case is that now there aretwo positive values of gain coefficient λ that correspond to the different roots of characteristic Eq.(1). We have obtained then the analytical solution that describes Stokes and anti-Stokes perturbations spectrum evolution in the undepleted cw pump field in each fiber principle axis.

a)*region of positive GVD:*
We show how depending on the initial pump intensity one can observe either MI spectrum with the Stokes components in the slow fiber axis and anti-Stokes components in the fast axis or Raman spectrum, or both processes together. It turned out that in this regime there is no decrease of exponential Raman gain. This result is quite different from the scalar case. However the calculated spectrum shape for large pump intensities exhibited more intensive Raman Stokes components in the slow axis in comparison with the fast one.

b)region of negative GVD:
We shall discuss various regimes of MI spectrum generation depending on the value of pump intensity with and without Raman nonlinearity influence. We show that for low pump intensities there are two separate spectral regions of MI amplification: one close to the zero frequency shifts and the other near the frequency shift $\Omega=\Delta/(|\partial^2 k/\partial\omega^2|)$and the peak MI gain value is about 1/2 of pump intensity. With the increase of pump intensity these two MI regions start to overlap. Under these condition the dependence of the frequency shift corresponding to the maximum of MI amplification on pump intensity experience a discontinuity- like change from the small frequency shifts to the frequency shifts larger than $\Omega=\Delta/(|\partial^2 k/\partial\omega^2|)$. In the limit of large pump intensities MI amplification parameters coincide with the regime of zero group velocity mismatch Δ [8], i. e. the maximum MI gain value for the sidebands in the same polarization with the pump is proportional to 5/3 of pump

intensity, while the peak gain for the sidebands whose polarization is orthogonal with respect to the pump is proportional to 1/3 of pump intensity. The analysis of the output spectrum shape showed that for small pump intensities the Stokes-anti-Stokes spectral components are generated in each fiber axis at the frequency shifts less than phase-matching frequency $\Omega=\Delta/(|\partial^2 k/\partial\omega^2|)$. The increase of pump intensity results in the change of MI spectrum shape : Stokes spectral components are now generated in the fast fiber axis, anti- Stokes components are in the fast axis and their frequency shift is larger than Ω. There is also an intermediate regime when there are two Stokes and two anti-Stokes sidebands at different frequency shifts in each fiber axis. In the limit of large pump intensities spectrum shape is similar to the case of $\Delta=0$ [8].

REFERENCES

1. A. Hasegawa and W. F. Brinkman, IEEE J. Quant. Electron., QE-16, 694 (1980).

2. S. Wabnitz, Phys. Rev. A, 38, 2018 (1988)

3. R. W. Hellwarth, Prog. Quant. Electron., 5, 1, Pergamon Press (1977)

4. E. A. Golovchenko, E. M. Dianov, P. V. Mamyshev and A. N. Pilipetskii, JETP Lett., 50, 190 (1990).

5. E. A. Golovchenko, P. V. Mamyshev, A. N. Pilipetskii, and E. M. Dianov, IEEE J. Quant. Electron., QE-26, 1815 (1990).

6. J. P. Gordon, Opt. Lett., 11, 662 (1986).

7. K. J. Blow and D. Wood, IEEE J. Quant. Electron., QE-25, 2665 (1989).

8. S. Trillo and S. Wabnitz, JOSA B, 6, 238 (1989).

9. J. E. Rothenberg, Phys. Rev. A, 42, 682 (1990).

10. P. D. Drummond, T. A. B. Kennedy, J. M. Dudley, R. Leonhardt and J. D. Harvey, Opt. Commun., 78, 137 (1990).

11. K. Stenersen and R. K. Jain, Opt. Commun., 51, 121 (1984).

Stimulated Raman scattering in optical fibers: spontaneous initiation and spatial propagation

Raymond J. Hawkins and R.H. Stolen[1]

Lawrence Livermore National Laboratory Livermore, California 94550, (415)-422-0581

Stimulated Raman scattering can be treated in either the frequency domain or the time domain. Traditionally, cw waves and long optical pulses have been treated in the frequency domain where the problem can be reduced to a set of coupled wave equations which include self and cross phase modulation as well as the Raman gain [1]. Frequency domain analysis, however, becomes intractable for ultrashort optical pulses where spectral bandwidths become comparable to the Raman frequency shift. Here a time domain approach is more appropriate.

In the time domain, the Raman gain spectrum is replaced by a Raman response function [2]. In the time domain there is a single equation of motion: self and cross-phase modulation and pulse walkoff are automatically included [2-4]. There is a price to pay for these advantages because it is necessary to follow the pulse evolution on a time scale less than that of the Raman response function ($\leq$ 20 femtoseconds). A large number of computational grid points are required once the pulse length is long compared to the ring-down time of the Raman response function. The fine structure is not a problem for ultrashort pulses.

The Raman response computational approach was introduced, in part, as a method for treating Raman scattering when the distinction between pump and Stokes broke down. This happens, for example, in the case of femtosecond optical pulses whose bandwidth exceeds the bandwidth of χ_3. The Raman response function has been used with considerable success to predict the propagation properties of many pulses in the femtosecond regime [2,3]. In these cases, the pulses were so short that they self-seeded the Raman process. Longer pulses do not have enough bandwidth to self-seed, and a proper treatment of spontaneous scattering is needed to describe the initiation of the Raman process. While the initiation of Raman scattering from noise has been used before in the time domain [4], the present work is, to the best of our knowledge, the first treatment in fiber optics to go beyond a simply phenomenological use of noise and to develop a direct linkage to the Raman response function.

The time-domain approach gives us the ability to study stimulated Raman scattering for optical pulses of arbitrary length. Raman gain in optical fibers is much simpler in the cw and ultra-short pulse limits. In the cw limit, the Raman gain spectrum can be traced out by measuring the amplification of a weak tunable signal. Amplification of a spontaneous noise background produces stimulated Raman scattering. In the opposite limit of ultrashort optical pulses, there is no distinct Raman band. Raman gain downshifts the average frequency and the pulse broadens spectrally by self-phase modulation. Our general goal is to use numerical simulation to examine the transition between these two regimes and, in particular, to understand the evolution of frequency chirp and of pulse shapes.

The propagation of pulses in single-mode optical fibers is described by the modified nonlinear Schroedinger equation, which we write in the usual normalized form [2]

[1]AT&T Bell Laboratories, Holmdel, New Jersey 07733, (908)-949-7852

$$-i\frac{2}{\pi}\frac{\partial u}{\partial(z/z_o)} = \pm\frac{1}{2}\frac{\partial^2 u}{\partial(t/t_o)^2} - (1-\alpha)|u|^2 u$$
$$-\alpha u\int_{-\infty}^{t} f(t-\tau)\left[|u(\tau)|^2 + F(\tau)\right]d\tau\,, \qquad (1)$$

where u is the (complex) amplitude envelope of the pulse, z is the distance along the fiber, and the plus (minus) corresponds to positive (negative) group-velocity dispersion (GVD). The time variable t is a retarded time measured in a reference frame moving along the fiber at the group velocity. The normalizing length z_o is defined by $z_o = \pi^2 c^2 t_o^2/(|D(\lambda_o)|\lambda_o)$, and the amplitude u is normalized such that $|u|^2 = 1$ corresponds to an effective intensity of $I_o = 10^{-7} nc\lambda_o/(16\pi n_2 z_o)$ W/cm^2. In these expressions t_o is a width parameter for the input pulse (defined below), $D(\lambda) = \lambda^2 \mathrm{d}^2 n/\mathrm{d}\lambda^2$ is the GVD in dimensionless units, n is the refractive index of the core material, n_2 is its nonlinear coefficient in electrostatic units (1.1×10^{-13} esu for silica), c is the speed of light in centimeters per second, and λ_o is the free-space wavelength. The term $|u^2|u$ in Eq. 1 is the instantaneous, 'electronic', portion of the nonlinear optical polarization density. Following the theoretical development of Stolen *et al.* [2], this has been extended to include the time-dependent 'nuclear' contribution [5,6] to the nonlinear optical polarization density. The coefficient α is the fraction of n_2 due to the nuclear contribution (18% for fused silica [5,6]) and $f(t-\tau)$ is the Raman response function of silica-core fibers [2]. The response function is normalized such that its integral is unity.

Physically, the terms on the right hand side of Eq. 1 correspond (from left to right) to GVD, self-phase modulation, and Raman amplification. The final term on the right hand side of Eq. 1 corresponds to spontaneous Raman scattering due to polarizability fluctuations. The response function formulation of the propagation problem given in Eq. 1 implies an expression for the noise input via the fluctuation-dissipation theorum the results of which [7] are:

$$< F(t) > = 0\,, \qquad (2)$$
$$< F(t)F(t') > = 2\gamma < q^2 > \delta(t-t')\,, \qquad (3)$$
$$< q^2 > = \frac{1}{\pi}\int_0^{+\infty} f''(\Omega)\coth\left(\frac{\Omega}{2T}\right)d\Omega\,, \qquad (4)$$
$$f''(\Omega) = \mathrm{Im}\left[\int_0^{+\infty} f(t)e^{i\Omega t}dt\right]. \qquad (5)$$

The ensemble average of the fluctuations and the strength of the fluctuations are stated in Eqs. 2 and 3. Equation 4 is a statement of the fluctuation-dissipation theorum that relates the strength of the fluctuations to the susceptibility (aka Raman gain curve) and the relaxation time γ. The usual relationship between the Raman response function and the Raman susceptibility [2] is given in Eq. 5, and the relaxation time γ ($= 2/T_2 \approx 220$ cm^{-1}) is determined by exploiting the similarity between the Raman response function and the response function for a harmonic oscillator. Thus, although stochastic, this is a completely determined numerical problem: there are no adjustable parameters.

To test the use of this approach in predicting the propagation properties of picosecond pulses in optical fibers, we have undertaken a numerical reproduction of the laboratory experiments of Raman scattering reported by Stolen and Johnson [8]. In these numerical experiments, we solved Eq. 1 using the split-step or beam-propagation method. The inital

fields were of the form $u(t/t_o, z/z_o = 0) = A\,\mathrm{sech}(t/t_o)$, having an intensity FWHM of $1.76t_o$ = 36ps, and the noise was of the form $F(t/t_o)$ = GASDEV$(t/t_o) \times \sqrt{2\gamma < x^2 >}$, GASDEV being a subroutine that generates Gaussian distributed deviates with zero mean and unit variance [9]

The predicted spectrum of a 36 ps, 200 Watt peak-power pulse after 21 meters of propagation in an optical fiber is shown below in Fig. 1. The pump portion of the spectrum shown the broadening characteristic of self-phase modulation and the asymmetric distortion characteristic of Raman scattering. The spectral development of the first Stokes pulse about 440 cm^{-1} is clearly evident. The initial development of the second Stokes pulse is also seen as the small bump about 880 cm^{-1}.

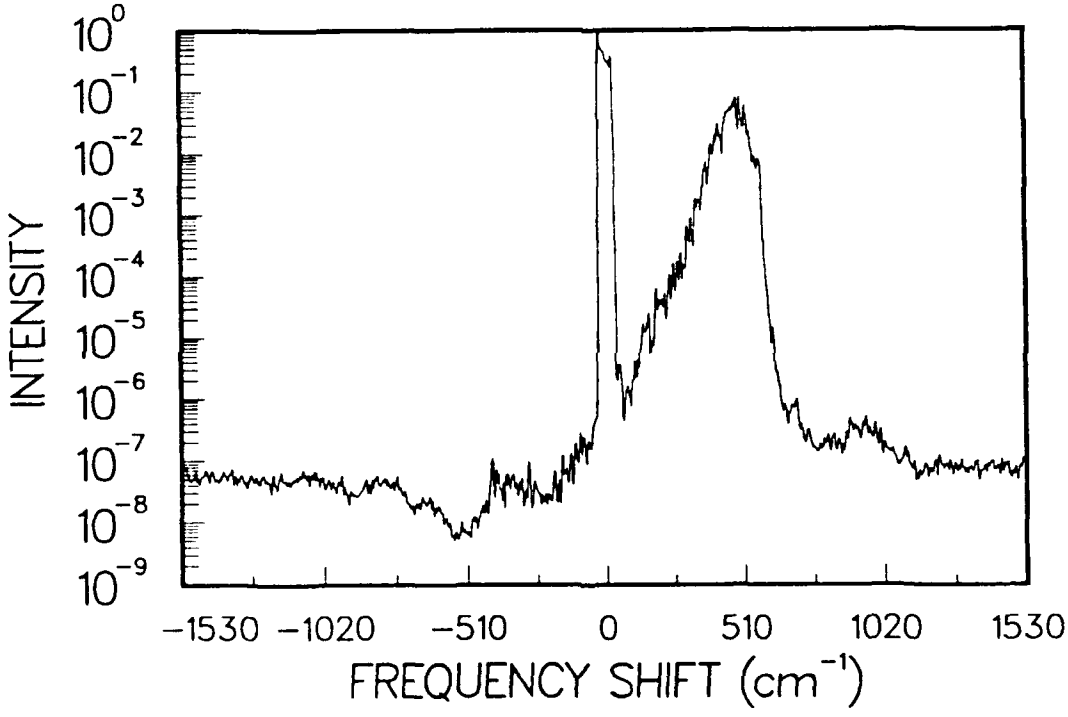

Figure 1

In summary, we have applied a time-domain response-function formalism that includes the buildup of SRS from spontaneous scattering to the numerical simulation of Raman scattering by picosecond optical pulses in single-mode fibers. This parameter-free polychromatic single-field approach is able to predict the experimentally observed impact of SRS on these pulses.

This work was performed, in part, under the auspices of the U.S. Department of Energy by Lawrence Livermore National Laboratory under contract W-7405-ENG-48.

REFERENCES

1. A. Penzkofer, A. Laubereau, and W. Kaiser, "High intensity Raman scattering," *Prog. Quant. Electr.* **6** , 55-140, (1979).

2. R.H. Stolen, J.P. Gordon, W.J. Tomlinson, and H.A. Haus, "Raman response function of silica-core fibers," *J. Opt. Soc. Am.* **B6** , 1159-1166 (1989).

3. A.M. Weiner, R.N. Thurston, J.P. Heritage, D.E. Leaird, E.M. Kirschner, and R.J. Hawkins, "Temporal and spectral self-shifts of dark optical solitons," *Opt. Lett.* **14** , 868-870 (1989).

4. K.J. Blow and D. Wood, "Theoretical description of transient stimulated Raman scattering in optical fibers," *IEEE J. Quantum Electron.* **QE-25** , 2665-2673 (1989).

5. R. Hellwarth, J. Cherlow, and T.-T. Yang, "Origin and frequency dependence of nonlinear optical susceptibilities of glasses," *Phys. Rev.* **B11** , 964-967 (1975).

6. R.W. Hellwarth, "Third-order optical susceptibilities of liquids and solids," *Prog. Quant. Electr.* **5** , 1-68, (1977).

7. L.D. Landau and E.M. Lifshitz, *Statistical Physics* , revised and enlarged by E.M. Lifshitz and L.P. Pitaevskii, 3rd ed. (Pergamon, New York, 1980), pp. 377-389, and H. Risken, *The Fokker-Plank Equation, Methods of Solution and Applications* , 2nd ed. (Springer-Verlag, New York, 1989).

8. R.H. Stolen and A.M. Johnson, "The effect of pulse walkoff on stimulated Raman scattering in fibers," *IEEE J. Quantum Electron.* **QE-22** , 2154-2160 (1986).

9. W.H. Press, B.P. Flannery, S.A. Teukolsky, and W.T. Vetterling, *Numerical Recipes* (Cambridge University Press, New York, 1986), pp. 202-203. The pulses were initialized in an array of 16384 elements spanning a time window of $t/t_o = \pm 5$. This corresponds to a time window of 204.5 picoseconds, a time-grid spacing of 12.5 femtoseconds, and a bandwidth of 2670 cm^{-1}.

A negative contribution to n_2 in silica fibers

R. H. Stolen
AT&T Bell Laboratories
Crawford Corner Road
Holmdel, NJ 07733-1918

and

W. J. Tomlinson
Bellcore
331 Newman Springs Road
Red Bank, NJ 07701-7040

The Raman interaction contributes about 18% of the nonlinear refractive index of silica optical fibers. By numerical simulation we previously demonstrated that this Raman contribution to the nonlinear refractive index is substantially reduced when the optical pulse width is less than the molecular resonance period.[1] A surprising result of those simulations was that the Raman contribution to the nonlinear index was actually negative for pulse widths less than 30 fsec. Here we show that the negative contribution can be traced to the time delay inherent in the Raman response.

In the simulations we use, as a measure of the effective nonlinear index, the pulse intensity necessary for the pulse to exhibit soliton-like propagation. The peak power of this fundamental soliton, P_o, depends on the pulse width, t_o, the dispersion, $D(\lambda)$, the effective core area of the fiber, A_{eff}, and the nonlinear index, n_2, as:

$$P_o = \frac{n\lambda^2}{16\pi^3 c} \cdot \frac{D(\lambda) A_{eff}}{n_2 t_o^2} \tag{1}$$

Thus a measurement of the soliton power is equivalent to measuring the nonlinear index because all the other parameters can be measured independently.

The Raman effect is included in the nonlinear Schrödinger equation by replacing the usual nonlinear term with an electronic term which is effectively instantaneous and a Raman term which is an integral over the Raman response function.[2]

$$n_2 I(t) \rightarrow n_2(electronic) I(t) + n_2(Raman) \int_{-\infty}^{t} f(t-t') I(t') dt' \quad , \qquad (2)$$

Our previous results for the Raman part of the effective nonlinear index are plotted in Fig. 1 as a function of input pulse width.[1] The Raman part of the nonlinear index shows not only the expected drop-off as pulse width is reduced, but is also clearly negative for pulse widths less than 30 fsec. The Raman interaction also introduces such features as self-frequency shift and nonuniform chirp. Even so, it is a reasonable approximation to search for a "best fit" soliton pulse.

The negative contribution to n_2 can be understood by looking at the phase as a function of time. This is just the usual treatment of self-phase modulation (SPM) except that the phase no longer depends instantaneously on the power of the pulse. The phase is retarded with respect to the pulse and can be calculated using Eq.(2). An instantaneous phase shift now appears only as the limit when the pulse is much longer than the Raman response time.

To see what happens as the pulse width becomes comparable to the response time, phase vs time was calculated for different pulse widths using only the Raman contribution to n_2. A Lorentzian response function was used with a resonant frequency and damping term chosen to approximately match the silica response function.[3] The response function is illustrated in Fig. 2a.

Figs. 2b-e show the pulse shape and calculated phase for several pulse widths. The quantity actually calculated was the Raman part of Eq. (2). This is related to the phase by the factor $2\pi L/\lambda$ where L is the fiber effective length and λ is the vacuum wavelength. When the pulse is short, the phase is retarded with respect to the pulse. By 2e, the medium has only started to respond near the end of the pulse. To compare the chirp in the different figures, we look at the phase near the peak of the pulse. On each figure, the phase is approximately expanded as a sum of linear and quadratic contributions.

A linear change in phase with time is a uniform frequency shift. This is just the Raman self-frequency shift. For an instantaneous response there is no uniform frequency shift. When the phase is retarded as in 2c, a uniform shift appears and grows larger as the pulse becomes shorter. When the pulse becomes extremely short the uniform shift diminishes and disappears for pulses much shorter than the response time.

It is this quadratic phase change which explains the negative n_2 for pulse widths less than 30 fsec. The quadratic phase change is the frequency chirp, which for an instantaneous response is the usual SPM chirp. We have defined an effective n_2 which is proportional to the frequency chirp. As the pulse gets shorter and the phase is retarded, this quadratic part changes sign so that the effective n_2 becomes negative. Once the pulse is much shorter than the response time, the quadratic part goes to zero.

The use of the phase-delay picture to explain the negative contribution to n_2 demonstrates the power of the time domain approach in dealing with ultrashort optical pulses.

REFERENCES

1. W. J. Tomlinson and R. H. Stolen, "The Raman contribution to the nonlinear refractive index of silica optical fibers," International Conference on Integrated Optics and Optical Fiber Communication (IOOC-89), Kobe, Japan, July 18-21, 1989, Paper 21C4-4.

2. R. H. Stolen, J. P. Gordon, W, J. Tomlinson, and H. A. Haus, "The Raman response function of silica-core fibers," J. Opt. Soc. B **6**, 1159-1166 (1989).

3. K. J. Blow and D. Wood, "Theoretical description of transient stimulated Raman scattering in optical fibers," IEEE J. Quantum Electron. **QE-25**, 2665-2673 (1989).

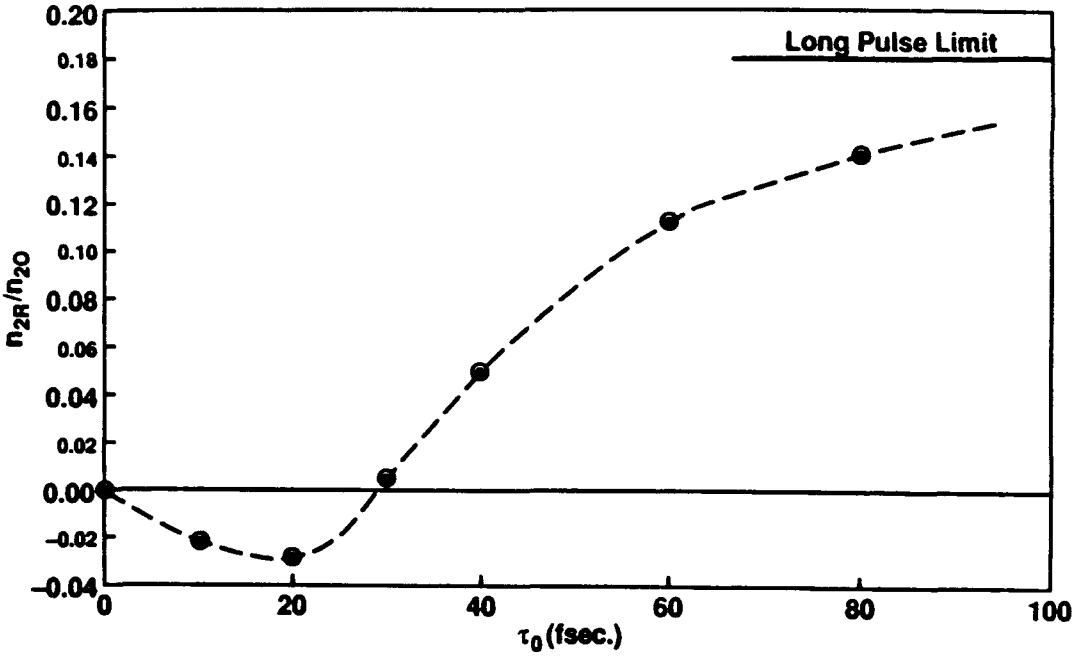

Fig. 1. Raman contribution to the effective nonlinear index of silica fibers.

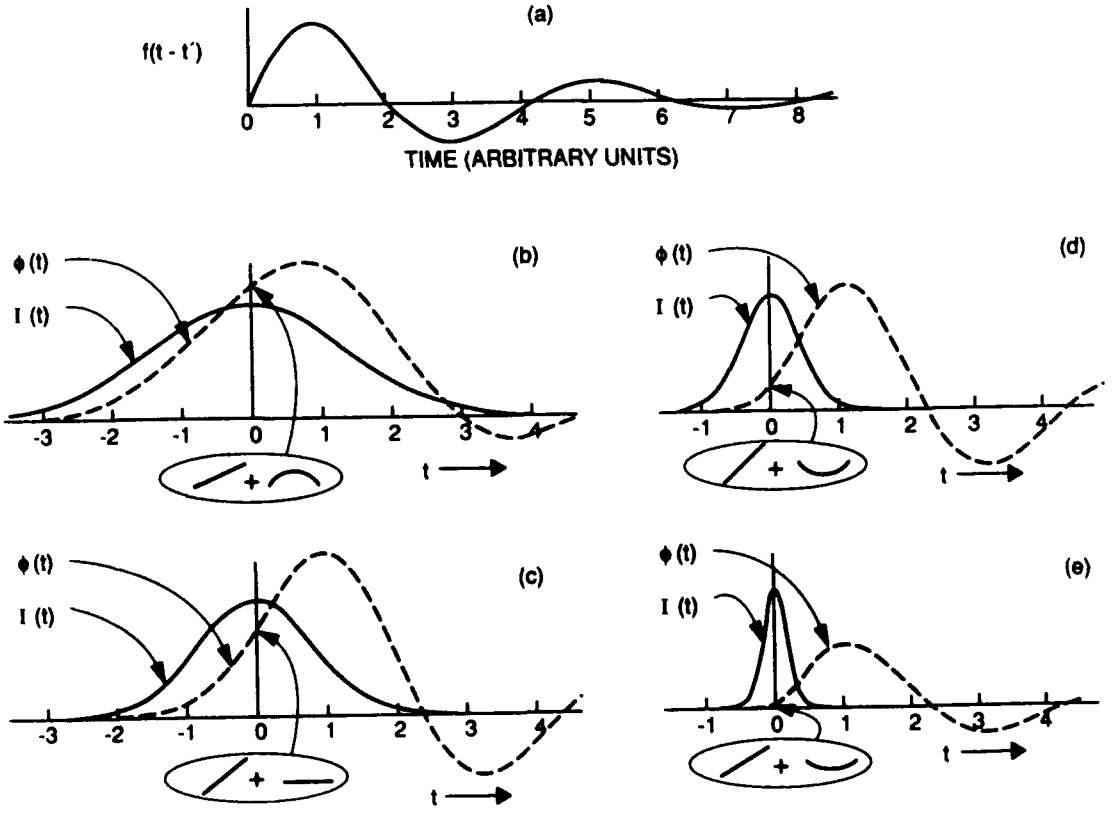

Fig. 2. Delayed phase for four pulse widths using a Lorentzian response function.

The soliton self frequency shift in telecommunications fibre

J.K.Lucek and K.J.Blow

BT Laboratories, Martlesham Heath, Ipswich, IP5 7RE, England.

Tel. +44 473 645941

Pulses of duration 800 fs (sech^2 FWHM) at 1550 nm are generated in an NaCl:OH laser having an actively stabilised external non-linear cavity [1]. These are coupled into lengths (several km) of standard telecommunications fibre (D=15 ps nm^{-1}km^{-1}, effective area = 75 μm^2). The spectral and time domain information about the pulses emerging from the fibres is compared with the results of exact calculations. It has been shown that the magnitude of the soliton self frequency shift [2] (SSFS) in a given length of fibre is proportional to the inverse fourth power of the pulse width when a single soliton is launched [3]. However, the pulse-width(s) of the soliton(s) that form(s) from an arbitrary launched pulse depends on the pulse power and shape. Consider a pulse launched in the form A sech t. The eigenvalues that describe the energies of the solitons that form are given by

$$\xi_j = A - j + 0.5 \qquad \xi_j > 0,\ j = \text{positive integer} \tag{1}$$

The pulse-width associated with each soliton is $\frac{\tau_0}{2\xi_j}$, where τ_0 is the pulse-width of the launched pulse. Hence by altering the launched pulse power (proportional to A^2), we alter the pulse-width(s) of the soliton(s) that form(s) and hence the magnitude of the SSFS that they undergo. Figures 1 and 2 show the experimental and calculated spectra generated by pulses with initial values of A=1.4 and A=1.7 respectively in a 10.6 km fibre. The features marked 'dispersive wave' represent the energy shed by the launched pulse in order to form the soliton(s). The figures show that the A=1.4 pulse generates one soliton (ξ_1) which undergoes a measurable SSFS and that the A=1.7 pulse generates two solitons, one of which (ξ_1) undergoes a measurable SSFS and the other (ξ_2), being relatively broad, does not. Figure 3 shows an example of the output from the fibre in

the time domain, as measured by a fast photodiode and sampling oscilloscope, when A>1.5. The ξ_1 soliton, which undergoes an appreciable SSFS, is retarded by 1.25 ns with respect to the ξ_2 soliton and the dispersive wave. This is in line with theoretical predictions and exact calculations given the sign and magnitude of the dispersion parameter.

In order to determine the fibre length dependence of the SSFS, pulses were launched into a fibre coupler that split the power equally between a 10.6 km length and another length, z, of the same type of fibre. The ratio of the SSFS in length z to that in 10.6 km is plotted in figure 4, along with results from a model [4] and exact calculations. The model uses the result from perturbation theory that the soliton broadens by a factor $e^{2\gamma z}$ after travelling distance z in a fibre of loss γ. It yields the result that the ratio of the SSFS at distance z_1 to that at z_2 is given by $\frac{1-e^{-8\gamma z_1}}{1-e^{-8\gamma z_2}}$. The experimentally determined ratios differ somewhat from those predicted, however measurements of the autocorrelation widths of the fundamental soliton at 2.1 km and 10.6 km show that it has undergone an excess broadening within the first 2.1 km corresponding to a loss of ≈30% of the launched energy, but between 2.1 km and 10.6 km broadens by a factor close to that expected from the fibre loss. This would have the effect of putting the measured points above the theoretical curve in figure 4 as has occurred.

REFERENCES

1. C.P.Yakymyshyn, J.F.Pinto and C.R.Pollock, Optics Letts 14 621 (1989)

2. F.M.Mitschke and L.F.Mollenauer, Discovery of the Soliton Self Frequency Shift, Optics Lett 11 659 (1986)

3. J.P.Gordon, Theory of the Soliton Self Frequency Shift, Optics Lett 11 662 (1986)

4. D Wood , Constraints on the Bit Rates in Direct Detection Optical Communication Systems using Linear or Soliton Pulses, IEEE J Lightwave Tech 8 1097-1106 (1990)

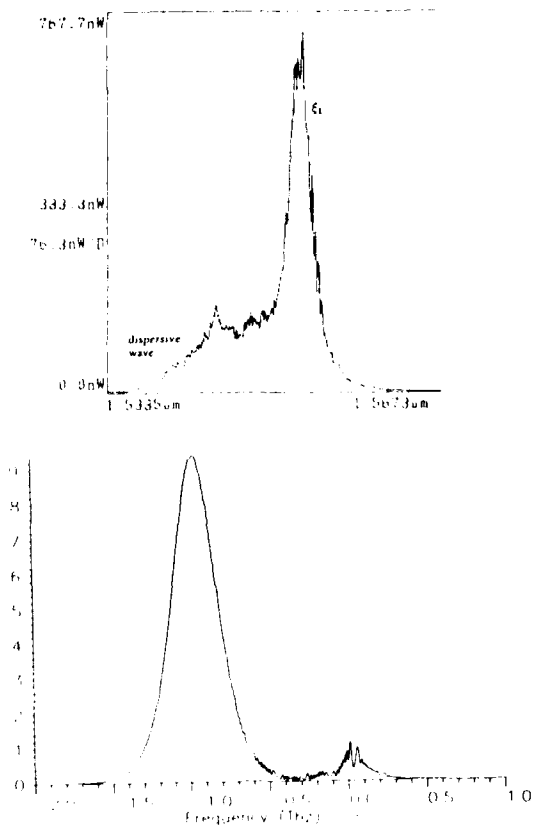

Figure 1

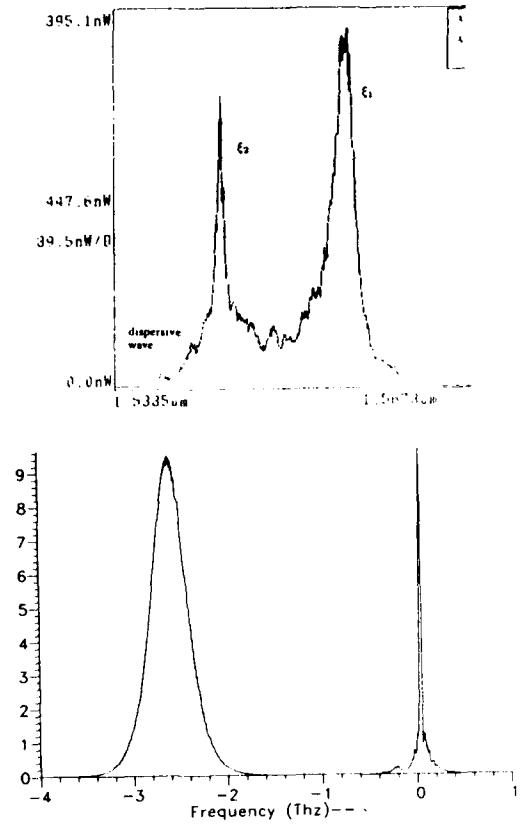

Figure 2

Figures 1 and 2: upper traces experimental, 5.85 nm per division, wavelength increases from left to right; lower traces computer simulation, wavelength increases from right to left (1 THz = 8 nm).

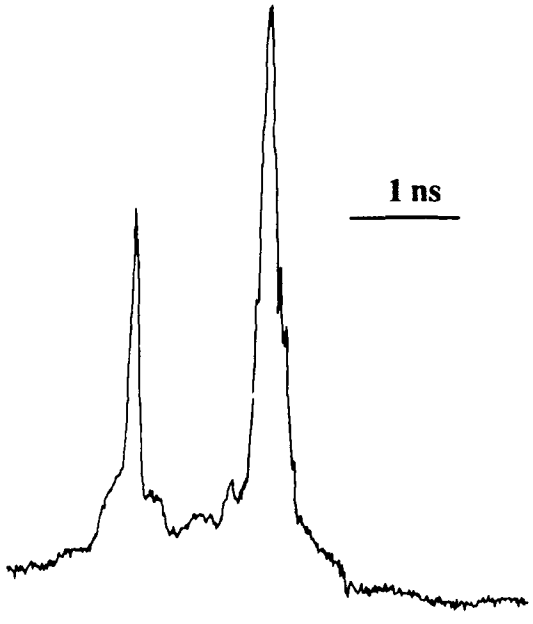

Figure 3

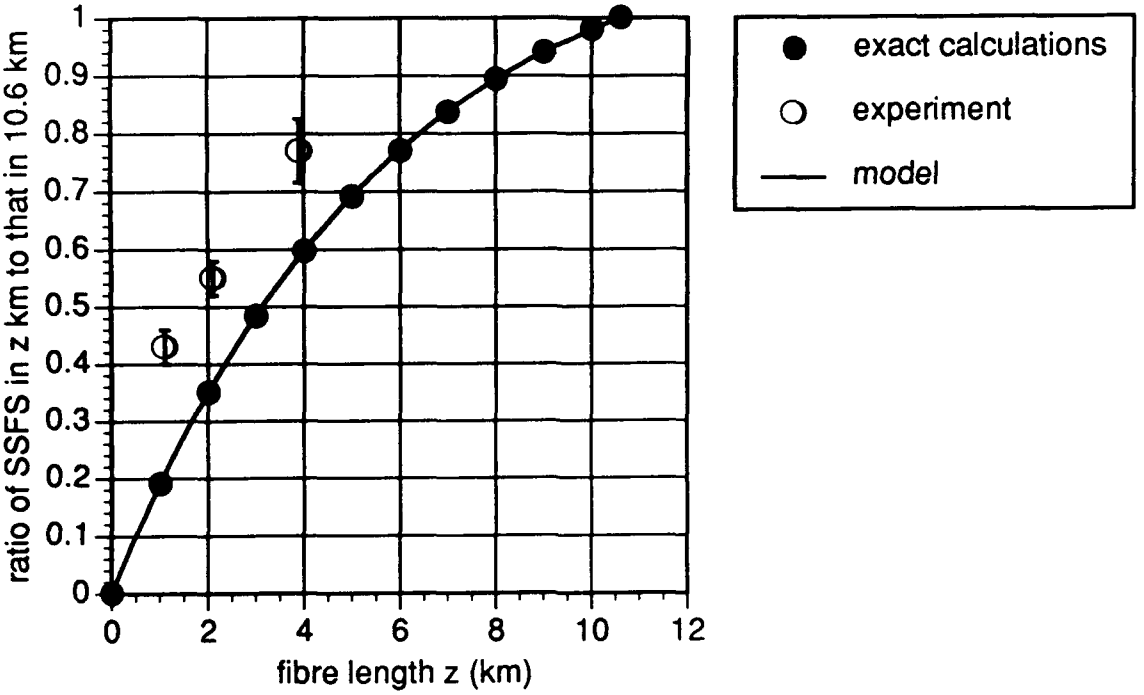
ratio of SSFS in z km to that in 10.6 km
1
0.9
0.8
0.7
0.6
0.5
0.4
0.3
0.2
0.1
0
0
2
4
6
8
10
12
fibre length z (km)
exact calculations
experiment
model

Figure 4

Generation of Spatio-Temporal Patterns and All-Optical Switching based on Coherently Induced Modulational Instability in Fibers

S. Trillo, S. Wabnitz

Fondazione Ugo Bordoni, Via B. Castiglione 59, 00142 Rome, Italy

1. INTRODUCTION

The appearance of modulational sidebands building up from noise has been reported when an intense cw or quasi-cw propagates in a fiber in the anomalous dispersion regime [1]. The modulation transforms the input wave into a train of pulses with ultra-high repetition rate. This process may be stimulated by seeding incoherently (i.e., by means of a different weak detuned laser) the modulational instability (MI) [2]. However the experiments and the early theory on MI [3] have led to the diffuse but erroneous belief that in the presence of MI the input wave becomes a train of solitons. On the contrary (temporally) periodic wave solutions of the nonlinear Schroedinger (NLS) equation have shown that the propagation is periodic also in space (a phenomenon known as Fermi-Pasta-Ulam recurrence [4]), leading to the formation of complex spatio-temporal patterns [5-7]. We show here that the nonlinear dynamics of modulated waves, which includes in principle the interaction of an infinite number of Fourier modes, is essentially locked to the simple interaction between three modes: the pump and the first symmetric sidebands. In this case a simple integrable one-dimensional equivalent oscillator model [8-9] enables one to unfold the role of a coherent modulation at the input in the generation of the spatio-temporal patterns. This suggests also the possibility of new experiments in wlhich the pulse train and switching among two logical state is controlled by the input phase relation between the pump and the sidebands.

Moreover we succesfully apply the present model to deal with the case in which the sidebands and the pump are linearly polarized along the orthogonal birefringence axes of a birefringent fiber [10]. In this case the domain of MI can be extended to the normal dispersion regime. We show that, in spite of the absence of analytical solutions for the coupled NLS equations, the predictions of the truncated model are in excellent agreement with numerical results.

2. THEORY

We consider the coupled NLS equations that describe the evolution of the linearly polarized envelope components u and v in a birefringent fiber, which read in dimensionless units,

$$\begin{aligned} i\frac{\partial u}{\partial \xi} \pm \frac{1}{2}\frac{\partial^2 u}{\partial t^2} + \frac{\Delta}{2}u + (|u|^2 + \frac{2}{3}|v|^2)u + \frac{1}{3}u^2 v^* = 0, \\ i\frac{\partial v}{\partial \xi} \pm \frac{1}{2}\frac{\partial^2 v}{\partial t^2} - \frac{\Delta}{2}v + (|v|^2 + \frac{2}{3}|u|^2)v + \frac{1}{3}v^2 u^* = 0, \end{aligned} \tag{1}$$

where Δ is the linear birefringence, the upper (lower) sign holds in the anomalous (normal) dispersion regime, whereas ξ and t are the longitudinal and temporal coordinates. Here we consider both the case of scalar or conventional MI, and the case of polarization modulational instability (MPI) in a birefringent fiber.

1) Let us consider initial conditions such that

$$u(\xi = 0, t) = 1 + b\,cos(\Omega t), v(\xi = 0, t) = 0, \tag{2}$$

where $b = \epsilon exp(i\phi_0/2)$, and $|\epsilon| \ll 1$. In this case the propagation is governed by the scalar NLS equation for the u component. By inserting eq.(2) in eqs.(1) and linearizing it with respect to b, one obtains the usual condition for modulational instability (MI) of the continuous wave solution $\Omega \leq 2$, whenever the propagation is in the regime of anomalous dispersion of the fiber [1]. Though in the regime of strong depletion higher order sidebands may be generated, the three-wave interaction gives an excellent description of the propagation whenever $1 < \Omega < 2$, so that higher order modes do not experience an initial exponential amplification. In other words we investigate the evolution of the initial conditions (2) over distances for which the approximation $|\epsilon| \ll 1$ fail. Let us consider the ansatz

$$u(\xi, t) = e^{\mp i\Omega^2\xi/4}(A_0(\xi) + \sqrt{2}A_1(\xi)\,cos(\Omega t)). \tag{3}$$

By substituting eq.(3) in eq.(1) and grouping terms vibrating with the same frequency we obtain two coupled ordinary differential equations for $A_0(\xi)$ and $A_1(\xi)$. It is convenient here to represent the evolution of the modulated wave by introducing a geometric representation based on a psedo-Stokes modulation vector $\mathbf{S} = (S_1, S_2, S_3)$, whose components read by definition

$$S_1 = (|A_0|^2 - |A_1|^2)/S_0; S_2 = (A_0^* A_1 + c.c.)S_0; S_3 = (iA_0^* A_1 + c.c.)/S_0. \tag{4}$$

Note that $S_0 = |A_0|^2 + |A_1|^2$ is a conserved quantity of eqs.(4), whereas S_0 is generally not conserved in the original system of eqs.(1). The evolution of the optical field in the fiber may be graphically displayed as the motion of the tip of the vector $\mathbf{S} = (S_1, S_2, S_3)$ on the sphere $\{\mathbf{S} : S_1^2 + S_2^2 + S_3^2 = S_0^2\}$. We obtain

$$\frac{d\mathbf{S}}{d\zeta} = (\mathbf{\Omega}_L + \mathbf{\Omega}_{NL}(\mathbf{S})) \times \mathbf{S}, \tag{5}$$

where $\zeta = S_0\xi$, $\mathbf{\Omega}_L = (\kappa/2, 0, 0)$, where $\kappa = \Omega^2/S_0$, is a dispersive contribution and $\mathbf{\Omega}_{NL} = (-7S_1/4 + 3/4, -S_2, S_3)$ accounts for the nonlinearity.

Figure (1) shows the projection of the solutions of eqs.(1) on the sphere of unity radius, with initial conditions (2), $\kappa = 1$, and the choice of anomalous dispersion. Each point on the sphere represents a different modulation state. For example, the points $\mathbf{S}_{p,s} = (\pm 1, 0, 0)$ represent the unmodulated pump and the sidebands, respectively. Points on the equator (i.e., on the $S_3 = 0$ plane) represent pure amplitude modulations (i.e., with $\phi = 0$), whereas points on the meridian with $S_2 = 0$ correspond to pure frequency modulations (i.e., $\phi = \pi$). All the remaining points represent mixed AM-FM modulation states. The vector $\mathbf{S}$ was evaluated from the first three Fourier components of the full numerical solution. The agreement with the prediction of eq.(5), in particular in the proximity of the separatrix trajectory that emanates from the unstable pump mode is excellent.

The insets in figure (1) show the intensities in one temporal period T that correspond to either an initial AM or FM wave ($\phi(z = 0) = 0, \pi$). As can be seen, in both cases a strong AM modulation periodically develops in the fiber. However, whereas the trajectory *inside* the separatrix evolves around the same stable AM eigenmodulation, the trajectory that lies *outside* the separatrix switches between the two stable AM

eigenmodulations that are time-shifted by half a period. As a result, a change from FM to AM of a weak initial modulation may result into orthogonal modulation states at the fiber output. They may be discriminated by cross-correlation with a reference pattern or by coherent detection. We anticipate that this effect has potential applications to all-optical information processing devices.

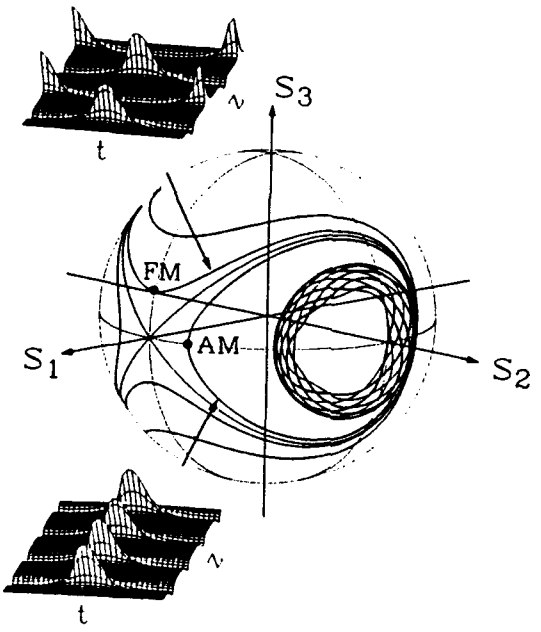

Figure 1: Modulational sphere and AM-FM switching in a dispersive nonlinear medium based on modulational instability.

2) When we set the initial conditions for eqs.(1) to

$$u(\xi = 0, t) = 1, v(\xi = 0, t) = b cos(\Omega t), \tag{6}$$

eqs.(1) describe the propagation of a modulated wave with sidebands orthogonally polarized with respect to the pump. With the ansatz

$$u(\xi, t) = A_0(\xi) e^{\mp i\Omega^2 \xi/4}; v(\xi, t) = \sqrt{2} A_1(\xi) e^{\mp i\Omega^2 \xi/4} cos(\Omega t). \tag{7}$$

from eq.(2) one obtains by following a procedure similar to the one outlined for the scalar case an integrable equation of the form (5) , with $\mathbf{\Omega}_L = (\kappa/2, 0, 0)$, $\kappa = \Delta/2 \pm \Omega^2/4$ and $\mathbf{\Omega}_{NL} = (3S_1/4 - 5/4, -S_2, S_3)$. In the present case AM/FM controlled switching between two temporal shifted patterns is still possible, once a polarizer at 45 degrees between the axes is placed at the output. However the output conversion may be controlled also by inducing a separatrix crossing by minimal changes of the initial modulation depth. This is shown in fig.2, where we report the evolution of one period of the modulation in the normal dispersion regime, for a pump along the slow axis, a weak frequency-modulation at the input and slightly different modulation depths (left and right). We anticipate that for other combination of pump orientation and sign of dispersion we have found situations in which the three-wave model is no longer valid and spatio-temporal chaos may result.

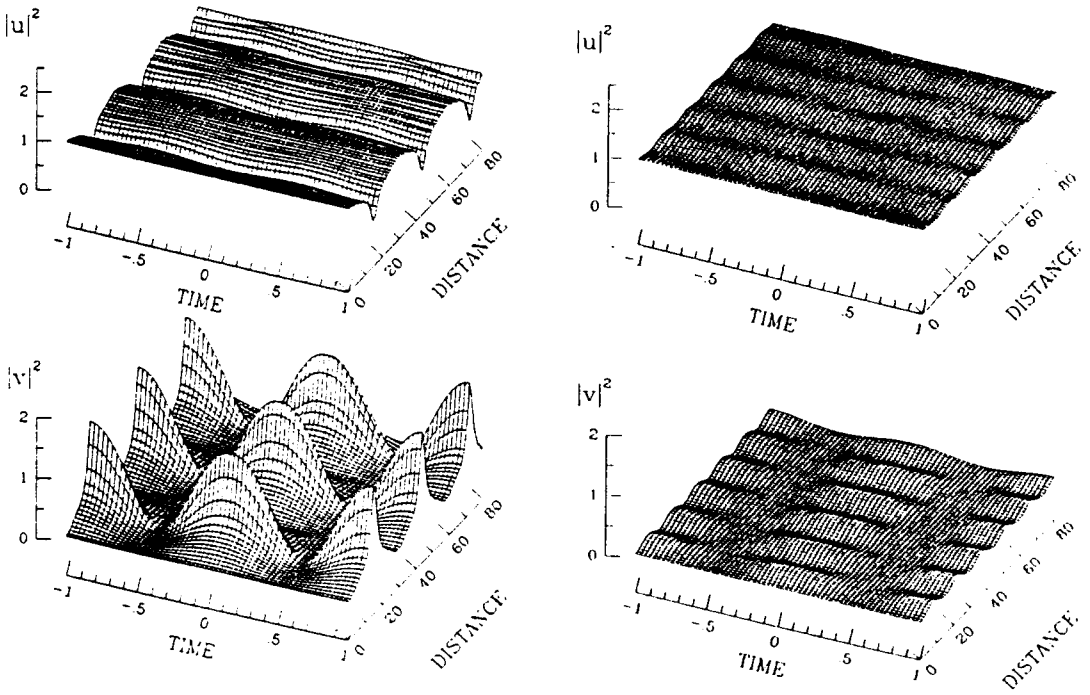

Figure 2: Evolution of one period of the time-periodic pattern of the two components of the field. Left: evolution in regime of strong coupling (inside the separatrix). Right: evolution in regime of weak coupling (outside the separatrix).

3. CONCLUSIONS

We have shown that a truncation to three Fourier modes may well describe the propagation of (both isotropic or polarized) modulated waves in the strong depletion regime. The characteristics of the generated spatio-temporal patterns generated through the coherently induced modulational instability lead to conceive novel schemes for all-optical information processing and switching.

This work was carried out in the framework of the agreement between Fondazione Ugo Bordoni and the Istituto Superiore Poste e Telecomunicazioni.

REFERENCES

[1] K. Tai, A. Hasegawa, and A. Tomita, Phys. Rev. Lett. **56**, 135 (1986).

[2] K. Tai, A. Hasegawa, J.L. Jewell, and A. Tomita, Phys. Rev. Lett. **56**, 135 (1986).

[3] A. Hasegawa, Opt. Lett. **9**, 288 (1984).

[4] E. Fermi, J. Pasta, and S. Ulam, in *Collected Papers of Enrico Fermi*, E. Segrè, ed. (Univ. of Chicago, Chicago, 1965), Vol. 2, p.978.

[5] E.R. Tracy, H.H. Chen, and Y.C. Lee, Phys. Rev. Lett. **53**, 218 (1984); E.R. Tracy, H.H. Chen, Phys. Rev. A **37**, 815 (1988).

[6] N.N. Akhmediev, and V.I. Korneev, Theor. and Math. Physics **69**, 1089 (1986).

[7] M.J. Ablowitz, and B.M. Herbst, SIAM J. Appl. Math. (April 1990).

[8] E. Infeld, Phys. Rev. Lett. **47**, 717 (1981).

[9] G. Cappellini, and S. Trillo, J. Opt. Soc. Am. B **8**, 824 (1991).

[10] S.Wabnitz, Phys. Rev. A **38**, 2018 (1988); S.Trillo, and S. Wabnitz, J. Opt. Soc. Am. B **6**, 238 (1989).

Monday, September 2, 1991

Erbium Lasers

MC 2:00pm–3:30pm
Palmerston Room

Roy Taylor, *Presider*
Imperial College, United Kingdom

Pulse Repetition-Rates in a Passive, Self-Starting, Femtosecond Soliton Fibre Laser.

D.J. Richardson, R.I. Laming, D.N. Payne
V. J. Matsas and M.W. Phillips.
The Optoelectronics Research Centre, Southampton University,
Southampton, U.K. SO9 5NH.
Tel. (0703) 593138, Fax. (0703) 593142.

Rare-earth doped optical fibres offer wide gain bandwidths and provide an ideal medium for the generation of ultra-short optical pulses. To date research in mode-locked fibre lasers has centered on active mode-locking schemes incorporating fast phase [1] and amplitude modulators [2]. However, the large non-linear effects obtainable in optical fibres make passive mode-locking an attractive proposition. A self-starting, passive mode-locking scheme based on the reflection properties of the Non-linear Amplifying Loop Mirror (NALM) [3] has recently been reported [4,5]. The system is capable of both picosecond/nanosecond duration square pulse operation [4] and ultra-short femtosecond soliton generation [5,6]. In this paper we discuss the various modes of operation of the laser and present results on pulse repetition rates, an *important* characteristic for a practical source of ultra-short solitons.

The laser configuration is illustrated in figure 1. The switching characteristic of the NALM dictates that the minimum loss per cavity round-trip pulse forms are either square pulses with a peak intensity determined by the switching power of the loop, or solitons. Both of these pulse forms can propagate in a non-linear medium with a constant phase across their entire envelope and this characteristic enables complete switching by the NALM [7]. In order to self-start, noise is required at the NALM input to enable either the square or soliton pulse forms to develop. The noise is provided by reducing the linear cavity loss to a level sufficient for the onset of CW lasing. This is achieved either by applying a birefringence induced non-reciprocal phase bias within the NALM or by arranging for asymmetric splitting at the NALM coupler. This latter option would permit the system to be constructed entirely of polarisation-maintaining fibre, thus improving system stability. Both square pulses with durations in the pico/nano -second range [3] and femtosecond soliton pulses [4,5] have been observed experimentally with the system operating at 1.55 μm. The shortest pulses so far generated had a duration of 320 fsec [4,5] and a corresponding time bandwidth product of 0.32 (see figure 2).

As well as having two distinct modes of pulse generation, the system has at least three distinct regimes of operation with regard to pulse repetition rates. During square pulse operation (which constitutes the most stable operation of the system), pulses are generated at the cavity round-trip frequency. In this regime the repetition rate is stable with regard to changes in input pump power, provided

that the pump power is not reduced to a level below which the pulsing cannot be sustained. The peak power of the square pulses remains clamped to the switching power of the NALM loop and, as the pump power to the system is increased, the extra power circulating in the cavity is taken up by a corresponding increase in pulse width. Square pulses generated with a 104m NALM at a variety of input pump powers are shown in figure 3 and illustrate the pulse broadening with increasing pump level.

The transition from the square pulse to the soliton regime of operation is most readily induced by changing the NALM phase bias. Three distinct modes of repetition rate behaviour have been observed. Firstly, as the NALM phase bias is slowly altered the square pulse is seen to break up into tightly-packed bunches of solitons, the bunches repeat at the cavity round-trip frequency. The situation is illustrated in figure 4. As the phase bias is adjusted close to the point at which the transition from square pulse to soliton behaviour occurs, large deviations from the expected 2:1 aspect ratio of the coherent spike to the pulse shoulder in the background free autocorrelation traces of the square pulses are observed. This observation indicates that substructure on a femtosecond timescale develops within the square pulse just prior to the transition to the soliton regime. Pulse repetition rates as high as 100 GHz (as determined from autocorrelation scans) have been observed within the pulse bunches.

Secondly the system can enter a soliton regime in which the solitons are no longer bunched, but occur seemingly randomly distributed over the entire cavity round-trip period, the pulse patterns repeating at the round-trip frequency. An example of this random pulsing is shown in figure 5a, where, since the detector response time (55 psec) is far longer than the pulse duration (500 fsec), the trace effectively displays the pulse energy. The pulse with twice the amplitude of the others is due to two pulses occuring within the detector response time and illustrates the quantisation of pulse energy associated with solitons being the preferred switching unit for system operation. Note that because of this energy quantisation, more pulses must circulate in the cavity if the pump power is increased, i.e. the average repetition rate must increase in order to obtain more output power. Moreover, no discernible change in the output soliton autocorrelation traces and spectra with input pump power have been observed with the system. This is in contrast to the square pulse mode in which the pulse peak-intensity is clamped and increased circulating energy is taken up by an increase in pulse duration.

By appropriate adjustment of input pump power and birefringence of the NALM it is possible to enter the third pulse repetition rate regime and obtain pure harmonic mode-locking as illustrated in figure 5b. However, in this mode the system is very sensitive to slight changes in pump power. Exactly what factors determine which of the three regimes of soliton generation is encountered are not yet understood. One possibility is that cross-phase modulation between counter-propagating pulse bunches within the NALM loop can play a significant role in its switching operation. The effects of cross-phase modulation would be maximised for tightly bunched pulse trains.

In conclusion, the various pulsing regimes of operation of the femtosecond soliton laser have been clarified. From a practical point of view, stabilisation of pulse repetition rates is an important goal. We have recently obtained encouraging results by incorporating within the system a pulse multiplier consisting of a re-circulating fibre ring delay line. Results of these experiments will be presented at the conference.

References

[1] J.D. Kafka, T. Baer and D.W. Hall: "Mode-locked erbium fibre laser", Opt. Lett. 14 pp 1269-1271, 1989.

[2] Fermann M.E., et al.: "Femtosecond fibre laser", Electron. Lett. 23 pp 1737-1738, 1990.

[3] Richardson D.J., Laming R.I. and Payne D.N.: "Very low threshold Sagnac switch incorporating an erbium doped fibre amplifier", Electron. Lett., 26 pp 1779 1990.

[4] Richardson D.J. et al.: "Self starting passively mode-locked fibre laser based on the amplifying sagnac switch", Electron. Lett., 27, p 542, 1991.

[5] I.N. Duhling III: "Subpicosecond all-fibre erbium laser", Electron. Lett., 27, p544, 1991.

[6] Richardson D.J. et al.: "320 femtosecond soliton generation with a passively mode-locked fibre laser" , accepted Electron. Lett. 1991.

[7] Doran N.J and Wood D.: "Non-linear optical loop mirror", Opt. Lett., 13 pp 56-58, 1988.

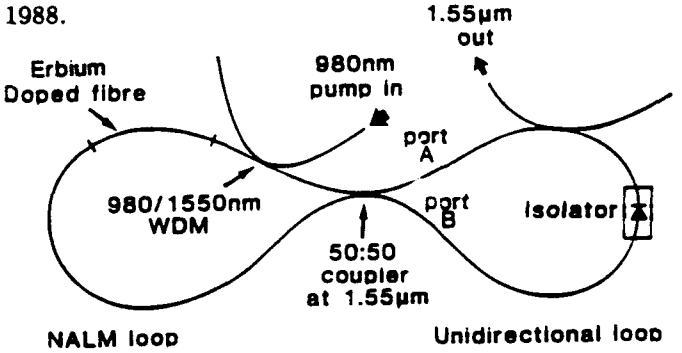

Figure 1)

Experimental configuration of the self-starting, passively mode-locked fibre laser.

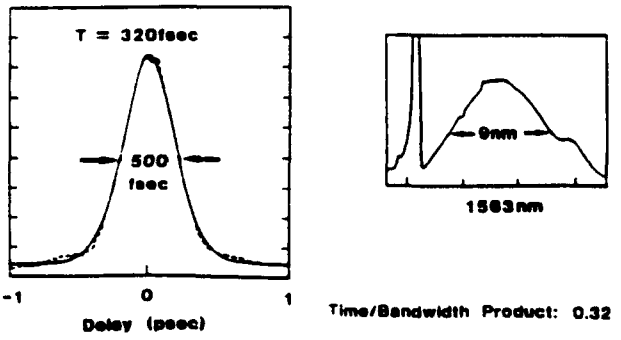

Figure 2)

Background free auto-correlation trace and optical spectra of 320 femtosecond soliton pulses. the solid line autocorrelation profile representa a non-linear least squares fit to the experimental data on the assumption of a $\mathrm{sech}^2 \tau$ pulse form.

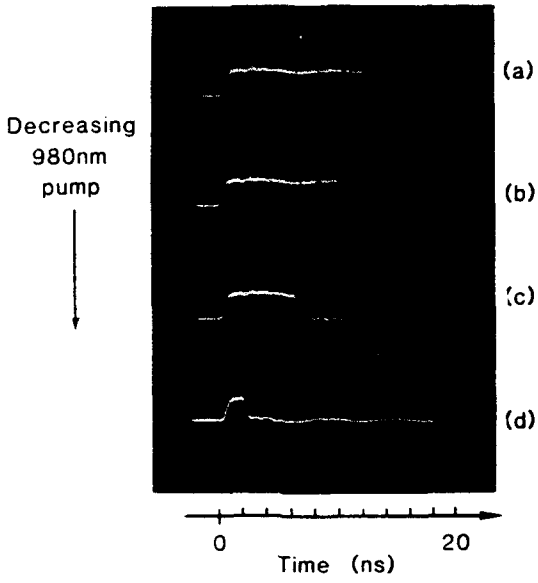

Figure 3) Output pulse shapes for 104 m mode-locked fibre laser as a function of pump power. Input 980 nm pump powers were (a)155 mW, (b)115 mW, (c)75 mW and (d)40 mW. The system self started at an input pump power of 80 mW.

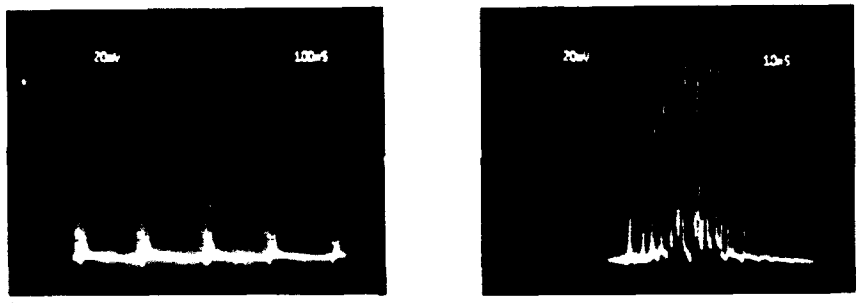

Figure 4) (a) Soliton pulse bunches circulating around the cavity at the cavity round trip frequency. (b) Exploded view of an individual soliton bunch.

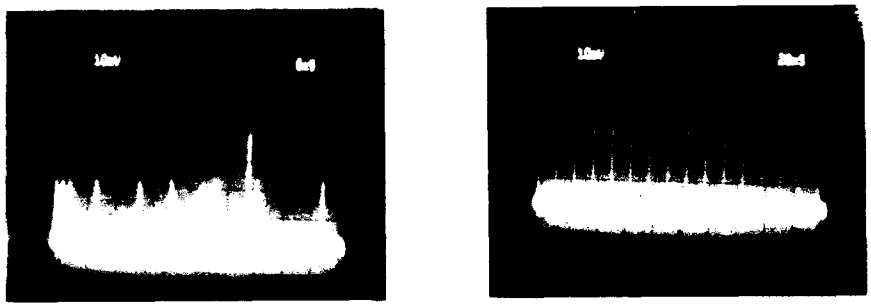

Figure 5) 450 fsec soliton pulse trains. (a) Pulses randomly spaced but well separated. The pulse of apparently twice the amplitude of the others is due simply to two pulses arriving within a time period less than the detector response time. (b) Pure passive, harmonic mode-locking (f=67.2 Mhz, the 16 th harmonic of the cavity round-trip frequency).

Interacting solitons in an erbium fibre laser.

R.P. Davey, N. Langford and A.I. Ferguson
Dept. Physics & Applied Physics, Strathclyde University, Glasgow, U.K.

Erbium doped fibres have become an important source and amplifier of ultra-short pulses in the 1.5μm region where soliton effects have important implications for long distance transmission of optical data. We report on the observation of multiple soliton interactions in a mode-locked erbium fibre laser. Complex interactions including repulsive and attractive forces have been observed over temporal separations of the order of 250ns , resulting in complex pulse-trains.

The cavity configuration is shown in figure 1, and is similar to that described elsewhere.[1,2] The gain was provided by a 2.5 metre length of erbium doped fibre, which was fusion spliced onto a 20 metre length of undoped fibre to ensure soliton pulse-shaping in the cavity. The 528nm pump was coupled into the erbium fibre through a cleaved facet which also acted as a 96% transmitting output coupler. The cavity was completed by a highly reflecting mirror and a bulk phase modulator provided modulation at 480 MHz.

Mechanical polarisation control discs were used to control the polarisation state within each fibre and the pulses were very sensitive to the alignment of these discs. The cavity length was not a crucial parameter and could be detuned by hundreds of microns with little effect on the pulses.

Two operating regimes were observed, neither of which gave pulses at the modulation frequency of 480 MHz. In fact, the modulator could often be turned off altogether and the pulses were self-sustaining.

In the first regime, the pulses were at a frequency of 4.6 MHz which corresponds to the cavity round trip time. Autocorrelations showed a 3ps feature on a large,noisy pedestal.

By adjustment of the polarisation control discs, the second regime could be obtained which gave pedestal-free autocorrelations of 2.5ps duration. Observation of the output on a fast photodiode showed complicated pulse-trains with periodicity corresponding to the cavity round trip time, as can be seen in figure 2, which also illurstrates the quantised nature of the pulse heights.

In this regime the number of pulses within the cavity was a linear function of output power. By reducing the pump level, pulses could be made to vanish one at a time, until for output powers of 2 mW, single pulses at 4.6MHz were obtained. The autocorrelation did not vary significantly during this process. The energy required to support a pulse within the undoped fibre can be calculated to be

16pJ per pulse, which compares well with the corresponding soliton energy of 18pJ. The pulses could form various complicated patterns and often executed complex motions as if attractive and repulsive forces existed between them. We believe this may be due to soliton interactions.

In conclusion, we have observed novel behaviour from a mode-locked erbium fibre laser. It is intriguing to speculate why this system behaves so differently to others reported previously[1], and this will be the subject of further research.

References

1 K. Smith et al: *Electron. Lett.*, 1990, **26**, pp.1149-50
2 Davey et al: CLEO'91 CFE2

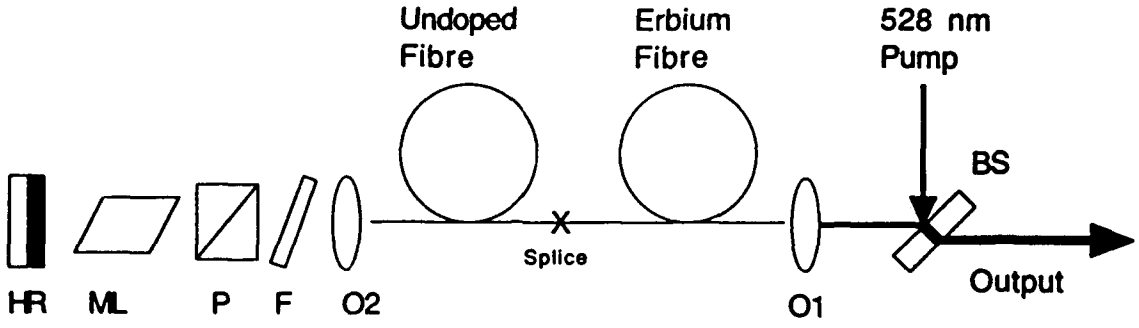

Figure 1. Cavity configuration. BS dichroic beam splitter, O1,O2 microscope objectives, F filter to absorb residual pump, P polariser, ML mode-locker, HR high reflector

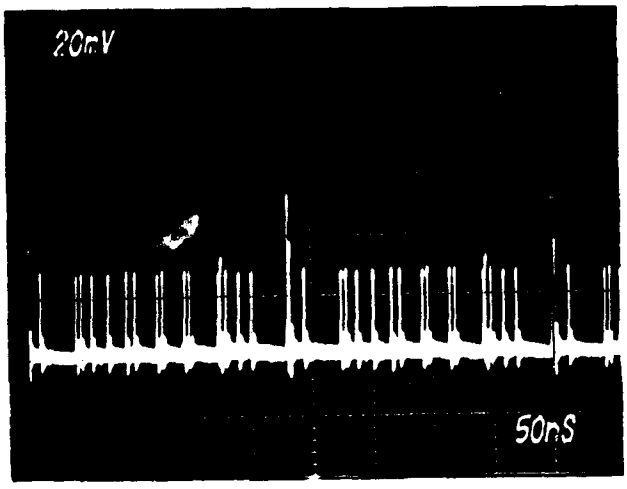

Figure 2. Soliton pulse-train observed on a fast photo-diode.

Noise in a passively mode-locked fiber laser

M.H. Ober, M. Hofer, F. Haberl and M.E. Fermann

Abteilung Quantenelektronik und Lasertechnik, IAEE
Technische Universität Vienna
Gusshausstr. 27/359/9, A-1040 Vienna, Austria
Tel. (0222) 58801 Ext. 3879
Fax. (0222) 5052666

Introduction

Passive modelocking of fiber lasers has recently been shown to be a viable technique for the generation of ultra-short optical pulses[1,2]. In fact pulse-widths as short as $38fsec$ have been generated with such lasers to date[3], which compares well with pulse-widths obtainable with much more complex bulk laser systems[4–8]. However, for practical applications not only the pulse-widths generated with a particular oscillator are important, but also its radio frequency (RF) noise characteristics. From the RF-spectrum of modelocked oscillators information about the amplitude-noise and timing jitter of the generated pulses can be inferred[9–12]. Here we choose to investigate the noise characteristics of a fiber laser passively mode-locked by nonlinear polarization evolution[2,3] due to the simplicity of the involved experimental set-up and its superior performance in short pulse generation compared to other fiber laser passive mode-locking schemes involving a nonlinear amplifying loop mirror[1,13].

Experimental

We used essentially the same experimental set-up as in Fig. 1b) of ref. 2, which consists of a Fabry-Perot cavity with an intra-cavity polarizer, a dispersive delay line and an active fiber attached to one of the two cavity mirrors. Polarization control is achieved by pressing the fiber with three piezoelectric cylinders. Here the output coupler had a reflectivity at the lasing wavelength of 54% and the dispersive delay line design elliminated any spatial frequency chirp at the fiber laser output. The high output coupling typically increases the long term stability of the mode-locked fiber laser, but causes an increase in obtainable pulse widths. A weakly-linearly birefringent silica fiber doped with $1700ppm\ Nd^{3+}$ was employed in the experiments. The fiber length was $40cm$, the core diameter was $5\mu m$ and the cut-off wavelength of the first higher-order mode $1\mu m$. With an absorbed pump power of $350mW$ from a Krypton laser a mode-locked laser power of $20mW$ was so obtained. Typical pulse-widths were $80fsec$ with a time-bandwidth product within 10% of the bandwidth limit. The pulse repetiton rate f_0 was $45.7MHz$. Under these conditions a stable mode-locking regime was found when coupling the laser pulses (intra-cavity) at $\approx 45^0$ to the fiber birefringence axes with a round-trip phase delay between these two axes of $\approx \pi$, i.e. the fiber was found to operate linearly as a quarter-wave plate rotating the polarization state by 90^0 in a double-pass. When modelocked the linear polarization rotation was cancelled by nonlinear pulse propagation in the fiber, thus a passive amplitude modulation of nearly 100% was obtained in the fiber laser. The RF-spectra were measured with a Rhode-Schwartz spectrum analyser with a $6Hz$ resolution bandwidth in a $100Hz - 2GHz$ span and an $8GHz$-bandwidth $InGaAs$ photodiode.

Results

The measured spectral noise density at the fundamental carrier frequency f_0 measured with a $500Hz$ resolution in a $100kHz$ span is shown in Fig. 1. Note that in this measurement the noise floor level in the $1-10kHz$ range is slightly enhanced compared to optimum mode-locking conditions. The single side-band total noise spectral density[11] at the fundamental carrier frequency and its 30th harmonic $L_1(f)$ and $L_{30}(f)$ are displayed in Figs. 2 and 3. The noise spectral density for $L_{30}(f)$ for frequency offsets < 2kHz is seen to be higher than for $L_1(f)$. This is due to the influence of phase noise which is additive to the total noise spectral density (for small phase fluctuations) and varies as n^2 with the order of the carrier harmonic frequency. From Figs. 2 and 3 it may be inferred that the phase noise is negligible at the first harmonic and therefore $L_1(f)$ essentially corresponds to the single side-band amplitude noise spectral density $L_A(f)$. The spectral feature in the frequency range from $2-10kHz$ stems from a noise band of the Krypton laser. This amplitude noise also dominates the total noise spectral density of $L_{30}(f)$ for frequency offsets larger than $2kHz$. Note that the shot-noise spectral density level (with respect to a photo-current of $1mA$) was at $-158dBc$. Thus at a frequency offset of $1kHz$ we obtain an amplitude noise spectral density $51dB$ above the shot noise level. The maximum sensitivity of our set-up was at $\approx 35dB$ above the shot noise level and thus a higher measurement sensitivity is required to resolve the spectral noise features at high frequency offsets. The single side-band phase noise $L_J(f)$ was inferred[9-12] from $L_1(f)$ and $L_{30}(f)$ and is shown in Fig. 4. $L_A(f)$ and $L_J(f)$ completely characterize the noise performance of the laser system and allow the calculation of the root mean square (rms) timing jitter σ_j and the rms amplitude fluctuations σ_a in a frequency band $f_{low}-f_{high}$. In this σ_j is given by

$$\sigma_j = \frac{1}{2\pi f_0}\left(\int_{f_{low}}^{f_{high}} 2L_J(f)df\right)^{1/2} \qquad (1)$$

and σ_a is calculated by substituting $L_J(f)$ with $L_A(f)$ in eq. (1) and omitting the factor $(1/2\pi f_0)$. In a $300Hz-10kHz$ band a rms amplitude fluctuation of 0.07% and a rms timing jitter of $200fsec$ are thus obtained. In a frequency band from $130Hz-20kHz$ the timing jitter was $300fsec$. These noise figures are approximately one order of magnitude lower than results obtained with colour center lasers[11,12]. We attribute the superior noise performance of the fiber laser mainly to the low noise of the employed Krypton pump laser and the stability of the polarization setting in the short fiber length employed, which did not require any adjustments for time periods of hours. Note, however, that a sharp rise in noise spectral density was observed for frequency-offsets $<100Hz$ and we are currently improving the measurement system to resolve these noise features. The main sources of timing jitter were drifts of the laser round-trip frequency due to low-frequency thermal variations in cavity length and thermal fiber vibrations at the butt-coupled launch mirror onto which the pump-light was focussed. We expect a further improvement in noise performance by employing laser diodes as the pump source and resorting to all-fiber cavity designs with cavity mirrors directly coated onto the fiber ends. Stable timing of the laser on a 1Hz scale would require active control of the cavity length[10], but could also be achieved by enclosing the fiber in a temperature stable environment.

Conclusions

In conclusion we have measured the noise performance of a modelocked fiber laser. The laser produces sub $100fsec$ pulses with a superior noise performance compared to colour center lasers. The results demonstrate that mode-locked fiber lasers are an attractive source for precision measurements on a femto-second scale and have potential as highly stable optical oscillators.

We are indebted to Prof. Seifert for lending us the RF spectrum analyser and to F. Krausz and A.J. Schmidt for stimulating discussions. This work was supported by the Fonds zur Förderung der wissenschaflichen Forschung in Österreich, project No. P8024-TEC

References

1. M.E. Fermann et al., Opt. Lett., **16**, 244 (1991)
2. M. Hofer et al., 'Modelocking with cross and self-phase modulation', to be publ. in Opt. Lett., Apr. 91
3. M. Hofer et al., 'Characterisation of ultra-short pulse formation in a passively modelocked fiber laser', subm. IEEE J. Quantum Electronics
4. L.F. Mollenauer and R.H. Stolen, Opt. Lett., **9**, 13 (1984)
5. J.A. Valdmanis and R.L. Fork, IEEE J. Quantum Electronics, **QE-22**, 112 (1986)
6. F. Krausz et al., Opt. Lett., **15**, 1082 (1990)
7. D.E. Spence, P.N. Kean and W. Sibbett, Opt. Lett., **16**, 42 (1991)
8. D.J. Delfyett et al., Opt. Lett., **15**, 1371 (1990)
9. D.v.d. Linde, Appl. Phys., **B39**, 201 (1986)
10. M.J.W. Rodwell, D.M. Bloom, and K.J. Weingarten, IEEE J. Quantum Electronics, **QE-25**, 817 (1989)
11. A. Finch et al., IEEE J. Quantum Electronics, QE-26, 1115 (1990)
12. U. Keller et al., Opt. Lett., **15**, 974 (1990)
13. I.N. Duling, 'All-fiber soliton laser modelocked with a nonlinear mirror', subm. Opt. Lett.

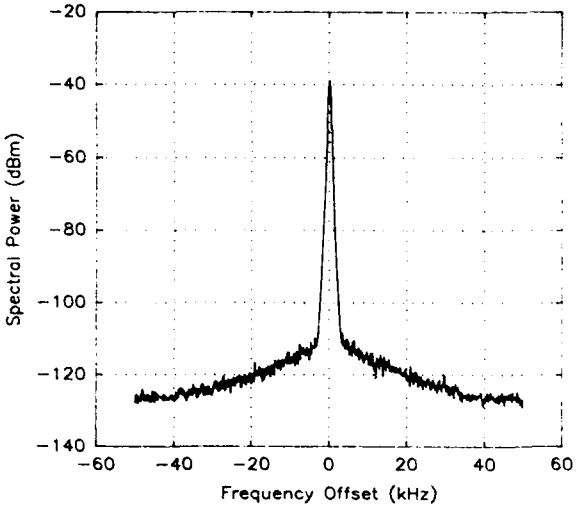

Figure 1:
Noise spectral density power as a function of frequency-offset from the fundamental laser round-trip frequency under imperfect mode-locking conditions. The spectral resolution is 500Hz.

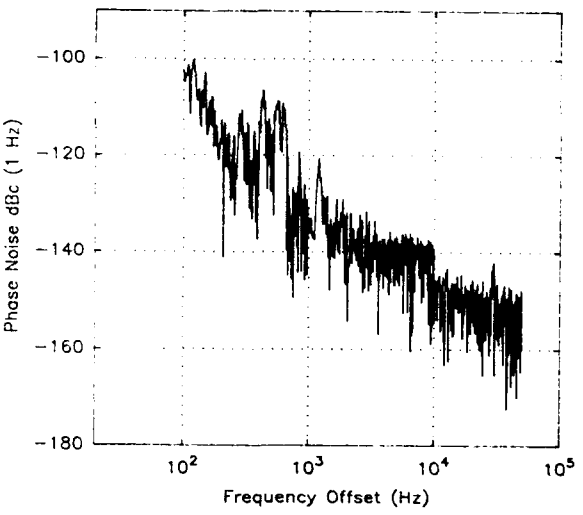

Figure 4:
Single side-band phase noise power $L_J(f)$ in a $1Hz$ bandwidth in dBc.

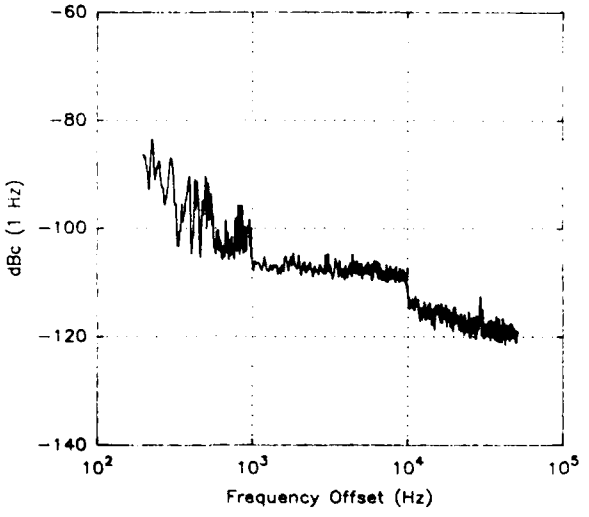

Figure 2:
Single side-band total noise power $L_1(f)$ (or amplitude noise power $L_A(f)$) in a $1Hz$ bandwidth in dBc, i.e. in dB below the carrier power at the fundamental laser round-trip frequency.

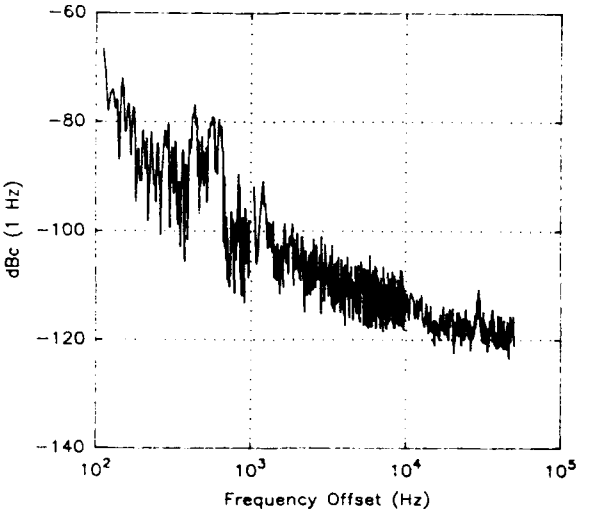

Figure 3:
Single side-band total noise power $L_{30}(f)$ in a 1Hz bandwidth in dBc at the $30th$ harmonic of the laser round-trip frequency.

Pulse Amplification and Shaping using a Nonlinear Amplifying Loop Mirror

E.J. Greer,* K. Smith, N.J. Doran, D.M. Bird and K.H. Cameron

British Telecom Research Laboratories, Martlesham Heath, Ipswich IP5 7RE, UK

* Laser Group, Physics Department, Imperial College, London SW7 2BZ

Summary

In recent work [1], we have studied the the shaping of picosecond-duration optical pulses by the intensity-dependent transmission characteristics of a nonlinear fibre loop mirror. We demonstrated both experimentally and theoretically the advantages to be gained from this pulse shaping, in particular pulse compression and pedestal suppression. In this paper, we report on a Nonlinear Amplifying Loop Mirror (NALM) which performs *both* amplification and intensity filtering functions. We believe that this work will be of significance to all-optical transmission systems [2] and to some of the novel erbium fibre soliton laser configurations now being investigated [3].

A schematic of the NALM configuration is shown in figure 1. The loop was constructed from a 30 m long diode-pumped erbium doped fibre amplifier (EDFA) and a length, L = 8.8 km of Corning dispersion shifted fibre. The dispersion zero of this fibre was around 1.55 μm and was chosen such that pulse shaping due to propagation effects would be negligible. Fibre polarisation controllers (PC) were also included in the loop in order to adjust the device to the desired reflection or

transmission mode.

It can easily be shown that for such a configuration the square pulse transmissivity, T, is given by

$$T = \frac{P_t}{P_i} = G\left\{1 - 2\alpha(1-\alpha)\left[1 + \cos[(1-\alpha)G - \alpha]\phi\right]\right\} \quad (1)$$

where ϕ ($=2\pi n_2 P_i L/\lambda A_{eff}$) is the nonlinear phase shift. P_t and P_i are the transmitted and input powers respectively, λ is the wavelength, n_2 is the nonlinear (Kerr) coefficient, A_{eff} is the effective fibre core area, and G is the power gain of the amplifier. Since the EDFA provided small signal gains of $\approx$30 dB, the calculated switching power, P_S, can be as low as $\approx$0.5 mW peak for the configuration described here. These powers are available from mode-locked semiconductor laser sources.

At the high repetition frequencies available from mode-locked semiconductor lasers, the average powers corresponding to these switching powers are comparable to the saturation powers of the erbium amplifier. We have conducted an experimental and theoretical study of the NALM response when amplifier saturation becomes important. Figure 2 shows the computed response of the NALM (dashed line) for sech^2 input pulses with a 20 dB (small signal) amplifier that saturates (i.e. G decreases by 3 dB) at an input power comparable to the calculated switching power ($P_S = 0.01$ with $n_2 L/\lambda A_{eff} = 1$). The full line in figure 2 represents the response of the EDFA in the loop. Theoretically, we find that although the action of the NALM sacrifices some overall gain (at best $\approx$3 dB), we achieve significant pulse compression (by $\approx \times 0.5$) and pedestal suppression. This is illustrated in figure 3 which compares

experimental autocorrelation traces at the input and output of the NALM for a mode-locked semiconductor laser generating ≈12 ps pulses at 2.5 GHz. Further data relating to the performance of the NALM will be reported.

References

[1] K. Smith, N.J. Doran and P.G.J. Wigley: "Pulse Shaping, Compression and Pedestal Supression Employing a Nonlinear-Optical Loop Mirror", *Opt. Lett.*, **15**, p. 1294 (1990).

[2] L.F. Mollenauer, B.M. Nyman, M.J. Neubelt, G. Raybon and S.G. Evangelides: "Demonstration of Soliton Transmission at 2.4 Gbits/s over 12000 km", *Elecron. Lett.*, **27**, p. 178, (1991).

[3] I.N. Duling III: "Subpicosecond All-Fibre Erbium Laser", *Electron. Lett.*, **27**, p. 544, (1991).

Figure Captions

Figure 1: The NALM Configuration

Figure 2: The $sech^2$ pulse response of the NALM (dashed line) and EDFA (full line).

Figure 3: Autocorrelation traces of (a) input pulses and (b) pedestal-free, compressed pulses transmitted through the NALM. (10 ps/horiz. div.).

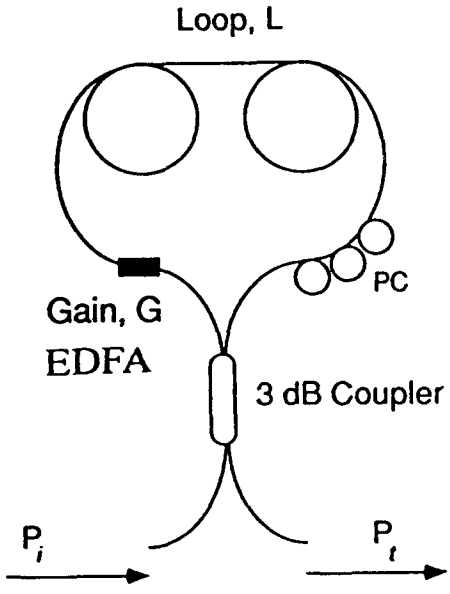

Figure 1

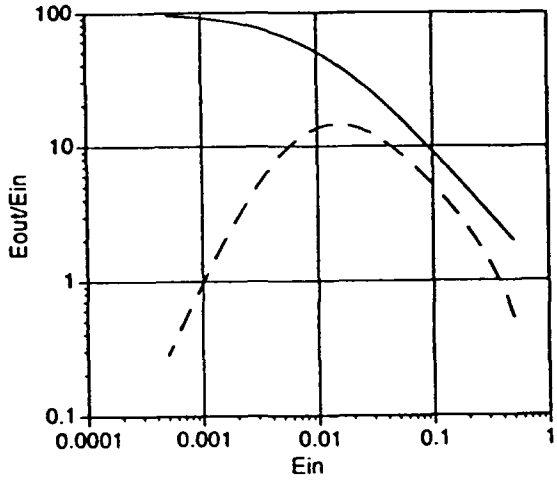

Figure 2

(a)

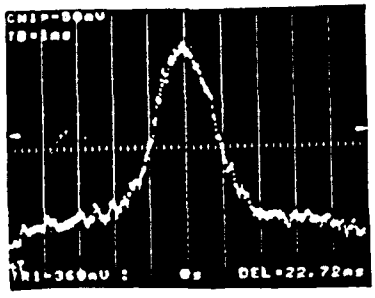

(b)

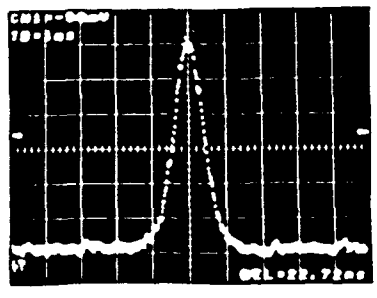

Figure 3

Soliton formation and propagation in a high gain fibre laser.

S.M.J.Kelly

Laser Optics Group, Department of Physics, Imperial College, London SW7 2BZ U.K

Telephone: 071–589 -5111 ext 6832, Fax 071–589–9463

K.Smith K.J.Blow N.Doran.

British Telecomm Research Laboratories, Martlesham Heath, Ipswich IP5 7RE U.K

A source that exploits both soliton shaping and broadband high gain within a single fibre environment is particularly appealing. Recently, Smith et al [1], demonstrated this simple idea with a mode–locked erbium fibre laser. Short picosecond structures with temporal spectral and power characteristics consistent with fundamental soliton shaping were observed. An important feature of the experiment was that only a short length of high gain single mode erbium doped fibre was used. This limit contrasts with previous studies [2] and leads to soliton behaviour that is significantly different from that commonly associated with propagation in long fibres with low gain [3]. The results presented here form part of a theoretical study aimed at understanding the stable behaviour of solitons reported in this short length high gain limit.

Our simple model is based on the experiment [1]. A uni–directional ring cavity is formed by a single mode fibre of length, z_a = 0.02km with laser transmission, T = 0.96, facilitated by discrete loss at one end. Pulse propagation is described by the nonlinear Schrodinger equation, with anomalous dispersion and driven by a constant pump term. The pump provides a distributed gain, $g \approx$ 700dB/km, that is nonsaturating of infinite bandwidth and uniformly distributed along the fibre. Successive cavity transits then lead to the (soliton) pulse experiencing a periodic energy profile, figure.1a, where the net gain is unity.

In a fibre based system with such large periodic variations one might expect the evolving soliton structure to be severely disturbed so that stable propagation is precluded. Our studies, however, reveal that when the single solition period is much greater than the amplification period, $Z_o >> Z_a$ a stable region exists. Here dispersionless single soliton–like behaviour can be realised even though there is a severe variation in the pulse intensity ! In this limit amplification takes place nonadiabatically, with the resultant soliton then understood in terms of averaged quantities. An example illustrating the fast nonadiabatic component as a stable solution is shown by figure 2a along with the almost constant pulse duration figure 2b. Here an initial pulse of the form A.sech(t/τ) was used, where A is not the usual soliton amplitude. This behaviour is quite uncharacteristic of that commonly associated with solitons propagating in the presence of gain [3] and will be discussed in detail.

Away from the stable region the soliton behaviour becomes progressively more complicated. Our studies have revealed two further regions exist. For the case where $Z_o > Z_a$ the evolution is dominated by pulse compression, energy shedding and the generation of a dispersive wave. Finally in the limit $Z_o \approx Z_a$, substantial reshaping of the initial soliton takes place which involves the symmetrical division of the initial structure into a number of less energetic components. An example of this is shown by figure.2c. The mechanism responsible for these features will be remarked on briefly.

[1] K.Smith, J.R.Armitage, R.Wyatt, N.J.Doran & S.M.J.Kelly, Electron. Lett., 1990 26 1149

[2] J.D.Kafka, T.Baer & D.W.Hall, Opt. Lett., 1989, 14 1269.

[3] K.J.Blow, N.J.Doran & D.Wood, JOSA B (1988) 5 381

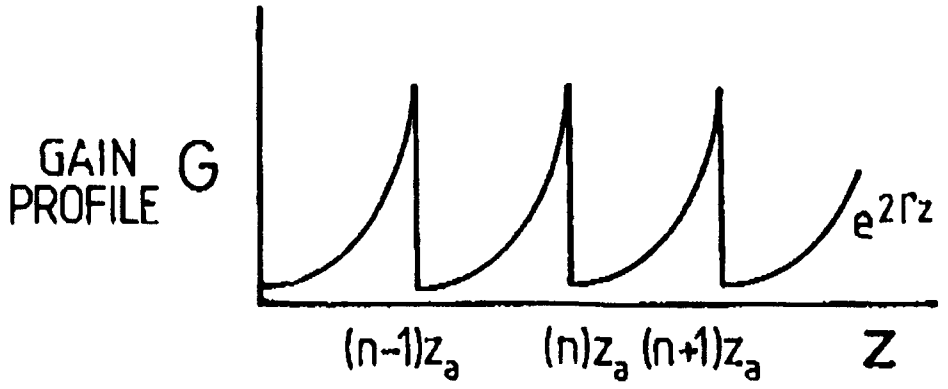

Figure.1a Periodic energy profile experienced by a soliton. The single pass gain $G = e^{2\Gamma z_a}$ (≈ 14dB) hence Γ = 700dB/km when distributed over a fibre length z_a = 0.02km.

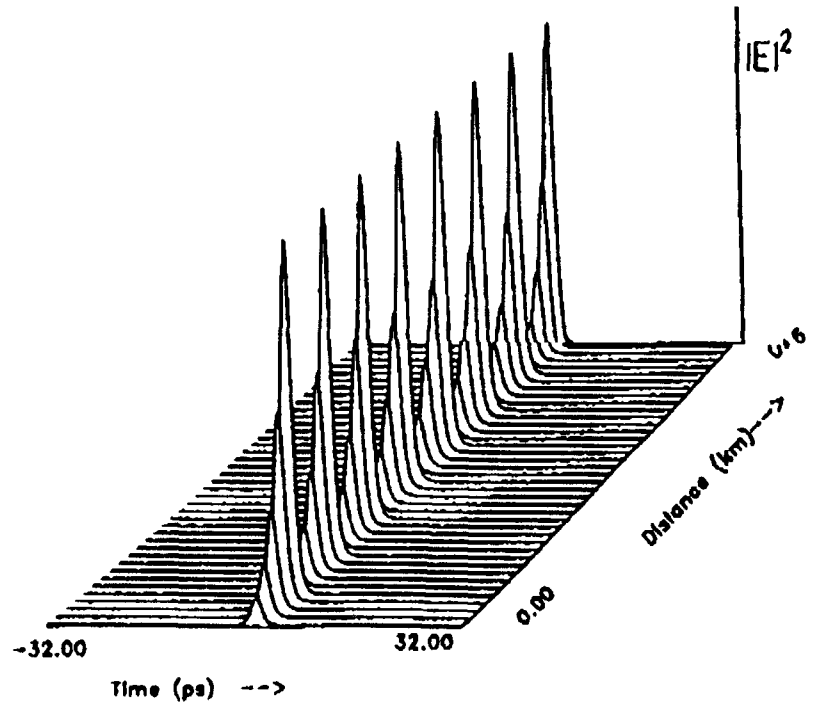

Figure.2a Computed single soliton intensity profile plotted at increments of $z_a/4$ illustrating the fast nonadiabatic component as a stable solution.

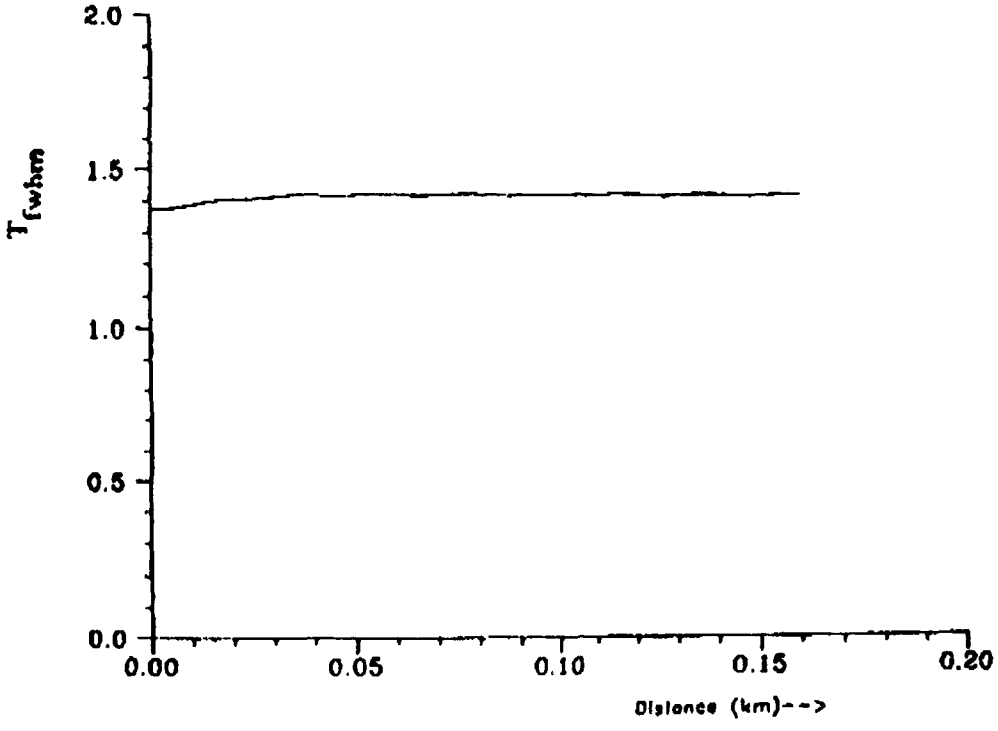

Figure.2b Behaviour of the pulse duration, $T_{fwhm} = 2\log_e(1+\sqrt{2}).\tau$, computed from the evolution in figure.2a. Note the almost constant trend indicating dispersionless propagation.

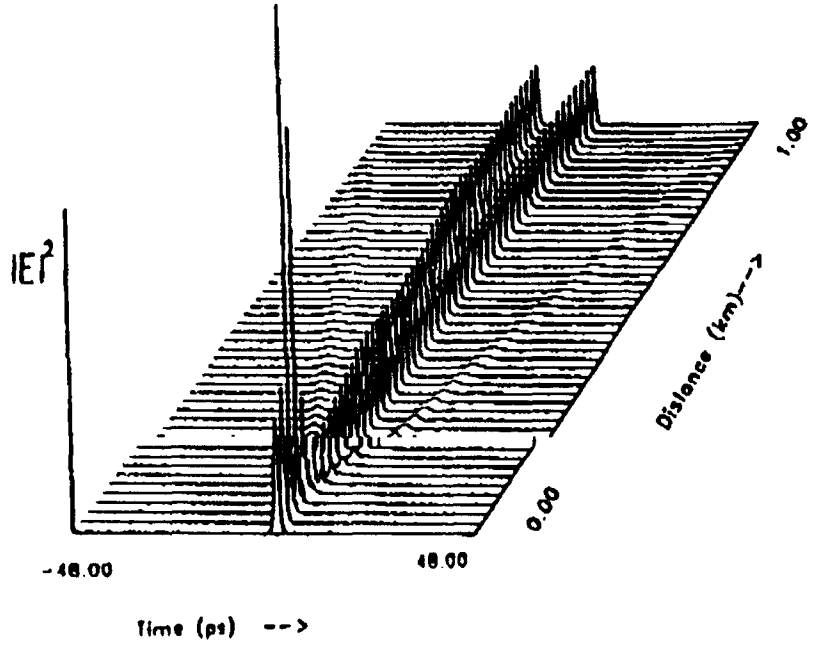

Figure.2c Soliton evolution displaying initial compression, followed substantial reshaping and ultimate breakup. Profiles plotted at increments of the amplification period, z_a.

Quantum Propagation in Optical Fibres

K.J.Blow†, *R.Loudon** and *S.J.D.Phoenix*†

†British Telecom Research Laboratories, Martlesham Heath

Ipswich, IP5 7RE, England

*University of Essex, Colchester, England

Tel: +44 473 643417

Quantum theory, as normally formulated, describes systems enclosed in an artificial box through its time evolution. In some systems, such as a laser, the box may be a physical element such as a cavity. In optical fibre communications the situation is somewhat different. The optical field is continuously generated by a source such as a laser. Once generated the field propagates along an optical fibre and is detected in some form of receiver at the far end. Quantum theory, with its reliance on Hamiltonian systems necessarily conserves the total energy in the system whereas fibre communication is better described as a balance between sources and sinks. Under these circumstances it may be more appropriate to describe the spatial evolution of the field [1], [2], [3]. In this paper we describe an approach to the study of quantum propagation in optical fibres. The discussion will be based on the description of single mode weakly guiding fibres so that a one dimensional scalar wave equation can be used to describe the electric field.

Without the quantization box the modes of the system are continuous in both the time and frequency domain which enables us to work directly with continuum operators rather than with their discrete counterparts. The positive frequency part of the

electric field is written [1], for a narrowband excitation,

$$\hat{E}^{+} = i\left(\frac{\hbar\omega}{4\pi\varepsilon_0 cA}\right)^{\frac{1}{2}} \int d\omega\, \hat{a}(\omega)\exp\{-i\omega(t - \frac{z}{c})\}, \tag{1}$$

where A is the mode area and ω_o is the central frequency of the wavepacket. The normally ordered Poynting vector is defined as

$$\hat{S}(z,t) = \frac{1}{\mu_0}\left\{\hat{E}^{-}(z,t)\hat{B}^{+}(z,t) + \hat{B}^{-}(z,t)\hat{E}^{+}(z,t)\right\} \tag{2}$$

and is conveniently expressed in terms of the Fourier transform $\hat{a}(t)$ of the destruction operator $\hat{a}(\omega)$

$$A\hat{S}(z,t) = \hbar\omega_0 \hat{a}^{\dagger}(t - \frac{z}{c})\hat{a}(t - \frac{z}{c}). \tag{3}$$

This has a particularly simple physical interpretation as the energy per photon multiplied by an operator representing the flux of photons per unit time.

In the study of χ_3 processes it will be necessary to evaluate operators of the form $\exp(\hat{O})$, where

$$\hat{O} = \int dt\, g(t)\hat{a}^{\dagger}(t)\hat{a}(t). \tag{4}$$

Using the noncontinuous operator representation we have proved the following continuous version of a single mode theorem [4],

$$\exp\{\int dt\, g(t)\hat{a}^{\dagger}(t)\hat{a}(t)\} = :\exp\left\{\int dt\, [e^{g(t)} - 1]\hat{a}^{\dagger}(t)\hat{a}(t)\right\}: \tag{5}$$

where the colons denote normal ordering.

The problem of quantum self phase modulation is exactly of the form of equation 4 where g(t) is related to the response function of the silica fibre [5], [6]. Using the theorem in equation 5 we have been able to calculate the squeezing spectrum of an arbitrary pulse propagating in a lossless fibre. The optimum squeezed noise (normalised to the shot noise) is shown as a function of distance in the figure. At small distances squeezing is observed but at large distances the pulse displays excess phase noise. The single mode theory of self phase modulation [7], predicts the formation of a number state at large powers and this is consistent with our observation since a number state can have no quadrature squeezing. In the figure we show the predicted squeezing for two different values of the medium response time. The onset of the enhanced quadrature noise is strongly dependent on this response time. This effect could be one additional source of noise in recent experimental measurments of squeezing in solitons [8].

REFERENCES

1. K.J.Blow, R.Loudon, S.J.D.Phoenix and T.J.Shepherd, Continuum Fields in Quantum Optics, Phys Rev A 42 4102-14 (1990)

2. N.Imoto, Interchanging Time and Space in Quantum Mechanics for Analyzing Spatial Evolution of a Propagating Electromagnetic Beam, Proc. 3rd Int. Symp. Foundations of Quantum Mechanics, 533-541, Tokyo (1989)

3. I.Abram, Quantum Theory of Light Propagation: Linear Medium, Phys Rev A 35 4661-72 (1987)

4. W.H.Louisell, Quantum Statistical Properties of Radiation (Wiley, New York 1973)

5. R.H.Stolen, J.P.Gordon, W.J.Tomlinson and H.A.Haus, Raman Response Function of Silica-Core Fibres, J Opt Soc Am B 6 1159-66 (1989)

6. K.J. Blow and D. Wood, Theoretical Description of Transient Stimulated Raman Scattering in Optical Fibres, IEEE J Quantum Electronics 25 2665-73 (1989)

7. M.Kitagawa and Y.Yamamoto, Number-Phase Minimum-uncertainty State with Reduced Number Uncertainty in a Kerr Nonlinear Interferometer, Phys Rev A 34 3974-88 (1986)

8. M.Rosenbluh and R.M.Shelby, Squeezed Optical Solitons, Phys Rev Lett 66 153-6 (1991)

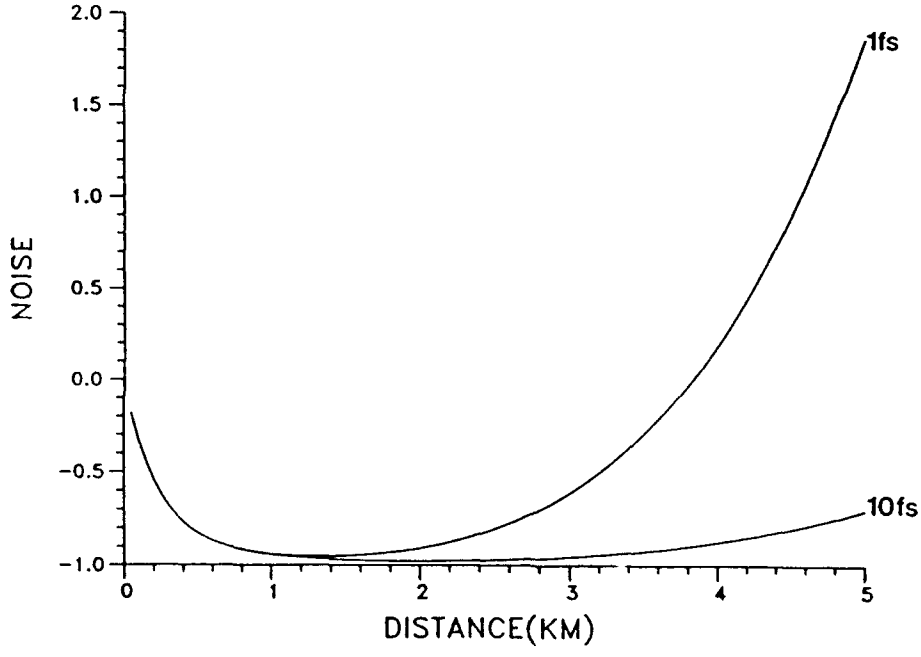

Monday, September 2, 1991

Nonlinear Optical Polymers

MD 4:00pm–5:30pm
Palmerston Room

George I. Stegeman, *Presider*
University of Central Florida, USA

Nonlinear optical polymers: Waveguide devices based on second order effects

Winfried H.G.Horsthuis, Gustaaf R.Möhlmann and Hans W.Mertens
AKZO Research Laboratories Arnhem,
Corporate Research, Applied Physics Department
P.O.Box 9300, 6800 SB Arnhem, the Netherlands

Introduction

In the past few years, organic materials have gained much interest for application in nonlinear optical devices. The initial scepsis towards these new materials has decreased, since interesting results have been obtained using these materials. The advantages of such materials, expected by early workers in the field, have partially been proven. High electro-optic coefficients have been reported, and reasonably well performing integrated optic devices have been realized [1]. Some other items, such as long term stability, mode matching and low cost production, still need further investigations and development. Nonlinear optic organic materials can be divided in several classes: organic (single) crystals, Langmuir-Blodgett films and several polymeric systems (solid-solutions, main-chain polymers, sidechain polymers). Until now, side-chain polymers appear to be the most promising class, mainly because of their attractive processing characteristics and the flexibility in molecular design.

Polymeric waveguides

The realization of waveguides using polymers is rather straightforward. Polymers are easily deposited on a substrate by spinning or dipping from a suitable solution, and subsequent curing [1]. Slab waveguides are formed either as a single layer on top of a transparent substrate, or as an optical multilayer structure on a suitable substrate, e.g. glass, silicon, gallium-arsenide etc. Such slabs provide one-dimensional confinement of the propagating light, provided the refractive index of the core layer is higher than those of the cladding layers. To obtain two-dimensional confinement, waveguiding channels are required, which can be realized by several techniques. Ridge and inverted ridge waveguides [2] can be formed by etching, analogous to the case of inorganic structures. However, polymers offer more possibilities using specific properties of the material. Photoinduced effects [3,4] are of particular interest since these offer simple means to realize channel structures. A very elegant way of channel formation is given by the photo-bleaching technique, which only requires the irradiation with suitable light to obtain a refractive index change. This technique can be used if the active groups in the polymer consist of substituted stilbenes, which exhibit a conformational change upon irradiation in the charge transfer band (TRANS to CIS isomerization) [4]. Channels realized by this method have smooth sidewalls, thereby minimizing the channel losses, and show no surface topography, which eases further processing on the structure.

Poling

Polymers incorporating nonlinear optical (nlo) moieties exhibit no spontaneous nlo effect, since the active groups will be oriented at random. To induce a bulk nlo effect, an alignment process is required. The alignment of the nlo active groups, which have a permanent dipole moment, can be induced by electric field poling. The polymeric layer is heated close to its glass transition point, where the molecular fragments have a high mobility. At this elevated temperature the layer is placed in a strong electric field, causing the dipoles to be oriented along the field lines. Finally, with remaining electric field, the film is cooled to ambient, freezing in the orientation of the active groups.

Several methods have been used to pole polymeric nlo films. Usually, thin electrodes are deposited on the substrate and on top of the polymeric film. The (DC) poling field is generated by a voltage difference between these two electrodes. Alternatively, a corona discharge can be utilized to charge the polymer surface. Recently, pulsed poling fields have also been reported [3] to induce locally inverted orientation of the active groups.

The poling efficiency and parameter dependency can be evaluated by several measurement techniques, either in transmission through thin films [5] or in waveguide structures [6].

To obtain high electro-optic coefficients in poled polymeric films, high electric fields are required. Fabrication of polymeric multilayers should therefore always be performed under clean room conditions, since contaminations will lead to electrical breakdown during poling. Field strengths up to 200 V/μm have been reached on relatively large surfaces (5 cm dia.). In such poled layers, electro-optic coefficients as high as 34 pm/V have been measured in the near infrared (off resonance condition).

Design of polymeric structures

Due to the specific properties of polymers, a flexible design of waveguide devices is possible. By tailoring the refractive indices of the different layers, the dimensions of the waveguide can be chosen: a low contrast ($\Delta n < 0.5\%$) permits relatively large single mode channels, a high contrast implies small size channels. Channel dimensions in the order of 6 to 8 μm (width and height) will increase the coupling efficiency with single mode optical fibres, however, a high confinement factor enables small radii of curvature for bent waveguides, resulting in a more compact design. A combination of both systems on a single substrate might even be feasible, due to the flexibility of processing techniques using this type of polymers.

Well known computational tools to evaluate waveguide and device designs, such as the Beam Propagation Method, can be used for polymeric systems.

Polymeric waveguide device fabrication

The realization of polymeric integrated optic devices has been demonstrated. Waveguides are made by channel formation in a polymeric sandwich, as described above. To obtain a nlo-active device, a poling step is required. At this stage, two

alternatives are available: the entire area of the polymer multilayer can be poled [1], or only a small portion of the polymer area is poled [3]. A disadvantage of the second option is that it will induce an abrupt change of the refractive index in the waveguide at the edge of the poled area, since in general poling gives rise to refractive index changes and birefringence [6]. This can result in scattering losses at these boundaries. The first method is, therefore, preferred.

After poling, a deposited top electrode layer needs to be patterned to form the driving electrodes. Finally, end-facets are prepared either by cleaving the substrate with the multilayer structure on it, or by subsequent sawing, grinding and polishing.

Device examples

Several groups have reported on polymeric nlo devices. These include phase and intensity modulators [1,2], spatial switches [1], railtaps [7] and frequency doublers [8,9]. Typical performances of intensity modulators (Mach-Zehnder interferometers) are $V\pi$ values down to 4.5 V [1], with extinction ratios better than -15 dB. High speed modulation up to 20 GHz (instrumentation limited) has been demonstrated in a polymeric Mach-Zehnder interferometer, too [10].
Directional coupler switches have been demonstrated, with switching voltages of the order of 8V, and an extinction ratio better than -15 dB [1].

Stability of polymeric devices

A most important issue is the long term stability of polymeric devices. Since the nlo effect is induced by the poling process at a certain temperature, the orientation of the active groups can also be destroyed at these temperatures. The absolute value of the glass transition temperature (Tg) therefore determines the maximum allowable temperature of the device under operation or storage. Usually, the device should be kept at a temperature well below the Tg. Typical Tg values of the present generation nlo polymers are between 70 and 160°C. At the Akzo Research Laboratories, the thermal relaxation phenomena of a typical nlo polymer (based on di-methyl-amino-nitro-stilbene) have been studied thoroughly [5]. The polar order relaxation rates have been measured at several temperatures. It can be concluded that for this polymer, with a Tg of 142°C, the long term use is expected to be limited to 60°C. Above this temperature, there is a noticeable decay of the electro-optic effect with time.

In order to improve the stability, different approaches can be chosen. Polymers with a high Tg will be useful at higher temperatures, for instance polyimides can have a Tg above 300°C, resulting in devices stable to at least 200°C.
A second option is the use of crosslinked polymers, in which the relaxation of active groups is limited by the network properties. Several groups have reported on progress in thermal stability using crosslinked nlo polymers [11,12].

References

[1] G.R.Möhlmann, W.H.G.Horsthuis, A.McDonach, M.J.Copeland, C.Duchet, P.Fabre, M.B.J.Diemeer, E.S.Trommel, F.M.M.Suyten, E.van Tomme, P.Baquero and P.van Daele, "Optically nonlinear polymeric switches and modulators", Proc.SPIE, **1337**, 1990, pp 215-225.

[2] D.R.Haas and Hong-Tai Man, "Polymeric electro-optic modulators", OSA Techn.Digest Series, **8**, 1991,p 133.

[3] P.R.Ashley and T.A.Tumolillo, "New poling techniques for electro-optic polymer devices", OSA Techn.Digest Series, **8**, 1991, p 87.

[4] M.B.J.Diemeer, F.M.M.Suyten, E.S.Trommel, A.McDonach, J.M.Copeland, L.W.Jenneskens, W.H.G.Horsthuis, "Photoinduced channel waveguide formation in nonlinear optical polymers", Electr.Lett., **26**, 1990, pp 379-380.

[5] C.P.J.M. Van der Vorst and C.J.M.van Weerdenburg, "Electro-optic measurements in poled polymer films between plane-parallel semitransparent metal electrodes", Proc.SPIE, **1337**, 1990, pp 246-257.

[6] W.H.G.Horsthuis and G.J.M.Krijnen, "A simple measuring method for electro-optic coefficients in poled polymer waveguides", Appl.Phys.Lett., **55**, 1989, pp 616-618.

[7] G.F.Lipscomb, R.S.Lytel, A.J.Ticknor, T.E.van Eck, S.L.Kwiatkowski and D.G.Girton, "Developments in organic electro-optic devices at Lockheed", Proc.SPIE, **1337**. 1990, pp 23-34.

[8] G.Khanarian and R.Norwood, "Efficient quasi phase matched second harmonic generation in a polymer waveguide", Proc.SPIE, **1337**, 1990, pp 44-52.

[9] G.L.J.A.Rikken, C.J.E.Seppen, S.Nijhuis and E.Staring, "Poled polymers for frequency doubling of diode lasers", Proc.SPIE, **1337**, 1990, pp 35-43.

[10] R.S.Lytel, "Applications of electro-optic polymers to integrated optics", Proc.SPIE, **1216**, 1990, pp 30-40.

[11] M.Reich, B.Reck, D.Y.Yoon, C.G.Willson, G.Bjorklund, "Novel second order nonlinear optical polymers via chemical crosslinking induced vitrification under electric field", J.Appl.Phys., **66**, 1989, pp 3241-3247.

[12] W.H.G.Horsthuis, P.M.van der Horst, G.R.Möhlmann, "Developments in high temperature stable nonlinera optical polymers", OSA Techn.Digest Series, **5**, 1990, p 23.

LARGE NONLINEAR PHASE SHIFTS IN A NITROBENZENE-CORED SINGLE-MODE FIBRE

Raman Kashyap, Neil Finlayson
BT Laboratories, Martlesham Heath, Ipswich IP5 7RE, UK.

SUMMARY

The availability of picosecond mode-locked pulses and low loss optical fibre has made it desirable to use the effects of self-induced phase-shifts for applications in all optical processing. There have been several successful demonstrations of all-optical switching in fused silica fibres in recent years. What is common amongst most of these devices is that they use long lengths of fibre, typically 25m to km, high optical powers or both. No demonstration of all optical switching in short lengths of optical fibre at relatively low powers has so far been demonstrated. This limitation is mainly due to the low nonlinearity of silica (3×10^{-20} m^2/W). Recently, 29cm long fibres made with new glasses have been reported which yield 17π nonlinear phaseshift with an input power of 1kW [1]. This paper reports on the observation of self-induced polarisation instabilities in 10cm lengths of nitrobenzene-filled silica-capillary single-mode waveguides. Large phase changes of at least 12π are reported at peak input powers of only 14W, with no saturation of the nonlinearity.

The optical fibre waveguide was manufactured using a 10cm long silica capillary with core and cladding diameters of approximately 1 4µm and 125µm respectively. It was filled with nitrobenzene via capillary action and sealed in using silica windows. The waveguide was single mode at 1064nm. Such devices have lasted several years and been used over many months without deterioration, or significant loss of the nitrobenzene. Fig. 1 shows the experimental layout. A Quantronix 117 mode-locked Nd:YAG laser, operating at 1064nm generating 200ps pulses at a repetition rate of 76 MHz was used in the experiments. A $\lambda/2$ plate and a polariser were used to control the input power launched into the capillary waveguide. A motorised $\lambda/2$ plate at the input was used to control the azimuth angle of the input polarisation. The light at the output end of the fibre was split into horizontal (H) and vertical (V) polarisation (relative to the optical table) and focussed onto two fast (< 90 ps rise time) photodiodes. It should be noted that the fast and slow fibre axes were oriented at an arbitrary angle α with respect to the table, so that the H and V polarisations were not necessarily the optimum polarisations to investigate the instabilities. The output was displayed on a fast sampling oscilloscope and also coupled to a boxcar averager for quantitative measurements.

Fig. 2a shows a series of transmittance curves at the H-port photodiode as a function of the input polarisation, with increasing input powers. For the V-port there is a complementary set of curves which is not shown. The lowest curve is for a peak power of 0.875 W. The output power has a

$\sin^2\theta$ dependence on the input azimuth angle θ. With increasing input power, the transmittance changes rapidly over certain angles. This feature is characteristic of a fast axis polarisation instability. The antisymmetric dependence of the output power on the azimuth angle is due to the angular misalignment of the fibre and analyser axes.

The theoretical response has been modelled using coupled mode-theory and is shown in Fig. 2b. Two free parameters are used to fit theory and experiment, namely the angle α and the ratio ρ of the fibre length to the polarisation beatlength. For this simulation the ratio was assumed to be 0.9 and α was found empirically to be 32^o with respect to the H-polarisation. There is good qualitative agreement between the simulation and the experimental results.

Fig. 3a shows the experimental transmittance of V- and H- polarisations as a function of the input power for an input polarisation azimuth angle of 60^o to the H-polarisation. This figure is equivalent to taking a cross-section of the response shown in Fig. 2 at approximately 90^o. Complete switching was not observed since the analyser was not set at the optimum position. The simulated response is shown in Fig. 3b. Good qualitative agreement is again observed. Each cycle in the transmittance curve corresponds to a *differential* nonlinear phase shift of 2π between the two eigenmodes. In addition, the eigenmodes experience a *common* phase shift. Consequently the most conservative estimate of the total phase shift is 12π. This number is in reasonable agreement with the calculated value of 13π based on the published n_2 of nitrobenzene [2]. We have calculated the figure of merit

$$w = \frac{I\, n_2}{\alpha\lambda} \qquad (1)$$

to be 60 at 1064nm.

We have reported here the first demonstration of single-mode nitrobenzene cored fibre waveguides. The experiments show that such fibres are excellent candidates for all-optical switching.

REFERENCES

1. M.A. Newhouse, D.L. Weidman and D.W. Hall, Opt. Lett., **15**, 1185, 1990.

2. P.P. Ho and R.R. Alfano, Phys. Rev. A **20**, 2170, 1979.

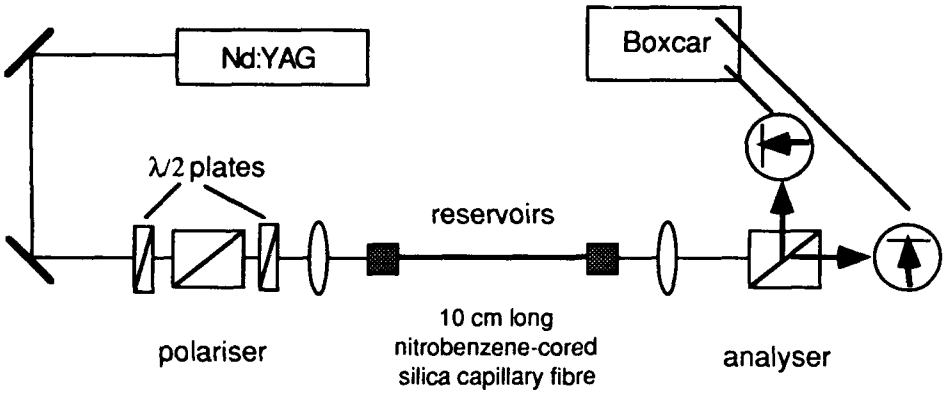

Fig. 1 Experimental setup.

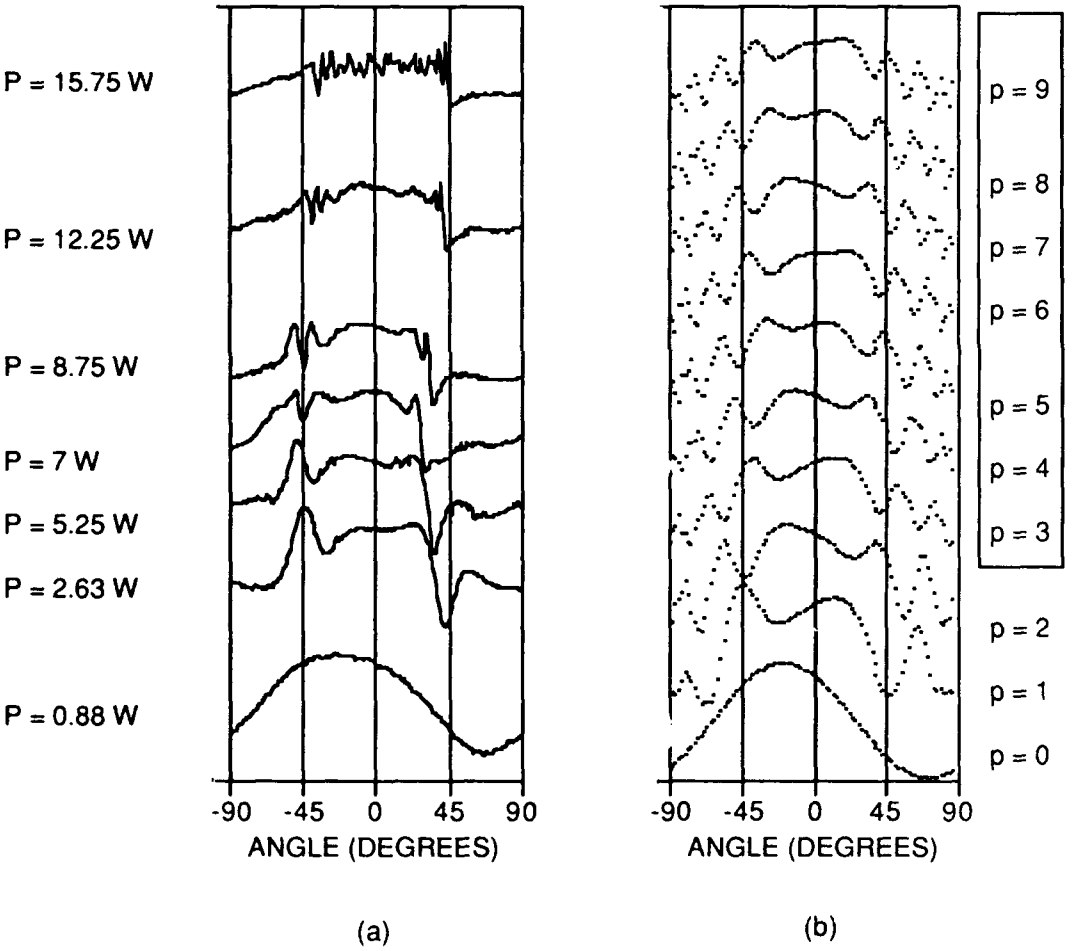

Fig. 2 Transmittance of the V polarisation as a function of input azimuth angle for increasing launched powers (a) experiment (b) theory.

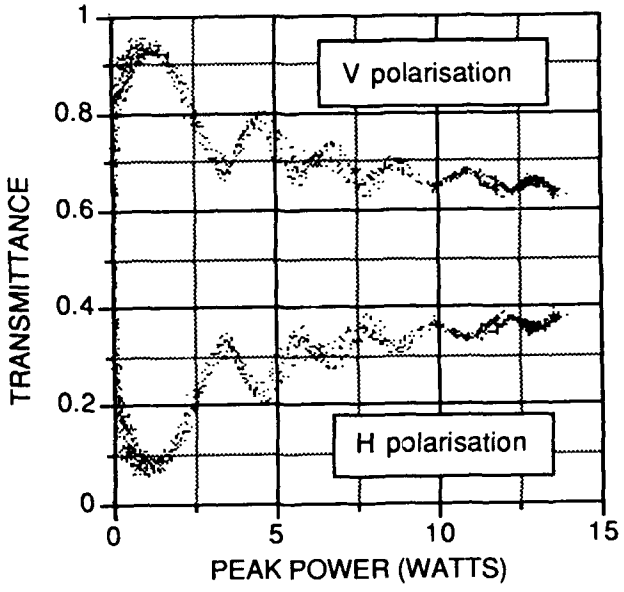

(a)

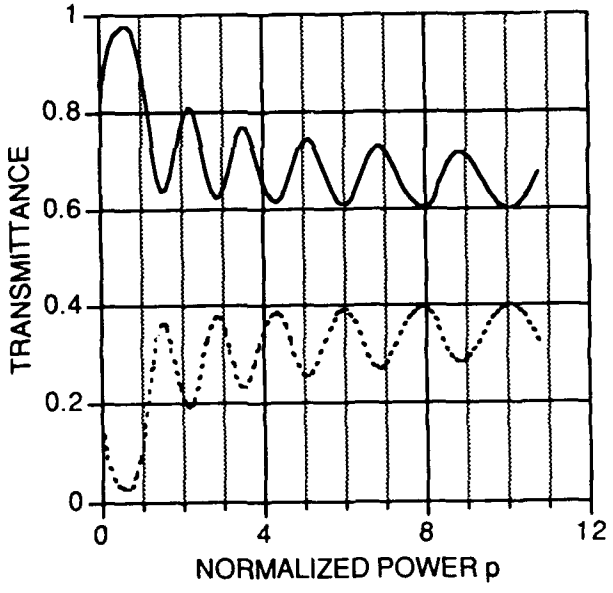

(b)

Fig 3 Transmittance in V and H polarisations as a function of peak power. (a) Experimental response (b) Theoretical response. Solid line - V polarisation. Dashed line - H polarisation.

Electrooptic Waveguide Grating Using New Nonlinear-Optic Polymer p-NAn-PVA

S. Ura, R. Ohyama*, T. Suhara and H. Nishihara
Dept. of Electron., Faculty of Engineering, Osaka University
Yamada-oka 2-1, Suita, Osaka 565, Japan
Tel. (06) 877-5111 ext.(5007)
* On sabbatical leave from Ube Industries, LTD.

1. Introduction

A new polymer p-NAn-PVA illustrated in Fig. 1 was developed by N. Ogata et al.[1] for implementing second-order nonlinear-optic (NLO) devices. p-NA (p-Nitroaniline) is introduced as side-chain to PVA (Polyvinyl Alcohol) main-chain via acetal-linkage, and second-order NLO effects emerge by electric-field induced side-chain alignment (poling). This polymer has some attractive features besides fabrication easiness. Large NLO susceptibility is expected since p-NA has large polarizability and is highly doped (x=0.82), and the relaxation is small in comparison with dispersive type NLO polymers because of the high glass-transition-temperature resulting from the acetal-linkage. In this paper, we report the fabrication and characterization of p-NAn-PVA waveguide and an application to electrooptic (EO) grating switch. The EO effects originate from second-order NLO susceptibility, and EO devices are one of important applications of such NLO polymer waveguides as well as wavelength converters.

2. Thin film waveguide

[Fabrication] DMF (Dimethylformamide) solution of p-NAn-PVA (6.6 wt%) was spin-coated on various substrates in the air of 80 ℃ and desolved by 2 step heating (110 ℃/30 min followed by 160 ℃/60 min) in order to obtain smooth and uniform thin film. Glass-transition-temperature T_g of the fabricated film was measured by differential calorimetry to be 115 ℃. It was confirmed from spectral transmittance that the absorption edge was 0.48 μm and there is no absorption at 0.83 μm. We can then use the thin film as waveguiding layer for a 0.83 μm laser diode (LD).

[Refractive index] A single-mode waveguide of 1.0 μm thick p-NAn-PVA guiding layer on a 1.0 mm thick Pyrex glass substrate was prepared. Some samples were poled by a corona-discharge method. The sample was set on a planar ground electrode and held at 140 ℃. High voltage of +5 kV was applied to a needle electrode set at 13 mm above the sample for 15 min and cut after sample cool-

ing. The poled film had birefringence with indices of 1.576 and 1.690 for beam-polarizations parallel and perpendicular to the film, respectively, while the index of unpoled film was 1.617.

[Propagation loss] Propagation losses for as-prepared (unpoled) and poled samples were 2.4 dB/cm and more than 12 dB/cm, respectively. We think that the loss increase by the poling process is due to surface roughness induced by corona-discharge and the loss can be reduced by improving the poling condition and/or by topping a cover layer.

[Electrooptic coefficient] Dependence of EO coefficient r_{33} on the poling electric field was measured. Subscript 3 represents the direction perpendicular to the film surface. In order to estimate the poling field quantitatively, we prepared samples, in which the NLO polymer was directly sandwiched between two planar electrodes, and measured the r_{33} by the reflection technique[2]. The r_{33} increases linearly against poling field. The maximum value was obtained to be 14 pm/V when the field was 120 V/μm, that is half of $LiNbO_3$ r_{33}.

[Relaxation] We monitored the relaxation of side-chain alignment by measuring the r_{33} reduction of the fabricated samples after leaving them at different temperatures. The dependences of the normalized r_{33} on time after poling are shown in Fig. . Although the r_{33} shows rapid fall for the sample held in the air of 100 °C (near the T_g=115 °C), the r_{33} reduction of the 70 °C sample saturates after initial 20 % fall. The r_{33} of the sample left at room temperature maintains more than 90 % of the initial value even after 100 hours.

3. Electrooptic grating switch

[Configuration] We fabricated a waveguide EO switch as an application of the p-NAn-PVA thin film and estimated the r_{33} of the film poled by the corona-discharge method. The EO switch was constructed by integrating interdigital switching electrodes and two linear and uniform grating couplers on a UV-adhesive/p-NAn-PVA/SiN/SiO_2 waveguide as shown in Fig. 3. A laser beam was coupled by a grating coupler to TM_0 mode in the waveguide, diffracted by an EO Bragg grating induced under the interdigital electrodes and coupled out by another grating coupler into the air. The EO grating efficiency can be controlled by the applied voltage, and the output beam switching is possible.

[Fabrication] The corrugation of the grating couplers was formed by electron-beam lithography and reactive ion etching of the 0.15 μm thick SiN layer (refractive index n_g=1.8) deposited by plasma

enhanced CVD on the SiO_2 optical buffer layer (n_b=1.46, thickness T_b=1.8 μm) RF-sputtered on a Cr-coated glass substrate. The p-NAn-PVA film of 1.0 μm thickness was coated on it and poled by the corona-discharge method with 140 °C and 5 kV. Then the InO_2 interdigital electrodes on a glass substrate, which were patterned by photolithography and wet-etching, were aligned and fixed by a UV adhesive (n_c=1.49, T_c=2 μm) on the p-NAn-PVA film. Specifications of the fabricated device are summarized in Table I. Switching voltage was applied to one of the interdigital electrodes against to the other connected with Cr counter electrode.

[Results] The output beams were monitored when a switching voltage of rectangular wave train was applied. Examples of the intensity variation of the diffracted beam are shown in Fig. 4. Intensities of both states were constant in the measurement range of switching frequency (from 10 Hz to 20 kHz). However, in the case of high switching voltage with low frequency, we observed a DC drift in diffraction efficiency. The efficiency increased as time advanced regardless of the polarity of the applied voltage, and the offset could be brought back to zero by applying slight reverse voltage. We think a main cause of the drift is a refractive index variation due to the electric-field induced side-chain alignment. The r_{33} was roughly estimated to be 9 pm/V, which consists with the results of the previous section.

4. Conclusion

Waveguides of a new polymer p-NAn-PVA were fabricated and an EO grating switch was demonstrated as an application. Guiding loss of a single-mode waveguide was less than 3 dB/cm. The obtained maximum r_{33} was 14 pm/V, of which relaxation was less than 10 % in 100 h after poling. Diffraction efficiency of the EO grating is controllable by the applied voltage and the switching is possible. The offset due to a DC drift, which was observed in the case of high voltage with low frequency, could be brought to zero by applying slight reverse voltage. The r_{33} and the SHG coefficient d_{33} are closely related, so that the results obtained for the r_{33} supports similar features for the d_{33} and may be useful in constructing SHG devices with p-NAn-PVA film.

[Acknowledgment] We would like to thank Prof. N. Ogata in Sophia Univ. and Mr. Yokoh in Ube Industries, LTD. for their supports in material discussion and supplying p-NAn-PVA solution.

[References]

1) N.Ogata, Y.Yokoh; Polymer Preprints Japan,vol.39,p.3468(1990).
2) C.C.Teng, H.T.Man; Appl.Phys.Lett.,vol.56,p.1734(1990).

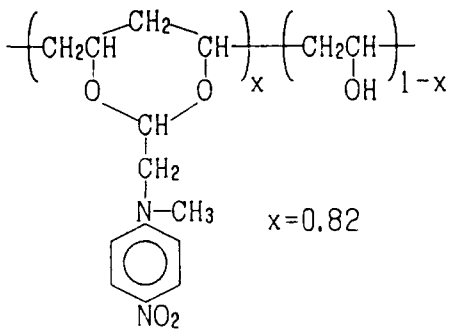

Fig. 1 Schematic of p-NAn-PVA.

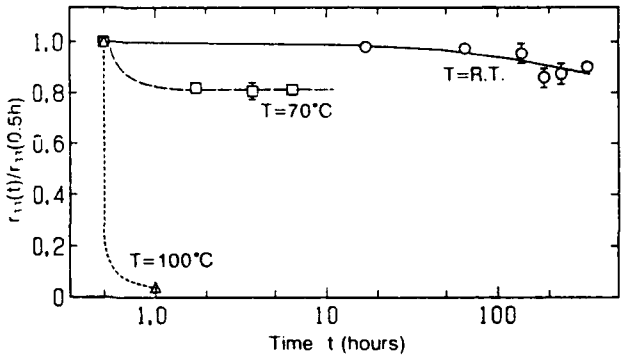

Fig. 2 Relaxation of EO coefficient.

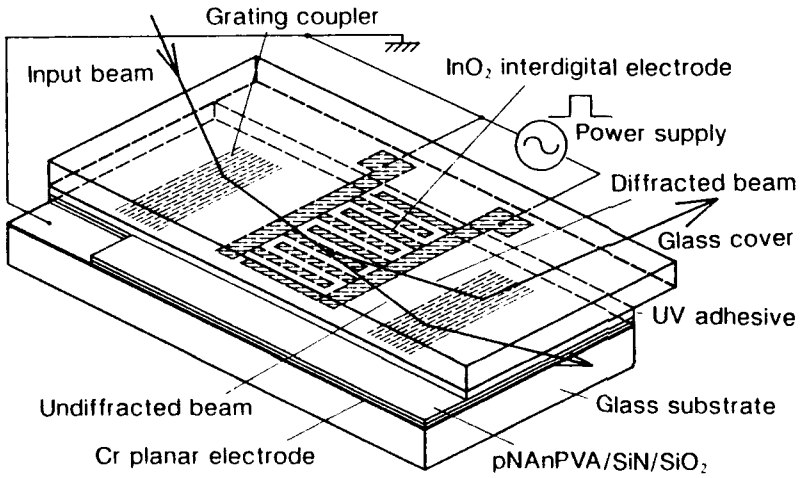

Fig. 3 Schematic of waveguide EO switching device.

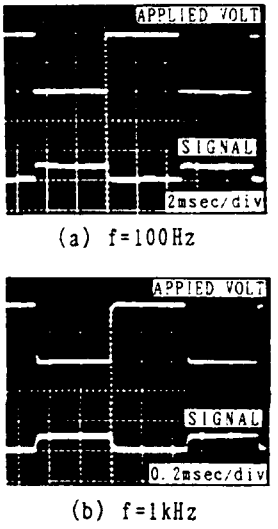

Fig. 4 Intensity of diffracted beam.

Table I Specifications of the fabricated EO switching device

Light source	Laser diode	Wavelength	λ=0.825	[μm]
Waveguide	UV-adhesive/pNAnPVA/SiN/SiO_2			
		Mode index	N=1.671	(TM_0)
Grating couplers	SiN layer corrugation	Aperture	0.5 x 2.0	[mm^2]
		Period	Λ_c=0.89	[μm]
		Output angle	θ=48	[Deg.]
Interdigital electrode	InO_2 patterning	Aperture	D=2.0	[mm]
		Coupling length	L=1.0	[mm]
		Period	Λ_e=20.0	[μm]
		Line width	W=4.0	[μm]
	Diffraction	Regime parameter	$Q=2\pi\lambda L/N\Lambda_e^2$=7.8	
		Angle	$2\theta_{IB}$=1.41	[Deg.]

New polymers for nonlinear optics

Manal u Kishimoto, Dechun Zou and Iwao Seo

Advanced Materials Laboratory,
Mitsubishi Petrochemical Co. Ltd.,
8-3-1 Chuo, Amimachi, Inashikigun, Ibaraki 300-03, Japan
[Tel. 0298-87-1022]

Summary

Poled polymer films with nonlinear optical (NLO) chromophores doped or covalently attached to the polymer chain have been the subject of recent study[1-3]. These materials have potential as electro-optic switching/modulator and second harmonic generator(SHG)[4,5]. Their usefulness is determined by their temporal stability and other physical and mechanical properties. For NLO processes, such as SHG, it is essential to achieve noncentrosymmetric molecular assemblies. In addition the material must provide ease of processability.

The poled polar polymer, vinylidene cyanide (VDCN) and vinyl acetate (VAc) copolymer (P(VDCN/VAc)), has recently been recognized as having NLO properties[6], in addition to its piezoelectric, pyroelectric and ferroelectric properties[7,8]. In particular, P(VDCN/VAc) has strong piezoelectric, pyroelectric activities and exhibits ferroelectric-like dielectric behavior. These strong activities and the dielectric anomalies are considered to be due to the existence of large C≡N dipole moments in the molecule and to the oriented polar molecules in polymer films poled by a high DC field. Under poling at a high DC electric field, the VAc unit located

between two VDCN units would facilitate the rotation of main chains, which ultimately causes the dipole orientation of the cyano group.

Recently, from the practical viewpoint of transparency and processability, a dye-attached polymer, where the dye molecules are incorporated into the main chain, is thought to be a promising candidate for nonlinear optics[2,3]. We report here an approach in which nonlinear chromophores are covalently linked to a glassy, film-forming macromolecule to produce, after alignment in an electric field, a new class of single-component polymeric NLO materials. Vinylidene cyanide copolymers were chosen as backbone because of their excellent transparency, relatively high glass transition temperature,Tg, (to help stabilize chromophore alignment) and amenability to varying kinds/levels of functionalization and processing. The functionalization of vinylidene cyanide and p-hydroxy vinyl benzoate copolymer was carried out with the chromophores 4-nitro-4'-oxo biphenyl (BP) and 4-nitro-4'-oxo stilbene (ST). Molecular structures of the chromophore substituted copolymers are shown in Fig.1 .

The polymer product was characterized for its thermal properties by differential scanning calorimetry (DSC) , thermal gravimetric analysis (TGA), and for chromophore content by proton NMR and ultraviolet/visible (UV/VIS) spectroscopy. The chromophore content of purified P(VDCN/VBZ-BP) and P(VDCN/VBZ-ST) were 10 90 mole percent (determined by NMR). The Tg of the copolymers were measured using a DSC at a scanning rate of 10°C/min . The results are given in Fig.1 .

Thin films of these copolymers were obtained by spin-coating onto ITO-coated conductive glass substrates. Film thicknesses measured by ellipsometry were from 0.1–1 μm. Films were poled at corona onset in air (2 μA at 7 kV) by a sharp tungsten needle tip one centimeter above the film. Films were poled for 0.5 hr at the poling temperature (Tp), then the heater

was turned off, and the film rapidly cooled to room temperature with the poling field on. After reaching room temperature , the poling field was removed. The Tp was selected so that Tp $\geq$ Tg .

The second-order nonlinear optical coefficient d_{33} of the corona-poled films were measured by the Maker fringe method with quartz as a reference. The experimental set up used for SHG measurements was Q-switched Nd:YAG laser operating at 1.064μm. The dependence of d_{33} on poling temperature Tp Tg (measured after aged for a month at room temperature in the absence of an electric field) is shown in Fig.2. Fig.2 provides an indication of the very large SHG effects that can be achieved with these functionalized polymers. Particularly striking is the large d_{33} value for P(VDCN/VBZ-ST).

Reference

1. K.D.Singer, M.G.Kuzyk, W.R.Holland, J.E.Sohn, S.L.Lalama, R.B.Comizzoli, H.E.Katz and M.L.Schilling, *Appl. Phys. Lett.*, **53**, 1800(1988).

2. Y.Chen, M.Rahman, T.Takahashi, B.Mandel, J.Lee, J.Kumar and S.Tripathy, *Jpn. J. Appl. Phys.*, **30**, 672(1991).

3. M.Eich, B.Reck, D.Y.Yoon, C.G.Willson and G.C.Bjorklunk, *J. Appl. Phys.*, **66**, 3241(1989).

4. A.F.Garito and Singer, *Laser Focus*, **80**, 59(1982).

5. J. Zyss, *J. Mol. Electron*, **1**, 25(1985).

6. H.Sato, T.Yamamoto, I.Seo and H.Gamo, *Opt. Lett.*, **12**, 579(1987).

7. S.Tasaka, K.Miyashita, M.Yoshikawa, S.Miyata and M.Ko, *Ferroelectrics*, **57**, 267(1984).

8. T.T.Wang and Y.Takase, *J. Appl. Phys.*, **62**, 3466(1987).

Fig.1 Chemical structure of Vinylidene cyanide copolymers

	Structure of copolymers
P(VDCN/VAc) Tg = 180 °C	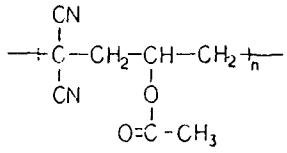
P(VDCN/VBZ-BP) Tg = 160 °C	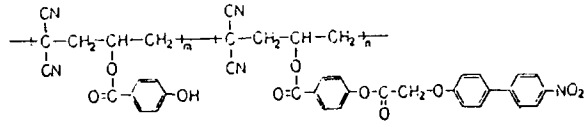
P(VDCN/VBZ-ST) Tg = 190 °C	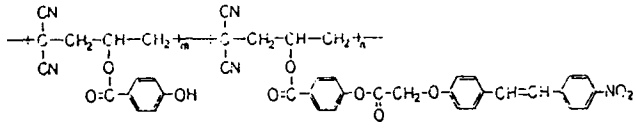

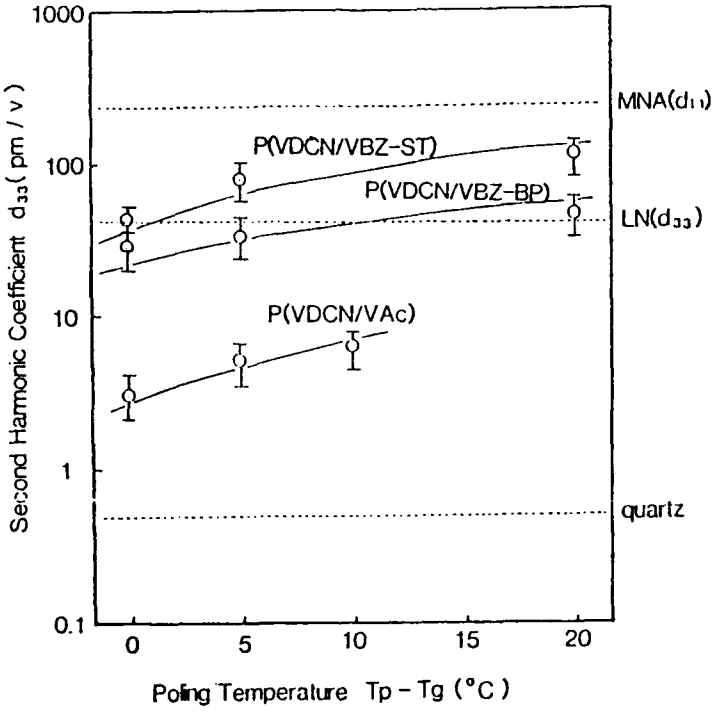

Fig.2 Poling temperature dependence of second harmonic coefficients (d_{33}) of VDCN family NLO polymers

Second harmonic generation from a polyurethane waveguide on a silver grating coupler

M. Kull *, J.-L. Coutaz, G. Vitrant, R. Reinisch

Laboratoire d'Electromagnetisme, Microondes et Optoélectronique (LEMO), ENSERG
BP 257, 38016 Grenoble, France. Tel. +33 76 87 69 76

and R. Meyrueix

Flamel Technologies, 33 ave. Dr. Levy, 69693 Venissieux Cedex, France

*Permanent address: Department of Physics II,
The Royal Institute of Technology, S-100 44 Stockholm, Sweden

1. Introduction

Organic waveguides are well suited for second harmonic (SH) generation [1]. We present here experimental results of SH generation from a polyurethane waveguide spin-coated on a silver grating coupler. As one of the waveguide boundaries is made from a metal it is possible to excite, in addition to guided modes, a surface plasmon (SP) at this boundary. We investigate the angular dependance of the SH generation from the polyurethane coated grating. The excitation of the electromagnetic resonances at the pump frequency lead to a large increase of the diffracted SH light intensity [2]. In order to study the wavelength dependence of the SH efficiency, we have employed two pump wavelengths - 1064 nm and 1318 nm. For the shorter wavelength pump, the SH falls within the absorption band of the polymer.

2. Experimental

The studied device is shown in fig. 1. A sinusoidal diffraction grating with a periodicity d = 1.67 μm and a groove depth of 80 nm is formed on a glass substrate by chemical etching. The grating has been covered with a 200 nm thick silver layer by evaporation. A 3 μm thick waveguiding film of a polyurethane with side chains (PUSC) is spin-coated on top of the grating. The film is poled by an applied field between the silver grating and an upper electrode. The polymer is red and absorbs light with wavelength up to 630 nm.
A mode-locked Nd:YAG laser is used as a pump source and the diffracted second harmonic light is detected by a photomultiplier tube (PMT). The sample and the detector are mounted on stepping motors for convenient scanning of the incident and the detected angles. By tuning the incident angle, θ, guided modes can be excited in the waveguide. It is also possible, in TM polarisation, to excite a surface plasmon which propagates at the boundary between the silver grating and the waveguide. The angular resolution is limited by the incident pump beam

divergence to 0.1°. A part of the incident fundamental beam is split off and frequency doubled in a thin KDP sample. This light is detected by a second PMT and serves as a reference, to compensate for intensity fluctuations of the laser. The signals from both PMTs are sent to a boxcar and finally a ratio of the two are taken by a computer. In the text below, the linear and nonlinear characteristics of the device are presented for two different fundamental wavelengths - 1064 nm and 1318 nm. For measurements of linear characteristics in the infrared the PMTs are replaced by InGaAs photodiodes.

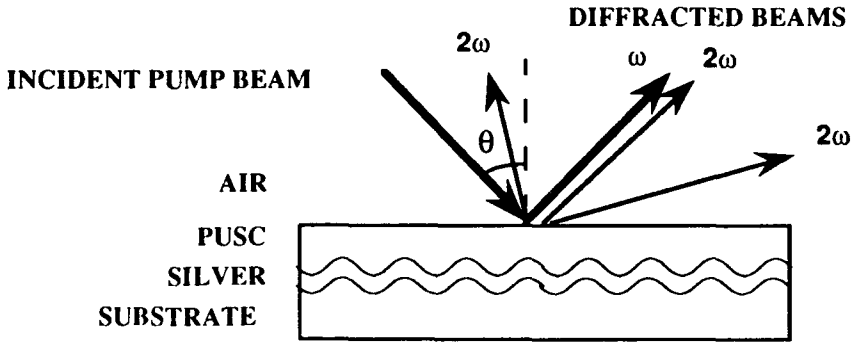

Figure 1. Schematic of the polymer waveguide coupled by a silver grating.

3. Results and discussion

At a pump wavelength of 1318 nm in TM polarization, three guided modes and the SP can be resonantly excited. This is shown in the upper trace of fig. 2, where the specularly reflected pump intensity as a function of the incident angle is plotted. The broad line at an incident angle of -53.3° is from light coupled to the SP propagating along the silver surface, whereas the three more narrow lines at -49.1°, -44.4° and -37.5° corresponds to light coupled to the guided modes TM_0, TM_1 and TM_2 respectively.

The modes and the plasmon are all coupled in the first order of diffraction of the grating, i.e. the conservation of the wavevector component which is parallell to the surface, k_{xi}, is given by: $k_{xi} + 2\pi/d = k_r$, where k_r is the wavevector of the excited resonance (guided modes or SP). The SH generated will be at λ = 659nm, which is just out of the absorption range of the polymer ($1/\alpha$ = 30 μm). Hence, it can also be coupled to resonances by the grating. Figure 3 shows four TM modes of the structure for this wavelength. For a fixed incident angle of -60° we observe 3 diffracted orders at 659 nm.

SH is produced as the sample is excited with modelocked pulse trains (400 ns FWHM, 6 ns between pulses and pulse duration of 120 ps) with a total energy of 0.2 mJ. The specularly reflected SH signal is shown in the lower trace of fig. 2 as a function of the pump incident angle. The largest efficiency is obtained as the SP is excited. The rather low efficiency as the TM_0 guided mode is excited is probably a combined effect of the relatively large beam divergence and a spatially

nonuniform waveguide. All SH is generated in TM polarization as is expected for a poled polymer with crystal symmetry $C_{\infty v}$ [1]. We have also confirmed that the measured SH intensity is proportional to the square of the fundamental intensity.

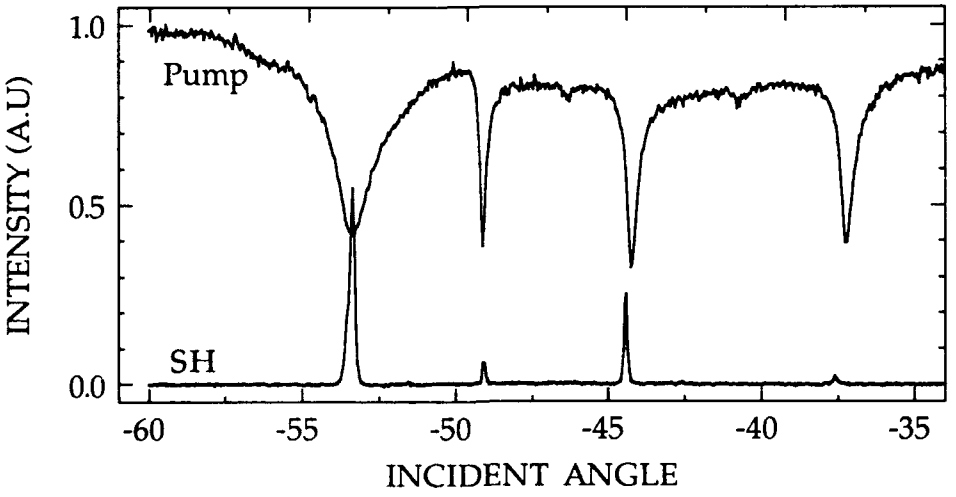

Figure 2. Specularly reflected fundamental intensity at 1318 nm (upper trace) and the corresponding specularly reflected second harmonic signal (lower trace). TM polarization.

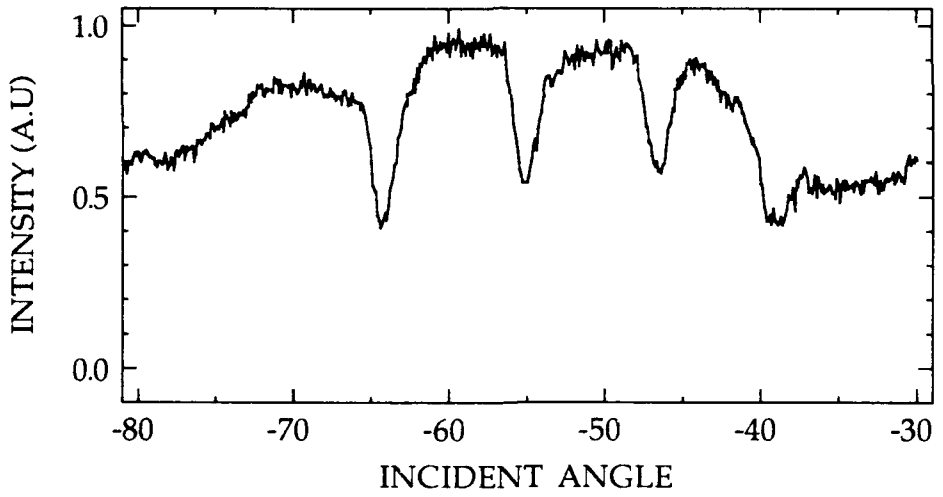

Figure 3. Specularly reflected intensity as the device is illuminated with light with a wavelength of 659 nm. TM polarization.

As we change the pump wavelength to 1064 nm, the situation changes dramatically. The waveguide now supports seven modes and also the SP can be excited. The SH light at 532 nm will now suffer from a large absorption in PUSC ($1/\alpha$ = 1 μm). Therefore green light which is incident on the device will be absorbed before it reaches the grating, and hence we do not observe any resonances at the SH wavelength. Neither can we observe linear diffraction of green light from the grating. This is in contrast to the observation of resonant coupling and linear diffraction of the SH wavelength as the pump is at 1318 nm. Still, as shown in fig. 4, we generate SH as the incident angle is scanned through

the pump field resonances. There is a stunning difference, as compared to the case of pumping with λ = 1318 nm. The specularly reflected SH signal now exhibits sharp *minima instead of maxima* as the pump is at resonance (marked by arrows in fig. 4). A possible explanation to this surprising result can be as follows:
Due to the large absorption at the SH wavelength, only the driven SH field contributes to the detected signal in specular reflection. Off resonance the incident pump beam propagates through the polymer and is specularly reflected at the silver grating and the SH light is produced by this beam. On the other hand, as pump light is coupled to a guided mode or a SP, the fundamental intensity shows a minimum in specular reflection. Therefore its contribution to the reflected SH light decreases and it can not contribute to the detected signal since the SH from the coupled resonance is not diffracted by the grating. Hence minima are observed in the SH reflected signal as the pump is resonantly excited. Numerical investigations are under way in order to support the observed phenomenon.

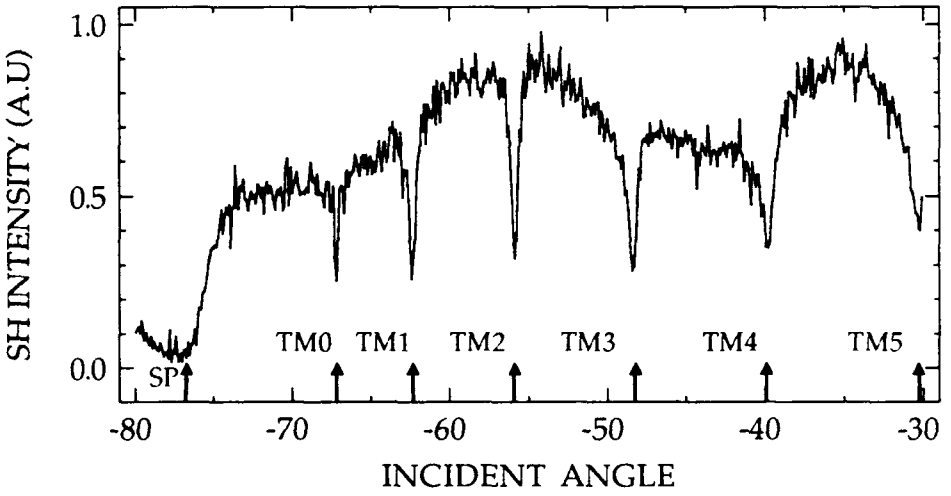

Figure 4. Specularly reflected second harmonic intensity as the device is pumped by light with a wavelength of 1064 nm. TM polarization. The arrows shows the measured angles at which the fundamental wavelength is coupled to the resonances.

In conclusion we have observed an increase of SH generation from a polymer waveguide as guided modes or a surface plasmon is coupled by a silver grating. If the SH wavelength falls within the absorption range of the polymer, the peaks of SH turns into dips. Finally, larger SH efficiencies are expected for phase-matched conditions.

References

[1] D. S. Chemla and J. Zyss (eds.) *Nonlinear Optical Properties of Organic Molecules and Crystals*, (Academic press, New York, 1986), vol. 1.
[2] R. Reinisch, M. Nevière, H. Akhouairy, JL Coutaz, D. Maystre, E Pic, Opt. Eng. **27**, 961 (1988).

Monday, September 2, 1991

Poster Session: 1

ME 5:30pm–7:00pm
Dirac Room

AN EFFICIENT FINITE ELEMENT SCHEME FOR HIGHLY NONLINEAR WAVEGUIDES

H E HERNANDEZ-FIGUEROA
Laser Optics & Spectroscopy Group
Department of Physics
Imperial College, London, SW7 2BZ, UK
Tel.: +44-71-2258840
Fax : +44-71-5899463

Since the late 70's the ***Beam Propagation Method*** (BPM) or ***Split-Step Fourier Method*** (SS/FM), has been widely used for solving the nonlinear partial differential equations which describe the propagation of spatial pulses through waveguide structures. By applying the Split-Step technique, the paraxial wave equation can be split in two propagating equations, one involving only linear terms and another including nonlinear ones. These two equations describe diffraction and nonlinear refraction respectively. In the SS/FM, diffraction is integrated by using the Fourier transform. However, the performance of this method is known to be seriously affected when abrupt variations of the refractive index are taken into account [1], and the problem tends to become even worse in the high nonlinear regime [2].

As an alternative, several authors [3], have reported the use of finite difference schemes for solving the diffraction effect instead of the Fourier Transform, in the picture of the Split-Step technique. Such an approach leads to the ***Split-Step Finite Difference Method*** (SS/FDM).

On the other hand, the reliability and high performance of the Finite Element Method (FEM) is well established in the analysis of linear guiding structures for microwaves and optical frequencies [4]. The most attractive features of this method, compared with the Finite Difference Method, are its capability to handle arbitrary shaped boundaries and the use of adaptive meshes [5]. For nonlinear optical guiding structures, the FEM has been used very recently, not only for the scalar but also for the vectorial case. Also, for evolutionary or propagating simulations, the FEM has been used in conjunction with the Step-by-Step (SbS) Method [6]. This makes use of the Galerkin criterion for the transversal coordinates, in conjunction with the finite difference Crank-Nicholson scheme for the longitudinal coordinate, such an approach leads to the ***Step-by-Step Finite Element Method*** (SbS/FEM).

Very recently there has been a surge of interest in analysing highly nonlinear waveguides (HNW) of arbitrary cross section [7], in order to study nonlinear transversal effects such as, symmetry breaking, multisoliton emission, spatial ring emission and filament formation. With all this in mind, in this paper, a novel FE scheme is introduced: the ***Split-Step Finite Element Method*** (SS/FEM). This new approach is based on the combination of the Split-Step technique and the Galerkin variational criterion for solving diffraction.

In this work we carried out a comparative assessment between our method and the SS/FDM. Although the analysis of the SbS/FEM is currently underway, early results have shown that this method tends to be slower than the SS/FEM due to at least two iterations in each step are necessary to allow the same large step-sizes along the propagating coordinate. These results will be reported in a separated paper.

As an example, we considered TE waves of frequency ω in a slab waveguide as illustrated in Figure 1. The refractive index in the various media is given by $n^2(x,|E|^2)=n_i^2+\alpha_i|E|^2$, i=c,f,s. Where E represents the usual slowly varying envelope of the electric field, and the subscripts c,f,s referring to the cladding ($x\leq -d$), film ($-d\leq x\leq d$), and substrate ($x\geq d$), respectively. For the results presented here we specifically set, following [8], $d=8c/\omega$, $n_c=n_s=1.55$, $n_f=1.57$, $\alpha_c=10^{-2}$, and $\alpha_f=\alpha_s=0$, which corresponds to a self-focusing Kerr-type nonlinear cladding.

The input beam profile was chosen as the linear zeroth-order transverse-electric (TE_0) mode of the waveguide, Figure 2. This situation could be reproduced experimentally, for instance, by prism coupling into the TE_0 modes of a linear waveguide section and interfacing this onto the nonlinear system [8]. On the other hand, the guided wave flux, S, was chosen as $S=0.45$ mW/m^2. Thus, according to [8], for this flux level the slab utilized here is known to emit, from the film to the cladding, two spatial solitons.

For both SS/FEM and SS/FDM, the length of the computational x-window was 300 units of c/ω, set from $x=-200\ c/\omega$ to $x=100\ c/\omega$, and the z-distance of propagation was 150 units of λ, where λ is the free-space wavelength. We checked the convergence for both methods, by decreasing the z-step, Δz, and increasing the total number of points N in the x-window, as much as: $\Delta z=0.01\lambda$ and N=2500. Then, we assumed as reference or 'exact' solution, E^{ex}, the one obtained from these values of Δz and N and plotted in Figure 2.

For the SS/FDM, we adopted a standard scheme, which makes use of a regular x-mesh [3]. On the other hand, for our method, it is possible to take advantage of a variable x-mesh, easily included in the FE code. Thus, for this purpose the x-window was divided in the following seven sub-intervals:[-200,-130], [-130, -80], [-80,-20], [-20,-8], [-8,8], [8,20], and [20,100], according to the power concentration. Besides, linear and quadratic FE functions were adopted.

In order to measure the degree of convergence of any approximate solution, E, at $z=150\lambda$, we defined the convergent absolute error, $e = \max|E-E^{ex}|$, where the maximum is taken for all the N points of the x-mesh. Thus, the restriction imposed was: $e<10^{-3}$. On the other hand, all our simulations were performed on an IBM/386 25MHz PC.

Our results, summarised in the Table 1, show that z-steps as large as 0.2λ for the SS/FDM and twice this value for the SS/FEM, can be used. These size z-steps are indeed large if

compared with the one reported in [2], for the SS/FM : 0.01λ. Taking into account only regular x-meshes, for Δz=0.2λ, the performance of both methods is quite similar. However, the situation changes remarkably when variable x-meshes are utilized. In this case, is possible to reduce drastically the number of points N, and consequently, the computational time for the SS/FEM.

From this example, we conclude that, our method constitutes a valuable and competitive numerical tool to simulate the propagation of spatial pulses in highly nonlinear waveguides. In addition, seems to be, that the use of quadratic FE functions, introduces considerable improvement. Also, the use of this novel scheme in the simulation of three dimensional problems is strongly recommended, since excellent accuracy should be obtained for this situation without recourse to expensive computing resources, like supercomputers.

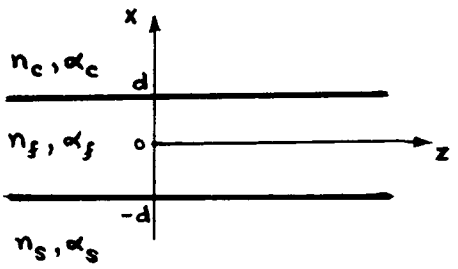

Figure 1. Nonlinear slab waveguide and coordinate system.

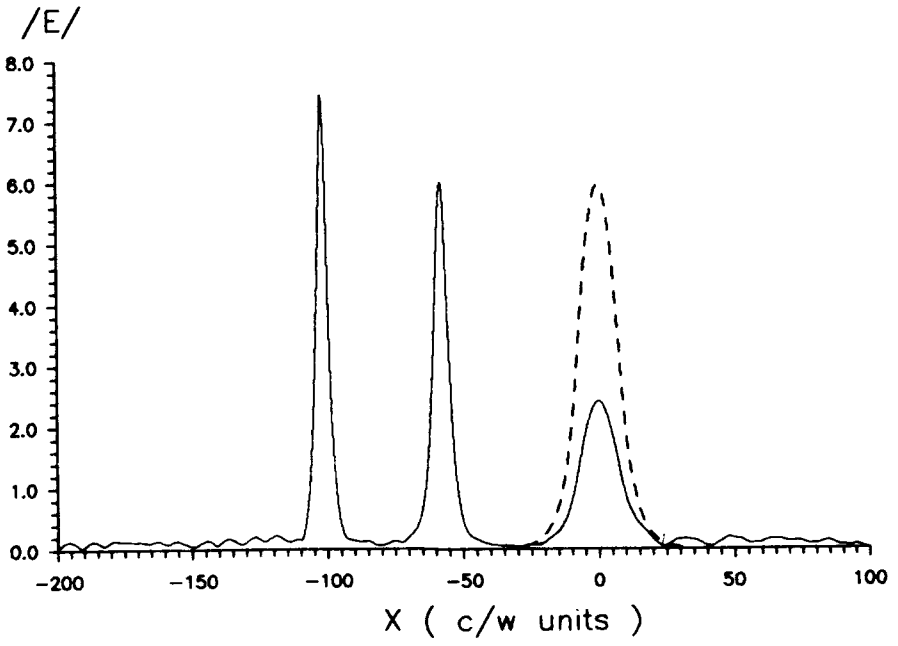

Figure 2. Modulus of the input beam profile at z=0 (dashed curve), and Modulus of the convergent solution at z=150λ: two spatial solitons emitted from the film to the nonlinear cladding (solid curve).

	Δz (λ)	x-Mesh	N	Time (min)
SS/FDM:	0.2	Regular	1200	45
	0.4	Regular	> 2500	--
SS/FEM:	(linear FE functions)			
	0.2	Regular	1500	50
	0.2	/60/200/150/150/160/70/60/	850	30
	0.4	Regular	> 2500	--
	0.4	/60/300/250/150/160/70/60/	1050	10
SS/FEM:	(quadratic FE functions)			
	0.2	Regular	1100	47
	0.2	/40/160/110/90/100/60/50/	610	26
	0.4	Regular	2000	20
	0.4	/40/240/170/130/100/60/50/	790	6

Table 1 Results obtained by using the SS/FDM and the SS/FEM. The numbers beetween slashes correspond to the number of points set regularly in each of the seven sub-intervals given in the text, respectively

REFERENCES

[1] Y. Chung and N. Dagli, IEEE J. Quantum Electron. QE-26, 1335 (1990).

[2] J.V. Moloney, J. Ariyasu, C.T. Seaton, and G.I. Stegeman, Opt. Lett. 11, 315 (1986).

[3] See, e.g., B.P. Nelson and D. Wood, IEEE J. Quantum Electron. QE-24, 1915 (1988).

[4] T. P. Young, Proc. IEE 135, Pt A, 135 (1988).

[5] R.D. Ettinger, F.A Fernandez and J.B. Davies, International Conference on Directions in Electromagnetic Wave Modeling, New York, Oct. 1990, Digest p. 48.

[6] K. Hayata, A. Misawa, and M. Koshiba, J. Opt. Soc. Am. B 7, 1268 (1990).

[7] See, e.g., D. R. Heatley, E. M. Wright, and G. I. Stegeman, Opt. Lett. 6, 291 (1991).

[8] E.M. Wright, G.I Stegeman, C.T. Seaton, J.V. Moloney, and A.D. Boardman, Phys. Rev. A 34, 4442 (1986).

Finite Element Analysis of Two-Transverse-Dimensional Bistable Nonlinear Integrated Optical Waveguides

B.M.A. Rahman,
Dept. of Electrical, Electronic and Information Engineering,
The City University,
Northampton Square, London EC1V 0HB, U.K.
Tel: +44-71-253-4399 Ext. 3808

F.A. Fernandez, R.D. Ettinger and J.B. Davies,
Dept. of Electronic and Electrical Engineering,
University College London,
Torrington Place, London WC1E 7JE, U.K.
Tel: +44-71-387-7050

There is considerable interest in the study of strong nonlinear effects in integrated optics for use in optical switching [1]. Nonlinear thin films have already been studied extensively by both analytical and numerical techniques. Only in more complex nonlinear waveguides, however, can one obtain very high power density for moderate input power through two-dimensional field confinement in a tiny cross-section.

Work on thin films has shown bistability for certain values of input power [2-4]. An additional solution at these powers lies on an unstable portion of the dispersion curve, as shown analytically [2]. In general, however, with two-dimensional cross-sections only numerical approaches are available. Besides, even in thin films practical solutions are two-dimensional [5,6]. Using variational and finite element methods, it was found that for thin films one can obtain both stable solutions in an incremental iterative approach [3,4]. In this approach, the field distribution found at one power is used as a prediction of the solution at an incremented (or decremented) power, which is then corrected by iterations for self-consistency. The finite element method is also well suited for two-dimensional cross-sections [7-9] and is a much more versatile method than the numerical iterative method described by Akhmediev et al. [6]. However, to the authors' knowledge, multiple solutions at the same power have not been reported before for two-transverse-dimensional waveguides.

This paper extends previous analyses of bistability in films to guides with two-dimensional field confinement. The rigorous vectorial method used for this purpose involves iterative application of the well-developed linear finite element approach for two dimensional cross-sections [10]. We have also incorporated recent techniques for adaptive remeshing [11] to great advantage.

An obvious but non trivial extension of the planar case is a strip-loaded two-transverse-dimensional nonlinear optical waveguide (shown as an inset in Fig. 1). The cladding has a saturable self-focusing optical nonlinearity with maximum possible refractive index change, $\Delta n_{sat} = 0.2$. We study the lowest order quasi-TM mode at a wavelength $\lambda = 0.515$ μm. All powers will be given in units of $1.169\ \lambda^2\ n_{lin} / (a\eta_0)$ where a is defined in eqn. (1). For $n_2 = 10^{-9}$ m^2/W, unit of power corresponds to 0.2 mW. The refractive indices are shown in the inset in Fig. 1. The assumed nonlinearity in the cladding has the form [8]:

$$\varepsilon = \varepsilon_{lin} + \Delta\varepsilon_{sat}\left(1 - \exp\left(-a|\mathbf{E}|^2 / \Delta\varepsilon_{sat}\right)\right) \tag{1}$$

with

$$(n_{lin} + \Delta n_{sat})^2 = \varepsilon_{lin} + \Delta\varepsilon_{sat} \tag{2}$$

Figure 1 illustrates the variation of effective index with increasing normalized total power for three different values of height b. For the strip height $b = 0.4$ μm, the result for the effective index variation with increasing total power is smooth. The curve reflects the drift of the mode into the nonlinear region as the refractive index inside the cladding becomes higher than the refractive index beneath. But with $b = 0.8$ μm, although the change is initially slower, the mode changes abruptly at a certain power (see point A in Fig. 2). Thereafter the mode is primarily guided by the nonlinearity of the cladding as in the previous case ($b = 0.4$ μm). When the strip height is 1.0 μm, the transition is even sharper. At very high powers, the strip height becomes irrelevant since the modes are almost solely confined to the nonlinear region.

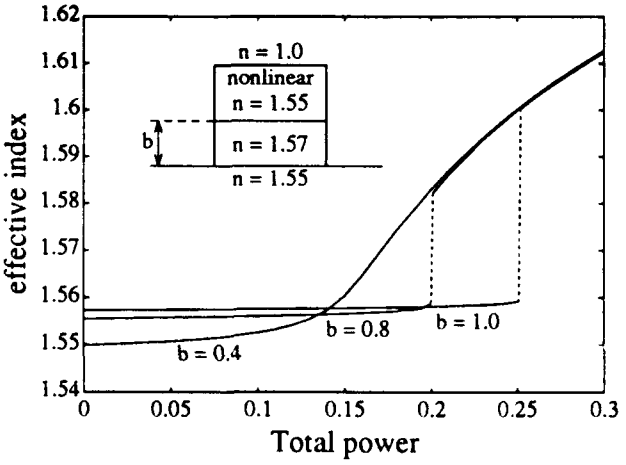

Fig. 1 Effective index versus total power for height $b = 0.4$, 0.8 and 1.0 μm. Width of each strip 2.0 μm, cladding height 1.0 μm.

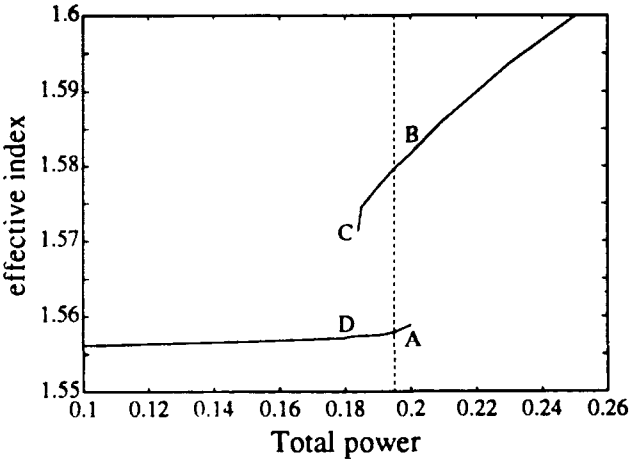

Fig. 2 Variation of effective index with increasing and decreasing power for $b = 0.8$ μm. (Note restricted scale for the total power, chosen to emphasize the switching region).

In Fig. 2 results for increasing and decreasing total power are plotted together for the case $b = 0.8$μm. For increasing power there is a sudden jump to the upper branch (from points A to B). However, when the power is reduced from a higher value on the upper branch, there is no change at point B. Instead, the upper branch continues to point C where further decrease of power

produces an abrupt return to the lower branch (point D). This behaviour is similar to that reported for thin films [3,4].

Figure 3 illustrates the variation of power in the linear strip of height $b = 0.8$ μm versus total power in the complete cross-section. As total power is increased from zero the power carried by the linear strip at first increases almost linearly, but at a certain total power the mode suddenly moves to the nonlinear cladding. Hence the power carried by the linear strip drops sharply. For decreasing total power, a jump back to the first branch occurs at a different value of total power. Points E and F correspond to two stable states with the same total power but very different characteristics. The vertical dotted line in Fig. 2 marks the effective indices of these two states. The corresponding field profiles are shown in Fig. 4 as contour plots of the power density (Poynting vector). Fig. 4a shows the mode primarily confined in the linear strip which carries 67% of the total power, whilst only 25% is in the cladding. In contrast, Fig. 4b shows the mode almost confined in the nonlinear cladding (just 17% of total power in the linear strip, 83% in the cladding).

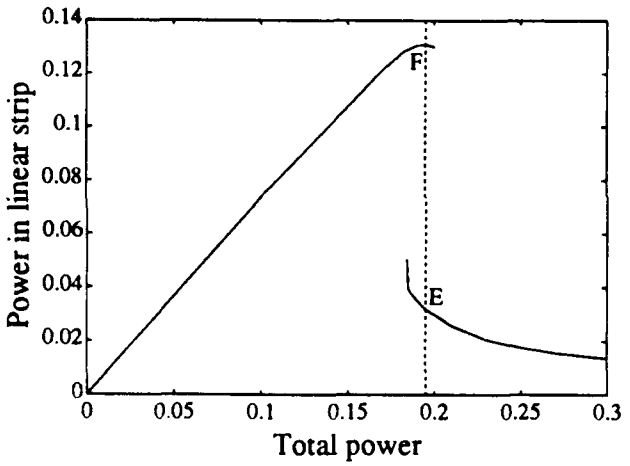

Fig. 3 Variation of power carried by the linear strip with increasing and decreasing total power.

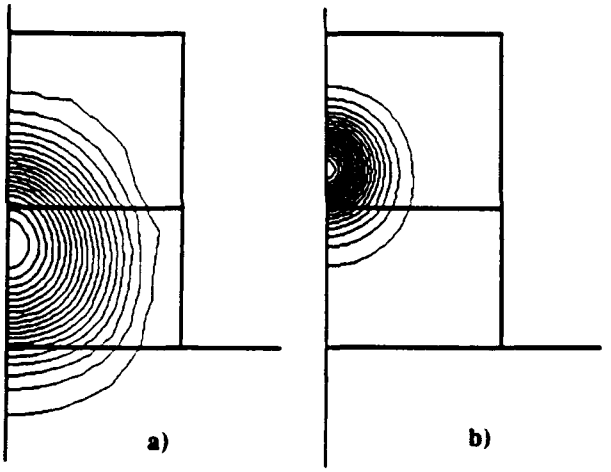

Fig. 4 Power contours of two stable states for the same total power 0.195. (a) mode confined in the linear strip (b) mode confined in the nonlinear cladding. (Only half of the cross-section is shown).

Of course any device based on this effect will suffer from a complex relation between applied input power and total transmitted power. Nevertheless, the clear result of our modal analysis is that both linear strip-guided and nonlinear cladding-guided states can exist at the same power.

The advantages of the present two-transverse-dimensional method include treatment of arbitrarily shaped waveguides with arbitrary refractive index profile, including tensor materials and a wide range of nonlinearities. This technique promises to be highly valuable for the design of practical nonlinear optical waveguides. The finite element method, in a vector field formulation, is much more versatile than the other available analytical and numerical methods, such as the iterative numerical method described by Akhmediev et al. [6]. Finally, a two-transverse-dimensional

approach allows study of high power density without the need for extremely high total power.

References

[1] G.I. Stegeman, E.M. Wright, N. Finlayson, R. Zanoni and C.T. Seaton, "Third order nonlinear integrated optics", *J. Lightwave Technol.*, **vol. LT-6**, pp. 953-970, 1988.

[2] G.I. Stegeman, E.M. Wright, C.T. Seaton, J.V. Moloney, T-P. Shen, A.A. Maradudin and R.F. Wallis, "Nonlinear slab-guided waves in non-Kerr-like media", *IEEE J. Quantum Electron.*, **vol. QE-22**, pp. 977-983, 1986.

[3] B.M.A. Rahman, J.R. Souza and J.B. Davies, "Numerical analysis of nonlinear bistable optical waveguides", *IEEE Photonics Technol. Lett.*, **vol. 2**, pp. 265-267, 1990.

[4] B.M.A. Rahman and J.B. Davies, "Finite element solution of nonlinear bistable optical waveguides", *Internat. J. Optoelectron.*, **vol. 4**, pp. 153-161, 1989.

[5] J.V. Moloney, "Modulational instability of two-transverse-dimensional surface polariton waves in nonlinear dielectric waveguides", *Phys. Rev. A*, **vol. 36**, pp. 4563-4566, 1987.

[6] N.N. Akhmediev, R.F. Nabiev and Yu.M. Popov, "Three-dimensional modes of a symmetric nonlinear plane waveguide", *Optics Comm.*, **vol. 69**, pp. 247-252, 1989.

[7] J.B. Davies, R.D. Ettinger, F.A. Fernandez, B.M.A. Rahman and J.R. Souza, "Variational and finite element solutions of TE modes in waveguides with nonlinear material", URSI National Radio Science Meeting, Boulder, Colorado, USA, 4-6 Jan. 1989.

[8] R.D. Ettinger, F.A. Fernandez, B.M.A. Rahman and J.B. Davies, "Vector finite element solution of saturable nonlinear strip-loaded optical waveguides", *IEEE Photonics Technol. Lett.*, **vol. 3**, pp. 147-149, 1991.

[9] F.A. Fernandez, R.D. Ettinger, J.B. Davies and B.M.A. Rahman, "Numerical study of the quasi-TE mode in optical waveguide with saturable nonlinear rectangular core", in Integrated Photonics Research 1991, Monterey, California, Tech. Digest Series (OSA), **vol. 8**, pp. 33-34, 1991.

[10] B.M.A. Rahman and J.B. Davies, "Finite-element solution of integrated optical waveguides", *J. Lightwave Technol.*, **vol. LT-2**, pp. 682-688, 1984.

[11] R.D. Ettinger, F.A. Fernandez and J.B. Davies, "Application of adaptive remeshing techniques to the finite element analysis of nonlinear optical waveguides", in "Directions in Electromagnetic Wave Modeling", H.L. Bertoni and L.B. Felsen, (eds.), Plenum Press, New York, 1991.

Analysis of TM-polarized nonlinear guided waves based on a conservation law

K. Gniadek and M. Rusek
Institute of Physics, Warsaw University of Technology, 00-662 Warsaw, Poland

In recent years, the properties of the transverse magnetic TM polarized guided waves in nonlinear layered structures have been investigated theoretically in a number of papers [1 - 4]. The presence of two electric field components, one parallel (E_z) and one orthogonal (E_x) to the boundaries of a thin film guiding structure makes the analysis of TM waves more complicated than for the transverse electric TE polarized waves. For simplify the analysis in some works was assumed that TM-wave nonlinearity arises only through one component electric field. The more elaborate is approximation referred to as longitudinal uniaxial approximation in which the nonlinearity is expressed as dependent only on the electric field component parallel to the boundary [1]. The more realistic is transverse uniaxial approximation in which the nonlinearity arises from the dominant transverse E_x component of the electric field [5]. In the few papers [6 - 7] has been investigated TM polarized waves / surface polaritons / propagating along the interface separating of two media, one / or both / of which is nonlinear with the general intensity dependent dielectric function. The effective method analysis of TM nonlinear guided waves is separation of the two electric field components E_x and E_z achieved by means of a conservation law. In this approach the properties of TM nonlinear guided waves can be study without the need to solve for the field profile [8]. Since the two field components E_x and E_z of TM wave are everywhere interrelated through the conservation law, then it is possible formally express one in terms of the other.

In this communication we analyse in detail the relationship between two components E_x and E_z utilizing the conservation laws

for TM guided waves in the linear film sandwiched between two lossless nonlinear media. The electric and magnetic field components are taken to have the form

$$E_j(x,z,t) = \tilde{E}_j(x)\exp[i(hz-\omega t)], \quad j = x,z$$
$$H_y(x,z,t) = \tilde{H}_y(x)\exp[i(hz-\omega t)] \qquad (1)$$

where h is propagation constant and ω is the angular frequency. E_x and E_z are the field components perpendicular and parallel to the film, respectively. Furthermore we suppose $\tilde{E}_j(x) = E_j(x)\exp[i\,\varphi_j(x)]$, where $E_j(x)$ and $\varphi_j(x)$ are all real variables. The dielectric subtensor of the nonlinear medium for the TM case reads as

$$\hat{\epsilon} = \epsilon_o \begin{bmatrix} \epsilon_{xx}(|E_x|^2, |E_z|^2) & 0 \\ 0 & \epsilon_{zz}(|E_x|^2, |E_z|^2) \end{bmatrix} \qquad (2)$$

where the elements ϵ_{xx} and ϵ_{zz} can depend on the intensity related to the components E_x and E_z in quite an arbitrary way.

Substituting (1) into Maxwell equations we get two conservation laws

$$\epsilon_{xx}E_xE_z\cos(\varphi_z - \varphi_x) = C_1 \qquad (3a)$$

$$F + \epsilon_{xx}E_x^2\left(1 - \frac{k_o^2}{2h^2}\epsilon_{xx}\right) = C_2 \qquad (3b)$$

where k_o is the free-space wave number. F is related to a free energy of the nonlinear medium and is determined from the particular mechanism of the nonlinearity. Conservation law (3b) is obtained provided that

$$\epsilon_{xx} = \frac{\partial F}{\partial(E_x^2)}, \quad \epsilon_{zz} = \frac{\partial F}{\partial(E_z^2)} \qquad (4)$$

and dF is an exact differential.

Equation (4) serves some restrictions on the type of nonlinear materials that can be used. The integration constants C_1 and C_2 have been set equal to zero because the nonlinear substrate /or cover / extend to infinity where $E_j = 0$. Equation (3a) express

the transversal component of the time-average Poynting vector $P_x = 1/2\ \mathrm{Re}(E \times H^*) = 0$. From (3a) / with $C_1 = 0$ / we see that two electric field components E_x and E_z are every where $\pm \pi/2$ out of phase. The conservation laws (3a and b) are key point of our analysis.

To be more specific, let us consider the case of cladding materials whose dielectric tensor has a nonlinear part proportional to the local intensity, i.e. $\epsilon_{xx} = \epsilon_{zz} = \eta = \epsilon + \alpha(E_x^2 + E_z^2)$. For this case the free energy F is given by

$$F = 1/4\ (E_x^2 + E_z^2)\left[2\epsilon + (E_x^2 + E_z^2)\right] \qquad (5)$$

and the conservation law (3b) becomes

$$E_z^2(\eta + \epsilon) = E_x^2\, f(\eta) \qquad (6)$$

where $f(\eta) = -2a\eta^2 + 3\eta - \epsilon$, $a = k_o^2/h^2$.
Equivalently (6) can be written as

$$E_x^2 = \frac{\eta - \epsilon}{f(\eta) + \eta + \epsilon}\ \frac{\eta + \epsilon}{\alpha} \qquad (7a)$$

or

$$E_z^2 = \frac{\eta - \epsilon}{f(\eta) + \eta + \epsilon}\ \frac{f(\eta)}{\alpha} \qquad (7b)$$

Thus all possible paths of the E_x and E_z in nonlinear region are curves determined by the parameter and each path crosses the circle with the radius $r = \left[(\eta - \epsilon)/\alpha\right]^{1/2}$ at one point. The analysis of the relationship between the field components E_x and E_z is based on detailed inspection of the conservation laws (3)and (7).

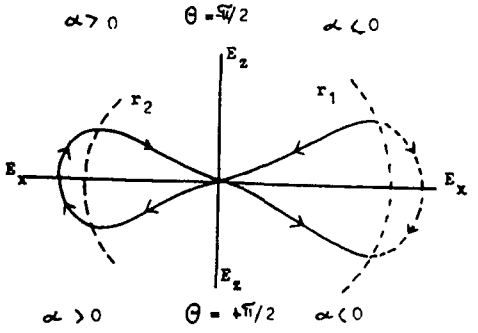

Fig. 1

Both the self-focusing ($\alpha > 0$) and self-defocusing ($\alpha < 0$) medium is considered. Qualitative illustration of the path in the $E_x - E_z$ space determined from the conservation laws is plotted in Fig. 1. /$\Theta = \varphi_z - \varphi_x$, $r_{1,2} = r(\eta_{1,2})$, where $\eta_{1,2}$ are the roots of the Eq. $dE_z/d\eta = 0$ /.

The paths start always at the central zero E_x, $E_z = 0$ which corresponds to $x = \pm\infty$. The end point at the path is determined by the boundary values of the field components E_{ox} and E_{oz}. Arrows indicate the direction of the transition on the particular section of the path.

For determining the dispersion relation we use the conservation laws (3) related to the linear film i.e. with $\alpha = 0$ and ϵ replaced by ϵ_f. The field components E_x^f and E_z^f in linear film are

$$E_x^f(x) = (h/q) A \sin\left[q(x - x_o)\right], \quad E_z^f(x) = A \cos\left[q(x - x_o)\right]$$

where $q^2 = k_o^2 \epsilon_f - h^2$. Matching the tangential components E_z and H_y at the boundaries $x = x_c$ and $x = x_s$ leads to dispersion relation

$$q(x_c - x_s) = tn^{-1}\left(\frac{q}{q_c}\right) - tn^{-1}\left(\frac{q}{q_s}\right) + m\pi \qquad (8)$$

where $q_r = q_r(h, A) = (\epsilon_f/\eta_{or})\left[f(\eta_{or})/(\eta_{or} + \epsilon_r)\right]^{1/2}$, $(r = s, c)$ is determined from relation between the boundary values of the field components E_x and E_z together with the conservation laws.

We conclude, that although the presented method does not leads to an exact analytical solutions it is applicable for analysis of the properties TM nonlinear guided waves for a large class of dielectric functions satisfying Eq. (4).

References

1. G.I. Stegeman, C.T. Seaton, J. Ariyasu, R.F. Wallis, and A.A. Maradudin, J. Appl. Phys., 58, 2453 (1985)
2. M.S. Kushwaha, Japan. J. Appl. Phys., 26, L1035, (1987)
3. U. Langbein, F. Lederer, D. Mihalache, D. Mazilu, Physica, 154C, 377, (1987)
4. A.D. Boardman, T. Twardowski, Opt. Comm., 74, 347 (1990)
5. C.T. Seaton, J.D. Valera, B.S. Svenson, G.I. Stegeman, Opt. Lett. 10, 149, (1985)
6. K.M. Leung, Phys. Rev., B32, 5093, (1985)
7. D. Mihalache, G.I. Stegeman, C.T. Seaton, E.M. Wright, R. Zanoni, A.D. Boardman, T. Twardowski, Opt. Lett. 12, 187,
8. R.I. Joseph, D.N. Christodoulides, Opt. Lett., 12, 826, (1987)

TE waves propagating in a nonlinear planar asymmetric converging waveguide Y junction

Sien Chi and Tian-Tsorng Shi
Institute of Electro-Optical Engineering
and Center for Telecommunications Research
National Chiao Tung University
Hsinchu, Taiwan, Republic of China

Summary:

Recently nonlinear waveguide junctions have been investigated intensively for their interesting switching behaviors[1,2]. The waves propagating in a nonlinear converging waveguide Y junction in which the two branches and the stem are single mode waveguides are less reported. For a linear case, the field injected into the thinner branch at a distance from the junction will not evolve into the fundamental mode of the stem, and the field injected into the thicker branch will propagate without loss[3]. Here we simulate the waves propagating in the Y junction with a nonlinear cladding by using beam propagation method[4], and we find that the field injected into the thinner branch is possible to transmit to the stem with a high efficiency.

The schematic structure of the considered Y junction is shown in Fig. 1. The permittivities of the nonlinear cladding which is shaded in the figure, the film, and the substrate are $2.4025 + \alpha |E|^2$ with $\alpha = 3.3776 \times 10^{-12}$ m^2/V^2, 2.4649, and 2.4025, respectively. The thicknesses of the stem, the thicker branch, and the thinner branch are 2.5, 2.5, and 1.5 μm, respectively. Wavelength is assumed to be 1.3 μm. The full angle of the junction is 0.1°, and the fields will propagate adiabatically in the junction with such a small angle.

Numerical results are shown in Fig. 2 to 5. In Fig. 2, a field with power equal to 0.165 W/mm is injected into the thicker branch and evolves into the fundamental mode of the stem. It is similar to the linear case which the field will transmit to the stem without loss. In Fig. 3, a field of 0.08 W/mm is injected into the thinner branch, and the field does not transmit to the stem but radiates to the cladding with a spatial soliton. In Fig. 4, a field of 0.165 W/mm is injected into the thinner end, the field couples from the thinner branch to the thicker branch near the joint of the two branches suddenly, and swings right and left for the successive propagation in the stem. The coupling efficiency of power is 75 % approximately. In Fig. 5, a surface-polariton of the nonlinear thinner branch is injected, which power is 0.185 W/mm. Because the field concentrates in the interface of the film and the cladding, it does not "see" the thicker branch. Thus, the surface-polariton maintains the shape very

well when the field propagates from the branch to the stem.

In conclusion, the field injected into the thinner branch of the nonlinear waveguide Y junction is possible to evolve into the fundamental mode of the stem by control its power. It can be used as the nonlinear combiner in the optical network.

References:

1. H. Fouckhardt, and Y. Silberberg, J. Opt. Soc. Am. B 7, 803 (1990).
2. G. I. Stegeman, and E. M. Wright, Opt. Quantum Electron. 22, 95 (1990).
3. M. Izutsu, Y. Nakai, and T. Sueta, Opt. Lett. 7, 136 (1982).
4. M. D. Feit, and J. A. Fleck, Jr., Appl. Opt. 19, 1154 (1980).

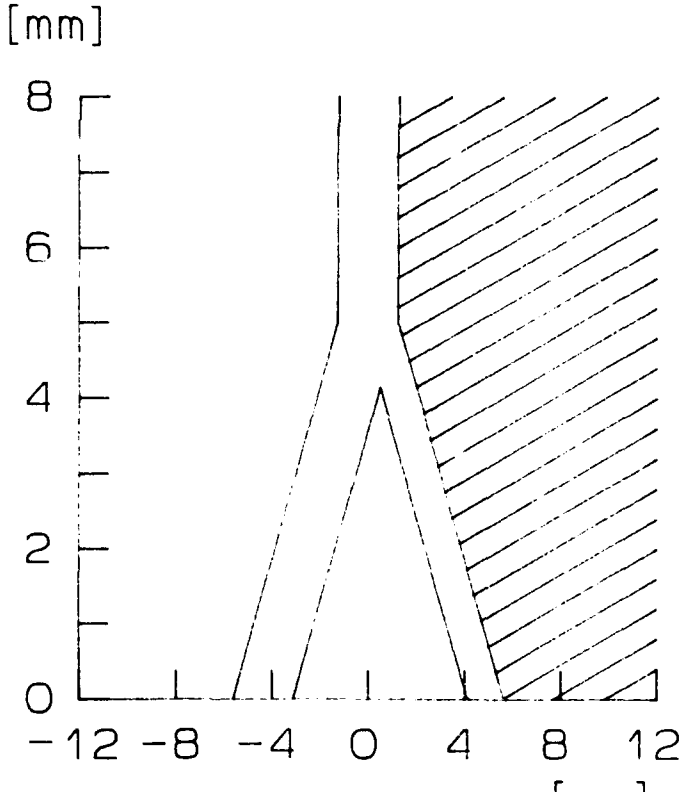

Fig. 1

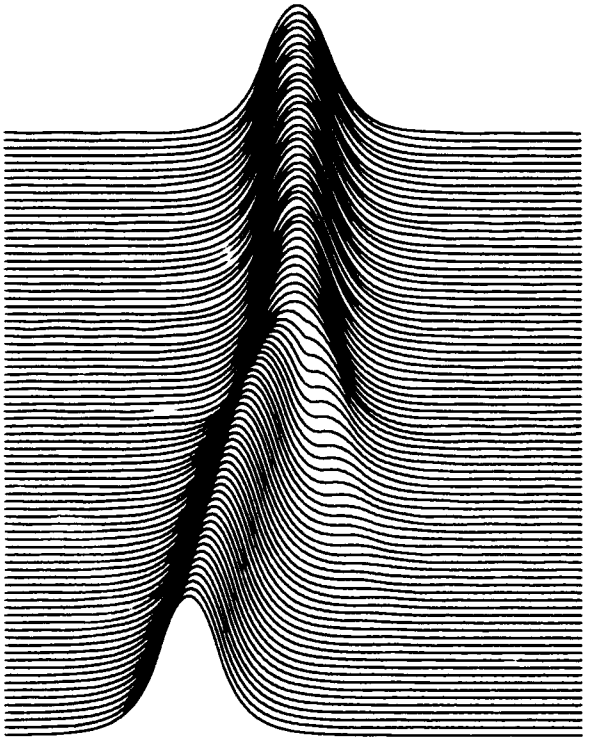

Fig.2

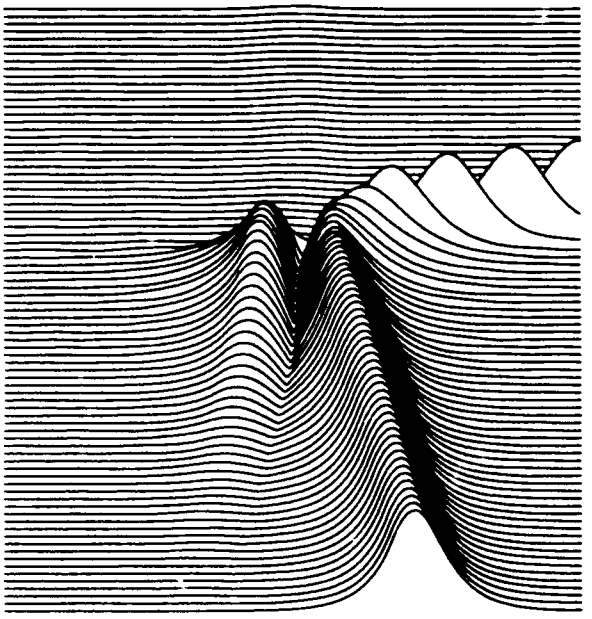

Fig.3

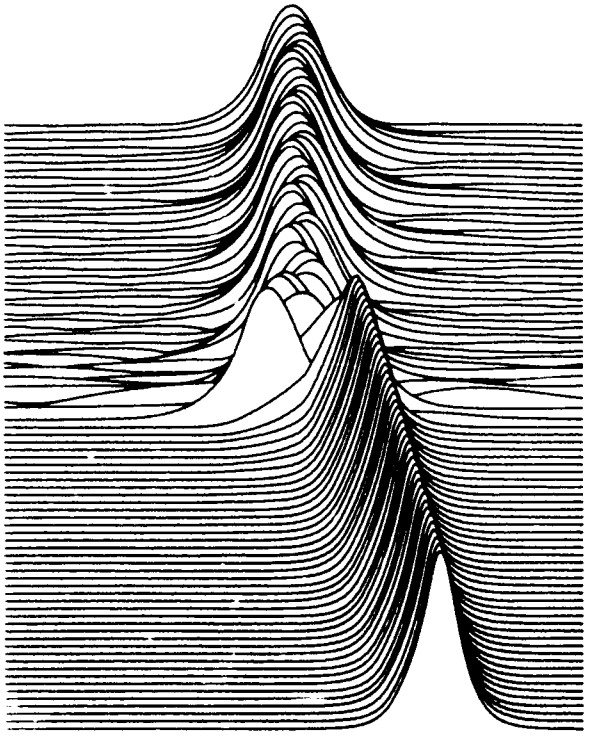

Fig.4

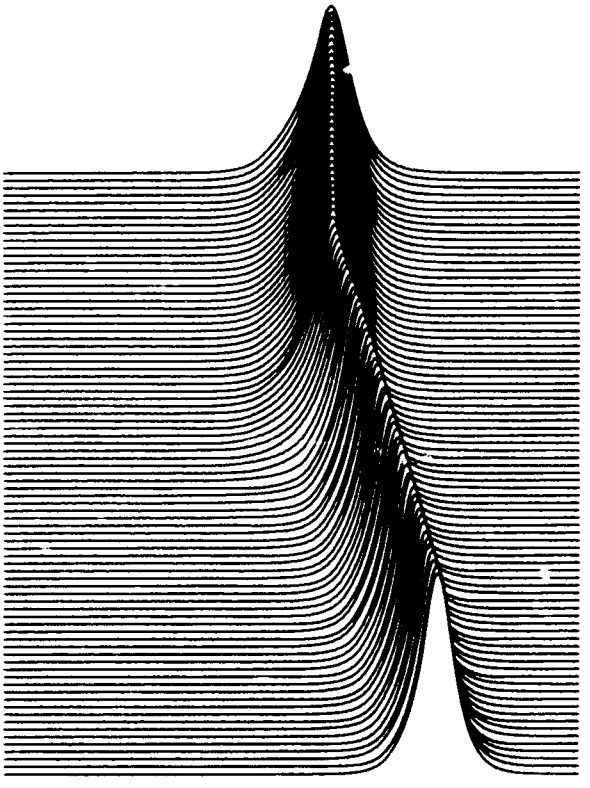

Fig.5

Spatial Soliton Propagation Through Periodically Modulated Layer in Nonlinear Medium

F.Kh.Abdullaev, A.A.Abdumalikov
Thermophysics Department of Uzbek Academy of Sciences
Tashkent-135 ,Katartal str.28,USSR.

Here we present a theory which describes the propagation of self-focused channel (spatial solitons) in the media consisting from thetwoself - focusing nonlinear media and the periodically-modulated thin linear film separating this media. Recently it was shown that propagation of spatial olitons at an oblique angle of incidence to an interface between nonlinear Kerr-like media may be represented as an equivalent particle moving in the effective potential[1].This theory predicts the nonlinear Snell's law of reflection and existence of nonlinear surface waves.It is possible to use the design of an all-optical power spatial scanner and an all-optical switch [2]. Existence of periodically - modulated thin film also leads to the new possibilities for such designs.

The problem we will consider is the propagation of spatial soliton in the z direction under angle ψ_i to linear film from the left hand of medium (see Figure 1).The wave equation in the dimensionless form which describes this problem is

$$iu_t + u_{xx} + 2|u|^2 u = \varepsilon\delta[x + f(t)]u \ . \qquad (1)$$

Here u is dimensionless envelope of electric field, $u = k\sqrt{\alpha/2n_o}E$, $t = z/2k$, k is the wavenumber, $n_1^2 = n_o^2 + \varepsilon\delta(x+f(t))$ describe the inhomogeneity of medium along boundary, $n^2 = n_o^2 + \alpha|E|^2$. Below we describe the evolution of incident beam in the form of spatial soliton

$$u(x,t) = 2\eta\, sech 2\eta(x - \bar{x}) exp[ivx/2 - 4i(\eta^2 - v^2/16)]. \qquad (2)$$

$$\bar{x} = -4\xi t \ , \ v = -4\xi .$$

Using perturbation theory for solitons [3],[4] we obtain the next equation for coordinate of soliton center (the beam average

position)

$$\frac{d^2y}{dt^2} = 2\eta f''(t) - \frac{\partial V}{\partial y}, \quad V(y) = \frac{V_o}{\cosh^2 y}, \qquad (3)$$

$$V_o = 8\varepsilon\eta^3, \quad y = 2\eta(\bar{x} + f(t)).$$

As follows from (3) the investigation of spatial soliton dynamics in the framwork of equation (1) is reduced to the investigation of a particle of unit mass in a field of effective anharmonic potential V(y) and external field f(t). At $\varepsilon > 0$ a soliton reflection (or transmission) from bounary is realized at $\varepsilon < 0$ the oscillating motion of soliton near inhomogeneity takes place. In the oscillating regime (nonlinear surface waves) an interaction with periodic field f(t) can lead to resonant motions of beam and spatial chaos in beam dynamics. The velocity of soliton is connected with the angle by relation $\psi_i = \tan^{-1}(v_i/2)$. The beam is reflected at $\varepsilon > 0$, $4\xi^2 < \eta\varepsilon$ and the solution is (f = 0) [5]

$$\bar{x}(t) = -\frac{1}{2\eta} arcsh[(\eta\varepsilon/4\xi_i^2 - 1)^{1/2} \cosh(8\eta\xi_i t)]. \qquad (4)$$

The beam is transmitted at $\varepsilon > 0$, $4\xi_j^2 > \eta\varepsilon$. The solution is

$$x(t) = -\frac{1}{2\eta} arsh[(1 - \frac{\varepsilon\eta}{4\xi_i^2}) \sinh(8\eta\xi_i t)] . \qquad (5)$$

The nonlinear surface wave appear at $\varepsilon<0$ and f=0. For the average position of this wave we have

$$\bar{x}(t) = \sinh^{-1}\left(\sqrt{\frac{2|V_o|}{|E|}} - 1 \; \sin[2|E|(t - t_o)]\right), \qquad (6)$$

$$E = \dot{\bar{x}}^2/2 + V(\bar{x}).$$

Let us study the motion type of spatial soliton. Expanding interaction Hamiltonian H_{int} into Fourier series we obtain in the action-angle (I,θ) variables (when $2\eta f''(t) = \varphi_o \sin\Omega t$) the expressions

$$I = I_{scp} \; 2\pi\sqrt{E}, \; I_{scp} = 2\pi\sqrt{2|V_o|}, \; H_{int} = v(\theta)f(t),$$

$$H_{int} = \varphi\sum_n H^{(n)}(I) exp(in\theta + i\Omega t). \qquad (7)$$

The condition of nonlinear resonance takes the form

$$(2m + 1)\omega(I) = \Omega \ , \omega(I) = (2\pi)^{-1}(I - I_{sep}). \qquad (8)$$

For large m follows for the distance between resonances

$$\delta\omega = |\omega_{m+1} - \omega_m| \approx 2\omega^2/\Omega \ , \qquad (9)$$

A nonlinear resonance width equals to

$$\Delta\omega = |4\varphi_o H^{(m)}_{int} \ d\omega/dI|^{1/2} \ , \qquad (10)$$

At $\alpha \cong m >> 1$ $H^{(m)} \approx 4\sqrt{\pi}/m$ and

$$(\Delta\omega)^2 = 32\sqrt{\pi}\ \varphi_o \omega(I)/\Omega \qquad (11)$$

In the case when the nonlinear resonance width is larger or the same is the distance between them, then one can expect the apperance of chaotic regime (Chirikov criterion [6]) i.e.

$$K = (\Delta\omega/\delta\omega)^2 = 32\varphi_o\Omega\sqrt{\pi}\ /(I - I_s)^3 \geq 1 \ . \qquad (12)$$

Hence is follows under any φ_o, Ω there exists a region in the separatrix vicinity where (12) is satisfied and the beam motion is chaotic(see Figure 2).If the initial values of soliton parameters corresponds to the stochastic region near separatrix then the beam oscillation amplitude stochastically grows andthe beam tramsmitted or reflected. The depinning length is

$$t_d \sim (16\varphi_o\Omega)^{-1/3}. \qquad (13)$$

In addition to adiabatic dynamics of beam there is also a possible emission of linear wave by beam at propagation along z-direction. The emitted field may be calculated with the perturbation theory based on inverse scattering transform [3],[4].The continuum spectrum is defined by the Jost coefficient $b(\lambda)$, where λ is the spectral parameter connected with the wavenumber of emitted field i.e. $k(\lambda) = \lambda/2$.Calculation was showed that the radiation maximal at $2\lambda^2 = 4\eta^2 - v^2 - n\Omega$.The energy emitted in the unit of length is

$$\frac{dE}{dt} = 2\pi\varepsilon^2\eta^2 \sum J_n\{2\varphi_o(\sqrt{v^2/4 - n\Omega} - v/2)\}^2, \qquad (14)$$

Equalizing the radiative losses to the amplitude changing we find that the soliton amplitude is damped: $\eta = \eta_o/(1 + A\eta_o t)$.

References

1.Acevec A.B.,Moloney J.V.,Newell A.C.J.Opt.Soc.Am.B5,559 (1988)
2.Varatharajan P.,Acevec A.B.,Moloney J.V.Appl.Phys.Lett.54,2631 (1989).
3.Karpman V.I.,Maslov E.M.JETP,73,537 (1987)(In Russian).
4.Kaup D.J.,Newell A.C.Proc.Roy.Soc.London A361,413 (1978).
5.Kivshar Y.S.,Kosevich A.M.,Chubykalo O.A.Phys.Lett.A,125(1), 35(1987).
6.Chirikov B.V.Phys.Rep.52,263(1979).

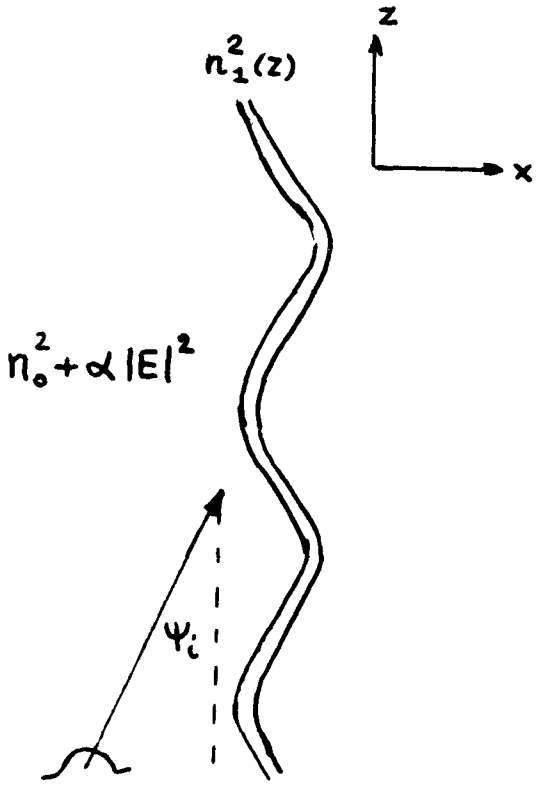

Fig.1

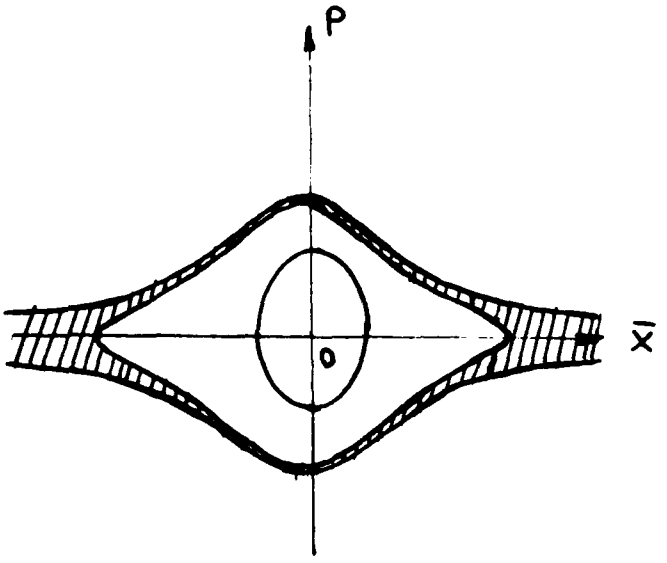

Fig.2

AMPLIFICATION OF NONLINEAR WAVES IN A SYMMETRIC PLANAR WAVEGUIDE

Akhmediev N.N., Mitskevich N.V.,

F.V.Lukin Research & Development Institute of Physical Problems, Zelenograd, 103460 Moscow, USSR

Nabiev N.N.

P.N.Lebedev Physical Institute of Academy of Sciences of the USSR, 53 Leninsky pr., 117924 Moscow, USSR

The study of nonlinear waves in layered structures proposed in Refs.[1] and [2] has become widespread, stimulated by the progress in the early 1980's. The possibility of using such waves in optoelectronic devices spurred advances in both theory and experiment [3-7]. Propagation of waves in nonlinear waveguides is usually considered in passive optical systems (a case of transparent media). In this work we consider for the first time the propagation of waves in nonlinear waveguides with optical gain in the guiding film.

We consider active film of thickness d with linear dielectric constant $\varepsilon_L' = \mathrm{Re}\ \varepsilon_L$ and with optical gain $g = \mathrm{Im}\ \varepsilon_L$ surrounded on both sides ($|x|>d/2$) by media with nonlinear dielectric constants of the form $\varepsilon_0 + \alpha|E|^2$. For a monochromatic TE polarized wave of a frequency ω propagating along z-axis we write the electric field in the form

$$E = \frac{1}{2}\left\{\sqrt{\alpha}\, A(x,z)\, \exp\left[i(\beta z - \omega t)\right] + \text{c.c.}\right\}. \qquad (1)$$

where β is the propagation constant. The slowly varying envelope function $A(x,z)$ obeys the following equation:

$$2i\beta\frac{\partial A}{\partial z} + \frac{\partial^2 A}{\partial x^2} - \left[\beta^2 - \varepsilon(x)\right]A + \alpha(x)|A|^2 A = ig(x)A \qquad (2)$$

where

$$\varepsilon(x)=\begin{cases}\varepsilon_L', & |x|<d/2\\ \varepsilon_o, & |x|>d/2\end{cases}, \quad \alpha(x)=\begin{cases}0, & |x|<d/2\\ 1, & |x|>d/2\end{cases}, \quad g(x)=\begin{cases}g & |x|<d/2\\ 0, & |x|>d/2\end{cases}$$

Stationary modes $A_o(x,\beta)$ of such a structure without gain, i.e. the solutions of Eq.(2) at $\partial A/\partial z=0$ and g = 0 have been comprehensively discussed in the paper [3]. The stability properties of these waves have been investigated in Ref.[7]. In this work we solved a more general problem of gaining of the stationary modes.

For the value β corresponding to increasing part of energy integral I dependence on β the field envelope A(x) and it's phase are changed upon propagation remaining close to stationary solution $A_o(x,\beta)$ but with changing β. This evolution can be described by the motion of representative point of a wave in the (I,β) space. The I value of representative point is calculated at each step of numerical simulations according to standard definition [3]. The β value of representative point is calculated at each step using the relation:

$$\beta(z) = \beta + (\Delta z)^{-1}\mathrm{Arctan}\,[A(x,z+\Delta z)/A(x,z)],$$

where β is the constant parameter of Eq.(2), Δz is the grid spacing along z. At small gain values $g<<\varepsilon_L'-\varepsilon_{NL}$ guided waves are propagated adiabatically changing, remaining close to stationary solution $A_o(x,\beta)$ with continuous changing of $\beta(z)$. The representative point moves along the stable branches of the $I(\beta)$ curves. These waves are remained stable in the ranges of the $I(\beta)$ dependence with positive slope. When the value of

energy integral passes through the maximum point of the N-shaped $I(\beta)$ curve the wave breaks up and spatial solitary waves are emitted. For symmetric initial conditions the radiation of two solitons is occurred from both sides of waveguide. If some asymmetry is existed in the layered structure or in initial conditions the symmetry breaking occurs at the point of splitting away of the branch of asymmetric modes on the I,β plane. This is in accordance with results of stability investigation in Ref.[7]. One soliton is emitted from the waveguide in this case. This process is repeated periodically along the z axis due to the gain.

REFERENCES

1. Alanakyan Yu.R. Zh.Techn.Fiz., 1967, v.37, p.817-821
2. Litvak F.G., Mironov V.A. Izv.vuzov, radiofizika, 1968, v.11, p.1911-1912.
3. Akhmediev N.N. Zh.Eksp.Teor.Fiz., 1982, v.83, p.545-553.
4. Seaton C.T., Stegeman G.I., Winful H.J. Optical Engineering, 1985, v.24, p.593-599.
5. Vach H., Seaton C.T., Stegeman G.I., Khoo I.C. Opt.Lett., 1984, v.9, p.238-240.
6. Akhmediev N.N., Nabiev R.F., Popov Yu.M. Optics commun., 1989, v.69, p.247-252.
7. Akhmediev N.N., Ostrovskaya N.V. Zh.Tekh.Fiz., 1988, v.58, p. 2194-2201.

Four-Wave Mixing Limitation In Multichannel Coherent Optical Communication

Johan Nilsson
Department of Physics II
Royal Institute of Technology
S - 100 44 Stockholm, Sweden, Tel: +46 8 790 9110

Milan Dado
Department of Telecommunication, University of Transport and Communication
Zilina, Czechoslovakia, Tel: +42 89 54962

Bozena Jaskorzynska
Institute of Optical Research
S - 100 44 Stockholm, Sweden, Tel: +46 8 790 9109

Introduction

Four-wave mixing (FWM) in a fiber is a nonlinear effect likely to impose severe restrictions on transmitted powers and channel spacing in optical frequency-division multiplexed (FDM) systems [1, 2, 3], hence limiting their information capacity. As a result of FWM waves at different frequencies can interact causing an inter-channel cross-talk. The efficiency of FWM is strongly dependent on the difference of phase velocities (phase-mismatch) between the interacting waves [4]. Therefore, it will mainly play a role in dispersion shifted (DS) fibres and for densely spaced channels as are possible in coherent systems.

FWM can be manifested in power transfer between channels [5] as well as in phase distortions of the multiplexed signals [6]. Both these effects deteriorate signal detectability in coherent systems. An evaluation of the maximum total power transfer due to FWM for un-modulated channels has been done in Refs. 1 and 2. From this, the degradation of receiver sensitivity has been estimated [1]. However, signal detectability in FSK and PSK systems will also be strongly dependent on both phase and amplitude distortions over a time slot corresponding to an information bit. We have earlier modelled the transmission of phase-modulated FDM signals influenced by FWM and calculated the resulting phase and amplitude distortions at the end of a fibre for different system parameters [6].

In the present paper we, as before, use the nonlinear Schrödinger equation to simulate multichannel coherent transmission in a quasi-monochromatic approximation [5, 6], accounting for group velocity dispersion, linear loss, and four-wave mixing in the fibre. However, we extend the model by including a frequency-shift-keying (FSK) phase-diversity receiver [7]. Furthermore, we evaluate the probability density function (PDF) of the fibre noise. This enables us to express the effect of FWM in terms of signal-to-noise ratio (SNR) or bit error-ratio (BER) degradation of the received signal. We asses the validity of our model by comparisons with the BER results of the first experiment systematically investigating the effect of FWM on signal detectability in a 16-channel FDM system [2]. The simulations presented here are made for frequency modulated signals in which the frequency varies sinusoidally with time, simulating an infinite ...010101... bit stream in each channel.

The effect of FWM is strongly dependent of the phase relations of the interacting waves [5]. In order to find a realistic PDF for each physical configuration, we collected statistics from 660 runs with randomly chosen optical phase relations of the signal lasers as well as random time delays between the time slots of different channels. For DS fibres, the PDF could be well described by a Gaussian function, from which the BER was calculated. The effect of FWM on the BER will also be influenced by the choice of receiver [3].

We used the model to investigate the deleterious effect of FWM for different fibre lengths, transmitted powers, peak frequency deviations, bit-rates, and number of channels. Examples of our simulations and a comparison with the experiment [2] are given below.

Comparison to experiment

To test our numerical model we simulated the experiment of Ref. 2 (see Fig. 7 of Ref. 2). The input power per channel was 0.46 mW, and the peak frequency deviation (PFD) was 1.8 GHz. We deduced the basic noise level of the receiver from the BER-measurements made without transmission fibre in Ref. 2 (cf. Fig. 8 of Ref. 2). We need to fit only one parameter (the modal spot-size to a radius r of 5 μm) to obtain good agreement (Fig. 1) with the experimental curve describing BER in the presence of FWM in the transmission fibre.

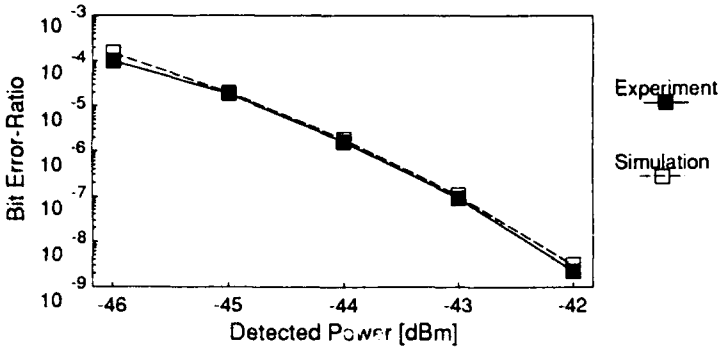

Fig. 1. Measured (solid squares) and simulated (empty squares) BER versus output power when the input power in the central of 16 channels was varied (attenuated). This corresponds to the middle curve in Fig. 8 of Ref. 2. (An attenuator was also used at the fibre output).

Numerical predictions for 16 channels in a DS fibre

The examples given here were all simulated for a 16-channel system in a DS fibre (D = -0.3 ps/km·nm at λ = 1.55 μm), with all channels modulated. The channel separation was 10 GHz. All channels carried the same power. The modal field was approximated by a Gaussian with r = 5 μm. Signal degradation was evaluated for channel number 7 (close to the centre of the total spectrum). The SNR values are given in the electrical domain at the output of the receiver.

In Fig. 2a, we show how noise, generated in the fibre, builds up along the fibre and degrades the SNR for different values of the channel input power. The SNR decreases when higher powers are used, showing the fibre nonlinearity plays a substantial role in the build-up of noise.

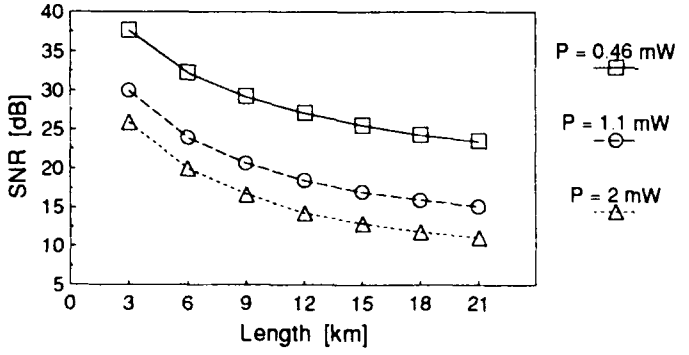

Fig. 2a. Degradation of the SNR due to fibre properties as a function of fibre length for different values of input power/channel P. Bit-rate 155 Mbit/s, PFD 1.8 GHz

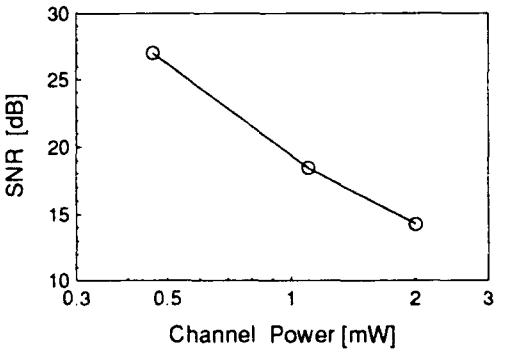

Fig. 2b. SNR as in Fig. 2a but plotted as a function of input power/channel P for a 12 km long fibre.

To closer examine the power dependence, we plot SNR vs. channel power for a 12 km long fibre in Fig. 2b. We found the slope of the SNR vs. P in dB to vary between -2.2 and -1.6 in the power range we examined with the receiver we used for these simulations.

We have also simulated degradation of the received signal for different values of the PFD. Higher PFD implies that the signal is less sensitive to distortions. Moreover, for larger PFD the power of a channel is distributed over a broader spectral range resulting in a lower spectral power density. Since FWM is a nonlinear process its efficiency, and hence the resulting signal distortions, are reduced. Therefore, as expected, signal degradation in the fibre decreases with increasing PFD. The maximum fibre length for which the bit-error-ratio due to fibre noise does not exceed 10^{-9} is plotted as a function of PDF in Fig. 3.

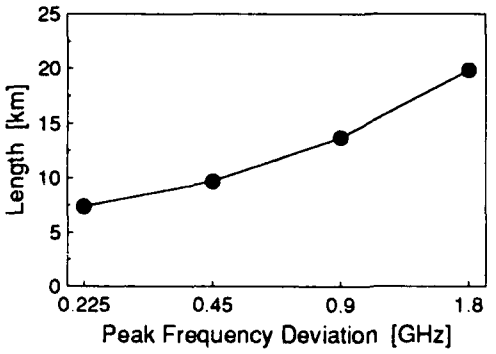

Fig. 3. Fibre length for which the BER resulting from fibre noise reaches 10^{-9} vs. peak frequency deviation. The power was 1.1 mW/channel, and the bit-rate was 155 Mbit/s.

In Fig. 4, we show the length dependence of the received signal degradation for different bit-rates. The output signal was low-pass filtered with a bandwidth proportional to the channel bit-rate (1.5 times the bit-rate). Therefore, in general, for higher bit-rates where the filter bandwidth is larger more noise is collected and the SNR decreases. The relative decrease of SNR with increasing bit-rate is plotted with in Fig. 5. The solid line corresponds to the case of a constant white noise level. We can see that for the simulated fibre noise (dashed and dotted lines) the decrease of SNR is slower. This can be mainly attributed to the reduction of the FWM-induced noise density in the fibre. For higher bit-rates the spectral power density decreases due to the broadening of the channel spectra, thus the efficiency of FWM drops.

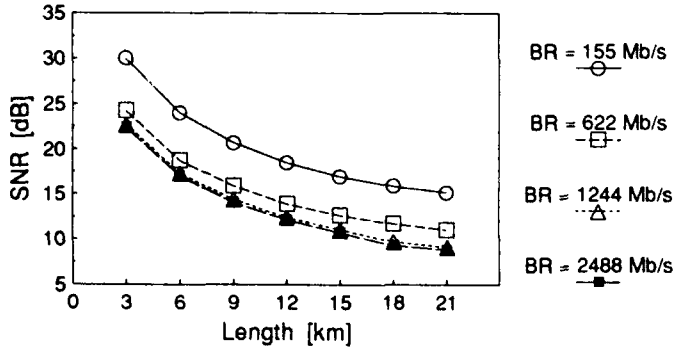

Fig. 4. Signal degradation vs. fibre length for different bit-rates (BR). Power 1.1 mW/channel, PFD 1.8 GHz.

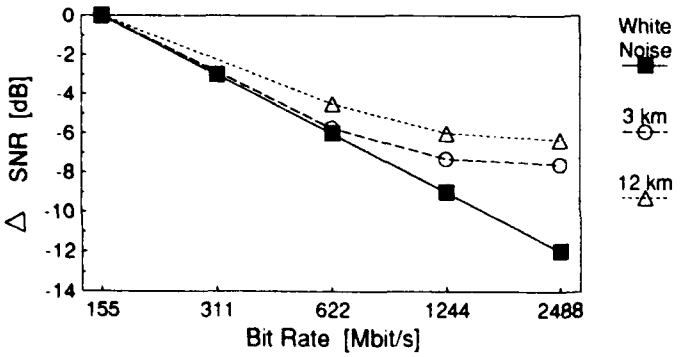

Fig. 5. Decrease Δ SNR of signal-to-noise ratio with increasing bit-rate for different fibre lengths. The solid line shows the behaviour due to the low-pass filter only, assuming a bit-rate independent white noise.

Conclusions

We modelled transmission affected by FWM in an optical fibre and coherent detection of frequency multiplexed FSK signals. We also calculated the probability density function (PDF) of fibre noise and the corresponding signal-to-noise ratios (SNR) and the bit error-ratios. We simulated the transmission and the resulting SNR degradation for various fibre lengths, transmitted powers, peak frequency deviations (PFD), bit-rates, and number of channels (not showed in this summary).

* We found the statistical properties of the FWM-induced noise to be well described by a Gaussian PDF for DS fibres.
* We showed that the model based on the quasi-monochromatic approximation of multichannel transmission and the Gaussian fit of the PDF gives results that are in a good agreement with the experiment reported in [2].
* SNR degradation predicted by the model for DS fibres is strongly dependent on the transmitted power, confirming the significance of the fibre nonlinearity in the build-up of noise.
* The dependence of SNR degradation on transmitted optical power was found to have a slope (using logarithmic scales) varying between -2.2 and -1.6 in the range 0.46 to 2.0 mW
* The rate of change of SNR with increasing bit-rate is slower than what can be attributed to the effect of increased bandwidth of the low-pass filter only. This can be explained by a reduction of the FWM-induced noise level as a result of channel spectra broadening for higher bit-rates.

We believe that the model presented here can be a helpful tool when designing high-power multichannel systems.

References

1. N. Shibata, Y. Azuma, and K. Nosu, "A consideration on single-mode fibers for frequency-division-multiplexing transmission systems", Proc. of IEEE GLOBECOM '89, Dallas, TX, 1989.
2. M. W. Maeda, W. B. Sessa, W. I. Way, A. Yi-Yan, L. Curtis, R. Spicer, and R. I. Laming, "The effect of four-wave mixing in fibers on optical frequency-division multiplexed systems", J. Lightwave Technol. vol. LT-8, pp. 1402-1408, 1990.
3. K. Inoue and H. Toba, "Error-rate degradation due to fiber four-wave mixing in four-channel fsk direct-detection transmission", IEEE Photonics Technol. Lett., vol. 3, pp. 77-79, 1991.
4. N. Shibata, R. P. Braun, and R. G. Waarts, "Phase-mismatch dependence of efficiency of wave generation through four-wave mixing in a single-mode optical fiber", IEEE J. Quantum Electron., vol. QE-23, pp. 1205-1210, 1987.
5. E. Lichtman, A. A. Friesem, R. G. Waarts, and H. H. Yaffe, "Exact solution of four-wave mixing of copropagating light beams in a Kerr medium", J. Opt. Soc. Am. B 4, 1801-1805, 1987
6. D. Schadt, D. Neveux, and B. Jaskorzynska, "Phase and intensity distortion induced by four wave mixing in multichannel coherent systems,", Proc. ECOC '89, vol. 1, TuP-7, pp. 470-473, Gothenburg, Sweden 1989.
7. R. Noe, W. B. Sessa, R. Welter, and L. G. Kazowsky, "New fsk phase-diversity receiver in a 150 Mbit/s coherent optical transmission system", Electron. Lett., vol. 24, pp. 567-568, 1988.

Poster Session: 2

MF 5:30pm–7:00pm
Castlereagh Room

Mixed states of optical solitons on different carrying frequencies.

L.M.Kovachev

Institute of Electronics, Bulgarian Academy of Sciences

Bulgaria,Sofia,1784,bull Lenin,72,tel:74311(653).

1. Introduction.

Investigating the nonlinear interactiors of the picosecond optical pulses with different frequencies in monomode optical fiber, one must take into consideration both linear effects, the dispersion and the group delay between waves. Besides, some additional nonlinear effects, as cross-phase modulation (CPM), four-photon parametric mixing (FPM), Raman amplifier (RA), appears. For optical pulses with soliton's powers as a rule, the group delay dominates among all other effects. Nevertheless there are some important cases, when it is possible to compensate group delay trough the nonlinear mechanisms.

2.Basic equations.

We assume that the slow-varying amplitudes of electric field for group packets satisfied the following relations between the carrying frequencies and wave numbers: $2\omega_3=\omega_1+\omega_2$; $2K_3-K_1-K_2=\Delta K$. In dimensionless coordinate system connected with the pump A_3, having in mind the Raman amplifications for picosecond pulses are obtained the next coupled equations [4]:

$$i\left(\frac{\partial A_1}{\partial z}+\frac{1}{v_1}\frac{\partial A_1}{\partial t}\right)=-\frac{1}{2}D_1\frac{\partial^2 A_1}{\partial t^2}+R_1\left(|A_1|^2A_1+2|A_2|^2A_1+2\alpha_1|A_3|^2A_1+\right.$$
$$\left.+\alpha_1^*A_3^2A_2^*\exp(i\Delta Kz)\right)$$
$$i\left(\frac{\partial A_2}{\partial z}+\frac{1}{v_2}\frac{\partial A_2}{\partial t}\right)=-\frac{1}{2}D_2\frac{\partial^2 A_2}{\partial t^2}+R_2\left(|A_2|^2A_2+2|A_1|^2A_2+2\alpha_2^*|A_3|^2A_2+\right.$$

$$+\alpha_2 A_3^2 A_1^* \exp(i\Delta K z)\Big) \qquad 2.1)$$

$$i\frac{\partial A_3}{\partial z}=-\frac{1}{2}\frac{\partial^2 A_3}{\partial t^2}+R_3\left(|A_3|^2A_3+2\alpha_3^*|A_1|^2A_3+2\alpha_3|A_2|^2A_3+2A_1A_2A_3^*\exp(-i\Delta K z)\right)$$

$$\alpha_i=\left(1+ig\frac{\omega_i}{\omega_3 R_i}\right);\ 1/v_i=\left(\frac{1}{u_i}-\frac{1}{u_3}\right)\tau/K_3''\ ;\ z=z;\ t=(t-z/u_3)/\tau\ ;\ A_i=A_i/A_3;$$

$$z=z/z_d;\quad R_i=z_d/z_i^{nl};\quad z_d=\tau_o^2/k_3'';\quad z_i^{nl}=n_2k_i|A_3|^2/2n_i;\quad D_i=k_i''/k_3''.$$

3. Influence of CPM ($\alpha_i=1$; $A_3=0$).

After the reduction, $\alpha_i=1$ and $A_3=0$, the system 2.4) is transformed to the NLS of two equations for two wave packets on different carrying frequencies. Equations for velocity and acceleration of center of weight of each wave τ_i and center of weight of the superposition of the packets $\bar{\tau}$ are derived in [1]. There are the next equations for nonlinear force $\ddot{\tau}_i(z,\Delta t)$ and potential $U_i(z,\Delta t)$ [2]:

$$\frac{\partial^2\tau_i}{\partial z^2}=\ddot{\tau}_i(z,\Delta t)=D_i\frac{R_i}{N_i}\int_{-\infty}^{\infty}|A_i(z,t+\Delta t)|^2\frac{\partial}{\partial t}\left(|A_j\ z,t\ |^2\right)dt \qquad 3.1)$$

$$U_i(z,\Delta t)-U_i(z,0)=\int_0^{\Delta t}\ddot{\tau}_i(z,dt)dt. \qquad i\neq j \qquad 3.2)$$

where N_i is the number of photons on each wave; Δt is distance between center of weight of the waves.Fig.1,2 shows the graphics of $\ddot{T}_2(\Delta t)$ and $U_{eff}(\Delta t)$ for one color soliton which does not change their shapes when passed one to another ($1/v\gg1$). If $\Delta\lambda'$ is spectral width of the wave packets, $\Delta\lambda''$ is spectral distance between pulses, it is obtained for the normalized group delay:

$$1/v=\tau_o/uK_2''\cong 0.27\ n_o\ \Delta\lambda''/\Delta\lambda' \qquad (n_o=1.43) \qquad 3.3)$$

The relations 3.3) determined a spectral bandwidth for self-confinement of solitons using the conditions $U_M>\frac{2}{(v)^2}$.

5. Influence of SPM and FPM (α=1).

Using the method of moments in [3] it is shown that the exchange of energy between the waves influence on their relative movement. For symmetrical multiplication $M=|A_1||A_2||A_3|^2$, there are an additional invariant:

$$\frac{d}{dz}\left(N_i\tau_i \right)= \frac{N_i}{v_i} +D_iP_i \qquad 4.1)$$

In the case when $1/v_i \cong D_i \cong 0$, i.e approximation of strong field, there are: $N_i\tau_i$=const. These equations give an additional criterion for self-confinement of the solitary like wave packets due to the exchange of energy between them during FPM.

6. Influence of the Raman resonance .

Fig 3.shows the evolution of the amplitudes of the pulses for parametric asymptotically *free soliton solutions* of the system 2.1) with small group delay between waves 1/v=1.5. As result it is obtained two different amplitudes and energies level for the signal waves and an asymmetrical mixed states of wave packets.

7. Discussion.

The numerical experiments and the calculations show, that all these effects of self-confinement between soliton like pulses in the case of wave synchronism, are possible for small group delay between waves: $1/v_1-1/v_2 \leq 5$. Taking into account the relations in &4. this leads to a spectral bandwidth for self confinement: $\Delta\lambda'' \leq 15\Delta\lambda'$, where $\Delta\lambda''$ is the spectral distance between A_1 and A_2. The condition shows that the waves are well spectrally separated. Thus this effect may be seen in a usual monomode optical fiber.

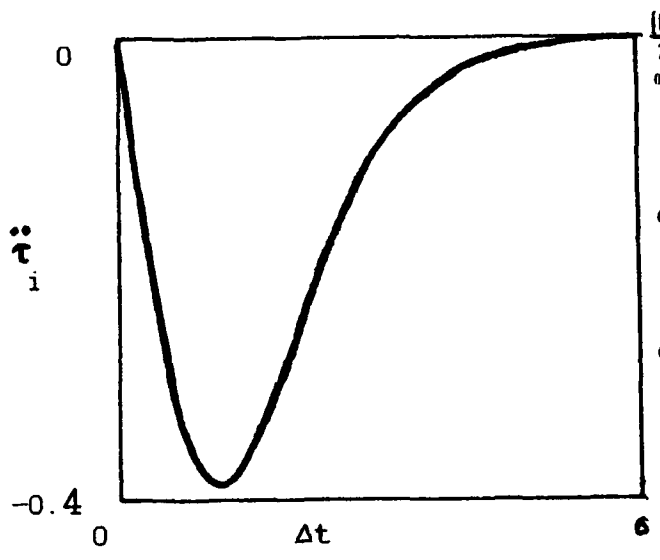

Fig.1.Effective force $\ddot{\tau}_i$ (Δt) for the soliton interaction.

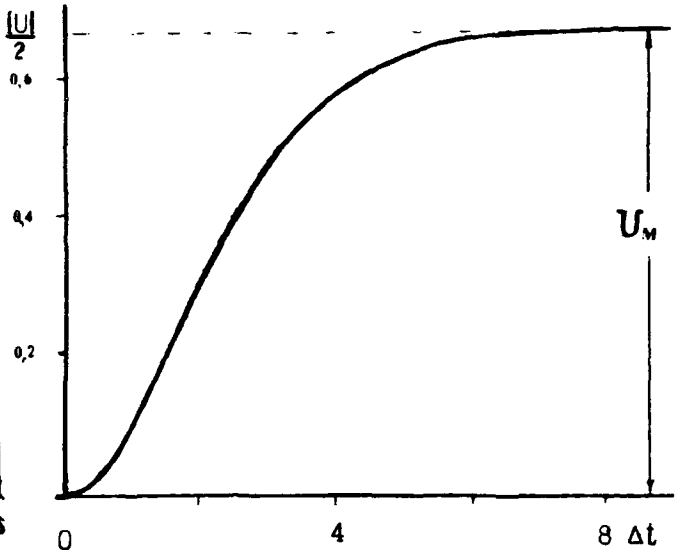

Fig.2.Effective potential $U(\Delta t)$ of $\ddot{\tau}$ (Δt) due to the CPM.

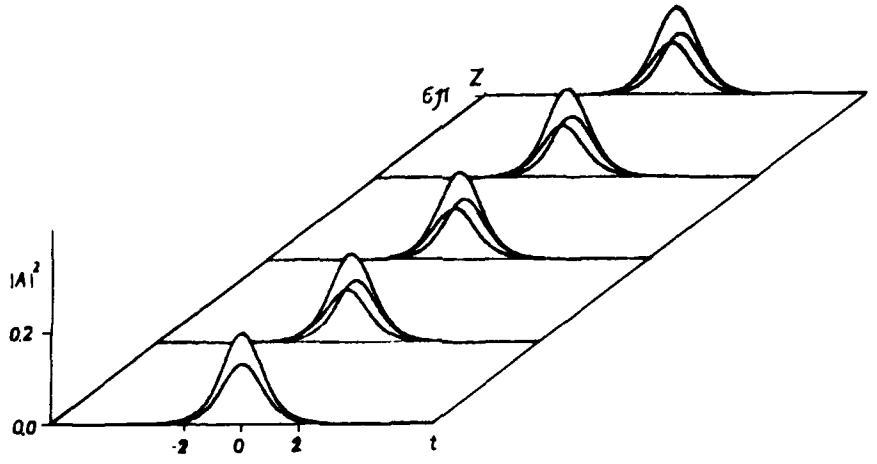

Fig.4. Evolution of the pulses in dynamics of system 2.1) for initial condition of the kind: $A_1(0,t)=A_2(0,t)=\sqrt{2/15}$ sech(t); $A_3(0,t)=\sqrt{1/5}$ sech(t); and $1/v=1.5$; $R_1=R_2=D_1=1$

R E F E R N C E S :

1.B.Grosignani,A.Cutolo .P.Di Porto JOSA 1982,72.9,p.1136.

2.V.V.Afanas'ev,L.M.Kovachev,V.N.Cerkin,Lett.JTP,16,14, 10(1990).

3.L.M.Kovachev,I.M.Uzunov.Jour.of Mod.Opt.,37,9,1453(1990).

4.L.M.Kovachev,Opt.and QE,21,429(1989).

PULSE PROPAGATION IN NONLINEAR OPTICAL FIBRES WITH SPATIAL INHOMOGENEITIES

E. Ryder, D.F. Parker and A.P. Mayer

Department of Mathematics, University of Edinburgh,
King's Buildings, Edinburgh EH9 3JZ, Scotland,
Tel. ++44 31 650 5049

1. INTRODUCTION

The propagation of envelope pulses in nonlinear optical fibres with carrier wave frequency in the monomode regime is described by a pair of nonlinearly coupled nonlinear Schrödinger equations (NLS) [1]. They can be derived from Maxwell's equations

$$\nabla\times\underset{\sim}{E} + \mu_0\dot{\underset{\sim}{H}} = 0 \ , \quad \nabla\times\underset{\sim}{H} - \dot{\underset{\sim}{D}} = 0 \quad \text{with} \quad \underset{\sim}{D} = \epsilon\underset{\sim}{E} + N|\underset{\sim}{E}|^2\underset{\sim}{E} \qquad (1.1)$$

using the technique of multiple scales [2]. In this derivation, the material properties of the fibre, i.e. the linear permittivity ϵ/ϵ_0 and the Kerr coefficient N, were taken to depend only on the radial coordinate r but not on the coordinate along the fibre axis. In this presentation, we consider gradual variations of these quantities along the fibre occuring on length scales larger than the wavelength of the carrier wave. Evolution equations are derived for the amplitudes of local fibre modes. In the derivation procedure, two stretched scales arise in a natural way, the scale on which pulse evolution takes place and an intermediate scale. Variations of ϵ and N on both scales are considered. Two cases are treated: Axisymmetric variations without limitation of magnitude and small deviations of the linear refractive index from axisymmetry giving rise to local birefringence.

Although the system of two coupled NLS equations is not integrable for realistic material coefficients even in the absence of birefringence and variations of material properties, it possesses solitary pulse solutions [3]. The scattering of such solitary wave solutions at a localised inhomogeneity of the system giving rise to a localised variation in certain coefficients of the evolution equations is investigated numerically.

2. EVOLUTION EQUATIONS WITH VARYING COEFFICIENTS

Following the method of multiple scales, we expand the electric field with respect to a small parameter ν,

$$\underset{\sim}{E} = \sum_{n=1}^{\infty} \nu^n \underset{\sim}{E}_n \tag{2.1}$$

and introduce stretched coordinates $Z_n=\nu^n z$, $T_n=\nu^n t$. ε and N depend on r and Z_m with m=1 or m=2. The field $\underset{\sim}{E}_1$ is then of the form

$$\underset{\sim}{E}_1 = e^{i\Psi} \sum_{\sigma=\pm} \underset{\sim}{E}_{\pm}(r,\theta,Z_m)\, A_\sigma(Z_1,T_1,Z_2,T_2,..) \ , \tag{2.2.}$$

where $\underset{\sim}{E}_{\pm}$ are orthogonal local modal fields of circular polarisation corresponding to the dielectric constant $\varepsilon(r,Z_m)$. The phase Ψ is connected with the frequency ω and local propagation constant $k(Z_m,\omega)$ via

$$\Psi = \nu^{-m} \int k(Z_m,\omega)\, dZ_m - \omega t \ . \tag{2.3}$$

The local propagation constant k itself is determined from the local dispersion relation with Z_m treated as a parameter. Considering the equations of second and third order in ν and making use of compatibility conditions for the resulting linear inhomogeneous field equations, as in [2], the following evolution equations for the amplitudes $A_{\pm}$ are obtained in the case m=2:

$$i\frac{\partial}{\partial Z_2} A_{\pm} = g(Z_2)\frac{\partial^2}{\partial \chi^2} A_{\pm} + \{f_1(Z_2)|A_{\pm}|^2 + f_2(Z_2)|A_{\mp}|^2\}A_{\pm} \ . \tag{2.4}$$

The retarded time χ depends on the local group slowness $S_g(Z_m,\omega)=\partial k/\partial\omega$ of the linear fibre modes,

$$\chi = T_1 - \nu^{1-m} \int S_g(Z_m,\omega)\, dZ_m \ . \tag{2.5}$$

The coefficients f_1 and f_2 in this pair of coupled NLS equations are connected with the local modal fields and the Kerr coefficient, which are now Z_2-dependent, in the same way as their counterparts in fibres that are homogeneous along the z-direction [2]. This is also the case for the dispersion coefficient $g(Z_2)$, if the local modal fields $\underset{\sim}{E}_{\pm}$ are normalised such that their associated energy flux is independent of Z_m.

If m=1, ε and N vary rapidly on the length scale of pulse evolution. We now make the additional assumption that these variations are periodic with a repetition length ℓ short on the scale of Z_2. Decomposing $A_{\pm}(Z_1,Z_2,..)=B_{\pm}(Z_2,..)+\nu b_{\pm}(Z_1,Z_2,..)$, it is found that the slowly varying part $B_{\pm}$ satisfies a pair of coupled NLS equations of the form (2.4) with,

however, constant coefficients, and the $b_\pm$ are bounded functions of Z_1. In addition, a linear term of the form $cB_\pm$ may appear associated with a change in phase velocity. Explicit expressions for the coefficients are given in the form of averages over a period ℓ.

With the same method that led to the evolution equations (2.4), the case is treated, in which the dielectric constant contains a small perturbation that varies gradually along the fibre and breaks the axial symmetry, $\varepsilon=\varepsilon_1(r)+\varepsilon_2(r,\theta,Z_2)$, while N is independent of z. If ε_2 is of second order in ν, we obtain the evolution equations

$$i\frac{\partial}{\partial Z_2}A_\pm = d_0(Z_2)A_\pm + d_\pm(Z_2)A_\mp + g\frac{\partial^2}{\partial\chi^2}A_\pm + \{f_1|A_\pm|^2 + f_2|A_\mp|^2\}A_\pm \ , \qquad (2.6)$$

where d_0 is real and the complex function $d_+=d_-^*$ is proportional to the overlap integral of ε_2 with $\underset{\sim}{E}_+^*\cdot\underset{\sim}{E}_-$. If ε_2 is of order ν, the following equations are obtained

$$i\frac{\partial}{\partial Z_2}B_\pm = p_\pm(Z_2)B_\pm + im_\pm(Z_2)\frac{\partial}{\partial\chi}B_\pm + g\frac{\partial^2}{\partial\chi^2}B_\pm + \{\tfrac{1}{2}(f_1+f_2)|B_\pm|^2 + f_1|B_\mp|^2\}B_\pm \qquad (2.7)$$

with four real functions $p_\pm$ and $m_\pm$ affecting phase and group velocity of the fibre modes, while the other coefficients in (2.7) are independent of Z_2. The amplitudes $B_\pm$ are connected to the $A_\pm$ through a unitary transformation which depends on an intermediate length scale and accounts for rapid changes of phase and polarisation.

3. PULSE EVOLUTION IN THE PRESENCE OF LOCALISED IRREGULARITIES

The coupled NLS equations (2.4) have, in the case of constant coefficients, solitary wave solutions of the form

$$A_\pm(\chi,Z_2) = \exp(-i\beta_\pm Z_2)\ F_\pm(\chi) \qquad (3.1)$$

with $F_\pm(\chi)$ being real functions that vanish exponentially for $\chi\to\pm\infty$ [3]. They are generalisations of vector solitons in the integrable system $f_1=f_2$ [4]. A special case is $F_+(\chi)\sim\mathrm{sech}\chi$, $F_-(\chi)=0$. The evolution of a pulse initially of this form, governed by equs. (2.6), is studied numerically with D=1, $f_1=1$, $f_2=2$, $d_0=0$, $d_+=i\mathrm{Sexp}\{-(Z_2-Z_2^0)^2/w^2\}$. The numerical results suggest that after passing the birefringent irregularity, the pulse is predominantly a solitary wave solution of the form (3.1) of altered polarisation, with small superimposed oscillations. For the integrable

case $f_2=f_1$ ([4], maxima of $|A_\pm|$ for Sw=0.2 shown dashed in figure) the final state is a vector soliton depending only on Sw. Otherwise, the final state can depend strongly on both S and w, as shown below for $f_2=2f_1$ and Sw=0.2: w=0.1 (solid), w=1.6 (dotted). For sufficiently large width w of the irregularity, the pulse regains its initial polarisation, a behaviour that can be understood in the framework of soliton perturbation theory.

Besides pulses of approximate sech-form, equs. (2.4) with constant coefficients possess a variety of solitary wave solutions with Z_2-dependence (3.1) for which analytic expressions can be given in the integrable case $f_1=f_2$ [5,6]. By allowing the cross polarisation to vary gradually with Z_2, we investigate to what extent solutions of the integrable system may be transformed adiabatically into corresponding solitary wave solutions for systems with $f_1 \neq f_2$.

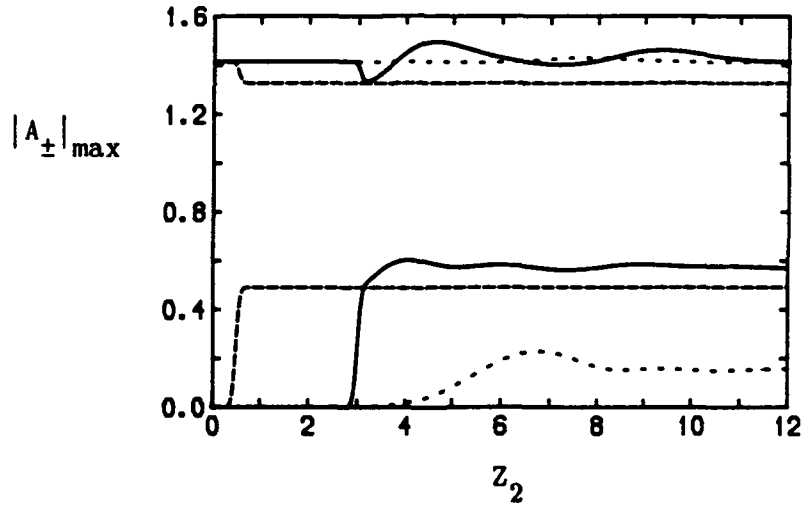

REFERENCES

1. G.P. Agrawal, "Nonlinear Fiber Optics", (Academic Press 1989), and references therein.
2. G.K. Newboult, D.F. Parker and T.R. Faulkner, J. Math. Phys. 30, 930 (1989).
3. D.F. Parker and G.K. Newboult, J. Phys. Colloq. 50, C3-137 (1989).
4. S.V. Manakov, Zh. Eksp. Teor. Fiz. 65, 505 (1973) [Sov. Phys. - JETP 38, 248 (1974)].
5. D.N. Christodoulides and R.I. Joseph, Opt. Lett. 13, 53 (1988).
6. M.V. Tratnik and J.E. Sipe, Phys. Rev. A 38, 2011 (1988).

Interactions between Solitons in a Monomode Fiber

Boris A. Malomed
P.P. Shirshov Institute for Oceanology of the USSR Academy of Sciences, 23 Krasikov Street, Moscow, 117259, USSR; phone (7-095) 124-7565

In the present work, pairwise interactions between solitons are considered in two models of a nonlinear monomode fiber. The first model is the simplest one to describe the competition between losses and gain in the fiber [1]:

$$iu_z + u_{tt} + 2|u|^2 u = i\gamma_0 u + i\gamma_1 u_{tt}. \quad (1)$$

The second model takes account of the intrapulse Raman scattering [2] :

$$iu_z + u_{tt} + 2|u|^2 u = -\epsilon u(|u|^2)_t . \quad (2)$$

Eqs.(1) and (2) are written in the standard notation [1,2] . The objective of our analysis of the model based on Eq.(1) is to investigate a possibility of existence of a bound state of two solitons separated by a temporal delay which is much larger than the widths of the solitons. For the model (2), the aim is to develop analysis of a collision between two solitons in the case when the frequency difference between them is much larger than their inverse widths. The approach to both models is based on the perturbation theory for the nonlinear Schrödinger (NS) solitons. The unperturbed soliton is taken in the form

$$u_{sol} = 2\eta\, \mathrm{sech}(2\eta(t + \Omega z)) \exp(-(i/2)\Omega t + 4i\eta^2 z - (i/4)\Omega^2 z), \quad (3)$$

where η and Ω are its inverse temporal width and frequency shift. As is known [3], the model (1) admits solitary-pulse solutions, that in the case $\gamma_1 \ll 1$ are close to the soliton (3) with $\Omega = 0$ and with

$$\eta^2 = 3\gamma_1/4\gamma_0 . \quad (4)$$

Using the exact solution for the pulse [3] or a perturbative expansion, one can see that in the case $\gamma_1 \ll 1$ the pulse has the form

$$u_{sol} = 2\eta\, \mathrm{sech}(2\eta\,(t - t_0)) \exp(4i\eta^2 z - ig|t - t_0| + i\phi_0), \quad (5)$$

where the phase constants t_0 and ϕ_0 have been introduced, and the small frequency

$$g = (4/3)\gamma_1\eta \equiv (2/3)\sqrt{3\gamma_1\gamma_0} \quad (6)$$

is generated by the terms on the right-hand side of Eq.(1). The term $g|t - t_0|$ in the pulse's phase will play a crucial role in the subsequent analysis. Let us consider the interaction between two solitons with a large temporal separation $T \equiv t_0^{(1)} - t_0^{(2)}$ between them,

$$\eta T \gg 1, \quad (7)$$

and with some phase difference $\phi \equiv \phi_0^{(1)} - \phi_0^{(2)}$. Following the known approach to the analysis of interaction between slightly overlapping solitons [4], we insert the linear superposition of the two solitons,

$$u(t,z) = u_{sol}^{(1)}(t,z) + u_{sol}^{(2)}(t,z), \tag{8}$$

into the potential term

$$H_{int} = -\int_{-\infty}^{+\infty} dt\, |u(t)|^4 \tag{9}$$

of the full Hamiltonian of the NS system, which accounts for the interaction between solitons. Thus we arrive at the effective potential of the soliton-soliton interaction, that is dominated by the contributions to the integral (9) from two regions where each soliton is overlapped with an exponentially weak "tail" of another soliton. At the leading order, the interaction Hamiltonian can be linearized with respect to the tail. So the effective potential is

$$U = -4\int_{-\infty}^{+\infty} dt |u_1(t)|^2 \mathrm{Re}(u_1(t)u_2^*(t)) + (1 \rightleftarrows 2), \tag{10}$$

where $u_1(t)$ is the soliton's wave form (5) with $t_0 = 0$ and $\phi_0 = 0$, and $u_2(t)$ is the asymptotic "tail" of the same wave form with $t_0 = T$ and $\phi_0 = \phi$:

$$u_1(t) = 2\eta \exp(4i\eta^2 z - 2\eta |t - T| - ig|t - T| + i\phi) . \tag{11}$$

Finally, inserting Eqs.(5) and (11) into Eq.(10) yields

$$U = -256\,\eta^3 \exp(-2\eta T)\cos\phi \cdot \cos(gT) . \tag{12}$$

Apart from the last multiplier, Eq.(12) coincides with the known expression [4] for the effective potential of the soliton-soliton interaction in the unperturbed NS equation. However, the last multiplier induces a drastic difference: It generates local minima of the potential, which are absent in the unperturbed case. The minima are located at

$$T = T_n \equiv (2n + 1)\pi/2g, \quad n = 0,1,2,\ldots , \tag{13}$$

$$\sin\phi = 0, \quad (-1)^n \cdot \cos\phi < 0 . \tag{14}$$

As it follows from the definition of g (Eq.(6)) and from the underlying assumption $\gamma_1 \ll 1$, the inequality (7) is satisfied at the points (13), i.e., the approximation employed is self-consistent. The minima of the potential correspond to locally stable bound states of the solitons. However, inserting Eqs.(13) and (14) into Eq.(12), one notices that the corresponding "binding energies"

$$-U(T=T_n) = 128g\eta^2 \exp(-(2n + 1)\pi\eta/g) = (512/3)\eta^3\gamma_1 \exp(-(2n +1)(3\pi/4\gamma_1) \tag{15}$$

are exponentially small, so that the stability of the bound states is very weak. Thus the bound states found by means of the perturbative analysis prove to be very feeble. One may expect that in a model with larger loss and gain coefficients they may be more robust. This issue requires numerical simulations. Anyway, a casual formation of bound sates may be very detrimental for operation of soliton-based fiber communication lines, so the detailed analysis of those states seems to be a worthwhile problem.

Let us proceed to the collision between solitons in the model (2). Recently, this problem was solved numerically in Ref.5. Here it will be solved analytically under the assumption

$$\Omega \gg \eta_1, \eta_2, \tag{16}$$

where η_1 and η_2 are the inverse widths of the colliding solitons, and $\Omega \equiv \eta_1 - \eta_2$ is their relative frequency (see Eq.(3)). From the general perturbation-theory analysis [6] it is known that, under the condition (16), the full wave form of the colliding solitons may be approximated by the same ansatz (8) that was employed above to analyze the interaction between the slightly overlapping solitons, although this time they are tightly overlapped during the collision. Next, we make use of the well-known relation between the soliton's energy,

$$E \equiv \int_{-\infty}^{+\infty} dt\, |u(t)|^2 , \tag{17}$$

and its inverse temporal width η:

$$E_{sol} = 4\eta . \tag{18}$$

So, for the first soliton we have the following expression for the perturbation-induced rate of change of its amplitude during the collision:

$$\frac{d\eta_1}{dz} = (1/4)\frac{d}{dz}E^{(1)}_{sol} \equiv (i/4)\epsilon \int_{-\infty}^{+\infty} dt\, u^{(1)}_{sol} u(|u|^2)_t + \text{c.c.} . \tag{19}$$

Inserting Eq.(8) into Eq,(19), one notes that the integrand becomes a sum of several terms. Analyzing contributions of these terms from the viewpoint of dependence on the large parameters $\Omega / \eta_{1,2}$ (see Eq.(16)), one concludes that the dominant term is that $\sim u^{(1)}_{sol} u^{(2)}_{sol} (u^{(2)}_{sol})^*_t$. Keeping it, one finally finds the collision-induced change of the soliton's amplitude as follows:

$$\delta\eta_1 \equiv \int_{-\infty}^{+\infty} dz \frac{d\eta_1}{dz} = -4\epsilon\eta_1\eta_2 \operatorname{sgn}\Omega . \tag{20}$$

Similarly, for the second soliton one obtains $\delta\eta_2 = -\delta\eta_1$. The latter relation complies with the fact that the total energy (17) remains the exact integral of motion of the model (2) (see the relation (18) between the energy and amplitude of the soliton). To compare the analytical result (20) with the numerical findings of Ref.5, note that, in the present notation, the simulations performed in Ref.5 corresponded to $\eta_1 = \eta_2 = 1/2$; in this case

Eq.(20) yields $|\delta\eta|/\eta = 2\epsilon$, which exactly coincides with the empiric formula extracted in Ref.5 from the numerical data for the case when the inequality (16) holds. Thus the soliton-soliton collision in the presence of the intrapulse Raman effect gives rise to the transfer of energy from the less downshifted soliton to the more downshifted one [5]. In the next approximation in ϵ, radiative losses of energy appear. They have been analyzed, under the same assumption (16), in Ref.7. The final expression for the collision-induced radiative losses of the soliton's amplitudes is [7]

$$\delta_{rad}\eta_{1,2} = -4\epsilon^2\eta_{1,2}\eta_{2,1}^2 \ .$$

In conclusion, let us note that another important perturbing term in the NS model of the monomode fiber may be the one taking account of the third dispersion [8]. In the presence of this term, the collision remains elastic in the first approximation. In the second approximation, the radiative losses have been recently analyzed in Ref.9. At last, if the third dispersion is added to the model (1), one can demonstrate that the existence and stability of the two-soliton bound states are not affected.

References

1. K.J. Blow, N.J. Doran, and D. Wood, Opt. Lett. **12**, 1011 (1987).
2. J.P. Gordon, Opt. Lett. **11**, 662 (1986); Y. Kodama and A. Hasegawa, IEEE J. Quant. Electron. **QE-23**, 510 (1987).
3. N.R. Pereira and L. Stenflo, Phys. Fluids **20**, 1733 (1977).
4. V.I. Karpman and V.V. Solov'ev, Physica **D3**, 487 (1981).
5. S. Chi and S. Wen, Opt. Lett. **14**, 1216 (1989).
6. B.A. Malomed, Physica **D15**, 374 (1985).
7. B.A. Malomed, Phys. Rev. **A41**, 4538 (1990).
8. P.K. Wai, C.R. Menyuk, Y.C. Lee, and H.H. Chen, Opt. Lett. **11**, 464 (1986).
9. B.A. Malomed, Phys. Rev. **A43**, 3114 (1991).

Cross-phase-modulation-induced nonelastic collisions of optical solitons.

A. Höök, M. Lisak, and D. Anderson,
Institute for Electromagnetic Field Theory, Chalmers University of Technology
S-412 96 Gothenburg, Sweden. Telephone: 46 31 721568

V. N. Serkin
Institute for General Physics, Academy of Sciences of the USSR
38 Vavilova Street, 117333 Moscow, USSR. Telephone: 7095 132 8306

Introduction. A new class of problems has recently appeared; nonelastic interaction of solitons at different polarization states or different wavelengths. Recently[1] it was predicted that the so-called effects of shadows should appear in the process of collisions between solitons in birefringent fibres. The same behaviour is observed in computer simulations of NLSE solitons at different wavelengths in single-mode fibres[2].

The purpose of this paper is to clarify the interaction dynamics of two colliding NLSE solitons. Using rough analytical methods together with numerical simulations the conditions for symbiotic soliton pair generation are studied.

Problem. The equations of motions for the incoherently coupled waves, assuming well-separated spectra can be taken as[3]:

$$i\frac{\partial u}{\partial z}+\frac{1}{2}\frac{\partial^2 u}{\partial t^2}+(|u|^2+2|v|^2)u=+iG|v|^2u \tag{1a}$$

$$i\frac{\partial v}{\partial z}+\frac{1}{2}\frac{\partial^2 v}{\partial t^2}+(|v|^2+2|u|^2)v=-iG|u|^2v \tag{1b}$$

where G is the normalized coefficient stimulated Raman scattering. First of all we consider the case G=0. Then we construct the Lagrangian of system 1:

$$L=L_u+L_v+L_{uv} \tag{2}$$

where

$$L_u=\frac{i}{2}\left(u\frac{\partial u^*}{\partial z}-u^*\frac{\partial u}{\partial z}\right)+\frac{1}{2}\left|\frac{\partial u}{\partial t}\right|^2-\frac{1}{2}|u|^4 \tag{3a}$$

$$L_v=\frac{i}{2}\left(v\frac{\partial v^*}{\partial z}-v^*\frac{\partial v}{\partial z}\right)+\frac{1}{2}\left|\frac{\partial v}{\partial t}\right|^2-\frac{1}{2}|v|^4 \tag{3b}$$

$$L_{uv}=-2|u|^2|v|^2 \tag{3c}$$

We now consider a rigid-body interaction between two pulses, i.e we assume that the waves will retain the shape of e.g. NLSE-solitons during the collision:

$$u=\eta_1\,\mathrm{sech}(\eta_1(t-vz))\exp\left(\frac{i}{2}(\eta_1^2-v^2)z+ivt\right) \tag{4a}$$

$$v=\eta_2\,\mathrm{sech}(\eta_2(t+vz))\exp\left(\frac{i}{2}(\eta_2^2-v^2)z-ivt\right) \tag{4b}$$

Substituting (4) into (3) and integrating the Lagrangian (2) over time one can obtain the variational equations for the soliton parameters[4]. As hinted, we assume that $\eta_1 = \eta_2 = \eta$. First we consider the case of two initially overlapping NLSE solitons and disregard the fact that the soliton form (4) is not an exact solution of the coupled NLSE's (1) around z = 0. One obtains that this state is bounded provided that the initial relative velocity is lower than a critical velocity, $v^2_{crit} = 4\eta/3$, which means that split-up should occur for v > 1.155.

If we compare with computer simulations we see that pulses are bound for initial velocities less than 1.05. This bound state is oscillative, which also is the case for the variational solutions; frictionless bouncing in a potential well[4]. However, it is also radiative; it looses energy by emitting dispersive waves. Above v = 1.05 the state splits in such a way that each of the pulses are splitted into two. The amplitudes of the splitted pulses will not be equal unless the initial velocity is increased to 1.13; the velocity at which symbiotic solitons thus may be formed, see Fig.1! Increasing the initial velocity beyond this value, the resulting amplitudes again become unequal.

If starting with well separated NLSE-solitons aimed towards each other, the general result is that one part of each pulse will continue and one part will be "reflected", or better, caught by the continuing part of the other wave. Generally, the two parts will have different amplitudes, but for a certain collision velocity, v = 0.16, the splitted amplitudes are all equal and a symbiotic state may again be formed; see Fig.2!

In this particular case the collision process is preferrably discussed in terms of the Hamiltonian corresponding to system (1). Denoting the initial velocity of each NLSE soliton by v' and the velocity of each symbiotic state by v", one obtains the relation $(v")^2 = (v')^2 + 2.5/6$. From the numerical solution, Fig.2, we see, however, that the process rather fulfils $(v")^2 = (v')^2 + 1.0/6$, i.e. the final 'kinetic energy' is lowered since part of the free energy is consumed by dispersive radiation and an oscillatory excitation of the bound symbiotic states. This simple form also suggests the existence of a reversed 'cut-off', i.e. the bound states will separate with a finite velocity even for zero initial velocity. The Hamiltonian approach also predicts the qualitative outcome if the initial NLSE solitons overlap initially. The new condition above then takes the form $(v")^2 = (v')^2 + 2.5/6 - X$, X > 0 where X represents the overlap integral in the Hamiltonian. Consequently, the final velocity of the separating bound states decreases. At higher relative velocity, v > 1.0, no trapping occurs and the particles pass through each other unaffected.

We have also investigated incoherent collisions in the presence of stimulated Raman scattering. When adding a small amount of SRS (e.g. G=0.04) to the collision in Fig.2 the pulse splitting process will be unaffected. On a longer scale, however, the two pulses in the Stokes wave will grow under the action of the SRS effect.

Increasing the Raman effect by, say, a factor of 5, Stokes pulse splitting will still occur but all energy is momentarily transferred in the collision and the pump wave becomes immediately depleted. The velocities of the Stokes pulses also looses their relative symmetry as seen in Fig. 3

Retaining this higher gain (G=0.2) and increasing the velocity, v= 0.65, conceptually new features of the interaction process emerge. The forward part of the Stokes pulse becomes ordinarily amplified. However, a secondary Stokes pulse emerges suddenly after some distance of propagation, well separated from the primary Stokes pulse and travelling with a velocity equal to the velocity of the pump pulse, see Fig.4. This "virtual absence" relies on the fact that a part of the pump energy is not immediately consumed but continues with its initial velocity and captures, through cross-phase modulation, a tiny fraction of the Stokes pulse, a fraction that will be amplified on a longer scale. At this end of the parameter space, we see also that the primarily amplified Stokes pulse is considerably compressed.

Conclusions. In this work, inelastic collisions beteween incoherently coupled waves have been investigated. The cross-phase modulation mechanism is able to (i) create symbiotic soliton pairs in a pulse collision process. The same mechanism can (ii) induce asymmetric pulse splitting of Raman amplified solitons. Finally, we suggest that (iii) cross-phase-modulation dominated collisions can be used to selectively split components from higher order solitons or Hasegawa bound states[5].

These effects could be experimentally observed if the dispersion length is comparable to the walk-off length. For example, if the pulse duration is 100 fs then L_{disp} $L_{walk\text{-}off}$ 50 cm. The parameters appear to be experimentally reasonable for picosecond pulses in dispersion-flattened optical fibres having low dispersion over a relatively large wavelength, 1.3-1.6 μm.

References

1. C. R. Menyuk, J. Opt. Soc. Am. B, 5, 392 (1988)
2. V. V. Afanasyev, E. M. Dianov, and V. N. Serkin, IEEE J. Quantum Electron., 25, 2656 (1989)
3. V. A. Vysloukh and V. N. Serkin, JETP Lett., 38, 199 (1983)
4. M. Lisak, A.Höök, and D. Anderson, J. Opt. Soc. Am. B, 7, 810 (1990)
5. A. Hasegawa, Opt. Lett., 5, 416 (1980)

Figure Captions

Figure 1. Splitting of two initially overlapping NLSE solitons of which only one is displayed. Initial separation = 0. Initial velocity, v= 1.13. The process is shown for $0 < z < 30$. $-20 < t < 20$

Figure 2. Collision of two initially well separated NLSE solitons, of which only one is displayed. Note the formation of two pulses with equal amplitude. Initial separation = 5. Initial velocity, v = 0.16. The process is shown for $0 < z < 54$. $-20 < t < 20$

Figure 3. Collision of two initially well separated NLSE solitons under the influence of Raman amplification. Initial separation = 5. Initial velocity = 0.1. Raman gain, G = 0.2. The process is shown for $0 < z < 80$. $-20 < t < 20$

Figure 4. Collision of two initially well separated NLSE solitons under the influence of Raman amplification. Initial separation = 5. Initial velocity = 0.65. Raman gain, G = 0.2. The process is shown for $0 < z < 18$. $-20 < t < 20$

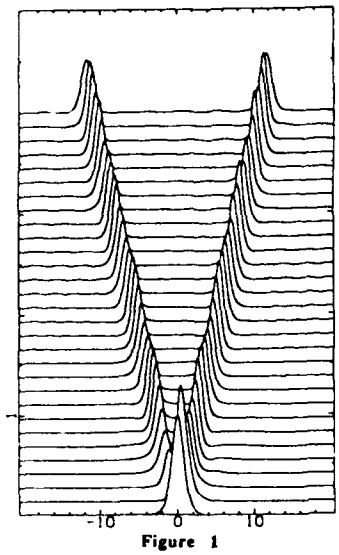

Figure 1

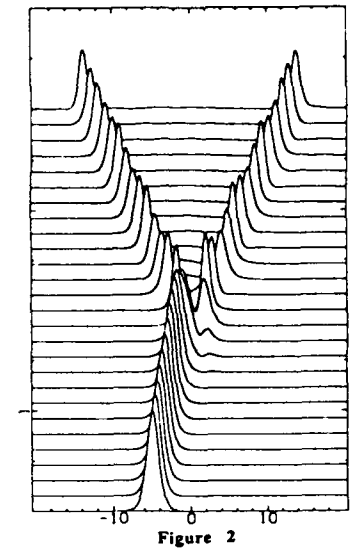

Figure 2

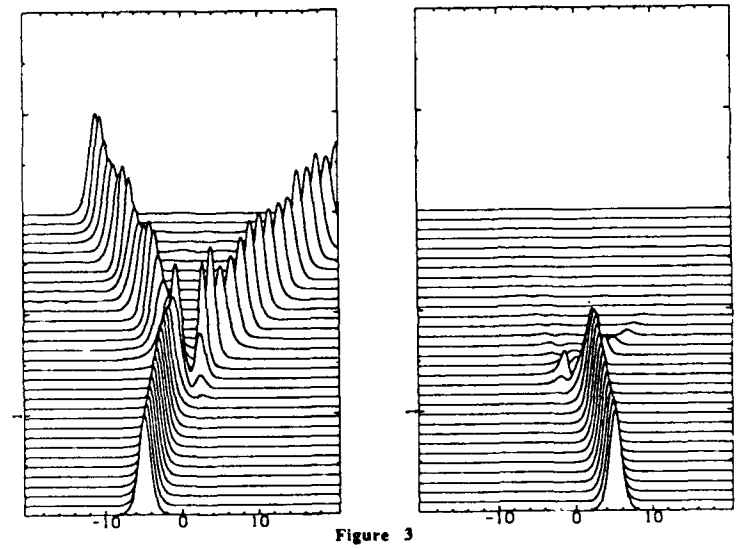

Figure 3

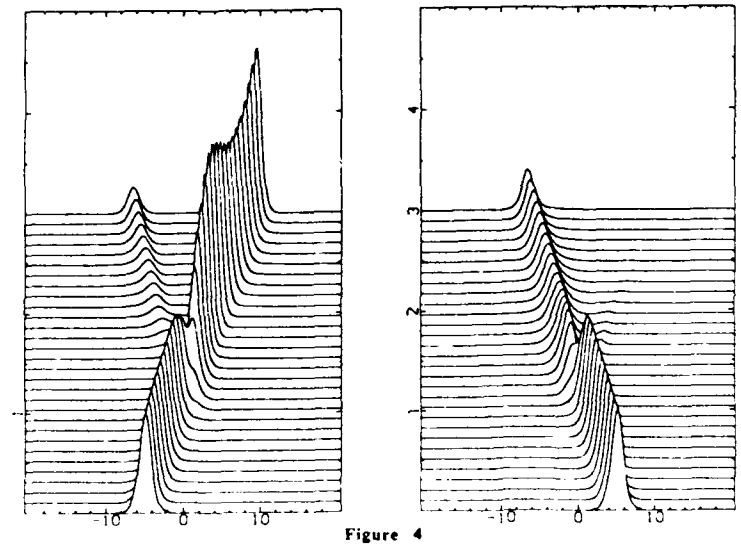

Figure 4

Erbium Fibre Soliton Laser Pumped by a Laser Diode

K. Smith, E.J. Greer,* R. Davey,** R. Wyatt, and N.J. Doran

British Telecom Research Laboratories, Martlesham Heath, Ipswich IP5 7RE, UK

* Laser Group, Physics Department, Imperial College, London SW7 2BZ

** Department of Physics, University of Strathclyde, Glasgow G4 ONG

Summary

We have recently reported on the generation of pulses as short as 1.2 ps from a mode-locked erbium fibre laser pumped by a frequency doubled Nd:YAG laser [1]. Experimental and theoretical evidence strongly supported the idea that soliton pulse shaping played a dominant role in the short pulse formation. In this paper, we review this earlier work and present preliminary data from a simple, compact totally integrated erbium fibre soliton laser pumped by a high-power laser diode.

The experimental arrangement of the fibre ring laser is shown in figure 1. As a pump source, we employed the output of a packaged/pigtailed GRINSCH InGaAsP MQW semiconductor laser [2]. The fibre pigtail of the MQW device was then spliced ("X" denotes a splice in figure 1) to fibre coupler C1, which permitted efficient coupling of the pump light into the 13 m long erbium fibre (Er). At the same time, C1 allowed the erbium emission to be coupled straight through to C2, which provided a 3 dB output coupling for the cavity. The fibre cavity was completed by an

integrated-optic lithium niobate phase modulator (PM) with a 3 GHz electrical bandwidth, insertion loss of ≈6 dB, and a switching voltage of ≈10 V [3]. Fibre polarisation controllers (PC) were also incorporated into the set-up in order to ensure correct polarisation of the light incident on the modulator.

Mode-locked operation was achieved by tuning the modulator drive frequency to a high harmonic of the fundamental cavity frequency. Figure 2(a) shows an autocorrelation trace of the counter-clockwise laser output recorded at an average (peak) power of 0.6 mW (≈0.3 W) and a repetition frequency of 810.6 MHz. An autocorrelation function of a 2.8 ps (FWHM) sech^2 intensity profile is an excellent fit to the experimental data as is clearly shown by the theoretical points depicted. The corresponding spectrum is shown in figure 2(b) from which a spectral width (FWHM) of 0.9 nm is measured. An inferred time-bandwidth product ($\Delta\tau\Delta\nu$) of 0.31 is also in excellent agreement with a sech^2 pulse shape. The measured temporal, spectral and power characteristics of the laser output are appropriate for fundamental solitons. In this work, drive frequencies were restricted to <1 GHz by the synthesiser/amplifier combination. However, the present configuration should be capable of generating soliton pulses at repetition frequencies ≈10 GHz. Further progress in this area will be reported.

References

[1] SMITH, K., ARMITAGE, J.R., WYATT, R., DORAN, N.J., and KELLY, S.M.J.: "Erbium Fibre Soliton Laser", *Electron. Lett.*, 1990, **26**, p. 1149

[2] COOPER, D.M., SELTZER, C.P., AYLETT, M., ELTON, D.J., HARLOW, M., WICKES, H., and MURRELL, D.L.: "High-Power 1.5μm All-MOVPE Buried Heterostructure Graded Index Separate Confinement Multiple Quantum Well Lasers", *Electron. Lett.*, 1989, **25**, p. 1635

[3] BT&D Technologies, Ltd. technical specifications.

Figure Captions

Figure 1: The experimental configuration of the Diode-Pumped Erbium Fibre Soliton Laser.

Figure 2: (a) Autocorrelation trace of 2.8 ps pulses obtained at a repetition frequency of 810.6 MHz (peak power $\approx$0.3 W) and (b) corresponding spectrum ($\Delta\nu$ = 111 GHz). The crosses in (a) represent the theoretical autocorrelation function of a 2.8 ps duration sech^2 intensity pulse.

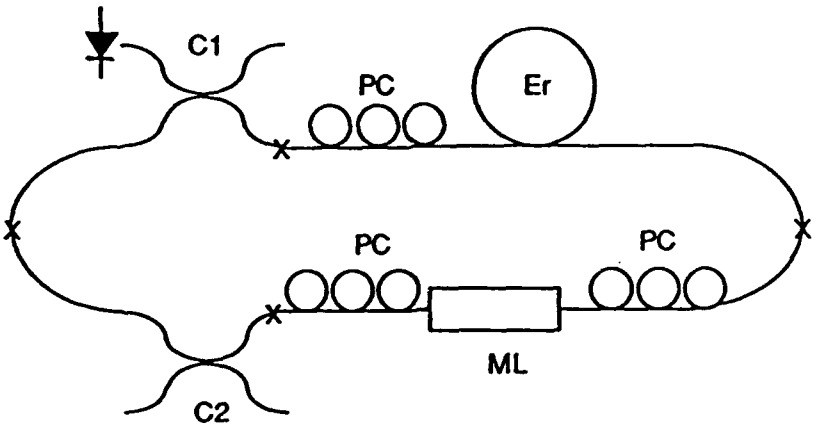

Figure 1

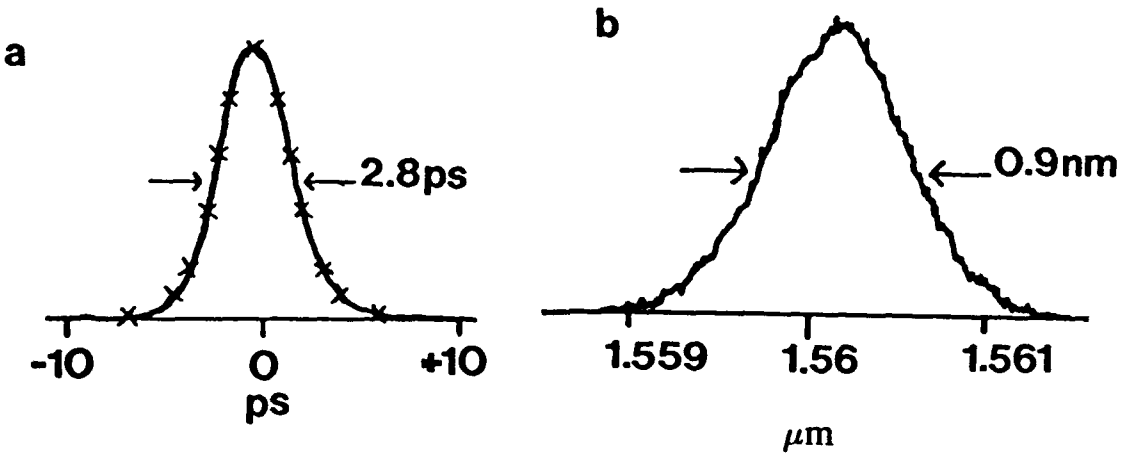

Figure 2

ULTRASHORT PULSE AMPLIFICATION IN ERBIUM-DOPED FIBRE AMPLIFIERS

D.V.Korobkin,Jr., I.Yu.Khrushchev, A.B.Grudinin, and E.M.Dianov

Optical Fibre Department,
General Physics Institute USSR Academy of Sciences,
Vavilov str. 38, 117942 , Moscow, USSR
Telephone:(095) 132-83-07

Erbium-doped optical fibres displaying broad gain bandwidth centred at the wavelength of minimum loss and negative group velocity dispersion make almost the ideal media for generation and amplification femtosecond range optical pulses. Several authors have studied both theoretically and experimentally the amplification of ultrashort pulses in such devices and have noted that not only resonant properties of fibre amplifier but also the Raman self-frequency shift are responsible for the net gain and pulse duration at the output of an amplifier[1-4].
The usual approach in a theoretical consideration treats resonant properties and Raman gain in a fibre amplifier independently, assuming similar nonlinear properties of rare-earth doped and undoped fibres. In this paper we present experimental results on Raman soliton amplification in an erbium fibre amplifier which indicate an influence of the erbium ions on the third order nonlinear susceptibility.

The basic experimental set up has been described elsewhere [2] and consisted of a mode-locked, Q-switched YAG laser which in combination with 100 m long ordinary fibre produced 80 fs Raman solitons in the region of 1.53μm. The erbium doped fibre was fusion spliced to the output end of the undoped fibre and was pumped with argon laser in a countertpropagating scheme.

Fig.1 shows autocorrelation traces of the output radiation at different pump power levels. The length of the fibre amplifier was 17 cm and the erbium ion concentration 1000 ppm. The shortest pulse duration was 34 fs. Spectra corresponding to 0.4 W and 2.3 W pump power are represented in Fig.2. The product of spectral width and correlation function width was 0.41 in each case. For $sech^2$-shape this value should be 0.49 indicating small shape distortion of the pulse during the amplification process. A small "blue" shift towards resonant gain centre was observed, indicating suppression the Raman self-frequency shift. However, such suppression is not stable and strongly depends on the amplifier length and pump level. Consequently it is impossible to keep an amplified femtosecond pulse under resonant gain curve, eventually it runs out of the gain bandwidth, that has been recently proved [2].

Since the shortest pulses obtained in the experiment were wider than predicted by the theory [3], the nonlinear properties of erbium-doped fibres have been studied in greater detail. For this purpose we firstly studied the stimulated Raman scattering process in a number of erbium-doped fibres with different rare-earth ion concentration. It has been found that with a 1.064 μm wavelength pump the Raman gain coefficient depends on the rare-earth ion concentration, decreasing with the growth of concentration of erbium ions. For example, in an erbium-doped fibre with concentration 75 ppm, Raman gain was approximately 40% less than in a comparable undoped fibre.

There is also slightly less Stokes component shift for doped fibres. Fig.3 represents spectra of second Stokes components in doped and undoped fibres with the same concentration germanium in the cores.

Similar experiments have been carried out with mode-locked and Q-switched YAP laser at 1.34 μm and pulsed chromium-erbium doped glass bulk laser at 1.54 μm and results will be reported on at the meeting.

Summary. We have studied the influence of Raman gain on amplification in erbium fibre amplifiers and have obtained pulses as short as 34 fs with shape slightly differ from a $sech^2$-form. The study of the Raman gain in erbium doped fibre have shown that resonant and Raman effects can not be considered as independent ones and that value of Raman gain in the doped fibre 40% less then in a comparable undoped fibre.

References.

1.M.Nakazawa, K.Kurokawa, H.Kibota, K.Suzuki, and Y.Kimura, Appl.Phys.Lett.57, 653, (1990)

2.A.B.Grudinin, E.M.Dianov, D.V.Korobkin,Jr., A.Yu.Makarenko, A.M.Prokhorov, and I.Yu.Khrushchev, JETP Lett.,51,135,(1990)

3.V.V.Afanas'ev, E.M.Dianov, A.M Prokhorov, V.N.Serkin, Sov.J.Pis'ma v Zhurnal Tech. Fiziki 16(18), 67, (1990).

4.G.P.Agraval, Opt. Lett. 16, 226, (1990).

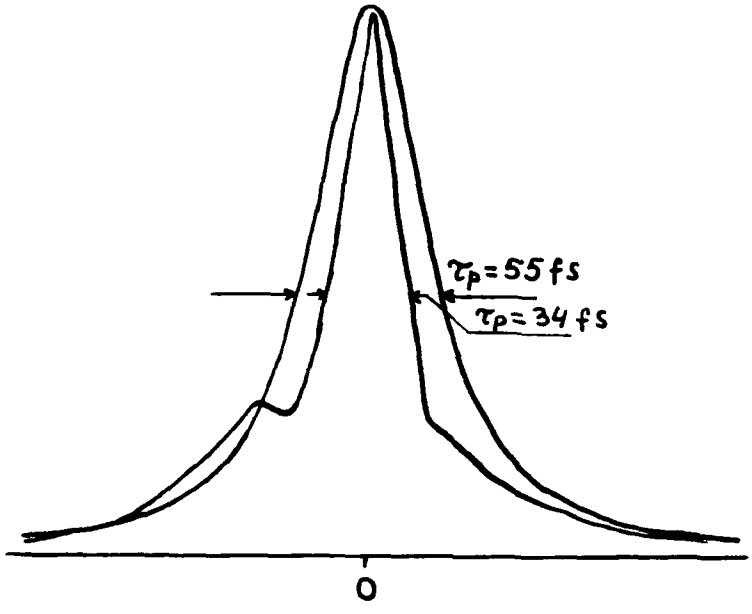

Fig.1 Autocorrelation traces of the output radiation at 1.54 μm. τ_p=34 fs corresponds to 2.3 W pump power, 55 fs- to 0.4 W.

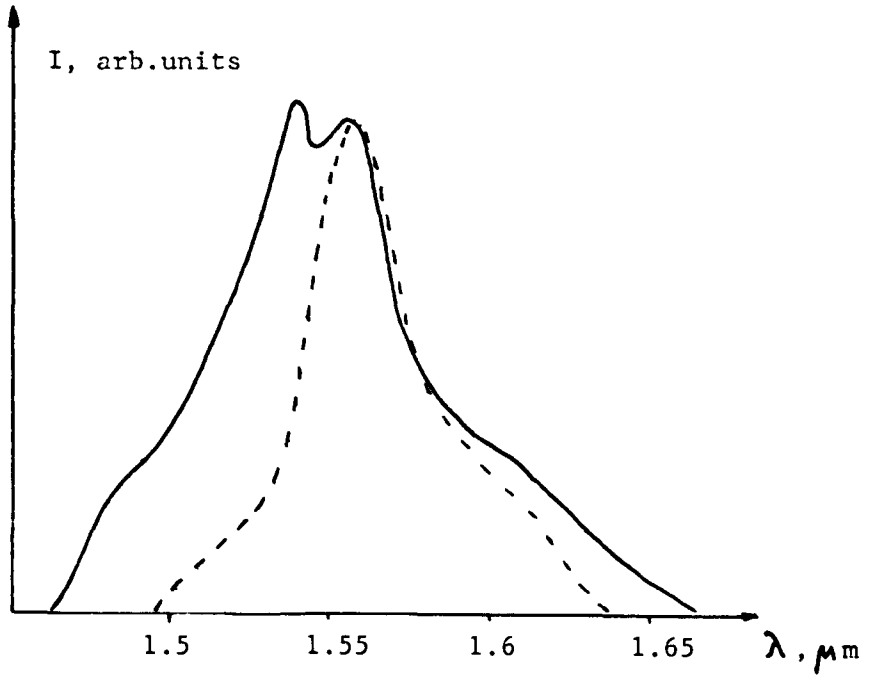

Fig.2 Spectra of amplified radiation. Pump power 2.3 W-solid line
0.4 W-dashed line

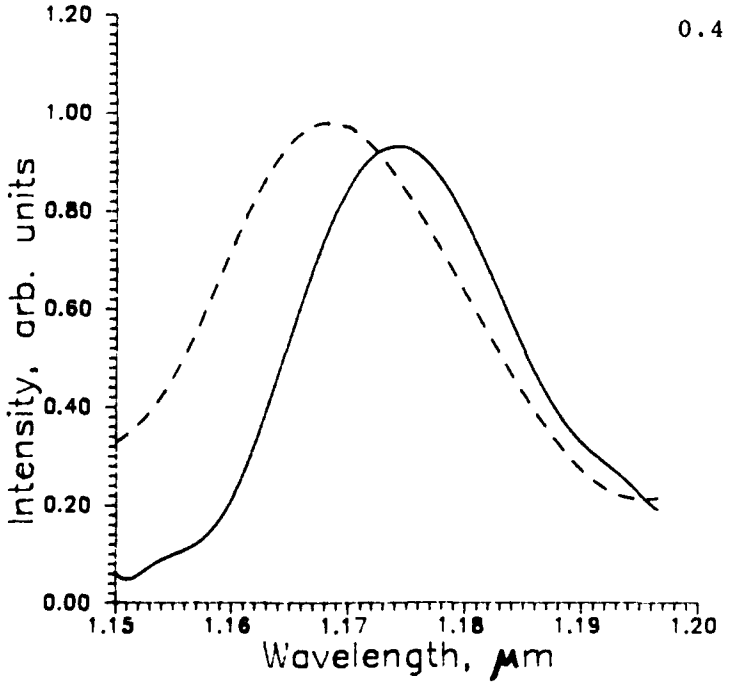

Fig.3 Spectra of second Stokes components.

Undoped fibre-solid line, doped fiber (700 ppm) -dashed line.

Poster Session: 3

MG 5:30pm–7:00pm
Boys Smith Room

PROPOSAL OF HIGH CAPACITY ALL OPTICAL TDMA NETWORKS

F. Matera, M. Romagnoli, M. Settembre, M. Tamburrini
Fondazione Ugo Bordoni, via B. Castiglione 59, 00142 Roma, ITALY

Abstract. Two scheme of all optical TDMA networks are proposed with the demultiplexed processing obtained by means of an optical gate based on the second harmonic generation process. The maximum throughput is obtained when solitons are used and is equal to 125 Gb/s.

Introduction. One of the techniques to access to a network is the Time Division Multiple Access (TDMA). Such a tecnique offers a good chance to obtain high throughput, in particular when a direct time multiplexing of optical pulses is used. TDMA is compatible with passive star network structures whereby the optical pulse frame is distributed to all users. Optical network experiments based on TDMA have shown a limitation of the throughput (10 Gb/s) because of the electrical contribution in the demultiplexing process [1]. In this work we present two complete schemes of all optical TDMA in a metropolitan area network (MAN) with a distance between each user and the central star of 10 km, and a dispersion shifted fiber with a chromatic dispersion of 1 ps/nm/km (1.3 ps^2/km) for two different regimes of pulse propagation: a) low power pulses travelling along the fiber and amplified at the gate input, b) optical solitons. The demultiplexed process is obtained by means of an AND optical gate based on a parametric two photon process, such a scheme overcomes the electronic bottleneck of the demultiplexing operation and it does not require very high input energy; in particular for a pulsewidth of 1 ps the minimum required energy content is 1 pJ. In the a) case the maximum throughput shows an upper limit of about 40 Gb/s, for 64 users at 622 Mb/s each, caused by the chromatic dispersion, while in case b) the throughput, essentially limited by the Stimulated Raman Scattering (SRS), is 125 Gb/s.

Optical gate. The bottleneck for high bit-rating in a TDMA based system is the demultiplexing process because of the speed limitations imposed by the detection electronics (10 Gb/s). The device that acts as a temporal demultiplexer is generally intented as an AND optical logic gate which, for a practical use, must fulfill the necessary requirements of high speed, energy efficiency, phase and polarization insensitivity and large extinction ratio. A variety of optical gates have been proposed but most of them satisfy partially the above requirements. For Kerr optical gates [2] pulse breaking up leads to a low extinction ratios. Such a problem may be overcome by exploiting the particle-like nature of solitons which allows a complete pulse switching as the pulse were an optical bit [3]. Unfortunately all the optical gates, until now demonstrated, present an energy switching larger than 1 pJ.

On the other hand, starting from the consideration that in an optical telecommunication network the demultiplexing process is localized at the user, a gate with an optical input and an electrical output can be considered sufficient. Starting from this point we think to use an optical gate based on the well-known phenomenon of the Second Harmonic Generation (SHG). In a SHG process two fields, at the fundamental frequency ω, E_1 and E_2, interact istantaneously in a non linear crystal generating a third field E_3 at the frequency 2ω. E_3 is generated only when E_1 and E_2 are simultaneously present, viceversa when only one field is present no signal is generated; therefore this provides an AND logic operation with the maximum on-off ratio.

When the depletion of the input fields is negligible the generated SH signal is proportional to the pair of the incoming signals through the power relation $P_3 = \Gamma P_1 P_2$, where P_1 and P_2 are the input power of the fields at the fundamental frequency, P_3 is the SH power and Γ is a constant that depends on the crystal characteristics.

With the SH gate most of the initial requirements for a good performance of the device may be accomplished although a polarization fluctuation may dramatically affect the amplitude of the generated SH signal; to obtain a gate insensitive to the input state of polarization the optical

scheme of fig.1, based on the polarization component separation followed by a suitable recombination in four nonlinear crystals, may be adopted [4].

Considering a KTP crystal, it can be verified that, for two equal input gaussian pulses with duration τ=1 ps, the input energy has to be about 1 pJ.

Pulse propagation in optical fibers. For the realization of high capacity networks the fiber limitations have to be taken into account; in particular in the regime of low power pulses the maximum bit-rate carried by a single channel is established by the chromatic dispersion [5].

On the contrary when the pulses propagate in the wavelength region of anomalous dispersion (negative group velocity), the nonlinear effect of Self Phase Modulation (SPM) can effectively reduce the dispersive pulse broadening and, for a known value of group velocity dispersion, this depends on the power of the pulse and on the input time width. When the nonlinearity compensates exactly the chromatic dispersion, pulse with a particular shape can propagate in the fiber without changing such a shape. This scenario corresponds to the evolution of the soliton. Because of this property, solitons seem particularly useful for optical communication. Unfortunately some problem limits their application and the main are losses, nonlinear interaction and Stimulated Raman Scattering (SRS).

Fiber losses can induce amplitude attenuation which is followed by a temporal readjustment that for soliton propagation results in a pulse broadening. The soliton pulses present a mutual interaction that can be neglected when the distance between two adjacent pulses is larger than eight times the width τ.

The SRS effect induces a continuous downshift of the pulse center frequency and as a result SRS produces a variable delay depending on pump power fluctuations [5].

The amplifier saturation may constitute another potential limit in the throughput of an optical communication system; for erbium doped fiber amplifiers (EDFA) the output saturation power level is around 100÷200 mW that for soliton transmission states a bit rate upper limit of 100÷200 Gb/s.

Proposal of the all-optical TDMA networks. In the all optical network that we propose in this section, the distance between user and central station is 10 km, the chromatic dispersion β_2 is 1.3 ps^2/km, the nonlinear coefficient $\gamma=\omega_0 n_2/(cA_{eff})$ (where n_2 is the nonlinear index, A_{eff} the effective core area, c the vacuum velocity and ω_0 the central frequency) is 4 rad/W/km and each user has an optical gate based on SHG. Two regimes of pulse propagations are considered: a) low energy pulses and b) optical solitons. In the a) case, low energy pulses (0.035 pJ) propagate through the network and are amplified before the optical gate to obtain the requested gating energy. According to the curves of fig. 4, when pulses with τ=10 ps and a power lower than 3.2 mW propagate in the fiber with the value of group velocity dispersion mentioned above, the condition to obtain a soliton is far away to be satisfied; a small compression of the pulse can be observed but in general may be considered a case of linear propagation. In this framework, considering an user bit-rate of 622 Mb/s, 64 users can simultaneously access the network. In the b) case, solitons propagate in the network and the requirement is that the power level must be kept constant. By means of the solitons, an higher bit-rate is possible allowing the network to have 200 users simultaneously communicating at the bit-rate of 622 Mb/s with a total throughput of 125 Gb/s. In particular the parameters determining this soliton regime are the pulse time duration τ = 1 ps, the energy W = 1.1 pJ, the peak power P = 1.0 W and a maximum average power P_{ave}= 140 mW.

A centralized laser distributes to all users a frame of pulses at 622 Mb/s (fig. 2); this frame could be obtained using a color center laser at the repetition frequency of 78 MHz, followed by four directional couplers at 3 dB and fiber optic delay lines, in such a way each pulse is splitted in eight output pulses with a loss deriving from the splitting of 3 dB. At the output of the divider an energy of 2.8 pJ for each splitted pulse is assumed [6]. Considering then the star sharing among 200 users (it is obtained using a part of the input-output of a 256x256 star coupler), the reduction of transmitted energy, considering also the coupler insertion losses, is 25 dB (19 dB for 64 users). In case a) at the star output the pulses present an energy of 0.035 pJ with a peak power of 3.2 mW. In case b), to obtain the requested energy and time width, optical amplifiers (A_0) for the soliton restoration are requested. Each user has two systems of

Ti:$LiNbO_3$ electrooptic 2x2 switches (S) with delay lines (DL), one for the transmission (D_T) that shifts the frame to the assigned time slot and the other for the reception (D_R) (fig. 3). The switching time of the electrooptic switches is of the order of the nanosecond. The transmitted signal is modulated by an intensity modulator (M) at the bit-rate of 622 Mb/s. The amplifier A_T compensates the loss of the fiber (2 dB), of the coupler C (3 dB), of D_T (3 dB) and of the modulator M (1 dB). A_R compensate the loss of C, of the fiber (2 dB), of D_R (3 dB), for the variable delay line L_R (1 dB) and provides the necessary power for the demultiplexing gate. The modulated signal reaches, through the fiber, the central node (figs.2 and 4) where all the signals are time multiplexed by the 256x256 star coupler #1 and the resulting signal is amplified to compensate couplers and fiber losses. Considering that, in the a) case, the star coupler loss is 19 dB, the fiber loss is 2 dB and 1 dB for the device L_R, that is used to synchronize the signals as we will explain later, the gain of the amplifier A_1 must be set at 22 dB (28 dB in the b) case). At the output of the amplifier the pulse is diveded into two equal parts, one of which, by means a coupler, is sent to a system to check the frame and the other to the star #2 to distribute the signal to all users. Another group of amplifiers (A_2) whose gain is set at 28 dB in b) case and 22 dB in a) case is located at the star output in order to compensate both the loss of the star coupler #2 and coupler (3 dB). The receiver is composed by an optical AND based on SHG with relative PIN FET photodiode. At the gate input the signal at high bit-rate from the central station and the strobe composed by pulses, at 622 Mb/s suitably delayed by D_R, are present. In the a) case an amplifier A_3 is necessary to obtain the requested gate energy. We set the A_3 gain equal to 20 dB in such a way that at the input gate the pulses present an energy of 2.2 pJ (the maximum average power is about 100 mW). Since for pulses of τ=10 ps the product W_1W_2 has to be larger than 10 pJ^2 [4], the gain of A_R must be set at 30 dB. In case b) the product W_1W_2 has to be larger than 1 pJ^2 [4] and indeed 11 dB of gain for A_R suffices.

Since very short pulses are used, a variety of time varying effects can disturb the synchronization of the signals. The current technology allows the source to mantain the time jitter below 1 ps [7]. For slowly varying effects the synchronization check among the users can be obtained in the central station by a system that has the same structure of a user.

Periodically each user can organize a self-synchronization operation which consists in sending its own pulses in an assigned time slot; the check system obtains the synchronization adjusting the delay line L_R. The frame, during the propagation after the check system, does not change its shape but can be shifted requiring a synchronization process in the reception. This process is made by the user that periodically sends pulses in the time slot of its own receiver and the synchronization is obtained by means of L_R that is located at the user station.

A system contained in the frame control checks also the amplification levels of A_1 and A_2's because in these amplifiers the power levels depend on the load of the network.

Conclusion. In this work we have shown that improving the gating process and choicing a suitable pulse propagation regime the overall throughput of telecommunication network may be raised by one orders of magnitude. In particular a novel optical gate based on Second Harmonic Generation, working with low energy and short pulse has been included in a scheme of optical TDMA network working in the regime of minimum pulse broadening. The resulting maximum throughput of 125 Gb/s can be obtained.

References.

1) P. R. Prucnal, D. J. Blumenthal, M. A. Santoro, Elect. Lett. Vol. 23 No 12, 1987, pp. 629-630.
2) S. Trillo, S. Wabnitz, J. Opt. Soc. Am. B Vol. 5 No 2, 1988, pp. 483-488.
3) C. E. Socchich, M. N. Islam, J. R. Sauer, Procs. of Photonic Switching, 6-8 March 1991, Usa pp. 136-139.
4) M. Romagnoli, F. Matera, M. Settembre and M. Tamburrini, Proceedings of the FOTONICA '91, Sirmione ITALY, 19-21 March 1991.
5) D. Wood, J. of Ligthwave Technology, Vol. 4 No 7, 1990, pp. 1097-1106.
6) M. Nagazawa, K. Suzuki, Y. Kimura, Optics Letters, Vol. 14 No 19, 1989, pp. 1065-1067.
7) A. J Taylor, J. M. Wiessenfeld, G. Eisenstein, R. S. Tucker, Appl. Phys. Lett. Vol. 49, N° 12, 1986 pp. 681-683.

Acknowledgment. Work carried out in the framework of the agreement between Fo. dazione Ugo Bordoni and the Italian PT administration and under the partial financial support of the National Research Council (CNR) in the frame of the Telecommunication Project.

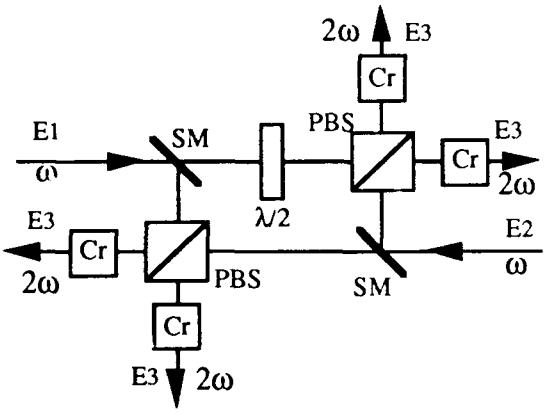

Fig. 1: Scheme of the polarization insensitive optical AND, PBS polarization beam splitter, SM semi reflecting mirror.

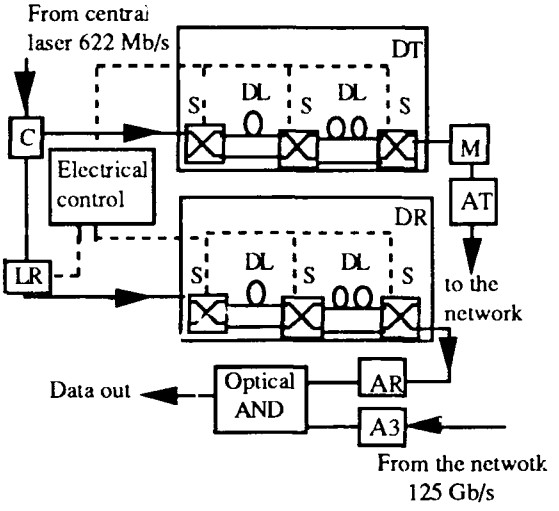

Fig. 3: scheme of an user station, A_T, A_R and A_3 optical amplifiers, C coupler, M intensity modulator, S optical switch, L_R delay line, dot line represents the electrical signal. A_3 is only present in a) case.

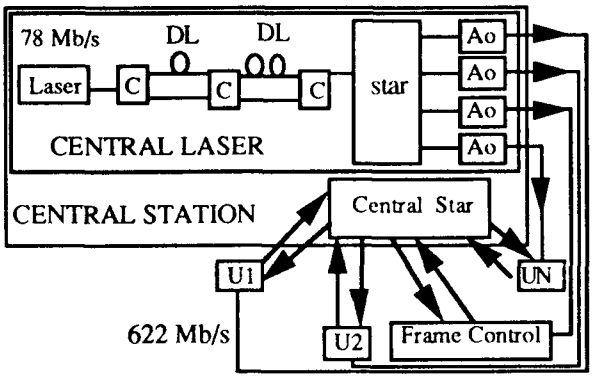

Fig. 2: Scheme of an all TDMA passive star network, C coupler, DL delay line, A amplifier.

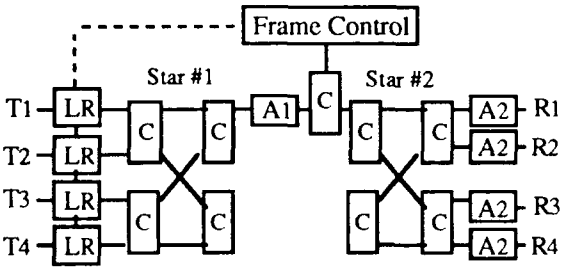

Fig. 4: scheme of the central node, A optical amplifiers, C coupler, T transmitters, R receivers, LR delay lines.

OPTICAL FIBER TRANSMISSION SCHEME WITH ULTRA-HIGH BIT-RATE CAPABILITY.

by
G. R. BOYER
M. A. FRANCO
M. K. JACKSON
and
A. MYSYROWICZ

Laboratoire d'Optique appliquée, Ecole Polytechnique-
Ecole Nationale Supérieure de Techniques Avancées,
Centre de l'Yvette, Chemin de la Hunière, 91120 Palaiseau, France.
Telephone (33-1) 60 10 03 18

Abstract : An optical fiber transmission scheme with 500 Gbit/s rate is demonstrated experimentally. Limitations of the system due to optical nonlinearities are observed and discussed.

Using present technology, optical pulses with duration ~ 50 fs are routinely obtained. It has already been demonstrated that such short pulses can propagate as stable solitons through long distance fibers, provided that the central pulse wavelength corresponds to an anomalous dispersion region of the fiber. Thus, in principal, a bit-rate of 5 THz can be envisioned. In practice, the bit-rate of such a transmission system is limited by soliton-soliton interactions, and by the pulse peak power which must be kept below the damage threshold. Since the soliton peak power obeys an inverse square law with respect to its time duration, the combined action of soliton-soliton interactions and maximum soliton intensity limit the transmission rate to a maximum value of the order of 500 Gbit/s.

It is interesting to consider transmission schemes that can operate in the normal dispersion region. However, in this case, normal dispersion is not compensated by self-phase modulation, leading to a rapid increase of the pulse duration. The recent development of pulse chirping techniques makes it possible to circumvent this difficulty in the following way. Femtosecond pulses are stretched before launching them in a fiber, then recompressed at the output of the fiber. Stretching causes a significant reduction in the peak intensity in the fiber, thereby reducing self-phase modulation and other nonlinear effects. In this way, the only remaining sources of dispersion are linear, and can be compensated even for pulses that overlap in the fiber.

We report the experimental study of the feasibility of this scheme. Pulses of 70 fs in duration, with a central wavelength of 620 nm delivered by a CPM dye laser and amplified by a copper vapour laser to a maximum peak power of 3 MW were split into pair of pulses with variable time separation using a Michelson interferometer with a translational mirror. These pairs of pulses were stretched to 60 ps by two anti-parallel gratings separated by a telescope of -1 magnification and coupled into a single-mode fiber (Figure 1).

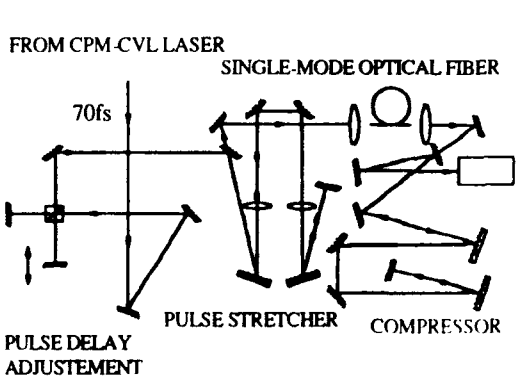

Figure 1. Sketch of the experiment

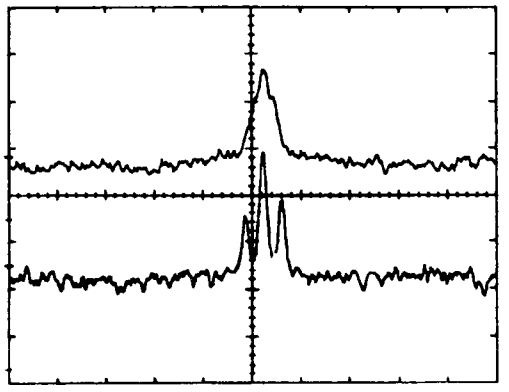

Figure 2. Autocorrelations of a pair of two sub-picosecond pulses transmitted across a 50m long single-mode fiber for delays of 1ps and 2ps between pulses, for the upper and lower curves, respectively. One division on the abscissa corresponds to 6.7ps

Note that the stretched pulses now overlap in time inside the fiber. The outgoing pulses were recompressed using a TREACY's grating pair and analyzed with an autocorrelator. Non-polarisation-preserving fiber strands, taken from the same fiber, of 4, 8, 16, 32 and 50 m in length and a 4 m long polarisation-preserving single mode fiber have been tested. The maximum fiber length was limited by the dimension of the gratings of our compressor. The maximum bit rate was estimated by measuring the minimum time interval still allowing detection of two pulses in the autocorrelation trace (Figure 2).

For low peak powers (0.1W) of the stretched pulses, this bit rate was found to decrease with the fiber length and is 500 Gbit/s for 50m. The limitation is given by the uncompensated third order dispersion of the fiber. For high peak power of the stretched pulses (1.7 W),an instability of the transmitted signal was observed, causing noisy autocorrelation signals. When the peak power was further increased, pulse break-up was observed. We have observed up to seven sub-pulses for a peak-power of 17 W (Figure 3). As expected, the use of a polarisation preserving fiber greatly improved the autocorrelation quality and the threshold for pulse break-up was found to be increased. As a result of stretching, no measurable spectral broadening was observed in the transmitted pulses, even at the highest powers. However we observed a noisy structure that can be attributed to nonlinear interaction (Figure 4).

It is interesting to extrapolate the performance of this scheme to other wavelengths, better suited to data transmission. The group velocity dispersion of our fiber was measured to be 330 ps/km/nm. For a pulse central wavelength of 1270 nm, the dispersion of a weakly guiding fiber is about 1.5 ps/km/nm. Thus a fiber length of more than 10 km could be compensated for group velocity dispersion by the compressor used in this experiment.

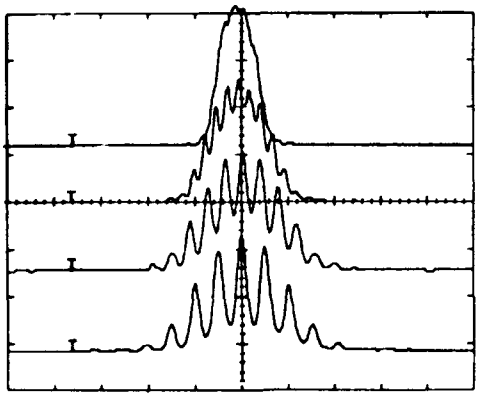

Figure 3. Pulse break-up for high peak power. Autocorrelation traces are shown for delays between the two pulses of 1, 2, 3 and 4ps for the curves in order from top to bottom. One division on abscissa corresponds to 6.7ps

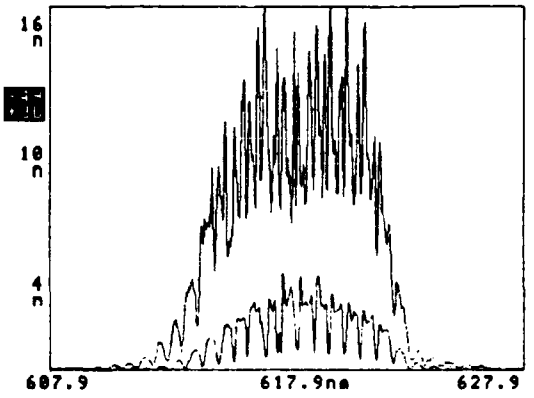

Figure 4. Spectra of two chirped 60ps pulses of a time delay of 2ps for a peak power of 1.4 and 2.8W. The nonlinear interactions cause the fringe structure of the coherent pulse pair

In conclusion we have demonstrated in the visible spectral range a new high bit-rate data transmission scheme providing 500 Gbit/s over 50 m in its preliminary version. Translated into a wavelength around 1300 nm, this experiment appears to be well suited for data transmission systems with a range of a few tens of km.

Distortion of a broadband-intensity signal during its transmission through a chain of lumped amplifiers due to their saturation

A.V. Luchnikov and A.N. Pilipetskii

General Physics Institute
Academy of Sciences of the USSR

38 Vavilov Street, Moscow 117942, USSR

Experiments on soliton pulse transmission through optical fiber on the distance of up to 10000 km [1] confirm the possibility of realization of ultra long high-bit-rate soliton communication systems. At the present moment it seems most reliable to compensate the optical fiber losses with the help of lumped erbium-doped fiber amplifiers, periodically placed along all the transmission distance. As the value of the erbium fiber amplifier saturation power is not very high (~ 0.5 mW), than the influence of the amplifier saturation could affect on the signal transmission in the soliton regime [2]. The amplifier saturation in soliton communication systems could result in decreasing of the soliton sequence signal-noise ratio. This effect can be accumulated after transmission through a large number of amplifiers (> 300 for L ≈ 10000 km [1]).

In the present paper we analyze theoretically the effect of signal-noise ratio decreasing in a soliton signal sequence during its transmission through a chain of erbium-doped fiber amplifiers.

In our calculations we used an ideal three level system (level of pump absorption, upper level of amplification transition, ground level) as a model of an erbium amplifier. Assuming that the signal bandwidth is much less than the amplifier bandwidth, the equation for the gain increment fluctuations $\delta\gamma_n$ in the n-th amplifier can be written as

$$\frac{\partial \delta\gamma_n}{\partial t} + \frac{\delta\gamma_n}{\tau_{eff}} = -\frac{\bar{\gamma}}{\tau}\left(I'_{fl} + i'_{n-1} \right) \qquad (1)$$

where t is time, τ - the longitudinal relaxation time of the amplification transition, $I'_{fl} = I_{fl}/I_{sat}$ - the path average fluctuation part of signal intensity normalized to saturation intensity of an erbium amplifier, $i'_{n-1} = i_{n-1}/I_{sat}$ - the path average noise part of the radiation intensity due to the influence of the amplifier saturation after n-1 amplifiers, $\bar{\gamma}$ - the value of the average gain increment of amplifier equal to the value of the optical fiber loss decrement between the amplifiers. The value τ_{eff} characterizing the dynamic amplifier response time in the presence of signal and pump is as follows

$$\tau_{eff} = \frac{\tau}{1 + (\omega_s/\omega_p)I'_{p0} + \bar{I}' - \bar{\gamma} - \beta} \qquad (2)$$

where ω_s, ω_p are the frequencies of signal and pump respectively, $I'_{p0} = I_{p0}/I_{sat}$ and $\bar{I}' = \bar{I}/I_{sat}$ - the input pump intensity and the mean path averaged intensity of signal , β - absorption coefficient of amplifier for a small signal in the absence of pump. Eq.(1) is obtained in the approximation of small perturbations of the gain increment $\delta\gamma_n \ll 1$.

Solving Eq.(1) we have obtained the relation for the dispersion of the soliton energy fluctuations σ_E normalized to soliton energy E in a random soliton sequence with the value of bit rate F (the probability of the soliton appearance is 1/2)

$$\left(\frac{\sigma_E}{E}\right)^2 = \frac{1}{\pi F}\int_0^{\infty} |f_\omega|^2 d\omega \qquad (3)$$

where function $|f_\omega|^2$ describes spectrum of the slowly varying in time envelope of the pulse energy perturbations in a random soliton sequence

$$f_\omega = 1 - \left(1 - \frac{E_{eff}}{1 + i\omega\tau_{eff}}\right)^N, \qquad (4)$$

$$E_{eff} = E'\bar{\gamma}\frac{\tau_{eff}F}{2}, \qquad (5)$$

where N - number of amplifiers, $E' = E/E_{sat}$ ($E_{sat} = I_{sat}\tau$ -

the saturation energy density of the amplification transition).

We have calculated $|f_\omega|^2$ as a function of ω for transmission rate F = 4 Gbits/s. The fiber and radiation parameters correspond to those experimentally realized in [1]: the input pump power P_p = 50 mW, $\bar{\gamma}$ = 1.6, E = $10^2 \cdot$nJ/cm^2, E_{sat}= 10 J/cm^2, D = 1.38 ps/(nm·km), A_{eff}= 35 μm^2, N = 350 (L $\approx$ 10000 km). Spectral behavior of $|f_\omega|^2$ essentially depends on the value of $\eta = E_{eff}N$. In our calculations $\tau_{eff} \approx 7 \cdot 10^{-3}\tau$ = $7 \cdot 10^{-5}$s and η = 0.8. Fig.1 shows the spectra $|f_\omega|^2$ for three different values of η: 0.1 « 1 (curve 1), 0.8 (curve 2), 2 (curve 3) and 10 (curve 4). With increasing of η the energy perturbation spectrum saturates at low frequencies, broadens and transforms from Lorenzian shape to a more complicated form. For η « 1 the expression for σ_E/E can be written as

$$\frac{\sigma_E}{E} = \left(\frac{\tau_{eff} F}{8} \right)^{1/2} \frac{E}{E_{sat}} \bar{\gamma} N . \qquad (6)$$

We have calculated $\sigma_E/E = 1 \cdot 10^{-3}$ with the help of Eqs. (3-5) for η = 0.8 and F = 4 Gbits/s.

In conclusion it should be noted that effect of saturation in erbium-doped amplifiers does not decrease considerably the signal-noise ratio of signal in soliton communication systems for a reasonable bit rate and transmission distance. The theory developed in this paper allows to calculate the crosstalk between different channels due to saturation in erbium-doped amplifiers in soliton communication systems with wavelength division multiplexing and could be applied to analysis of instabilities in multipass amplifying systems such as mode locked erbium-doped fiber laser.

A.V.Luchnikov would like to acknowledge A.N.Starodumov for his fruitful discussions which have lead to the joint creation of the idea of the effect discussed in this paper.

1. L.F.Mollenauer, M.J.Neubelt, S.G.Evangelides, J.P.Gordon, and L.G.Cohen, Opt. Lett., v.15, 1203 (1990).
2.M.Nakazawa, Y.Kimura, and H.Kubota, J. Appl. Phys., v.66, 2803 (1989).

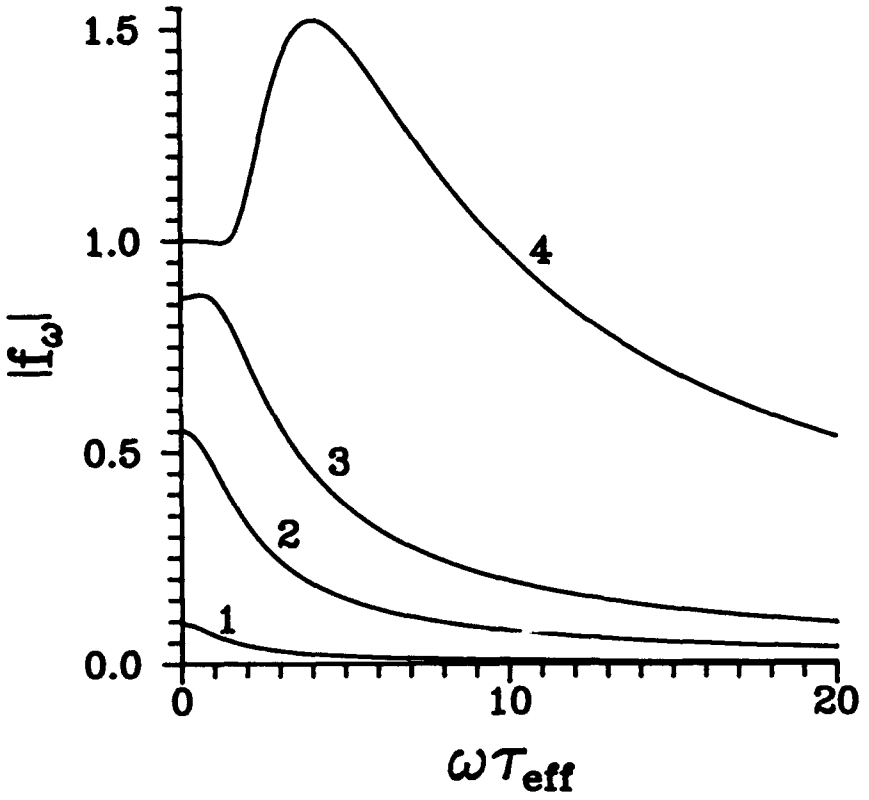

Figure 1

THE GAIN SATURATION BY THE RANDOM PULSE TRAIN AND NOISE CHARACTERISTICS OF LONG-DISTANCE SOLITON-BASED SYSTEM

A.N.Starodumov

General Physics Institute, Academy of Sciences of the USSR,
38 Vavilov Street, Moscow 117942, USSR, tel. (095) 132-83-78

In this work we investigate the degradation of the signal-to-noise power ratio (SNR) at the output of the communication line caused by the random fluctuations of a gain in lumped optical amplifiers. There are a few sources of gain fluctuation: effect of pump modulation, random deviiation of Erbium concentration from one amplifier to the next and others. In [1] Kubota et al. have considered by numerical simulation the soliton propagation over long distance taking into account the gain fluctiation (±1,5%). It was pointed out that the pulse width fluctuation over 9000 km was within ±10%, and the pulse shape was clearly distinguished from noises.

In our paper we discuss another source of noise, connected with the random character of soliton sequence. The information bearing solitons modulate by random way the gain owing to saturation. The effect of saturation for every pulse is very small ($\sim 10^{-6}$–10^{-8}) but the changes of the inversion population can be accumulated for the time of Erbium relaxation ($\tau_{21} \sim 10^{-2}$ s). We evaluate the degradation of the SNR and show that the power fluctuations due to random gain greater or of order amplified spontaneous emission [2]. Note, that this noise has a fundamental nature and is connected with the random character of the information process.

We consider a random sequence of pulses with τ_0 (τ_0 is the FWHM of the pulse), peak intensity I_0. The probabilities of "1" (soliton present) and "0" (no soliton present) are both equal to 1/2 in bit period T. Pulse duration is supposed to be much shorter than bit period $5\tau_0<T$. The time-averaged intensity of optical radiation is $< I_L>= I_0\frac{\tau_0}{2T}$.

To calculate gain coefficient, we use an ideal 3-level model for Er-doped fiber amplifier . Since nonradiative life-time $\tau_{32}<<\tau_{21}$, we can assume that $P_3<<P_2, P_1$, where P_i- population in the level i (i=1,2,3). Then the changes of inversion $P= P_2-P_1$ is given by equation

$$\frac{\partial P}{\partial t} =-\left[2\sigma_{21}\frac{I_o}{h\nu} + \frac{1}{\tau_{21}} +\sigma_{13}\frac{I_p}{h\nu_p}\right]P + \left[\sigma_{13}\frac{I_p}{h\nu_p} - \frac{1}{\tau_{21}}\right]N_0 \qquad (1)$$

where σ_{21}, σ_{31}- emission and absorption cross-section for transitions 2→1, and 1→3 respectively, N_0- total concentration of Er ions, I_p- pump intensity, $h\nu$, $h\nu_p$- information photon and pump photon energies, respectively. Note, to achieve an inversion population at any point in a fiber, it is neccesary that $I_p>I_{th}= \frac{h\nu_p}{\sigma_{31}\tau_{21}}$. In general case pump intensity is changed along the amplifier, but we assume $I_p=(z,t)=const$, because of the insignificant pump depletion for EDFA in soliton-based long distance system with parameters as in [2].

We have calculated from (1) the fluctuations of inversion for a random pulse train and determined intensity fluctuations at the output of communication system. The SNR at the output of the system is described as

$$SNR =\left\{ \frac{8T}{\tau_{21}}\left[\frac{<I_L>}{I_S} + \frac{I_P}{I_{th}} +1\right]\right\}^{1/2} \frac{\varepsilon_S}{\varepsilon_p} \quad (\alpha L)^{-1} \qquad (2)$$

where $I_s=(2\sigma_{21}\tau_{21})^{-1}$, $\varepsilon_p, \varepsilon_s$-pulse and saturation energies.

The SNR was evaluated for the soliton-based communication system with parameters τ_o=22ps, D=3 ps/nm/km, fiber loss coefficient α=0.057 km^{-1}, effective fiber core areas 35 μm^2, distance L=10000km, T=200ps.

Pump power. As it can be seen from (2) the SNR depends on pump power of optical amplifiers. It is explained by the fact that the saturation intensity of 3-level amplifier depends on pump intensity. To increase SNR it is desirable to use more powerful pump. Fig.1 illustrates the degradation SNR ratio with decreasing pump power— curve (a) correspond to pump power 50 mW and curve (b) 20 mW.

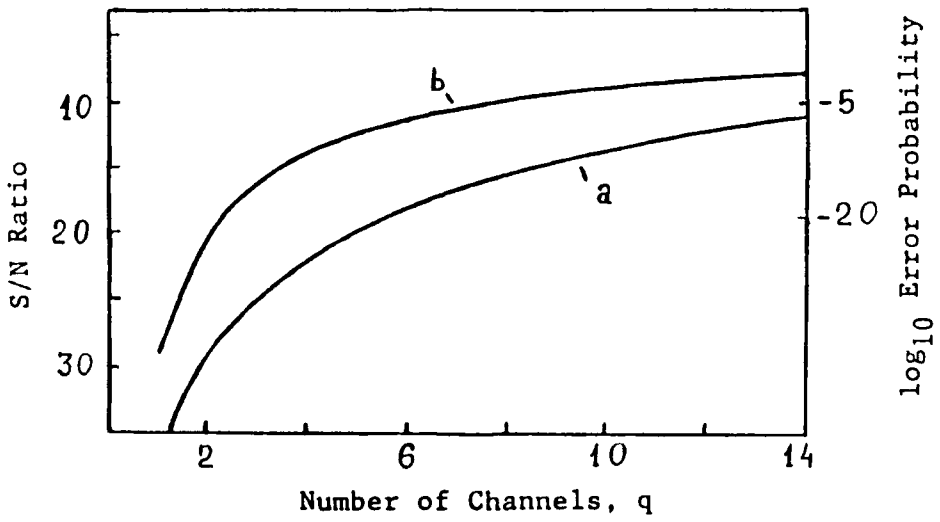

Fig.1 Signal to noise ratio dependence on number of channels. Pump power 50 mW (a), 20 mW (b) τ_0 = 22 ps, D = 3 ps/nm/km, L = 10000 km, α = 0.057 km^{-1}, T^{-1} = 5 GHz.

Wavelength division multiplexing. As the soliton trains of different frequencies move with different velosities, then the

resultant gain for one fixed pulse is changed from one amplifier to another.The gain fluctuation is accumulated over time interval $\sim\tau_{21}$ and determined by $\tau_{21}/T \simeq 10^7$-10^8 pulses. If the difference of velosities is small and the distance over which pulses pass through one another is large ($\approx$ 100 km) compared to amplifier spacing, the changes of pulse train from one amplifier to another are determined by a small part (10^2-10^3) of the whole quantity of pulses causing gain fluctuations. Thus one can assume that the gain fluctuations in each amplifier is determined approximately by the same random soliton train.Since information bearing soliton trains of different frequencies are mutually independent the resulting signal to noise ratio can be described as $SNR_q \approx q^{1/2}SNR$ (it was taken into account that $\langle I_L \rangle \ll I_p I_s / I_{th}$ to avoid cross talk between channels). The SNR and error probability dependence on number of channels q are shown in Fig.1. Note that the error probability is increased if we take into account the fluctuations of pump and is decreased for fibers with low dispersion.

In conclusion we have investigated the new factor limiting information capasity of soliton-based communication lines. The degradation of the signal to noise ratio at the output of high bit-rate communication line owing to random gain saturation increases the probability of errors up to 10^{-9}-10^{-7}.

References

1. H.Kubota, M. Nakazawa, IEEE J. Quantum Electron., vol. 26, pp.692-670, 1990.

2. J.P.Gordon, L.F.Mollenauer, submitted for publication in joint issue of IEEE J. Quantum Electron. and Lightwave Tech. on Optical Amplifires.

INFLUENCE OF SELF-PHASE MODULATION ON ULTRA LONG-SPAN OPTICAL TRANSMISSION AT ZERO DISPERSION.

S.F. Carter, E.G. Bryant, and J.V. Wright.
Submarine Systems Section
BT Laboratories,
Martlesham Heath, Ipswich, UK.
IP5 7RE
Tel: 0473 646990.

Introduction.

There appear to be two distinct approaches to the design of future ultra long-span optically-amplified transmission systems. In the first, the signal wavelength is chosen to give operation in the region of anomalous dispersion. This is consistent with soliton operation, although other pulse shapes may propagate with little degradation. This paper is concerned with the second approach, where the operating wavelength is chosen to lie very close to the dispersion minimum. Self-phase modulation is now a source of potential impairment, and must be controlled.

We examine the likely performance of a system of length, 6000km, operating at a line-rate of 5Gb/s, with a single-channel intensity-modulated NRZ pulse format. This is carried out using a computer program which implements a split-step Fourier[1] technique to simulate the simultaneous propagation of signal and ASE noise along a multi-amplifier system. A 32-bit psuedo-random data sequence is used to modulate the signal, while a Gaussian random number generator is used to generate a white-noise signal at each amplifier. The degradation after transmission is estimated from the opening of the received data "eye", after processing by a lowpass filter with raised-cosine frequency-response. An equivalent optical penalty is derived from this opening.

System Parameters.

While maintaining a specified signal/noise ratio, the nonlinear phase-shift, ϕ for a step intensity change along a multi-amplifier chain, can be shown to depend on the amplifier spacing, L, the fibre loss,α, and the amplifier gain, G, by:

$$\phi \propto \frac{(G - 1)^2}{\alpha G L} \qquad \text{where: } G = \exp(\alpha L)$$

On this basis a system with an amplifier spacing of 40km was selected for modelling. This employs 150 amplifiers and gives a nonlinear phase-shift only a factor of 1.32 greater than the limiting case of distributed amplification (see fig 1). Other parameters were: fibre loss, 0.22dB/km, fibre effective area, Aeff: 40 x 10^{-12} m^2, dispersion-slope: 0.067 ps nm ^{2} km^{-1}, nonlinear coefficient, n_2: 3.2 x 10^{-20} m^2/W, signal wavelength: 1550nm, and amplifier noise-figure: 7dB.

For all the results presented here the following additional conditions apply: Based on an estimate of likely insertion losses, an attenuation of 2dB was added to the input

of each amplifier; this gives an equivalent degradation of the noise figure. A bandpass filter of width 4nm was also included at each amplifier. The peak signal level was 2.2mW; a straightforward linear noise analysis indicates that this gives an operating margin of more than 7dB above the 1E-9 error-rate level.

Results.

The first set of results are for values of dispersion ranging from -0.1 to +0.1 ps nm^{-1} km^{-1}, equivalent to operation over a wavelength range of 1.5nm (188GHz) either side of the fibre dispersion-minimum. Penalties are shown in fig 2. Previously[2] the general observation has been made that pulse-broadening occurs in the normal regime, with compression and multi-pulse formation in the anomalous regime. This behaviour is reflected in these results, though an additional phenomena is now apparent in the region very close to the dispersion-zero. This is caused by cross-phase modulation (XPM) between signal components in the region of zero-dispersion, where strong phase-matching enhances the efficiency of the process[3]. This is supported by an examination of the evolving optical spectrum as the signal propagates; the spectrum initially evolves gradually until significant power straddles zero-dispersion, whereupon a rapid increase in spectral growth results. Significant optical power is then absorbed by the bandpass filters, and the time-domain pulses become distorted. The asymmetry of the effect relative to the dispersion-zero is caused by the more rapid spectral broadening that occurs anyway in the anomalous regime.

In the presence of ASE noise the effect is even more significant, due to additional XPM between the signal and noise. Fig 3 shows the penalty as a function of dispersion. In all the simulations including ASE noise the penalty is slightly over-estimated, as the additive effects of noise are present on the received signal as well as the degradation due to nonlinear interaction. However, it is apparent that the constraints on acceptable performance are tight.

Marcuse[4] has suggested a technique to allow operation at zero-dispersion by reducing the efficiency of phase-matching. This involves constructing each inter-amplifier span from a number of shorter spans of varying dispersion, but with a sum of zero. These are arranged with their dispersion values following a "sawtooth" configuration. There is merit in the technique, but in practice it is likely to involve considerable expense in manufacturing fibre with a range of dispersion-zero values, and in assembling each section to tight tolerance on overall dispersion. We have investigated a similar technique whereby alternate inter-amplifier spans are assigned different values of dispersion. The resulting penalties, with and without ASE noise, are shown as a function of the mean dispersion by the dotted curves in figs 2 & 3 respectively. Here the dispersion value oscillates with alternate spans taking values of 0.5 ps nm^{-1} km^{-1} either side of the mean. There is clearly some improvement over the results for uniform dispersion, but this is not enough to allow operation at exactly zero-dispersion.

We have also investigated the effect of providing dispersion compensation at the output of the system. The wavelength is chosen to lie in the normal regime, where the XPM effects are small. The signal at the output of the system then undergoes dispersion of equal but opposite sign to that encountered over the total span of the transmission fibre. In practice this could be accomplished by a relatively short span of step-index fibre. All the results shown are for a system fibre dispersion of -0.1 ps nm^{-1} km^{-1}, requiring approximately 38km of step-index fibre for compensation. Received optical pulses (unfiltered) and corresponding data "eyes" (filtered) are

shown in fig 4, with and without dispersion compensation, with no ASE noise included. Also shown are corresponding received eyes with ASE included in the simulations. The technique is clearly effective in restoring the eye-opening, in this case giving an improvement of about 5dB.

Finally, we introduced statistical variation in the values of dispersion in each inter-repeater span. We used a standard deviation of 0.25 ps nm^{-1} km^{-1}, which we believe to lie within the range of achievable manufacturing tolerances. Using a mean value of -0.1 ps nm^{-1} km^{-1} together with dispersion-compensation, only minimal additional degradation over the above results was noted.

Discussion.

Dispersion compensation has often been advocated for applications in linear systems, e.g. [5]. It is remarkable however that the technique works in this instance, where self-phase modulation clearly has a large influence over the optical signal, evident by considerable broadening of the optical spectrum. Indeed, in the absence of any self-phase modulation, the values of dispersion used in these simulations would have produced only a very modest eye-closure.

Conclusions.

We have used a simulation technique to identify the regime of possible operation for a 6000km optically-amplified transmission system at 5Gb/s. While satisfactory operation may be possible at a wavelength a few tenths of a nanometer below the dispersion-minimum, there is a fine balance between degradation due to XPM, and excessive eye closure due to the interaction of self-phase modulation with normal dispersion. Techniques to reduce the XPM effect have been examined, but they either introduce the need for elaborate fibre selection, or are relatively ineffective. We have investigated system operation in the normal regime to minimise XPM, combined with dispersion-compensation to restore the eye-opening. We believe this technique to be compatible with fibre production tolerances.

References.

1)Agrawal: "Nonlinear Fiber Optics", Academic Press, p44.

2)Bryant et al.: "Influence of Kerr-Effect on Long-Span Optical Transmission", IEE Colloquium on Non-Linear Effects in Fibre Communications, Nov '90.

3)Hill et al.: "CW Three-wave Mixing in Single-mode Optical Fibers", J. Appl Phys. Vol. 49 No. 10 pp 5098-5106.

4)Marcuse: "Single-Channel Operation in Very Long Nonlinear Fibers With Optical Amplifiers at Zero Dispersion", J. Lightwave Tech., LT-9, No. 3, 1991.

5)Cimini et al: "Optical Equalization to Combat the Effects of Laser Chirp and Fiber Dispersion", J. Lightwave Tech., LT-8, No. 5, 1990.

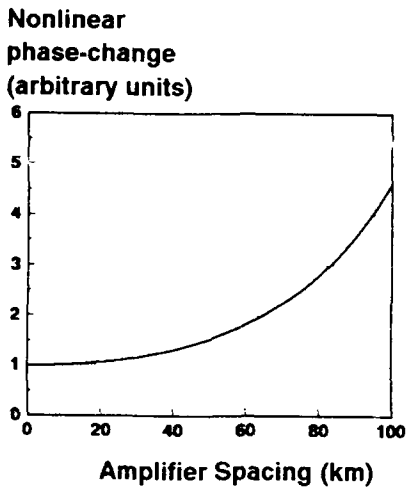

Fig 1: Nonlinear phase-change as function of amplifier spacing.

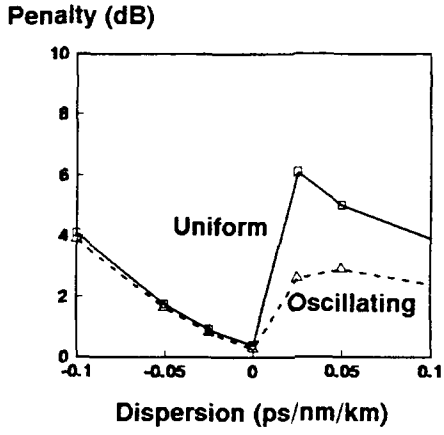

Fig 2: Penalty versus dispersion (uniform and oscillating) - no ASE.

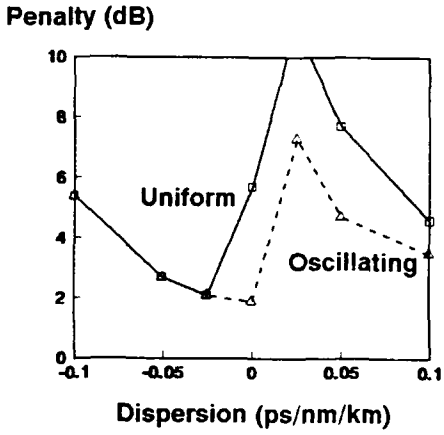

Fig 3: Penalty versus dispersion (uniform and oscillating) - with ASE.

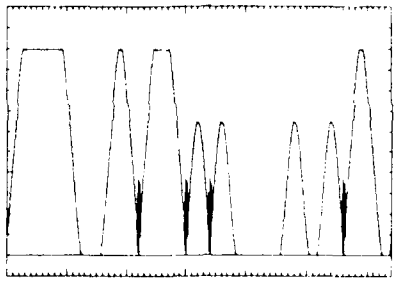

Fig 4a: Received pulses D = -0.1 ps/nm/km no ASE.

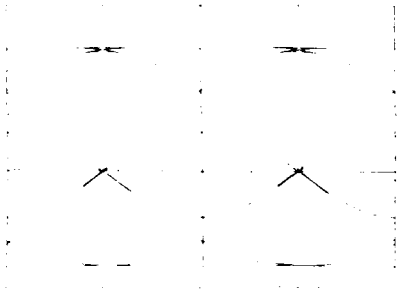

Fig 4b: Received eye D = -0.1 ps/nm/km no ASE.

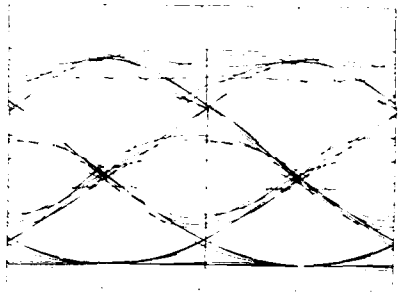

Fig 4c: Received eye D = -0.1 ps/nm/km with ASE.

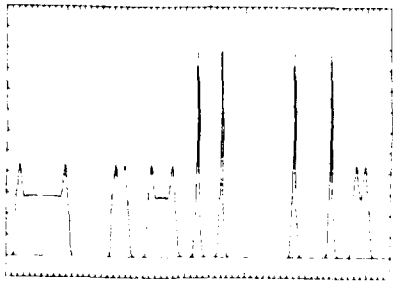

Fig 4d: Received pulses D = -0.1 ps/nm/km no ASE, with dispersion-compensation.

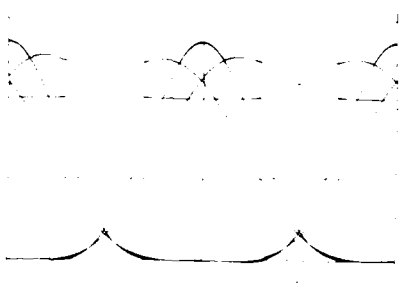

Fig 4e: Received eye D = -0.1 ps/nm/km no ASE, with dispersion-compensation.

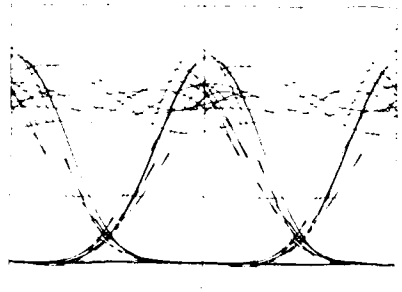

Fig 4f: Received eye D = -0.1 ps/nm/km with ASE and dispersion-compensation.

Electrostrictional Interaction of Optical Pulses in Long Distance Soliton Communication Systems

E. M. Dianov, A. V. Luchnikov, A. N. Pilipetskii, and A. M. Prokhorov

General Physics Institute
Academy of Sciences of the USSR
38 Vavilov Street, Moscow 117942, USSR

Mollenauer et al. have experimentally demonstrated the transmission of optical solitons in a single mode fiber over large distance up to 10000 km [1]. One of the limitations to the transmission rate in the soliton regime of propagation is an interaction between optical pulses. Besides the well studied short-range Kerr-like interaction, Smith and Mollenauer experimentally discovered the interaction of the two periodic trains of 55-ps solitons shifted in time on several dozens of soliton widths for propagation distance of 3000 km [2]. In [3,4] we suggested and developed the theory or a mechanism of long-range interaction of solitons - electrostrictional interaction. According to this theory an optical pulse excites an acoustic wave, propagating in transverse direction to the fiber axis. This leads to the temporal perturbation of the fiber effective refractive index. In consequence, the following optical pulses become phase-modulated and change their carrier frequency. That results in additional temporal shift of solitons. We have obtained a good quantitative agreement [4] with experimental results of [2] on interaction of two soliton pulse trains.

For the case of soliton transmission systems we have shown that electrostrictional long-range interaction leads to random temporal shifts of pulses [5]. The expression for the mean-square deviation of the optical pulse arrival time σ_τ is approximated by:

$$\sigma_\tau = 1.38 \cdot 10^{-2} D^2 F^{3/2} L^2 \left(1 - \frac{1.18}{F} \right)^{1/2} . \qquad (1)$$

where σ_τ is in ps, D in ps/(nm·km), F is the bit rate in Gbits/s, L is the propagation distance in thousands of km. This expression has been obtained assuming (i) Gaussian profile of the fiber mode with effective cross section A_{eff}= 35 μm^2, (ii) $F \cdot \tau_{sol}$= 0.2 (τ_{sol} is the soliton FWHM duration) to make the short-range soliton interaction negligibly small [1].

Besides the value of dispersion σ_τ, to calculate bit error rate (BER)in transmission system, one should also know the probability distribution of the pulse temporal shifts τ from their average shift $<\tau>$. Fig.1 demonstrates the calculated numerically gystogramm of the $(\tau - <\tau>)/\sigma_\tau$ value distribution after a random sequence of 500000 pulses passing through the fiber of length of 10000 km (F = 5 Gbits/s, $<\tau>$ = 10.2 ps, σ_τ = 25.8 ps). This dependence is well approximated by Gaussian distribution with dispersion σ_τ (Fig.1, dashed line).

Fig.2 shows BER as a function of transmission rate F due to electrostrictional interaction of optical pulses for L = 10000 km and three values of the fiber dispersion: 1.38 (1, solid), 1 (2, solid) and 0.5 ps/(nm·km) (3, solid). In these three cases the transmission rate is limited to 4, 5 and 8.5 Gbits/s respectively. For comparison the dashed curves in Fig.2 represent the dependencies of BER due to timing jitter caused by the amplified spontaneous emission from erbium-doped fiber amplifiers on the bit rate F (D = 1.38 (1), 1 (2) and 0.5 ps/(nm·km) (3) respectively; L = 10000 km). These curves were calculated according to the theoretical results of Gordon and Mollenauer [6].

Spectral multiplexing of a number of channels was suggested in [7] to increase the information capacity of soliton communication systems. We have calculated the value of timing jitter in each channel of soliton communication system with spectral multiplexing. The value of the square of dispersion σ_n^2 of the soliton pulses arrival time in the n-th channel is

$$\sigma_n^2 = \sigma_{nn}^2 + \sum_{k \neq n} \sigma_{kn}^2 , \qquad (2)$$

where σ_{nn}^2 is due to electrostrictional interaction of solitons within the n-th channel (see Eq.(1)) and the terms σ_{kn}^2

describe the influence of other channels through the electrostriction on the n-th channel timing jitter

$$\sum_{k\neq n}\sigma_{nk}^2 = \left(\frac{D\lambda}{c}\right)^2\left(\frac{L}{\alpha}\right)^2 F\int_0^\infty \delta n^2(t)dt \sum_{k\neq n}\frac{1}{(n-k)^2}\,. \qquad (3)$$

where λ is the radiation wavelength, c - velocity of light, $\alpha = D\,\Delta\lambda$ - the group velocity mismatch between neighbouring channels with spectral interval $\Delta\lambda$ between them. $\delta n(t)$ is the magnitude of perturbation of the fiber mode effective refractive index excited by the soliton pulse through electrostiction (the response function of electrostrictional interaction). The expression for σ_n can be written as $\sigma_n = \sigma_{nn}(1+\varepsilon)$. Numerical calculations show that ε which is maximal for channel lying in the center of transmission spectrum is of $2\cdot10^{-2}$ (D = 1 ps/(nm·km), αL = 10 ns, number of channels is of 5).

In conclusion, it shoud be stressed that to achieve a higher bit rate transmission fibers with as low dispersion as possible should be used. Wavelength division multiplexing in soliton communication systems does not increase considerably the bit error rate due to electrostrictional interaction of optical pulses.

1. L.F.Mollenauer, M.J.Neubelt, S.G.Evangelides, J.P.Gordon, J.R.Simpson, and L.G.Cohen, Opt.Lett., 15, 1203 (1990).
2. K.Smith, L.F.Mollenauer, Opt.Lett., 14, 1284 (1989).
3. E.M.Dianov, A.V.Luchnikov, A.N.Pilipetskii, and A.N.Starodumov, Opt.Lett., 15, 314 (1990).
4. E.M.Dianov, A.V.Luchnikov, A.N.Pilipetskii, and A.N.Starodumov, Soviet Lightwave Communications, 1, 37 (1991).
5. E.M.Dianov, A.V.Luchnikov, A.N.Pilipetskii, and A.M.Prokhorov, submitted to Soviet Lightwave Communications.
6. J P Gordon and L F Mollenauer, the joint issue of IEEE J. Quantum Electron. and J. Lightwave Tech. on Optical Amplifiers.
7. L.F.Mollenauer, S.Evangelides, COST 217 International Workshop: Nonlinear Effects in Fibers, Mons, Belgium 1990.

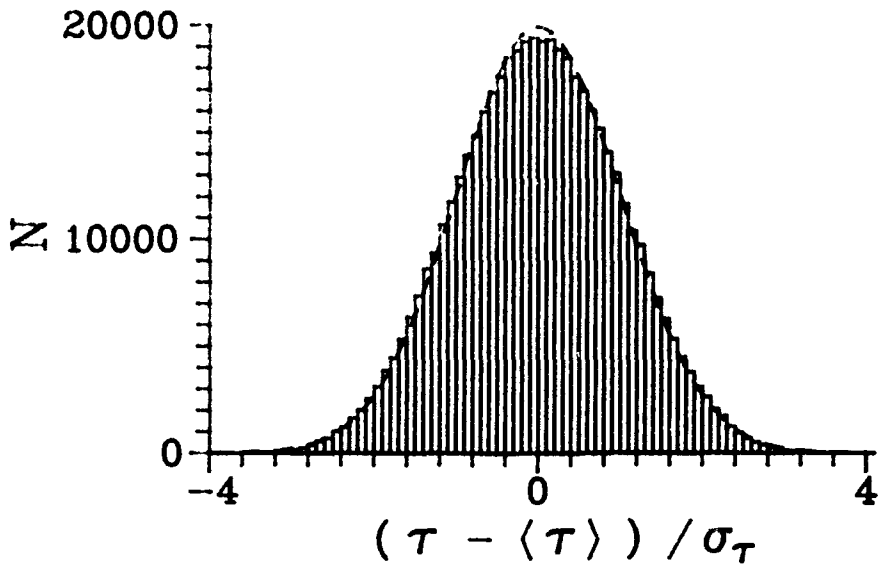

Figure 1

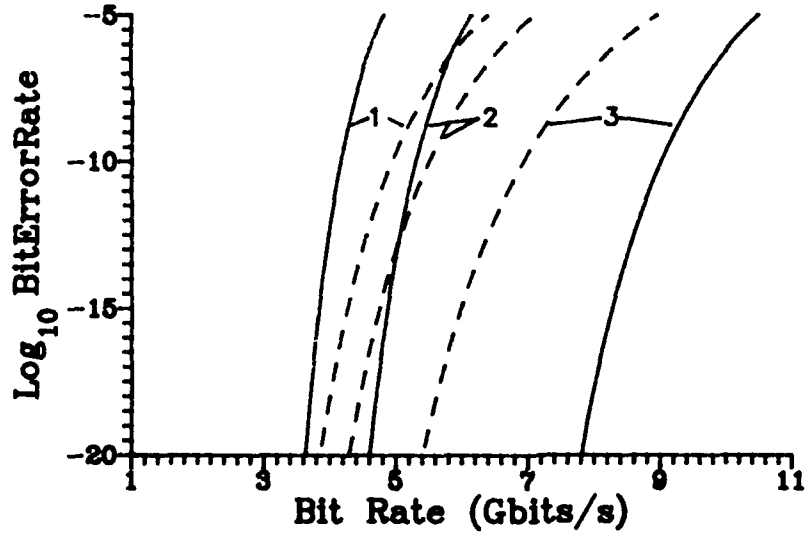

Figure 2

Tuesday, September 3, 1991

Erbium-Doped Fibers and Amplifiers

TuA 9:00am–10:30am
Palmerston Room

Roger H. Stolen, *Presider*
AT&T Bell Laboratories, USA

Coherent Effects in Er-doped Fibers: Photon-Echo with Femtosecond Pulses

Y. Silberberg, V. L. da Silva, J.P. Heritage, E.W. Chase, M.A. Saifi, and M.J. Andrejco

Bellcore, 331 Newman Springs Road, Red Bank, New Jersey 07701

Optical fibers have proven to be one of the most important nonlinear media, even though in most cases the nonlinearity exploited is the notoriously weak Kerr effect of the silica-based fiber. By using doped fibers, new, stronger nonlinearities are possible. These stronger effects could allow for new phenomena and applications. Coherent effects, in particular, should be important when pulses shorter or comparable to the dephasing time of the impurity ions propagate in the fiber. Here we report, for the first time, the observation of accumulated photon-echo and free induction decay during the propagation of femtosecond pulses in Er doped fibers at 4.2°K.

A basic photon-echo experiment consists of applying two pulses to a sample with resonant absorbing atoms and observing the radiated pulse (echo) which is delayed with respect to the second pulse by a time equal to the separation of the two exciting pulses. Photon echo is usually explained in terms of dephasing and rephasing of inhomogeneously broadened group of two-level absorbers [1]. In an *accumulated* photon-echo experiment, the pair of pulses is repeated many times within the radiative lifetime of the level involved, thereby enhancing the resulting echo [2].

A simple and intuitive way to understant these effects is obtained by considering the frequency domain picture shown in Fig. 1. Two short pulses with a separation of τ (Fig. 1a) are characterized by a sinusoidally modulated spectrum (1b) with a modulation period $\Delta\omega = 2\pi/\tau$. This modulated spectrum saturates the absorption line. For an inhomogeneously broadened absorber, a population grating is formed, with a shape that corresponds to the excitation spectrum (1c). The output spectrum is obtained by transmitting the input spectrum through this absorption grating (1d). The result is a distorted spectrum that is not purely sinusoidal: It contains higher order terms, which on transforming back to the time domain yield harmonics of the basic period τ, or echo terms (1e). This picture suggests a complete equivalence between photon echo and holography, and indeed this technique is sometimes refered to as time domain holography.

Photon echo has been proposed as a basis for time domain optical memory and optical signal processing [3], and several demonstrations have been reported in bulk crystals and gases [3-5]. In such applications, one of the short pulses in Fig. 1 is replaced with a more complicated signal. It can easily be shown that the longest signal that can be recorded is of the order of the homogeneous lifetime T_2, the time resolution is the inhomogeneous lifetime T_2^*, and the storage time is the radiative lifetime T_1. Most rare-earth absorption lines in solid hosts are inhomogeneously broadened at low temperatures. The homogeneous, inhomogeneous and fluorescence lifetimes for the $I_{13/2} - I_{15/2}$ transition of erbium in aluminosilicate fibers at 4.2°K were measured to be 80 psec, 0.6 psec, and 10 msec, respectively [6]. The use of Er-doped fibers for these applications offer a major advantage in term of significant simplification of alignment and cooling requirements, as well as compatibility with many highly developed fiber-based components.

In our experiment, depicted in Fig. 2, a NaCl:OH^- color-center laser with additive-pulse mode-locking is used as the optical pulse source for the photon-echo experiment. These pulses are less than 200 fsec long and can be tuned into the $I_{15/2} - I_{13/2}$ transition of the Er ions at 1.53 μm. The laser pulse repetition rate is 82 MHz while the Er relaxation time T_1 is 10 msec. That means that approximately 10^6 pulse-pairs are coupled into the fiber within T_1. The fiber used had a silica cladding and an Er-doped germanium-calcium-aluminum silicate core [7], with a diameter of 5μm. The peak absorption was 10 dB/m at 1.530 μm at room temperature. A 4.5 m section of this fiber was coiled to a 4 cm diameter, spliced to dispersion shifted fiber pigtails and immersed in liquid helium. Note that using a fiber system eliminated the need for windows, vacuum and other difficulties associated with cryogenic optical systems.

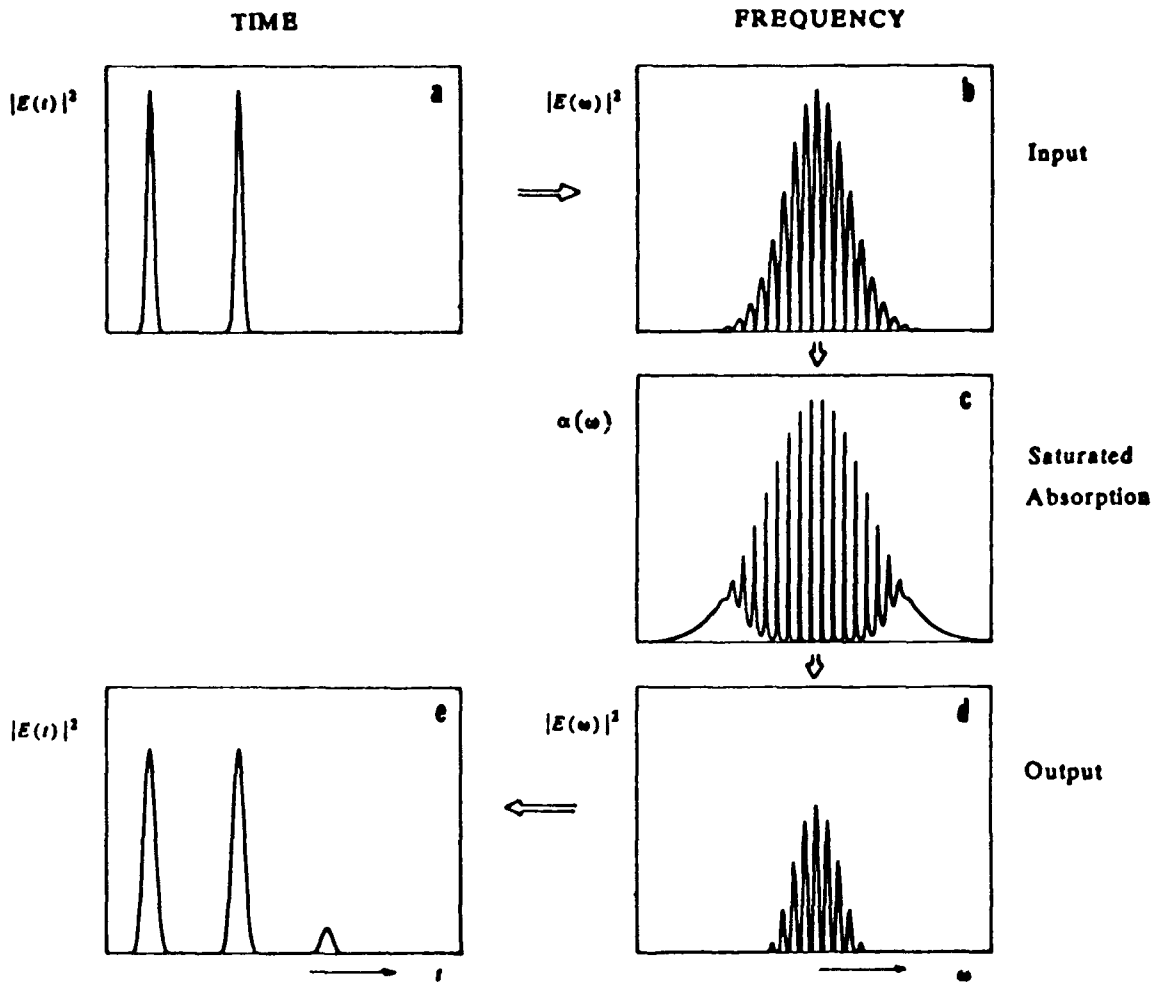

Fig. 1. Photon echo in the frequency domain.

A Michelson interferometer was used to generate a pulse pair which was coupled to the fiber. The average power coupled to the fiber was about 4 mW. In some experiments, an erbium doped amplifier was used to amplify the input pulses before they entered the cooled fiber. The 3 m long amplifier, made from the same fiber, was pumped by a 532 nm doubled Nd:YAG laser. Besides amplifying the pulses, the erbium-doped amplifier ensures that they are spectrally matched to the erbium transition. The output from the tested fiber was time-resolved by cross-correlating it with a delayed pulse of the laser, as shown in Fig. 2. No additional optical pumping was supplied other than that provided by the pulse pair, so that the erbium fiber under test acts as an absorber in this experiment.

Figure 3 shows the cross-correlation trace when the two input pulses are separated by 25 psec. As expected, an echo is observed 25 psec after the second pulse. Note also the free-induction decay emission that follow each of the pump pulses. The echo pulse duration is about 800 fsec. It is likely that this pulse is broadened by the dispersion in the fiber, estimated to be about 10 psec/Km nm. The echo duration was measured to be only 500 fsec in a 0.8 m long fiber, where dispersion effects should be minimal. Since the excitation pulses are only 200 fsec in duration, this echo duration is a signature of the 10 nm inhomogeneous linewidth. Although we did not measure the value of the homogeneous lifetime T_2 in our fiber, it seemed to be significantly longer than the 80 psec measured in aluminosilicate fibers [6], as we could not detect a significant drop in echo intensity even for pulse separations of 200 psec. This difference can be attributed to the special glass composition of the fiber in our experiment [7]. The echo intensity in the 4.5 m long fiber was about 50 times weaker than the transmitted excitation pulses. It was considerably stronger than the echo generated in a 0.8 m long fiber. This suggests that the echo is generated along the entire fiber length.

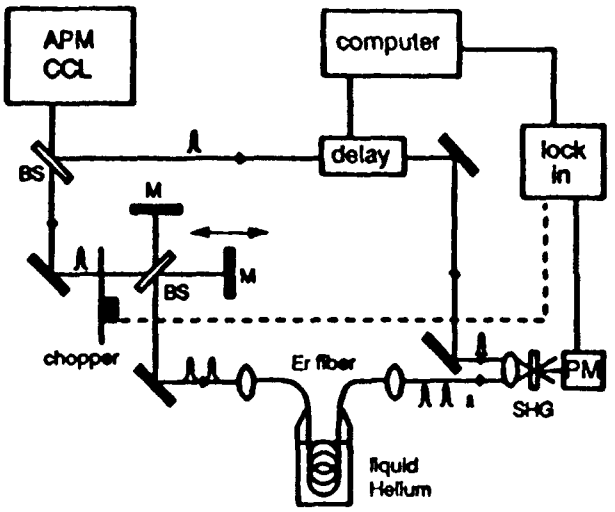

Fig. 2. Experimental setup for observation of photon-echo in an Er-doped fiber.

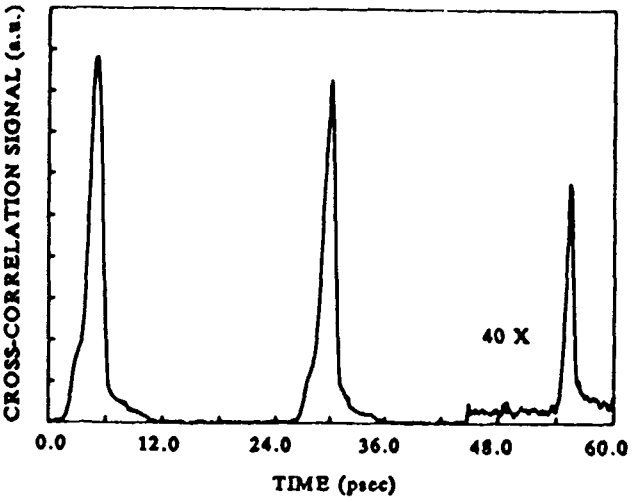

Fig. 3. The cross-correlation signal showing the two excitation pulses, separated by 25 psec, and the echo signal. The echo is amplified 40 times compared with the excitation pulses.

Er-doped fibers could be used for time domain processing of optical pulses. One of the simpler schemes is that for time domain optical memory as was first suggested by Mossberg [3]. In this configuration the echo is recorded between an information-containing data pulse (possibly a sequence of pulses) and a single write pulse. A third pulse, the read pulse, is used to recall the stored information by stimulating an echo. Although in our experiment the echo is generated through the accumulating effect of many pulses, we can still demonstrate the correlation between the shapes of the echo and the excitation pulses, which provides the basis for these signal processing applications. In our experiment the second excitation pulse serves also as the read pulse. For this purpose, we substituted one of the excitation pulses by a double- peaked pulse. This double pulse, with 3 psec separation, was obtained by exploiting the birefringence of a 10 mm long KTP crystal, which was introduced into one of the arms of the interferometer. The relative intensity of the two peaks was adjusted by rotating the crystal. A polarizer was inserted before the fiber in order to assure that both excitation pulses were linearly polarized in the same direction. An Er-doped fiber amplifier was used in this experiment to amplify the input pulses before they enter the fiber under test, in order to enhance the generated echo.

Figure 4(a) shows the echo generated when the double-pulse is the first to enter the fiber. Ideally, the echo in this case should be a time-reversed replica of the first excitation pulse. Figure 3 clearly demonstrates the time-reversal property, although it is also evident that the ratio of the two peaks is distorted. Figure 4(b) shows a similar experiment where the double pulse was arriving second. The echo clearly shows a triple peaked signal; in the small signal limit, this echo can be shown to be the autoconvolution of the second excitation pulse [3]. Again, we observed significant distortion of the echo pulse shape, particularly when the excitation intensity was increased. We believe that the distortions are the result of higher nonlinear effects induced in a strongly saturated system.

In conclusion, we have observed, for the first time, photon echo in Er doped fibers. We have verified that the complex pulse shapes can be stored and recalled, suggesting that erbium doped fibers could be used for femtosecond time-domain optical signal processing. Our data suggest that the erbium-doped fiber system is suitable for processing complex signals with maximum duration of hundreds of picoseconds, with resolution of about 0.5 psec.

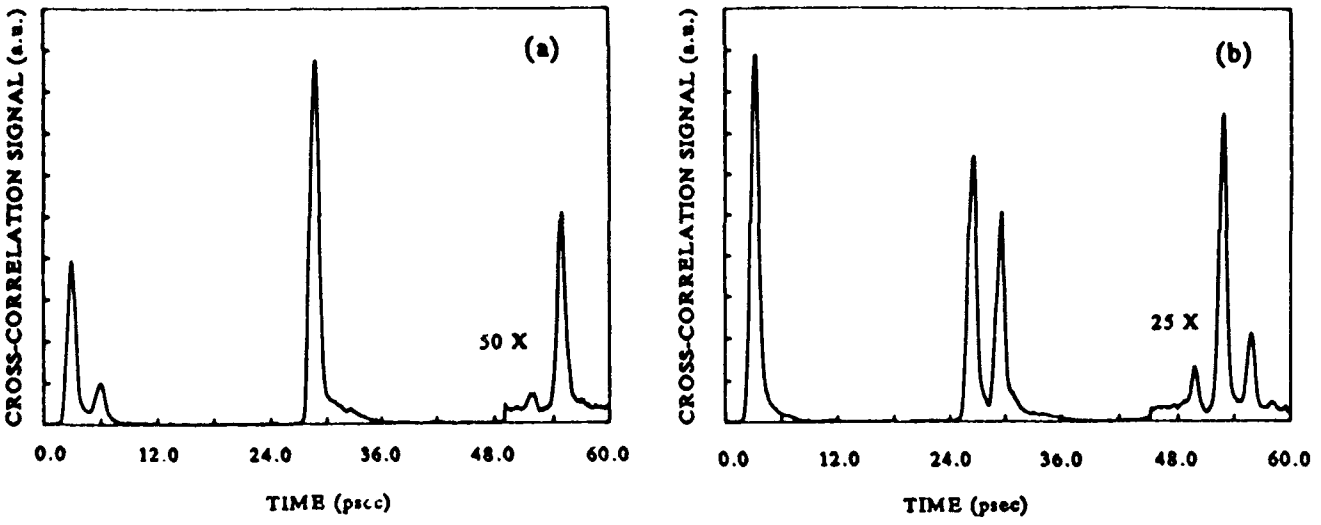

Fig. 4. (a) An echo experiment with a double-peaked leading pulse. The echo is a time-reversed replica of the leading pulse. (b) An echo experiment with a double-peaked trailing pulse. The triple-peaked echo is the auto-convolution of the second pulse. Distortions are caused by higher order saturation effects.

References

1. L. Allan and J. H. Eberly, *Optical Resonances and Two Level Atoms*, Wiley, New York, 1975.
2. W.H. Hesselink and D.A. Wiersma, J. Chem. Phys. 75, 4192 (1981).
3. T.W. Mossberg, Opt. Lett. 7, 77 (1982); N.W. Carlson, L.J. Rothberg, A.G. Yodh, W.R. Babbitt, and T.W. Mossberg, Opt. Lett. 8, 483 (1983); N.W. Carlson, Y.S. Bai, W.R. Babbitt, and T.W. Mossberg, Phys. Rev. A 30, 1572 (1984); Y.S. Bai, W.R. Babbit, N.W. Carlson, and T.W. Mossberg, Appl. Phys. Lett. 45, 714 (1994); W.R. Babbitt and T.W. Mossberg, Opt. Comm. 65, 185 (1988).
4. A. Rebane, R. Kaarli, P. Saari, A. Anijalg, and K. Timpmann, Opt. Comm. 47, 173 (1983); A. Rebane, J. Aaviksoo, and J. Kuhl, Appl. Phys. Lett. 54, 93 (1989).
5. M.K. Kim and R. Kachru, Opt. Lett. 12,, 593 (1987); M.K. Kim and R. Kachru, Opt. Lett. 14, 423 (1989).
6. E. Desurvire, J.L. Zyskind, and J.R. Simpson, IEEE Phot. Tech. Lett. 2, 246 (1990).
7. M.A. Saifi, M.J. Andrejco, W.I. Way, A. Von Lehman, A.Y. Yan, C. Lin, F. Bilodeau, and K.O. Hill, in the Technical Digest of the Optical Fiber Communication Conference 1991, paper FA6.

THE SOLITON FREQUENCY STABILIZATION AND RAMAN SELF-FREQUENCY SHIFT SUPPRESSION IN FIBERS DOPED Er AND Tm IONS

E M Dianov, K K Konstantinov, A N Pilipetskii,
A.N. Starodumov.

General Physics Institute, Academy of Sciences of the USSR
38 Vavilov Street, Moscow 117942, USSR

The possibility of the Raman self-frequency shift [1-3] suppression is of great interest for both the high bit rate communication lines and the lasers with fiber cavities [4]. In the communication lines for picosecond pulses the frequency shifts are small. Frequency drift toward a maximum of the gain profile in an active fibers can compensate to some extent the effect of self-frequency shift. The possibility of frequency stabilization by the effect of frequency pulling under the gain profile was investigated by Blow et al [5]. The frequency pulling to some fixed frequency was predicted instead of the growing with the fiber length soliton frequency shift. The suppression of self-frequency shift due to Raman amplification in the field of external pump wave was experimentally investigated by Gouveia-Neto et al [6].

The processes of picosecond and femtosecond pulse amplification differ considerably. We present here the results of investigation of the ultrashort soliton pulse (~ 100 fs) self-frequency shift suppression in a fiber doped by Er and Tm ions.The SRS and Er gain spectra have a wide bandwidth (~ 440 cm^{-1} and ~ 150 cm^{-1} respectively). We used the causal response functions to describe both an Er and Raman spectra. In contrast to [5] it gives us the possibility to consider more correctly the situation with the femtosecond pulses where frequency bandwidth of the pulse is not too small compared to the gain and Raman spectra. Our calculations have shown that the effect of frequency pulling under the maximum of the amplification line does not permit to compensate for the self-frequency shift for such short pulses. To attenuate the influence of Raman self-scattering and stabilize the frequency

we have introduced in our calculations an additional absorption line in the Stokes spectral region. Such an absorption line may be created by Tm ions. We have revealed that the additional absorption does not guarantee the stabilization of the soliton frequency. It turned out that the stabilization took place only for fixed pulse duration and carrier frequency of the soliton. When the input soliton parameters differ from the optimum the mutual influence of Raman self-scattering, amplification and absorption lines results in an unusual regime of soliton propagation : the soliton carrier frequency and energy oscillate near some fixed values with the fiber length.

We have used the experimentally obtained shapes of the absorption and luminescence lines for Er [7]. Fig 1 demonstrates the process of adiabatic amplification of the fundamental soliton with the parameters $\lambda_0 = 1.55$ μm, $\tau_0 =$ 100 fs in active fiber doped only Er ions with concentration N - $3.1*10^{17}$ cm^{-1}. The soliton propagating through the fiber increases the energy. Pulse duration is shortened that leads to growing of Raman self-frequency shift. The pulse continuously changing the carrier frequency passes through the amplification line. The soliton spectrum comes out from the gain line and the carrier frequency shifts continuously into the Stokes region. Fig. 1 illustrates the iimitation of the output energy due to

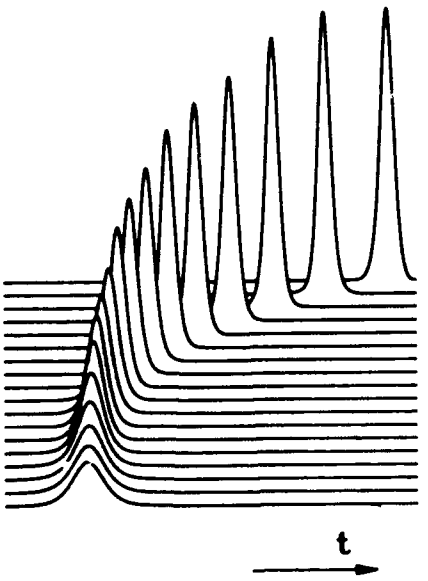

Fig. 1

SRS self-frequency shift. The growing time delay corresponds to the Stokes frequency shift for the fiber with negative dispersion. It should be noted that the group velocity dispersion associated with Er ions may be large enough, but in our case we can neglect it because the concentration of Er ions is rather small. Fig. 2 depicts dependencies of the central pulse frequency on the fiber length for different input pulse durations in fiber doped both Er and Tm ions with concentration $N_1 \sim 1.7 * 10^{18}$ cm^{-3} and $N_2 \sim 2 * 10^{18}$ cm^{-3} respectively. The input pulse wavelength is 1.565 mm. When the pulse duration is great (curves a, b) (so the Raman self-scattering is small) the central pulse frequency is dragged under the amplification line of Er for the first moment.

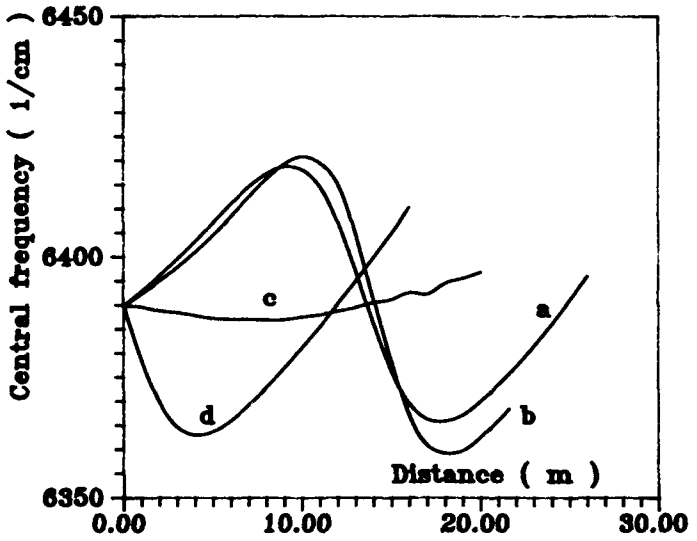

Fig. 2

On the contrary when the input pulse duration is less (curves d) at the first stage the Raman scattering prevails on the effect of frequency pulling under the amplification profile and the soliton loosing the energy and broadening shifts to the Stokes region. Then, as in previous case, the influence of

Raman self-scattering decreases and the central soliton frequency is pulled under the amplification profile. Nevertheless when the soliton with some fixed input parameters (wavelength and energy) is launched into the fiber, the soliton energy and carrier frequency don't change considerably during the propagation through the fiber (curve c). These parameters are determined from the following conditions [5]. Firstly, the amplification of one part of the pulse must be fully compensated by the absorption of the other one. Otherwise the pulse energy will either grow or decrease. Secondly, the rate of pulse spectrum pulling in anti-Stokes region toward the peak of the gain should be exactly equal to the Raman self-frequency shift rate to the Stokes region. If these two demands are violated, the pulse either comes out of amplification line and exhausted in absorption line, or it's frequency and energy oscillate along fiber length. In our case to realize the soliton propagation with stable energy and carrier frequency it is necessary to launch in fiber the soliton pulse with $\lambda \sim 1.565$ μm, $\tau_{FWHM} \sim 85$ fs.

REFERENCES

1. Dianov E.M.,Karasic A.Ya., Mamyshev P.V. et al, JETP Lett. 41,242 (1985).
2. F.M. Mitschke, L.F. Mollenauer. Opt. Lett., 11, 659 (1986).
3. J.P.Gordon. Opt. Lett., 11, 662 (1986).
4. X. Zhu, P.N. Kean, W. Sibbet., Opt. Lett., 14, 1192 (1989).
5. K.J. Blow, N.J. Doran, D. Wood. J. Opt. Soc. Am. B, 5,1301 (1988).
6. A.S. Gouveia-Neto, A.S.L. Gomes, J.R. Taylor., Opt. Lett., 14, 514 (1989).
7. Belov A.V., Gurjanov A.I., Gusovskij D.D. et. el. Sov. High purity substances., 3, 205 (1990).

THE ROLE OF THE SOLITON SELF FREQUENCY SHIFT IN THE AMPLIFICATION OF FEMTOSECOND FUNDAMENTAL SOLITONS USING Er-DOPED FIBERS

W. Hodel, J. Schütz, and H. P. Weber
Institute of Applied Physics, University of Bern
Sidlerstrasse 5, CH-3012 Bern
Phone 031 65 89 51; Fax 031 65 37 65

1. Introduction

Recently there has been considerable interest in the amplification of solitons with the use of Er-doped fiber amplifiers because of their possible application in long distance optical communication systems. Among the many advantages of this type of active fiber are the high gain (> 30 dB) in the 1500 nm region, the wide gain bandwidth (in the order of 30 nm), the polarization independent gain and the high saturation output power. Especially the large bandwidth makes Er-doped fibers attractive candidates for the amplification of ultrashort pulses (with pulse durations in the order of 100 fsec). Whereas some authors have reported on experimental results of short pulse amplification [1,2,3,4], only little theoretical work has been done in this field up to now [5]. Agrawal [5] and earlier Blow et al [6] have pointed out that bandwidth-limited amplification of ultrashort solitons results in a suppression of the soliton self frequency shift (SSFS). This, however, is in contrast to recent experimental results which show that the SSFS is gain enhanced [1]. We will present numerical results for the amplification of ultrashort fundamental solitons in Er-doped fibers based on an extended version of the nonlinear Schrödinger equation which takes into account the influence of group-velocity dispersion (GVD) including higher order dispersion, self phase modulation, the Raman self scattering effect and the frequency dependent gain and phase shift provided by the fiber amplifier. Our calculations clearly demonstrate the deleterious influence of the SSFS on the amplification of 100 fsec solitons: the energy gain that can be extracted from the amplifier is limited to very small values because the SSFS rapidly shifts the pulse spectrum outside the gain bandwidth.

2. The Numerical Model

The propagation of ultrashort pulses in an undoped fiber is governed by an extended version of the nonlinear Schrödinger equation which for the electric field amplitude A has the form

$$i\,dA/dz - 1/2\,k''\,d^2A/dt^2 - i/6\,k'''\,d^3A/dt^3 = -\,n_2k\,A\,[(1-\alpha)\,|A|^2 + \alpha \int_0^\infty h(t')\,|A(t-t')|^2\,dt'] \quad (1)$$

The second and third term on the left hand side describe the influence of group-velocity dispersion (GVD) and higher order dispersion, respectively. The first term on the right hand side describes self phase modulation and the second term represents the Raman-self scattering process using the response function approach (α = 0.2 and h(t') is the dimensionless normalized response function which we take as a single sided exponential with a decay time of 70 fsec). In our

model the nonlinear differential equation (1) is solved by the split-step Fourier technique. In this way the effects of amplification can easily be taken into account in the frequency domain. For the sake of simplicity the gain profile is assumed to have a Lorentzian shape centered at 1540 nm with a spectral width of 30 nm (3.8 THz). The associated frequency dependent phase shift is calculated using the Kramers-Kronig relations. Note that the values for the gain parameter G given below are defined as the peak intensity gain for the case where additional nonlinear and dispersive effects (which lead to temporal and spectral reshaping of the pulses) as well as bandwidth effects (which are important for pulses with a spectral extent larger than the gain bandwidth) are negligible. Since such pulse shaping effects cannot be neglected when amplifying ultrashort solitons we will characterize the efficiency of amplification by the net energy gain. Note also that saturation effects are neglected in equ. (1) because the saturation energy for fiber amplifiers is in the order of 1 μJ and therefore much larger than the pulse energy for sub-picosecond pulses which typically is in the order of a few nJ or less.

3. Numerical Results

We have numerically studied the amplification of 100 fsec fundamental solitons for values of the gain parameter up to G = 200 (23 dB). The dispersion parameters of the amplifying fiber are assumed to be those of a standard telecommunication fiber (GVD parameter D = -15 psec/(km·nm), third order dispersion parameter $k''' = 6 \cdot 10^{-5}$ psec^3/m at 1540 nm). The fiber length (2.7 m) corresponds to approximately ten soliton periods (the soliton period is 26.8 cm) so that the amplification - at least for not too large values of G - should be adiabatic. In the following we will briefly summarize the main features of ultrashort soliton amplification. The temporal and spectral shapes after amplification are shown in Fig. 1 (a) and (b) as a function of the gain parameter G.

Since the peak power of a fundamental soliton scales inversely with the square of the pulse duration the amplification causes a pulse compression in the time domain. In the frequency domain this is accompanied by a spectral broadening and an enhancement of the (differential) soliton self frequency shift which is inversely proportional to the fourth power of the pulse duration. As a consequence the pulse spectrum rapidly shifts outside the gain bandwidth and the amplification of these frequency components stops. The further evolution of the pulse is governed only by the combined effects of dispersion, self phase modulation and Raman self scattering. It is important to note that the resulting Stokes shifted pulses are fundamental solitons: the maximum deviation of the numerically calculated time bandwidth products from the ideal value for a sech^2 pulse is only 2%. Figure 1 (b) shows that during the formation of the Raman solitons some energy is left behind at the original frequency propagating ahead in time of the shifted soliton pulse. In an undoped fiber this energy would evolve into a dispersive wave. In the active fiber these frequencies experience gain and are progressively amplified which leads to the generation of a second pulse at the original wavelength (see Fig.1a). It can be anticipated that for sufficiently large gains this process would repeat itself and a train of solitons at different wavelengths would be produced. Figure 2 shows the resulting energy gain for both pulses (total energy gain) and for the Raman soliton only. It should be pointed out that the maximum energy gain for a 100 fsec pulse calculated without additional nonlinear and dispersive effects is only 75 because the width of the pulse spectrum is approximately the same as the gain bandwidth. It is nevertheless evident that the maximum achievable energy gain is limited to very small values (< 4) due to the gain enhanced soliton self frequency shift.

Although efficient amplification of ultrashort fundamental solitons in an Er-doped fiber is hardly possible due to the enhanced SSFS, this effect can be used to

generate Raman solitons over a large wavelength range using very short pieces of fiber (negligible fiber loss!). The centre wavelength of these Raman solitons can thereby be tuned by choosing the appropriate gain. This fact is illustrated in Fig. 3 which shows the frequency shift of the Raman soliton as a function of the gain parameter G.

4. Discussion and Conclusions

Our numerical results clearly demonstrate that the soliton self frequency shift plays a major role in the amplification of ultrashort fundamental solitons in Er-doped fiber amplifiers: efficient amplification is no longer possible when the pulse duration is in the order of 100 fsec. It is important to note in this respect that the SSFS will therefore also limit the amplification efficiency of initially longer pulses. The pulse compression during the amplification process may result in pulses as short as 100 fsec before the pulse has travelled along the entire amplifier length.
We have also shown that the SSFS is distinctly gain enhanced. This is in agreement with recently published experimental results [1] but contradicts theoretical predictions that bandwidth limited amplification should lead to a suppression of the SSFS [5,6]. In both of these theoretical models the gain profile is approximated by a parabola. This approximation is certainly valid as long as all the spectral components are located in the vicinity of the gain peak which, however, does not hold anymore if the SSFS becomes large. In the parabolic gain profile approximation frequencies far away from the gain peak experience an artificial loss and are suppressed. In our opinion this analytically introduced loss - and not the bandwidth limited amplification - is responsible for the observed suppression of the SSFS. It should be mentioned in this context that a straightforward way to reduce the SSFS would be to use a fiber with a small dispersion (the differential SSFS is proportional to the fiber GVD parameter). If we take a value of $D = -1.5$ psec/(km·nm) instead of $D = -15$ psec/(km·nm) used in the calculations the amplifier length of 2.7 m would correspond to only one soliton period. Preliminary numerical results show that in this case the amplification induces severe pulse distortions and pulse break up even for small values of the gain parameter G. Further details will be given in the talk.

5. References

[1] "Femtosecond erbium-doped optical fiber amplifier" by M. Nakazawa, K. Kurokawa, H. Kubota, K. Suzuki, and Y. Kimura, APL 57 (7), 1990.
[2] "Amplification of femtosecond pulses in Er^{3+}-doped single-mode optical fibers" by I. Yu. Khrushchev, A. B. Grudinin, E. M. Dianov, D. V. Korobkin, V. A. Semenov, and A. M. Prokhorov, Electron. Letters 26 (7), 1990.
[3] "Decay of femtosecond pulses during amplification in single-mode optical fibers doped with Er^{3+} ions" by A. B. Grudinin, E. M. Dianov, D. V. Korobkin, A. Yu. Makarenko, A. M. Prokhorov, and I. Yu. Khrushchev, JETP Letters 51 (3), 1990.
[4] "Femtosecond soliton amplification in Erbium doped silica fiber" by B. J. Ainslie, K. J. Blow, A. S. Gouveia-Neto, P. J. G. Wigley, A. S. B. Sombra, and J. R. Taylor, Electron. Letters 26 (3), 1990.
[5] "Effect of gain dispersion and stimulated Raman scattering on soliton amplification in fiber amplifiers" by G. P. Agrawal, Opt. Letters 16 (4), 1991.
[6] "Suppression of the soliton self-frequency shift by bandwidth-limited amplification", K. J. Blow, N. J. Doran, and D. Wood, J. Opt. Soc. Am. B 5 (6), 1988.

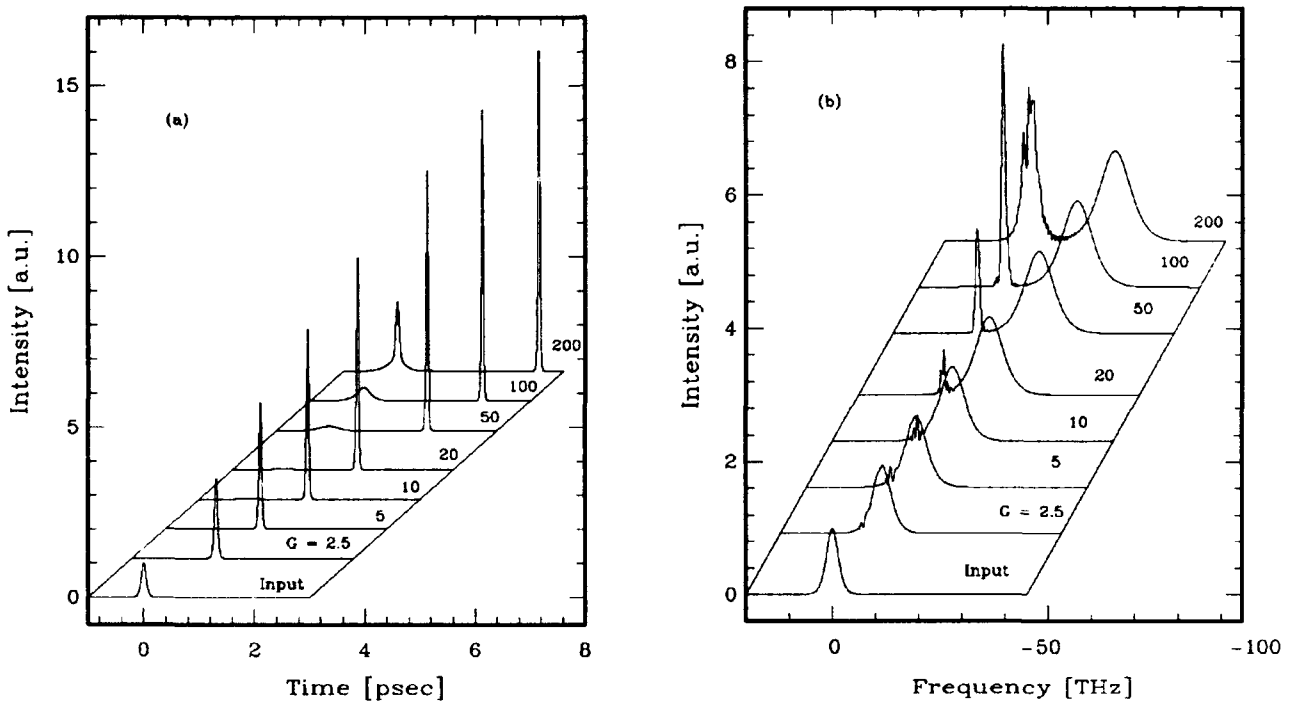

Figure 1: The temporal (a) and spectral shapes (b) after amplification of an initially 100 fsec soliton as a function of the gain parameter G.

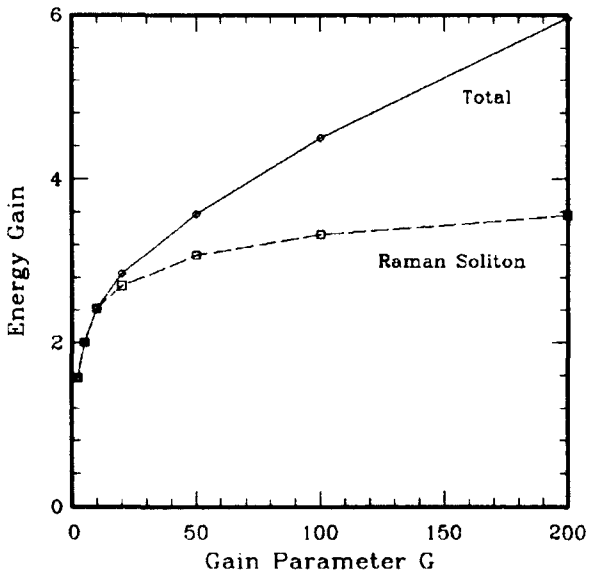

Figure 2: The total energy gain and the energy gain of the Raman soliton as a function of the gain parameter G.

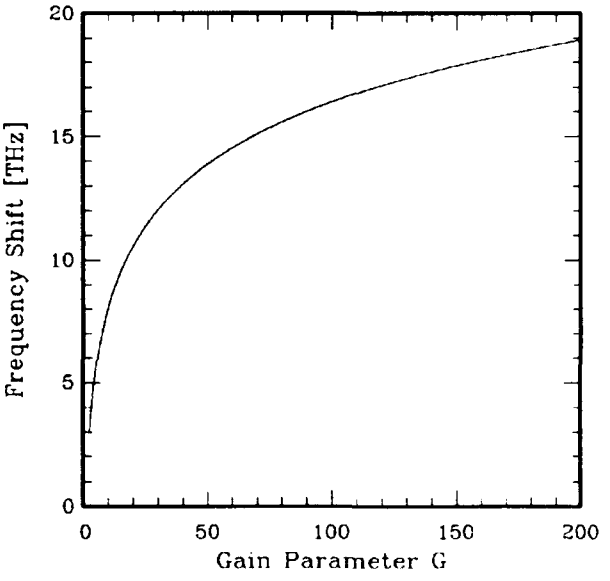

Figure 3: The frequency shift of the Raman soliton as a function of the gain parameter G.

Theory of Ultrashort Soliton Amplification in Erbium-Doped Fibers

I.R. Gabitov

L.D. Landau Institute for Theoretical Physics, Kosygina 2, 117334 Moscow, USSR

M. Romagnoli, and S. Wabnitz

Fondazione Ugo Bordoni, Via B. Castiglione 59, 00142 Rome, Italy

1. INTRODUCTION

The use of active fiber lasers and amplifiers for soliton generation and transmission seems to offer a breakthrough towards the application of nonlinear optics to all-optical information processing systems. As far as picosecond solitons are concerned, erbium-doped fibers simply behave as linear amplifiers. However, it is very important to understand what is the lower bound to the time width of a soliton that can be amplified in practice. Moreover, the amplification of ultrashort pulses is subject to both Raman and coherent effects which may add novel interesting physical effects to the soliton dynamics.

Several recent experiments [1-3] have reported the amplification of femtosecond solitons in erbium-doped fibers. The spectral width of these solitons was comparable to the linewidth of the amplifier. As a consequence, the observed gain was reduced with respect to the gain measured for weak continuous wave signals. It was also observed that the amplified soliton time width may remain essentially unchanged. Indeed, the pulse shape is determined by two competing and opposite factors. From one side, the anomalous dispersion of glass and the Kerr effect lead to pulse compression for solitons or order higher than one. On the other hand, the pulse spectrum experiences a finite bandwidth gain. This leads to preferential amplification of the on-resonance pulse spectrum components, which would lead to pulse broadening. As we shall see, the balancing between these two effects is unstable.

In fact, in ref.[3] it was observed that upon increasing the pumping (or linear gain) above a certain threshold value, the soliton is subject to a sudden temporal compression, with substantial spectral reshaping. We study here by numerical and analytical means this pulse collapse and the subsequent pulse train formation, that is activated by the development of a self-modulation instability. This instability originates from the breaking of the uniform soliton phase. As we shall see, a train of equispaced ultrashort pulses with different amplitudes is generated by the instability. We study the collision process among these pulses in the presence of Raman self-scattering. We anticipate that a single compressed and amplified soliton may eventually exit from the fiber.

2. THEORY

Soliton propagation in the presence of finite bandwidth gain may be studied by introducing linear gain and gain dispersion in the nonlinear Schrödinger (NLS) equation [3-5]. Indeed, previous numerical studies have shown that the presence of a soliton compression effect may still be captured by this relatively simple model [3-5]. However, that approximation is only valid in cases where the spectral width of the pulse is much narrower than the amplifier bandwidth [6]. This condition is clearly not satisfied with pulsewidths of 200 fs or shorter [1-3]. Moreover, the instability generates a train of compressed pulses with typical widths of 50 fs. Therefore a correct analysis of femtosecond soliton dynamics in erbium-doped fibers requires that the coherent nature of the

interaction between field and atoms is retained, along with intrapulse Raman scattering effects [7].

The coupled equations for the single mode electric field E in the fiber and the polarization P and population inversion W of the system of two-level atoms (that is supposed to be the homogeneously broadened) in the active fiber read, in dimensionless units,

$$\begin{aligned} \frac{\partial E}{\partial z} + \frac{i\beta''}{2}\frac{\partial^2 E}{\partial t^2} &= iR\left(\rho|E|^2 + (1-\rho)\int_{-\infty}^{t}|E(\tau)|^2 f(t-\tau)d\tau\right)E + P \\ \frac{\partial P}{\partial t} &= \frac{P}{T_2} + EW \\ \frac{\partial W}{\partial t} &= -\frac{1}{2}(PE^* + EP^*). \end{aligned} \tag{1}$$

where $1-\rho \simeq 0.2$ is the fractional Raman contribution to the nonlinear index of glass [7], R is the the Kerr effect coefficient, and β'' is the host glass group velocity dispersion (GVD). Furthermore, $f(t)$ is the Raman response function of silica [7], and T_2 is the dephasing time of the atomic polarization.

Even in the absence of Raman effects, the system of coupled NLS and Maxwell-Bloch equations (1) is, in general, nonintegrable by means of the inverse scattering transform. For some special values of the physical parameters in eqs.(1), however, the above system is integrable and soliton solutions exist. We will discuss these cases and present some new relevant extensions of the theory of integrability to the system (1) (with $\rho = 1$).

3. RESULTS

In the following we present numerical solutions of eqs.(1) that simulate the experimental conditions in ref.(3), which permits us to establish the validity of the present model. We have at the input of the inverted atomic system a pulse that is close to a N=1 soliton of the NLS equation

$$\begin{aligned} E(z=0,x,t) &= A_0\sqrt{\beta/R}sech(t) \\ P(z,t=-T) &= 0, W(z,t=-T) = 1. \end{aligned} \tag{2}$$

Here T is half of the computational temporal window.

Figures (1-2) show the calculated pulses and spectra at two successive distances along the fiber. We have considered a fiber dispersion of $D = -5ps/nm \cdot km$, and an input pulse width at half maximum $\tau_0 = 250fs$. The estimated homogeneous linewidth of the erbium transition at $\lambda = 1.55\mu m$ is of $10nm$, which leads, in real units, to $T_2 \simeq 250fs$. The doping concentration was set to $N = 5 \times 10^{18}cm^{-3}$, whereas the atomic dipole moment of erbium is $\wp = 2.5 \times 10^{-20}esu$.

Figure (1) shows the output pulse profile and spectra after 1.5 and 3 m of erbium doped amplifier, for a linear gain of 4.2 dB/m and with $A_0 = 1.4$. As can be seen, the soliton collapses down to a width of about 40 fs, whereas in the frequency domain the soliton spectrum exhibits three distinct spectral peaks. The relative height of these peaks depends on the ratio between the input pulsewidth and T_2.

Figure (2) separately illustrates the effects of the coherent soliton dynamics after the compression, and the effects of including Raman self-scattering. Here the fiber length

is 6m and the gain is 7 dB/m. The figure on the left has been calculated without the Raman term in eqs.(1), whereas in the next figure the Raman effect is included. In the absence of the Raman effect, a train of pulses is generated. These are not independent solitons: rather, the train may be thought as a chain of infinitely many coupled solitons, in analogy with the self-similar pulse trains from a two-level amplifier in the absence of GVD and Kerr effect. Indeed, we may introduce a new analytical description of this pulse-train generation effects, on the basis of the self-similarity properties of eqs.(1).

Figures (2-3) show that in the presence of the Raman effect the higher intensity leading pulse of the train gains energy from multiple inelastic collisions with the other pulses. Eventually, this soliton separates from the background owing to soliton self-frequency shift. Figure (3) shows the broad and rapidly oscillating down-shifted spectrum that is associated with the emerging soliton.

4. CONCLUSIONS

In summary, we discuss both analytically and numerically the nonlinear dynamics of femtosecond soliton compression, soliton train generation and collision in erbium-doped fiber amplifiers.

This work was carried out in the framework of the agreement between Fondazione Ugo Bordoni and the Istituto Superiore Poste e Telecomunicazioni.

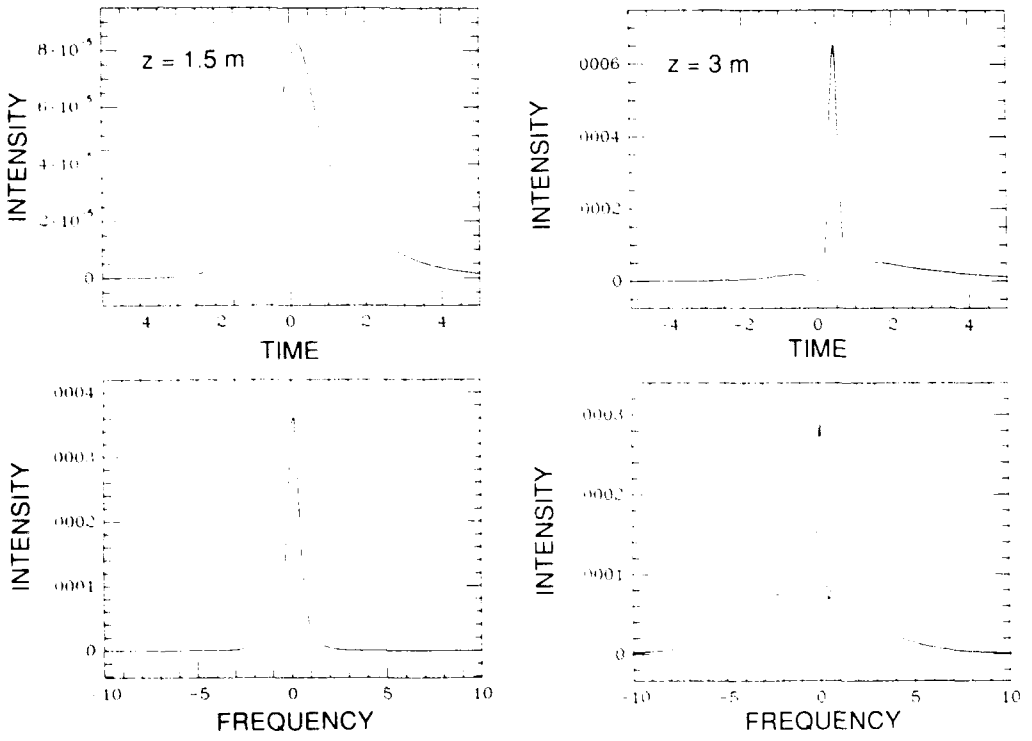

Figure [1]: Output pulse profiles and spectrum of the pulse at two successive distances in the fiber.

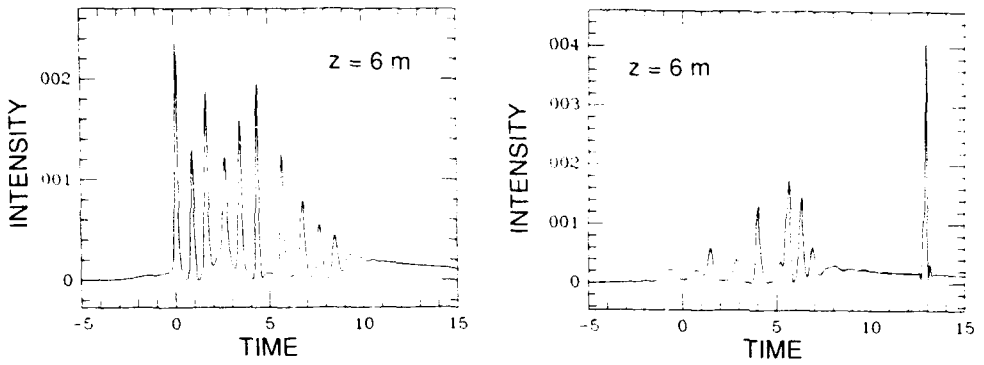

Figure [2]: Time-domain output waveforms without (left) and including Raman effect (right).

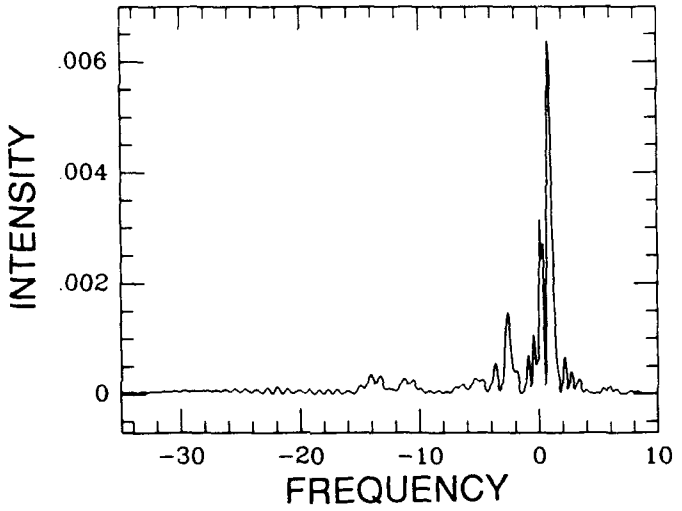

Figure [3]: Spectrum associated with the above figure (right).

REFERENCES

[1] B.J. Ainslie, K.J. Blow, A.S. Gouveia-Neto, P.G.J. Wigley, A.S.B. Sombra, and J.R. Taylor, Electron. Lett. **26**, 186 (1990).

[2] I.Yu. Khrushchev, A.B. Grudinin, E.M. Dianov, D.V. Korobkin, V.A. Semenov, and A.M. Prokhorov, Electron. Lett. **26**, 456 (1990); A.B. Grudinin, E.M. Dianov, D.V. Korobkin, A.Yu. Makarenko, A.M. Prokhorov, and I.Yu. Khrushchev, JETP Lett. **51**, 135 (1990).

[3] M. Nakazawa, K. Kurokawa, H. Kubota, K. Suzuki, and Y. Kimura, Appl. Phys. Lett. **57**, 653 (1990); M. Nakazawa, K. Kurokawa, H. Kubota, and E. Yamada, Phys. Rev. Lett. **65**, 1881 (1990).

[4] K.J. Blow, N.J. Doran, and D. Wood, J. Opt. Soc. of Am. **B 5**, 381 (1988).

[5] G.P. Agrawal, Opt. Lett. **16**, 226 (1991).

[6] I.V. Mel'nikov, R.F. Nabiev, and A.V. Nazarkin, Opt. Lett. **15**, 1348 (1990).

[7] E.M. Dianov, A.Ya. Karasik, P.B. Mamyshev, A.M. Prokhorov, V.N. Serkin, M.F. Stelmakh, and A.A. Fomichev, JETP Lett **41**, 294 (1985); F.M. Mitschke, and L.F. Mollenauer, Opt. Lett. **11**, 659 (1986).

THEORY OF FEMTOSECOND SOLITON AMPLIFICATION IN RARE-EARTH-DOPED FIBERS

V.V. Afanasjev, V.N. Serkin
Academy of Sciences of the USSR, General Physics Institute
38 Vavilov Street, 117942 Moscow USSR
Telephone: (095) 132 83 06, Telex: 411074 LIMEN SU, Fax: (095) 135 02 70

V.A. Vysloukh
Moscow State University, Physics Department, 119899 Moscow USSR
Telephone (095) 939 30 91

Recent demonstrations of the transmission of optical solitons amplified using the Raman process [1] or the amplification process in the rare-earth-doped fibers [2, 3] promise not only prospects to all-optical high speed transmission systems, but also to femtosecond laser systems.

In this paper we analyze the influence of Kerr and Raman nonlinearities on the dynamics of femtosecond solitons amplification in rare-earth-doped fiber. Raman self-frequency shift transfers the central soliton frequency far from the gain bandwidth and as a result the process of soliton amplification is finished. Our main purpose is to discuss utmost degrees of femtosecond soliton compression and amplification in rare-earth-doped fibers and to investigate optimal conditions of soliton transmission with conserving high signal-to-noise ratio.

The process of amplification of light pulses is describe by the well known Bloch eqs.:

$$\frac{\partial^2 P^{amp}}{\partial t^2} + \frac{2}{T_2^{amp}}\frac{\partial P^{amp}}{\partial t} + \Omega_0^2 P^{amp} = -2N^{amp}E\frac{\Omega_0}{h}|d|^2; \tag{1}$$

$$\frac{\partial N^{amp}}{\partial t} + \frac{N^{amp} - N_0}{T_1^{amp}} = \frac{2}{h\Omega_0}E\frac{\partial P^{amp}}{\partial t}. \tag{2}$$

For correct description of soliton self-frequency shift in the time domain, it is possible to use the model of two coupled oscillators with parametric interaction between nucleus and electrons of molecule. From this model one can derive the equation for Raman polarization and molecular vibrations Q:

$$\frac{\partial^2 Q}{\partial t^2} + \frac{2}{T_2^{Ram}}\frac{\partial Q}{\partial t} + \Omega_{Ram}^2 Q = \frac{1}{2M}\frac{\partial \alpha}{\partial Q}n < E^2 > . \tag{3}$$

Period of molecular oscillations $T^{Ram} = 2\pi/\Omega_{Ram}$ in silica core fibers is about 75 fsec, therefore it is necessary to solve exactly eq. (1-3) without using slowly varying approximation (SVA). Standard procedure of SVA for electromagnetic wave E (but not for molecular wave Q, when supposing that $N^{amp} \approx N_0 = const$), provides the following system of eqs.[4]:

$$i\frac{\partial \psi}{\partial z} = \frac{1}{2}\frac{\partial^2 \psi}{\partial \tau^2} + i\frac{GP}{2} + \delta n_{eff}\psi; \tag{4}$$

$$\gamma_{amp}\frac{\partial P}{\partial \tau} + P(1 + i\Delta\Omega\gamma_{amp}) = \psi; \tag{5}$$

$$\mu^2 \frac{\partial^2 Q}{\partial \tau^2} + 2\mu\gamma \frac{\partial Q}{\partial \tau} + Q = |\psi|^2; \tag{6}$$

$$\delta n_{eff} = \delta n_{Kerr} + \delta n_{Ram}; \delta n_{Kerr} = (1-\beta)|\psi|^2; \delta n_{Ram} \equiv Q. \tag{7}$$

Variables in eq. (4 - 7) are measured in soliton units (see more detailed [5]).

A key role in the process of short pulse amplification in rare-earth-doped fibers is played by the relationship between the amplification length Z_{amp} and dispersion length Z_{disp}. This relationship is determined by a parameter $G = Z_{amp}/Z_{disp}$.

If the gain is sufficiently small using a perturbing technique, one can obtain the one-soliton solution of (4 - 7) with adiabatically varying form-factor $\kappa = \kappa(z)$ and velocity $V = V(z)$ caused by frequency-dependent gain and Raman self-shifting effect:

$$\psi(z,\tau) = \kappa(z) sech[\kappa(z)(\tau - V(z)z)] exp[-iV(z)\tau + i(V^2(z) - \kappa^2(z))z/2]. \tag{8}$$

The soliton form-factor $\kappa(z)$ defines not only soliton's amplitude, but also its duration $\tau_s(z) = 1/\kappa(z)$ and energy $W_s(z) = 2\kappa(z)$.

The soliton energy increases as $\kappa(z)$, and it means that soliton adiabatically transfers to another soliton, so-called, Raman high-energy soliton. The degrees of soliton intensity increasing and compression may be obtained from very simple condition of overlapping of soliton spectrum and gain bandwidth. If we use the original physical parameters this means that the intensity and pulse width of the forming soliton are:

$$I_{out}/I_0 \approx \sqrt{15\tau_0^4 g_{amp}/\tau_d k_\omega'' T_2^{amp}} = \sqrt{15G/\gamma_{amp} 2\mu\gamma 3}; \tau_0/\tau_{out} \approx \sqrt{I_{out}/I_0}. \tag{9}$$

Where $\tau_d \approx 6$ fsec is the Raman delay time, $T_2^{amp} \approx 100$ fsec determines a finite gain bandwidth, k_ω'' - group velocity dispersion parameter and g_{amp} - gain per length.

For example, 100 fsec initial soliton at $\lambda = 1.5\mu$m in erbium doped fiber with $g_{amp} = 10^{-2} cm^{-1}$ may be adiabatically compressed to about $\tau_{out} = 30$ fsec with increasing intensity up to 10. In case on non-adiabatic amplification process ($G \geq 1$) a one-soliton pulse transforms, generally, into a multisoliton one. Besides, the energy of the non-soliton component of the radiation grows the non-adiabatic regime of pulse amplification and the process of new solitons arising is illustrated in Fig. 1 ($G = 1, \tau_0 = 100$ fsec, $\gamma_{amp} = 1$). The dynamics of the Fourier-spectrum transformation is shown in Fig. 2. In the Fourier-spectrum, one can see separation of components connected with the soliton and carrying the main share of energy. This is so called Raman high-energy soliton (see Fig. 1). The other part of the Fourier-spectrum, which corresponds to the central frequency of the input pulse, continues to be amplified, and acquires a rather complex structure. In the time domain, additional pulses appear.

Dependencies of the degree of compression τ_0/τ_{out} on the initial duration are given in Fig. 3 ($T_2^{amp} = 100$ fsec). The solid lines depict the asymptotical dependencies corresponding to formulae (9), the circles ($\circ, \bullet$) are the results of numerical experiments. The dependence with $G = 0.2$ is in a good agreement (the regime is close to the adiabatic one). The asterisk ($*$) show the result [7], which agree well with the calculations.

However the results of our numerical experiment posed a number of questions. What are the parameters of the soliton formed? Will the pulse formed at the center of the gain bandwidth be a soliton? If so, what will its parameters be? To answer these and similar

questions we have applied numerical techniques based on the inverse scattering transform [6]. This technique allows one to find the number of solitons in the pulse and to calculate their parameters, namely, form-factors κ_i, defining soliton amplitudes and durations, velocities (central frequencies) V_i, coordinates of the center and phases. The method applied also allows one to calculate important characteristics of the amplification process such as maximum degree of compression τ_0/τ_{out}, energy coefficient of amplification $\kappa_1(z)/\kappa_1(0)$, signal-to-noise ratio.

Analysis of the soliton parameters in case of non-adiabatic amplification (Fig. 4, $G = 1$, $\tau_0 = 100$ fsec, $\gamma_{amp} = 1$) shows, that during the amplification process the two additional solitons (with form-factors κ_2, κ_3) are appear. The dependence of the form-factor κ_1 of the Raman high-energy soliton reaches saturation owing to the escape of frequency from the center of the amplification line.

The results of calculations of energy amplification coefficient are shown in Fig. 5 ($\tau_0 = 100$ fsec, $\gamma_{amp} = 1$). The saturation of the form-factors dependent on G can be seen. Note, that growth of G by an order results in twofold energy growth in Raman high-energy soliton. The utmost amplification dependent on G is illustrated by the curve "Limit" (Fig. 6, $\tau_0 = 100$ fsec, $\gamma_{amp} = 1$). Introducing a noise-to-signal ratio $N_s = (W_0 - W_s^1)/W_s^1$, where $W_0(z)$ is the total energy of the pulse and $W_s^1 = 2\kappa_1$ is energy of the Raman high-energy soliton, we have investigate the dependence of the maximum amplification coefficient $\kappa_1(z)/\kappa_1(0)$, with which the noise does not exceed a given level, on G parameter (Fig. 6, the noise level, is indicated near the curves). The key peculiarity of these dependencies is the existence of a distinct optimum, shifting towards small G as N_s decreases.

Thus, combining analytical methods based on inverse scattering transform and numerical techniques, one can describe in detail the dynamics of femtosecond soliton amplification and calculate the conditions of optimum amplification.

References

[1] L.F. Mollenauer and K. Smith, *Opt. Lett.*, **13**, p. 675 (1988).

[2] L.F.Mollenauer, M.J. Neubelt, S.G. Evangelides, G.P. Gordon, J.R. Simpson and L.G. Cohen, *CLEO'90*, **PDP 17**, p. 633 (1990).

[3] M. Nakazawa, K. Suzuki and Y. Kimura, *Opt. Lett.*, **14**, p. 1065 (1989); M. Nakazawa, Y. Kimura and K. Suzuki, *Electron. Lett.*, **25**, p. 199 (1989); M. Nakazawa, Y. Kimura, K. Suzuki, H. Kubota, *J. Appl. Phys.*, **66**, p. 2803 (1989).

[4] V.V. Afanasjev, E.M. Dianov, A.M. Prokhorov and V.N. Serkin, *Pisma Zh. Teh. Fiz.*, **16**. p. 67 (1990) (in Russian) (Sov. Phys. JTP Lett.).

[5] V.V. Afanasyev, V.A. Vysloukh and V.N. Serkin, *Opt. Lett.*, **15**, 489 (1990).

[6] V.A.Vysloukh and I.V. Cherednik, *Dokl. Akad. Nauk*, **289**, p. 336 (1986) (in Russian) (USSR Academy of Sciences Reports).

[7] M. Nakazawa, K. Kurokawa, H. Kubota, K. Suzuki and Y. Kimura, "A femtosecond erbium-doped optical fiber amplifier" *Appl. Phys. Lett.*, (1990).

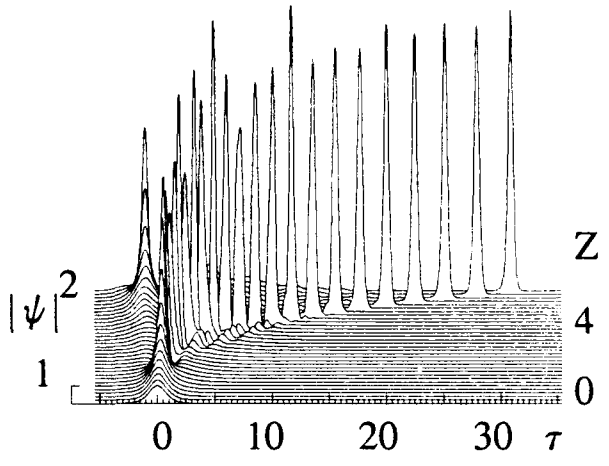

Fig.1

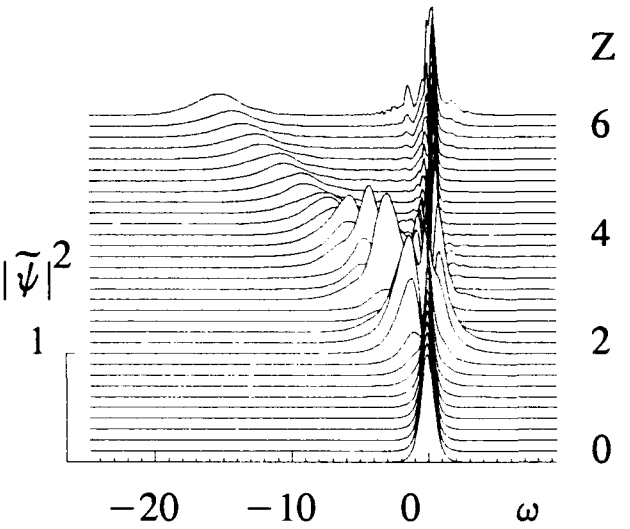

Fig.2

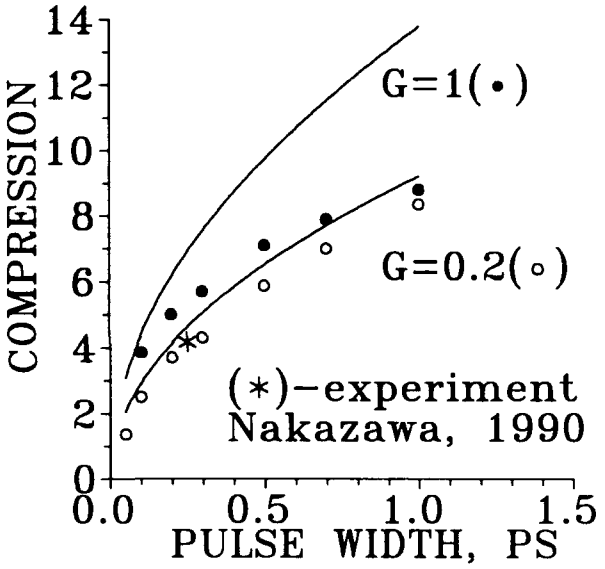

Fig.3

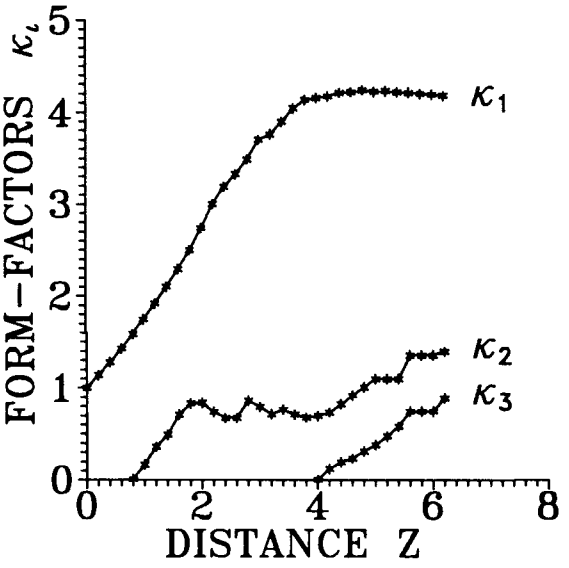

Fig.4

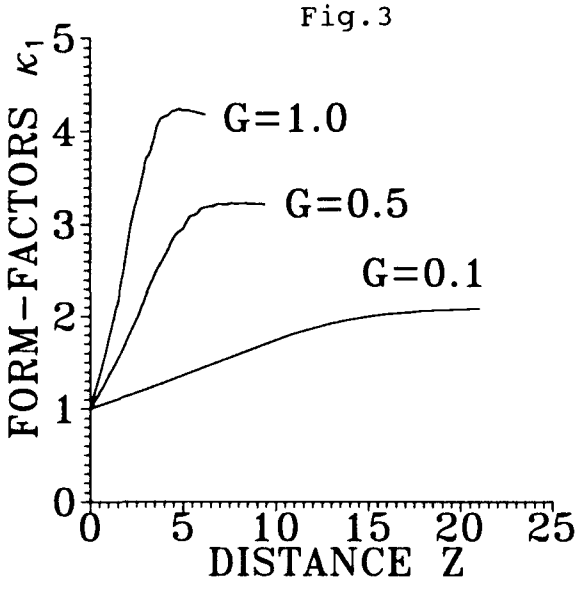

Fig.5

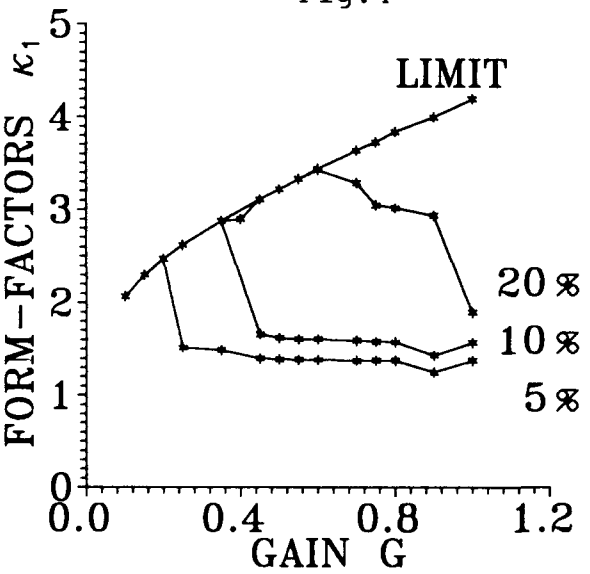

Fig.6

Tuesday, September 3, 1991

Semiconductors

TuB 11:00am–12:45pm
Palmerston Room

Allan D. Boardman, *Presider*
University of Salford, United Kingdom

Nonlinear Guided Waves in Semiconductors:

Induced Focusing and Directional Coupling

H. M. Gibbs, G. Khitrova, R. Jin, C. L. Chuang, and J. Xu
Optical Sciences Center
University of Arizona
Tucson, AZ 85721 USA
602-621-2941

Recently, Agrawal[1] suggested a novel focusing effect in a self-defocusing medium. The transverse spatial gradient of the field amplitude of a strong pump beam induces a refractive index profile that can result in focusing and deflection of a weak beam. Below the band edge of a semiconductor, the optical nonlinearity is self-defocusing; far enough above the decreased absorption, the nonlinearity is self-focusing, but the >100 μm length and large absorption there ($\alpha \simeq 1$ μm^{-1}) of a semiconductor waveguide result in no transmission.[2] Hence *induced* focusing is especially intriguing in a passive semiconductor waveguide because *self*-focusing cannot occur.

The planar waveguide structure was grown in our Riber 32P molecular beam epitaxy machine on an undoped GaAs (100) substrate maintained at 600° C as follows: first a 1-μm GaAs buffer for growth smoothing, then a 3-μm $Al_{0.3}Ga_{0.7}As$ bottom cladding of lower index than the guide material and thick enough to prevent evanescent-tail absorption in the substrate, followed by a 1.2-μm guide region consisting of 100 periods of 9.7-nm GaAs/9.9-nm $Al_{0.3}Ga_{0.7}As$ multiple quantum wells, topped by a 1.0-μm top cladding of $Al_{0.13}Ga_{0.87}As$ with a 10-nm GaAs cap layer. The substrate was then ground away to reduce the sample thickness to 40 μm, after which the sample was cleaved to a length of 127 μm. We have etched such planar-waveguide structures to form two-dimensional waveguides and directional couplers and have studied their nonlinear (defocusing) behavior extensively.[3-5]

To observe induced focusing, we use 10-ps pulses cavity-dumped at a 4 MHz rate from a modelocked Stryl-9 dye laser synchronously pumped by an actively modelocked Nd:YAG laser. The pump and probe pulses have energies of 150 and 1.5 pJ and are polarized perpendicular and parallel to the growth axis, respectively. Use of 10-ps pulses with 30-ps delay between them avoids carrier diffusion that would otherwise reduce or eliminate transverse effects with dimensions of a few microns or less. Field-amplitude interference effects are not present because of orthogonal polarizations and the absence of temporal overlap between pump and probe. The nonlinearity here is cumulative, so the induced focusing (Agrawal's cross modulation) is mediated through the spatial profile of carriers (and refractive index) prepared by the pump pulse; this index profile persists much longer than the pump-probe delay time.

We have observed both induced focusing effects predicted by Agrawal. In the first effect, a Gaussian-profile pump induces focusing for a probe of the same profile but displaced by about one beam waist. Figure 1 shows the probe guide-exit transverse profile (perpendicular to the growth axis) with and without the pump. The second effect is induced focusing without deflection by using a twin-peak pump pulse followed by a concentric Gaussian probe pulse; see Fig. 2.

For the computations, the slowly-varying envelope A_I of the intense pump electric field [$E_I = A_I e^{i(k_I z - \omega_I t)} + c.c.$] is assumed to satisfy the standard paraxial-wave equation:

$$\frac{\partial A_I}{\partial z} + \frac{n_I}{c}\frac{\partial A_I}{\partial t} + \frac{1}{2ik_I}\left[\frac{\partial^2}{\partial x^2} + \frac{\partial^2}{\partial y^2}\right]A_I =$$

$$-\frac{ik_I}{2}\left[\left[\frac{n_I(x,y,z,|A_I(t)|^2)}{n_{I0}}\right]^2 - 1\right]A_I - \frac{\alpha_I}{2}A_I \qquad (1)$$

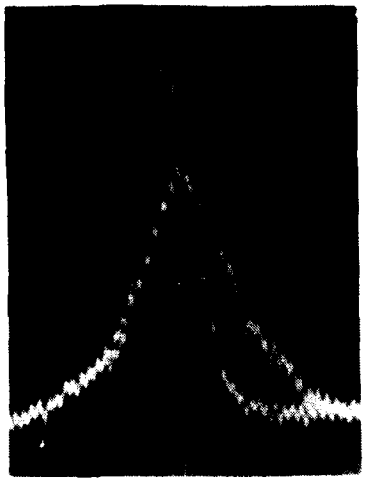

Figure 1. Induced focusing of a probe pulse following a pump pulse displaced to the right by one beam waist. The guide-exit horizontal profile of the probe is shown without the pump (lower-peak broader trace) and with the pump.

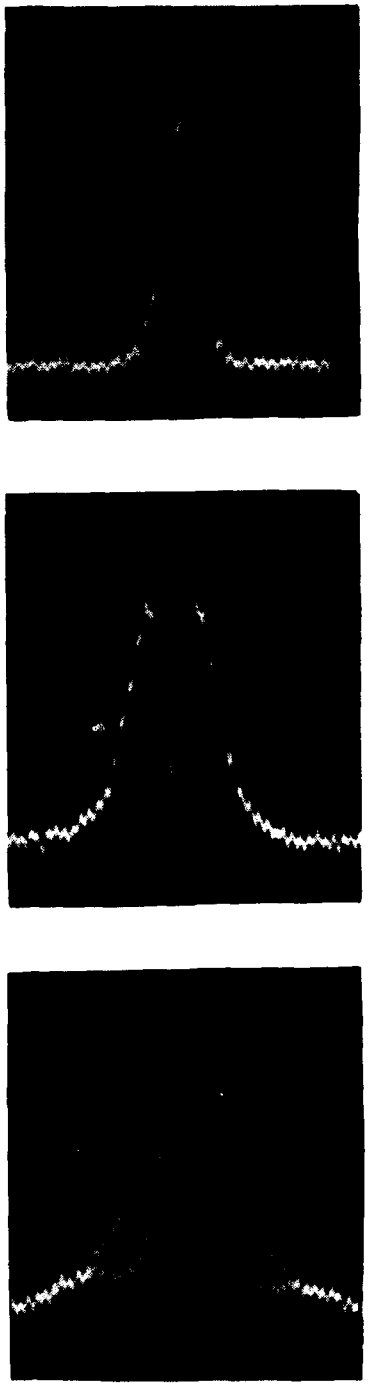

Figure 2. Induced focusing of (a) a probe input pulse by (b) an input twin-peak pump is shown in (c) without the pump (lower-peak broader trace) and with the pump.

where $n_l = n_{l0} + \delta n_l$, δn_l is the change in refractive index because of the carriers generated by absorption of some of the pump intensity $|A_l(t)|^2$ and is computed using the plasma theory,[6] obtaining the carrier density from

$$N(x,y,z,t+\delta t) = N(x,y,z,t) + \int_t^{t+\delta t} \frac{\alpha_l(x,y,z,t')|A_l(x,y,z,t')|^2}{\hbar\omega_l}\,dt', \qquad (2)$$

where the carrier lifetime of a few nanoseconds is much longer than the 30-ps delay between the 10-ps pump and probe pulses. One uses the plasma theory to compute α_l and δn_l for the next δz, etc. Because the weak probe amplitude A_w is much weaker than A_l, it induces no self-defocusing or nonlinear absorption. Consequently, the A_w propagation satisfies an equation identical to Eq. (1) without the time derivative and where $n_w(x,y,z)$ and $\alpha_w(x,y,z)$ are the values induced in the medium by the cumulative effect of the pump pulse:

$$\frac{\partial A_w}{\partial z} + \frac{1}{2ik_w}\left[\frac{\partial}{\partial x^2} + \frac{\partial}{\partial y^2}\right]A_w = -\frac{ik_w}{2}\left[\left[\frac{n_w(x,y,z)}{n_{w0}}\right]^2 - 1\right]A_w - \frac{\alpha_w}{2}A_w \qquad (3)$$

Note that A_l is polarized perpendicular to the growth axis (seeing both heavy- and light-hole absorptions) whereas A_w is polarized parallel to the growth axis (seeing only the light-hole absorption), as a result, n_w, n_{w0}, and α_w are different from n_l, n_{l0}, and α_l. In the modeling, the bulk GaAs plasma theory is used, so different detunings from the band edge are taken for A_l and A_w. Equations (1)-(3) are solved by alternations between free-space diffraction by fast Fourier transformation and nonlinear encoding of amplitude and phase changes in the usual way,[7] using the parameters of our waveguide.

Equations (1)-(3) have the same structure as those we have used to describe the copropagation of a strong pump beam and also two weak probe beams leading to the emission of a cone of light around the pump beam in the far field.[8] Indeed, even the physics is quite similar; conical emission occurs because weak light (generated by Raman amplification of resonance fluorescence plus four-wave mixing) on the defocusing side of the AC Stark-shifted absorption line propagates through the spatial refractive index profile induced by the strong pump beam.

The steady-state limit of Eqs. (1) and (2) have been solved for our ridge-waveguide nonlinear directional coupler using the plasma theory to describe either a passive[9] or gain medium. Using the parameters of our strip-loaded geometry (typically 2-μm strips with 2 μm in between and 0.7 μm etch depth with the same sample described above) and published refractive indices, we find good agreement between computations and experiment for the linear coupling length ($\simeq$ 1 mm), crossover energy, high-energy contrast, etc. The computed linear contrast is higher than measured (typically 1:3 to 1:5).

In summary, Agrawal's prediction of induced focusing in a self-defocusing medium has been clearly demonstrated using the band-edge optical nonlinearity of GaAs/AlGaAs multiple quantum wells. This novel effect illustrates that the spatially-dependent nonlinearities induced by an intense pump beam can have very different effects upon a weak probe.

References

1. G. P. Agrawal, Phys. Rev. Lett. **64**, 2487 (1990).
2. Y. H. Lee, A. Chavez-Pirson, S. W. Koch, H. M. Gibbs, S. H. Park, J. Morhange, A. Jeffrey, N. Peyghambarian, L. Banyai, A. C. Gossard, and W. Wiegmann, Phys. Rev. Lett. **57**, 2446 (1986).
3. R. Jin, C. L. Chuang, H. M. Gibbs, S. W. Koch, J. N. Polky, and G. A. Pubanz, Appl. Phys. Lett. **53**, 1791 (1988).
4. R. Jin, J. P. Sokoloff, P. A. Harten, C. L. Chuang, S. G. Lee, M. Warren, H. M. Gibbs, N. Peyghambarian, J. N. Polky, and G. A. Pubanz, Appl. Phys. Lett. **56**,993 (1990).
5. S. G. Lee, P. A. Harten, R. Jin, B. Fluegel, K. E. Meissner, C. L. Chuang, R. Binder, S. W. Koch, G. Khitrova, H. M. Gibbs, and N. Peyghambarian, Phys. Rev. B **43**(2), 1719 (1991).
6. L. Banyai and S. W. Koch, Z. Phys. **B63**, 283 (1986).
7. J. V. Moloney, M. R. Belic, and H. M. Gibbs, Opt. Commun. **41**, 379 (1982).
8. J. F. Valley, G. Khitrova, H. M. Gibbs, J. W. Grantham, and Xu Jiajin, Phys. Rev. Lett. **64**, 2362 (1990).
9. H. M. Gibbs, G. Khitrova, Xu Jiajin, R. Jin, C. L. Chuang, and S. W. Koch, "Nonlinear Directional Coupler Beam-Propagation Computations with Two Transverse Dimensions and Plasma Theory," CLEO '91, Baltimore, May 12-17, 1991.

Ultrafast Optical Kerr Effect in Active Semiconductor Waveguides

C.T. Hultgren and E.P. Ippen

Department of Electrical Engineering and
Computer Science and Research Laboratory
of Electronics
Massachusetts Institute of Technology
Cambridge, MA 02139

Active optical waveguides offer interesting possibilities for performing nonlinear functions in photonic circuits. By varying the injected carrier density one can change not only the linear components of gain and index of refraction but also the nonlinear ones. Some studies of ultrafast gain dynamics in AlGaAs[1] and InGaAsP[2] diode laser amplifiers have been performed previously. Four-wave mixing experiments with large frequency detunings in diode lasers [3,4] have provided frequency domain measurements of the magnitude of the nonlinear susceptibility of $\chi^{(3)}$. The effect of dynamic index changes has also been revealed by the chirp and spectral changes experienced by ultrashort pulses traveling through amplifiers[5]. In this paper we discuss direct measurements of optically induced changes in index of refraction in active AlGaAs waveguides. With femtosecond pump-probe measurements sensitive, separately, to induced phase and amplitude changes, we have studied the relative amplitudes of these dynamics as functions of wavelength and injection current. We observe nonlinearity due to changes in carrier number, carrier heating and, for the first-time, a large above-bandgap ultrafast optical Kerr effect. An interesting aspect of this latter, instantaneous nonlinearity is that it may be utilized without change in carrier number, by operating near the wavelength of nonlinear transparency (where stimulated emission equals absorption).

In our experiments, we used femtosecond pulses from a synchronously-pumped, cavity-dumped dye laser followed by a fiber/grating-pair pulse compressor. The devices studied were channeled-substrate planar (CSP) AlGaAs diode lasers (Hitachi HLP 1400), biased below lasing threshold. A novel time-division interferometer (TDI) used in conjunction with the standard pump-probe technique enables accurate measurement of the pump-

induced refractive index changes in the diode laser.[6,7] Figure 1 illustrates the TDI arrangement. In addition to the variably-delayed pump and probe pulses, a third, reference pulse is also transmitted through the active waveguide. Afterwards, an imbalanced interferometer delays the well-advanced reference pulse so that it overlaps the probe pulse. A $\pi/2$ optical phase difference bias between the probe and reference is maintained by a low-frequency stabilization circuit. At this point, the amplitude of the probe-reference interference is linearly proportional to the phase shift induced on the probe by the pump. The pump is chopped at a frequency beyond the cut-off of the stabilization circuit and the signal is detected in a lock-in amplifier. Note that amplitude changes are canceled out by the balanced detection scheme. The gain dynamics are observed separately, for reference, by simply blocking the reference and monitoring the probe transmission to one detector.

Pulses traveling through the diode waveguide may experience either gain or absorption, depending upon their wavelength and the level of diode injection current. Under conditions of gain, the pump pulse induces a decrease in carrier density due to stimulated emission. The corresponding reduction in gain, and increase in refractive index, persists for a time on the order of a nanosecond (the carrier lifetime). Similar long term changes, with opposite signs because carriers are being created, are observed when the wavelength is tuned into the absorption regime, higher into the band. Between these two regimes, at the point of nonlinear transparency, the long-lived changes can be avoided. Figure 2 shows experimentally observed changes in amplitude and phase induced near this point. The amplitude dynamic (lower curve) shows the gain being transiently compressed by the pump pulse. Its recovery is comprised of an initial component, too rapid to resolve, followed by a 1.7 psec component that is consistent with previous results attributing such behavior to nonequilibrium carrier heating[1]. The optical phase change (upper curve) observed under the same conditions also has a very rapid intial component followed by a 1.7 psec tail. The difference is the change in sign between components. The 1.7 psec component shows a positive change in index of refraction associated with the carrier heating term. On the other hand, the initial unresolved component represents a negative change in index. It must have a different origin. Since the two effects tend to cancel each other near zero delay, we fit the data to a sum of two components and determine their individual magnitudes. The peak probe phase shift (averaged over the pulse) associated with the faster component is

about -0.2π. This corresponds to a modal index change of -2.5x10^{-4}. Since the pump pulse has a peak intensity of 150 Mw/cm^2 in the waveguide, we infer an intensity dependence of the refractive index of approximately -5x$10^{-12}$$cm^2$/W.

Our experiments were performed with orthogonally polarized pump and probe pulses. Thus, the Kerr coefficient that we measure is $n_{2\perp}$. The ultrafast component we observe is of the same (negative) sign as, but larger than, those measured previously in a below-bandgap study of AlGaAs waveguides[6]. It is consistent with those values if one assumes that the resonant enhancement of $n_{2\perp}$, observed as the wavelength was tuned toward the bandgap energy, continues into the band. The observed positive index change due to carrier heating is consistent with a simple Kronig-Kramer analysis based on the temperature dependence of the gain. At this conference we will also present recent data obtained at different wavelengths and diode currents and will discuss in more detail the physical mechanisms underlying the observed behavior.

This work was supported in part by the AFOSR under contract F49620-88-C-0089, by NSF under grant EET-8815834, and by DARPA through the National Center for Integrated Photonics Technology.

[1] M. P. Kesler and E. P. Ippen, Appl. Phys. Lett. 51, 1765 (1987).

[2] K. L. Hall, J. Mark, E. P. Ippen, and G. Eisenstein, Appl. Phys. Lett. 56, 1740 (1990).

[3] R. Nietzke, P. Panknin, W. Elsaesser and E. Goebel, IEEE J. Quant. Electron. 25, 1399 (1989).

[4] S. Murati, A. Tomita, J. Shimizu, M. Kitamura and A. Suzuki, Appl. Phys. Lett. 58, 1458 (1991).

[5] G. P. Agrawal and N. A. Olsson, IEEE J. Quant. Electron. 25, 1399 (1989).

[6] M. J. LaGasse, K. K. Anderson, C. A. Wang, H. A. Haus and J. G. Fujimoto, Appl. Phys. Lett. 56, 417 (1990).

[7] K. K. Anderson, M. J. LaGasse, C. A. Wang, J. G. Fujimoto and H. A. Haus, Appl. Phys. Lett. 56, 1834 (1990).

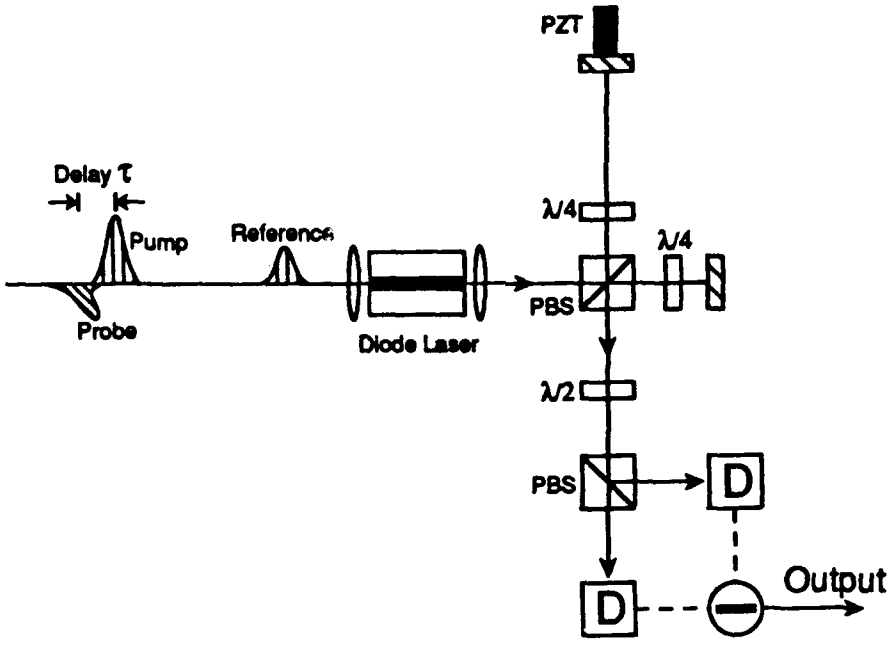

Figure 1: Experimental arrangement for time division interferometric pump-probe studies.

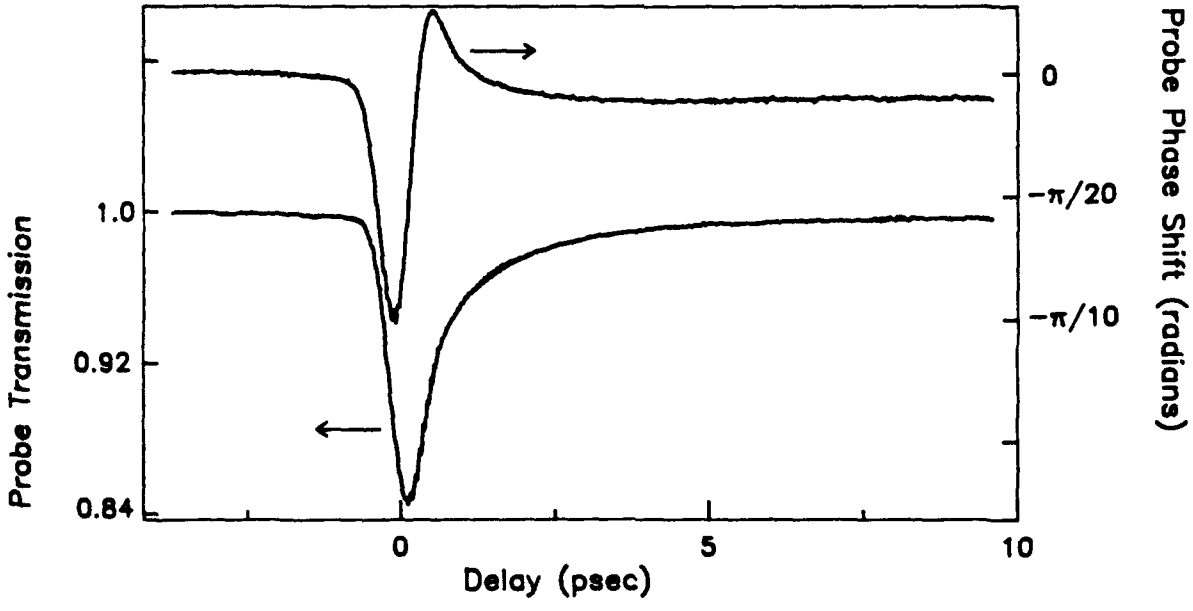

Figure 2: Experimental observations of dynamic phase (upper trace) and amplitude (lower trace) changes near nonlinear transparency.

All-Optical Modulation by Interaction between Interband- and Intraband-Lights in n-Doped Quantum Well Structure

Susumu NODA, Tetsuro OKUDA, Takao YAMASHITA, and Akio SASAKI

Department of Electrical Engineering, Kyoto University
Kyoto 606, JAPAN
TEL: +75-753-5298

I. INTRODUCTION

There is great interest in nonlinear optical phenomena in a quantum well structure. Although there are various energy levels in the quantum well structure, most of nonlinear devices with the quantum well structure only utilize either interband or intraband electron transition. The interband transition is the transition from a valence band to a conduction band, and the intraband transition is the transition between the first and the second quantized energy levels in a conduction or a valence band. When we utilize both of the interband- and the intraband-transitions simultaneously, the freedom of the device synthesis is greatly increased, and light-controlled optical devices which are indispensable for the future optical signal processing and optical computing can be realized.

We have recently proposed and demonstrated theoretically very fast all-optical modulation by the simultaneous utilization of the interband and the intraband transitions in n-doped quantum well structure [1,2]. Nonlinear third-order optical absorption caused by the interaction between interband- and intraband-lights is utilized in the modulation. In this paper, we demonstrate experimentally the all-optical modulation by using a guided-wave structure. In the following, the modulation principle, the guided-wave structure, and the modulation characteristics are described.

II. Principle and Guided-Wave Structure

The principle of the all-optical modulation using n-doped quantum well structure is illustrated in Fig.1. The energy level E_{c1} is filled with electrons with n-doping, and therefore the absorption coefficient for the light with photon energy of E_{c1}-E_v (interband-light) is very small (a). However, when the light with the photon energy of E_{c2}-E_{c1} (intraband-light) is irradiated to the quantum well, the electrons in the E_{c1} level are excited to the E_{c2} level and thus the absorption coefficient for the interband-resonant light is increased (b). The E_{c2} level is the virtual level in the extended state. Therefore, the interband-light can be modulated by changing the intensity of the intraband-light due to the nonlinear third-order process. The response time of this modulation is determined by the electron relaxation time from E_{c2} to E_{c1} levels (1-10ps) and very fast modulation speed can be expected.

The guided-wave structure fabricated to demonstrate the

all-optical modulation is illustrated in Fig.2. The interband-light propagates through the ridge-waveguide structure with n-doped multiple quantum wells. The intraband-light is incident to the quantum wells from the substrate side through 45° gratings since the element of the electric field parallel to the quantized direction is necessary for the absorption of the intraband-light. The interband-light is modulated by the intraband-light when it propagates through the ridge-waveguide structure.

The wafer for the guided-wave structure was grown by MBE. $Al_{0.23}Ga_{0.77}As$ cladding, multiple quantum well, and $Al_{0.23}Ga_{0.77}As$ cladding layers were successively grown on a GaAs substrate. The multiple quantum well was composed of 50 periods of GaAs wells (50Å) and $Al_{0.23}Ga_{0.77}As$ barriers (150Å), and was uniformly doped with silicon ($n=2\text{-}3x10cm^{-3}$). The wafer was mechanically thinned to 100μm and 45° gratings with 2μm period were formed on the substrate side for the incidence of the intraband-light. The epilayer side was processed to the ridge waveguide structure in which the interband-light can propagate. Au/Cr electrode was deposited on the ridge side, and the device was bonded on a silver heatsink with the up-side down configuration.

III. Experimental

The all-optical modulation characteristics were investigated through the following three-step experiments: 1)the estimation of the absorption for the interband-light which propagates through the ridge waveguide structure; 2)the estimation of the absorption for the intraband-light; and 3)the investigation of the absorption change for interband-light by the interaction with the intraband-light.

The absorption coefficient for the interband-light propagating through the waveguide was measured by using various semiconductor lasers with the different lasing wavelengths of 780, 825, 830, and 850nm. Figure 3 shows the absorption coefficient measured for these wavelengths. It can be seen that the gentle curve indicating reduced absorption due to the n-doping is obtained.

The absorption coefficient for the intraband-light was measured by the Fourier transform infrared spectroscopy (FTIR) method. For the measurement, a wafer with the same quantum well structure as the modulator wafer but with larger numbers of wells and barriers (500period) was used to improve S/N ratio. From the measurement, it was found that the absorption peak existed at about 10.6μm with the half width of 60meV.

The experiment for the interband-light modulation by intraband-light was done by using the following two light sources. A semiconductor laser with 827nm lasing wavelength was used for the interband-light. The wavelength was selected by comparing the result shown in Fig.3 and the theoretical analysis [3]. A transverse electric atmospheric (TEA) CO_2 laser with the wavelengths around 10.6μm was used for the intraband-light. The emitted pulse shape from the TEA CO_2 laser with the mixed gas of CO_2:N_2:He=1:1:3 was as shown in Fig.4. In order to avoid the

heating of the device due to the long tailing of the CO_2 laser pulse, the interband-light was also supplied by the pulse form as shown in Fig.4. The modulation characteristics of the interband-light by the intraband-light was measured by the combination of a charge coupled device (CCD) camera and a photomultiplier to obtain large sensitivity. Due to the slow response speed of the measurement system, the experimental modulation characteristics here were not real time but average ones. The modulation characteristics obtained in the experiments are shown in Fig.5. It is seen in the figure that the interband-light was modulated by the incidence of the intraband-light with the intensity of 100-200kW/cm^2 and that the modulation depth was about 60%. The modulation depth is almost coincident with the theoretical value.

IV. Summary

We have shown experimentally the interband-light modulation by the intraband-light in n-doped quantum well guided-wave structure for the first time. This result indicates that the nonlinear optical absorption by the interaction between interband and intraband-lights is useful for the all-optical modulation. By using a light source with much shorter pulse width for the intraband-light and by using much faster measurement system such as a streak camera system, we can expect to confirm that the modulation speed is very fast (1-10ps).

References

[1] S. Noda, T. Uemura, T. Yamashita, and A. Sasaki, J. Appl. Phys. 68, 6529 (1990).
[2] S. Noda, T. Uemura, and A. Sasaki, Tech. Digest Nonlinear Optics: Materials, Phenomena and Devices, Hawai, USA, 1990, paper TP19.
[3] S. Noda, T. Uemura, T. Yamashita, and A. Sasaki, unpublished.

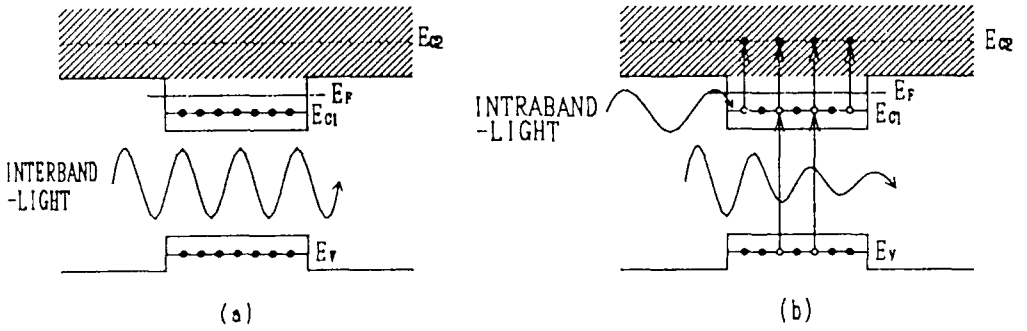

Fig.1 Principle of all-optical modulation using n-doped quantum well.

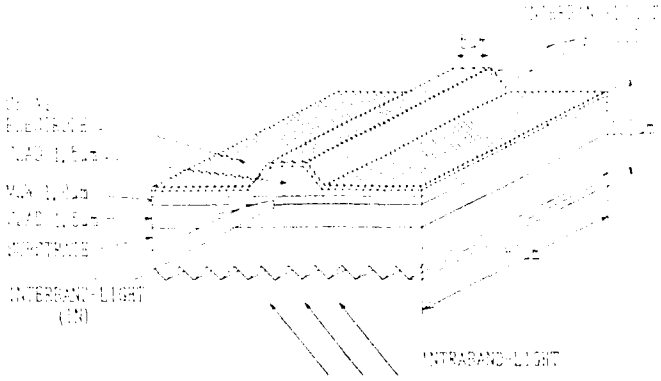

Fig.2 Schematic diagram of fabricated guided-wave structure.

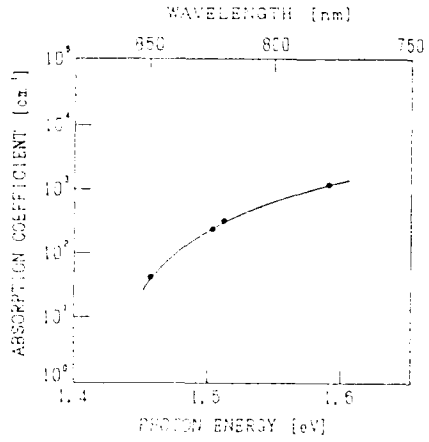

Fig.3 Absorption coefficient for interband-light without intraband-light.

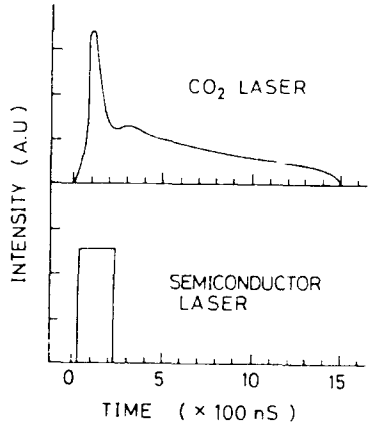

Fig.4 Pulse shapes of TEA CO_2 laser (intraband-light) and semiconductor laser (interband-light) used for modulation experiment.

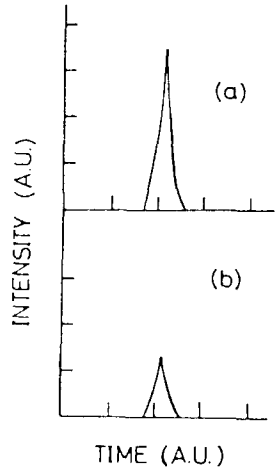

Fig.5 Modulation characteristics. (a) and (b) express the interband-light intensities without and with incidence of intraband-light (100-200kW/cm^2) respectively.

Nonlinear refraction and absorption of an InGaAs Single Quantum Well in an InGaAsP waveguide

J.E. Ehrlich, D.J. Goodwill, D.T. Neilson, A.C. Walker

Department of Physics

Heriot-Watt University

Edinburgh, Scotland, UK EH14 4AS

031-451-3023

C.I. Johnston, W. Sibbett

Department of Physics and Astronomy

University of St. Andrews

St. Andrews, Scotland, UK KY16 9SS

Semiconductor quantum-well structures can provide enhanced nonlinear effects compared to those observed in bulk material. The largest irradiance-induced refractive changes occur at wavelengths nearly resonant with the band edge or exciton absorption. If such a nonlinearity is to be effectively exploited in a waveguide configuration, the absorption due to the active quantum-well layers must be diluted to ensure sufficient transmission. Although this produces, all else being equal, a proportional drop in the effective nonlinearity (n_2), it does permit operation at, or near to, the optimum wavelength where the figure-of-merit n_2/α is maximized. In addition to the possible device potential of nonlinear optical waveguides, this configuration also permits investigation of the nonlinearity using light polarized both parallel (TE) and perpendicular (TM) to the quantum well. We present here measurements of nonlinear absorption and refraction, associated with electron-hole pair excitation, in an InGaAs Single Quantum Well (SQW) centered

within a strip-loaded, non-absorbing InGaAsP waveguide.

The samples used were 0.8μm thick InGaAsP waveguides (bandgap of 1.1μm) with a 7.0nm SQW of InGaAs (hh-e transition of the n=1 level of the quantum well at 1.51μm). Ribs, ranging in widths from 2.0 to 6.0 μm, were etched into the InP cover layer to form strip-loaded waveguides. The samples were cleaved to lengths of 300-900μm, such that the natural reflectivity of the uncoated facets could form a Fabry-Perot (FP) cavity. A cw NaCl-OH^- color center laser (tunable over λ=1.46-1.65μm) was end-fire coupled into the waveguide, while an acousto-optic modulator (AOM) was used to generate quasi-cw (1.5ms long) triangular pulses. The output power was monitored as a function of the incident power at various wavelengths. For photon energies near the bandgap, strong absorption saturation was observed at powers above 5.0mW (Fig.1). This power level was sufficiently low to permit observation of this saturation using a tunable, external-cavity diode laser. At photon energies less than the bandgap, the absorption was sufficiently small to create a FP cavity with finesse of 2.2. An irradiance-dependent refractive index could be observed as the FP resonance condition was modified with changing incident power (Fig.2). The three curves in Fig.2 correspond to different initial cavity tuning conditions, which were set by slightly heating the sample with an external source. It was found that the index change induced optically was of the opposite sense to that obtained by direct heating of the sample. This indicated that the mechanism was electronic excitation, rather than a thermal effect. The observed lack of any optically-induced thermal effects, despite the relatively long duration of the input pulse, contrasts strongly with our experience with similar GaAs/GaAlAs SQW waveguides, where illumination times have to be kept down to microseconds to avoid thermal nonlinear phenomena.

The P_{in}/P_{out} measurements were fitted to the FP transmission equation, which included a saturable absorption and saturable nonlinear index of refraction of the form $\alpha = \alpha_0/(1 + N/N_{sat}) + \alpha_{NS}$ and $n = n_0 + \sigma_0 N/(1 + N/N_{sat})$, where α_0 and n_0 are the linear absorption and refractive index, α_{NS} is a background, non-saturating absorption (such as a waveguide loss

term), σ_0 is the nonlinear refractive cross-section at low carrier density, N is the carrier density and N_{sat} is the saturation density. In this model, an average intensity within the cavity was assumed. For TE polarization at 1600nm, values of $\alpha_0 = 160cm^{-1}$, $\sigma_0 = -0.9x10^{-19}cm^3$ and $N_{sat} = 2.0x10^{17}cm^{-3}$ were deduced for the quantum well. At 1486nm (in the bandgap), no FP cavity resonances were observable due to the large absorption, and thus the average intensity approximation was no longer valid. Instead, a good fit was obtained by considering a single pass through a series of discrete elements with a saturating absorption. Values of $\alpha_0 = 1.65x10^4cm^{-1}$ and $N_{sat} = 6.8x10^{17}cm^3$ at 1486nm were obtained. In these calculations, a carrier lifetime of 10ns was assumed. Comparable results were obtained for TM polarization, but at shorter wavelengths since the principal absorption edge is now the n=1 lh-e transition.

For the refractive tuning, the low saturation density limits the refractive index change and thus inhibits switching and bistability for device lengths up to 2mm, assuming the natural facet reflectivity. If the facet reflectivities were increased to 90%, bistability is predicted for operation close to the bandedge, where the refractive cross-section is maximum. Further studies of this nature should lead to complete characterization of this structure and permit the design of fully optimized nonlinear waveguide devices for the 1.55μm wavelength.

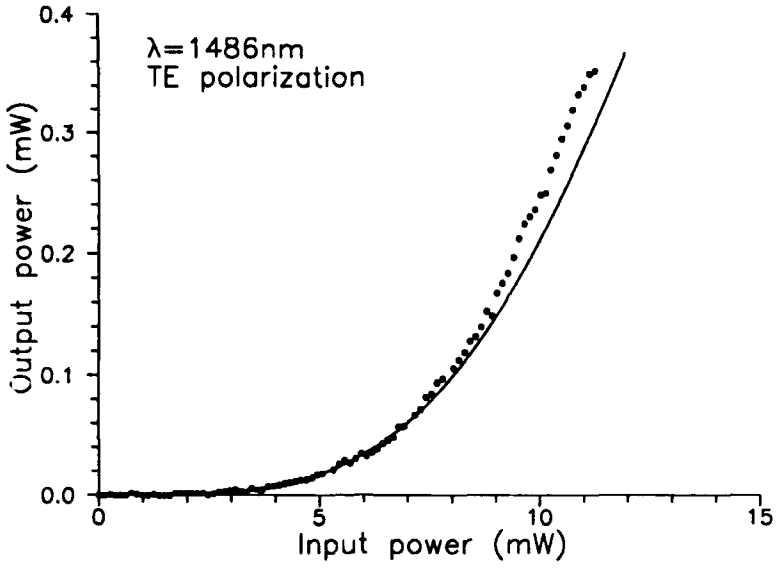

Fig.1 Output power vs input power at a wavelength shorter than the InGaAs SQW bandedge, showing absorption saturation. The points are experimental data, the solid line is the fitted curve.

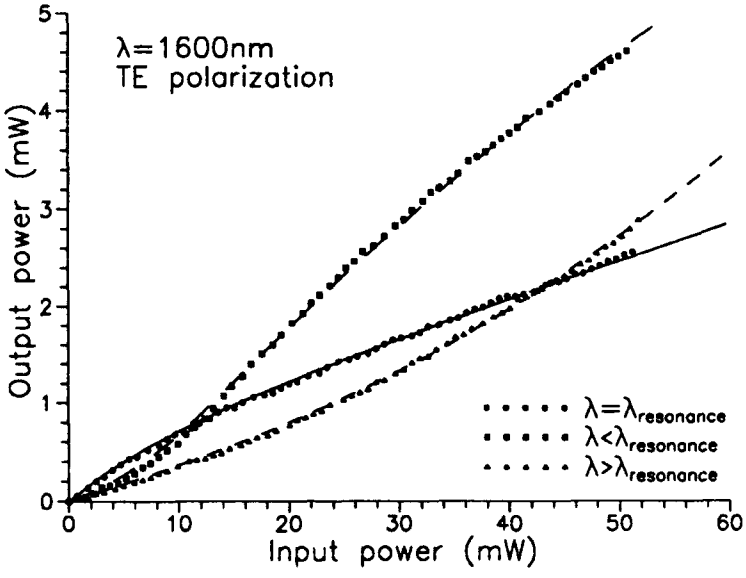

Fig.2 Output power vs input power at a wavelength longer than the bandedge, showing tuning of the FP cavity resonance due to an optically-induced electronic nonlinear refractive index change. The three separate curves correspond to different initial cavity detunings. The points are experimental data, the lines are the fitted curves.

Nonlinear optical properties of a single quantum well waveguide and a nonlinear asymmetric interferometer

K. Al Hemyari , B. S. Bhumbra* and C. N. Ironside
Department of Electronics and Electrical Engineering
University of Glasgow,
Glasgow G12 8QQ.
U. K.

The quantum well semiconductor laser has been shown to be the semiconductor laser of choice for efficiency and thereby high power applications. The key advantage of nonlinear devices fabricated in quantum well waveguides is that they can be easily integrated with quantum well lasers. Nonlinear optical effects in GaAs/AlGaAs quantum wells have been of considerable interest for sometime (see ref(1) for a recent review). In guided-wave formats some nonlinear devices have been demonstrated; a nonlinear directional coupler has been fabricated and characterised (2),(3) and a saturable absorber for a mode-locking semiconductor laser.(4) has also been demonstrated.

This paper describes the nonlinear optical properties of a GaAs/AlGaAs a single quantum well waveguide and the fabrication and operation of a nonlinear optical device, the asymmetric Mach-Zehnder interferometer.

Figure (1)
Single quantum well wafer

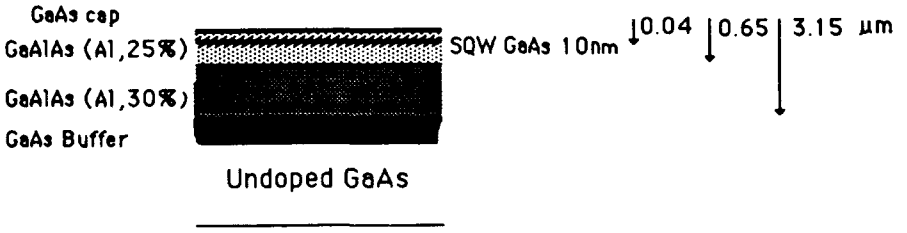

Caption: *The single quantum well material used in this paper.*

We have investigated both the refractive and absorptive nonlinearity of quantum well waveguides fabricated in the material shown in figure (1)

In fig(2) we show the refractive nonlinearity of a quantum well waveguide which was by measured using an interferometric technique(5). This interferometric technique has allowed, for the first time, direct measurement of the refractive nonlinearity in single quantum well waveguides

Figure 2
Refractive nonlinearity

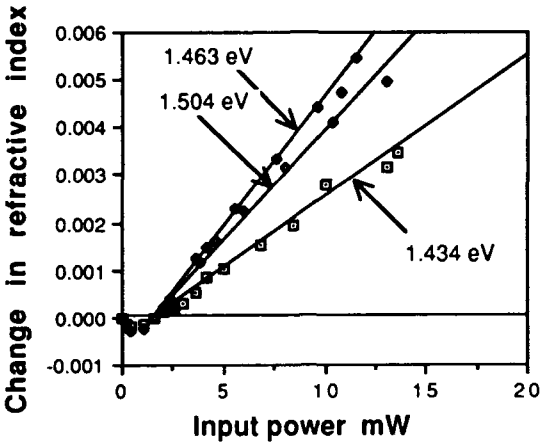

Caption: *The refractive nonlinearity in a single quantum well waveguide. Measured with a CW source with TE polarisation.*

The electronic and thermal refractive nonlinearities have different signs the electronic refractive nonlinearity is negative and the thermal refractive nonlinearity is positive. It can be seen from figure (2) that at low powers the electronic part of the refractive nonlinearity is apparent but it saturates and the thermal part of refractive nonlinearity becomes dominant at higher powers. The value of electronic refractive nonlinearity, n_2, is 1.4×10^{-12} m^2/W

Figure (3a)
Absorptive nonlinearity

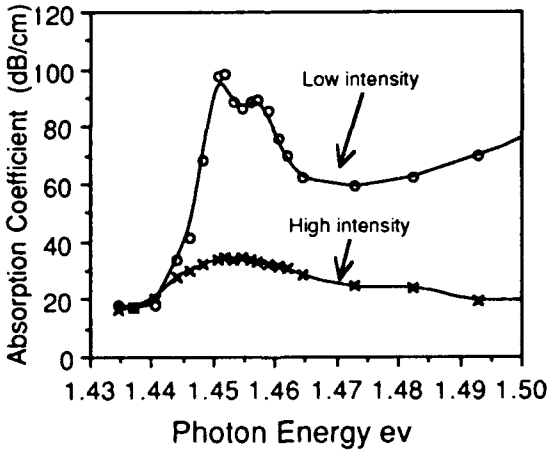

Figure(3b)

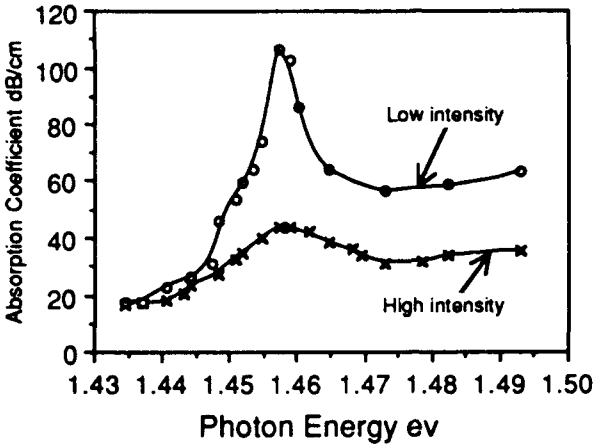

Caption: *Saturation of the exciton peak in a single quantum well waveguide with a CW source (a) TE and (b)TM polarisations Low intensity corresponds to 20 μw (6.6 10^6 W/m^2) in the waveguide and high intensity 10 mW (3.3 10^9 W/m^2).*

In figure (3) we show the absorptive nonlinearity for both TE and TM polarisations for a single quantum well waveguide. In the TE polarisation the heavy and light hole transitions are apparent and in the TM polarisation only the light hole transition is obvious which agrees with theory and previous observations (6). These measurements have been carefully calibrated by a sequential cleaving technique.

Figure(4)
Integrated Asymmetric Mach-Zehnder Interferometer

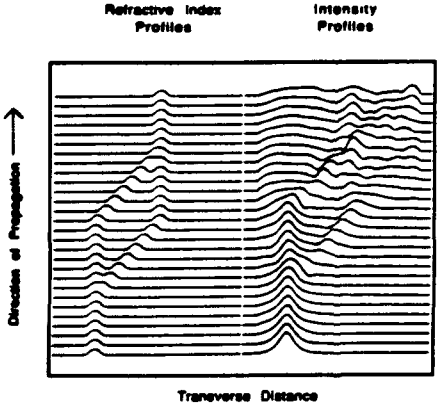

Caption: *The layout of the integrated nonlinear asymmetric Mach-Zehnder interferometer. The diagram on the right shows the operation of the device as modelled by a nonlinear beam propagation method.*

Figure (4) shows one version of the asymmetric Mach-Zehnder interferometer which employs asymmetric Y-junctions to split unevenly optical intensity between the two arms of the interferometer. In fig(4) the operation of the device is modelled

by a nonlinear beam propagation method. The device modulates because the difference in intensity in each arm results in a different phase shift in each arm via the refractive nonlinearity. The integration of a nonlinear interferometer with a quantum well semiconductor laser would enable the implementation of an integrated coupled cavity mode-locking scheme for semiconductor lasers.

The operation of an asymmetric Mach-Zehnder interferometer has been investigated under CW conditions. The pump was a CW Ti: sapphire laser operating at a photon energy of 1.46 eV and the probe laser was a semiconductor laser at a photon energy of 1.495 eV. With a pump power of 30 mW a modulation of the probe has been observed of around 15%. The modulation under these CW conditions is largely due to the thermal nonlinearity. The saturation of the electronic nonlinearity is typical of resonant nolinearities and means that complete fast switching in this device is not possible unless unrealistically long devices are employed. However, for applications such as mode-locking it is not necessary to have complete switching and a modulation of a few percent may be sufficient

Other versions of the asymmetric Mach-Zehnder interferometer can be fabricated which do not necessarily require asymmetric Y junctions for their operation. One version employs an electric field to unbalance the nonlinearity in each arm of the interferometer. The operation of this device is currently being investigated under pulsed and CW conditions. In other versions the nonlinearity can be unbalanced by selective disordering of the quantum wells which is used to control the exciton energy in each arm of the interferometer.

In conclusion both the refractive and absoprtive nonlinearities of a single quantum well waveguide have been measured and all-optical modulation has been observed in a nonlinear integrated interferometer albeit thermal in origin. Currently under investigation is the operation of an interferometer where the nonlinearity in each arm is unbalance by an electric field and the fabrication of an interferometer where the band-gap in each arm is adjusted by impurity induced disordering

References

(1) S. Schmitt-Rink, D. S. Chemla and D.A.B. Miller Adv. Phys. 38. 89-188 1989.
(2) P. Li Kam Wa, P. N. Robson, J. P. R. David, G. Hill, P. Mistry, M. A. Pate and J. S. Roberts, Electron Lett 22, 1129 1986.
(3) R. Lin, J. P. Sokoloff, P. A. Harten, C. L. Chuang, S. G. Lee M. Warren, H. M. Gibbs, N. Peyghambarian, J. N. Polky, and G. A. Pubanz Appl. Phys. Lett. 56 993-995 1990.
(4) S. Sanders, L. Eng, J. Paslaski, A. Yariv "108 GHz passive mode locking of a multiple quantum well semiconductor laser with an intracavity absorber" Appl. Phys. Lett 56 310-311 1990
(5) D. Cotter,C. N. Ironside, B. J. Ainslie and H. P. Girdlestone Optics letts. 14, 317-319, 1989.
(6) J. S. Weiner, D. S. Chelma, D.A.B. Miller, H. A. HAus, A. C. Gossard, W. Weigman and C. A. Burrus Appl. Phys Lett 47 664-667 1985.

NONLINEAR DIRECTIONAL COUPLER BASED ON RB:KTP-WAVEGUIDES

K.S.Buritskii, E.M.Dianov, V.A.Maslov,

V.A.Chernykh, E.A.Shcherbakov

General Physics Institute, U.S.S.R. Academy of Sciences

38 Vavilov Str.,Moscow, 117942, U.S.S.R.

telex 411074 LIMEN SU, phone (095)1328231

To create ultrahigh-speed long-distance optical fiber communication systems of new generation particularly soliton transmission lines and to implement information optical processing systems into practice it is necessary to develop different functional devices having less than 10 ps high-speed characteristics[1]. The best variant is the application with this aim of light-controlled integrated optical switches and gates, as the pulses of less than 10 fs duration are obtained precisely by the optical methods. Promising from this point of view is the switch based on nonlinear coupled optical waveguides previously used experimentally in the integrated-optical variant on lithium niobate [2] and gallium arsenide [3] base as well as in quartz fiber light guides [4,5].

Taking into consideration the fact that up till now there is no universal material satisfying all the requirements necessary for performing optical switching of ultrashort light pulses the search for new materials of high enough third order nonlinearity, low loss and high optical damage resistance is of paramount importance. One of the most perspective crystals from this point of view is potassium-titanyl phosphate (KTP) possessing unique properties and permitting to obtain low loss optical waveguides losses by comparatively simple way (by means of ion exchange).

The aim of the studies was the realization of nonlinear light switching in coupled channel Rb:KTP waveguides.

As is generally known [7,8] nonlinear directional coupler is a system of two identical waveguides brought into sufficiently close proximity that their fields overlap (see Fig.2). When one of them is excited by low optical signal, light power at the coupler output is distributed between two waveguides in the following way, depending on their coupling coefficient:

$$P_0(L)=P_1(0)\sin^2((\Delta\beta^2+\kappa^2))^{1/2})L) \qquad (1)$$

$$P_1(L)=P_1(0)\cos^2((\Delta\beta^2+\kappa^2))^{1/2})L) \qquad (2)$$

where $\Delta\beta$ - is the difference of propagation constants in two waveguides ($\Delta\beta$ = 0 for identical waveguides); κ - coupling coefficient; L - coupler length. When light power in excited channel increases crystal refractive index changes according to Kerr law:

$$n=n_0+n_2I \qquad (3)$$

where I - light intensity in a waveguide, n_2 -nonlinear coefficient ($n_2 \approx 3\ 10^{-12}$ cm^2/kW for KTP) As the identity of waveguides is disturbed and the value of detuning is proportional to the light intensity, the signal at the output of the directional coupler depends nonlinearly on the input signal:

$$P_1(L)=P_1(0)(1+cn(2\kappa L;P_1^2(0)\Delta\beta_2/4\kappa)) \qquad (4)$$

where cn(x;y) - Jacobi elliptic function; $\Delta\beta_2=c^2\varepsilon_0 n_0 n_2^2 E^4(x,y)\,dxdy$, E(x,y)- normalized distribution waveguide mode field.

The system of coupled waveguides based on KTP crystal was produced for the experiment. The waveguides of 6 μm in width directed along Y axis the spacing between them being 4 μm, were obtained by Rb^+ ion exchange from $RbNO_3$ melt into the substrate of KTP Z-cut within 15 min at a temperature of 350°C. The waveguides were monomode at 1.06 μm for TE- polarized radiation. The light source was laser Quantronix-116, operating in Q-switch and mode locking regime. The duration of pulse train was 200 ns, a that of a single pulse in a train 200 ps, while frequency of pulse sequence in a train amounted to 100 MHz. Maximum irradiation peak power was 500 kW.

Single-mode anisotropic polarization maintaining fiber was used to couple beam into a channel waveguide. Light from the fiber was fed into Rb:KTP waveguide through the polished endface by means of a system consisting of two 20x microobjectives. Light peak power in front of input microobjective did not exceed 10 kW and was controlled adjusted by shifting the fiber input endface. At the waveguide output the signal was registered by the fast photodiode (the bandwidth being 2 GHz) and the boxcar integrator (Fig.1).

In the linear mode (at low input signal) at the output of the studied directional coupler almost all the light power was concentrated in the initially excited waveguide (the length of waveguides - 7 mm; the ratio of signals at the output being 10:1). The increase of input signal results in phase detuning between waveguides and the rate of light switching changes. In every laser pulse train peak power varies from zero to some maximum value. Correspondingly while measuring power value in each pulse from a train for two waveguides (in one of them the output power increases when increasing input power P(0), in the other - it decreases) it is possible to determine the switching state for every value of input power. Fig. 3 shows the distribution of pulse amplitudes in a train of two coupled waveguides for the following cases: linear transmission of switching pulse train through the directional coupler (the ratio of signal amplitudes in two channels being 10:1) (a) and nonlinear switching (b) of light power (the ratio of signal amplitudes is 2.25:1 at maximum input peak power of 5 kW). Consequently in case of input signal increase from 0 to 5 kW about 40 percent of light power was switched from one waveguide

to the other.

Thus the present paper for the first time presents the data on the nonlinear coupling (in a subnanosecond range) in a directional coupler based on Rb:KTP waveguides.

References.

1. N.K.Cheung. Techn. ,Dig. OFC'90, p.WF1, San Francisko, 1990.
2. A.Lattes, H.A.Haus, F.J.Leonberger, E.P.Ippen.IEEE J.QE-19, 1719(1983).
3. P.Li Kam Wa, J.E.Sitch, N.J.Mason, J.S Roberts, P.N.Robson. Electr. Lett., 21, 26(1985).
4. D.D.Gusovskii, E.M.Dianov, A.A.Mayer et al. Sov. J. QE-14, 1144(1987).
5. Y.Silberberg, A.M.Weiner, S.R.Friberg, B.G.Stez, P.W.Smith. Techn. Dig. IGWO'88, p.WC3, Santa Fe, 1988.
6. J.D.Bierlein, H.Vanherzeele. JOSA B6, 622(1989).
7. A.A.Mayer. Sov. J. QE-9, 2296(1982).
8. S.M.Jensen. J. QE-18, 1580(1982).

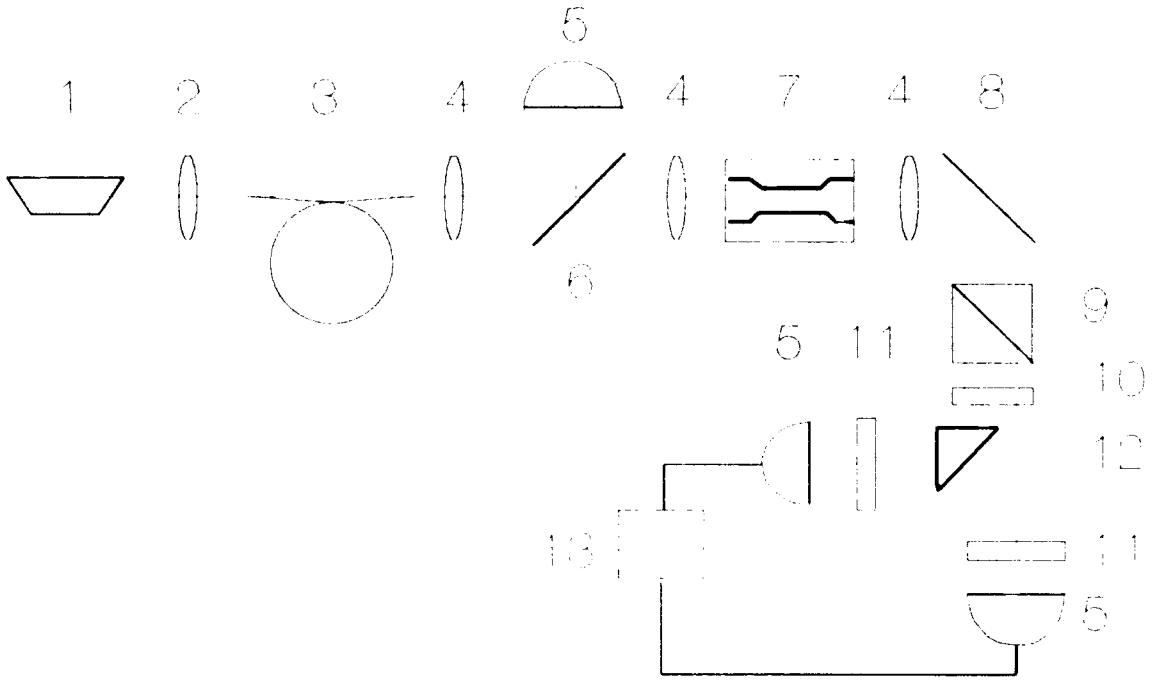

Fig.1. Experimental setup: 1-Nd:YAG-laser, 2-lens(f=10 mm), 3-single-mode anisotropic fiber, 4-microobjective, 5-photodiodes, 6-beamsplitter, 7-nonlinear directional coupler, 8-mirror, 9-polarizer, 10-filter, 11-attenuator, 12-total reflection prism, 13-boxcar integrator.

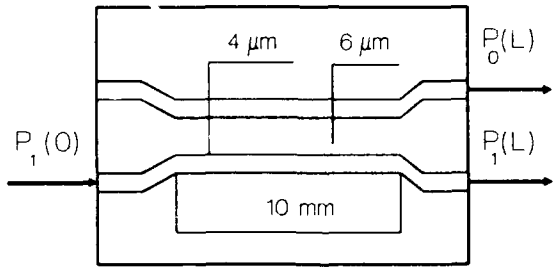

Fig.2. Schematic of the directional coupler

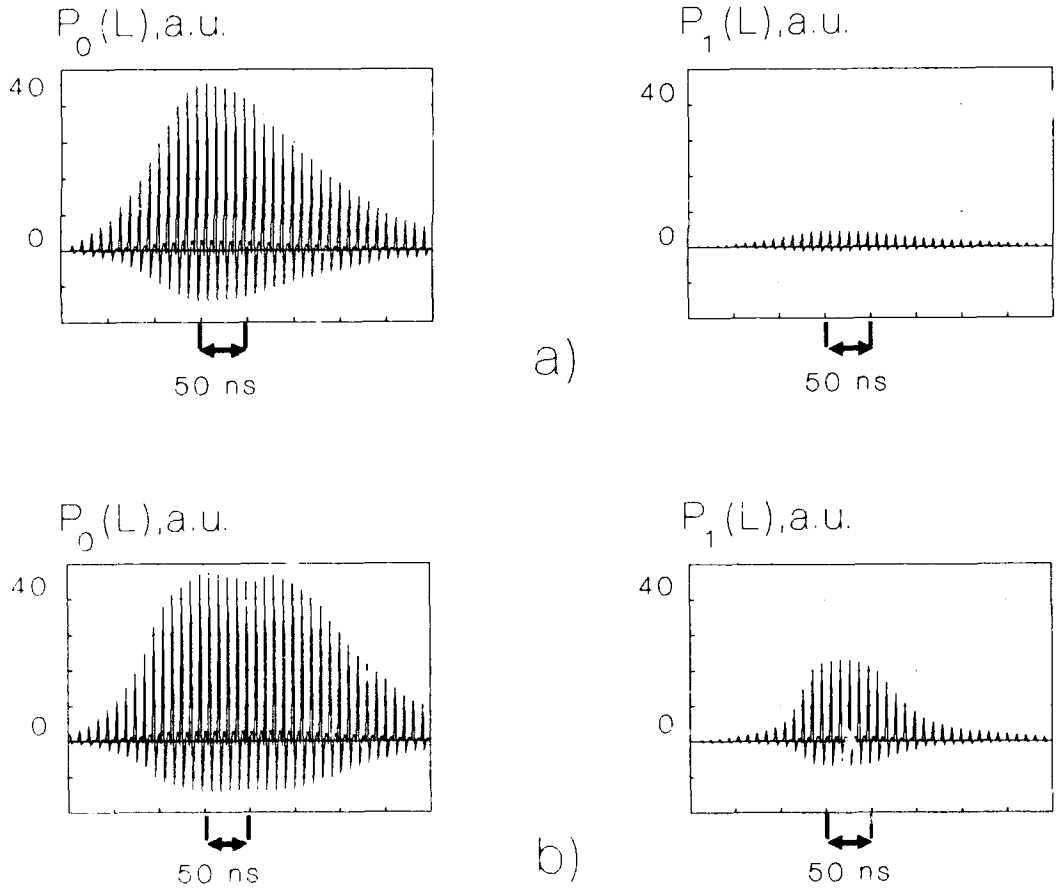

Fig.3. Output pulse amplitude vs time dependence in channels 0 and 1 in linear (a) and nonlinear (b) regimes. In each plot pair (a) and (b) vertical scale is the same.

Tuesday, September 3, 1991

Multiphoton Effects

TuC 2:00pm–3:30pm
Palmerston Room

G. Arvidsson, *Presider*
Royal Institute of Technology, Sweden

Prospects for Nonlinear Organics in Guided Wave Optics

George I. Stegeman
Center for Research in Electro-Optics and Lasers, University of Central Florida, 12424 Research Parkway, Suite 400, Orlando, FL 32825, Tel. (407-658-3916)

Although it has been known for some time that organic materials can have large second and third order nonlinearities [1], it is only within the last five years that there has been a concentrated effort to try to make nonlinear devices out of them. This has been at least partly due to many misconceptions about organic materials which have been proven inaccurate. For example it was widely believed they have low damage thresholds, poor optical properties such as transmission, are not easily processible into device structures etc. In this paper we will review the linear and nonlinear properties of organic materials, how waveguides can and have been made out of them and some of the initial nonlinear devices which have reported.

Appropriately engineered organics can have second order coefficients much larger than their inorganic counterparts [1]. For example, the d_{33} coefficient = 34 pm/V of lithium niobate is one of the largest known for inorganic media. By way of comparison, the largest coefficient in DAST has a maximum coefficient of 460 pm/V! The trade-off however, is that the edge of the optical transparency window moves to progressively longer wavelengths with increasing activity, and solving this problem is one of the outstanding challenges to using these materials for doubling GaAs lasers.

Another problem is to fabricate waveguides from single crystal materials. There are two options: 1) to make channels out of single crystal materials by ion-exchange, ion milling, etching etc. This approach has not yet been used to make waveguide channel doublers. What has been done is to grow

organic materials directly into waveguide geometries, for example as the core of single mode fiber [2]. In fact that particular case has shown efficient doubling using the Cerenkov technique.

One of the unique features of using organic nonlinearities is that one can construct non-centrosymmetric media without resorting to single crystal growth. This can be achieved using poling in which a strong DC field is used, under appropriate conditions, to orient molecules which have both large linear dipole moments and second order hyperpolarizabilities [3]. The result is a net macroscopic second order coefficient. Activities in excess of 50 pm/V have been created in waveguide films in this way, and efficient, phase-matched second harmonic generation has been demonstrated [4].

This fabrication technique also highlights one of the waveguide fabrication techniques unique to organic materials. Namely, during the poling process a preferential orientation is imparted to optically anisotropic molecules. Therefore electric fields create regions of higher index for one polarization, and lower index for the orthogonal polarization. Therefore lightguide circuits can be made which are defined by electrode patterns.

There are other techniques for writing channel waveguides which work well with organics and not with other materials. For example, illumination with light can lead to trans-cis photoisomerization [5], breaking of bonds [6] etc. which lead to local changes in the refractive index. Typically, the refractive index and the nonlinearity are reduced by illumination at the appropriate frequency. The unilluminated regions form the waveguides which are nonlinear.

The non-resonant, ultrafast third order nonlinearities of selected organic materials are typically at least one order of magnitude larger than those associated with dielectrics or semiconductors [7]. This is certainly true for conjugated polymers in which electron orbitals are delocalized over many

atoms. The largest values range from 10^{-12} to a few times 10^{-13} cm^2/W [8]. The lowest attenuation coefficients are less than 0.1 cm^{-1},occurring typically between 1000 and 1400 nm. Although it was initially believed that many of these conjugated polymers would be insoluble and therefore not useful for spinning waveguide films, there has been progress in developing spinnable versions of the some of the most nonlinear materials [9].

Two material figures of merit have been identified which materials must satisfy in order to be useful for devices. They are $W = \Delta n_{sat}/\alpha\lambda$ where Δn_{sat} is the maximum index change, and $T = 2\beta\lambda/n_2$ where β and n_2 are the two photon and nonlinearity coefficients respectively [10]. $W > 2$ and $T < 1$ are desirable, and one of the principal problems is that the wavelength dependence of these parameters have not been measured. However, there are a few isolated cases which indicate that there will be spectral windows in organics in which the figures of merit will be satisfied [8,10]. Unfortunately the one attempt to make a switching device reported to date failed because strong two photon absorption occurred at the wavelength used, namely 1060 nm [11].

In summary, nonlinear organic materials are starting to make an impact in nonlinear guided wave physics and devices, as discussed in this paper.

References

1. Many chapters in Nonlinear Optical Properties of Organic Molecules and Crystals, Vols I and II, edited by D.S. Chemla and J. Zyss (Academic, Orlando, 1987)

2. T. Uemiya, U. Uenishi, Y. Shimizu, S. Okamoto, K. Chikuma, T. Tohma and S. Umegaki, SPIE Proceedings, **1148**, 207 (1989)

3. G. Khanarian, R.A. Norwood, D. Haas, B. Feuer and D. Karim, Appl. Phys. Lett., **57**, 977 (1990).

4. X.F. Cao, L.P. Yu and L.R. Dalton, Technical Digest of the 1990 Optical Society of America annual meeting, paper ThE3, pp 165 (1990).

5. Y. Shi, W.H. Steier, L. Yu, M. Chen and L.R. Dalton, Appl. Phys. Lett., **58**, 1131 (1991)

6. K.B. Rochford, R. Zanoni, Q. Gong and G.I. Stegeman, Appl. Phys. Lett., **55**, 1161 (1989)

7. C. Sauteret, J.-P. Hermann, R. Frey, F. Pradere, J. Ducuing, R.H. Baughman and R.R. Chance, Phys. Rev. Lett., **128**, 606, (1976)

8. D.M. Krol and M. Thakur, Appl. Phys. Lett., **56**, 1406 (1990); S.T. Ho, M. Thakur and A. Laporta, IQEC Digest, paper **QTUB5**, 40-2 (1990)

9. H. Vanherzeele, J.S. Meth, S.A. Jenekhe and M.F. Roberts, Appl. Phys. Lett., **58**, 663 (1991)

10. K.B. Rochford, R. Zanoni, G.I. Stegeman, W. Krug, E. Miao and M.W. Beranek, Appl. Phys. Lett., **58**, 13 (1991).

11. P.D. Townsend, J.L. Jackel, G.L. Baker, J.A. Shelbourne III, S. Etemad, Appl. Phys. Lett., **55**, 1829 (1989).

NONLINEAR ABSORPTION PROCESSES AT HALF THE BAND GAP IN GaAs BASED SEMICONDUCTORS

A. Villeneuve and G.I. Stegeman
CREOL, Univ. of Central Florida
Orlando, FL 32826, USA

G. Scelsi*
Microelectronics Sciences Laboratories
Columbia University
New York, N.Y. 10027, USA

C.N. Ironside and J.S. Aitchison
Department of Electronics and Electrical Engineering
University of Glasgow
Glasgow, G12 8QQ, U.K.

J.T. Boyd
Department of Electrical and Computer Engineering
University of Cincinnati
Cincinnati, Ohio 45221, USA

The utility of the ultrafast nonlinearity in semiconductor waveguides operated below the band gap is limited by two photon absorption β ($\alpha = \beta I$ where I is the intensity) which does not allow a nonlinear 2π phase shift over one absorption length.[1] However, the two photon coefficient should be zero below half the band gap, potentially allowing for all-optical device operation there.[2,3] Here we report the first measurements of two photon absorption in GaAs waveguides in the vicinity of half the band gap.

A tunable, synchronously pumped mode-locked NaCl:OH color center laser was used to produce 8-12 picosecond pulses between the wavelengths of 1.48 and 1.74 microns. The waveguides were 1.1 cm long and consisted of a 1.3 μm layer of GaAs grown onto a 2.7 μm thick layer of $Al_{0.1}Ga_{0.9}As$ which was itself deposited on a GaAs substrate. The guide was defined by two grooves made by direct laser writing to a depth $\approx$ 0.5 μm [4]. The guide is single mode at 1.3 μm for a center-to-center width between the grooves larger than 8 μm. The guides used had a width of 10 μm.

Single beam experiments were performed first by using a half-wave plate and a polarizer to vary the power into the waveguide. The average power was measured before and after the waveguide and $1/T \propto \beta$, where T is the transmission, was plotted versus input pulse energy [5]. The slope of the resulting curve gave the two photon coefficient, and the low power waveguide loss was estimated from the intercept of the curves at zero input. Since the waveguides were near cut-off at the longest wavelengths studied, the linear loss also increased with increasing wavelength and had to be normalized out of the data. Finally, we assumed a Gaussian temporal pulse shape in converting the pulse width and energy

values to intensity [6].

The results for β, after correcting for the factors discussed above, are shown in Fig 1 versus wavelength. As expected, the two photon coefficient falls to zero at half the band gap, i.e. 1.74 μm. We found that the wavelength dependence of the decrease agreed well with theoretical predictions[7]. However, the magnitude of the measured β was consistently a factor of about 4 higher than predicted, suggesting the presence of other contributing factors such as free carrier absorption of the photogenerated carriers.

The free carrier contribution to the absorption was measured using orthogonally polarized pump-probe beams. A strong pump was transmitted through the sample which created carriers by two photon absorption. A time-delayed, orthogonally polarized probe beam (<1% of the pump beam) was then coupled into the channel waveguide and its transmission was monitored as a function of probe delay. A plot of probe transmission is show in Fig. 2 for low and high intensities of the pump beam. At low intensities, since the absorption due to free carrier absorption can be neglected, the two photon absorption produces a response which is symmetrical in time with a width given by the input pulse width. At high intensities there is in addition a tail at longer times which corresponds to free carrier scattering, i.e. by the carriers excited by the strong pump beam. Therefore there was a strong contribution to the measured β from free carrier scattering. Note that this free carrier contribution also adds to the peak of the effective two photon absorption.

Further analysis was performed to verify that extra absorption was due to free carrier scattering. If these carriers are generated by TPA then the number of carriers generated Δn is proportional to I^2. Since free carrier scattering is itself proportional to I, the net process should be even higher order in intensity, i.e. $dI/dz = \gamma I^3$ so that the effective absorption α scales as I^2. At a time delay of 40 ps (4x the pulse width), the absorption contribution should be solely due to free carrier absorption and should therefore scale quadratically with intensity. This is verified by the data shown in Fig. 3.

There are other factors which identify the additional absorption process as free carrier scattering. The absorption does not fully decay back to zero before the next pulse arrives (in 13 ns). From the residual signal we estimate a decay time of 7-10 ns, times typical of free carrier lifetimes. Finally, by assuming a λ^2 dependence of the free carrier scattering cross-section σ on wavelength, we estimated the free carrier absorption coefficient $\alpha = \sigma\Delta n \approx 0.14$ cm^{-1} at $\lambda = 1.56$ μm for an average power of 230 mW and $\sigma = 5.5\times10^{-18}$ cm^2 at 1.06 μm [8]. When compared to the experimentally measured value of 0.48 cm^{-1} which also includes the coupling losses, the agreement is reasonable.

In summary, we have found that both two photon absorption and free carrier scattering contribute to the nonlinear loss just

above half the band gap in GaAs waveguides for picosecond pulses. At half the band gap, the two photon coefficient goes to zero.

This research was supported by NSF (EET-8814663).

(*) On leave from Dipartimento di Ingegneria Elettrica & IAIF-CNR, Universite di Palermo

References:

1. J.S. Aitchison, M.K. Oliver, E. Kapon, E. Colas and P.W. Smith, Appl. Phys. Lett. 56, 1305 (1990).
2. K.W. Delong, K.B. Rochford, and G.I. Stegeman, Appl. Phys. Lett. 55, 1823 (1989).
3. K.W. Delong and G.I. Stegeman, Appl. Phys. Lett., 57, 2063 (1990).
4. A.E. Willner, M.N. Ruberto, D.J. Blumenthal, D.V. Podlesnik and R.M. Osgood, Jr., Appl. Phys. Lett. 54, 1839, (1989)
5. A. Villeneuve, M. Sundheimer, N. Finlayson, G.I. Stegeman, S. Morasca, C. Rigo, R. Calvani and C. De Bernardi, Appl. Phys. Lett. 56, 1865, (1990)
6. W.L. Smith, in CRC Handbook of Laser Science and Technology, Edited by M.J. Weber (CRC, Cleveland, Ohio, 1986), Vol. 3, p229.
7. M. Sheik-Bahae, D.C. Hutchings, D.J. Hagan and E.W. Van Stryland, IEEE. J. Quant. Elec., 27, (6), June 1991
8. G.C. Valley, T.F. Boggess, J. Dubard and A.L. Smirl, J. Appl. Phys. 66, 2407, (1989)

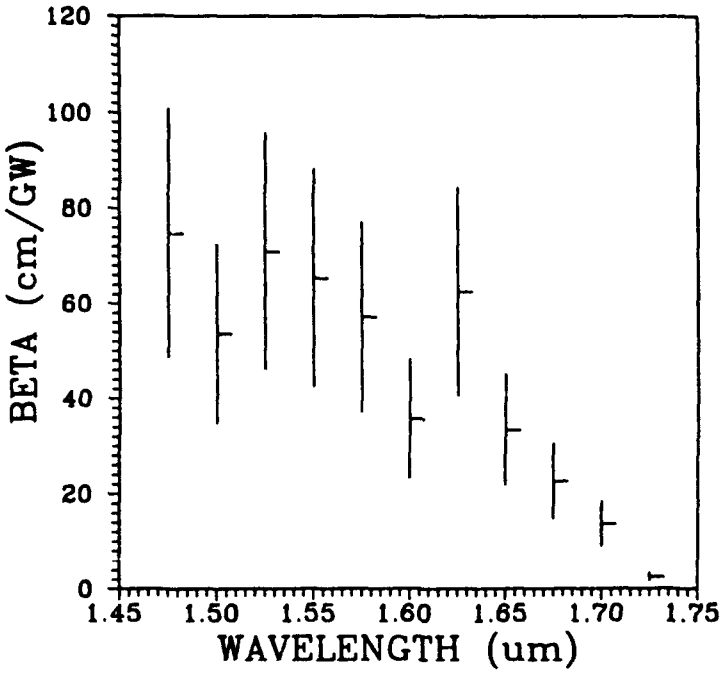

Figure 1. Two photon absorption coefficient β versus wavelength. The error bars show a 30% error.

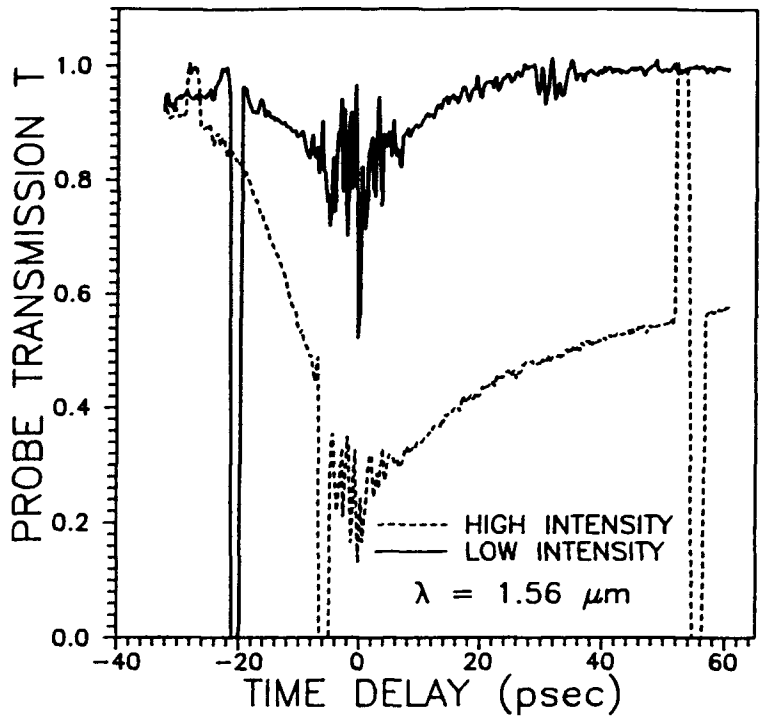

figure 2. Probe transmission with low and high intensity pump versus time delay between probe and pump.

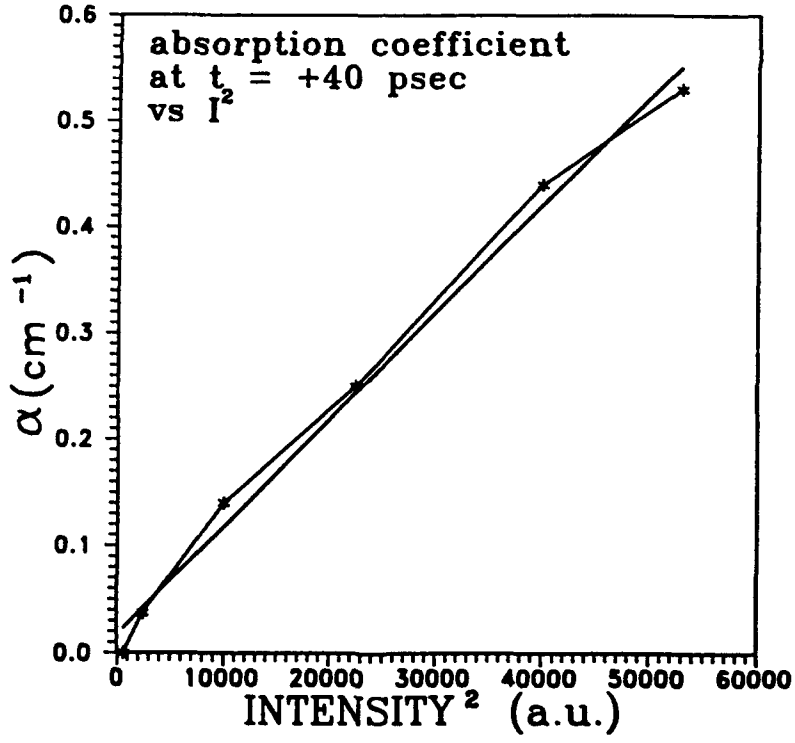

Figure 3. Free carrier absorption coefficient versus pump intensity squared at +40 psec.

Measurement of High Frequency Electro-Optic Coefficient in Ferroelectric Liquid Crystal Materials

J.Y.Liu, †M.G.Robinson, K.M.Johnson and D.Doroski

Center for Optoelectronic Computing Systems,
Department of Electrical and Computer Engineering,
University of Colorado, Boulder, CO 80309.
Tel: 303) 492-2820

†Sharp Laboratories of Europe
Neave House, Winsmore Lane,
Abingdon, Oxon OX14 5UD
United Kingdom.

Ferroelectric liquid crystals (FLC's) form the thermodynamically stable Smectic C* liquid crystalline phase that is non-centrosymmetric and has macroscopic polar order. The symmetry (C_2) implies that FLC materials can exhibit second order nonlinear properties such as the linear electro-optic(EO) effect and second harmonic generation (SHG). In most FLC's designed for optical modulation applications these nonlinearities are small[1,2], but in principle could be made large by specifically synthesizing liquid crystal molecules which self-assemble in such a way that functional groups with large microscopic hyperpolarizabilities, β's, are oriented along the polar axis. By adopting this approach to produce second order nonlinear material, the problems associated with processing organic single crystals are avoided. Furthermore, the flexibility of the liquid crystal technology can be used to design materials with specific refractive indices for phase matching purposes and waveguide design. Waveguides in this material system are particularly interesting as they allow a significant increase in optical propagation length with high electric field generation capability; both important attributes for nonlinear optical phenomena. Preliminary work has already been carried out on waveguide structures whose possibilities are numerous owing to the ability to successfully align FLC's on many different substrates (including Si)[3].

Conventional EO process in FLC's involve molecular reorientation which leads to response times less than microseconds. This paper, however, focuses on the linear electro-optic effect (Kerr effect), which arises from excitations in the molecular electronic structure that can be affected on a nanosecond time scale. Recently, we reported the novel FLC materials with large 2nd order nonlinearities of this nature using SHG{$\chi^{(2)}_{22}$(W314) = 1/4 $\chi^{(2)}_{22}$ ($LiNbO_3$)}[4]. With these new nonlinear materials, novel modulation schemes through the expected large FLC linear electro-optic

should be possible. To demonstrate and measure high speed EO effect a prism coupled FLC cell is prepared as shown in Figure 1. Two high index prisms (SF10 glass) coated with transparent electrode Indium-Tin-Oxide(ITO) are used as the cell walls. A thin polyvinyl alcohol(PVA) layer, which acts as both an aligning layer and a cladding medium, is then spun on top of the ITO prisms. The thickness and the refractive index of the PVA layer is measured using ellipsometry techniques and are found to be 1.5 μm and 1.514 respectively. After buffing the PVA, which defines the direction of the FLC optical tensor, the prisms are brought together to form a cell of ≈ 8 μm wide using polyspheres and UV optical adhesive. This prism module is heated to a temperature sufficient to maintain the FLC in its isotropic phase and capillary filled.

With a d.c. field across the PVA/FLC/PVA region, the FLC molecules are fixed with their optical axis along the z-direction. A HeNe laser beam(λ=0.6328 μm) with its polarization perpendicular to the incident plan (TE polarization) is launched into the prism cell. The transmission is then measured as a function of incident angle and shown in Figure 2. The coupling peaks, which refer to waveguide TE eigenmodes, occur when the component of the wave vectors parallel to the gap are equal for the wave in the prism and the wave in the FLC layer. At the position of the peaks, guided radiation propagates for a distance varying from 2 to 10 mm before coupling evanescently into radiation modes.

To demonstrate the high frequency EO effect a high voltage (20-300V), high frequency (0-200KHz) pulse train is applied to the prism module. To insure that the FLC molecules do not flip to an alternative state, a bias voltage of 20 V is always applied across the cell. The electro-optic effect for C_2 symmetry in the FLC materials can be expressed by:

$$n'_z = n_z - \frac{n_z^3 r_{32} E_y}{2}$$

for electric fields applied along in the y-direction. This small change of the refractive index will modulate the effective index, or propagation constant β, of the waveguide modes. Recall that the propagation constant is related to the incident angle through the relationship $\beta = k n_p \sin(\theta_p)$, where $k = 2\pi/\lambda$, n_p is the refractive index of prism, and θ_p is the incident angle. Thus the small change of θ_p will shift the position of the waveguide mode. By fixing the incident angle at a specific mode where 50% transmission occurs, intensity modulation can be detected using an avalanche photodiode. A typical result is shown in Figure 3a. The EO coefficient r_{32} calculated from above experiment is found to be ≈0.3 pm/V for the commercially available SCE9 with significantly increased values expected for novel materials to be measured in the near future. Due to the large capacitance of the PVA/FLC/PVA films used in these initial experiments the modulation frequency was limited to 10k Hz. By patterning the electrode, the capacitance of the module can be reduced

and improved frequency response is expected. This future work will be presented at the conference.

Theoretical analysis indicates that this prism coupled waveguide technique is very sensitive as compared to alternatives such as the direct interferometric measurement of phase modulation, or Fabry-Perot multiple reflection interferometry. For experimental conformation of measured results however, this latter measurement technique is also used on Fabry-Perot etalon FLC cells prepared as follows.

A thin Al layer (200 Ä) with reflectivity 85% is coated on a pair of 1" diameter optical flats. Photolithographic techniques are used to form 2 mm diameter electrodes in the Al layer; the small size being necessary to reduce the cell capacitance. PVA (400 Ä) is spun coated onto the substrates as an aligning layer. The flats are then brought together to within 8 μm to form the cell which is filled under vacuum with FLC SCE9. A d.c. biased, high voltage pulse train is applied to the FLC cell and the modulated transmission of a HeNe laser beam is measured (see Figure 3b). Initial experiments indicate the two measurements are consistent within experimental error although it can be seen from Fig.3 that this latter method is indeed less sensitive than the former prism coupling technique. However, due to the smaller capacitance of the Fabry-Perot cell and the low resistance of its Al electrodes, we are able to modulate the field up to 200k Hz. Results indicate that the measure EO effect persists to this frequency as expected, and should be present at much higher frequency(GHz). Experiments at greater frequencies are being planned at the present time.

In conclusion, a prism coupling waveguide technique is presented for the measurement of high frequency EO effects in ferroelectric liquid crystals. Measurements indicate an electro-optic coefficient r_{32} of 0.3 pm/V for SCE9; a commercially available FLC material. Higher nonlinearities are expected for novel specially synthesized materials now under investigation.

Reference:

1. J.Y.Liu, M.G.Robinson, K.M.Johnson,& D.Doroski, Opt. Lett.,**15**, 267 (1990).

2. A.Taguchi, Y.Oucji, H.Takezoe, & A.Fukuda, Jpn. J. Appl. Phys. **28**, 997 (1989).

3. J.Y.Liu, M.G.Robinson, K.M.Johnson,& D.Doroski, OSA Annual Meeting, Tech. Dig. TuZ2, Boston MA., Nov. 1990.

4. J.Y.Liu, M.G.Robinson, K.M.Johnson,& D.Doroski, Proc. Int. Symp. Nonlinear Optical Material, El Paso, Texas,Oct. 1990.

5. S.J. Elston & J.R.Sambles, Appl. Phys. Lett. **55**, 1621 (1989).

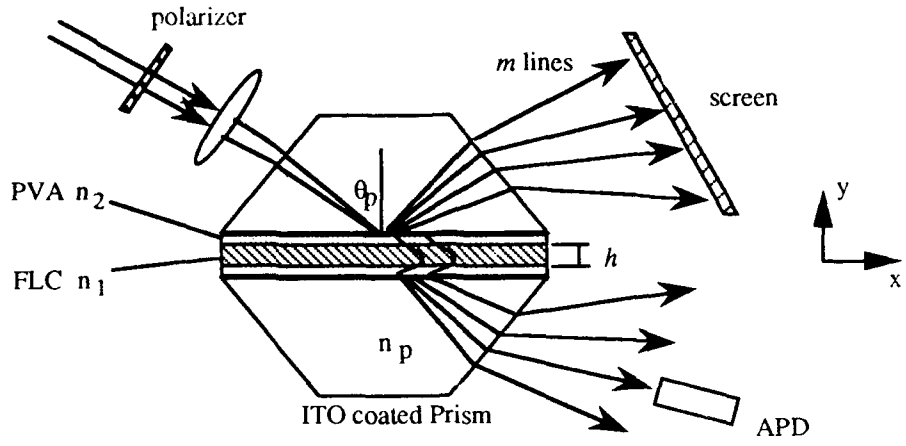

Fig.1 Prism Coupled FLC Waveguide

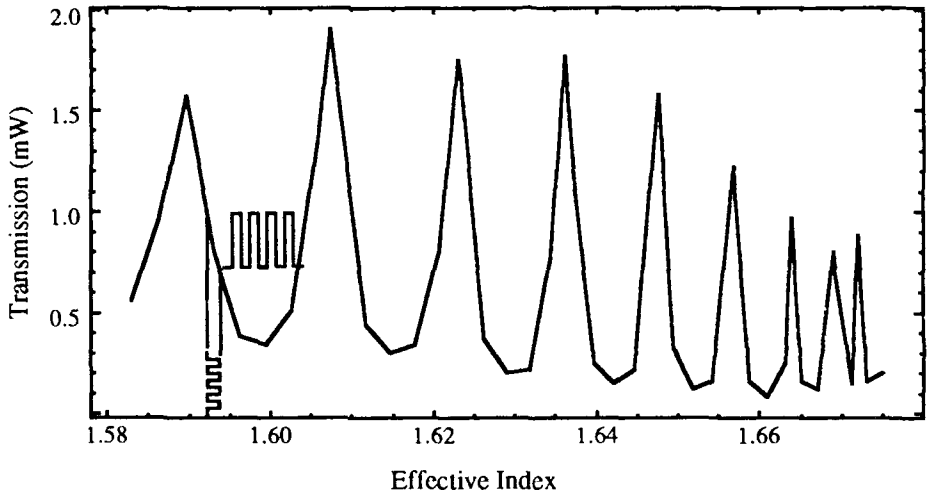

Figure 2. Typical transmission of the prism coupled FLC waveguide cell. A waveguide mode is intensity modulated by a high voltage pulse train through the electro-optic effect.

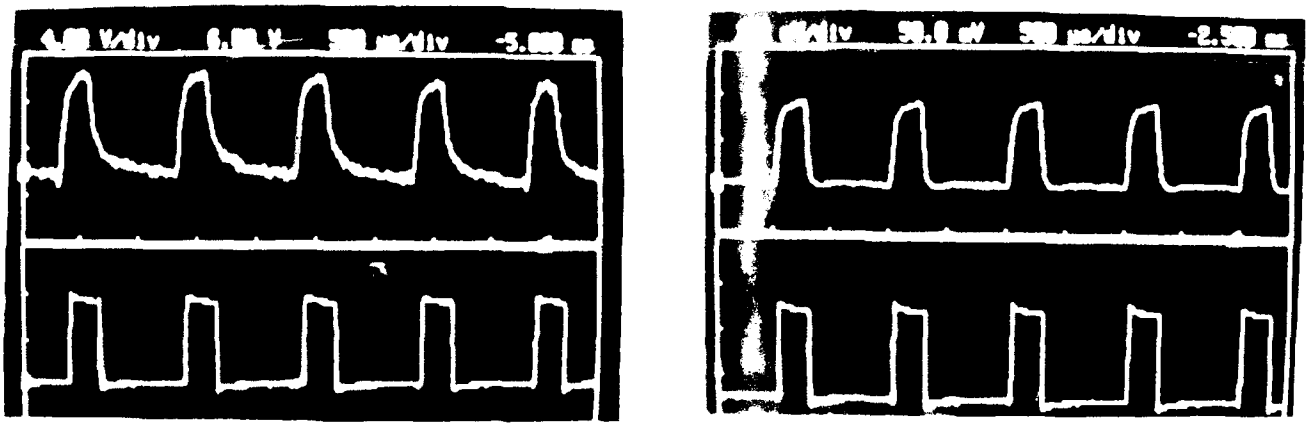

(3a) Prism Coupled FLC Cell.

(3b) Fabry-Perot Cell.

Figure 3. 200 V voltage pulase train was applied to prism coupled and Fabry-Perot cells. The sensitivity of 3a is higher than 3b for an order of magnitude.

Quasi-Phase-Matched Second-Harmonic Generation in Lithium Tantalate Waveguides : Experiments and Simulations

Henrik Åhlfeldt, Gunnar Arvidsson and Bozena Jaskorzynska
Institute of Optical Research
S-100 44 Stockholm, Sweden; telephone +46 8 790 7287

Introduction

Several materials and methods are investigated in the search for devices for efficient frequency doubling of infra-red diode lasers to blue. Such compact light sources would find important applications in i.e. optical data storage, displays and spectroscopy.

For efficient second harmonic generation (SHG), the phase-matching condition must be fulfilled. In the quasi-phase-matching (QPM) scheme, phase matching is accomplished by periodic modulation of the non-linear properties of the material. Quasi-phase-matched SHG of blue light in waveguides has been demonstrated in lithium niobate [1],[2], in polymers [3] and recently very encouraging results have been obtained in KTP [4]. Lately there have also been reports on quasi-phase-matched SHG of blue light in lithium tantalate waveguides [5], [6].

In a ferroelectric material, like lithium niobate, lithium tantalate or KTP, the modulation of the non-linear coefficient is obtained by periodic reversal of the ferroelectric domains. Two different methods have been demonstrated for periodic domain inversion in lithium tantalate. The first method uses electric fields applied by interdigital electrodes to induce periodic domain reversal [6], and the other technique is built on periodic proton exchange followed by heat treatment below the Curie point [5]. The domain inverted waveguides analyzed in this paper were fabricated using the second method.

The shape of the reversed domians is not the same in the different materials. KTP seems to exhibit laminar domain-inverted regions, similar to the ideal case shown in Fig. 1. In lithium niobate, the domain boundaries show a triangular shape as indicated in Fig.2. The shape of the domain boundaries in lithium tantalate is instead semicircular or somewhat elliptic. This is shown schematically in Fig. 3, whereas Fig. 4 shows a micrograph of a periodically domain inverted lithium tantalate sample.

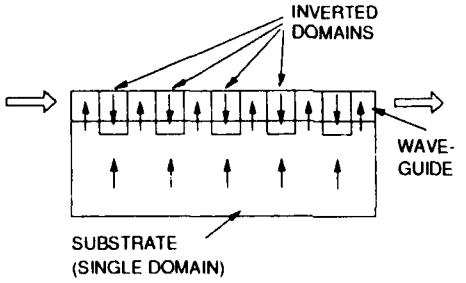

Fig. 1. The ideal waveguide structure in $LiNbO_3$ or $LiTaO_3$ for quasi-phase-matching. The waveguide passes regions with alternating domain orientation, corresponding to alternating sign of the effective nonliner coefficient.

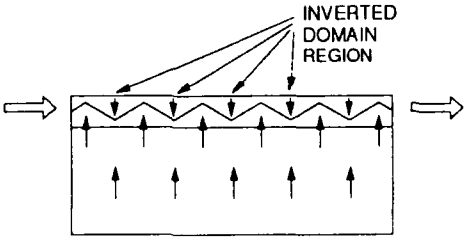

Fig. 2. The actual waveguide structure used for quasi-phase-matched SHG in $LiNbO_3$.

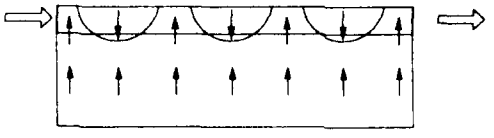

Fig. 3. The actual waveguide structure used for quasi-phase-matched SHG in $LiTaO_3$.

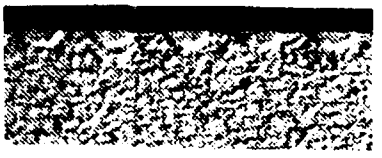

Fig. 4. The etched y-face of a periodically domain inverted lithium tantalate sample. The period is 12 μm.

The influence of the triangular shape of the domain boundary on the conversion efficiency for QPM SHG in lithium niobate has been reported previously [7]. In this paper we present calculations on the conversion efficiency for QPM SHG in lithium tantalate. We report on some experimental results and make comparisons to the lithium niobate case.

Theory: Influence of the shape of the domain boundary on the conversion efficiency

The period of modulation required to phase-match generation of blue light in $LiTaO_3$ is ~3.5 μm. To facilitate the photolitographic process a modulation with a lower periodicity, used in a higer order, is often considered. The periodic modulation of the nonlinearity along the waveguide can be decomposed in spatial Fourier components, and the conversion efficiency depends on the relevant Fourier coefficient [7]. For the waveguide structures which we consider, the duty cycle of the modulation, and thus also the relevant Fourier coefficient, varies with the depth. Therefore the Fourier coefficient has to be included when evaluating the conventional overlap integral over the cross section of the waveguide, as shown in Ref 7. The expression for the n-th Fourier coefficient $c_n(z)$, in the case of elliptical boundaries is:

$$c_n(z) = \frac{2}{\pi \cdot n} \sin\left\{ n\frac{2\pi}{T} \cdot b \cdot \sqrt{1-(z/a)^2} \right\} \qquad \text{for} \qquad -a \le z \le 0$$

$$c_n(z) = 0 \qquad \text{otherwise}$$

The geometrical parameters used are explained in Fig 5. In an ideal laminar structure the function $c_n(z)$ would be constant. For example: in a laminar structure with 50% duty cycle used in first order we would have $c_n(z)=c_1(z) \equiv 2/\pi$.

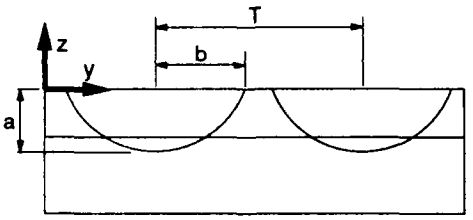

Fig. 5. The geometrical parameters, used to describe the domain inverted regions for $LiTaO_3$. Note that the duty-cycle refers to the value at the surface.

Experiments

Quasi-phase-matching waveguides have been fabricated in c-cut $LiTaO_3$ using a one-step fabrication procedure based on periodic proton exchange followed by heat treatment below the Curie temperature [5]. Slab and channel waveguides were characterized by prism coupling. Third order quasi-phase-matched SHG experiments were carried out using a Styryl 9 dye laser as fundamental light source. For a 12 μm wide channel waveguide a normalized conversion efficiency of 0.4 % W^{-1} cm^{-2} was measured. Using a 6 μm wide channel guide, a value of 2 % W^{-1} cm^{-2} was obtained. The near fields were measured at the fundamental and second harmonic wavelength. The channel waveguides used were multimode for the fundamental wavelength, which made it difficult to launch the light exclusively into the lowest order mode, and this may have decreased the conversion efficiencies.

Numerical results

Using the experimentally determined effective indices, refractive index profiles were determined for the waveguides. It was found that the slab waveguides with very good accuracy had a gaussian index profile. Therefore a model commonly used for graded index titanium-diffused waveguides was used for the channel waveguides for numerical calculation of the field distributions. The calculated distributions showed good agreement with the measured near-fields. Using such data, calculations of the conversion efficiencies were carried out for various geometrical parameters for the domain-inverted regions. In Figs. 6 and 7 results are shown for a 12 μm channel waveguide, and for varying duty-cycle.

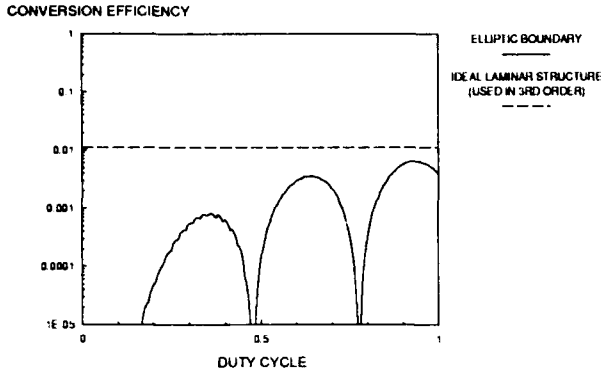

Fig 6. Calculated conversion efficiency for a waveguide length of 1 cm and fundamental power of 100 mW as function of the duty-cycle for the domain-inverted regions (cf Fig 5). 3rd order QPM. Modal fields (cf fig 7) fitted to the experimental case. (a/b)=0.8

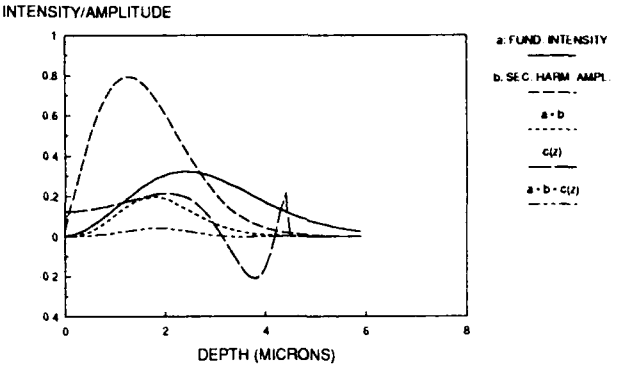

Fig 7. Modal fields in depth and the shape of the function $c_n(z)$ for the optimal duty-cycle according to Fig 6.

Three maxima can be observed in Fig 6. The two minima corresponds to cases in which the duty cycle - at the depth in the waveguide, where the modal distributions are concentrated - takes a value (1/3 and 2/3 respectively) such that the third Fourier coefficient $c_3(z)$ passes through a zero-point as function of z.

In our experimental case we have a duty-cycle of 0.8, which according to Fig. 6 is close to a minimum. The measured conversion efficiency is in good agreement with the calculated value. By increasing the duty-cycle it should be possible to increase the conversion efficency by one order of magnitude. Calculation showed that for this limited mode confinement the conversion efficency is not more effficient when going to 2nd or 1st order QPM. Calculations with other, realistic, waveguide profiles have, however, given conversion efficencies up to at least 35 % W^{-1} cm^{-2} using 3rd order QPM, and still higher values for 1st order, see Figs 8 and 9.

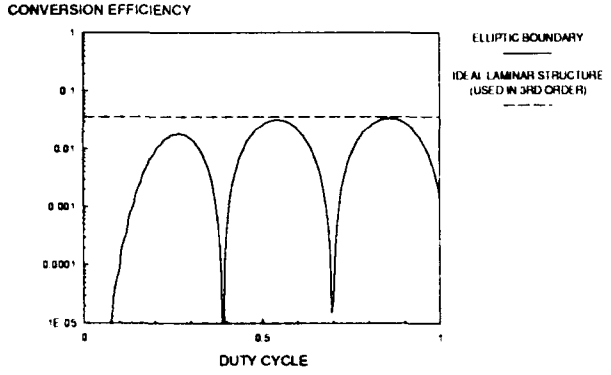

Fig 8. Calculated conversion efficiency as function of the duty cycle for another modal distribution than in Fig 6 and 7. Third order QPM. Same fundamental power and waveguide lenght as in Fig 6. (a/b)=0.8

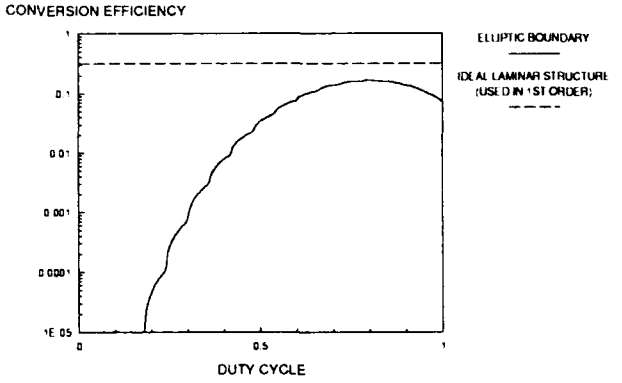

Fig 9. As in Fig 8, but for 1st order QPM.

Discussion

The mode confinement, in particular in depth, is essential for high conversion efficency. As the modulation depth in 1st order QPM is only a third of the modulation depth in 3rd order QPM, this is particularly important when working with 1st order QPM. In order to gain by going to 2nd or 1st order QPM a tight mode confinement is more important for $LiTaO_3$ than for $LiNbO_3$. This is related to the following two factors: firstly, in $LiNbO_3$ the domain boundary may be buried without geometrical changes, which is not possible in $LiTaO_3$. Secondly, the shape of the $c_n(z)$ function for 3rd order QPM, makes it possible to efficiently utilize interaction between modal fields over a larger depth in $LiTaO_3$, than in $LiNbO_3$. The second factor indicates that it should be easier to come close to the theoretical limit, corresponding to an ideal laminar structure, when using 3rd order QPM in $LiTaO_3$, as compared to $LiNbO_3$.

Conclusions

The shape of the periodic domain boundary that is obtained during domain reversal by heat treatment is more promising in $LiTaO_3$ than in $LiNbO_3$. In particular it should be more easy to come close to the theoretical limit when using third order quasi-phase-matching. In order to utilize the possibility of a more efficient interaction by going to first order QPM, it is, however, critically important to obtain a very tight mode confinement. To achieve an improvement compared to our first experimental results, the duty cycle is an essential parameter to optimize. A better mode confinement is also important and can be obtained for example by fabricating the channel waveguide separately after obtaining domain inversion.

References

1. J. Webjörn, F. Laurell and G. Arvidsson, "Blue light generated by frequency doubling of laser diode light in a lithium niobate channel waveguide", *IEEE Photon. Technol. Lett.*, vol. 1, pp. 316-318, 1989.
2. E. J. Lim, M. M. Fejer, R. L. Byer and W. J. Kozlovsky, "Blue light generation by frequency doubling in periodically poled lithium niobate channel waveguides", *Electron. Lett.*, vol. 25, pp. 731-732, 1989.
3. G. Khanarian *et al.*, "Phase-matched second-harmonic generation in a polymer waveguide", *Appl. Phys. Lett.*, vol. 57, pp. 977-979, 1990.
4. C. J. van der Poel, J. D. Bierlein, J. B. Brown and S. Colak, "Efficient type I blue second harmonic generation in periodically segmented $KTiOPO_4$ (KTP) waveguides", *Appl. Phys. Lett.*, vol. 57, pp. 2074-2076, 1990.
5. H. Åhlfeldt, J. Webjörn and G. Arvidsson, "Periodic domain inversion in lithium tantalate", in Integrated Photonics Research, 1991, Technical Digest Series, (Optical Society of America, Washington, DC, 1991), pp. 60-61.
6. S. Matsumoto, E. J. Lim, M. M. Fejer and H. M. Hertz, "Second-harmonic generation of blue light in a periodically poled $LiTaO_3$ waveguide", in Integrated Photonics Research, 1991, Technical Digest Series, (Optical Society of America, Washington, DC, 1991), p. 97.
7. G. Arvidsson and B. Jaskorzynska, "Periodically domain-inverted waveguides in lithium niobate for second harmonic generation: influence of the shape of the domain boundary on the conversion efficiency", Intern. Conf. on Materials for Non-linear and Electro-optics, Cambridge, UK, 1989, *Int. Phys. Conf. Se. No.* **103**, 47 (1989).

GRATING COUPLERS FOR KERR-TYPE NONLINEAR WAVEGUIDES : A SIMPLIFIED THEORY

R. Reinisch*, P. Vincent**, M. Nevière**, G. Vitrant*

* : Laboratoire d'Electromagnétisme, Microondes et Optoelectronique, Ecole Nationale Supérieure d'Electronique et de Radioélectricité de Grenoble, 23 avenue des Martyrs, BP 257, 38016 Grenoble Cédex, France. Tel : (33) 76876976, Fax : (33) 76433796
** : Laboratoire d'Optique Electromagnétique, Case 262, Faculté des Sciences et Techniques de St-Jérome, 13397 Marseille Cédex 13, France. Tel : (33) 91288388, Fax : (33) 91674428

We consider grating induced optical bistability (OB) arising from the resonant excitation of a given nonlinear guided mode. In that case it can be shown, using the coupled-mode formalism[1], that in the whole bistable domain :

a) the transverse field map of the resonantly excited nonlinear guided mode corresponds to that of the associated linear one *which is known.*

b) the Kerr-type nonlinearity *only* modifies the longitudinal wavevector component.

Thus the rigorous theory of diffraction[2], previously used to study grating-induced plane wave OB[3], can be replaced by a much more simple one which works as follows :

i) determine the *complex* longitudinal wavevector component of the linear *leaky* guided mode p, β_p^L, through the solution of the associated linear homogeneous *grating* problem[2] ,

ii) use the rigorous theory of diffraction in linear optics[2] to determine the in-coupling efficiency, t_p, of the incident plane wave,

iii) use the coupled-mode formalism to derive the analytical expression[4] of the complex nonlinear longitudinal wavevector component β_p^{NL}.

Considering a plane wave incident on a Kerr-type grating coupler, points i) to iii) show that the knowledge of the guided field amplitude, A_{gw}, no longer requires a complicated numerical integration, as in ref. 3, but can be obtained in a simple analytical way by the following expression :

$$A_{gw} = A_i \frac{t_p}{\beta - \beta_p^{NL}} \qquad (1a)$$

with :

A_i : amplitude of the incident plane wave

$\beta = k_0 \sin\theta$

θ : angle of incidence

$$\beta_p^{NL} = \beta_p^{L} + \xi_p |A_{gw}|^2 \qquad (1b)$$

ξ_p : nonlinear coefficient derived from the theory of ref.(4).

Moreover, we have found that the reflected amplitude, B_n, of any *radiated* diffracted order, n, can be obtained very easily : it suffices to replace, in the *linear* expression[2] of B_n, the linear zero, β_z^L, by the nonlinear one, β_z^{NL}, where β_z^{NL} *has the same intensity dependence as* β_p^{NL}. This is a consequence of a). We then get the following expression of the reflectivity of a propagating diffracted order n:

$$B_n = r_n \frac{\beta - \beta_z^{NL}}{\beta - \beta_p^{NL}} A_i \qquad (2a)$$

where r_n is derived from the rigorous theory of diffraction in linear optics[2]

and

$$\beta_z^{NL} = \beta_z^{L} + \xi_p |A_{gw}|^2 \qquad (2b)$$

The following is worth noting : the range of validity of this method is only determined from the knowledge of the rigorous solution of the *linear* regime which requires a much lower computation time than the nonlinear theory of ref.3. Indeed the modal formalism presented here applies whenever the associated linear transmittivity can be approximated by a lorentzian in the vicinity of the nearest electromagnetic resonance.

When this criterium is fulfilled the agreement is very good : we consider a nonlinear grating coupler (fig.1); the results are plotted figs. 2a and 2b for a wavelength of 1.06 µm. The angles of resonance and incidence are respectively : 47.73° and 47.33°.

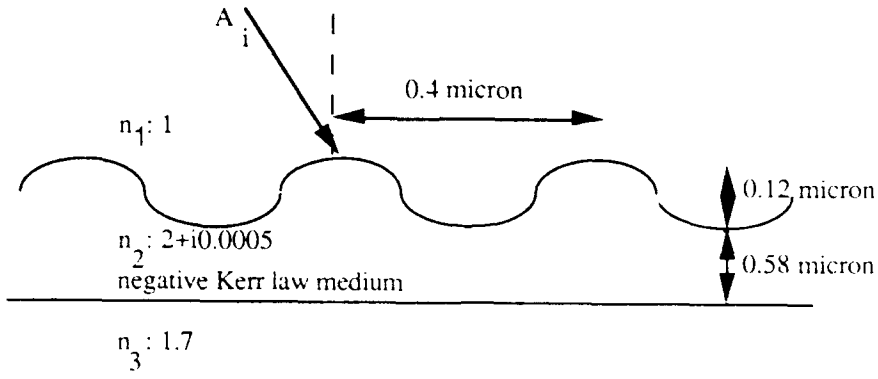

fig.1

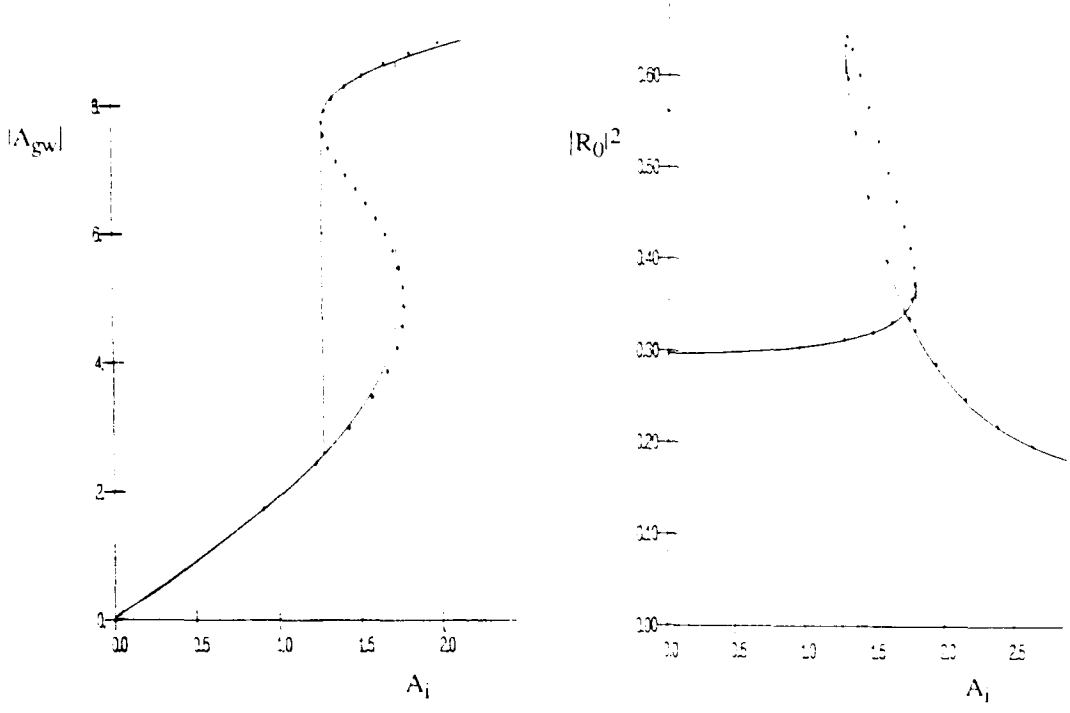

fig.2

a

$|A_{gw}|$ as a function of A_i

full line : theory of ref. 3

dotted curve : derived from eq. 1a

b

Reflectivity $|R_0|^2$ as a function of A_i

$(R_0=B_0/A_i)$

full line : theory of ref. 3

dotted curve : derived from eq. 2a

Let us emphasize that this method takes rigorously into account the groove depth (δ) of the grating. Thus this method is *not a perturbative one with respect to* δ. This is due to the fact that only the nonlinear term is taken perturbatively into account through the relations (1b) and (2b). The effect of the grating is linear and is dealt with by an exact linear calculation of the diffracted orders[2].

In the case of finite width incident beam(s), diffraction induced transverse effects (along x) in Kerr-type grating couplers can be analyzed using the following equations (directly derived from eqs 1a and 2a) :

$$j\frac{d\mathcal{A}_{gw}(x)}{dx}+(\beta_p^{NL}-\beta)\mathcal{A}_{gw}(x)=-t_p\mathcal{A}_i(x)$$

$$\mathcal{B}_n(x)=r_n\mathcal{A}_i(x)+\frac{r_n}{t_p}(\beta_p^{L}-\beta_p^{L'})\mathcal{A}_{gw}(x)$$

$\mathcal{A}_{gw}(x)$: guided wave amplitude

$\mathcal{B}_n(x)$: reflected amplitude

To summarize, we have shown that the simultaneous use of both the rigorous theory of diffraction in linear optics[2] and the coupled mode formalism[1] provides a convenient mean for studying the response of nonlinear grating couplers. This method, whose accuracy can be easily checked, allows an easy access, *not only to the guided wave* (i.e. to a resonantly excited evanescent diffracted order) but also to the *radiated* diffracted orders. This leads to the possibility of studying the influence of transverse effects on the field map of diffracted orders *whatever their type, evanescent or radiated, may be.*

References

(1) H. Kogelnik "Theory of dielectric waveguides" in *Integrated Optics*
Ed. T.Tamir, Springer-Verlag (New-York, 1975)

(2) *Electromagnetic Theory of Gratings*
Ed. R. Petit, Springer-Verlag (New-York, 1980)

(3) P. Vincent, N. Paraire, M. Nevière, A. Koster, R. Reinisch
J. Opt. Soc. Am. B2, 1106 (1985)

(4) G. Vitrant, M. Haelterman, R. Reinisch
J. Opt. Soc. Am. B7, 1319 (1990)

Novel Effects

TuD 4:00pm–5:00pm
Palmerston Room

Yaron Silverberg, *Presider*
Bellcore, USA

REMOTE NONLINEAR SWITCHING AND LARGE NONLINEAR EFFECTS IN RESONANT OPTICAL WAVEGUIDES

Falk Lederer, U.Trutschel, M.Mann, Ch.Wächter
Friedrich-Schiller-Universität Jena
Faculty of Physics and Astronomy
Institute of Solid State Physics and Theoretical Optics
Max-Wien-Platz 1, phone +(37)78 82 26161
0-6900 Jena
Germany

1. INTRODUCTION

Waveguide configurations are promising candidates for all-optical switching and modulation due to the combination of diffractionless propagation of the fields (large interaction length) and the strong confinement of power . Both peculiarities enhance the effectivness of the nonlinear processes that produce the needed induced index change.
The phenomena on which nonlinear guided wave devices are based can be categorized as weakly and strongly nonlinear. When the nonlinear contribution to the refractive index is much smaller than any variations in the linear refractive index that define the waveguide the guided field profile is assumed to be unchanged and perturbation methods can be used to describe the nonlinear mode coupling. The most studied weak nonlinear device to date has been the nonlinear directional coupler where the intensity of the input signal determines the routing of this signal, thus representing an all-optical switch.
In the case of large nonlinearities where the induced refractive index changes are comperable with the index discontinuities the very guiding mechanism is affected. The large induced index changes result in the arising of nonlinear guided waves (NGW) which exhibit power-dependent field profiles and propagation constants and can be unstable in certain domains of the nonlinear dispersion curve. If one attempts to excite an unstable NGW (e.g. via end fire coupling) it cannot be captured by the guide and the power is expelled e.g.via a spatial soliton leaving no guided power at the waveguide output. Hence, there is a large difference in the transmission for either low or high input powers. This device may be used as an all-optical modulator.
The desirable material property required is an off-resonant pure dispersive, and thus ultrafast, Kerr nonlinearity (local dependence of the induced index change on the intensity as $\Delta n_{NL} = n_2 I$) because resonant nonlinearties are accompanied by absorption which can provide serious limitations to all-optical devices. Unfortunately, dispersive nonlinearities are relatively weak and saturate in many materials at relatively

the conventional guiding mechanism basing on total internal reflection as well as the related evanescent coupling between adjacent waveguides do not meet these requirement optimum. The guiding mechanism is relatively stable against induced index changes and the evanescent coupling is weak and restricts the separation of the coupler elements to few micrometers.
This is the motivation to investigate novel guiding schemes which rely on resonance effects as Fabry-Perot action or Bragg reflection. We intend to show that these schemes fit better to all-optical requirements because the guiding mechanism itself can be affected very sensitively by nonlinear index changes lifting some stringent material requirements.

2. THE REMOTE NONLINEAR ARROW-COUPLER

An ARROW (Anti-Resonant Reflecting Optical Waveguide) consits of a low-index film sourrounded by a few (typical two or three) cladding and substrate films of high-index material. The guided waves are essentially leaky waves with propagation losses of about 0.4 dB/cm for a well-designed ARROW.
A combination of two identical ARROW's constitutes an ARROW-directional coupler having the peculiarity that the fields in the coupling region are sinusoidal rather than evanescent. This has the consequence that the coupling behaviour reproduces periodically with increasing guide separation. Thus, even in the linear regime this device can be used as a remote coupler up to distances of some ten μm [1]. A typical power transfer between the guides is shown in Fig.1.

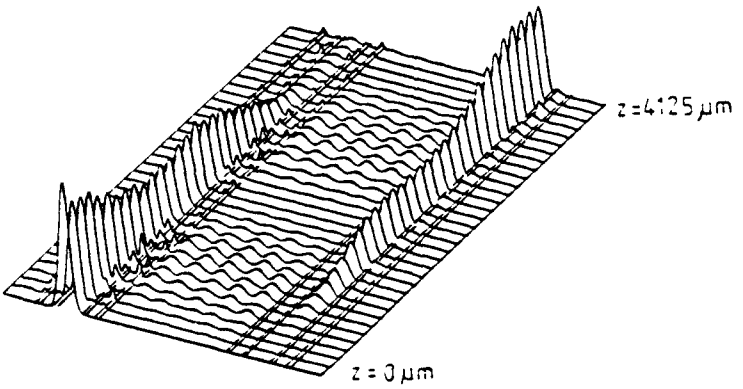

Fig.1 Linear ARROW-coupler with 15.6 μm guide separation

Until now, remote coupling was only reported in the strong nonlinear regime using spatial solitons [2].
Endowing any coupler component with a Kerr-like nonlinearity the device can be used as a remote all-optical switch. The switching characteristic was calculated using a coupled supermode theory [3] and is plotted in Fig.2. It is clearly shown that the switching characteristic is steeper than that of conventional nonlinear directional couplers which can be attributed to the resonant guiding mechanism.

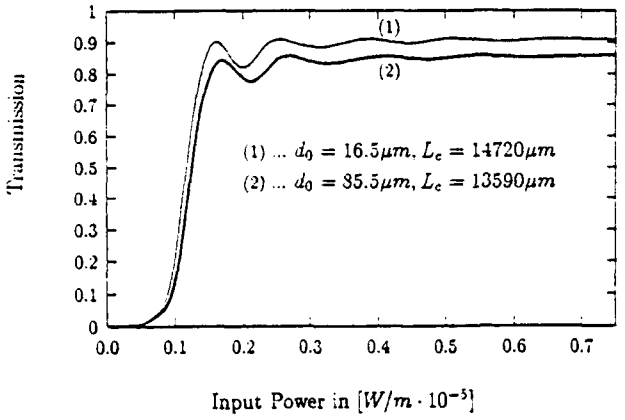

Fig.2 Output- versus input power of a remote ARROW-coupler for different guide separations (n_2 = 10^{-15} m^2/W)

3. THE NONLINEAR ARROW-CUT-OFF MODULATOR

The radiation losses of a single ARROW change abruptly altering the optical thicknesses of the high-index cladding films. This is the basis in designing a nonlinear cut-off modulator [4]. When these films exhibit a self-focusing or defocusing Kerr nonlinearity the refractice index can be controlled by the power localized within these films. When the ARROW is initially in a low-loss state it can be tuned into a high-loss one increasing the power. This applies also for the reversed situation. A numerically calculated input-output characteristic is depicted in Fig.3. There are some indications that the distinction between weak and large nonlinear effects loses some ground for ARROW-geometries because very small changes in the refractive index affect the guiding mechanism.

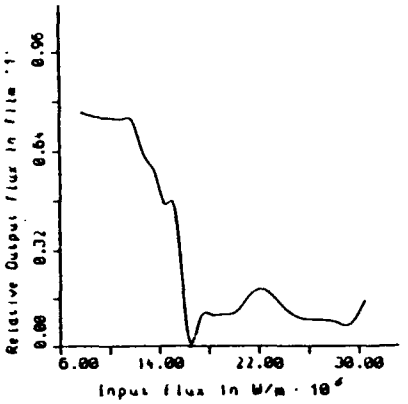

Fig.3 Output power of a nonlinear ARROW in dependence on the input power (device length = 125 μm ,n_2 = 10^{-15} m^2/W)

4. THE NONLINEAR BRAGG REFLECTION WAVEGUIDE

A Bragg reflection waveguide (BRW) consists of a low-index film in contact with two semi-infinite high-index periodic superlattices. Bragg reflection within the stop gap of the superlattices constitutes the guiding mechanism. Only when the propagation constant is situated within this stop gap guided waves can propagate. When the central film is nonlinear nonlinear Bragg guided waves may emerge the propagation constants of which are subject to a power-dependent dispersion relation. We discuss the corresponding dispersion curves and investigate the stability of NGW's situated on different branches. The majority of NGW's turns out to be unstable and evolve into spatial solitons captured in the central film [5]. Furthermore the stop gap can be shifted changing the guided power. This effect can also be exploited for cut-off modulation.

5. CONCLUSIONS

The nonlinear cut-off and switching behaviour have been investigated for ARROW- and Bragg reflection waveguides. The resonant character of the guiding mechanism offers some potential for novel all-optical schemes.

REFERENCES

1. M.Mann, U.Trutschel, Ch.Wächter, L.Leine, F.Lederer Opt.Lett.(1991) accepted for publication
2. D.R.Heatley, E.M.Wright, G.I.Stegeman Appl.Phys.Lett.**53**(1988)172
3. Y.Silberberg, G.I.Stegeman, Appl.Phys.Lett.**50**(1987)801
4. M.Mann, U.Trutschel, F.Lederer, Ch.Wächter, L.Leine J.Opt.Soc.Am.B (1991) accepted for publication
5. Ch.Wächter, F.Lederer, J.Opt.Soc.Am.B, subm.for publication

Photonic Bloch Waves and Field Microstructure in Nonlinear Gratings: An Intuitive Approach

P.St.J. Russell,
Optoelectronics Research Centre,
University of Southampton,
Southampton SO9 5NH, U.K.

1. Introduction

Coupled wave theory is commonly used in numerical simulations of reflection from nonlinear grating structures. By contrast, the complementary photonic Bloch wave (PBW) approach has rarely been adopted, perhaps the only example being recent work on gap solitons[1,2]. Bloch wave theory[3,4] offers an alternative physical intuitive picture that encourages one to think in terms of field microstructure, leading to a range of simple explanations for the behaviour of light in linear gratings. In this paper the dispersion relation and field microstructure of *nonlinear* Bloch waves are found, and used to clarify the physical mechanisms that lead to regions of bistability, instability and oscillation for incidence of a monochromatic plane wave on a nonlinear grating half-space.

2. General nonlinear dispersion relation

The nonlinear Bloch waves are the grating's normal modes. In the two-wave approximation they are modelled by a pair of superimposed plane waves of constant amplitude:

$$E(z,t) = \frac{1}{2}\left(V_f \exp\{-j\mathbf{k}_f \cdot \mathbf{r}\} + V_b \exp\{-j\mathbf{k}_b \cdot \mathbf{r}\}\right)\exp(j\omega t) + \text{c.c.} \tag{1}$$

whose k-vectors are related by Floquet's theorem $\mathbf{k}_f = \mathbf{k}_b + \mathbf{K}$ where $|\mathbf{K}| = 2\pi/\Lambda$ is the grating vector and Λ its period. V_b and V_f are the field amplitudes and f and b are forward and backward labels. This pair of waves propagates through the grating with a fixed group velocity or decay rate. Putting (1) into Maxwell's equation, assuming a linear grating described by $\chi^{(1)} = \chi_o^{(1)} + \chi_m^{(1)}\cos(Kz)$, $\chi_m^{(1)} > 0$, and making standard approximations, it is straightforward to show that the field amplitudes obey:

$$\begin{pmatrix} -\delta_f + \Delta(|V_f|^2 + |V_b|^2) & \kappa + \Delta V_b^* V_f \\ \kappa + \Delta V_b V_f^* & \delta_b + \Delta(|V_f|^2 + |V_b|^2) \end{pmatrix} \begin{pmatrix} V_f \\ V_b \end{pmatrix} = \begin{pmatrix} 0 \\ 0 \end{pmatrix} \tag{2}$$

where $\kappa = \chi_m^{(1)} k_o/4n_o^2$, and the nonlinear dephasing parameter Δ is

$$\Delta = \left[3\chi^{(3)}\omega\mu S_o/8(1+\chi_o^{(1)})\right). \tag{3}$$

where S_o is the incident Poynting vector. δ_f and δ_b are the corrections to the mean linear wavevector k_o needed to yield $\mathbf{k}_f$ and $\mathbf{k}_b$, i.e.,

$$\mathbf{k}_n^2 = (k_o + \delta_n)^2.$$

Solutions of (2) are easily found algebraically for a given boundary condition, yielding up to three different $(\delta_f, \delta_b, V_f/V_b)$ sets and hence three different nonlinear Bloch waves.

For a purely distributed feed-back (DFB) structure (Figure 1), $\mathbf{k}_b$ and $\mathbf{k}_f$ are anti-parallel, and we write

$$\gamma = \delta_f = (\delta_b + \vartheta) \tag{4}$$

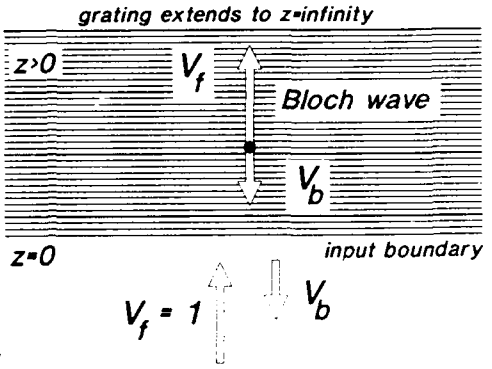

Figure 1: Boundary condition at DFB half-space.

where $\vartheta = 2k_o - K = 2n_o(\omega - \omega_B)/c \approx 4\pi n_o(\lambda_B - \lambda)/\lambda_B^2$ and λ_B is the vacuum Bragg wavelength. The parameter γ is the perturbation to k_o that appears in the vicinity of a Bragg condition, i.e., $k_f = k_o + \gamma$.

As written, the matrix equation (2) illustrates succinctly the various regions of behaviour. At $\Delta = 0$, the standard linear dispersion relation is obtained, as illustrated in Figure 1 for Bloch waves with group velocities pointing into the grating. Floquet's theorem forces the field microstructure (created by interference) to mimic the grating structure. Fast and slow PBW's exist, for which the optical power is partially or fully redistributed by interference into, respectively, the low and high refractive index regions of the grating. For linear gratings, the ramifications of this picture are fully explored in a separate article[4].

As the nonlinearity rises, the mean wavevectors in the grating are increased by $\Delta(|V_f|^2 + |V_b|^2)$ (on-diagonal matrix elements) and the effective grating strength by $\Delta V_b V_f^*$ (off-diagonal matrix elements). The fringe microstructure of the Bloch wave, having the same periodicity as the grating, acts either to enhance or reduce the grating strength. A fast PBW in a grating with a positive Δ will experience a gradual diminution in grating strength, leading to modulational instability when the induced nonlinear grating cancels the linear one at

$$\kappa = -\Delta V_b^* V_f. \tag{5}$$

The slow PBW's, on the other hand, will experience a nonlinear enhancement in grating strength as the power is raised. Concurrently with these effects, the average refractive index of the material rises. The full picture is thus of a complex interplay of Bragg condition dephasing and grating enhancement/depletion.

3. Dispersion diagrams

This behaviour may be summarised graphically on a k_f-ϑ diagram, as depicted on Figure 2 for the special case of plane-wave incidence on a DFB half-space (Figure 1). Under these circumstances the boundary condition at $z = 0$ is very simple: $V_f = 1$ (the normalised amplitude of the incident plane wave) and $V_b = \pm\sqrt{\eta}$ where $0 \leq \eta \leq 1$ is the reflection efficiency. For each value of ϑ, the matrix equation is then solved for permitted values of γ and V_b and the results plotted on the k_f-ϑ diagram. A succession of different cases is now explored: (a) In the absence of a grating, the solution is the straight line $(\gamma + \theta)/\kappa = -\Delta/\kappa - \vartheta/2\kappa$ expected of a monochromatic plane wave travelling into the grating half-space. It is the sloping (-..-..) line on the diagrams. (b) Introducing a linear grating, the usual stop-band opens up at the Bragg condition. The branches with negative group velocities ($\partial k_f/\partial\vartheta < 0$) are suppressed - they play no role in the grating half-space. On its red-shifted branch, the k-vector is longer than predicted in (a), i.e., the PBW is a slow one. The opposite is true on the blue-shifted branch. As mentioned above, this behaviour is the result of the periodic PBW field microstructure; power is redistributed into low/high index regions. (c) Increasing the optical nonlinearity or the input power level, two effects are seen: i) as expected from very simple considerations, the Bragg condition shifts to lower frequencies owing to the nonlinear increase in the average propagation constant; ii) the stop-band branches gradually develop distortions owing to the appearance

of a nonlinear grating through interference of the backward and forward waves in the Bloch wave. These distortions are most severe where the nonlinear grating is strongest, i.e., close to the band edges where the fringe visibility is greatest.

4. Refractive index profiles

The linear, nonlinear and nett refractive index profiles across the grating planes are plotted in Figure 2 for ten different Bloch waves. In cases 1 and 3, the nett grating strength is zero, meaning that the forward and backward waves are no longer bound together – this will cause modulational instability. In cases 1,3 and 5 the nonlinear grating strength actually *exceeds* the linear, reversing the sign of its grating ripple: a fast Bloch wave turns into a slow. In all these cases the Bloch waves are likely to be unstable since the nonlinear grating equals or dominates over the linear.

On the slow stop-band side at intermediate levels of nonlinearity, parameter regimes exist where the nonlinear PBW is "evanescent", whereas the linear PBW is propagating. This occurs at $\vartheta/2\kappa = -2.5$ for $\Delta/\kappa = 1$ in Figure 2. The analysis here is not valid in these regions, since evanescence is not compatible with stability for nonlinear waves, for the level of optical nonlinearity will fall off as the PBW amplitude decays; at some point inside the DFB structure the PBW will start to propagate, causing light to leak through and violating the evanescent condition. It is likely that instability and oscillation will occur in this range.

For high levels of nonlinearity, the stop-band ceases to exist, although the region of modulational instability (approximately between points 3 and 5) widens. On the red-shifted stop-band branch, however, bistability arises where two or more travelling-wave solutions exist, with high and low reflection states.

5. General discussion and conclusions

To observe the effects described here, the nonlinear index change must be comparable to the index modulation depth of the linear grating. The two waves bound together by the grating forms an entity insensitive against weak perturbations. Slight changes in refractive index ($\Delta/\kappa \ll 1$) will slow down or speed up the Bloch wave without disturbing its field microstructure or group velocity dispersion. This occurs for example on the edge of the blue-shifted stop-band, where the negative GVD of the linear Bloch waves is undisturbed by the nonlinear index changes needed for gap soliton formation. A quite different situation occurs when $\Delta/\kappa \sim 1$, for now the nonlinear index perturbation is comparable to the grating index modulation and the Bloch wave entity is susceptible to gross distortions in its normal mode shape. This is reflected in the stop-band distortions seen in Figure 2. An interesting aspect of this regime is that the optical path length does not determine whether strong nonlinear effects are seen or not; they are caused by modal shape distortions and not cumulative phase delays between co-propagating waves.

For a grating of modulation depth 10^{-5} at $\lambda_B = 1\mu m$ in an optical fibre with $n_2 \approx 3 \times 10^{-8}$ μm^2/Watt and a core area of 1 μm^2, a power level of a few 100 Watts would result in the behaviour depicted in Figure 2. In order not to straddle the whole stop-band at once, the incident bandwidth would need to be of the order of 10^{-6} of the optical base frequency, i.e., some 0.3 GHz.

In conclusion, the nonlinear PBW approach leads to an easily solvable algebraic dispersion relation, a clear field-microstructural explanation for PBW behaviour, and may be used to delineate regions of stability and instability for incidence on a grating half-space.

References

1. J.E. Sipe and H.G. Winful, Optics Letters **13** (133-134) 1988.
2. C.M. de Sterke and J.E. Sipe, Phys.Rev.Lett. **63**(811) 1989.
3. P.St.J. Russell, Phys.Rev. A **33** (3232-3242) 1986.
4. P.St.J. Russell, J.Mod.Optics, in press.

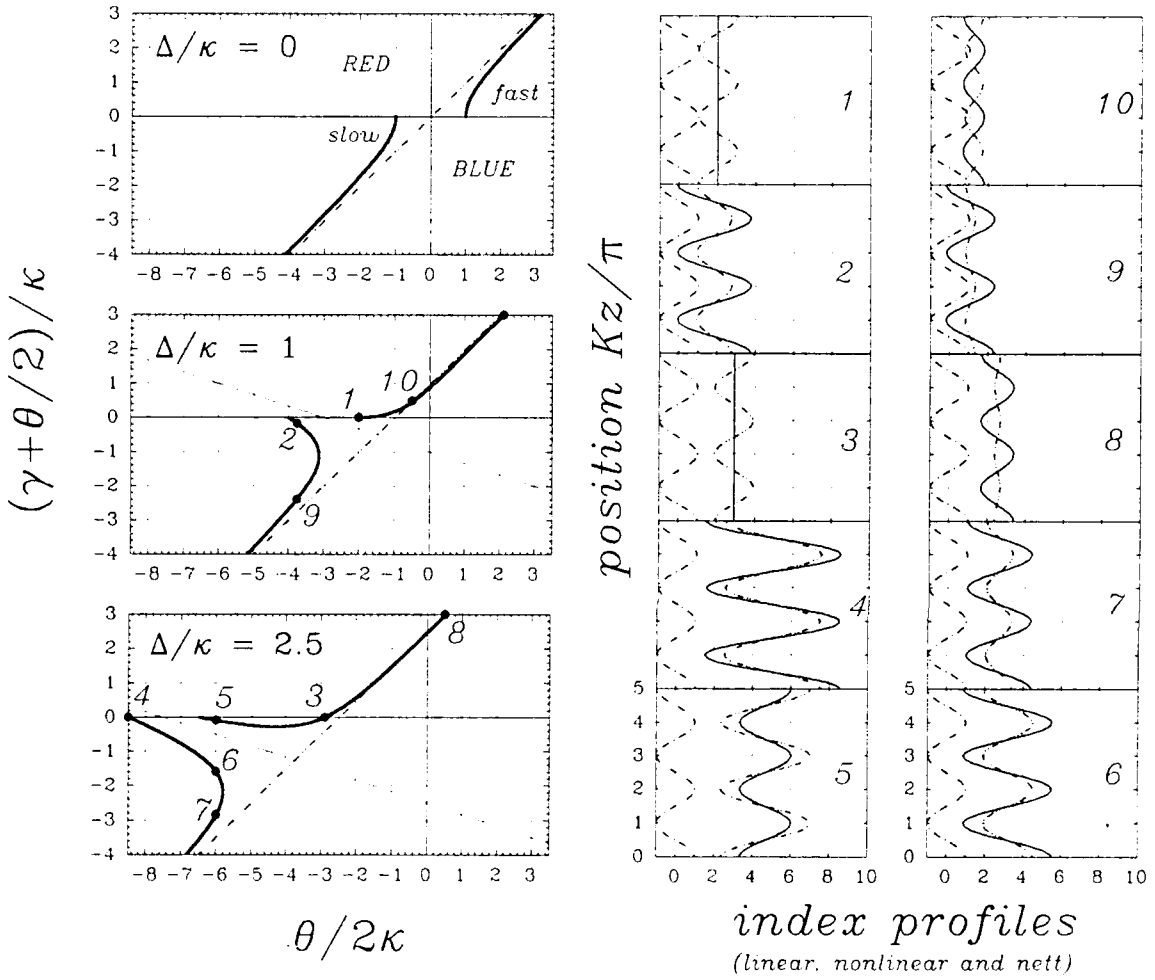

Figure 2: Stop-bands and refractive index profiles for several different cases. The slanting (-..-..) lines on the stop-band diagrams are the solutions for a plane wave in an isotropic nonlinear medium. The loci of forward travelling Bloch waves alone are included (the backward travelling waves do not appear in a half-space). The refractive index profiles show the original grating (-.-.), the nonlinear index change (-..-..) and the nett index profile (—). Cancellation of the linear grating occurs at points 1 and 3, where modulational instability is expected. All the nonlinear distortions in the stop-band shape can be understood from these index modulation patterns. The branches (terminating at 4 and 5, and 1 and 2) are algebraically asymptotic to the dashed lines $(\gamma + \vartheta/2) = -\Delta - \vartheta/6$.

EXPERIMENTAL OBSERVATION OF PICOSECOND DARK SOLITON PROPAGATION OVER 1KM FIBER IN THE NEAR INFRARED

Ph. Emplit, J.-P. Hamaide* and M. Haelterman
Service d'Optique Théorique et Appliquée, Université Libre de Bruxelles
50 av. F.D. Roosevelt, CP 194/5, B-1050 Bruxelles, Belgium

* permanent address: Alcatel Alsthom Recherche, DPE, Route de Nosay
F-91460 Marcoussis, France

In 1973, Hasegawa and Tappert predicted that the nonlinear refractive index of silica fibers can compensate for Group Velocity Dispersion (GVD), resulting in the so-called optical solitons which propagate without distortion.[1,2] Both "bright" and "dark" solitons were identified that correspond to the negative and positive GVD regions of the spectrum, respectively. Since then, owing to their potential applications in high bit-rate fiber telecommunication systems, optical solitons have been intensively investigated both theoretically and experimentally. Soliton propagation of bright pulses has been verified in a large number of experiments and the possibility of its application in long haul fiber transmission has been demonstrated.

However, the difficulty in generating negative pulses has hardly limited the number of experimental observations of dark solitary wave propagation in fibers. A first experiment on the demonstration of dark soliton propagation was performed in the picosecond regime at 600nm but did not provide clear-cut results because the corresponding characteristic length for soliton propagation Z_0 exceeded the attenuation length of the fiber.[3] More recently experimental observations on dark and gray solitons have been achieved in the femtosecond regime for which the soliton characteristic length (Z_0=0.3m) and the 620nm-wavelength are not compatible with applications to long distance soliton-based optical transmission systems.[4-6] In our communication we report on experimental observations of picosecond dark soliton propagation on a fiber length up to 1 km.

The experimental arrangement is depicted in Fig. 1. We started with 3.2-psec, 850-nm pulses from a mode-locked Ti:Sapphire Tsunami laser. Pulses are tailored by a spatial amplitude and phase filtering technique that provides 5.2-psec (FWHM) dark pulses on a 35-psec (FWHM) square shaped background pulse.[3] Even- and odd-symmetry dark pulses as well as odd-symmetry dark pulses interaction were investigated. We present here measurements on propagation of odd-symmetry dark pulses that correspond to the NLSE dark-soliton solution.[2]

The generated 5.2-psec odd-symmetry dark pulses are launched into a 960m long single-mode optical fiber. This length corresponds approximately to 2.5 X the length Z_0 characteristic of these pulses. Although the fiber attenuation corresponding to the working wavelength (2dB/km at 850nm) is not negligible over such a distance, our computer simulations have exhibited a soliton-like adiabatic behavior with pulse shape and amplitude close to those of the fundamental dark-soliton solution of the Nonlinear Schrodinger Equation (NLSE). At low input power we observed substantial broadening of the dark pulses due to GVD, but at powers corresponding to the first order soliton we verified a distortion-free propagation. Such a result which is in quantitative agreement with numerical predictions, constitutes a first evidence for long-distance dark soliton propagation and tends to demonstrate its possible application to optical fiber telecommunication.

Observation and control of the dark pulses were performed in both temporal and spectral domains by means of streak camera and spectrograph measurements. Due to the high sensitivity of the output pulse spectrum with respect to initial conditions (input pulse shape and amplitude) the systematic spectral analysis, which is an original aspect of our experiment, turned out to be a very efficient regulation tool.

Fig.2(a) presents the measured input pulse intensity profile. The streak camera resolution is 6.7psec and does not allow for the observation of the complete dip that corresponds to the target hyperbolic tangent shape. Also the square shape of the broader carrier pulse is not visible. However, the input pulse shape can be properly checked by means of spectral measurements. The shaped pulse spectrum is presented in Fig.2(b), it has been measured by means of a spectrograph and a photodiode array with a resolution of 0.02nm. Experimental results for this odd-symmetry dark pulse propagation are presented in Figs 3(a to f). Curve (a) is the temporal profile of the pulse at the output of the fiber at very low power (i.e.: in the linear regime). Because of GVD we observe a broadening of the dark pulse up to a factor of 2, while its spectrum remains unchanged as shown in Fig.3(b).

At an input peak power of 0.55W that corresponds to the fundamental dark soliton, the temporal dark peak narrows to its original duration, while the background pulse broadens giving rise to a triangular shape. Also, due to self-phase modulation acting on the background pulse, the spectrum broadens (the two main peaks move appart and small wings appear). This particular situation is illustrated in Figs. 3 (c) and (d).

Curves (e) and (f) show the results obtained at twice the ampitude of the fundamental dark soliton, i. e., at a peak power of approximately 2.1W at the intput of the fiber. At this power, the dark pulse would normally tend to the stable second order ESNL dark-soliton solution which means that its width would decrease by a factor of 2. On curve (e) we observe indeed a narrowing of the dip as compared to the first order soliton (curve

(c)), but due to finite background and losses, the factor of 2 is not reached. All the results presented here are in excellent quantitative agreement with our computer simulations.

In summary, we have investigated nonlinear propagation of picosecond dark pulses over 1 km single-mode fiber in the near infrared. Odd-symmetry dark pulses were shown to propagate without distortion at the power corresponding to the NLSE fundamental dark soliton. Our results constitute a first evidence of dark soliton propagation over fiber length compatible with optical telecommunication systems. Further data relating to even-symmetry dark pulses propagation and dark solitons interaction will be reported.

This work was supported by the IAP-10 program of the Belgian Government.

References

[1] A. Hasegawa and F. Tappert, Appl. Phys. Lett. 23, p.142 (1973).

[2] A. Hasegawa and F. Tappert, Appl. Phys. Lett. 23, p.171 (1973).

[3] P. Emplit, J.P. Hamaide, F. Reynaud, C. Froehly and A. Bartélémy, Opt. Commun. 62,p.374 (1987).

[4] D. Krokel, N.J. Halas, G. Giuliani, and D. Grischkowsky, Phys. Rev. Lett.60, p.29 (1988).

[5] A.M. Weiner, J.P. Heritage, R.J. Hawkins, R.N. Thurston, E.M. Kirschner, D.E. Leaird, and W.J. Tomlinson, *Phys. Rev. Lett. 61*, p.2445 (1988).

[6] R.N. Thurston and A.M. Weiner, J. Opt. Soc. Am. B8, p.471 (1991).

Figure Captions

Fig.1: Experimental set-up. The shaped pulses consist of an intensity depression separating two steps of opposite phases. Fiber: non-polarization-preserving 960-m single mode fiber, dispersion 3.49 10^{-26} sec^2/m, losses 2dB/km, effective area 28.3 μm^2, effective nonlinear index 2.66 $10^{20} m^2/W$

Fig.2: Odd-symmetry input pulse streak camera measurement (a) and spectrum (b).

Fig.3:Temporal intensity profiles and spectra of the pulses after propagation through the fiber. Measurements are given as a function of the intput pulses peak power; (a,b): P_{in}=0.04W (linear regime); (c,d): P_{in} = 0.55W; (e,f): P_{in} = 2.1W.

Fig. 1

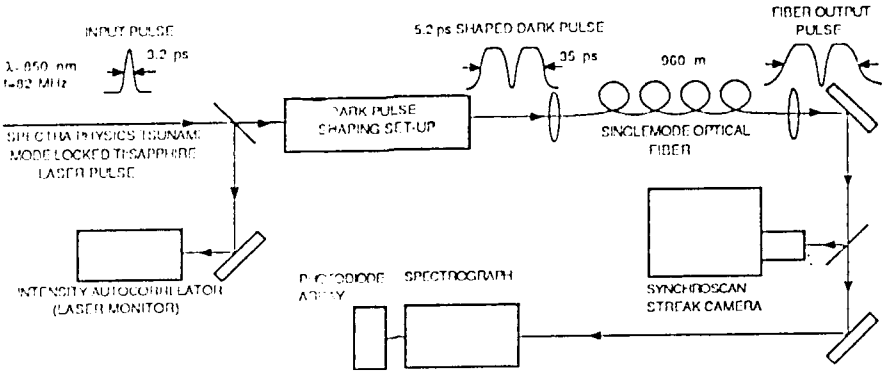
INPUT PULSE
3.2 ps
5.2 ps SHAPED DARK PULSE
35 ps
960 m
FIBER OUTPUT PULSE
DARK PULSE SHAPING SET-UP
SINGLEMODE OPTICAL FIBER
INTENSITY AUTOCORRELATOR (LASER MONITOR)
SPECTROGRAPH
SYNCHROSCAN STREAK CAMERA

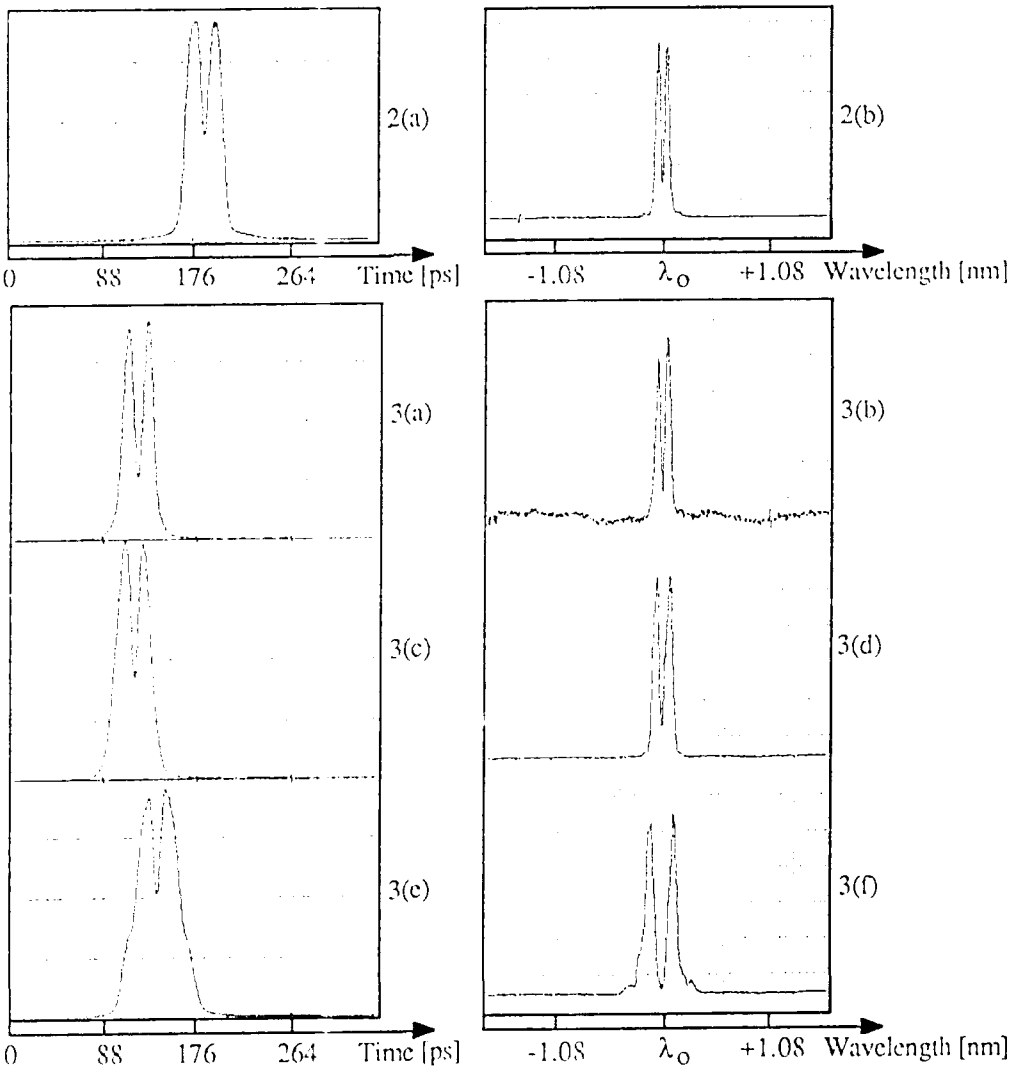
2(a)
2(b)
0
88
176
264
Time [ps]
-1.08
λ_o
+1.08
Wavelength [nm]
3(a)
3(b)
3(c)
3(d)
3(e)
3(f)
0
88
176
264
Time [ps]
-1.08
λ_o
+1.08
Wavelength [nm]

HE_{1m} self-guided modes : vector solutions and stability

J.-L. Archambault, S. Lacroix
Ecole Polytechnique de Montreal, departement de génie physique, P.O Box 6079, station A, Montréal, Qc, Canada, H3C 3A7. Ph.: (514) 340-4124 Fax: (514) 340-3218

A.W. Snyder
Optical Sciences Centre, Australian National University, GPO Box 4, Canberra ACT 2601, Australia. Ph.: (61) (6) 249 2626 Fax: (61) (6) 249 5184

Self-focusing in a medium of intensity-dependent refractive index has been extensively studied since the 60's. A particular case of self-focusing is the self-guided mode for which the natural tendency of a light beam to diffract is exactly compensated by the presence of a positive Kerr-law nonlinearity. A self-guided mode can also be seen as a mode of the waveguide it induces [1]. In this paper, we present a study of the HE_{1m} self-guided modes of circular cross-section in an ideal (homogeneous, non-saturable and without absorption) Kerr-law nonlinear medium. Although scalar theory predicts, within its domain of validity, that these modes are unstable, our exact vectorial analysis shows that they are stable to cylindrical perturbations. This result is in accordance with the recent work of Chen and Snyder who established the need of taking into account the polarization of self-guided cylindrical TE and TM modes [2].

The electrical field **E** of a wave in a uniform medium obeys the vector wave equation

$$\nabla^2\mathbf{E} - \nabla(\nabla\cdot\mathbf{E}) + k^2 (n_0^2\,\mathbf{E} + \mathbf{P}^{NL}/\varepsilon_0) = 0 \qquad (1)$$

where k and ε_0 are respectively the wavenumber and permittivity in free-space and n_0 is the linear part of the refractive-index. The nonlinear polarization, $\mathbf{P}^{NL}$, can be written in terms of the **E**-field

$$\mathbf{P}^{NL} = A\,|\mathbf{E}|^2\,\mathbf{E} + \frac{B}{2}\,\mathbf{E}^2\,\mathbf{E}^* \qquad (2)$$

where A and B are the material's Kerr coefficients [3]. By definition, the intensity profile of a circularly symmetric self-guided mode is invariant along its direction of propagation, $\hat{\mathbf{z}}$, and in the azimuthal direction, $\hat{\boldsymbol{\theta}}$. The field must therefore have a simple harmonic dependence on both cylindrical coordinates θ and z. The **E**-field of the HE_{1m} self-guided mode is thus expressed as

$$\mathbf{E}(r,\theta,z) = \{e_r(r)\,\hat{\mathbf{r}} \pm i\,e_\theta(r)\,\hat{\boldsymbol{\theta}} + i\,e_z(r)\,\hat{\mathbf{z}}\}\exp[i\,(\pm\theta+\beta z)] \qquad (3)$$

where e_r, e_θ and e_z are real functions of r only, and β is the propagation constant of the mode. In addition, e_r and e_θ are both maximum and equal in r=0 while $e_z(0)$=0. The field of Eq. 3 is primarily circularly polarized, the ± sign indicating left- or right-hand polarization. The left- and right-hand solutions are degenerate. We emphasize the fact that the primarily $\hat{\mathbf{x}}$ or $\hat{\mathbf{y}}$ polarized vector modes would not have a circularly symmetric modal intensity [1]. For the sake of simplicity, we only present results of the case where B=0 in Eq. 2. For other cases of physical interest with $B\neq0$, the results are almost identical, since $\mathbf{E}^2 << |\mathbf{E}|^2$ when **E** is primarily circularly polarized.

Using Eqs. 2 and 3, the three vectorial components of Eq. 1 reduce to three coupled, one-dimensional, differential equations in e_r, e_θ and e_z. These three equations are then solved numerically and the HE_{1m} modes are found as the discrete, bound solutions. In a given nonlinear material, there is an infinite number of solutions for each HE_{1m} mode, with one degree of freedom, e.g. spotsize, power or propagation constant. Two examples of HE_{11} field distributions are shown in Fig. 1.

HE_{11} self-guided solutions of the scalar and vector wave equations are compared in Fig. 2. In both cases, we see that there are no restrictions on the spotsize radius, σ, of the mode. The major difference is that the scalar self-guided mode is only defined for one specific power, P_S [4], while its vector counterpart can carry any power P above P_S. This result is crucial as it is responsible for the stable or unstable nature of the solution. The scalar and vector solutions coincide only in the weak-guidance limit, when $\sigma\rightarrow\infty$ and $\Delta\rightarrow 0$, where $\Delta=(n_{max}^2-n_0^2)/n_{max}^2$ is the profile height parameter and n_{max} the refractive index in $r=0$. The results obtained for the higher-order HE_{1m} solutions are very similar, except that the powers needed to excite them are higher (e.g. $P(HE_{12})\approx 6.6\ P(HE_{11})$).

We are able to describe analytically the properties of the HE_{11} self-guided mode using a first-order gaussian approximation. If a waveguide is weakly-guiding (small Δ), the vector fields of its modes can be expanded in powers of $\Delta^{1/2}$ [5]. At the zeroth order, the field of a mode is TEM and obeys the scalar wave equation. The first-order correction, in $\Delta^{1/2}$, is longitudinally polarized. Considering only these first two terms, the components of Eq. 3 become

$$e_r(r) \approx e_\phi(r) \approx \Psi(r)\ ;\ e_z(r) \approx \Psi'(r)/kn_0 \tag{4}$$

where $\Psi(r)$ is the corresponding solution of the scalar wave equation. The field distribution of the fundamental, scalar, self-guided mode is well described by a gaussian function. This gaussian field induces a waveguide with a gaussian refractive-index profile, satisfying the self-guidance condition [6]

$$V = k\,\sigma_g\,\sqrt{n_{max}^2-n_0^2} = 2 \tag{5}$$

where V is the waveguide parameter and σ_g the spotsize radius of both the mode and the waveguide. The field distribution may then be written as

$$\Psi(r) = \frac{\sqrt{2\varepsilon_0/A}}{k\,\sigma_g}\,e^{-r^2/2\sigma_g^2} \tag{6}$$

The power of the scalar, gaussian mode, given by

$$P_{s,g} = 2\pi\,n_0\,c\,\varepsilon_0\int_0^\infty \Psi^2\,r\,dr = \frac{2\pi\,n_0\,c\,\varepsilon_0}{A\,k^2} \approx 1.1\,P_S \tag{7}$$

is independent of σ_g. Its propagation constant is equal to [6]

$$\beta_g = \sqrt{k^2n_0^2 + 1/\sigma_g^2} \tag{8}$$

Using Eqs. 4, 6 and 8, we can calculate the power of the first-order gaussian field, P_g, and deduce an approximate expression for the spotsize of the HE_{11} self-guided mode as a function of power

$$\sigma_g(\hat{P}) = \frac{1}{kn_0}\sqrt{\frac{1}{\hat{P}-1}} \tag{9}$$

where $\hat{P}=P/P_S=P_g/P_{s,g}$. The results obtained from Eq. 9 are compared to the scalar and vector numerical results in Fig. 2 which shows a good agreement between the vector and first-order gaussian results.

The problem of predicting the stability of self-guided modes to perturbations can be reduced to a simple physical argumentation. A self-guided mode is a light beam of shape, spotsize and power chosen to produce an equilibrium between diffraction and self-focusing. For a light beam with more power but the same spotsize, self-focusing overcomes diffraction and the beam compresses as it propagates. Similarly, a beam with less power than the mode expands as it propagates. From these simple facts, it is possible to predict the evolution of a beam that is close to being a self-guided mode, by looking at the mode's σ vs. $\hat{P}$ diagram, as shown in Fig.3. The $\sigma(\hat{P})$ characteristic curve of the mode separates the σ-$\hat{P}$ plane in two regions. A beam in the region left of the curve has a tendency to diffract, while a beam in the right region tends to self-focus, as indicated by the arrows. Since we have assumed that the nonlinear medium has no absorption, a beam can only evolve along a vertical line on the σ-$\hat{P}$ diagram, if there is no radiation loss. Let us assume that a beam is launched with power $\hat{P}_0$ and spotsize $s_0=s(z=0)$, which is close to the self-guidance value, $\sigma(\hat{P}_0)$. Opposing arrows at power $\hat{P}_0$ indicate that $s(z)$ will oscillate around $\sigma(\hat{P}_0)$ as the beam propagates and thus that the self-guided solution is stable to cylindrical perturbations. It is then easy to see that the condition for stability is simply $\sigma'(\hat{P})<0$. The scalar result of Fig. 2 is therefore characteristic of an unstable solution, while the vector result shows stability. It is important, however, to notice that the tolerance on the power of a stable light beam is as small as the slope of $\sigma(\hat{P})$ is large. For a beam of spotsize radius larger than the wavelength, a very small loss of power would move the beam from the stable ($\hat{P}>1$) to the unstable ($\hat{P}<1$) region of the σ-$\hat{P}$ plane. In practice, only beams of extremely small spotsize could remain stable over a significant distance of propagation in the presence of absorption or other loss mechanisms.

The exact vector mode calculations lead us to believe that, contrary to what has previously been observed experimentally or predicted from the scalar theory, the circularly symmetric HE_{1m} self-guided modes of an ideal Kerr-law nonlinear medium should be stable. Moreover, the first-order gaussian approximation is sufficient to describe the essential features of the vector solution: field shapes and stability diagram. The actual observation of these modes in an absorbing medium would however require beams of very small spotsize.

References

1. A. W. Snyder, J. D. Mitchell, L. Poladian and F. Ladouceur, "Self-induced optical fibers: spatial solitary waves", Opt. Lett. **16**, 21-23 (1991).
2. Y. Chen and A. W. Snyder, "TM type self-guided beams with circular cross-section", Electron. Lett. **27**, 565-566 (1991).
3. P. D. Maker, R. W. Terhune and C. M. Savage, "Intensity dependent changes in the refractive index of liquids", Physical Review Letters, **12**, 507-509 (1964).
4. R. Y. Chiao, E. Garmire and C. H. Townes, "Self-trapping of optical beams", Physical Review Letters, **13**, 479-482 (1964).
5. A. W. Snyder and J. D. Love, *Optical waveguide theory*, chapter 32 (Chapman and Hall, London, 1983).
6. Idem, chapter 15.

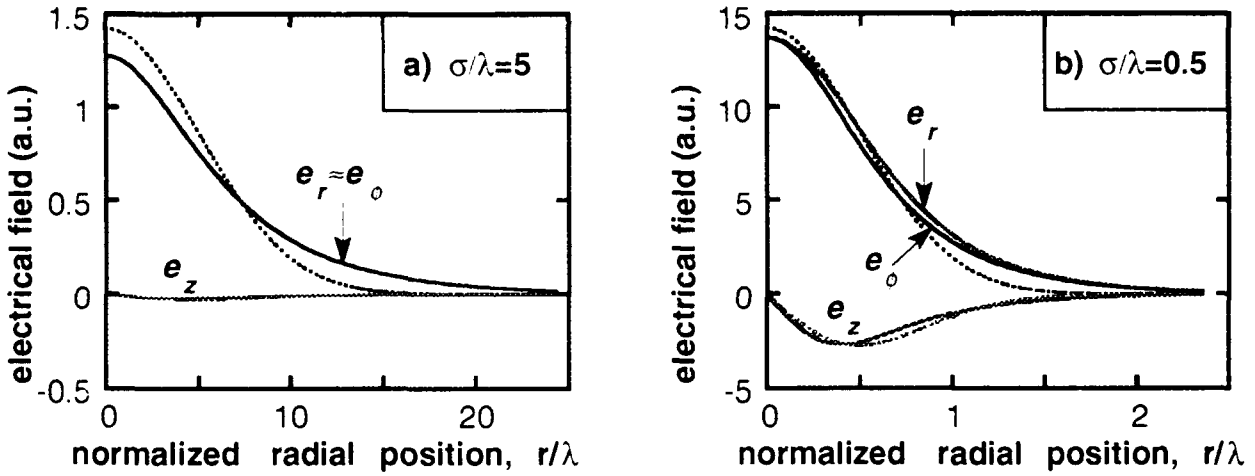

Fig. 1 Field components of HE_{11} self-guided modes are shown in solid lines. Dashed lines are first-order gaussian field components (Eq. 4). Fig. 1a) is the almost circularly polarized mode of a weakly-guiding waveguide: large spotsize, small Δ, negligible e_z and $e_r=e_\phi$. The field of Fig. 1b) is more intense in $r=0$ and induces a larger Δ; e_z is significant and e_r can be distinguished from e_ϕ. $\lambda=2\pi/kn_0$ is the wavelength in the medium.

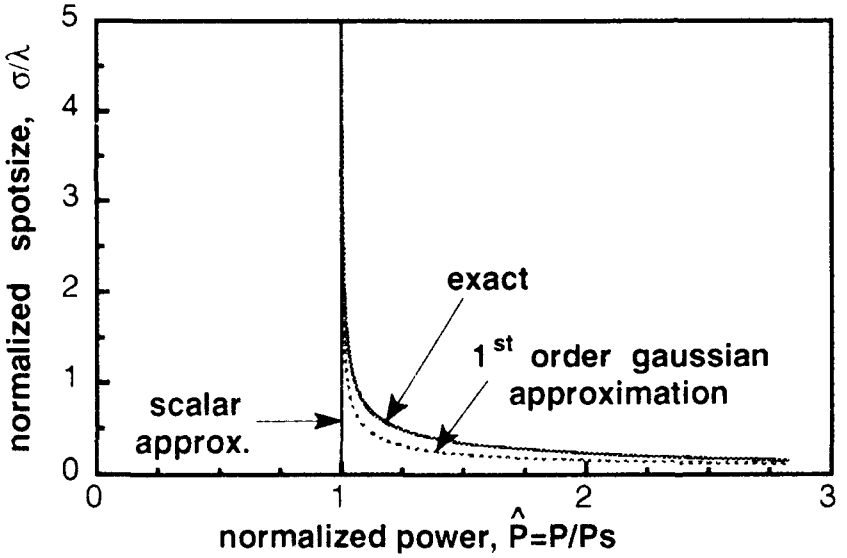

Fig. 2 Spotsize versus power for the HE_{11} self-guided mode. The scalar and and first-order gaussian (in dashed line) approximations are compared to the exact vector solution. The first-order gaussian curve is obtained from Eq. 9.

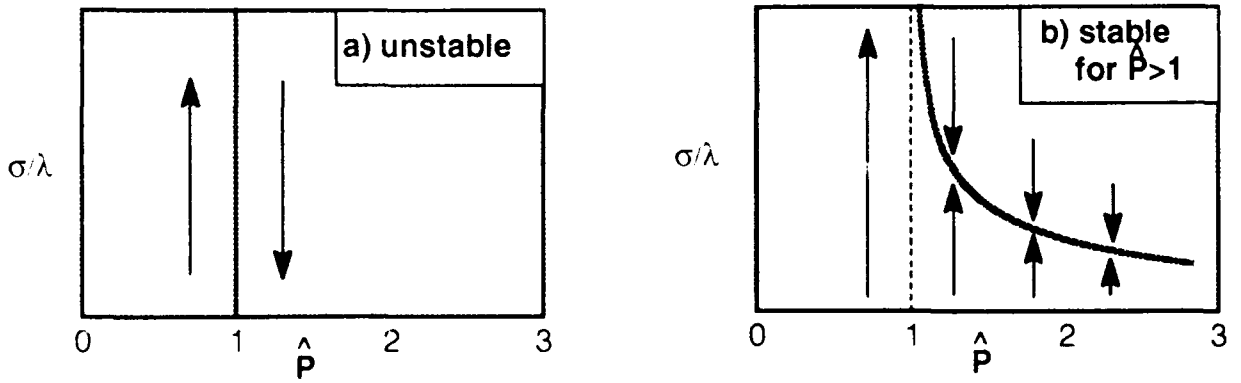

Fig. 3 Beam evolution diagrams for a) the scalar result and b) the vector result of Fig. 2.

Limitation for Transmission Capacity in Soliton - based Optical - fibre Communications due to Stimulated Brillouin Scattering.

Carlos Montes

Laboratoire de Physique de la Matière Condensée, U.R.A.- C.N.R.S. n° 190
Université de Nice-Sophia Antipolis, Parc Valrose, 06034 Nice Cedex, France
Phone : (33) 93 52 99 78 ; Fax : (33) 93 52 99 19 ; Telex : 970 281 F

and

Alexander M. Rubenchik

Institute of Automation and Electrometry, USSR Academy of Sciences,
Siberian Branch, 630090 Novosibirsk, U.S.S.R.

For long-distance data communication based on coherent optical transmission in single-mode optical fibres, the use of soliton pulses as information carriers has raised a large interest since the NLS soliton concept (solution of the nonlinear Schrödinger equation) in dispersive optical fibres by Hasegawa and Tappert [1] and its first experimental verification by Mollenauer et *al.* [2]. High bit rate transmission capacity may be achieved by this technique if the minimum distance between solitons (5 to 10 times their width) avoids the interaction between them [3]. Recent experiments have demonstrated: (i) soliton transmission over more than 4000 km in a non-shifted-dispersion single-mode fibre (hereafter called n.d.-s.f.) in which losses are periodically compensated by Raman gain [4], and over 9000 km in a dispersion-shifted fibre [5] (hereafter called d.-s.f.); (ii) generation and transmission of high-bit rate optical solitons (up to a repetition rate $f_{bit} = 20$ GHz) in dispersion-shifted fibres, losses being compensated by amplification in an Er^{3+} - doped fibre, using a color-center laser [6(a)], or a directly modulated distributed-feedback laser diode [6(b)].

However, in all these successful experiments the propagation of **rather short trains of solitons ($N_{bit} < 2$ kbit) was studied.** The soliton's width τ_0 varying as the inverse of its amplitude E_0, and the separation between solitons being necessary to avoid interaction between them, a large information rate requires correspondingly higher laser intensity. Then the question arises : for high enough optical intensity and for continuous data transfer can stimulated Brillouin scattering (SBS) distort the information transmission? We show [7] that for n.d.-s. fibers and random phase solitons the information may be perturbed above some power threshold ($P_{thr} \simeq 1$ W) at a distance $L_c \simeq 400$ km for currently high bit rates ($f_{bit} \simeq 22$ GHz). For this reason it appears interesting to use d.-s. fibers : SBS information degradation will be moved to distances $L_c > \simeq 400$ km at $f_{bit} \simeq 440$ GHz (cf. figure).

SBS is a parametric instability which is able to deeply modify and deplete the signal envelopes when the intensity of the stimulated backscattered Stokes waves attains their

level. The SBS threshold condition is proportional to the signal amplitude and width (which can be considered as the pump for SBS) and inversely proportional to the separation between pulses. Once the threshold is reached, even though the action of one pump soliton only produces extremely small Stokes and sound waves, their step by step amplification due to the interaction with the consecutive solitons prevails over their spontaneous damping. This cumulative effect for both the sound wave and the backscattered Stokes wave leads to the nonlinear SBS interaction stage where the information is perturbed. Until now this effect has been neglected for soliton-based optical-fibre communication due to its small growth rate compared to the dispersion penalty for high f_{bit} transmission capacity and also to the small optical power level P used in actual fibre-systems ($P \sim$ few mW). Even if the small number N_{bit} of solitons (digits) in trains demonstrated until now is not sufficient to stimulate Brillouin scattering up to a detectable level, it is interesting to evaluate SBS limitation for a continuous train of digits in low dissipation fibres, where losses are compensated by additional gain effects [4]-[6].

Two main situations are analysed by studying analytically and numerically the time dependent coherent three-wave equations for SBS with periodic signal pulse input [7] : (1) **coherent** case where the solitons have the same phase; and (2) **random** case where the phase of each soliton randomly changes with respect to that of the neighbouring solitons. In a n.d.-s. fiber and for a train of well separated solitons, the SBS thresholds (for 0.2 dB/km optical attenuation) range from a peak power $P_{thr} \simeq 1$ mW at $f_{bit} \simeq 0.7$ GHz for the coherent case (1) [point **A** in the figure] to $P_{thr} \simeq 860$ mW at $f_{bit} \simeq 20$ GHz for the random phase case (2) [point **B** in the figure]. For a soliton train of peak power $P = 1$ W at $f_{bit} = 22$ GHz the maximum number of bits N_{bit} transmitted without perturbation by SBS, ranges from only 50 kbit for case (1) to 45 Mbit for case (2). The corresponding critical fibre length L_c which is required for strong perturbation of the soliton profile at a continuous signal input (hereafter called *signal damage length*) is inversely proportional to f_{bit} or to f_{bit}^2 (cf. figure).

Let us summarize the analytical basis for these results. The spatio-temporal SBS dynamics is described by the coherent nonlinear 3-wave model which takes account of the sound wave inertia. The "slowly varying" amplitude envelope of the soliton acting as the pump wave E_p, the backscattered Stokes wave E_S and the acoustic wave E_a satisfy :

$$(\partial_t + \frac{c}{n}\partial_x + \gamma_p)E_p = -\gamma_0 E_S E_a \; ; \; (\partial_t - \frac{c}{n}\partial_x + \gamma_S)E_S = \gamma_0 E_p E_a^* \; ; \; (\partial_t + \gamma_a)E_a = \gamma_0 E_p E_S^*$$

where γ_p, γ_S and γ_a are respectively the damping constants for the soliton, Stokes and acoustic waves. γ_0 is the SBS coupling constant [8] given by $\gamma_0 = \left(\frac{\epsilon_0 c n_0^7}{2\rho_0 c_a}\right)^{1/2} \frac{\pi p_{12}}{\lambda}$ [$\simeq 20.8$ m s^{-1} V^{-1}, for an optical fibre of fused silica with refractive index $n_0 = 1.44$, an elasto-optic coefficient $p_{12} = 0.286$, a sound velocity $c_a = 5.96 \times 10^3$ m s^{-1}, an unperturbed fibre density $\rho_0 = 2.21 \times 10^3$ kg m^{-3} and a pump wavelength $\lambda = 1.55$ μm]. We neglect the pump attenuation γ_p since we can assume that losses are restored by periodic repeaters (or additional gain effects) which do not interact with the scattered waves, the Stokes and acoustic damping rates being respectively $\gamma_S = 4.7 \times 10^3$sec^{-1} and $\gamma_a = 5 \times 10^7$sec^{-1}. In order to obtain the instability growth rate γ, we solve the eigenvalue problem for periodic step pump functions formed by narrow square pulses of amplitude E_0 and width a separated

from each other by a distance $b \gg a$. For sech-like soliton pump pulses $E_p = E_0/cosh(\frac{t-t_0}{\tau_0})$ we perform numerical computation of the SBS equations. By measuring the one-soliton width τ_0, which is inversely proportional to the pump amplitude E_0, in characteristic SBS time units $\tau = (\gamma_0 E_0)^{-1}$, which are also inversely proportional to E_0, we can define a useful dimensionless soliton width a only dependent on the fibre parameters by the following mean value

$$a = \frac{1}{\tau}\int \mathrm{sech}\Big(\frac{t-t_0}{\tau_0}\Big)dt = \pi\frac{\tau_0}{\tau} = \frac{\pi}{2}\Big(\frac{\varepsilon\lambda n_0^7}{\rho_0 c_a n_2}\Big)^{1/2} p_{12}\sqrt{D},$$

where $D = |k''|(2\pi c/\lambda^2)$ is the group velocity dispersion (GVD). For D =21 psec/nm/km (n.d.-s.f.) and for the given data, the above formula yields $a \simeq 6.7 \times 10^{-4}$. [Whereas for d.-s.f. we can have D =1 psec/nm/km and $a \simeq 1.4 \times 10^{-4}$]. For the same n.d.-s.f. data and for an effective cross section $S = 25\ \mu\mathrm{m}^2$, the one-soliton peak power is given by $P[\mathrm{W}] \simeq 4.7\times 10^{-14}\big[E_0[\mathrm{V/m}]\big]^2 \simeq 5\big[\tau_0[\mathrm{ps}]\big]^{-2} \simeq 10^2\big[\tau[\mathrm{ns}]\big]^{-2}$. In order to avoid interaction between solitons we shall take the separation rate $(a+b)/a = 20/\pi$ between them. Then the bit rate f_{bit} depends on the peak power P, namely $f_{bit} = \frac{\gamma_0 E_0}{a+b} \simeq 2.24 \times 10^{10}\sqrt{P[W]}$ (for n.d.-s.f.) or $f_{bit} \simeq 10^{11}\sqrt{P[W]}$ (for d.-s.f.)

We shall obtain threshold bit rates f_{bit}^{thr}, for both cases (1) and (2), by defining $(a+b)_{thr}$ as the separation (periodicity) needed for SBS instability. Let us give simple expressions (the explicit values calculated for the n.d.-s.f. case) :

(1) **coherent** case : SBS threshold $\gamma_0 E_0 \geq \frac{a+b}{a}(\gamma_S\gamma_a)^{1/2}$ (typically $P > 1$ mW), namely $f_{bit}^{thr} = \frac{\gamma_0 E_0}{(a+b)_{thr}} = (\gamma_S\gamma_a)^{1/2}/a$ (typically $f_{bit}^{thr} \simeq 0.7$ GHz). For $\frac{\gamma_a}{\gamma_0 E_0} \ll \frac{a}{a+b}$, which needs very high pump powers $\big[P \gg 270(\frac{a+b}{a})^2\ \mathrm{mW}\big]$, the growth rate is $\gamma = \frac{a}{a+b}\gamma_0 E_0 = af_{bit}$. This yields a signal damage length $L_c[\mathrm{m}] = 10(c/n_0)/\gamma = 10\frac{c}{n_0 a f_{bit}} \simeq 140/\sqrt{P[\mathrm{W}]}$. For $\frac{\gamma_a}{\gamma_0 E_0} \gg \frac{a}{a+b}$, which is satisfied for pump powers $P \ll 270(\frac{a+b}{a})^2$ mW, the growth rate is $\gamma = (\frac{a}{a+b})^2\frac{(\gamma_0 E_0)^2}{\gamma_a} = \frac{(af_{bit})^2}{\gamma_a}$ yielding $L_c[\mathrm{km}] = 10(c/n_0)/\gamma = 10\frac{1}{(af_{bit})^2}\frac{c\gamma_a}{n_0} \simeq 466/P[\mathrm{mW}]$.

(2) **random phase** case : The computed SBS mean growth rate verifies very well a formula deduced from Lichtman *et al.* [9] for SBS gain concerning phase shift keying (PSK), namely $\gamma = \frac{a^2}{2(a+b)}\gamma_0 E_0 = \frac{a^2 f_{bit}}{2}$. This imposes a more stringent threshold $\gamma_0 E_0 \geq \frac{2(a+b)}{a^2}\gamma_S$ for well separated solitons (typically $P_{thr} > 1$ W). The threshold bit rate is also independent of the pump amplitude $f_{bit}^{thr} = \frac{\gamma_0 E_0}{(a+b)_{thr}} = \frac{2\gamma_S}{a^2} = \frac{8}{\pi^2}\frac{\rho_0 c_a n_2}{\varepsilon p_{12}^2 \lambda n_0^7}\frac{\gamma_a}{D}$ ($\sim$ 22 GHz for the given data), and fixes an upper limit for the information rate transmitted along the n.d.-s. fibre. The signal damage length is $L_c[\mathrm{km}] = 10(c/n_0)/\gamma = 20\frac{c}{a^2 f_{bit} n_0}$ ($\simeq 400/\sqrt{P[\mathrm{W}]}$ for n.d.-s.f. and $\simeq 8 \times 10^3/\sqrt{P[\mathrm{W}]}$ for d.-s.f.).

The figure shows in log-log scales the minimal signal damage length L_c due to SBS for different bit rates, for both coherent and random cases, and in the last case for n.d.-s.- and d.-s. fibres. To each bit rate f_{bit}, and for the choosed separation between solitons, the soliton peak power is written in the right y-axis for n.d.-s.fibres. Points **A** and **B** determine respectively for the coherent and the random cases the threshold bit rates, under which there is no signal damage even for very long fibres. Since **no** SBS has been observed until now in optical transmission experiments, we shall conclude that conditions in these experiments are closer to the random case, where much more higher bit-rates and peak

powers are required. Because $a \propto \sqrt{D}$ and $L_c \propto (a^2 f_{bit})^{-1}$, the situation is much more comfortable with respect to SBS degradation for d.-s. fibers, as can be seen on the graph: upper right line. Note that for this d.-s. fiber (D = 1 psec/nm/km) the peak power corresponding to the bit rate f_{bit} is divided by a factor 21 (as is shown on the right y-axis scale).

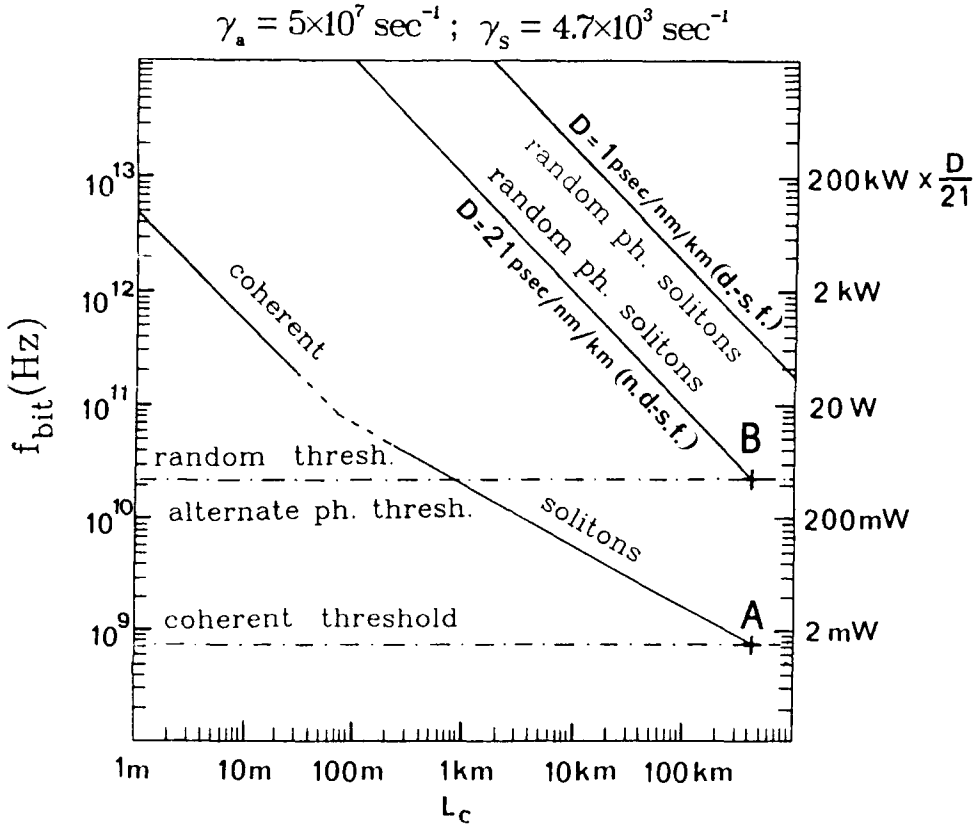

[1] A. Hasegawa and F. Tappert, Appl. Phys. Lett. **23**, 142 (1973).

[2] L.F. Mollenauer, R.H. Stolen, and J.P. Gordon, Phys. Rev. Lett. **45**, 1095 (1980).

[3] A. Hasegawa and Y. Kodama, Proc. IEEE **69**,1145 (1981).

[4] L.F. Mollenauer and K. Smith, Opt. Lett. **13**, 675 (1988).

[5] S. Evangelides, L.F. Mollenauer, and M. Neubelt, COST 217 International Workshop: Nonlinear effects in fibers, Mons (Belgium), Oct. 23-24 (1990).

[6] M. Nakazawa, K. Suzuki, and Y. Kimura, Opt.Lett. (a) **14**, 1065(1989); (b) **15**, 588(1990).

[7] (a) C. Montes, O. Legrand, A.M. Rubenchik, and I.V. Relke, in *Nonlinear World*, World Scientific, p. 1250 (1990); (b) C. Montes and A.M. Rubenchik, IEEE Colloquium "Non-linear effects in fibre communications", Savoy Place, London (U.K.), 20 Nov. 1990.

[8] D. Cotter, J. Opt. Commun. **4**, 10 (1983).

[9] F. Lichtman, R.G. Waarts, and A.A. Friesem, IEEE J. Lightwave Techn. **7**, 171 (1989).

Tuesday, September 3, 1991

Poster Session: 4

TuE 5:30pm–7:00pm
Dirac Room

Nonlinearity Enhancement in a Four Layer GaAs/GaAlAs Waveguide

Shaomei Chen, Chaengjun Liao, Huaichen Jin
and Zhaohong Huang

Institute of Quantum Electronics
South China Normal University
Guangzhou,510631, Tele.(020)516911-2540
The People's Republic of China

The photorefractive effect in semiconductor materials is attractive for processing low intensity near-infrared optical signals which are important for optical communication and optical computing. Photoinduced large nonlinearity in GaAs materials has been extensively studied in bulk material. A few is desl with optical waveguide of GaAs materials though the signal amplification in GaAs waveguide via two wavemixing has been proposed.

The large photorefractive in bulk GaAs materials is due to photo-induced gratings. The large electro-optical coefficient of the GaAs is responsible for the photo-induced gratings. The electric field between the fixed positively charged center and the diffussion electrons causes large birefrigence.The fixed positively charged centers are from the ionization of the native defect EL_2.These deep level defects are at about 0.8eV below the conduction band.Light of 1.06μm can excite and ionize EL_2 to offer fixed positive charged centers and free electrons. The free electrons has a distribution according to the distribution of the light intensity.

The number of the free electrons from photo-ionized deep level defects is much larger in the bright area than in the dark area. The free electrons begin to diffuse from bright area to the dark area. A electric field between the diffused electrons and the fixed positive charged centers was built up that the index grating due to electro-optical kerr effect is formed if two beams interfere each other in the material. We proposed here there is also nonlinearity enhancement in optical waveguide even if there is no grating formed in the waveguide.

The four layer GaAs/GaAlAs wave guide we analyzed is shown in Fig.1. The waveguide is designed for single guided mode at wavelength of 1.06μm. It is charaterized with twinlayer core layer. A barrier of 0.035 eV is formed at the interface in the twin-layer core of the $Ga_{0.75}Al_{0.25}As/GaAs/Ga_{0.97}Al_{0.03}As/Ga_{0.75}Al_{0.25}As$ to facilitate the free electron diffusion to one side of the waveguide. This directional diffusion creates an electric field at a fixed direction to optimize the photo-induced refractive index change. If the incident light is at wavelength of 1.5μm, then the ionization of the deep level defects is only in the GaAs layer. The suitable deep level dopants can also be chosen to meet this needs. The direction of the inner

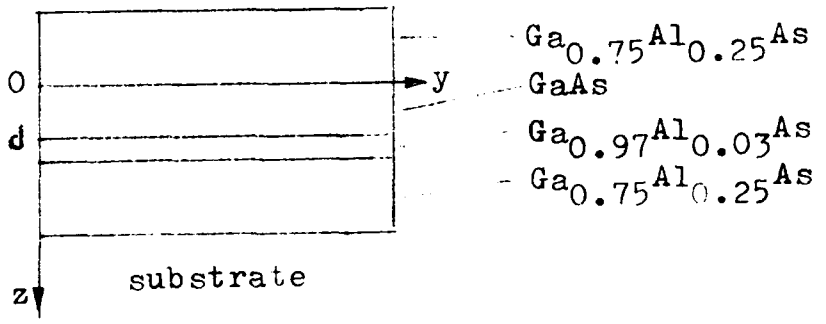

Fig.1 Four layer optical waveguide with twinlayer core layer.

built electric field is in the direction (100).

The barrier is at the position near the peak intensity of the fundamental guided mode where only one peak intensity can exist in the waveguide. We choose the thickness of the GaAs layer to set the interface at the position where the intensity of the guided wave has fallen down to 80% of the peak intensity of the guided power in the waveguide. The most of the free electrons will produced in the GaAs layer and will diffuse to the boundary of GaAs/$Ga_{0.75}Al_{0.25}As$. The photo-induced electric field can be calculated

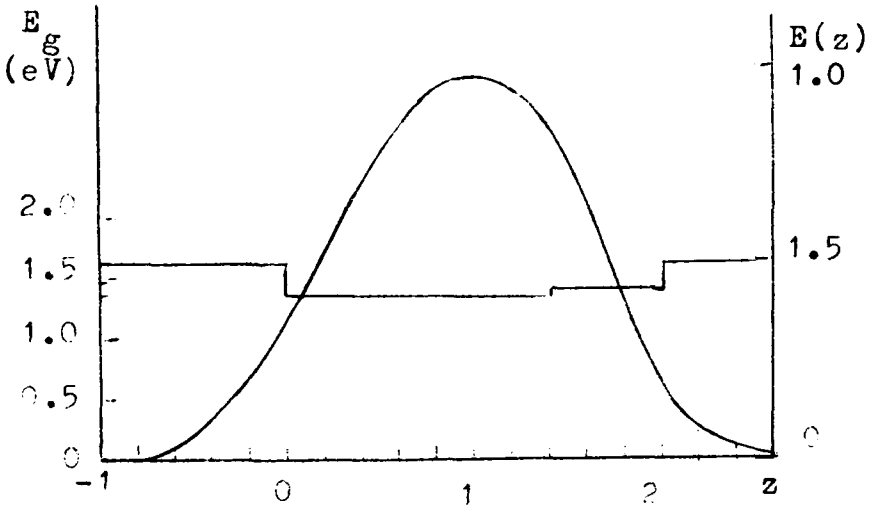

Fig.2 The band diagram and the intensity distribution of the guided TE_0 mode in the four layer waveguide.

$$E_{in}=(NeL/\varepsilon\varepsilon_0)\left[kL/(1+k^2L^2)\right]$$

where L is $d/2\pi$. N is the free electron density produced by photo-ionization. The power density in waveguide can be much larger that in the bulk. Two photon absorption will dominate the process and offer more free electrons. We expected that less power will be needed to build up a inner built electric field as strong as that in the bulk material.

The four layer waveguide may grow by liquid phase epitaxy technique. A mini-prism may be integrated with the waveguide in a single pass liquid phase epitaxy technique

such as we indicated in the other paper we contributed to the topical meeting.

We believe that the photo-induced nonlinearity enhanced by the twin-layer core waveguide structure will find variety of practical uses of nonlinear quided wave devices.

References

1. H. Rajbenback, B. Imbert, J.P. Huignard and S. Mallick, Opt. Lett. 14,1(1989)78;
2. M.B. Klein. Opt. Lett., 9,8(1984)350;
3. Jefferson Strait and A.M. Glass. Applied Optics 25,3 (1986)338.

Large Non-Resonant Nonlinearities in DANS Based Polymer Waveguides: Role of Microscopic Cascading

Gaetano Assanto, George I. Stegeman
Center for Research in Electro-Optics and Lasers, University of Central Florida, 12424 Research Parkway, Orlando, FL 32826 (USA), Tel. (001-407)658-6800

Manuel B. Marques
Centro de Fisica da Universidade do Porto (INIC), 4000 Porto (Portugal).

William E. Torruellas
Raytheon Research Division, 131 Spring Street, Lexington, Massachussetts 02173 (USA)

Winfried H.G. Horsthuis, Guus R. Möhlmann and E.W.P. Erdhuisen
AKZO Research Laboratories, Arnhem, Corporate Research, Applied Physics Department, P.O. Box 9300, 6800 SB Arnhem, The Netherlands

Polymers can exhibit both large and fast nonresonant third-order nonlinearities which rely on π-electron delocalization and conjugation, as well as good physical and chemical properties suitable for the fabrication of nonlinear integrated optics devices. Soluble polymers with strong charge transfer states such asymmetrically suostituted 4-dialkylamino-4'-nitro-stilbene (DANS) and 4-dialkylamino-4'-nitro-diphenylbutadiene (DAN2) side-groups were originally developed for electro-optic applications because of their large second order nonlinearities and low propagation losses in waveguide form.[1] Using nonlinear grating coupling we found a large value for n_2, the Kerr coefficient. Measurements and analysis of the spectral dispersion of third harmonic generation indicate that the dominant contribution to the nonlinearity is due to the local cascading of second order nonlinearities.[2]

There are two possible contributions to the third order nonlinearity in materials containing non-centrosymmetric molecules, namely the direct third order electronic nonlinearity, and also a term due to the cascading of two second order nonlinearities.[2] This second term occurs when a local (at an individual molecule) field at the second harmonic due to $\chi^{(2)}(2\omega;\omega,\omega)E(\omega)^2$ mixes with the fundamental field via

$\chi^{(2)}(\omega,2\omega,-\omega)E(2\omega)E^*(\omega)$ to produce a field at ω. This leads to an index change proportional to $\chi^{(2)}(\omega;2\omega,-\omega)\chi^{(2)}(2\omega;\omega,\omega)|E(\omega)|^2E(\omega)$. The contribution to n_2 scales quadratically with the magnitude of the second order susceptibility, hence the name "cascading nonlinearity". Note that since the mechanism is operative at a molecular level,[2] this nonlinearity still occurs with randomly oriented molecules for which there is no net second order susceptibility.

Thin polymer films were spin-coated from a 0.2μm filtered cyclopentanone solution onto fused-silica substrates with two ion-milled gratings of periodicity Λ=0.6 μm and 1cm apart. After spinning, the samples were cured in air at 140^{0}C for about 1 hour. The guiding properties of the films (i.e. propagation losses and effective indices) were characterized at low powers. Indices at 1.064μm were $\cong$1.62 for DANS and 1.64 for DAN2.

First n_2 and the two photon coefficient (TPA) β were measured at 1.06 μm using nonlinear distributed coupling, a technique which has been used successfully for evaluating nonlinearities in slab waveguides.[3,4] Since a nonlinear change in index due to n_2 modifies the effective index of a guided mode, increasing the incident power changes both the coupling efficiency and optimum coupling angle for grating coupling to waveguides.[3] Note that the shift of the angular resonance is substantially independent of absorptive nonlinearities (such as two-photon absorption) which, instead, affect the waveguide throughput. As a result the two photon coefficient can also be measured. We used a Q-switched mode-locked Nd-YAG laser generating 30ps pulses at 1.064 μm at 10 Hz, and monitored both the light coupled out from the second grating after propagation, and the light transmitted through the sample at the input. Figure 1 shows some typical data collected via the output grating of a DANS waveguide with the input coupler set at the optimum low-power incidence angle. The linear input coupling efficiencies η ranged between 10 and 17% in all the samples. Next, we measured η vs coupling angle, at fixed excitation energies. In Fig. 2 we show typical results of experiments performed on DANS. The coupling dip shifts towards smaller (negative) angles, with $\Delta\theta$>0, indicating a positive n_2. The measured shifts were $\Delta\theta\cong+0.015^0$ for DANS and $\cong+0.040^0$ for DAN2, when the pulse energy was increased from 5 μJ to 350 or 500 μJ, respectively. The analysis yielded n_2 and TPA values of $+7\pm1\times10^{-8}$ cm^2/MW and 0.-2 cm/GW for DANS, and $n_2\cong+1.9\pm0.1\times10^{-7}$ cm^2/MW and $\alpha_2\cong$0-2 cm/GW for DAN2. Note that the largest Kerr coefficient, $+2\cdot10^{-7}$ cm^2/MW, is comparable to reported values for waveguides in PMMA-MNA[5] and poly-4BCMU.[6] The small TPA coefficients show little two-photon

enhancement of n_2 and the large uncertainties in β indicate that this technique is not suited for measuring it accurately.

The origin of the nonlinearity was investigated by tunable third-harmonic-generation in a Maker-fringe arrangement.[7] Fig.3 shows the dispersion in the magnitude of $\chi^{(3)}(3\omega;\omega,\omega,\omega)$ for a 0.1μm thick DANS film, as well as theoretical calculations based on a two-level model for the nonlinearity. Although none of the detailed fits to the spectral dispersion of the data are acceptable, inclusion of the cascading term (solid line) improves the fit to the peak magnitude by a factor of two relative to the no-cascading case (dotted line). These results indicate that second order local cascading dominates the third order nonlinearity in these materials and that the resulting non-resonant third order nonlinearities are large.

References

1. G.R. Möhlmann and 12 co-authors, SPIE Proc. V.1147, 245 (1989).
2. G.R. Meredith, Chem.Phys.Lett. **92**, 165 (1982).
3. G. Assanto, M.B. Marques, and G.I. Stegeman, J.Opt.Soc.Am. B **8**, 553 (1991).
4. R. Burzynski, B.P. Singh, P. Prasad, R. Zanoni and G.I. Stegeman, Appl. Phys. Lett., **53**, 2011 (1988).
5. M.J. Goodwin, C. Edge, C. Trundle, and I. Bennion, J.Opt.Soc.Am. B 5, 419 (1988).
6. P.D. Townsend, G.L. Baker, N.E. Schlotter, C.F. Klausner, and S. Etemad, Appl.Phys.Lett. **53**, 1782 (1988).
7. W.E. Torruellas, R. Zanoni, G.I. Stegeman, G.R. Möhlmann, E.W.P. Erdhuisen, and W.H.G. Horstuis, J. Chem. Phys., **94**, 6851 (1991).

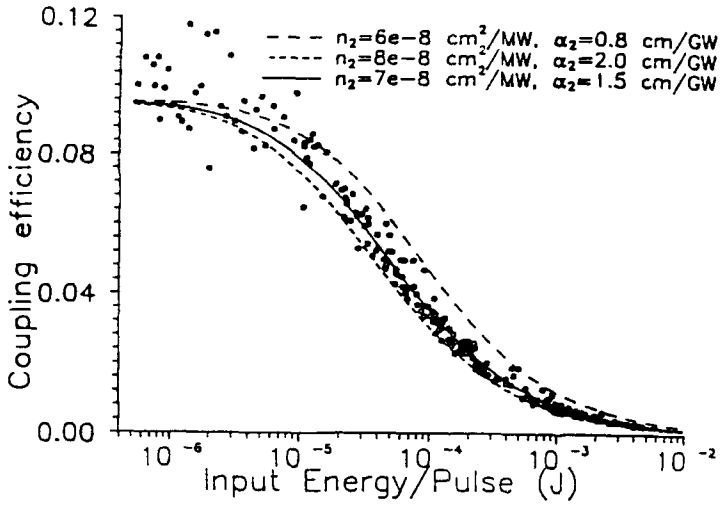

Figure 1

Throughput efficiency versus input pulse energies for a DANS sample. The circles are experimental data points, and the curves are numerical calculations.

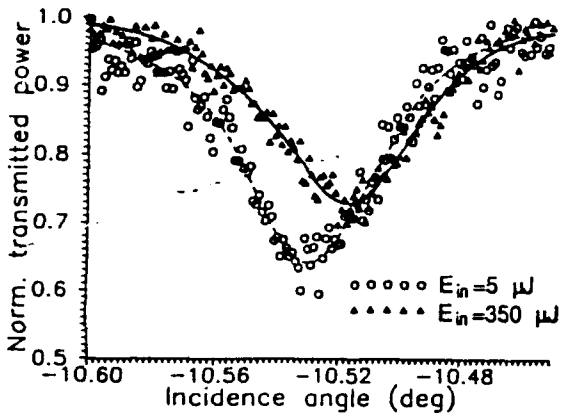

Figure 2

Normalized transmitted power through the input grating versus incidence angle for a DANS waveguide at low (5μJ, circles) and high (350μJ, triangles) input energies. The lines are a guide to the eye. The angular shift is ≅ +0.015°.

Figure 3

Spectral dispersion of $\chi^{(3)}(3\omega;\omega,\omega,\omega)$ for a DANS sample. The solid and dotted line fits were obtained with and without the second-order cascading term respectively.

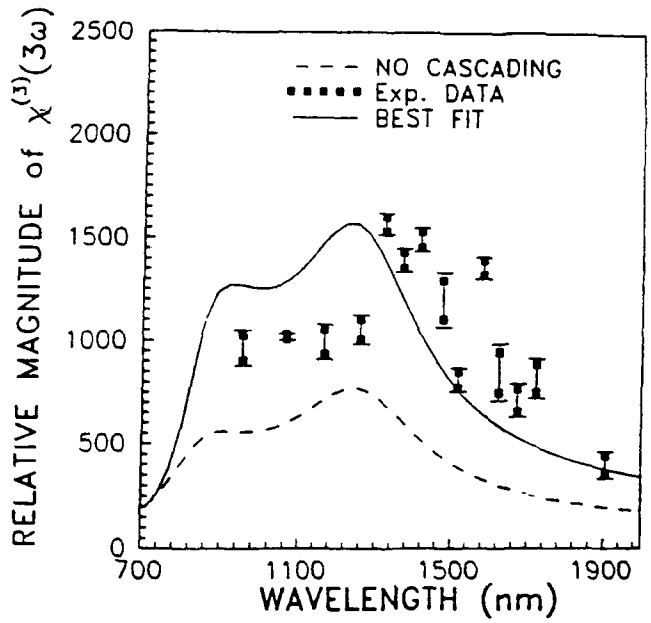

Characteristics of Annealed Proton Exchanged Waveguides for Quasi-Phase-Matched Frequency Conversion in Periodically-Poled $LiNbO_3$ Waveguides

M. M. Fejer, M. L. Bortz, and E. J. Lim
Stanford University

Ginzton Laboratory
Stanford University
Stanford, CA 94305
(415) 725-2160

Nonlinear frequency conversion in waveguides has been investigated since the first days of integrated optics, but practical applications were hampered by a lack of suitable pump lasers and the often inconvenient phase-matching characteristics of the available waveguides. Recent developments in high power (> 100 mW) single-mode diode lasers and quasi-phase-matching techniques have led to renewed interest in waveguide frequency conversion. Periodic modulation of the optical properties of a nonlinear medium, quasi-phase-matching, is an attractive technique as it decouples phase-matching from birefringence and thus allows any interaction within the transparency range of the medium using any component of the nonlinear susceptibility tensor. The most efficient form of quasi-phase-matching involves periodic reversal of the sign of the nonlinear susceptibility ($\chi^{(2)}$) of the medium, with a period equal to an odd multiple of the coherence length of the interaction. In ferroelectrics, such a *periodic sign reversal* in $\chi^{(2)}$ can be accomplished by periodic reversals in the orientation of the spontaneous polarization. Periodic incorporation of dopants has been found to induce domain reversal in several ferroelectrics, e.g. Ti or Li in $LiNbO_3$, H in $LiTaO_3$, and Rb and Ba in KTP, leading to rapid progress in device demonstrations in these material systems. [1 – 5] Several milliwatts of blue light generated by quasi-phase-matched (QPM) frequency doubling have been demonstrated in $LiNbO_3$[3],[6], KTP [4], and $LiTaO_3$ waveguides [5], as has QPM difference frequency generation of 2.1 μm radiation in $LiNbO_3$ waveguides. [7]

The efficiency of waveguide frequency conversion devices depends on the magnitude of the nonlinear coefficient of the medium, the refractive index profile of the waveguide, the dispersion of this profile, and, for QPM interactions, the form of the modulation of the nonlinear susceptibilities. In this paper, we present measurements and modeling of these quantities in annealed proton-exchanged (APE) waveguides in $LiNbO_3$ substrates with domain reversals created by in-diffusion of patterned Ti films, and the implication of the results for the conversion efficiencies of visible and infrared nonlinear devices.

Most of the QPM devices in $LiNbO_3$ and $LiTaO_3$ use APE waveguides, which are attractive for nonlinear optical applications because they, unlike Ti-indiffused waveguides, are more resistant to photorefractive damage than bulk $LiNbO_3$. These waveguides guide only extraordinary-polarized modes and thus are inappropriate for birefringently phase-matched interactions. However, APE waveguides are well suited to QPM interactions, which generally use only extraordinary modes in order to take advantage of the large d_{33} coefficient of $LiNbO_3$. An additional advantage of APE is the low process temperatures, typically below 400°C, which minimizes interactions between the domain patterning and the waveguide fabrication.

The basic fabrication process for these devices [1] consists of first creating a substrate with periodically reversed domains by patterning a Ti grating on the $+z$ face of a $LiNbO_3$ substrate, indiffusing the film at a temperature (1100°C) close to but below the Curie temperature, and cooling the substrate to room temperature. Domain reversal with the same periodicity as the grating

occurs in the doped regions, with a cross-section that is typically triangular and penetrates to a depth somewhat smaller than the period of the grating (Fig. 1) For ease of fabrication, domains three coherence lengths long (third order quasi-phase-matching) are typically used. Channel waveguides are formed in this substrate with an Al mask by proton exchange in benzoic acid, followed by removal of the mask and annealing at 333°C to drive in the protons and lower the maximum concentration.

It is useful to describe the efficiency of waveguide frequency doublers according to

$$P_{2\omega}/P_{\omega} = \eta P_{\omega} L_{eff}^2 \quad , \tag{1}$$

where $P_{2\omega}$ and P_{ω} are the powers at the second harmonic and the fundamental, and η [%/W-cm^2] is a normalized conversion efficiency accounting for the mode overlap and the nonlinear susceptibility. The effective length of the device, L_{eff}, is the length over which phasematching is maintained. Typical results for third order QPM channel waveguide devices for SHG of 410 nm radiation show $\eta \approx 40-60\,\%/\mathrm{W-cm^2}$, substantially smaller than the theoretically predicted efficiency ≈ 300 %/W-cm^2.

The normalized conversion efficiency of QPM waveguide devices depends on the overlap of the modal fields with the periodic modulations of the nonlinear coefficient. As the duty-cycle of the inverted domains is depth dependent, the overlap calculation is often sensitive to small errors in the modal fields and the domain shapes. For the purposes of optimizing this overlap, a model for the dependence of the waveguide parameters on the processing conditions is essential. Several characteristics of the APE process render such modeling difficult. Both the index of refraction and the diffusion coefficient of protons in $LiNbO_3$ are nonlinear functions of the proton concentration. The concentration-dependent reduction in the nonlinear susceptibility in proton exchanged (PE) $LiNbO_3$ further complicates the modeling.

Recent reports suggest that the nonlinear susceptibility is reduced by approximately 50% in PE waveguides, and recovers gradually with annealing. [8]–[10] These results suggest that it should be possible to create large index difference ($\Delta n \approx 0.12$) shallow waveguides with tight mode confinement and good overlap with the shallow domains characteristic of first order gratings, and thus produce very efficient devices. Our efforts to build devices using PE waveguides were unsuccessful, with no visible second harmonic produced even with kilowatts of 1.06 μm radiation launched into the as-exchanged waveguide from a Q-switched Nd:YAG laser. We were thus led to investigate the effect of proton exchange on the nonlinear susceptibilities in a simpler, non-waveguide geometry. The difficulty in this measurement is to eliminate the contribution to the second harmonic generation of the $LiNbO_3$ substrate, which could be large compared to that of the thin film of PE material. This was accomplished by focussing 532 nm radiation on the surface of an x-cut crystal and observing the backward propagating 266 nm second harmonic radiation. This backward wave is generated in a layer within a wavelength of the air/$LiNbO_3$ interface; the short absorption length of the 266 nm radiation eliminates any signal generated at the interface between the proton-exchanged layer and the substrate. The backward second harmonic produced in crystals with a PE layer was 10^{-4} that from untreated substrates, suggesting that the nonlinear susceptibility of the PE layer is very small. This observation is consistent with our device results, but contradicts the conclusions of the earlier studies. The results of Ref. [10] for surface SHG with a 1.06 μm fundamental may be reconciled with ours if the contribution of the PE/substrate interface is incorporated into their analysis. The source of the discrepancy with Refs. [8] and [9] is not clear, but may have to do with the rather complicated deconvolution of the linear and nonlinear effects necessary for their analysis. We are currently extending our study to include the recovery of the nonlinear coefficient with annealing.

For modeling the waveguide fabrication process, the dependence of the diffusion coefficients and the refractive index change on the proton concentration are needed. Planar waveguides were exchanged to various depths (d_e) in pure benzoic acid, and annealed at 333°C for times (t_a). Using prism coupling and IWKB analysis, we determined the refractive index profiles as a function of the processing conditions. The $1/e$ depths (d_a) and the surface index change (Δn_a) of the annealed

waveguides are plotted in normalized form *vs* a normalized process parameter $\tau \equiv t_a/d_e^2$. For long τ the depth increased as $\sqrt{\tau}$, as would be expected for linear diffusion with $D_0 = 0.55\ \mu m^2/hr$. For short times, the diffusion is highly nonlinear, but can be accurately predicted with a concentration dependent diffusion coefficient given by

$$D(C) = D_0[a + (1-a)\exp(-bC)] \tag{2}$$

where the best fit is obtained with $a = 0.1$ and b = 12. The results obtained by numerical solution of the diffusion equation with this diffusion coefficient and initial step profile characteristic of the exchange process are shown in Fig. 2. These results are extracted under the assumption that the change in the refractive index is proportional to the proton concentration at least up to 70% of the surface concentration after exchange, a conclusion that is supported by the constant area under the refractive index profile with annealing over this range of concentrations, and by the success of the model in predicting the modal properties over a broad range of processing conditions. We are currently extending this work to *x*-cut substrates, in order to obtain the other independent diffusion coefficient for modelling channel waveguide fabrication. By repeating the measurements at several wavelengths the plot of the dispersion in Δn_a shown in Fig. 3 was obtained.

A final issue that arises in understanding the effect of APE on the efficiency of QPM devices is the changes that the APE process induces in the domain structure. As the processing is at temperatures 700 K below the Curie temperature, we expected that such effects would be negligible. However, recent studies have shown that domains change after APE from their initial triangular form to a more circular form similar to that observed in $LiTaO_3$ crystals (Fig. 1). The mechanism for this modification, and the dependence of the effect on process conditions, is not yet clear.

With the results for the dependence of the diffusion coefficients, the refractive indices, the nonlinear susceptibility and the domain structure on proton concentration, and the dispersion of the index, it will be possible to accurately model the performance of QPM frequency conversion devices in APE $LiNbO_3$ waveguides. Results for the recovery of the nonlinear susceptibility with annealing and measurements of the diffusion coefficient in the *x*-direction will be reported, as will be optimized designs based on these data. We expect to observe substantial increases in the conversion efficiency in these optimized devices.

REFERENCES

[1]. E. J. Lim, M. M. Fejer, R. L. Byer, and W. J. Kozlovsky, *Electron. Lett.* **25**, 731-732 (1989).

[2]. J. Webom, F. Laurell, and G. Arvisdsson, *IEEE Photon. Technol. Lett.* **1**, 316 (1991)

[3]. N. Nada, O. Kawakubo, and K. Watanabe, paper CTuV7, CLEO '91, Baltimore, May 1991.

[4]. C. J. van der Poel, J. D. Bierlein, and J. B. Brown, *Appl. Phys, Lett.*, **57**, 2074 (1990).

[5]. K. Yamamoto, K. Mizuuchi, T, Taniuchi, paper CPDP23, CLEO '91, Baltimore, May 1991.

[6]. E. J. Lim, M. L. Bortz, and M. M. Fejer, paper PD-11 Integrated Photonics Research, Monterey, April 1991.

[7]. E. J. Lim, M. M. Fejer, and H. M. Hertz, paper CTuV2, CLEO '91, Baltimore, May 1991.

[8]. T. Suhara, H. Tazaki, and H. Nishihara, *Electron. Lett.* **25**, 1326 (1990).

[9]. R. W. Keys, A. Loni, and R. M. de la Rue, *Electron. Lett.* **26**, 624 (1990).

[10]. X. Cao, R. Srivastava, R. V. Ramaswamy, and J. Natour, *IEEE Photon. Technol. Lett.* **3**, 25 (1991).

[11]. M. L. Bortz, E. J. Lim, and M. M. Fejer, submitted to *Opt. Lett.*

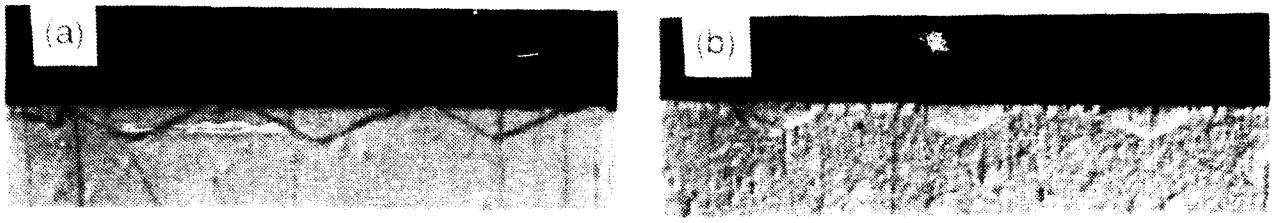

Fig.1. Inverted ferroelectric domains revealed by etching the polished y -face of z-cut plates. (a) Prior to proton exchange. (b) after annealed proton exchange process. Note change from triangular to semi-circular shape.

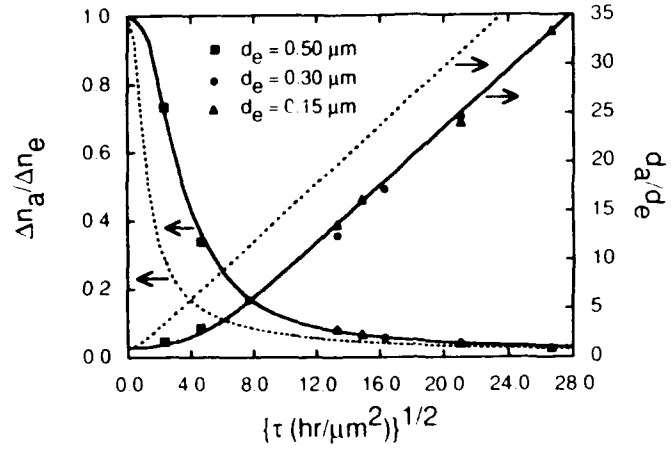

Fig. 2. Waveguide depth after annealing, d_a, normalized to the exchange depth, d_e, and surface refractive index change after annealing, Δn_a, normalized to surface index change of the PE waveguide, Δn_e, plotted *vs* square root of anneal time, t_a, normalized according to $\tau \equiv t_a/d_e^2$. Dashed lines calculated with asymptotic linear diffusion coefficient, $D_0 = 0.55$ μm^2/hr. Solid lines calculated with nonlinear diffusion coefficient given in the text.

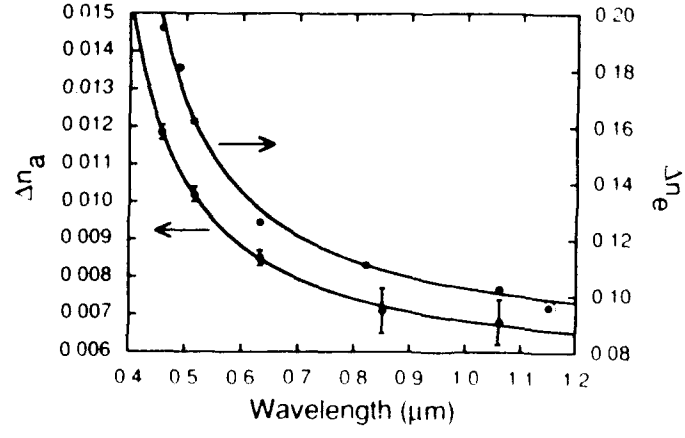

Fig. 3. Dispersion of the surface refractive index change in proton-exchanged and annealed proton-exchanged waveguides.

Flowing Afterglow Synthesis of Polythiophene Films

Peter Haaland and James Targove

Air Force Institute of Technology, Wright Patterson AFB, OHIO, *USA*

1 Introduction

Polymers of aromatic heterocycles such as thiophene and pyrrole have been actively investigated for their promising electrical and optical characteristics. However the use of these materials in waveguide structures has been constrained by morphological and synthetic barriers. Specifically, larger oligomers are less soluble causing multiphase chemical kinetics and irregular morphology in the metal-catalyzed coupling syntheses.[1] Electrochemical preparation methods also produce grainy or fibrillar material, most probably because the heterogeneous boundary conditions on film growth change as insulating or semi-conducting material is deposited on the electrodes. [2] We report here a synthetic approach to the polymeric heterocycle polythiophene using electronically excited argon metastables to activate organic precursors. This method is seen to produce dense, uniform films with desirable thiophene linkages and excellent optical properties.

Polythiophene films have been studied extensively as third-order nonlinear materials. Third harmonic generation measurements of magnitude and phase in the 950–1904 nm range have shown that polythiophenes have a $\chi^{(3)}$ which is comparable to that of polyacetylenes [3, 4] while degenerate four-wave mixing at 602 nm has demonstrated sub-picosecond response times [5]. However, optical measurements have primarily been performed on alkylated polythiophenes which are more soluble and thus more easily cast into uniform films.

Plasma Assisted Chemical Vapor Deposition (PACVD) has also been used to generate polythiophene films. [6] This technique injects thiophene directly into an electrical discharge. Since the time scales for chemical reaction and diffusion in these reactors are short compared to the gas residence time a lot of parasitic chemistry can occur. The resulting films therefore typically contain a nonaromatic hydrocarbon component which would inhibit conjugation length and therefore $\chi^{(3)}$.

2 Film Deposition

The vapor pressure of thiophene is sufficiently high (tens of torrs at room temperature) that one can exploit gas phase kinetics to generate polymer precursors. A schematic drawing of our reactor is shown in figure 1. Thiophene is entrained in a flow of argon and injected downstream of a flowing plasma. The main argon flow is excited with 10-30 watts of rf power at 13.56 MHz which generates electrons, ions, radiation, and metastable argon atoms in the discharge region. The electrons and ions diffuse and recombine in microseconds. At typical

flow velocities of centimeters per second only metastables are left in the flow when the organic is introduced. This greatly reduces the ring decomposition observed in traditional PECVD. Typical deposition rates for this method are 0.25-1 $\AA s^{-1}$ for high-quality film deposition at a total system pressure of approximately 0.5 torr.

The organic precursors have ionization potentials well below the energy of the argon metastable (11.6 eV), and the profile of the deposit is changed by electrostatic boundary conditions (we observe film thickness variations on a spatial scale comparable to a Debye length). We therefore hypothesize that the mechanism of film formation involves Penning ionization of the precursor by the argon metastable. The resulting molecular ion is transported to the surface by ambipolar diffusion and deposits as film. The other species produced by the decomposition of thiophene are conveniently stable gases (acetylene, ethylene, diacetylene, and H_2S), which are exhausted with the main argon flow.

3 *Film Characteristics*

The films grown by this technique appear smooth under Nomarski microscopy for film thicknesses of several microns. Atomic force microscopy confirms this smoothness, with a measured RMS roughness of 5 $\AA$ over one μ^2 areas. This is in contrast to electrochemically grown films, which typically exhibit a fibrillar structure for thicknesses of several microns.

Large nonlinear susceptibilities require extensive π conjugation along the carbon backbone of the thiophene polymer chains. 2-5 polymerization accentuates this conjugation, while 2-4 polymerization tends to limit the extent of the conjugation. The films grown using thiophene precursor exhibit a mixture of 2-4 and 2-5 polymerization based on infrared absorption bands at both 790 and 680 cm^{-1}. Changing to a less volatile (2,5)-dichlorothiophene precursor results almost exclusively in the desirable $\alpha - \alpha'$ linkages (figure 2).

The stoichiometry of a deposited film on a beryllium substrate has been assessed using Rutherford Backscattering Spectrometry [7]. A typical film composition is $C_{4.0}S_{0.85\pm.04}Cl_{0.33\pm.03}$. From this stoichiometry one infers an average chain length of approximately five thiophene units if the chains are terminated by chlorine atoms.

The absorption coefficients of films deposited from thiophene and dichlorothiophene precursors are shown in fig 3. The latter film exhibits an absorption edge at approximately 600 nm, typical of well-conjugated polythiophene. In contrast, the bandgap of the film from thiophene precursor has shifted to about 500 nm, as expected for the $\alpha - \beta$ linkages present.

The refractive index of the films was determined by spectroscopic ellipsometry. A 300 nm thick film on glass was measured at 70 degrees angle of incidence for wavelengths between 300 and 800 nm. The $tan\Psi$ data was well fit by an isotropic film model with a dispersion relation of the form $n2 = 2.69 + 0.04\lambda^2 + 0.0062\lambda^4$ where λ is in μ.

Initial waveguide experiments were performed with a 6000 $\AA$ thick film deposited on an oxidized silicon substrate. 700 nm light from a Ti:Sapphire laser was edge coupled into the waveguide and observed to propogate over 5 cm, the length of the substrate. Waveguide loss measurements are underway.

4 Summary

We have illustrated a new gas-phase synthetic route to dense, uniform, organic polymer films using the activation of a volatile precursor by metastable argon atoms. This method should be compatible with microelectronic practices such as CVD and ion etching. The addition of organic material outside the active plasma is shown to be essential to the controlled production of optical- quality films. The $\alpha - \alpha'$ polythiophene films produced by reaction of 2,5 dichlorothiophene with Ar^* have been characterized by optical absorption, spectroscopic ellipsometry, Rutherford backscattering, infrared absorption, and atomic force microscopy. Waveguide propogation has been observed, $\chi^{(3)} \approx 10^{-11} esu$ at 602 nm on an early sample, and additional nonlinear optical measurements are in progress.

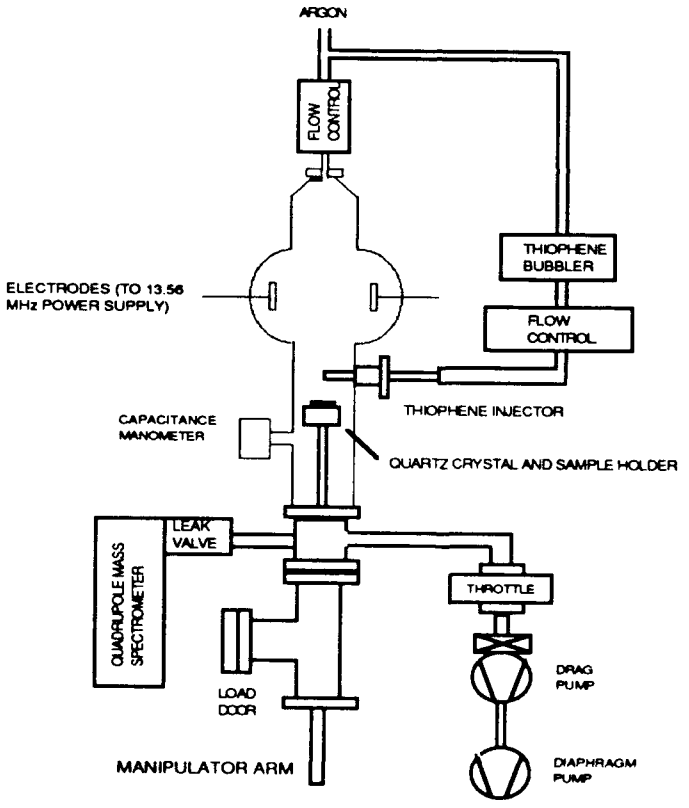

Figure 1: Schematic drawing of the flowing afterglow deposition system

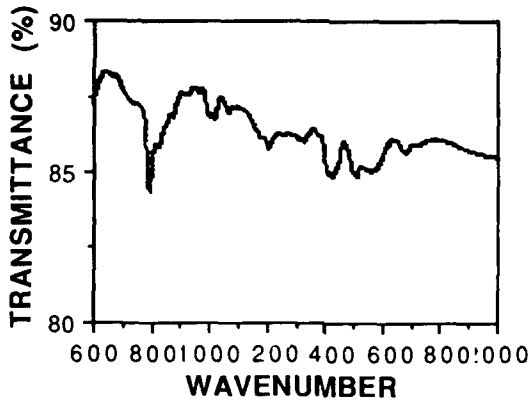

Figure 2: Infrared absorption spectra of polythiophene films using 2,5 dichlorothiophene precursor. The line at 790 cm^{-1} is characteristic of the $\alpha - \alpha'$ linkage, while absorption at 680 cm^{-1} is characteristic of an $\alpha - \beta$ linkage

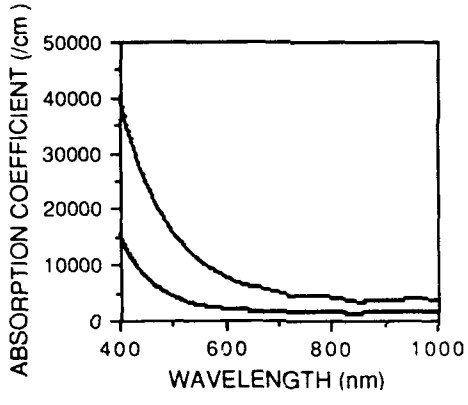

Figure 3: Absorption spectra of polythiophene films formed using thiophene and 2,5 dichlorothiophene precursors in the flowing afterglow reactor.

References

[1] T. Skotheim, *ed.*, **Handbook of Conducting Polymers, (NY:Marcel Dekker)**, chapter 9, 1986.

[2] A. Yassar, J. Roncali, and F. Garnier, *Macromolecules*, **22**, 804 [1989].

[3] R. Dorsinville, L. Yang, R. Alfano, R. Zamboni, R. Danieli, G. Ruani, and C. Taliani, *Optics Letters*, **14**, 1321, [1989].

[4] W. Torruellas, D. Neher, R. Zanoni, G. Stegeman, F. Kajzar, and M. Leclerc, *Chem. Phys. Lett.*, **175**, 11 [1990].

[5] B. Singh, M. Samoc, H. Nalwa, and P. Prasad, *J. Chem. Phys.*, **92**, 2756, 1990.

[6] K. Tanaka, K. Yoshizawa, T. Takeuchi, and T. Yamabe, *Synthetic Metals*, **38**, 107 [1990].

[7] J. Leavitt, University of Arizona, 1990.

Instabilities of a dispersive nonlinear all-fiber ring cavity

Réal Vallée
Michel Piché

Centre d'optique photonique et laser (COPL)
Université Laval (Pav. Vachon) G1K 7P4
Canada
TEL.: (418) 656-2454
FAX.: (418) 656-2623

Nonlinear optical cavities have been proposed for many applications such as bistability and optical switching. They have recently found an important application as the fast modulating element in coupled-cavity mode-locking. In this paper, we address the problem of the dynamical instabilities at the output of an all-fiber ring cavity synchronously pumped by a pulse train from a sync. pumped dye laser. Our analysis is based on a numerical simulation of the Nonlinear Schroedinger (NLS) equation and is primarily *intended to explain recent experimental results*[1].

The system under consideration is depicted in figure 1 (extracted from reference(1)). The electric field inside the cavity after N round trips (E_N) can be described by the following equation:

$$E_N = \gamma_o\{\sqrt{1-\kappa}E_{IN}\exp(j\,\phi_E) + j\,\sqrt{\kappa}\,\exp(j\phi_o)\,P(E_{N-1})\} \qquad (1)$$

where κ is the intensity coupling coefficient, γ_o the amplitude losses and j explicitly represents the phase shift of $\pi/2$ across the coupler. Note that Φ_E, the external phase factor, also appears explicitly in order to allow for the existence of a chirp (i.e. $\varphi_E = \omega_o t + Ct^2$). E_{in} therefore represents the amplitude of the electric field (namely A_o sech(t) at the input of the cavity). The operator $P(E_{N-1})$ represents the propagation of the pulse along the fiber according to the beam propagation method (BPM) applied to the NLS equation. Finally φ_o is the static phase shift of the cavity.

In the case of a cw input the nonlinear ring cavity is well known to show bistability, period-doubling and chaos[2]. However, when it is synchronously pumped by a train of pulses the whole sequence of dynamical instabilities is likely to occur within each single pulse (for a medium with a very fast nonlinearity like an optical fiber). This gives rise to new phenomena as the group velocity dispersion (GVD) starts filtering out the very fast oscillations resulting from the intrinsic instabilities of the system. Accordingly, a trade-off

between local and global constraints will result from the interplay between the GVD and the instabilities. This situation is depicted in figure 2 where the output of the cavity is computed from equation(1) for 1 psec (FWHM) input pulses and for different values of β_2 (the GVD parameter). For a negligibly[3] small β_2 (fig. 2a) the output of the system is characterized by a period-2 solution on the "cavity time scale" since it alternates between pulse(1) and pulse(2) from one iteration to the next. However a very fast oscillation (in the femtosecond time-scale) appears on top of these pulses in such a way that a period-2 scheme is also followed on the "pulse time scale". (Note that the energy of these two pulses is essentially the same). A comparison with figure 2b where β_2 is increased to 2 $psec^2/km$ readily shows that these fast oscillations are limited by GVD which simply acts as a time constant for the system. For a larger value of β_2 (corresponding to the nominal value for a silica fiber at 600 nm) the output of the system remains in a stable state as is shown on fig. 2c. In this case the continuity constraint imposed by the GVD is such that the instability on top of the pulse is averaged out by the stable lower part of the pulse so that the pulse is globally stable. For a higher input power the system eventually reaches a global period-2 state where the energies of the two pulses are now clearly distinct (which fortunately allows for an experimental verification using an electronic detector).

Group velocity dispersion also plays an indirect role in increasing the threshold of instability when chirped input pulses are considered in the analysis. (As a matter of fact in the experiment GVD is a constant while the chirp parameter C is, at least in principle, allowed to vary.) This is extremely important since the typical unstable behavior of the all-fiber ring cavity, as experimentally observed, was characterized by the sudden appearance of "bubbles" in the envelope of the output pulse train. Numerical simulations as well as indirect experimental evidence have shown that such a behaviour could be explained neither by an internal phase (Φ_o) drift nor by input power fluctuations. Indeed these bubbles can only be explained if the amount of chirp in the input pulse is allow to vary from one pulse to the next. Using values of C ranging from 0.0 to 1.0 typical experimental results can readily be reproduced. Moreover one can infer interesting information about the evolution of the chirp out of a sync. pumped dye laser.

Relevance of these results to coupled-cavity mode-locked lasers will be discussed.

REFERENCES

(1) R. VALLÉE. "Temporal instabilities in the output of an all-fiber ring cavity", Opt. Comm., 81(6), 419 (1991).

(2) K. IKEDA, "Multiple-valued stationary state and its instability of the transmitted light by a ring cavity" Opt. Comm., 30(2), 257 (1979).

(3) For such a small β_2 the higher order dispersion term β_3 obviously becomes predominant. This ideal dispersionless is shown for comparison purpose.

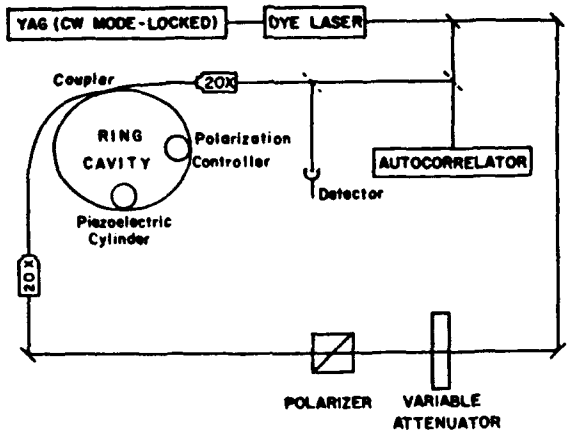

Fig. 1 Experimental set up of the all-fiber ring cavity

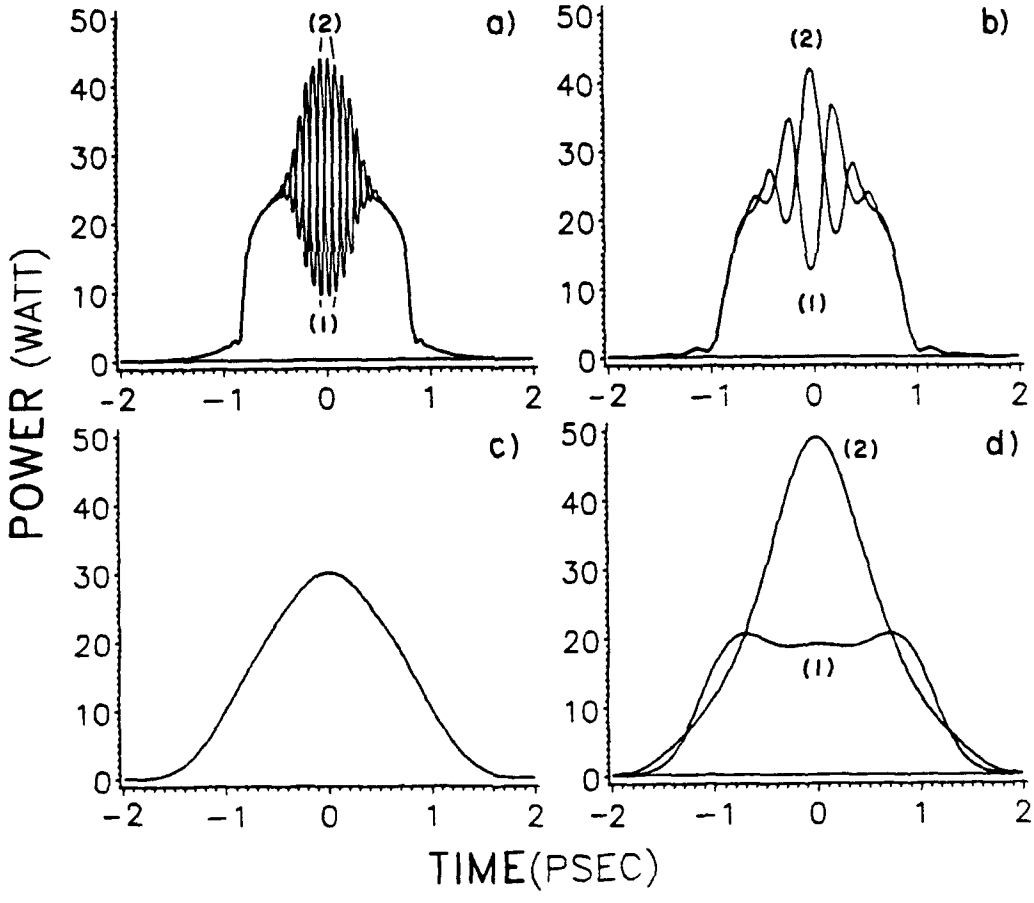

Fig. 2 Output pulses as computed from (1) for:

a) $A_o = 8.5\ w^{1/2}$, $\beta_2 = 0.2$ psec^2/km

b) $A_o = 8.5\ w^{1/2}$, $\beta_2 = 2$ psec^2/km

c) $A_o = 8.5\ w^{1/2}$, $\beta_2 = 50$ psec^2/km

d) $A_o = 10.5\ w^{1/2}$, $\beta_2 = 50$ psec^2/km

The other parameters are: $\tau_p = 1$ psec (FWHM), L (cavity length) = 2.65 m., $\lambda_o = 600$ nm, $C = 0$, $\Phi_o = \pi$, $\kappa = 0.5$.

DOUBLY NONLINEAR FIBRE LOOP LASERS

P. E. Langridge and W. J. Firth
Department of Physics and Applied Physics
University of Strathclyde, Glasgow G4 0NG, Scotland

Over the last decade, fibre-based devices incorporating single or multiple linear directional couplers have been the subject of theoretical and experimental investigation. These include fibre resonators [1-6] and linear [4] and nonlinear [7] loop mirrors. Except in [6] and [7], the devices involve linear propagation of a continuous wave (cw) or long pulse input. Only [7] studies operation with narrow pulses. Fibres have been incorporated in laser systems since the development of the soliton laser [8]. Recently, lasers with rare earth doped (neodymium [9] or erbium [10]) fibres as the active medium have been developed. All the above laser systems involve linear coupling to and from the fibre.

Here, we consider a novel type of passively mode-locked fibre laser in the form of a loop resonator with nonlinear coupling to and from the active medium. The first device studied consists of a nonlinear directional coupler (NLDC) [11,12] with amplification and nonlinear pulse-shaping occurring in a length of fibre connecting the output of one channel of the coupler to the input port of the same channel. Acting on results obtained for this configuration led to the inclusion of a second NLDC to improve the output from the device.

Pulse propagation around an amplifying, dispersive nonlinear fibre loop closed by a nonlinear directional coupler [11,12] was numerically studied using the split-step Fourier method [13] with absorbing boundaries implemented as suggested by If et al. [14].

With a single coupler, a very sharp threshold is observed between decay and growth of a seed pulse. A finite gain bandwidth was included, which has a saturation effect and allows a steady state to be reached. The behaviour above threshold is illustrated in figure 1. Fluctuations in the energy become negligible after approximately 30 circuits. The steady-state output intensity profile consists of a central pulse with 'shoulders' and low intensity radiation leading and trailing the main pulse. The steady state output is not strictly dependent on the form of the initial pulse launched.

The above simulations suggested that a double coupler configuration should produce a larger and cleaner output. Figure 2 shows the steady state output from the extra coupler after 140 round trips. Comparing with Figure 1, a marked improvement in the peak output intensity occurs with shoulders no longer present. In the figure, low intensity radiation is present but is approximately 1000 times less than the peak value.

P. E. Langridge acknowledges support through a SERC studentship. This work is supported in part by SERC Grant GR/F 75087.

References

1. L. F. Stokes, M. Chodorow and H. J. Shaw, Opt. Lett. 7, 288 (1982).
2. P. Urquhart, Appl. Opt. 26, 456 (1987).
3. M. Brierley and P. Urquhart, Appl. Opt. 26, 4841 (1987).
4. P. Urquhart, J. Opt. Soc. Am. A 5, 803 (1988).
5. Y. H. Ja, Opt. Commun. 75, 239 (1990).
6. T. V. Babkina, F. G. Bass, S. A. Bulgakov, V. V. Grigor'yants and V. V. Konotop, Opt. Commun. 78, 398 (1990).
7. N. J. Doran and D. Wood, Opt. Lett. 13, 56 (1988).
8. L. F. Mollenauer and R. H. Stolen, Opt. Lett. 9, 13 (1984).
9. M. W. Phillips, A. I. Ferguson and D. B. Patterson, Opt. Commun. 75, 33 (1990).
10. J. D. C. Jones and P. Urquhart, Opt. Commun. 76, 42 (1990).
11. S. M. Jensen, IEEE J. Quant. Electron. QE-18, 1580 (1982).
12. S. Trillo, S. Wabnitz, E. M. Wright and G. I. Stegeman, Opt. Lett. 13, 672 (1988).
13. T. R. Taha and M. J. Ablowitz, J. Comp. Phys. 55, 193 (1984).
14. D. Yevick and B. Hermansson, Opt. Commun. 47, 101 (1983).
15. F. If, P. Berg, P. L. Christiansen and O. Skovgaard, J. Comp. Phys. 72, 501 (1987).

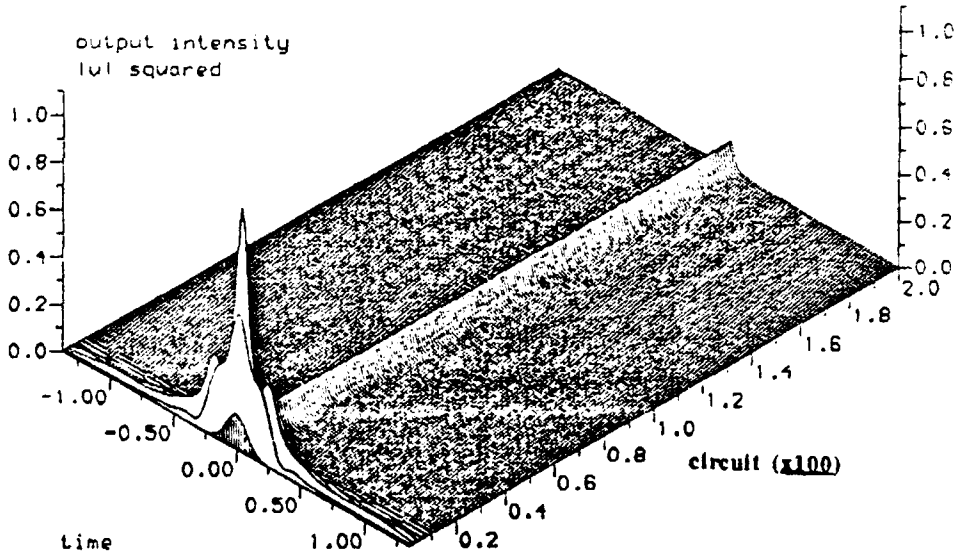

Figure 1
Evolution of a single seed pulse (shaded) injected into a nonlinear fibre loop with nonlinear coupler over 200 round trips. After transients, the pulse shape settles to a steady state consisting of a pulse plus background "ripples".

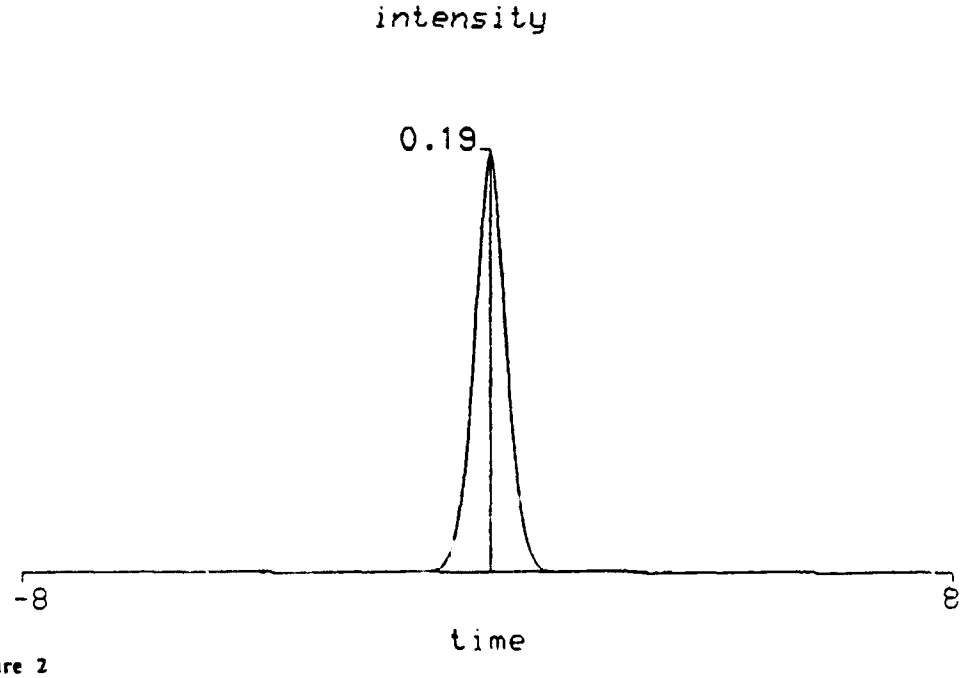

Figure 2
Steady state pulse shape emitted from a second nonlinear coupler inserted into the fibre loop. Note the absence of background.

FIBER-OPTICAL ELEMENT FOR ULTRASHORT PULSES CONTROL AND SWITCHING

D.V. Khaidarov

Thermal Physics Department, Uzbek Academy of Sciences
Chilanzar "C", ul. Katartal 28, Tashkent, 700135, USSR.
Telephone (371 2) 76-66-78. Telex 116162 TLAZO SU.

Fiber optical interferometers are outlook for ultrafast all - optical light control and switching. Here the fiber - optical loop is discussed as an element for fundamental soliton self-switching and for ultrashort pulses formation.

The loop is the two beam interferometer which consists of single - mode directional coupler with two output ports joined by single mode fiber with a length L [1] (Fig.1). In the FOL radiation passes through the coupler, then, after splitting, propagates in the loop along opposite directions, returns back to the coupler and interferes there. In the linear case loop transmittivity β_0 is connected with the splitting ratio of the coupler $\alpha(\lambda)$: $\beta_0(\lambda)=(2\alpha(\lambda)-1)^2$. In general part of the radiation β guided to the loop output depends on the phase difference φ between counterpropagating radiations which causes switching: $\beta=\beta_0+(1-\beta_0)sin^2(\varphi/2)$.

Optical solitons are the most convenient pulses for using in such devices due to their quasi-particle propagation which makes possible high contrast and avoidance of the pulse break-up under switching. Here the passage of the fundamental soliton through the fiber-optical loop is discussed in contrast to [1] where soliton like pulses with varying amplitude (nonfundamental solitons) were considered at the loop input.

Amplitude of the soliton at the input port is described by the expression $q_0(\tau)=sech(\tau)$ ($\tau=t/\tau_0$ - normalized time). When the solitons dispersive length $L_d=\tau_0^2/|\partial^2 k/\partial\omega^2|$ is much longer then the coupler one ($(L_d \gg 1)$) the nonlinearity in the coupler doesn't influence on the soliton coupling ratio. This fact has been tested numerically. Thus the nonlinear phase increases and the pulse shape modifies only in the loop.

PASSAGE OF THE SOLITON THROUGH THE LOOP. Case 1: $\alpha<0.25$ (or $\alpha>0.75$). After the coupler only one perturbed soliton propagating in one direction in the loop is formed [3] and the switching is not the case. At the loop output soliton $q(\tau)$ with the form factor $\varkappa=(2\sqrt{\alpha}-1)^2$ is derived $q(\tau)=\varkappa sech(\varkappa\tau)$. The duration T and the energy E of this soliton are concerned with initial ones $T/\tau_0=\varkappa^{-1}$; $E/E_0=\beta=\varkappa$ (Fig. 2,3).

Case 2: $0.25<\alpha<0.75$. Two counterpropagating solitons are formed and interfere in the coupler. It is necessary to take into account the soliton's phases $\varphi_{1,2}=\varkappa_{1,2}^2\xi/2$ [3]; where $\xi=L/L_d$, $\varkappa_{1,2}=(2\sqrt{\alpha_{1,2}}-1)$, $\alpha_1=\alpha$, $\alpha_2=1-\alpha$. Soliton's phase difference φ is expressed as $\varphi=2(\alpha_1-\sqrt{\alpha_1}+\sqrt{\alpha_2}-\alpha_2)\xi$. The value of the β may be calculated by the expression:

$$\beta = E/E_0 = \alpha_1\varkappa_1 + \alpha_2\varkappa_2 \pm \sqrt{\alpha_1\alpha_2}\,\varkappa_1\varkappa_2\int\{sech(\varkappa_1\tau')sech(\varkappa_2\tau')\}d\tau'$$

Upper sign - maximal β, lower - minimal. The switching contrast $K=\beta_{max}/\beta_{min}$ is maximal near the point $\alpha=0.5$ ($\alpha=0.45$, $K\approx30$). At $\alpha=0.45$ and $\xi\approx500$ ($L=L_d\xi\approx100$m) switching could be observed for the solitons with energy difference only about 5%.

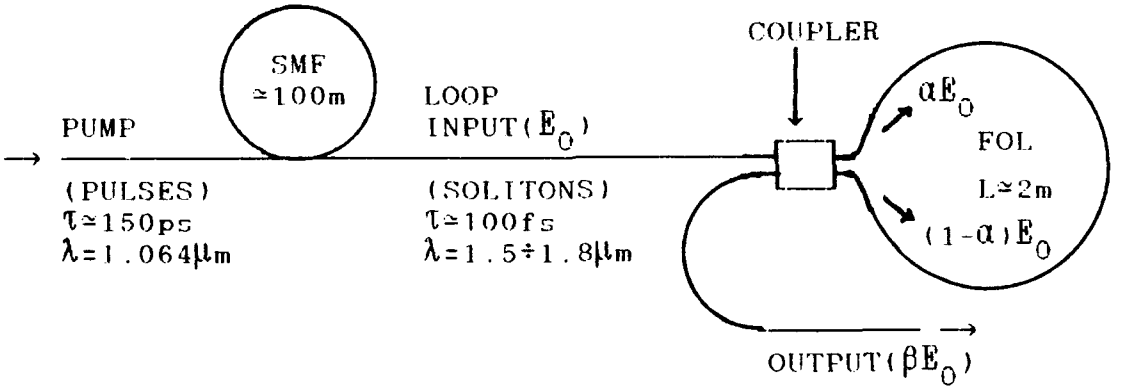

Fig.1:Scheme of the experiment and FOL configuration.

In the experiments solitons with duration $\tau_0=100\div200$fs ($\lambda=1.5\div1.8\mu$m) were formed via cascade Stimulated Raman Scattering (SRS) in the single-mode fiber [2]. Dispersive length L_d of the formed solitons was 10÷30cm in the whole spectral region. Q-switched and mode-locked CW Nd:YAG laser ($\lambda=1.064\mu$m) was used as a pump source. SRS generator and the loop were designed from one piece of the single-mode fiber. The coupler with length

l≈0.5cm and losses about 0.1dB per pass have been used. Experimental data of the soliton transmission through our loop (L=2m, ξ≈15) are in agreement with the theoretical curves (Fig. 3,4). The deviation β from β_0 is observed at the point $\alpha\approx0.3$ corresponding to the first transmission maximum.

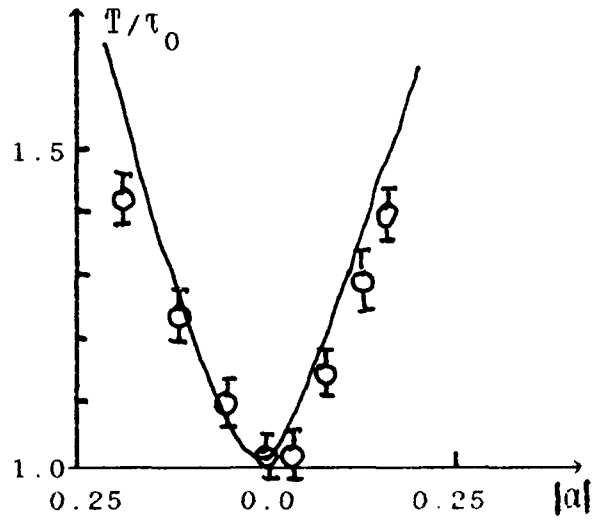

Fig.2: Soliton duration.

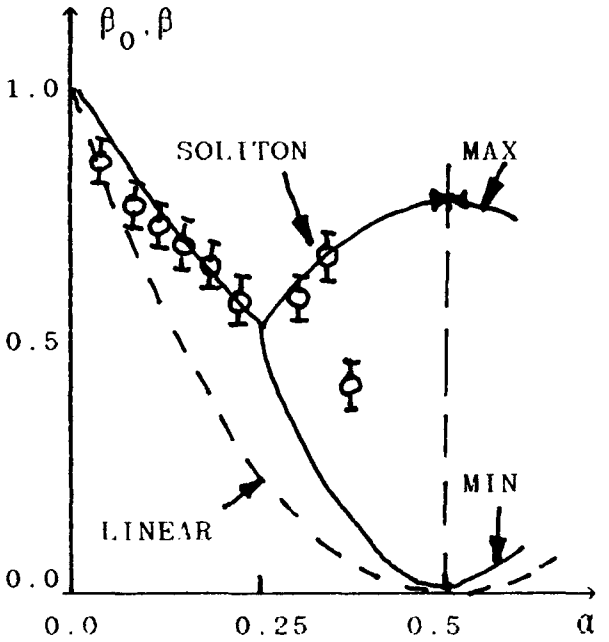

Fig.3: Loop transmission.

THE SOLITON INTERACTION WITH THE CW RADIATION AT THE OTHER WAVELENGTH IN THE LOOP. The nonreciprocal phase shift φ of the CW radiation could arise under cross phase modulation (XPM) from soliton propagating in the loop in one direction. This situation could be realized by using spectral selective coupler with coupling ratio for soliton $\alpha=1$, and for CW radiation $\alpha=0.5$. Under this conditions from the CW radiation high contrast pulses are formed with the intensity envelop described in the nondispersive approximation by the following expression: $I(\tau)=I' sin^2(\varphi(\tau)/2)$, where I' intensity of the CW radiation at the input of the loop. Nonreciprocal phase difference $\varphi(\tau)$ is given by the following expression:

$$\varphi(\tau) = (\eta/\gamma)\int_{\tau-\gamma}^{\tau} sech^2(\tau')\, d\tau'$$

where $\eta=4\pi n_2 I_0 l/\lambda$; $\gamma=\Delta L/\tau_0$; n_2 - nonlinear refracted index; I_0 - soliton peak intensity; $\Delta=(1/u-1/u_0)$; u, u_0 - group velocities at the wavelengths of the CW radiation (λ) and the soliton (λ_0).

To take into account dispersive evolution of the radiation in the loop the computer simulations have been done. It showed that formed pulse is of minimal duration and maximal intensity at $\eta \simeq \pi$ ($L \approx 0.75 L_d$) for soliton and pulse wavelengths 1.6μ and 1.06μ. Pulse has nonconstant phase during its envelop: frequency chirp exists, and pulse could be effectively compressed to about one half of the soliton duration (Fig.4).

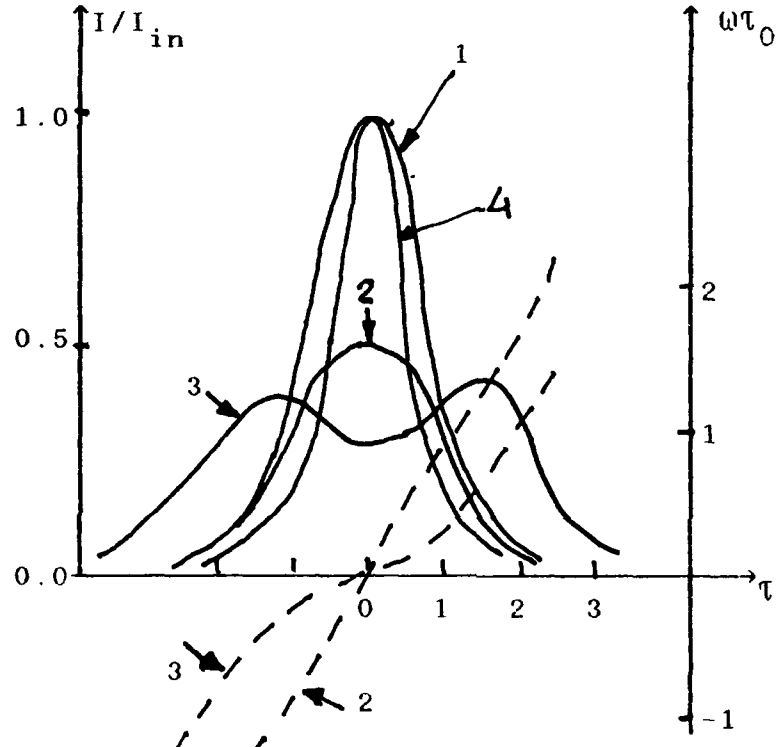

Fig.4: Soliton (1) and generated pulse at $\gamma=0$. 2: $\eta \simeq \pi$; 3: $\eta \simeq 2\pi$. Compressed pulse (4) at $\gamma=0$, $\eta \simeq \pi$
Intensity solid line, pulses chirp - dashed line.

Besides the above mentioned ways for use of the fiber-optical loop it could be used as a nonlinear mirror in the fiber lasers or in the additive pulse mode-locked (APM) lasers. By using of the loop as a mirror one could avoid additional discrete optical elements in the devices and consequently, decrease optical losses. Some our experiments connected with use of the loop as a mirror in the APM YAG laser will be described.

REFERENCES

1.Blow K.J., Doran N.J., Nayar B.K.//Opt.Lett.,1989,V.14,P.754.
2.Grudinin A.B. et al. JETP Lett.//1987,V.45,P.211.
4.Satsuma J.,Yajima N.,Progr.Theor.Phys.Suppl.//1974,V.55,P.284.

Poster Session: 5

TuF 5:30pm–7:00pm
Castlereagh Room

THE SPATIO-TEMPORAL DYNAMICS OF THE LIGHT PULSES IN THE NONLINEAR WEAK-GUIDING OPTICAL WAVEGUIDES

L.A.Melnikov, R.G.Bauer

Chernyshevsky State University, Astrakhanskaya,83, Saratov, 410071, USSR

The formation of the solitons owing to self-phase modulation (SPM) occurs at relatively small intensities [1]. In this cases the transverse beam profile may be considered as very close to the spatial profile of the fundamental mode. For shorter pulses or larger intensity when $n_2 I/\Delta n \cong 1$ ($n_2 I$ is the nonlinear part of refraction index, Δn is the difference of core and cladding index) it is needed to include into consideration other third-order effects such as self-focusing (SF) [2]. For the pulse parameters control it is interesting to investigate the transmission of the ultrashort pulses in periodical waveguides. In the step-index waveguides the transverse structure of fields is strongly dependent from excitation of modes of continuous spectrum of transverse wavenumber, and it is useful to derive the corresponding expressions.

1. For the parabolic graded-index fiber the envelope of the electric field obeys the equation (in dimensionless variables z/l, r/a, t/τ)

$$2i\partial\Psi/\partial z+\nabla_\perp^2\Psi+(V-r^2+4R|\Psi|^2)\Psi+\sigma\partial^2\Psi/\partial t^2=0 \qquad (1)$$

where V is the characteristic frequency, $R=l/l_c$, $l_c=\Delta n/2n_2V$, $\tau=l\beta''$, $\sigma=sign\beta''$, l is the diffraction length, a is the core radius, β'' is the group-velocity dispersion. Usually pulse duration τ_p is much more larger than τ and we can solve Eq.(1) in two step. First we omit the dispersion at the distances comparable to l and we find the approximate solution through the trial solution $\Psi=A(z,t)exp(-P(z,t)r^2/2)$. The equations satisfied by this subsidiary functions have been obtained using the method from Ref.3 and may be written as follows:

$$2idA/dz+(V-2P)A+3R|A|^2A=0, \quad idP/dz=P^2-1+\eta R|A|^2, \quad \eta=ReP, \qquad (2)$$

with the solution $A(z,t)=A(0,t)[\eta(z,t)]^{1/2}\times$ $\times\ exp(iVz/2-i\int dz'\eta(z')[1-3R|B|^2])$, where $B=A/\eta^{1/2}$, $\eta(z)=\eta(0)\times$ $\times\ (\cos^2 z+\eta^2(0)(1-R|B|^2)\sin^2 z)^{-1}$. It should be noted that B is a constant along z, but strongly depends from t. It is worth to mark that the SF critical power in Eqs.(2) is four times larger than in aberrationless approximation of Ref.2b. This leads to the correct sign of the "chirp" in our treatment in difference from the results of Ref.2b. At the second step we find a variation of A due to group-velocity dispersion and nonlinear chirp. Using Eq.(1) with $r=0$ we have:

$$2i\partial A/\partial z+\sigma\partial^2 A/\partial t^2+\{V-2P(z,t,R|A|^2)\}A+4R|A|^2A=0, \quad (3)$$

At a small R and after averaging on z Eq.(3) is reduced to the nonlinear Schrodinger equation. In Fig.1a,b we demonstrate the evolution at the fiber axis of the initial pulse $\Psi(0,r,t)=exp(-0.1t^2-r^2/2)$ for $\sigma=1$, $R=0.6$ (a) and $\sigma=-1$ $R=0.6$ (b). Due to SF and waveguiding the beam minimum (intensity maximum) is observed at $z\cong\pi/2$.The evolution of pulses after this maximum depends from the sign of dispersion. At the negative dispersion the regime corresponds to the disturbed multi-soliton oscillation (Fig.1a). At $\sigma=-1$ we have observed ordinary pulse spreading (Fig.1b).

2. In the periodic waveguide where $V(z)=V(1+m\cos\Omega z)$ and for $R\ll 1$ we have observed the destroying of N-soliton regimes at a value of Ω near to the soliton beat frequency. In Fig.2a,b the evolutions of 3-soliton and 1-soliton pulses are shown at $m=0.2$ and $\Omega=4$. It should be marked that modulation slightly varied 1-soliton pulse but strongly modified the N-soliton regimes. It is interesting to pointed out the similarity among the regimes in periodic waveguides and in fiber with SF.

3. The nonlinear propagation of an ultra-short pulse in a step-index fiber may be considered as the evolution of a pulse in the condition of longitudinal transient regime which is characterized by the excitation of leaky modes and spatial wave. The existence of these modes of continuous spectrum of transverse wave number continuum is determined the transversal field structure [4]. Using the decomposition of the Fourier transformation of pulse field in terms of guided modes $\varphi_0(r,\omega)$ and continuum modes

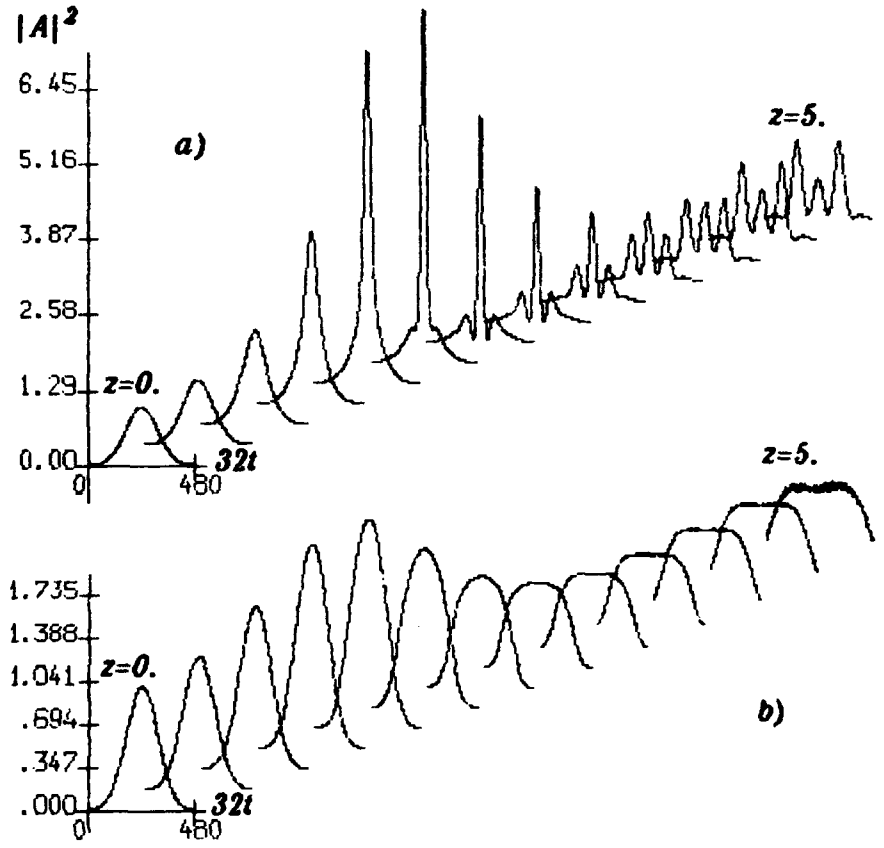

Fig.1. Pulse evolution in parabolic graded-index fiber with self-focusing, self-phase modulation and group-velocity dispersion. a) σ=1, R=0.6, b) σ=-1, R=0.6

$\Phi(q,r,\omega)$ and excluding the equations for continuum mode amplitudes we obtain the equation for fundamental mode envelope including the effects of radiated field:

$$2i\partial A/\partial z+\beta''\partial^2 A/\partial t^2+2R|A|^2A+4iR^2\Big[\int_0^\infty dqF(q)\int_0^z dz'\{|A(z)A(z')|^2 \times$$

$$\times A(z')C(q,z-z') - A(z)^2|A(z')|^2A^*(z')D(q,z+z')\}\Big] =0. \quad (4)$$

Here $F(q)$ is connected with the normalization integral of q-th mode, C,D are the products of overlapping integrals of fundamental and q-th modes including phase factors. The whole field in the

waveguide may be written as follows:

$$E(z,r,t)= [A(z,t)\varphi_0(r,\omega_0)+(id\varphi_0/d\omega)(\partial A/\partial t)-$$
$$-(1/2)(d\varphi_0/d\omega^2)\partial A^2/\partial t^2+\dots]\exp(-i\omega_0 t+i\beta(\omega_0)z) \quad (5)$$

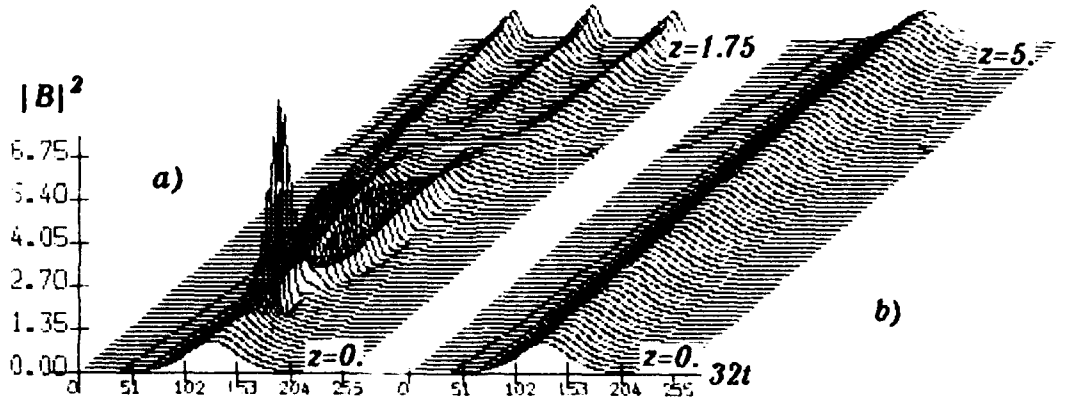

Fig.2. The N-soliton regimes in periodic waveguide. a) N=3, b) N=1

This models of nonlinear pulse propagation in optical wave guides allow to estimate the contributions of SF in graded or step-index fibers and the stability of soliton regimes in the fibers with modulated parameters. This results may be useful for the analysis of pulse-control devices based on the nonlinear waveguides.

REFERENCES

1. S.A.Akhmanov, V.A.Vysloukh, and A.S.Chirkin. -Optics of femtosecond laser pulses. Moscow, 1988 (in Russ.).
2. a) V.A.Vysloukh, and T.A.Matveeva. Izv.Vuz., Radiophys., **28**,101(1985) (in Russ.). b) J.T.Manassah, P.L.Baldeck, and R.R.Alfano. Opt.Lett. **13**, 589(1988).
3. V.L.Derbov, L.A.Melnikov, and A.D.Novikov. Kvant.Elektr., **14**, 2529(1987) (in Russ.).
4. A.W.Snyder, J.D.Love. -Optical waveguide theory. London, Chapman and Hall, 1983.

Soliton Propagation in Media with Non-central Symmetry

Qi Guo, Chang-jun Liao, and Shong-hao Liu,
Institute of Quantum Electronics, South China Normal University,
Guangzhou 510631, P. R. China.
Tel. 020-516911-2540

The second-order susceptibility $\chi^{(2)}$ describes the energy transfer of second-order nonlinear optical effects in media with non-central symmetry. In the waveguides made of this kind of media, however, if the phase-matching condition is not satisfied, the effects are very weak in the propagation distance that the wave interaction length is much longer than the coherent length (the wave interaction length can be very long, when the guides have low loss.). It is theoretically demonstrated here for the first time that the waveguides in this case can support the envelope solitons described by nonlinear Schrödinger equation (NLSE).

For simplification, we limit ourself to one-dimensional linear polarized wave propagation. With the limitation, the polarization P in the media is[1]

$$P(z,t)=\varepsilon_0\Big[\int_{-\infty}^{\infty}\chi^{(1)}(t-\zeta)E(z,\zeta)d\zeta+\int_{-\infty}^{\infty}\chi^{(2)}(t-\zeta,t-\eta)E(z,\zeta)E(z,\eta)d\zeta d\eta$$
$$+\int_{-\infty}^{\infty}\chi^{(3)}(t-\zeta,t-\eta,t-\theta)E(z,\zeta)E(z,\eta)E(z,\theta)d\zeta d\eta d\theta\Big]$$
$$+\quad\text{higher terms.}\qquad(1)$$

In terms of reductive perturbation method[2], which is one of the

asymptotic methods describing far fields[2], and has been successfully applied to discuss the soliton propagation in optical fibers[3], the solution of one-dimensional Maxwell wave equation (ODMWE) [1,4] is supposed as:

$$E(z,t)=(1/2)\sum_{m=-\infty}^{\infty}\sum_{n=1}^{\infty}\varepsilon^{n}u_{m}^{(n)}(\xi,\tau)\exp[im(\beta z-\omega t)], \qquad (2)$$

where $u_m^{(n)}$ are the slowly varying envelopes, ξ and τ are slow variables ($\xi=\varepsilon^2 z$, $\tau=\varepsilon(t-\beta' z)$, $\beta'=\partial\beta/\partial\omega$), and ε is a small parameter($\ll 1$). $u_p^{(n)}(p\neq\pm 1)$ are called as the pth-order self-harmonics, and their phase-matching condition is satisfied automatically, which is different from the harmonic generations[1].

Substitution of Eq.(1) and (2) into the ODMWE, following the same but easier step in ref.[3], we have:

$$E=\varepsilon(1/2)u_1^{(1)}\exp[i(\beta z-\omega t)+C.C.+o(\varepsilon), \qquad (3)$$

with dispersion relation $\beta(\omega)=\omega n_0(\omega)/c$, and $u_1^{(1)}$ is described by

$$i\frac{\partial}{\partial\xi}u_1^{(1)}-\frac{\beta''}{2}\frac{\partial^2}{\partial\tau^2}u_1^{(1)}+\frac{\beta\bar{n}_2}{n_{01}}|u_1^{(1)}|^2u_1^{(1)}=0, \qquad (4)$$

where $\beta''=\partial^2\beta/\partial\omega^2$. Here $\bar{n}_2$ is effective nonlinear-index coefficient (NIC) defined as

$$\bar{n}_2=n_2+(\bar{\chi}^{(2)})^2[2/(c^2\beta'^2-n_{00}^2)-1/(n_{02}^2-n_{01}^2)]/(4n_{01}), \qquad (5)$$

where n_2 is NIC, $n_{0m}=n_0(m\omega)$ linear refractive index at frequency $m\omega$, the relation between n_2 and $\bar{\chi}^{(3)}$ that $n_2=3\bar{\chi}^{(3)}/(8n_{01})$ [4] is used, and $\bar{\chi}^{(n)}$ is the n-dimensional Fourier transform of $\chi^{(n)}$ (n=2,3).

Eq.(4) is also the NLSE, except the effective NIC $\bar{n}_2$ is

instead of the NIC n_2, i.e., envelope solitons can propagate in the waveguides, too. The main difference between the waveguides and the fibers is that $\bar{n}_2$ might be negative, but n_2 in the fibers is positive. So, it is possible that bright solitons[4] can exist in the normal-dispersion regime for the waveguides. We should note that, similarly to the fibers[3], it is expected that a reduction factor should be multiplied to the coefficient of the last term of Eq.(4) for the three-dimensional guided waves.

Analogy of Eq.(4) with the NLSE in the fibers also shows that the nonlinear refractive index (NRI) in this case can be expressed as

$$n(\omega, |E|^2) = n_0(\omega) + \bar{n}_2 |E|^2 . \qquad (6)$$

The appearance of the effective NIC is due to the additional contribution of $\chi^{(2)}$ to the NRI. $\chi^{(2)}$ has been known to be unable to directly devote to the NRI[5]. It is found here, however, that the second-order and zero-order self-harmonics can be generated at the second-order in ε because of non-zero $\chi^{(2)}$. The interaction of them and the wave itself will give the additional refractive work.

The optical waveguides in which the soliton propagation predicted above can be experimentally demonstrated are thin-film waveguides and crystal fibers[6]. It is expected that the conventional glass fiber can also be as the candidate since the high-efficiency second harmonic generation has been found to be exist if the fiber is illuminated with pump radiation for several hours[7]. Because one can follow the standard procedure to study

the wave propagation when a self-organized $\chi^{(2)}$ grating is introduced[4], Eq.(4) can directly be applied to this case provided that $\chi^{(2)}$ in the efficiency NIC is substituted by the grating.

By use of Eq.(6), our results can be easily extended to study the other nonlinear optical effects connected with the NRI in the media with non-central symmetry.

It is expected that our find will result in some further theoretical and experimental researches, and quest for applications.

REFERENCE

[1] Y. R. Shen, The Principles of Nonlinear Optics (John Wiley & Sons, Inc., New York, 1984), Chap. 1,3,6, and 7.

[2] T. Taniuti and K. Nishihara, Nonlinear Waves (Pitman Publishing Inc., Marshfield, Massachusetts, 1983), p.p.114-130.

[3] Y. Kodama and A. Hasegawa, IEEE J. Quantum Electron., QE-23, 510(1987).

[4] G. P. Agrawal, Nonlinear Fiber Optics (Academic Press, Inc., Boston, 1989), Chap. 2 and 5, and p.p.319-325.

[5] W. L. Smith, in CRC Handbook of Laser Science and Technology, edited by M. J. Weber, (CRC Press, Inc., Boca Raton, Florida, 1986), Vol.3, Part 1, Sec. 1.3, p.259, and reference therein.

[6] M. Fejer, et al., Laser Focus, 21, 60(1985), and references therein.

[7] U. Osterberg and W. Margulis, Opt. Lett., 11, 516(1986).

ON THE MECHANISMS OF COHERENT PHOTOVOLTAIC EFFECT FOR SECOND HARMONIC GENERATION IN GLASS FIBERS

V.O.Sokolov, V.B.Sulimov
Institute of General Physics
of the Academy of Sciences of the USSR,
38 Vavilov Street, Moscow, 117942

Different models have been suggested for photoinduced second-harmonic generation in silica fibers [1,2]. The model with charge carriers redistribution in the core of the fiber due to coherent photovoltaic effect was proposed in [3-15]. The coherent photovoltaic effect means that direct current appears in the glass under coherent pump and second-harmonic light waves. Theory of this effect was proposed in [16] but the expressions presented there are too complicated to get estimations of photocurrent and also the semiclassical method used there is not adequate to the phenomena. One of the possible mechanism of such effect was proposed in [4-8,11,13,15] but there is no consistent calculation of the photocurrent. So, the question on the microscopic mechanisms of coherent photovoltaic effect is still open.

Our aim is to find the direct current as a linear response to the external second-harmonic field in the electron subsystem of silica created by the external pump wave with frequency Ω. Linearizing the density matrix with respect to second-harmonic field $\vec{\mathcal{E}}_{2\Omega}$ the current density can be expressed through the averaged commutator of the current density and velocity operators. The averaged commutator was expressed through second harmonic of the non-equilibrium two-electron Green's function, for which the equation can be written in the ladder-type approximation [17-19]. This integral equation contains the one-electron non-equilibrium Green's functions, which can be found by perturbations with respect to the pump wave amplitude $\vec{\mathcal{E}}_{\Omega}$ [20]. Solving the equation we obtained next expression for the direct current density created due to electron excitation from the localized states to conduction band:

$$j^{\beta}_{DC}= \frac{e^2\pi N}{4(\hbar\Omega)^2m^2}\sum_{\vec{p}} p^{\beta}\,\tau_p Re\left[(\vec{p},\vec{\mathcal{E}}_{2\Omega})D^{*}_{ip}D^{*}_{pi}\right](n_i-n_p)\delta(E_p-E_i-\hbar\Omega)+$$

$$+\frac{e^2\pi N}{4(\hbar\Omega)^2m^2}\sum_{\vec{p}} p^{\beta}\,\tau_p Re\left[(\vec{p},\vec{\mathcal{E}}^{*}_{\Omega})D^{*}_{ip}(\omega_{ip}/\Omega)(e\vec{x}_{ip},\vec{\mathcal{E}}_{2\Omega})\right](n_i-n_p)\times \qquad (1)$$

$$\times[\delta(E_p-E_i-\hbar\Omega)-\delta(E_p-E_i-2\hbar\Omega)].$$

Here N is the defect concentration, m is the effective mass ($m \approx m_0$ for SiO_2), $|\vec{p}\rangle$ is a delocalized state of electron with impulse $\vec{p}$ (plane wave), $|i\rangle$ is a localized orbital of the defect, E_p is the energy level in the conduction band, E_i is the energy level of the defect in the gap of silica, n_i and n_p are the equilibrium occupation numbers of the $|i\rangle$ and $|\vec{p}\rangle$ states, respectively; τ_p is the transport relaxation time, $D_{ij}=(\omega_{ij}/2\Omega)(e\vec{x}_{ij},\vec{\mathcal{E}}_{\Omega})$, $\omega_{ij}=(E_i-E_j)/\hbar$, $\vec{x}_{ij}=\langle i|\vec{x}|j\rangle$.

It is easy to recognize in all terms of (1) the usual expression for the drift part of current density [21] but with some non-equilibrium distribution function of the electrons photoexcited to the conduction band from localized states. This leads to the next interpretation of the discussed phenomena.

The transition probability P(t) between two states n → m under biharmonic excitation

$$\hat{V}(t) = \hat{h}\,exp(-i\Omega t)+\hat{h}^{+}exp(i\Omega t) + \hat{H}\,exp(-i2\Omega t)+\hat{H}^{+}exp(i2\Omega t), \quad (2)$$

contains not only constant term but also time dependent ones varying with pump (Ω) and second-harmonic (2Ω) frequencies:

$$P(t) \propto \frac{h_{mn}h^{*}_{mn}}{(\omega_{mn}\mp\Omega)^2+\delta^2} + \frac{h_{mn}h_{nm}}{(\omega_{mn}\pm\Omega-i\delta)(\omega_{mn}\mp\Omega+i\delta)}\,exp(\pm i2\Omega t) + \quad (3)$$

$$+\left[\frac{h^{*}_{mn}H_{mn}}{(\omega_{mn}\mp\Omega-i\delta)(\omega_{mn}\mp2\Omega+i\delta)} + \frac{H^{*}_{nm}h_{nm}}{(\omega_{mn}\pm\Omega+i\delta)(\omega_{mn}\pm2\Omega-i\delta)}\right]exp(\pm i\Omega t),$$

where the summation over the double signs is implying and terms $\propto H^2$ and also terms $\propto exp(\pm i3\Omega t)$ were neglected. We consider here the adiabatic growth of excitation (2) (δ is the

adiabatic parameter) from $t = -\infty$, when the system was in the state n. The expression (3) shows, that the distribution function of the electrons in the conduction band must contain time dependent terms:

$$\Delta n_p(t) = \Delta n_1(p)\cos(\Omega t) + \Delta n_2(p)\cos(2\Omega t+\varphi). \qquad (4)$$

We can see from (3) that first term in (4) appears due to the impurity ionization by the interference of the second-harmonic and the pump fields. The second term in (4) appears due to the excitation of electrons only by pump wave. The direct current can be obtained from general expression

$$\vec{j} = e\, n(t)\, \mu\, \vec{\mathcal{E}}(t) \qquad (5)$$

by two ways. First, field $\vec{\mathcal{E}}$ in (5) is electric field of second-harmonic wave and n(t) is second term in (4). Second, field $\vec{\mathcal{E}}$ in (5) is electric field of pump wave and n(t) is first term in (4). This leads to (1), where first term describes the drift of non-equilibrium electrons under second-harmonic field, and second term describes the drift of non-equilibrium electrons under pump field. It can be seen from (3) that second mechanism takes place when energy difference between electron levels is either $\hbar\Omega$ or $2\hbar\Omega$. This agrees with the second term in the right-hand side of (1). The electron excitation due to interference of pump and second-harmonic waves with absorption of the energy $2\hbar\Omega$ was discussed in [4-8,11,13,15]. The first term in the right-hand side of (1) was discussed in [2,10,14].

We estimate current density about 10^{-6} A/cm^2 for the defect concentration $N \approx 2\times10^{11}$ cm^{-3} (plain waves for conduction band and hydrogen-like localized wave function) under fields $\mathcal{E}_\Omega \approx 3\cdot10^8$ V/m and $\mathcal{E}_{2\Omega} \approx 3\cdot10^7$ V/m.

For this phenomena we propose some germanium defects. Their characteristics were obtained by MNDO method in cluster approximation.

REFERENCES

1. U.Osterberg and W.Margulis, Opt.Lett. 11, 516 (1986).
2. Sokolov V.O., Sulimov V.B. Izvestia AN SSSR, ser.Fizicheskaia

54, 2313 (1990) (in Russian).
3. Dianov E.M. et al. Sov.J.Quantum Electron, **16**, 887 (1989).
4. Zel'dovich B.Ya., Chudinov A.N. Pis,ma Zh.Teor.Fiz., **50**, 554 (1989) (in Russian).
5. Anoikin E.V. et al. Pis'ma Zh.Tech.Fiz., **15**, 78 (1989) (in Russian).
6. Dianov E.M. et al. Proc.Integ.Phot.Res., Hilton-Head, South Caroline, March 26-28, 1990. USA. Paper MJ1. P.46.
7. Baranova N.B. et al. Proc.CLEO'90, 21-25 May, 1990, Anaheim, California, Paper CFJ2, P.518.
8. Anoikin E.V. et al. Opt.Lett., **15**, 834 (1990).
9. Dianov E.M. et al. Sov.J.Quantum Electron. **17**, 926 (1990).
10. Dianov E.M. et al. Sixth Europhysical topical conference: Lattice defects in ionic materials, Groningen, The Netherlands. 3-7 sep. 1990. P.338.
11. Baranova N.B. et al. Opt.Comm. **79**, 116 (1990).
12. Dianov E.M. et al. Tech.digest of OSA Annual Meeting, Boston, 1990, Paper TuU4.
13. Anderson D.Z. et al. Tech.digest of OSA Annual Meeting, Boston, 1990. Postdeadline Papers, Paper PDP24. P.57.
14. Dianov E.M. et al. Proc. Conference on quantum chemistry of solids, 26-30 Nov. 1990. Riga. P.190.
15. Baranova N.B. et al. Zh.Eksper.Teor.Fiz., **98**, 1857 (1990) (in Russian).
16. Entin M.V. Phys.Tech.Semicond. **23**, 1066 (1989) (in Russian).
17. Keldysh L.V., Zh.Eksper.Teor.Fiz., **47**, 1515 (1964) (in Russian)
18. V.B.Sulimov, deposed in VINITI, No.2588-78(1978); Ref.Zh.Fiz. **11E**, 257 (1978) (in Russian).
19. V.B.Sulimov, Thesis, Moscow State University, Phys. Faculty, 1979 (in Russian).
20. V.B.Sulimov, Physica Status Solidi (b) **96**, 507 (1979).
21. J.M.Ziman, Principles of the theory of solids, Cambridge, Univ.Press, 1964.

Correlation of UV-radiation with the process of second harmonic generation in Ge-doped optical fibers

F.B.Baikabulov, P.V.Chernov, S.K.Isaev, L.S.Kornienko, A.O.Ribaltovsky, Yu.P.Yatsenko

Physics Department of Moscow State University
Moscow,117234,USSR,tel.(095)939-31-94

To clarify the mechanism of second harmonic generation (SHG) in Ge-doped optical fibers, it is very important to know what leads to formation of permanent X(2) grating. Some of the reports [1-3] considered strong internal dc fields to be the main reason for writing such gratings. In other papers [4-6] a lot of attention is paid to formation and orientation of color centers and permanent defects. In this great role can play UV-radiation due to simultaneous generation of the third or fourth harmonics .

We present here some additional evidence of strong correlation between the preparation process for the induced SH and parametric generation of third and fourth harmonic in Ge-doped fibers.

1.We used silica fibers that were single mode at 1064 nm and supported 3-4 modes at 532 nm. With proper matching it was possible to excite only the fundamental mode for both waves. The core was doped with 10-11 mol% GeO_2 and the cladding was doped with 1-2 mol% P_2O_5 and F. In some experiments we use also fibers with smaller concentration of GeO_2.

A Q-switched and mode-locked Nd:YAG laser operating at 1064 nm was used as a pump source. Trains of 100 ps IR pulses with peak power of 20 kW and repetition frequency 1,2 kHz run through KTP crystal to generate SH. Then the both seed waves passed through a polarizer and were coupled into the fiber. The light emitted from the fiber was analyzed with a monochromator.

2.To optimize the process of seeding we investigated first the influence of fiber length and intensity ratio for seed SH and IR waves P_2/P_1. In our experiments the conversion efficiensy reaches maximum 0.1 % for optimal fiber lengths not exceeding 15-20 cm. In a broad range of the seed SH intensities with IR wave power kept constant the conversion efficiency has the same saturation level but the time of achieving this level varied from a few minutes to 20 minutes when P_2/P_1 ratio decreased from 1/50 to 1/1000.

The most interesting result is: immediately after the two seed waves are launched into the fiber the TH and FH generation at 355 nm and 266 nm starts. TH and FH pulses corresponded to pump pulses in duration and broke off at once when any of two seed waves (IR or SH) was suppressed. The TH signal from the output end of the fiber was 10^4-10^5 times weaker than the seed SH signal. FH signal was 10^3- 10^4weaker than the TH one. We relate this to strong absorption at 266 nm in glass. We observed also UV fluorescence in the 380-410 nm region with a weak peak at 396 nm.It emerged either from the fiber end or from side surface. The fluorescence pulses had

exponentially decaying tails of 0.1ms duration.

All three types of UV radiation are strictly correlated with the processof seeding.The stronger UV radiation at the beginning of the seeding process the faster saturation level of the induced SH was reached. Fig.1 shows a typical dependence of preparation time on the intensity of 396 nm radiation. Using four fibers with different percentage of GeO_2 we revealed strict correlation between GeO_2 concentration and UV radiation. Fig.2 demonstrates sharp decreasing of generated TH with decreasing GeO_2 concentrationM(mol%).

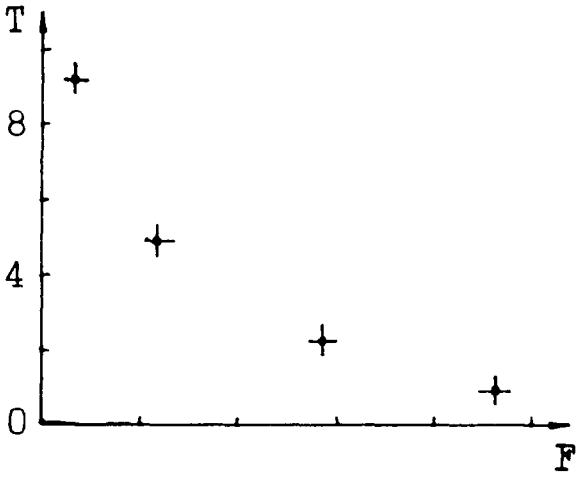

Fig.1. Preparation time T(min) vs fluorescense intensity F(a.u.)

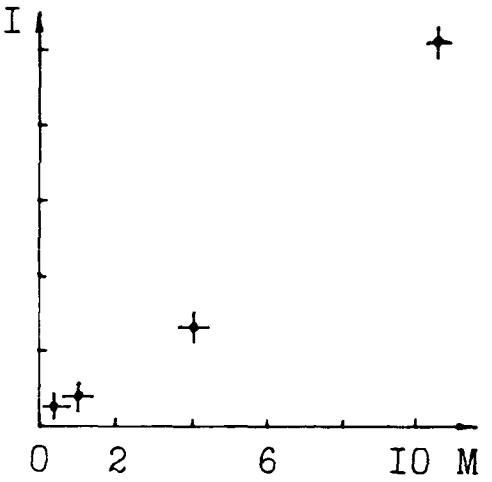

Fig.2. TH intensity I(a.u.) vs GeO_2 concentration M

3.The fact that TH and FH emission strictly depends on the simultaneous presence of IR and SH pumping indicates four-wave parametric mechanism of their formation through X(3) .As it has been already discussedin [5] such processes can be very effective in media with resonance levels close to TH or FH frequences.In [5] P-doped fiber was considered. It

is well known that Ge-doped fibers have a sharp absorption line at 242 nm and 10^3 weaker line at 330 nm. These lines are connected with the excitation of covalent bonds in oxygen deficient germano-silicate glass.Excitation of these bonds gives rise to fluorescence peaked at 396 nm with relaxation time 0.105 ms. Thus, parametric TH and FH processes can be resonant and effective.

We should take into account and speculate that TH and FH can break covalent bonds and form well-known Ge-E' centers which can be oriented according to interference pattern of two seed waves. New experiments are in progress to check these speculations.

In conclusion,we have found that the process of seeding is accompanied from the very beginning by generation of third and forth harmonics. This generation is parametric and involves fundamental and second harmonics photons of seeding waves.The fluorescence discovered at 400 nm shows that parametric generation can have resonant character connected with excitation of covalent bonds in oxygen deficient germano-silicate glass . A strict correlation is revealed between UV-radiation and seeding time of induced SH.

References

1. R.Stolen, H.Tom, Opt.Lett. 12, 585 (1987).
2. V.Mizrahi, Y.Hibino,G.Stegeman, Opt.Commun. 78, 283 (1990).
3. E.Dianov, P.Kazansky, D.Stepanov, Kvant.Electr. 16, 887 (1989).
4. J.Gabriagues, H.Fevrier, Opt.Lett. 12, 720, (1987).
5. A.Krotkus, W.Margulis, Appl.Phys.Lett. 52, 1942, (1988).
6. U.Osterberg, Electr.Lett. 26, 103, (1990).

THEORY OF PHOTO-INDUCED SECOND-HARMONIC GENERATION CAUSED BY PHASE TRANSITION IN DEFECTS SYSTEM IN SILICA GLASS

E.M.Dianov, V.O.Sokolov, V.B.Sulimov

General Physics Institute of the USSR Academy of Sciences
38 Vavilov St., Moscow, USSR SU 117942 Phone 132 8303

To describe inducing of non-zero macroscopic second-order susceptibility in a centro-symmetric media such as the glass we suppose that a pump wave excites electrons from certain "donor" states in the middle of the v-SiO_2 forbidden gap to defect states near the conduction band edge and the conformation of each defect changes significantly owing to pseudo-Jahn-Teller effect with a certain number of electrons placed in the proper state of the defect. Our cluster calculation performed by MNDO method proves the pseudo-effect to occur in Ge and Al atom substituted for the Si one and in ≡Ge-O-Ge≡ diatomic center with a certain defect state occupied by two electrons or by one electron, respectively. The relaxed conformation of the defects is stable since their spontaneous decay is forbidden. We suppose that a phase transition occurs owing to cooperative pseudo-Jahn-Teller effect in the system of defects created in the glass by the pump wave, that it is described by a vector order parameter $\vec{\eta}$ and that it is caused by small relaxation of each of the defects with non-zero polarizability b^{ω}. Under these assumptions macroscopic second-order susceptibility is proved to be $\chi^{(2)}_{ijk} = \chi^{(2)}(\eta_i\delta_{jk} + \eta_j\delta_{ik} + \eta_k\delta_{ij})$ where $\chi^{(2)} \equiv nb^{\omega}\delta R/R$, $\delta R/R$ being mean relative atomic displacement in relaxed defect, n being defects concentration. Bloembergen's relations [1] are valid for $\chi^{(2)}_{ijk}$ since $\chi^{(2)}_{xxy} = \chi^{(2)}_{xyx} = \chi^{(2)}_{yxx} = \chi^{(2)}\eta_y$, $\chi^{(2)}_{yyy} = 3\chi^{(2)}\eta_y$. So the results of [2] are explained by our theory and therefore those do not prove the SH generation to be caused by strong electrostatic field induced in the glass by the pump wave, as supposed in [2]. Our computer simulation of the defects results in $\delta R/R \sim 0.1$. The defect polarizability may be estimated as $b^{\omega} \sim (\nu d)^3(\eta\omega)^{-2}$ with d being mean value of dipole matrix element in the defect, ν being number of the

defect states. Since $\nu d \sim 1e$, one finds for wavelength ~ 1 μm: $\nu d \sim 5 \cdot 10^{-18}$ CGS and $b^{\omega} \sim 10^{-28}$ CGS. Assuming the mean order parameter to be $\eta \sim 0.1$ one obtains $\chi^{(2)} \sim 10^{-30} \cdot n$ CGS $\sim 10^{-12}$ CGS for $n \sim 10^{18}$ om^{-3} in good agreement with experimental data (see review in [3]).

Relaxed conformation of pseudo-Jahn-Teller center is characterized by a vector $\vec{J}$. While relaxing the defect in point $\vec{R}^a$ induces atomic displacements in glass interacting with another one in the point $\vec{R}^b$. Energy of the interaction is $U^{ab} = - U^{ab}_{sp} J^a_s J^b_p$ where $\vec{R}^{ab} = \vec{R}^b - \vec{R}^a$. The U^{ab} can be found explicitly only using a certain microscopic model of defect. However owing to randomness of the glass host one is only to estimate a typical value of the mean interaction energy. For $R^{ab} \gg (V^d)^{1/3}$, V^d being defect's volume, the principal term is $U^{ab} \sim (\Lambda V^d)^2 \tilde{\lambda}^{-1} (R^{ab})^{-3}$ with $\tilde{\lambda}$ being averaged elastic constant of the glass ($\tilde{\lambda} \sim E/3$, $E \sim 7 \cdot 10^{11}$ $erg \cdot om^{-3}$ being Young's modulus of silica glass). Assuming $(R^{ab})^{-3} \sim n$ we conclude that it is the product ΛV^d which is to be estimated. Three different approaches yield the estimations of one and the same order: $\Lambda V^d \sim 10$ eV.

We prove the interaction energy to decrease approximately as R^{-3} if $R \gg (V^d)^{1/3}$. Hence with $R^{ab} \sim n^{-1/3}$ the principal term leads to the estimation of the mean interaction energy of the two defects: $U_{sp} \sim (\Lambda V^d)^2 n \tilde{\lambda}^{-1} \sim 10^{-33} \cdot n$. For $n \sim 10^{19}$ om^{-3} the interaction energy is $U_{sp} \sim 10^{-2}$ eV ~ 100 K and hence the phase transition in the defects system is possible at room temperature. In mean field approximation critical temperature of the phase transition is found to be $T_c = 2zU/3 \sim 100$ K for $n \sim 10^{18}$ om^{-3}, U being the mean interaction energy, $z \sim 30$ being the number of nearest defects giving rise to the mean field. At $T \leqslant T_c$ a ferromagnet-like ordered state arises characterized by non-zero mean vector $\langle \vec{J} \rangle$ being an order parameter of the phase transition: $\vec{\eta} = \langle \vec{J} \rangle$.

Using Landau's theory of phase transitions one obtains in the absence of the external field for $T \leqslant T_c$: $\vec{\eta}^2 = a(T_c - T)/2B$, i.e. a uniform order degenerated with respect to the $\vec{\eta}$ direction, a and B being constants of the theory. Hence both

directional and spatial dependencies of $\vec{\eta}(\vec{r})$ are determined by the effective external field $\vec{h}(\vec{r})$ affecting the order parameter. In Landau's theory generalized susceptibility $æ_{ij}$ describing order parameter response to external field in vicinity of phase transition is $æ_{ij} = \lim_{h\to 0} \delta\eta_i/\delta h_j = æ\,\delta_{ij}$, where $æ = [4a(T_c-T)]^{-1}$ if $T \leqslant T_c$ or $æ = [2a(T-T_c)]^{-1}$ if $T > T_c$. Owing to singularity of the susceptibility æ in the phase transition point, the system is strongly influenced by any weak external field and the spatial dependence of the order parameter $\vec{\eta}(\vec{r})$ coincides with that of the $\vec{h}(\vec{r})$ field.

The effective external field arises owing to second-harmonic (SH) wave interacting with non-linear dipole polarization of the defects induced by the pump wave. The oscillating dipole moments $d_i^{2\omega}(\vec{R}^a)$ induced in the defects interact with any SH wave coherent with the pump one. There are two essential cases: (i) interaction with an "external" SH wave generated in the glass owing to non-dipole or non-bulk second-order processes or used for seeding and (ii) interaction with an "internal" SH wave generated owing to the induced macroscopic susceptibility $\chi^{(2)}_{ijk}$.

In the case (i) the effective external field is

$$\vec{h}_1(\vec{r}) = -\frac{\chi^{(2)}_{ijk}\, I^{\omega}(I^{2\omega})^{1/2}}{2n}\left[\vec{e}_1(2+\xi_3)\cos(\Delta\vec{k}\vec{r}) - \vec{e}_2(2-\xi_3)\sin(\Delta\vec{k}\vec{r})\right]$$

where $\Delta\vec{k} = 2\vec{k}^{\omega}-\vec{k}^{2\omega}$, ξ_3 is the pump wave Stokes parameter and $\vec{e}^{\omega} = \vec{e}_1+i\vec{e}_2$ being its polarization vector ($\vec{e}_1\vec{e}_2 = 0$). In general, $\vec{h}_1(\vec{r})$ is a helical field and gives rise to helical spatial dependence of order parameter and susceptibility:

$$\vec{\eta}(\vec{r}) = \eta\left[\vec{e}_1\cos(\Delta\vec{k}\vec{r})-\vec{e}_2\sin(\Delta\vec{k}\vec{r})\right],$$

$$\chi^{(2)}_{ijk}(\vec{r}) = \chi^{(2)}\Big[\left[e_{1_i}\cos(\Delta\vec{k}\vec{r})-e_{2_i}\sin(\Delta\vec{k}\vec{r})\right]\delta_{jk} +$$

$$+ \left[e_{1_j}\cos(\Delta\vec{k}\vec{r})-e_{2_j}\sin(\Delta\vec{k}\vec{r})\right]\delta_{ik} + \left[e_{1_k}\cos(\Delta\vec{k}\vec{r})-e_{2_k}\sin(\Delta\vec{k}\vec{r})\right]\delta_{ij}$$

So helical spatial grating of second-order susceptibility with spatial period $(\Delta k)^{-1}$ is formed in the defects system.

In the other case (ii) the effective field is

$$\vec{h}_2 = \frac{4\pi}{n}\left[\frac{\chi^{(2)} I^{\omega}_{\omega}}{k^{2\omega}_{c}}\right]^2 \left\{L^2\vec{\eta} + 4(1+\xi_3)\left[\vec{\eta} - \frac{(\vec{k}^{\omega}\vec{\eta})\vec{k}^{\omega}}{(k^{\omega})^2}\right]\right\}(\vec{k}^{2\omega}\vec{r}) \sin(\Delta\vec{k}\vec{r}),$$

L being degree of linear polarization of the pump wave. Hence the effective field $\vec{h}_2$ results in an additional term in effective Hamiltonian of the defects system breaking at $T \leqslant T_c$ the isotropy of initial interaction so that the final Hamiltonian is of the same kind as that of easy-plane ferromagnet.

In experiments with no seeding one obtains $h_1 \sim 10^{-13}$ eV for quadrupole SH generation in the bulk glass or $h_1 \sim 10^{-10}$ eV for core-cladding boundary SH generation in optical fibres [4], and in experiments with seeding $h_1 \sim 10^{-7}$ eV. One obtains as well $h_2 \sim 10^{-10}$ eV or $h_2 \sim 10^{-14}$ eV in experiments without seeding and in those with seeding respectively. Both h_1 and h_2 fields are too weak to orientate the defects if no phase transition occurs, but those strongly influence the defects system in vicinity of the phase transition owing to generalized susceptibility æ singularity.

Using our theory we have managed to explain various experimental peculiarities concerning the photo-induced SH generation in doped silica fibres. Detailed discussion as well as some other interesting results see in [5]. Thus we believe the theory to explain practically all main experimental facts known now.

[1] S.S.Jha, N.Bloembergen Phys.Rev. **171** 891 (1968)

[2] V.Mizrahi, Y.Hibino, G.I.Stegeman Opt. Comm. **78**, 283 (1990)

[3] V.O.Sokolov, V.B.Sulimov Izvestia AN SSSR, ser.Fiz. **54**, 2313 (1990) (in Russian).

[4] R.W.Terhune, D.A.Weinberger J.Opt.Soc.Am. , **4**, 661 (1987)

[5] E.M.Dianov, V.O.Sokolov, V.B.Sulimov Submitted to Soviet Lightwave Comm. **1** (1991) .

Distributed out-coupling of second harmonic generation in a waveguide

Z. Weissman, A. Hardy and E. Marom
Faculty of Engineering, Tel Aviv University,
Ramat Aviv 69978, ISRAEL.

Frequency doubling of diode-laser light has been studied recently, to obtain compact short-wavelength coherent sources (e.g. green and blue) for various applications.[1] In some materials, a strong optical nonlinearity is coupled with strong absorption and large dispersion, both of which prevent an efficient out-coupling of the SHG radiation. In many cases the harmonic absorption is strong, whereas the fundamental absorption is weak. This is typical to semiconductors in the vicinity of the band-gap, as well as to some organic materials, which strongly absorb in the green/blue region. In order to benefit from the large nonlinearity of these waveguide materials, it is essential to overcome absorption and dispersion. Whereas dispersion effects may be reduced by using various phase-matching techniques, absorption remains a problem. Here we propose a new way to reduce the effects of harmonic absorption in an SHG waveguide, as well as those of the dispersion.

We recently[2] proposed to use a resonant first-order corrugation (in ω) as a selective reflector(ω)/radiator(2ω) for SHG waveguide resonators. By working off-resonance (see Fig. 1) the reflectivity of the grating in ω can be significantly reduced, whereas the radiative out-coupling in 2ω remains virtually the same, with the radiated harmonic wavefront somewhat tilted from the normal to the surface.

Due to the distributed out-coupling, the generated harmonic photons are constantly extracted through the grating before being absorbed significantly. In addition, the radiated harmonic photons are less affected by possible phase-mismatch in the waveguide. On the other hand, the gradual field extraction prevents second harmonic power buildup. As a result, the conversion efficiency is roughly proportional to the length L - rather than to L^2.

To illustrate the potential of the proposed scheme, we consider the $TM_0^{(\omega)} \rightarrow TE_0^{(2\omega)}$ conversion in a three-layer air/GaP/AlP waveguide, described in Fig. 1. The conversion efficiency ($= P_{out}^{(2\omega)} / P_{in}^{(\omega)}$) was calculated by using the method of Ref. [1]. For comparison, we calculated the conversion efficiency for an equivalent noncorrugated waveguide, with the same power density. The results for the two cases are plotted in Fig. 2, as a function of L. It is clear that the corrugated waveguide is more efficient than the noncorrugated one, particularly as L increases.

Finally, to asses the quality of the radiated harmonic beam, we calculated the far-field pattern for L=0.8mm. We note (see Fig. 3) that most of the beam energy is contained in a main narrow lobe. The angular width of the main lobe is approximately 1mrad, i.e. very close to the

diffraction limit.

To conclude, a nonresonant first-order corrugation (in ω) reduces the destructive effects of strong harmonic absorption and (to a lesser extent) dispersion, through a distributed out-coupling of the second harmonic power. The resulting harmonic beam has a narrow angular spectrum in the longitudinal dimension and thus the beam can be focused easily. By using such a grating scheme, some semiconductor and organic waveguide materials could be used more efficiently for frequency doubling of laser-diode light.

References

1. For example: M.K. Chun and L. Goldberg, IEEE Lasers and Electro-optics society 1990 Annual meeting (Boston), Paper ELT8.2.

2. Z. Weissman, A. Hardy, E. Marom and S.R.J. Brueck, Jour. Appl. Phys., 1209, **69**, 1991.

figures

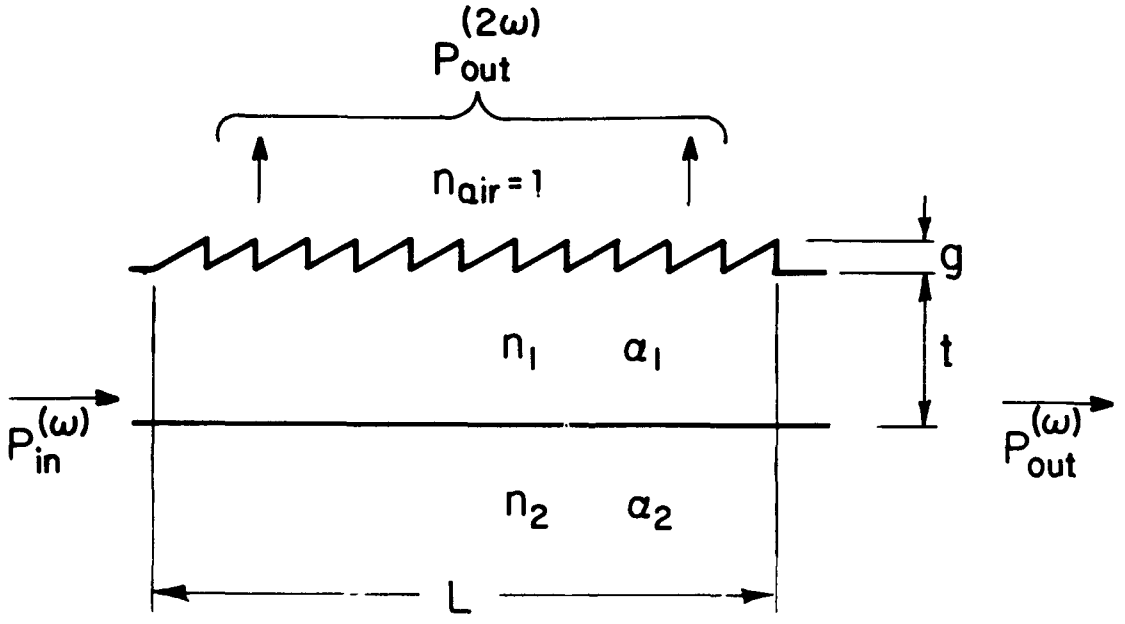

Fig. 1 A corrugated waveguide with distributed out-coupling of the SHG power.

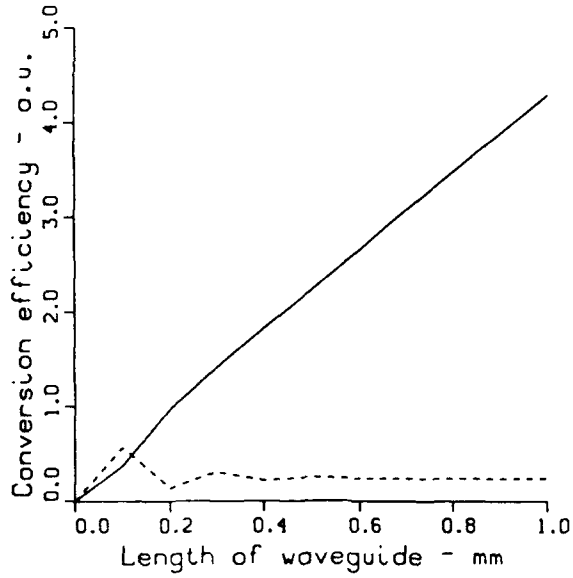

Fig. 2 Conversion efficiency of corrugated (solid line) and noncorrugated (dashed line) waveguide. Referring to Fig. 1b and to the formulation of Ref. 2, the data is as follows: $g = 0.1\mu m$, $t = 0.3\mu m$, $n_1^{(\omega)} = 3.105$, $n_1^{(2\omega)} = 3.482$, $n_2^{(\omega)} = 2.76$, $n_2^{(\omega)} = 2.95$, $\alpha_1^{(\omega)} = 0.1cm^{-1}$, $\alpha_1^{(2\omega)} = 63cm^{-1}$, $\alpha_2^{(\omega)} = 0.1cm^{-1}$, $\alpha_2^{(2\omega)} = 12cm^{-1}$, $\delta^{(\omega)} = 10^4 cm^{-1}$, $d_1^{(2\omega;\omega,\omega)} = 0.5d_1^{(\omega;2\omega,-\omega)} = 99 \cdot 10^{-6} \frac{m}{V}$.

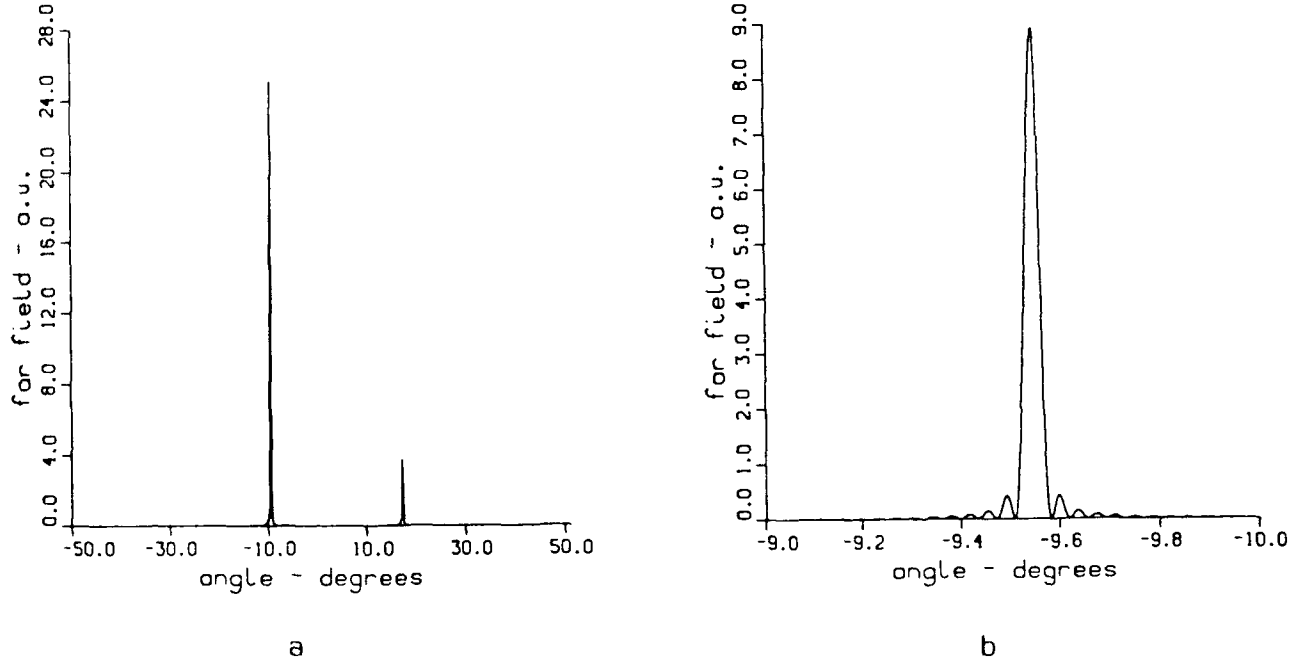

Fig. 3 The far-field pattern of the harmonic beam, for L=0.8mm (the angle is from the normal to the surface): a. Global view. b. Magnified view of the main lobe.

Poster Session: 6

TuG 5:30pm–7:00pm
Boys Smith Room

NONLINEAR CDS GRATING COUPLER : C.W. AND PULSED OPERATION

M.Bertolotti, F.Michelotti ,C.Nisio, E.Fazio, G.Assanto(*), C.Cali'(+)

Dipartimento Di Energetica , Universita' di Roma I, Via Scarpa 16 ,00161 Roma, Italy
and
GNEQP of CNR
(*) CREOL , Orlando, Florida , U.S.A.
(+) CRES, Via regione Sicilia, Monreale, Palermo and Univesrita' di Palermo, Italy

Distributed couplers , such as prisms and gratings, have been largely employed in conjunction with nonlinear planar waveguides in order to study the nonlinear properties of the structures , suitable for all optical devices in integrated optics.
In the present work we report an experimental investigation of a semiconductor nonlinear grating coupler realized onto a planar linear waveguide, where the grating is burried between the guide and the substrate (the periodicity is 0.8 μm) but over the guide ,in correspondence of the grating , there is a thin layer (200 A) of CdS. A single mode ($\lambda = 0.632\mu$m) is supported by the guide while two modes are present if an Ar laser or the second harmonic of Nd-Yag pulsed laser is used .

Radiation is coupled out through a prism . Input coupling effects have been studied in both temporal c.w. and pulsed regime versus input power .
In c.w. operation all the obtained results are interpreted in terms of optothermal dispersive and absorbitive effects, while in the ps time domain electronic nonlinear behaviour of the CdS is the main responsible of the refractive index change of CdS.

Polarization induced switching and bistability in a nonlinear prism coupler.

Jan DANCKAERT *, Guy VITRANT ** and Raymond REINISCH **.

* Applied Physics Department (TONA/TW), Vrije Universiteit Brussel
Pleinlaan 2, B-1050 Brussel, Belgium, tel. 32-2.641.35.69.

** Laboratoire d'Electromagnétisme, Microondes et Optoélectronique (LEMO-ENSERG)
B.P. 257, 38016 Grenoble Cédex, France, tel. 33-76.87.69.76.

Polarization may be an interesting parameter in optical computing devices [1]. Polarization induced irradiance switching was proposed as a new switching mechanism in nonlinear Fabry-Perot (NLFP) etalons under oblique incidence [2]. In this context, the stationary response of Fabry-Perot etalons containing an anisotropic medium exhibiting a diffusive Kerr-type nonlinearity was investigated [3]. Here, we will adress the question of the influence of polarization on the response of a nonlinear prism coupler (NLPC), where the waveguide shows a diffusive third order nonlinearity.

Prism coupling of light into integrated nonlinear optical waveguides has been the subject of extensive theoretical and experimental investigation over the past few years [4]. It is established that in the case of a diffusive nonlinearity, both plane wave and finite beam calculations yield a bistable optical response in good agreement with the experimental observations [5].

Since a NLPC is equivalent to a nonlinear Fabry-Perot resonator (NLFP) under oblique incidence [6], the modal theory developed to study the dynamical behaviour of the NLFP [7,8] applies here. In fact, the behaviour of all types of nonlinear planar resonators can be described by this equation :

$$2i\omega_0 (\partial\beta_m^2/\partial\omega^2) \frac{dA_g}{dt} + \left[\beta_m^2 - \beta_0^2 + \eta U \right] A_g + i\kappa_m^2 A_g = i\xi A_i(t) \qquad (1)$$

Here A_g (A_i) is the guided (incident) field amplitude, $\beta_m^2 - \beta_0^2$ is the detuning from the m^{th} resonance, κ_m is the resonance width, and depends on the device parameters, as does ξ. The nonlinear term is described by U, where η is the sign of the nonlinearity.

For a diffusive nonlinearity, also the response for TM polarized light is governed by the same equation. The linear, stationary response curves for TE and TM polarized light of the NLPC under study here (Fig. 1a) are shown in Fig. 1b.

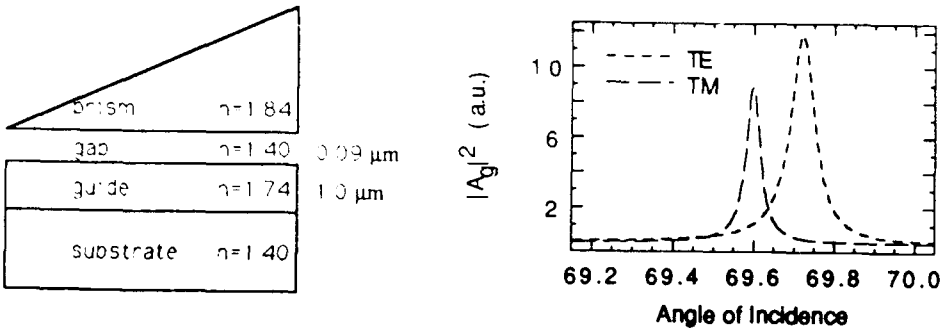

Fig.1. a. Structure and parameters of the NLPC under consideration.
b. Linear and stationary response for TE and TM polarized incident light.

The nonlinear and time-dependent response of a NLPC, subject to an incident plane wave of arbitrary polarization (characterized by a polarization angle ϕ, where $\phi = 0°$ (90°) for TE (TM) polarization), is given by two equations of the same kind as Eq (1). These two equations, one for each polarization component, are coupled through the nonlinear term, which depends on the total waveguide irradiance (TE and TM).

In the dynamical regime, we solved these equations numerically, together with a Debye equation for the nonlinear term U (γ is proportional to the nonlinear refractive index n_2):

$$\frac{\partial U}{\partial t} = -\frac{U}{\tau} + \gamma \left(|A_g^{TE}|^2 + |A_g^{TM}|^2 \right) \qquad (2)$$

We observed several interesting phenomena relying on a change of the polarization state of the incoming wave. In Fig. 2 an example of polarization induced irradiance switching is shown, i.e. the NLPC, initially in the high-TE state, is switched down, by changing the polarization angle from 0° (point labeled 1) to 90° (label 2) and back (label 3) and keeping the incident irradiance constant. The device cannot be made to switch up again using the same switching mechanism, i.e. by only changing the polarization angle. This is a dynamical confirmation of previous conclusions drawn from an analysis of the stationary response for a NLFP etalon [2].

Next, we consider the dynamic (Fig. 3b) response of the same device for a different detuning (stationary response is shown in the inset). Here, an example of polarization induced bistability is presented, where the guided wave irradiance of both the TE and the TM component describe a full hysteresis cycle as a function of the polarization angle, the incident irradiance again being kept constant. Also the total irradiance describes a hysteresis cycle (not shown on the figure), but with a much smaller contrast than the TE and TM ones. Notice that a change of about 5° in the polarization state of the input beam is sufficient to create a change of more than 50° in the polarization state of the guided wave.

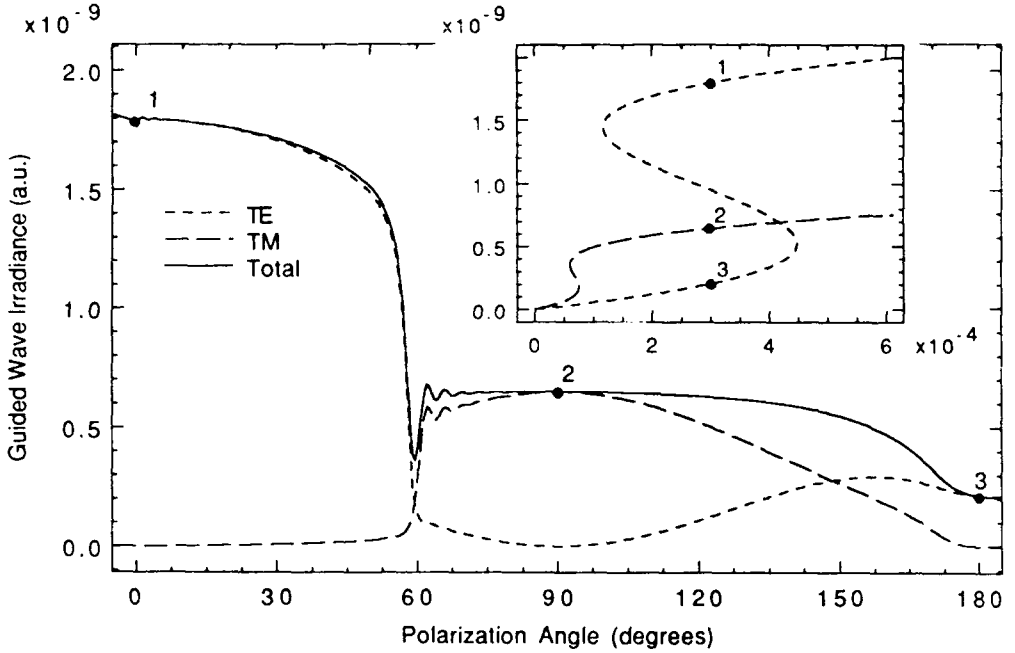

Fig. 2. Polarization induced irradiance switching. The stationary response curves for TE and TM are shown in the inset. The incident angle is 69.55°, the Debye time 5ps, and the incident irradiance was fixed at a value of $3\ 10^{-4}$. The nonlinearity was taken to be negative.

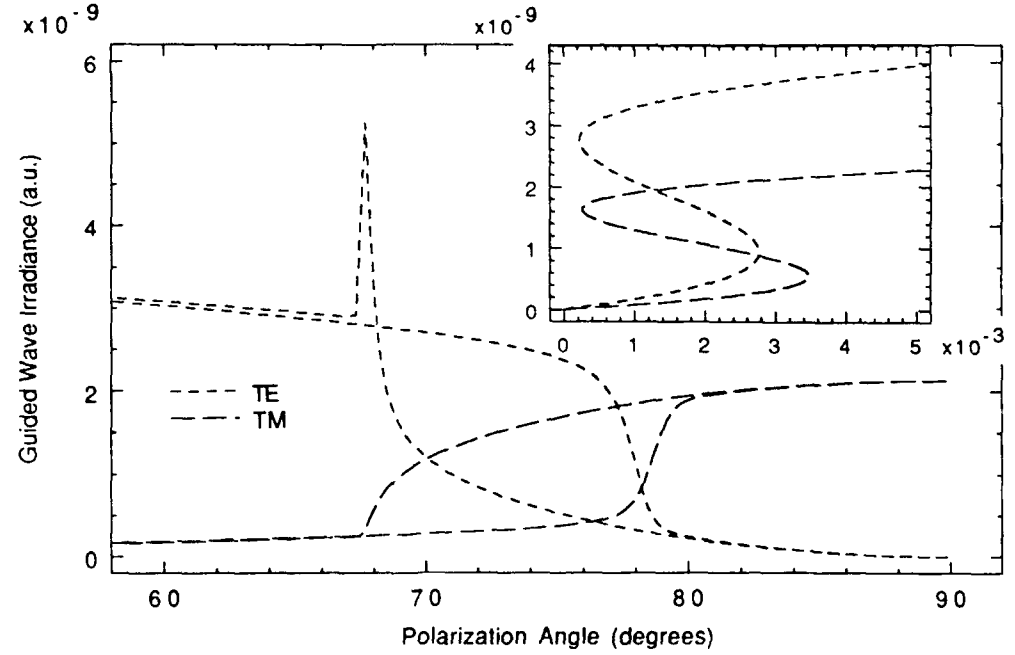

Fig. 3. Polarization bistability. In the inset, the stationary response curves for an incident angle (detuning) of 69.4° for TE and TM are shown. The dynamic response was plotted with a Debye time of 50 ps and at a fixed value of the incident irradiance of $3\ 10^{-3}$.

To summarize, we have investigated the influence of polarization on the dynamic plane wave response of a prism coupler with a waveguide exhibiting a diffusive nonlinearity. Examples of polarization induced irradiance switching and polarization optical bistability were shown. These phenomena can be used in devices for polarization logic, for transducers from polarization logic to irradiance logic and back, and as a tool to investigate the nonlinear properties of materials. We wish to stress that the modal theory used here is valid for all planar resonators of sufficiently high finesse. Hence it can also be applied to nonlinear grating couplers, and to nonlinear Fabry-Perot etalons filled with an isotropic medium under oblique incidence or with a medium exhibiting an intrinsic anisotropy.

REFERENCES :

1. A. Korpel and A.W. Lohmann, Applied Optics **25**, 1528, 1986.
2. H. Thienpont, L. Peirlinckx, M. Smedts and I. Veretennicoff, *Optical Computing 88*, Proc. SPIE **963**, 148 (1989) ; H. Thienpont, Ph.D. dissertation (Vrije Universiteit Brussel, Brussels, Belgium, 1990).
3. J. Danckaert, H. Thienpont, V. De Schutter, W. Lintermans, I. Veretennicoff, *ECOOOSA'90 Quantum Optics*, to be published by A. Hilger (London, 1991).
4. G.I. Stegeman et al., IEEE J. of Lightwave Tech. **6**, 953, 1988 ; and references therein.
5. G. Vitrant, R. Reinisch, J.C. Paumier, G. Assanto, G.I. Stegeman, Optics Lett. **14**, 898 (1989).
6. M. Haelterman, G. Vitrant and R. Reinisch, J. Opt. Soc. Am. **B7**, 1309 (1990) ; G. Vitrant, M. Haelterman and R. Reinisch, J. Opt. Soc. Am. **B7**, 1319 (1990).
7. M. Haelterman and G. Vitrant, Technical Digest on Nonlinear Dynamics in Optical Systems, (post-deadline paper PdP5, O.S.A., 1990).
8. G. Vitrant, M. Haelterman, G. Martinelli, A. Barthélémy, C. Froehly, *ECOOOSA'90 Quantum Optics*, to be published by A. Hilger (London, 1991).

Paper Withdrawn

Nonlinear bent directional couplers with asymmetrical distribution of nonlinearity

Mirosław A. Karpierz

Institute of Physics, Warsaw University of Technology
Koszykowa 75, 00-662 Warszawa, Poland

Recently, the nonlinear directional couplers have been extensively investigated as optical devices for ultra high-speed data processing [1-7]. They were analyzed for parallel waveguides [2-5] as well as for configuration with bending waveguides [5-6], which is more insensitive with respect to fabrication tolerances of the device length. In most of previously analyzed nonlinear directional couplers there was assumed the symmetrical distribution of nonlinearity. However, it has been shown that for asymmetrically placed nonlinear material the required switching power is lower than for symmetrical case [7].

In this paper the influence of asymmetry of nonlinear refractive index distribution for transmission characteristics of nonlinear bent directional coupler is analyzed. The coupled mode theory [8] is used and numerical results show that the critical power is strongly dependent on asymmetry of nonlinearity distribution.

The TE-type electric field in the investigated nonlinear bent directional coupler (fig. 1.) may be expressed in the form:

$$E(x,y,z) = a_1(z)\, \mathcal{E}_1(x,y,z) + a_2(z)\, \mathcal{E}_2(x,y,z) , \qquad (1)$$

where $\mathcal{E}_j$ (j=1,2) are the normalized modes of the isolated waveguides and a_j are their complex amplitudes. It is taken into consideration the Kerr-type nonlinearity with the electric permittivity $\varepsilon=\varepsilon_L+\varepsilon_{NL}|E|^2$, and it is assumed that a distribution of a linear part of electric permittivity ε_L is symmetrical (i.e. linear waveguides are identical). Then the coupled mode

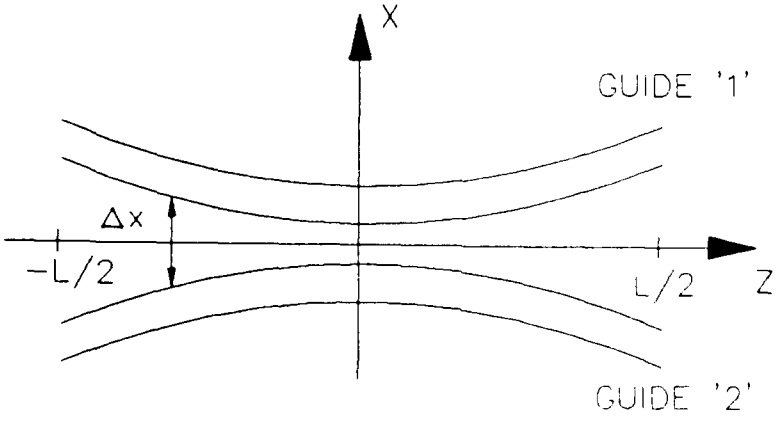

Fig. 1. Schematic diagram of a nonlinear bent directional coupler.

equations for amplitudes a_1 and a_2 can be written in the form:

$$\begin{aligned} ia_1' &= \beta a_1 + qa_2 + w_1|a_1|^2 a_1 , \\ ia_2' &= \beta a_2 + qa_1 + w_2|a_2|^2 a_2 , \end{aligned} \qquad (2)$$

where the prime indicates differentiation with respect to z and β is a linear propagation constant. The linear coupling coefficient q is assumed to be slowly dependent on z: $\partial q(z)/\partial z << q/L$ (where L is an effective length of a coupler).
Consequently w_j (j=1,2) are the nonlinear coefficients defined as follows:

$$w_j = \frac{\omega}{\mathcal{P}} \varepsilon_0 \iint dxdy \; \varepsilon_{NL} \mathcal{E}_j^4, \quad j=1,2 \qquad (3)$$

and there were neglected in eq. (3) the remained nonlinear coefficients:

$$\iint dxdy \; \varepsilon_{NL} \mathcal{E}_1^m \mathcal{E}_2^{4-m} \cong 0, \quad m=1,2,3.$$

In the symmetrical distribution of nonlinear electric permittivity (i.e. for $\varepsilon_{NL}(-x)=\varepsilon_{NL}(x)$, $\varepsilon_{NL}(-y)=\varepsilon_{NL}(y)$) the coefficients (3) are identical $w_1=w_2$ but for asymmetrical distribution of nonlinearity $w_1 \neq w_2$. Following this it is convenient to introduce dimensionless coefficient of asymmetry $\eta = (w_1-w_2)/\varphi_0$ where $\varphi_0=(w_1+w_2)$. The absolute value of this coefficient $|\eta| \leq 1$ is proportional to the asymmetry of nonlinear medium distribution ($\eta=0$ for symmetrical cases) and the sign depends on waveguide in which nonlinearity is greater. The nonlinearity in the waveguide '1' correspond to $\eta>0$ and nonlinearity in the waveguide '2' correspond to $\eta<0$ respectively. It is assumed additionally that both parameters φ_0 and η are constant and independent on z ($d\varphi_0/dz = d\eta/dz = 0$).

Equations (2) are conveniently rewritten in terms of the real dimensionless parameters analogous to the Stokes parameters:

$$\begin{aligned} S_0 &= (|a_1|^2+|a_2|^2)\varphi_0/q_0, \\ S_1 &= (|a_1|^2-|a_2|^2)\varphi_0/q_0, \\ S_2 &= (a_1 a_2^* + a_1^* a_2)\varphi_0/q_0, \\ S_3 &= -i(a_1 a_2^* - a_1^* a_2)\varphi_0/q_0, \end{aligned} \qquad (4)$$

where $q_0 = q(z=0)$. Then the evolution equations for parameters (4) are found from eq. (2) in the form:

$$\begin{aligned} S_1' &= -2qS_3, \\ S_2' &= \frac{1}{2} q_0 (S_1+\eta S_0) S_3, \\ S_3' &= 2qS_1 - \frac{1}{2} q_0 (S_1+\eta S_0) S_2 \end{aligned} \qquad (5)$$

and S_0 = const.

The eqs (5) may be solved for arbitrary function q(z) slowly varying with respect to z. In this paper there are analyzed bending waveguides analogous to that from paper [5], i.e. for $\Delta x \sim z^2$ and then

$$q(z) = q_0 \exp[-\gamma z^2], \tag{6}$$

where γ is constant.

Figure 2 presents the nonlinear cross power transmission $I_2(L/2)/I_1(-L/2)$ versus input intensity for various values of asymmetry coefficient η. There were used the dimensionless intensities $I_j=|a_j|^2\varphi_0/q_0=(S_0\pm S_1)/2$ where j=1,2 correspond to the intensity in waveguide '1' and in waveguide '2' respectively. As an boundary condition it was assumed that the light is initially launched to the waveguide '1' i.e. $|a_2|=0$ and consequently $S_1(-L/2)=S_0=I_1(-L/2)$ and $S_2(-L/2)=S_3(-L/2)=0$. The numerical results were done for parameters of bending waveguides $\gamma=0.9$ and $q_0=1.7$. Such values allows to cross-state transmission for low input intensities and correspond to typical semiconductor-doped glass directional coupler structures [5].

The results plotted in fig.2. show that the critical value of input power appears to be strongly dependent on asymmetry of nonlinear refractive index distribution. For $\eta>0$ the switching power is lower then for symmetrical configuration. Respectively for $\eta\cong-0.3$ the transmission is almost independent on input intensity, but for the case $\eta=-1$ the nonlinear effect appears approximately at the same input intensity as for $\eta=1$. Such behavior leads to nonreciprocity in switching characteristics between channels in nonlinear directional coupler. This can be the basis of construction logic gates for signals incoming from various waveguides.

REFERENCES

1. G.I.Stegeman and E.M.Wright, Opt. & Quantum Electron. vol.22, No.2, pp 95-122 (1990)
2. S.M.Jensen, IEEE J.Quantum Electron. vol. QE-18, No.10, 1580-1583 (1982).
3. A.A.Maier, Sov.Quantum Electron. vol.9, No.11, 2296-2302 (1982).
4. S.Trillo and S.Wabnitz, Appl.Phys.Lett. vol.49, No.13, 752-754 (1986).
5. V.Leutheuser, U.Langbein, and F.Lederer, Opt. Commun. vol.75, No.3,4, pp 251-255 (1990).
6. M.Guntau, T.Possner, A.Brauer, and P.Dannberg, Proc.SPIE vol.1513, *ECO'91* (1991).
7. M.A.Karpierz, D.F.Clark, I.Andonovic, and B.Culshaw, Proc.SPIE vol.1085, *Optical fibers and their applications* (1989).
8. D.Marcuse, *Theory of dielectric optical waveguides*, Academic Press, New York 1974.

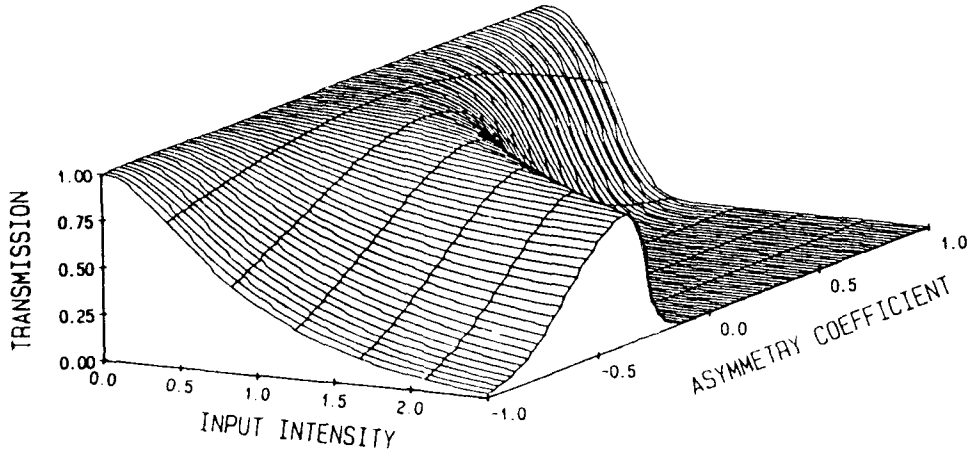

(A)

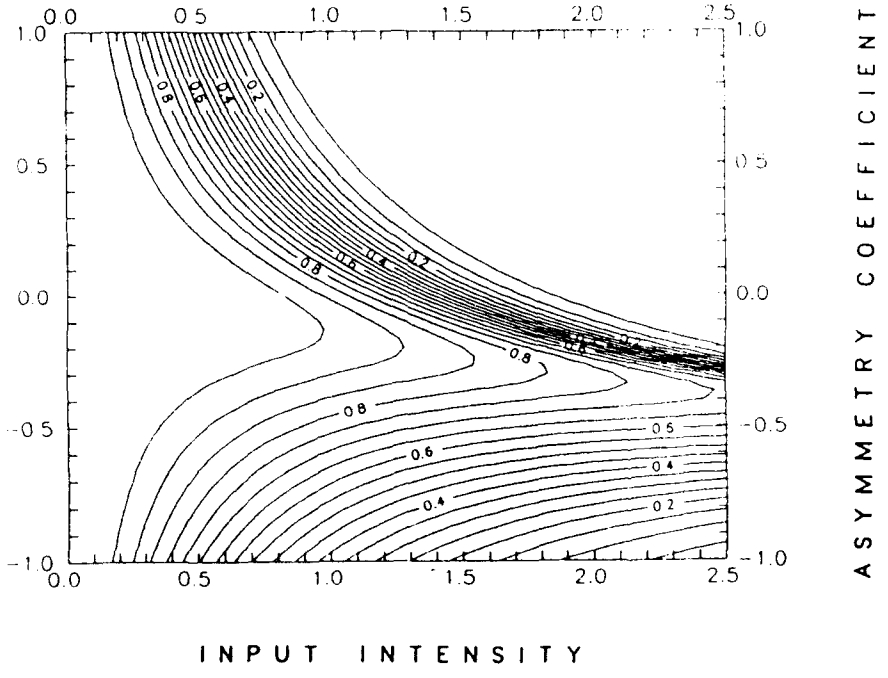

(B)

Fig. 2. Cross power transmission characteristics versus coefficient of asymmetry η (A) and contour lines corresponding to them (B).

Directional Couplers with Varying Placement of Nonlinearity in Quaternary Semiconductors

C. P. Hussell, R. Srivastava, and R. V. Ramaswamy
Photonics Research Laboratory, Department of Electrical Engineering
University of Florida, Gainesville, FL 32611
Phone: (904) 392-0990 Fax: (904) 392-4765
and
M. Bloemer, and P. Ashley
U.S. Army Missile Command
Redstone Arsenal, AL 35898
Phone: (205) 876-4685 Fax: (205) 876-4759

The large optical nonlinearities exhibited by III-V multiple quantum well (MQW) materials[1] have afforded some optimism in achieving large all-optical switching ratios with low threshold power and short device length. By using multiple quantum wells in the coupling as well as the guiding regions, Kam Wa et al. was the first to demonstrate partial switching between two parallel GaAs/AlGaAs MQW channel waveguides.[2] This device, however, exhibited very high loss. Cada et al. argued that much better performance in terms of lower loss may be achieved by placing the MQW nonlinear medium in the coupling region only,[3] but the experimental device still exhibited only partial switching.[4] Several approaches to solve the problem of the nonlinear directional couplers in semiconductors have been proposed and since no general exact analytical treatment including absorption and nonlinear saturation is available, approximations or numerical simulation must be used. In this regard, Caglioti et al.[5] presented a more complete analytical estimate for the characteristics of nonlinear directional couplers for operation above the resonance with large detuning.

In this paper, we consider the potential characteristics of a nonlinear directional coupler in quaternary III-V semiconductor materials using realistic values of the nonlinearity and study its role as a function of its location within the directional coupler. These compounds are important because they are useful in the region of two important communications wavelengths: 1.3 and 1.55μm. To take advantage of the large absorptive nonlinearities in these materials, we consider the case when the device is operated just below the bandgap; ie., with small detuning below the resonance. This contrasts most previous analysis. In our analyses, we use the beam propagation method (BPM) to simulate such a device using realistic values for all the material properties. We choose not to use the standard coupled-mode approach since, in the case of negative nonlinearity, the coupling increases with power and the theory breaks down for large coupling. We simulate the response of devices using two different placements of the MQW nonlinearity: in the guiding regions of the two waveguides and in the coupling region only.

The model for the nonlinear refractive index and saturation is assumed to be given by $n^2=n_b^2+\delta\chi$ where n is the total complex index (including absorption), n_b is the total complex index at very high powers ($E\rightarrow\infty$), and $\delta\chi$ is the resonant contribution to the susceptibility, which, for a saturable two-level system can be written as[6]

$$\delta\chi = \frac{q_1(\delta_t+i)}{1+\delta_t^2+q_2E^2} \approx -\frac{2n_b\Delta n_{sat}}{1+I/I_{sat}},$$

where δ_t is the normalized detuning from resonance, q_1 and q_2 are real constants determining the maximum index change and the saturation intensity respectively, and E is the electric field amplitude. The approximation is based on the premises that

$$n = n_o + \frac{\Delta n_{sat}(I/I_{sat})}{1+(I/I_{sat})},$$

where n_0 is the low power complex refractive index, Δn_{sat} is the maximum complex index change at the specified detuning, I is the local intensity, and I_{sat} is the saturation intensity. This approximation turns out to be very good since Δn_{sat} is considered to be much lower than n_0. These constants are related by

$$q_1 = -\frac{2n_o\Delta n_{sat}(1+\delta_t^2)}{(\delta_t+i)} \text{ and } q_2 = \frac{n_o(1+\delta_t^2)}{2\eta_o I_{sat}},$$

where η_0 is the free space impedance. For all the modeling in this paper, we assume that δ_t=1. Since the imaginary part of n_0 can be neglected, this implies that the imaginary and real parts of Δn_{sat} are equal.

The specific quaternary material system considered in our investigation is InGaAsP/InP and MQWs made from these materials. Very low loss was achieved for bulk InGaAsP layers on InP by McIlroy et al.[7] Therefore, for our analysis, we consider the absorption and nonlinear index only in the MQW layers and neglect them in the InGaAsP and InP layers. The linear indices for $In_{1-x}Ga_xAs_yP_{1-y}$ and InP are well known.[8] In order to operate at a wavelength of λ=1.3μm, slightly longer than the bandgap wavelength, we chose the arsenic fraction to be y=0.47 and the gallium content to be x=0.1894y/(0.4184-0.013y) for proper lattice match with InP. This gives an index of 3.424 for the InGaAsP layers and an index of 3.210 for InP at the chosen wavelength. Since refractive index data are scarce for MQW layers in these materials, we approximate these using the method of Born and Wolf[9] for the calculation of the mean refractive index. This approach is reasonable in the region where the excitonic contribution to the low-power refractive index can be ignored. With a ratio of the well to barrier thickness of 2.5, the index of the MQW layer is 3.273 for TE modes and 3.267 for TM modes. The power dependence for the refractive index and absorption of these materials are also not well known. Therefore, we borrow the data from ternary MQW materials expecting the values for the saturated absorption and refractive index to be similar. According to Park et al.,[1] for MQWs in GaAs/AlGaAs, the low power absorption coefficient just below the bandgap is about 1000 cm^{-1} and the saturated index change is as large as -0.10. According to Miller et al.,[4,10] the low power absorption coefficient just below the bandgap is about 1000 cm^{-1}, the saturation intensity is about 200 W/cm^2, and the maximum change in the refractive index is about 2×10^{-3}. Accepting these values for InGaAsP/InP materials is justified since the same nonlinear mechanisms are expected to be dominant in each case.

Figure 1 shows the first device structure under consideration. It consists of the MQW nonlinearity placed only in the guiding regions. The low-power coupling length l_c=532μm. We

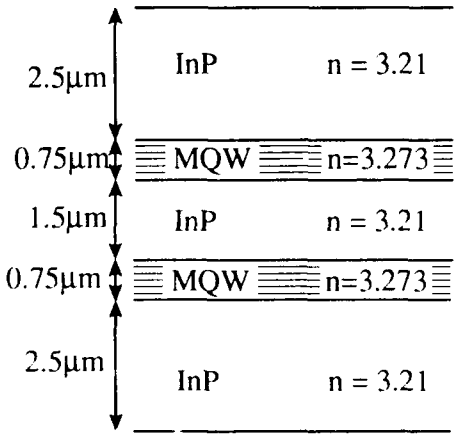

Figure 1. Device structure with MQWs in the guiding regions.

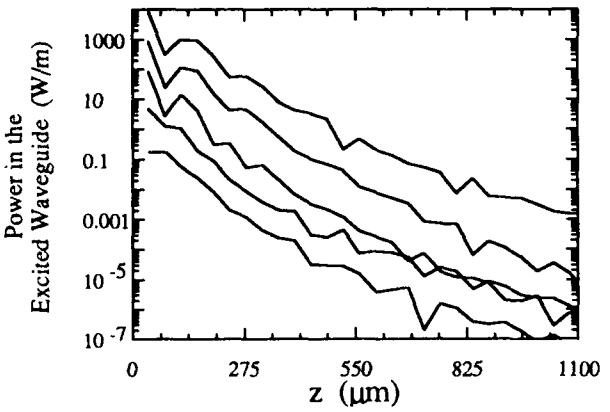

Figure 2. Result of propagation through the device of figure 1 with an absorption coefficient of 333cm^{-1}.

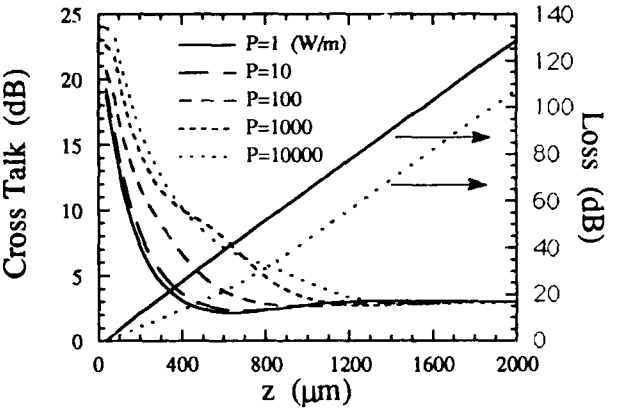

Figure 4. Result of propagation through the device of figure 3 with an absorption coefficient of 1000cm^{-1}.

start with an estimate of the low-power absorption for the MQW regions of 333cm^{-1}, i.e., the low power refractive index n_o=3.273-3.445×10^{-3}i. From the data above, Δn_{sat}=-2×10^{-3}. Figure 2 shows the power remaining in the excited waveguide versus length along the propagation direction z of the directional coupler for varying powers over several orders of magnitude. No switching is observed.

Figure 3 shows the second device structure under investigation in which the MQWs are placed only in the coupling region and l_c=609μm. The waveguides are formed by the two InGaAsP

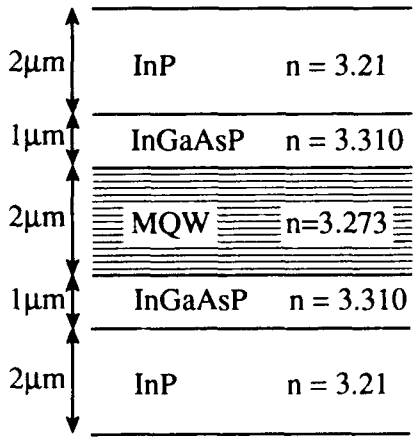

Figure 3. Device structure with MQW in the coupling region only.

layers with arsenic fraction of y=0.21 which have refractive indices of 3.310. Taking a more conservative estimate for the low-power absorption coefficient for the MQW region of 1000cm^{-1}, figure 4 shows the cross talk for input powers over several orders of magnitude and the loss for the two extreme cases, calculated using

$$\text{cross talk} = -10\log\left[\frac{P_2}{(P_1+P_2)}\right]$$

and

$$\text{loss} = -10\log\left[\frac{(P_1+P_2)}{P_{in}}\right],$$

versus propagation length along the device. P_1 is the power in the waveguide excited, P_2 is the power coupled to the other waveguide, and P_{in} is the total input power. Partial switching is observed only for $z=l_c$. This result is in excellent agreement with the experimental results of Cada et al.[4] At low power, at best only about 3dB cross talk may be achieved, but at high power, much better (10dB) switching is observed. Figure 5 shows the results when the low-power absorption coefficient is 333cm^{-1} (all other parameters are assumed to be the same). In this case, reasonably good switching is achieved at $z=l_c$ and $z=2l_c$. For this case, figure 6 shows the cross talk versus power for one, two and three coupling lengths. The curve for two coupling lengths exhibits a better switching fraction and sharper switching characteristics, but at the cost of increased losses.

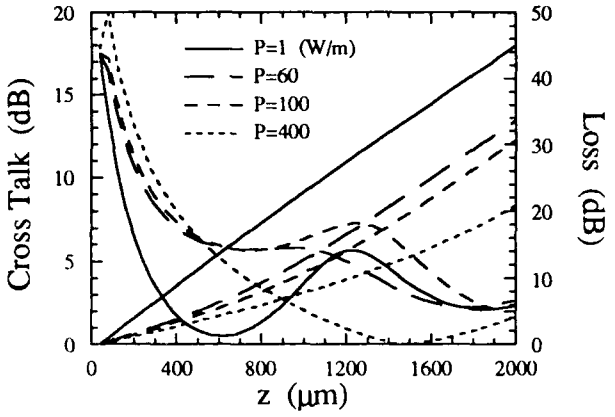

Figure 5. Result of propagation through the device of figure 3 with an absorption coefficient of 333cm^{-1}.

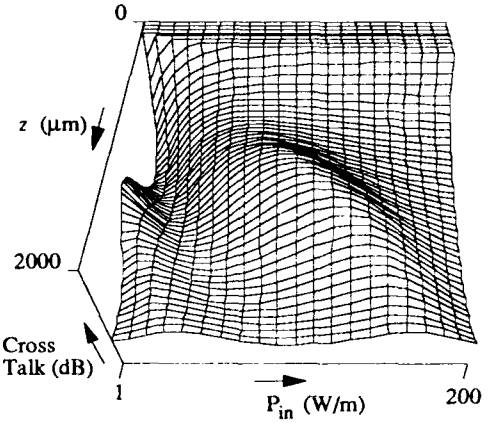

Figure 7. Surface plot of the cross talk versus power and device length.

These results are in qualitative agreement with those of Caglioti et al.[5] for positive nonlinearity. This may be contributed to the fact that with the nonlinearity placed in the coupling region only, the modes become more guided as the power increases as in the case with positive nonlinearity in all layers. Finally, figure 7 shows a surface plot of the cross talk versus power and device length. From this, it is observed that at either coupling length the switching characteristics are not sharply dependent on the actual device length since the plot is slowly varying.

In conclusion, we have supported the claim of Cada et al.[3] that the performance of devices in these materials is more easily optimized if the MQW nonlinearity is placed in the coupling region only. For the data we used, based on measurements in ternary materials, we observe that the quality of the device is marginal at best. However, it is a worth while endeavor to measure the nonlinear properties of these materials since, as we (and others) have shown, the characteristics improve drastically as loss is decreased.

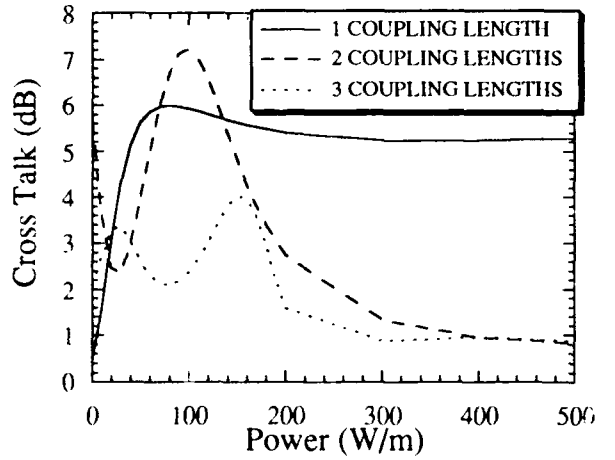

Figure 6. Cross talk versus power for the device of figure 3 with an absorption coefficient of 333cm^{-1}.

References:

[1] S. H. Park, et al., *Appl. Phys. Lett.*, vol. 52, pp. 1201-1203, 1988.

[2] P. Li Kam Wa, et al., *Electron. Lett.*, vol. 21, pp. 27-, 1985.

[3] M. Cada, et al., *Appl. Phys. Lett.*, vol. 49, pp. 755-757, 1986.

[4] M. Cada, et al., *J. Opt. Soc. Am. B*, vol. 5, pp. 462-466, 1988.

[5] E. Caglioti, et al., *J. Opt. Soc. Am. B*, vol. 5, pp. 472-482, 1988.

[6] L. Thylen, E. M. Wright, and G. I. Stegeman, *J. Opt. Soc. Am. B*, vol. 5, pp. 467-471, 1988.

[7] P. W. A. McIlroy, et al., *Electron. Lett.*, vol. 23, pp. 701-703, 1987.

[8] B. Broberg, and S. Lindgren, *J. Appl. Phys.*, vol. 55, pp. 3376-3381, 1984.

[9] M. Born and E. Wolf. *Principles of Optics*. Oxford, England: Pergamon Press, 1980.

[10] D. A. B. Miller, et al., *Appl. Phys. Lett.*, vol. 41, pp. 679-681, 1982.

NONLINEAR DIRECTIONAL COUPLER SWITCHED BY THE EXTERNAL WAVE

Ewa Weinert-Rączka
Institute for Physics, Technical University of Szczecin,
Al.Piastów 19, 70-310 Szczecin, Poland, Tel 0048-91-39114.
Jan Petykiewicz
Institute for Physics, Warsaw University of Technology,
ul. Koszykowa 75, 00-662 Warszawa, Poland.

A typical Nonlinear Directional Coupler (NLDC) permits power dependent energy transfer between two adjacent waveguides. The output of the device can be controlled by the input power solely for high energy signals. For weak fields NLDC works like a linear coupler with the output dependent only on the device design. NLDC working with weak modes and controlled by a strong field at a different frequency guided by the central region of the coupler was proposed by Lederer et al. [1] .

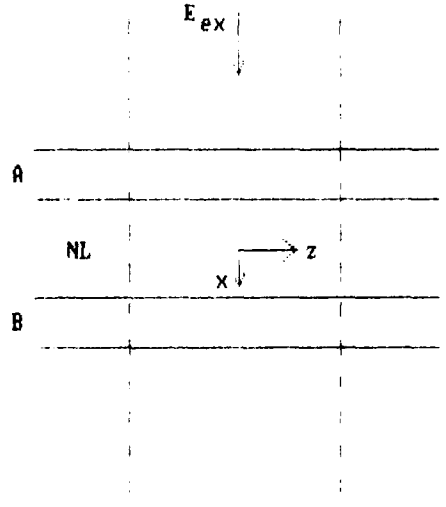

Fig.1. Geometry of the problem

The coupler considered here has the geometry of a traditional parallel NLDC [2] sketched in Fig.1. The central region of the coupler, where the evanescent fields of two guided modes overlap exhibits a local nondispersive Kerr nonlinearity. For weak guided modes a periodic power exchange between two waveguides occurs similarly as in the linear coupler. The nonlinear mode of operation is obtained with the help of a strong field incident from outside on the couplers surface. As a result of the interaction between the external wave and the guided field the power dependent changes of a coupling coefficient are obtained.

The external wave is taken as a strong y-polarized field at the frequency ω propagating in x direction. Its parameters inside the central region of the coupler are given by

$$E_{ex} = E_{ex}(z)\exp(i\omega t - i\gamma x) + c.c., \qquad (1)$$

where $E_{ex}(z)$ describes the slowly varying amplitude and γ is the propagation constant. The x dependence of the amplitude due to a self-focusing in the narrow central region was neglected.

The y-polarized weak field propagating in a coupler consisting of two identical weakly coupled monomode waveguides can be represented by a sum of single waveguides modes.

$$E_g = A(z)E_A(x)\exp(i\omega t - i\beta z) + B(z)E_B(x)\exp(i\omega t - i\beta z) + c.c. \quad (2)$$

where $E_A(x)$, $E_B(x)$ and β represent the transverse configurations and propagation constant of the modal fields of guides A and B in isolation, respectively.

The polarization due to the nonlinear response of the central region material is

$$P^{NL} = \chi(x)E_{ex}|E_{ex}|^2 + \chi(x)E_g|E_{ex}|^2 \quad (3)$$

where the non-phase matched terms and the terms proportional to $|E_g|^2$ were neglected. After application of the Coupled Mode Theory Methods [2,4] to the field propagating along the coupler the following set of differential equations is obtained:

$$dA(z)/dz = i\eta(z)A(z) + i\varkappa(z)B(z), \quad (4)$$

$$dB(z)/dz = i\eta(z)B(z) + i\varkappa(z)A(z), \quad (5)$$

where $\eta(z) = \eta_0 + \eta_N|E_{ex}(z)|^2$ and $\varkappa(z) = \varkappa_0 + \varkappa_N|E_{ex}(z)|^2$. Constants η_0, η_N, $\varkappa_0$ and $\varkappa_N$ for a symmetric coupler are given by the following overlap integrals:

$$\eta_0 = \omega\varepsilon_0\int[\varepsilon(x)-\varepsilon^A(x)]|E_A(x)|^2dx, \quad (6)$$

$$\eta_N = \omega\varepsilon_0\int\chi(x)|E_A(x)|^2dx, \quad (7)$$

$$\varkappa_0 = \omega\varepsilon_0\int[\varepsilon(x)-\varepsilon^A(x)]E_A(x)E_B^*(x), \quad (8)$$

$$\varkappa_N = \omega\varepsilon_0\int\chi(x)E_A(x)E_B^*(x)dx, \quad (9)$$

where $\varepsilon^A(x)$ and $\varepsilon^B(x)$ are the dielectric functions of the isolated waveguides A and B. Changes in modal overlaps due to the optical Kerr effect are assumed to be negligible.

The solution of coupling equations (4,5) takes the form:

$$A(z) = A_0\exp[i\Phi(z)]\cos[\Psi(z)] + iB_0\exp[i\Phi(z)]\sin[\Psi(z)], \quad (10)$$

$$B(z) = iA_0\exp[i\Phi(z)]\sin[\Psi(z)] + B_0\exp[i\Phi(z)]\cos[\Psi(z)], \quad (11)$$

where $\Phi(z)=\eta_0 z+\eta_N F(z)$, $\Psi(z)=\varkappa_0 z+\varkappa_N F(z)$ and $F(z)=\int|E_{ex}(z)|^2dz$. Constants A_0 and B_0 are the initial amplitudes.

When the external wave amplitude is constant inside the whole coupler, $E_{ex}(z) = E_0$, then $F(z)=|E_0|^2z$, and the solution of the coupling equations is similar to the results obtained for NLDC controlled by the wave guided in central region of the coupler [1]. An increase of the external wave power, accomplished by changing the value of $\varkappa$ can drive the device from the parallel state (for $\varkappa=n\pi/L$ the input and output signals are in the same guide) to the crossed state (for $\varkappa=(2n+1)/2L$ the input and output signals are in different guides). L denotes here a length of the coupler.

Numerical results present the solutions of the coupling equations for the external wave envelope in a form of a gaussian beam $|E_{ex}(z)|^2=|E_0|^2\exp(-z^2/R^2)$. The intensity of the field in the waveguide B versus normalized distance $z'=z\pi/\varkappa_0$ for $B_0=0$ and for different values of a relative nonlinear coupling coefficient $I_{NL}=\varkappa_N|E_0|^2/\varkappa_0$ is shown in Fig.2.

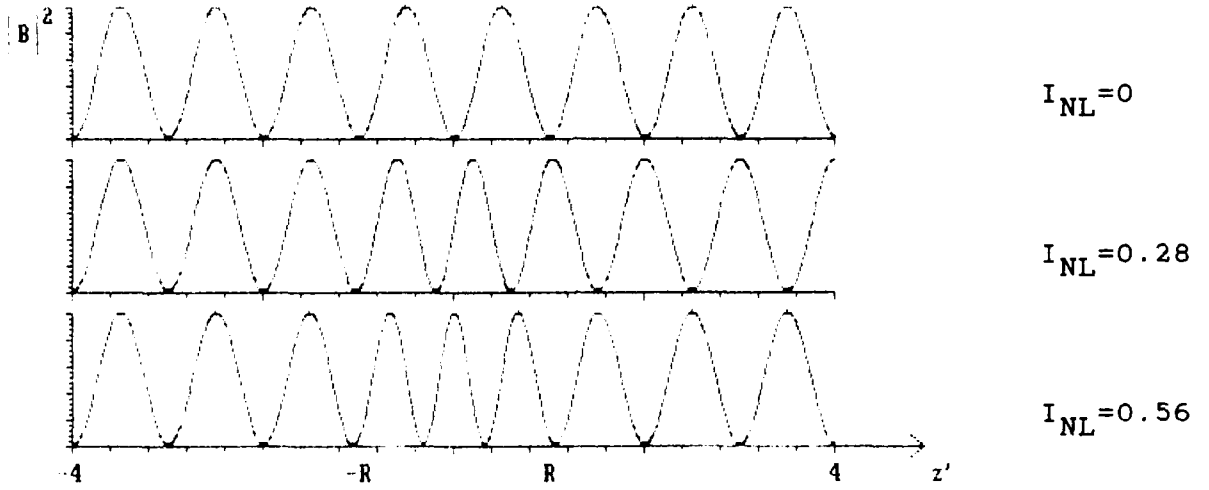

Fig.2. Intensity of the field propagating in the second waveguide versus a normalized distance $z'=z\pi/\varkappa_0$ for $R=\pi/\varkappa_0$ and different values of I_{NL}.

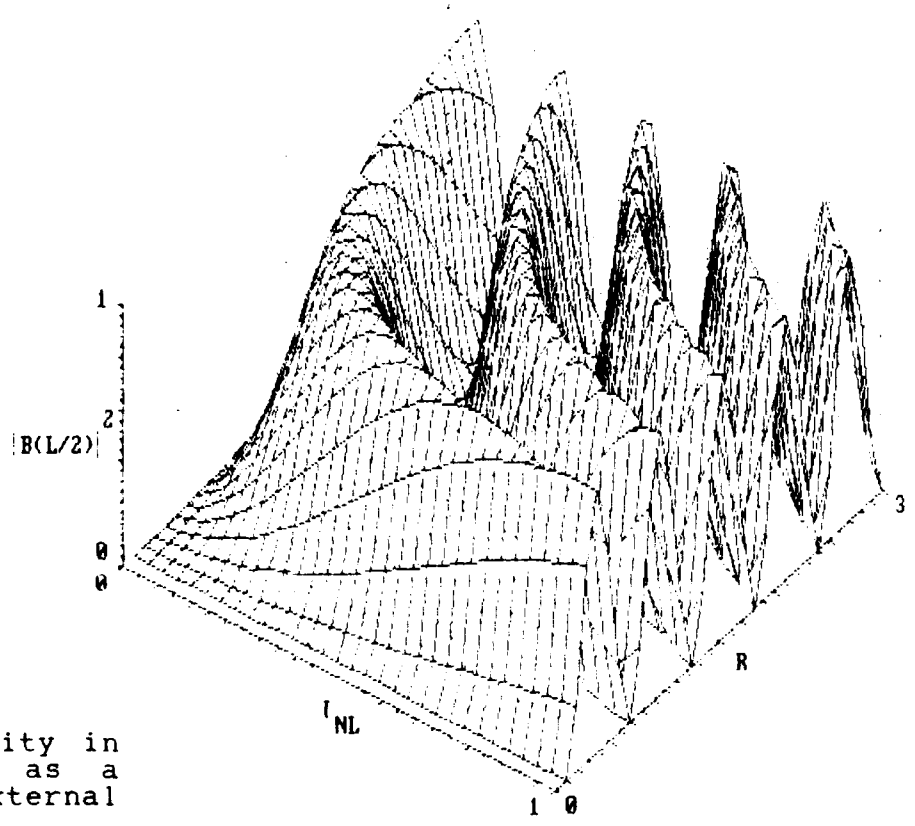

Fig.3.
The output intensity in the waveguide B as a function of the external wave parameters.

The output intensity in the second waveguide $|B(L/2)|^2$ as a function of the relative nonlinear coupling coefficient I_{NL} and the radius R of the external wave is sketched in Fig.3. Figure 4 presents the output intensity versus the relative nonlinear coupling coefficient for few different radii. Remembering that I_{NL} is proportional to the external wave intensity it is easy to see that the minimal switching intensity of the coupler can be considerably reduced by increasing the radius of the external wave. This radius can be chosen during the experiment.

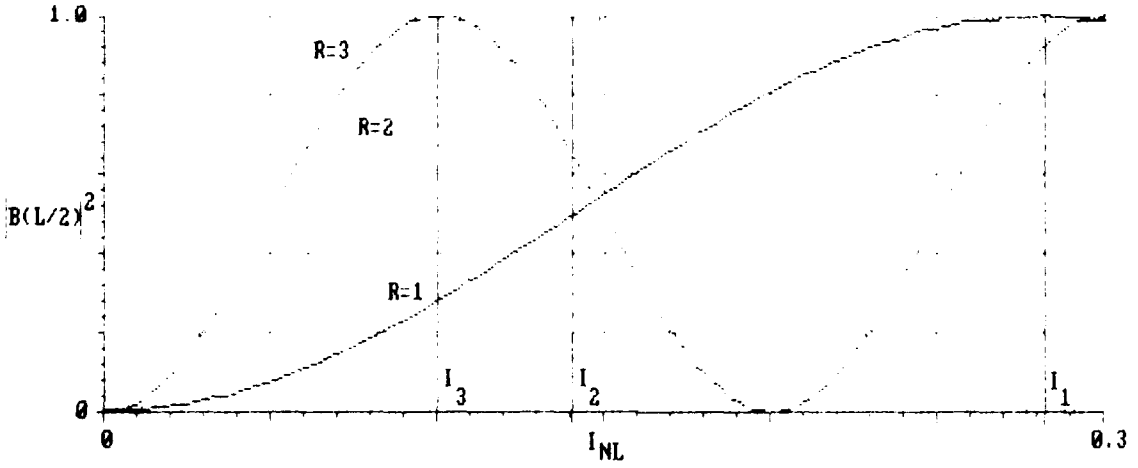

Fig.4. The output intensity in second waveguide versus the relative nonlinear coupling coefficient for the different radii of the external wave. Minimal values of I_{NL} sufficient for switching the coupler are marked.

The final result is that one can switch the weak field in the nonlinear directional coupler from the guide A to B by changing the intensity and/or the radius of the strong external field. The advantage of the operation proposed here is that it can be realized in a traditional nonlinear directional coupler without any special preparation.

References

[1] F.Lederer, M.Bertolotti, C.Sibilia, V.Leutheuser, Opt.Commun. 75, 2116, (1990).

[2] S.M.Jensen, IEEE J.Quantum. Electron. QE-18, 1580, (1982).

[3] H.Kogelnik, Theory of dielectric waveguides, in Integrated optics, ed. T. Tamir (Springer, Berlin, 1979).

Nonlinear switching characteristics of an ARROW–based Directional Coupler

U. Trutschel, M. Mann, C. Wächter, F. Lederer, L. Leine
Friedrich–Schiller–University
Faculty of Physics and Astronomy
Max–Wien–Platz 1
O–6900 Jena
Federal Republic of Germany

ARROW's (Antiresonant Reflecting Optical Waveguides) attracted a considerable interest within recent years [1]. Contrary to conventional waveguiding the underlying mechanism consists in phase – matched Fabry–Perot–action rather than total internal reflection. In this paper we show that the inclusion of the optical nonlinearity into an ARROW–based directional coupler scheme leads to novel all–optical switching characteristics.

The structure under consideration is depicted in fig. 1. ARROW A and B are separated by a layer of arbitrary thickness d_0. In contrast to conventional directional couplers the coupling mechanism is nonevanescent (see fig.1). Due to this peculiarity the coupling length turns out to be a periodic function of the spacing distance d_0, as we have shown elsewhere [2].

We describe the nonlinear coupling within the framework of a supermode theory. In fig. 2a the propagation constants of several supermodes are plotted in dependence on the spacing layer thickness d_0 where one can recognize that either two or three of them apply to a certain d_0. The propagation constants of these excited supermodes determine the coupling length for a given d_0. (As an example the modes at $d_0 = 89.8\mu m$ are labeled.) In dependence of the shape and the location of the input beam different combinations of two supermodes can be excited leading to different coupling lengths for a fixed d_0 (see fig. 2b). This behaviour has serious consequences concerning the nonlinear input–output– characteristic.

In this paper we will concentrate to an example of a situation dealing with three supermodes. When the nonlinearity sets in the supermodes get detuned and couple with each other. Using the coupled mode theory the output characteristic was investigated in dependence on the input power for $d_0 = 89.80\mu m$ as well as $d_0 = 90.00\mu m$ and $90.20\mu m$ (in every case three supermodes exist). Consequently we have to consider six combinations of these three supermodes at the three selected thicknesses. As it can be recognized from fig. 3a – c the output characteristic looks completely different for different supermode combinations. Case 1a reflects the familiar nonlinear switching behaviour, that is after exceeding a certain *critical power* (labeled in fig. 3 by little

arrows) no energy exchange between the two channels takes place. Case 1b shows that a periodic power exchange between the two channels is maintained. Consequently *no critical power* exists.
The case 2a shows a qualitatively different behaviour. At first the familiar nonlinear switching characteristic of a traditional waveguide coupler can be recognized. Surprisingly at higher powers the device returns to a periodic power exchange. That means that *two critical powers* exist. The switching behaviour in case 2b is the same like case 1b, that means no critical power exists.
Case 3a also shows the usual switching behaviour with a relatively high critical power because there is at lower input powers a very small region with power exchange. Finally, in case 3b again two critical powers exist like in case 2b. But the region without energy exchange now is smaller than in case 2b and therefore energy exchange starts at lower input powers.
We want to emphasize that we are able to compute exactly the critical power(s) at *every* thickness d_0 using only the two conservation laws of the coupled amplitude equations. The switching characteristic depends in a sensitive manner on the spacing layer thickness d_0 and on the combionation of different supermodes at a definite thickness. This sensitivity could be a possibility in implementing an optical sensing system.
In conclusion we have shown that nonlinear remote switching is achievable in ARROW–directional couplers without taking advantage of spatial solitons which emerge only for very strong nonlinearities [3]. Until now the here investigated configuration is not completely understood but should have some potential in all–optical switching as a qualitative novel device.

References

[1] T. Baba, Y. Kokubun, T. Sakaki, K. Iga; Journ. Lightw. Techn. 6, 1440–1445 (1988) and references therein

[2] M. Mann, U. Trutschel, C. Wächter, L. Leine, F. Lederer; *" An ARROW-based directional coupler"* submitted to Opt. Lett.

[3] D. R. Heatley, E. M. Wright, G. I. Stegeman; Appl. Phys. Lett. 53, 172–174 (1988)

Figures

Fig. 1a, b shows geometry, refractive index distribution and field profiles of eigenmodes of the coupler.
In Fig. 2a the real part of the propagation constants of the modes necessary for coupler design is drawn. Fig. 2b shows the coupling length in dependence of spacing layer thickness d_0.
The nonlinear switching characteristics are shown in Fig. 3a – c. In Fig. 3a case 1 (thickness $d_0 = 89.8\mu m$), in Fig. 3b case 2 ($d_0 = 90.0\mu m$) and in Fig. 3c case 3 $d_0 = 90.2\mu m$ is depicted. In every case excitation of supermodes I and II (II and III) corresponds to case a (b).

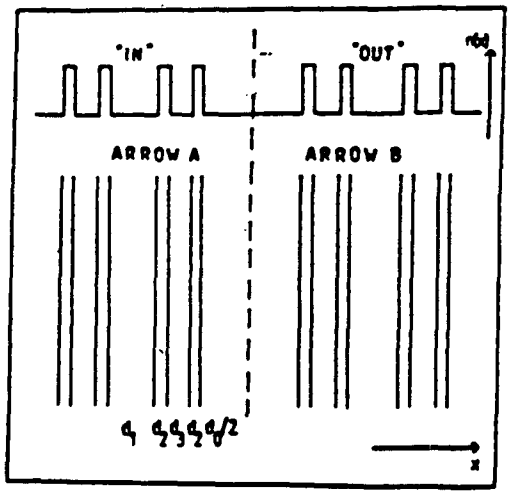

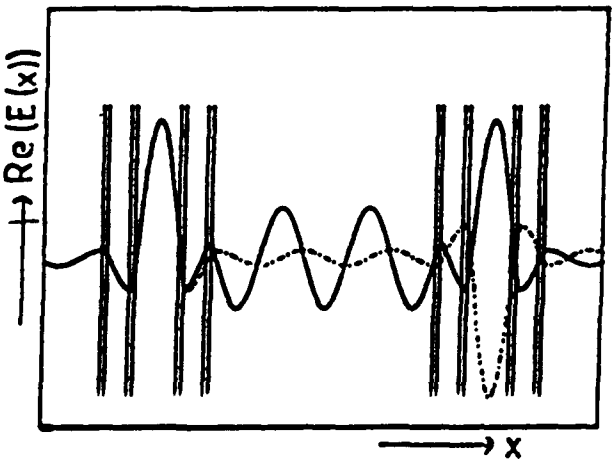

Fig. 1 a , 1 b

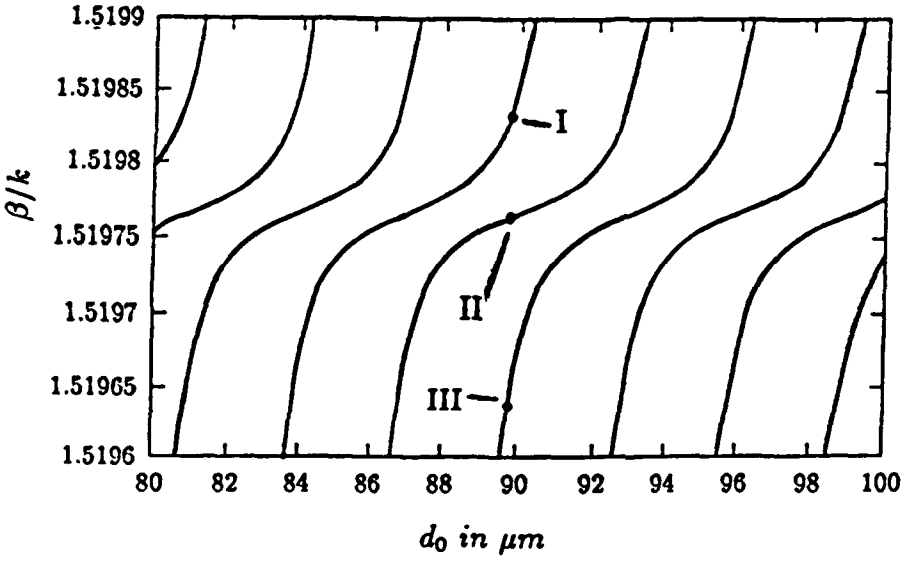

Fig. 2 a

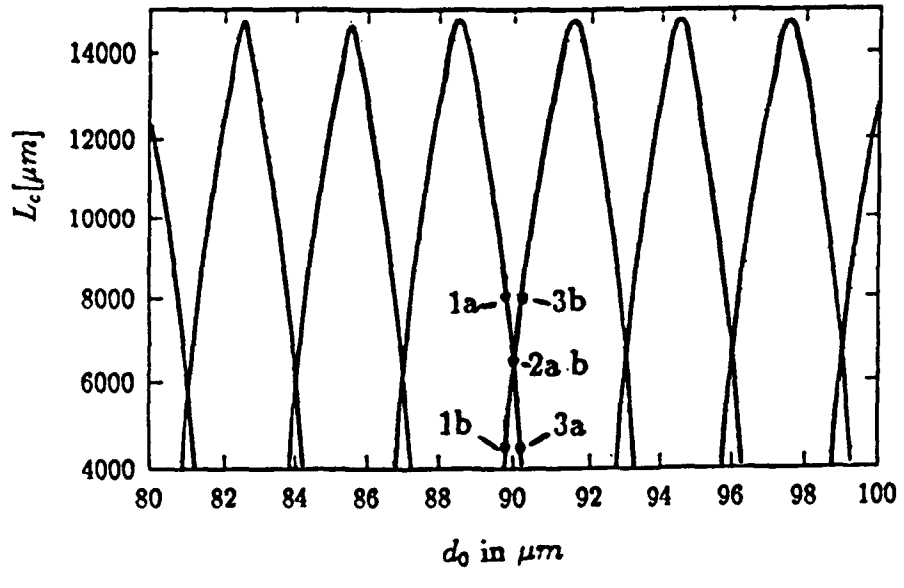

Fig. 2 b

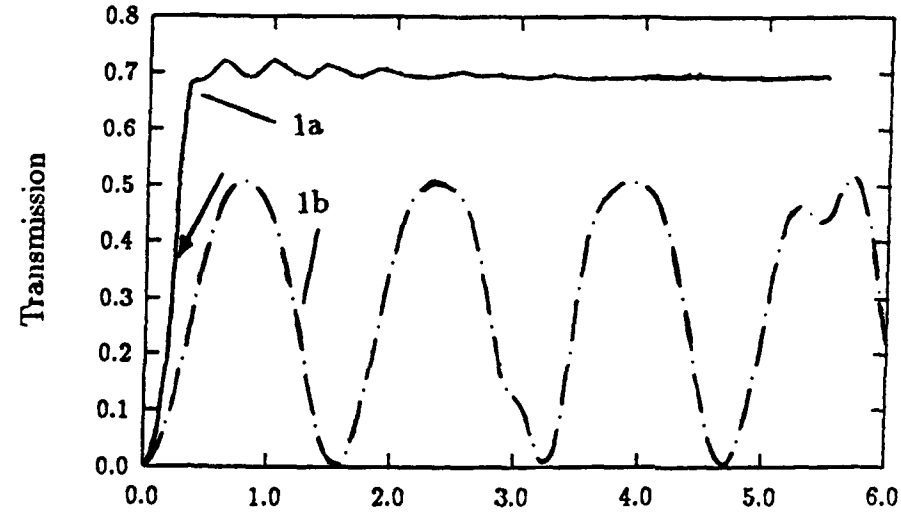

Fig. 3 a

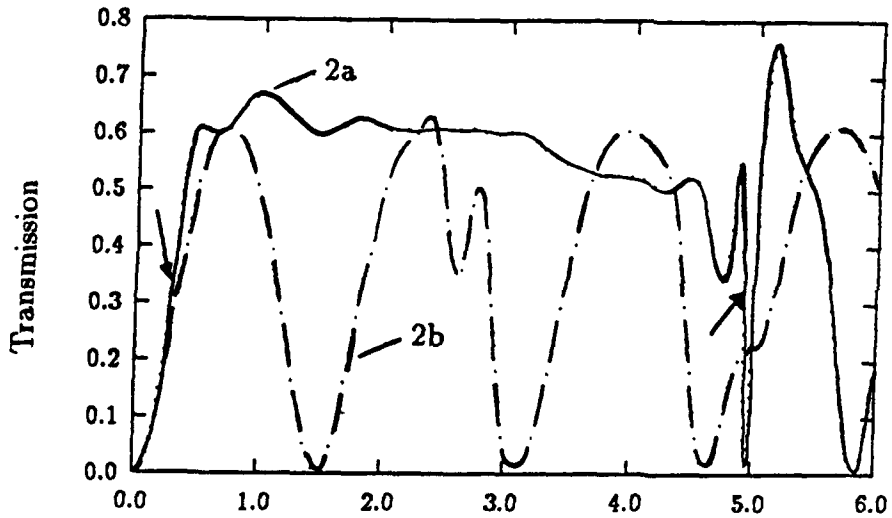

Fig. 3 b

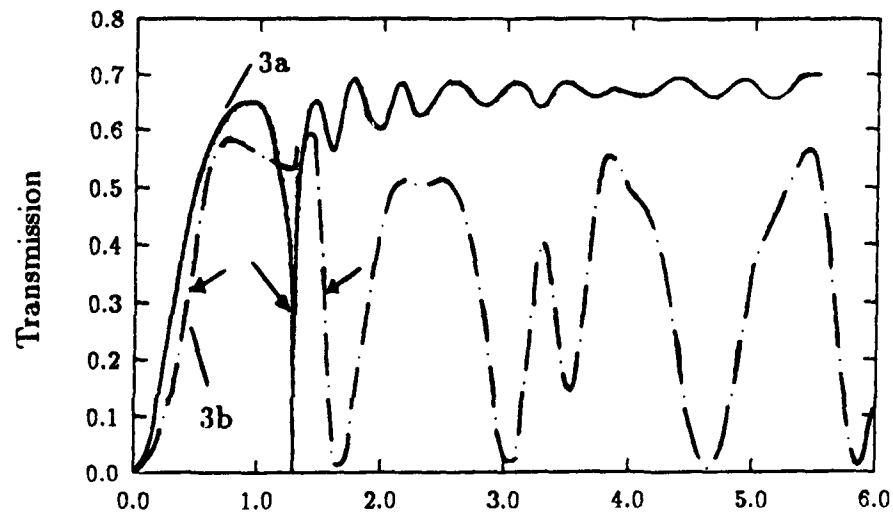

Fig. 3 c

Fiber Switches: 1

WA 9:00am–10:45am
Palmerston Room

Philip Russell, *Presider*
University of Southampton, United Kingdom

All-Optical Switching in Optical Fibre Devices

K.J.Blow

British Telecom Research Laboratories

Martlesham Heath

Ipswich, IP5 7RE

England

Tel: +44 473 643417

A number of fibre based devices have been shown to be capable of performing all-optical switching. These include, polarisation discriminators [1], Mach-Zehnder interferometers [2], Sagnac interferometers [3] and coherent couplers [4]. The crucial feature common to these devices is the existence of two modes which can propagate independently in the linear regime. Polarisation based devices and couplers are described by a simple set of coupled equations which can either be in terms of the local modes (mode of a single core for the coupler, circular modes for polarisation) or the global (true) modes (symmetric and antisymmetric modes of the coupler, linear modes for polarisation). The latter choice exemplifies the connection with the interferometer based devices since the linear coupling operation is described in terms of the beating of the true modes in much the same way as the linear properties of the interferometer are described in terms of the beating between the fields in the two arms.

In order to achieve all-optical switching it is necessary for the device to exhibit some nonlinearity. The most successful devices use the intrinsic, although small, Kerr

nonlinearity of Silica. The modification of the refractive index is described by the following equation

$$n = n_0 + n_2 I \tag{1}$$

where n_0 is the linear refractive index of the guide, n_2 is the Kerr coefficient and I is the optical intensity. The devices generally work by inducing an intensity dependent phase shift which alters the interferometric beating to produce an intensity dependent switching.

Two generic forms of switching are usually considered. Self-switching occurs when the optical response of the device depends on the intensity of the signal beam (self phase modulation). This can also be thought of as intensity dependent routing. Cross-switching occurs when the optical response is controlled by the intensity of a control beam (cross phase modulation). In this case the routing of the signal is determined by the control beam. Self switching has a major problem when pulsed light is considered. The optical nonlinearity of Silica responds on femtosecond timescales and for the most part can be considered instantaneous. This leads to pulse distortion since the optical response of the device changes with the local intensity of the signal. Solitons are one possible way to overcome this problem [5], [6] but restrict the fibre properties and the required power levels. Cross-switching offers some rather simpler solutions to the pulse distortion problem. The simplest is to make the control pulse long compared to the signal pulse so that a quasi-CW control pulse is seen. Another possibility is to use the group velocity dispersion of the fibre to arrange for the control pulse to walk through the signal pulse. In this way the signal sees an integrated control pulse which only places a restriction on the control pulse energy.

In this talk we will discuss some of the more recent results obtained using cross-switching to perform all-optical demultiplexing. The demultiplexer is a fibre loop mirror with a dichroic coupler so that the control pulse propagates in only one direction round the loop [7]. Demultiplexing of signals at 20GHz line rate down to 2.5GHz is demonstrated.

Other recent examples of self-switching will be shown such as a long fibre based Mach-Zehnder and a many beat length polarisation switch.

REFERENCES

1. T.Morioka and M.Saruwatari, Ultrafast All-Optical Switching Utilizing the Optical Kerr Effect in Polarization-Maintaining Single-Mode Fibres, IEEE JSAC 6 1186-98 (1988)

2. I.H.White, R.V.Penty and R.E Epworth, Demonstration of the Optical Kerr Effect in an All-Fibre Mach-Zehnder Interferometer at Laser Diode Powers, Electron Lett 24 340 (1988)

3. N.J.Doran and D.Wood, Nonlinear-Optical Loop Mirror, Optics Lett 13 56-58 (1988)

4. S.R.Friberg, A.M.Weiner, Y.Silberberg, B.G.Sfez and P.W.Smith, Femtosecond Switching in a Dual-Core Fibre Nonlinear Coupler, Optics Lett 13 904-6 (1988)

5. N.J.Doran, K.J.Blow and D.Wood, Soliton Logic Elements for All-Optical Processing, SPIE 836 238-43 (1987)

6. K.J.Blow, N.J.Doran and B.K.Nayar, Experimental Demonstration of Optical Soliton Switching in an All-Fibre Nonlinear Sagnac Interferometer, Optics Lett 14 754-6 (1989)

7. K.J.Blow, N.J.Doran, B.K.Nayar and B.P.Nelson, Two-Wavelength Operation of the Nonlinear Fibre Loop Mirror, Optics Letts 15 248-50 (1990)

All Optical Gigabit Switching in a Nonlinear Loop Mirror using Semiconductor Lasers

B. P. Nelson, K J Blow, P D Constantine, N J Doran, J K Lucek
I W Marshall and K Smith

British Telecom Research Laboratories
Martlesham Heath
IPSWICH IP5 7RE

In a recent paper [1] we demonstrated an all-optical demultiplexer using a nonlinear optical loop mirror (NOLM) in which a signal at one wavelength is used to switch a signal at a different wavelength [2], [3]. The switching signal in that case was generated from a modelocked Nd-YAG laser at 1.32um operating at 76 MHz and the switched signal was a gain switched DFB laser operating at 1.56um at 1 GHz. The purpose of this present work is to extend the optical switching into the gigabit regime while, at the same time, avoiding high power laser systems.

The first target is to reduce the switching power required so that semiconductor lasers may be used throughout the device. This can be achieved by increasing the length of the fibre loop used in the NOLM. The loop employed in the current experiment was 6.4 km of standard dispersion shifted fibre and stability measurements showed no significant drift over an hour. With this loop the peak power required for complete switching is approximately 160 mW. This means that for example with a 10ps pulse the switching power is only 1.6pJ.

The switching signal was generated from a gain switched DFB laser driven at 2.5 GHz. The resulting pulses were then compressed using 700m of negative group delay dispersion fibre. The full width half maximum (FWHM) of the pulses was 27ps when displayed on a fast photodiode(p/d)/sampling oscilloscope detection system. Deconvolving the detection system response implies a pulse width of ~16ps. These pulses were then amplified using a diode pumped erbium amplifier which resulted in an average output power of 20mW. Even allowing for losses in the following couplers this is sufficient power to provide switching in a 6.4km NOLM.

The signal source was a mode locked diode laser operating at 1.56μm with a repetition rate of 10GHz. These pulses were interleaved using a fibre Mach-Zehnder to produce a 20GHz pulse train. The two wavelengths were then combined using a WDM coupler and launched into the loop. The loop is constructed from a coupler which has a 50:50 coupling ratio for the 1.56μm signal and 100:0 for the 1.53μm switching signal. The polarisation controllers in the loop allow us to operate the loop either in "reflecting" or "transmitting" mode [1]. In reflecting mode the loop output is zero for the 1.56μm signal, in the absence of the switching pulses, and the complete signal is reflected. The injection of the switching pulses causes the signal pulses to be switched to the output of the loop. In transmitting mode the situation is reversed and the switched out pulses are reflected. The output of the loop is connected to a filter which passes the 1.56 μm

signal and blocks the switching pulses. The remaining signal is amplified and detected on a photodiode then displayed on a sampling oscilloscope. A schematic diagram of the apparatus is shown in figure 1.

In order to establish the switching width of this configuration the modelocked signal source was replaced with a cw source operating at the same wavelength (1.56μm). The 'effective' width of the switching pulse is determined by a combination of the differences in the group delay between the two wavelengths and the initial pulse width. The loop was set up in reflecting mode and the width of the pulse switched from the cw source was measured as 33ps on the oscilloscope which deconvolves to 25ps. The initial pulse width was 16ps thus indicating a difference in dispersion between the two wavelengths of 3 ps/km. This establishes that with this set-up we should be able to demultiplex at up to 40Gbit. Having established the suitability of the switching pulse width the cw source was replaced by the modelocked laser. In order that switching takes place it is necessary to synchronise the two trains of pulses. This was accomplished by having an adjustable delay in one arm of the clock pulses which drive the two sources.

In figure 2 we show the results. Figure 2(a) shows the modelocked, 1.56 "signal" pulse train at 20 GHz. Figure 2(b) shows the switched output with the loop in 'reflecting' mode that is a transmission of only those pulses coinciding with the switching pulses i.e. every eighth pulse. Figure 2(c) shows the result when the loop is set up in the 'transmitting' mode and clearly shows every eighth pulse being switched out. There is still a small residual component of the switched out pulse. This is because we may not be quite at the total switching energy. Increasing the amplification of the 1.53 pulses will result in more complete extinction.

We have shown that the NOLM is capable of switching at the multigigabit rate and have demonstrated stable operation at the silica loss length (e.g. 6 km) allowing this ultrafast all-optical processing to be performed entirely with semiconductor sources. This device is also capable of a number of nonlinear processing functions including pulse insertion, wavelength translation, logic and all-optical memory.

REFERENCES

1. K.J.Blow, N.J.Doran and B.P.Nelson, Demonstration of the Nonlinear Fibre Loop Mirror as an ultrafast all-Optical Demultiplexer, Electron Lett 26 962-4 (1990)

2. M.C.Farries and D.N.Payne, Appl Phys Lett, Optical Fibre Switch Employing a Sagnac Interferometer, 1 25 (1989)

3. M.Jinno and T.Matsumoto, Ultrafast Low Power and Highly Stable All-Optical Switching in an All Polarisation Maintaining Fibre Sagnac Interferometer, IEEE Photonics Tech Letts 2 349 (1990)

Fig 1

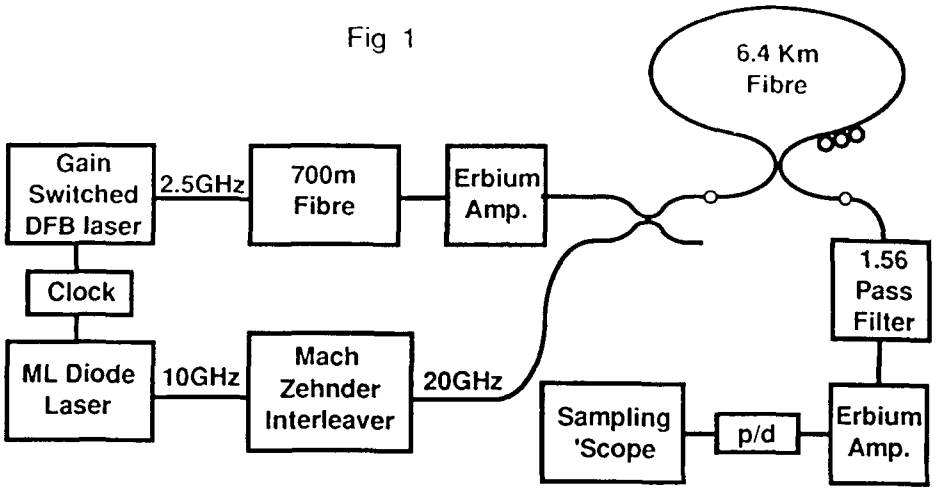

Fig 2

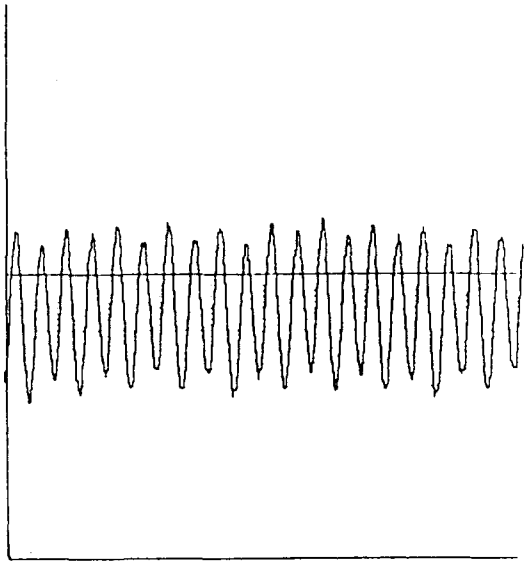

a)

b)

100 ps/div

c)

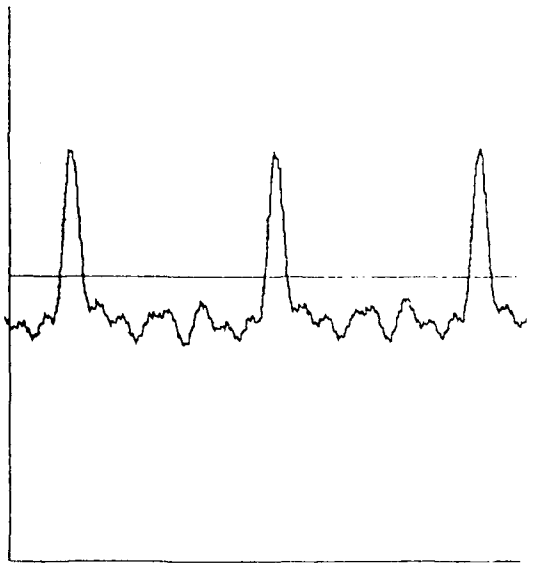

100 ps/div

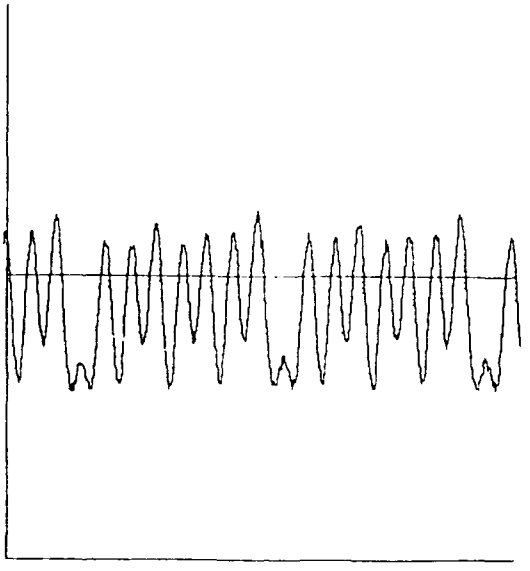

100 ps/div

All-optical logic gates based on cross-phase modulation in a nonlinear fiber interferometer

J.-M. Jeong and M.E. Marhic

Department of Electrical Engineering and Computer Science

Northwestern University

2145 N. Sheridan Rd., Evanston, IL 60208

Phone: (708) 491 7074

All-optical logic gates have been demonstrated using nonlinear waveguide devices. In such devices, optical fibers are increasingly used, since their optical Kerr effect is very fast, and their low-loss waveguide structure allows a long interaction length and relatively low power. For example, an AND gate based on intensity-dependent polarization rotation [1], XOR and AND gates based on soliton trapping [2], a NOR gate based on soliton dragging [3], and AND, NOT, XOR, and XNOR gates [4] have been demonstrated in polarization-maintaining fibers.

We propose and demonstrate all-optical logic gates, capable of performing all eight two-input logic functions (ON, AND, OR, XOR, NAND, NOR, XNOR, INV) in a versatile arrangement. The basic component of the logic gate is a nonlinear Sagnac interferometer based on cross-phase modulation between a signal and a pump with two different wavelengths. The configuration is similar to that of Ref. 4., but in the latter the AND is not exactly gating of two input control beams but just switching of a probe beam by a pump beam. We place three WDM couplers at the center, the beginning, and the end of the fiber loop, as shown in Fig. 1(a); as a result, we can truly obtain two-input logic functions.

In the Sagnac interferometer, the reflected light corresponds to the inverted logic ($\overline{O}$) and the transmitted light is for the non-inverted logic (O). The output powers are given by

$$O = P_s \cos^2(\frac{\Delta\Phi}{2}), \qquad \overline{O} = P_s \sin^2(\frac{\Delta\Phi}{2}), \tag{1}$$

where P_s is the power of the signal, and $\Delta\Phi = QP_pL$ is the nonlinear phase-shift difference between the two counterpropagating signal beams, produced by the pump pulses; Q is the fiber nonlinear coefficient, P_p is the power of the pump, and L is the interaction length. To obtain the various logic functions, high-power pumps are injected into one or two of the three possible input ports A, B, and C. Table I shows the inputs used for particular functions, and the entries correspond to the nonlinear phase shifts induced by the pumps in the fiber lengths which they traverse. It is assumed throughout that a logic threshold equal to $P_s/2$ is used at the outputs to make clean binary decisions from the outputs of the interferometer.

The experimental setup is shown in Fig.1(b). For the pump pulses, we used a frequency-doubled Nd:YAG laser at the wavelength of 532nm, repeatedly Q-switched at 1-5kHz, producing pulses with 100-200W peak

$\Delta\phi_a$	$\pi/3$	$2\pi/3$	0	π	0	0
$\Delta\phi_b$	$\pi/3$	$2\pi/3$	π	0	π	0
$\Delta\phi_c$	0	0	π	0	0	π
O	AND	OR	XOR	ON	ON	ON
$\overline{O}$	NAND	NOR	XNOR	INV	INV	INV

Table 1: Phase shifts required for various functions

power. Pulse lengths were 150nsec fwhm. For the signal, a CW He-Ne laser was used, operating at the wavelength of 633nm. The power-coupling ratio of the WDM coupler was 99% at 532nm and 5% at 633nm. We used normal single-mode fibers and polarization controllers (PC) instead of polarization-maintaining fibers, which were used in other Sagnac interferometer logic gates [4]. BS1, BS2, fiber loop, and WDM coupler constitute a Sagnac interferometer. BS2 was used instead of WDM coupler 1 in Fig.1(a). We used a red filter to separate the pump and the signal at the output of the fiber loop instead of WDM coupler 3 in Fig 1(a).

In a typical experiment, we adjusted the optics to obtain a high-contrast interference pattern for the CW signal and located the PMT at the dark fringe for the non-inverted logic function (O). Then we injected the pump pulses into the inputs A and B for the AND and OR functions, according to the input truth tables, and measured the resulting signal output waveforms. Blocking and injecting the pump pulses correspond to input logic '1' and '0', respectively. For the XOR function, inputs B and C were used, where the net nonlinear phase shift due to counterclockwise (input B) and clockwise (input C) pump pulses are subtracted. Either input B or C was used for the ON function. For the inverted logic function ($\overline{O}$), which is the reflected light in Fig. 1(a)., the PMT was located at the bright fringe.

The modulated signal outputs are shown in Fig.2. The solid line is the theoretical output of the non-inverted logic function, and the dashed line is the inverted logic function. Circles and squares are the measured data at the dark and bright fringe, respectively. The peak powers of the input pump pulses were approximately 0.13 W, 0.25 W, 0.38 W, and 0.38 W for the AND (NAND), OR (NOR), XOR (XNOR), and ON (INV) functions, respectively. Fig. 2(a) shows the AND and NAND functions with approximately a 3:1 logic level '1'/'0' contrast ratio, as expected. Fig. 2(b) shows the OR and NOR functions. When both inputs A and B are present, the total nonlinear phase shift, $\Delta\Phi$, is $4\pi/3 > \pi/2$, and this causes the dip at the center of the signal, due to the nonzero rise and fall time of the pump pulses; the use of square pump pulses would avoid this dip. Fig. 2(c) shows the XOR and XNOR functions. We see that the net nonlinear phase shift is almost canceled, showing approximately a 16:1 contrast ratio. In Fig. 2(c) we see the ON and INV functions when either input B or C was used.

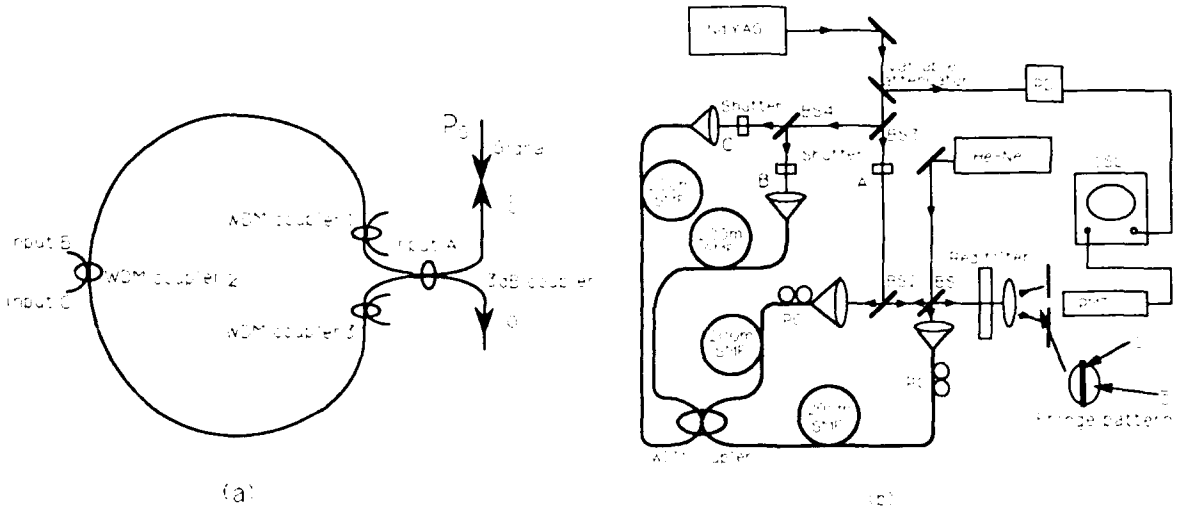

Figure 1: (a) The basic schematic of logic gates in a Sagnac interferometer. The power-coupling ratio of WDM coupler is 100% at the wavelength of the pump and 0% at the wavelength of the signal. (b) Experimental setup.

In conclusion, we have proposed and demonstrated all-optical logic gates, capable of performing all eight two-input Boolean functions, in a two-wavelength single-mode fiber Sagnac interferometer. *This nonlinear* interferometer configuration has some advantages over other previously demonstrated fiber logic gates: it does not need any other external optics such as output polarizer, Fabry-Perot band-pass filter, and correlator, to observe logic functions, and shows the inverted and non-inverted logic functions simultaneously. The logic gates demonstrated here show four more logic functions, including the AND, NAND, OR, and NOR functions, than other Sagnac interferometer logic gates.

References

[1] Y. Kimura, K.-I. Kitayama, N. Shibata, and S. Seikai, *Electron. Lett.*,**22**, pp.277-278, 1986.

[2] M. N. Islam, *Opt. Lett.*,**14**, pp.1257-1259, 1989.

[3] M. N. Islam, *Opt. Lett.*,**15**, pp.417-419, 1990.

[4] M. Jinno and T. Matsumoto, *Opt. Lett.*,**16**, pp.220-222, 1991.

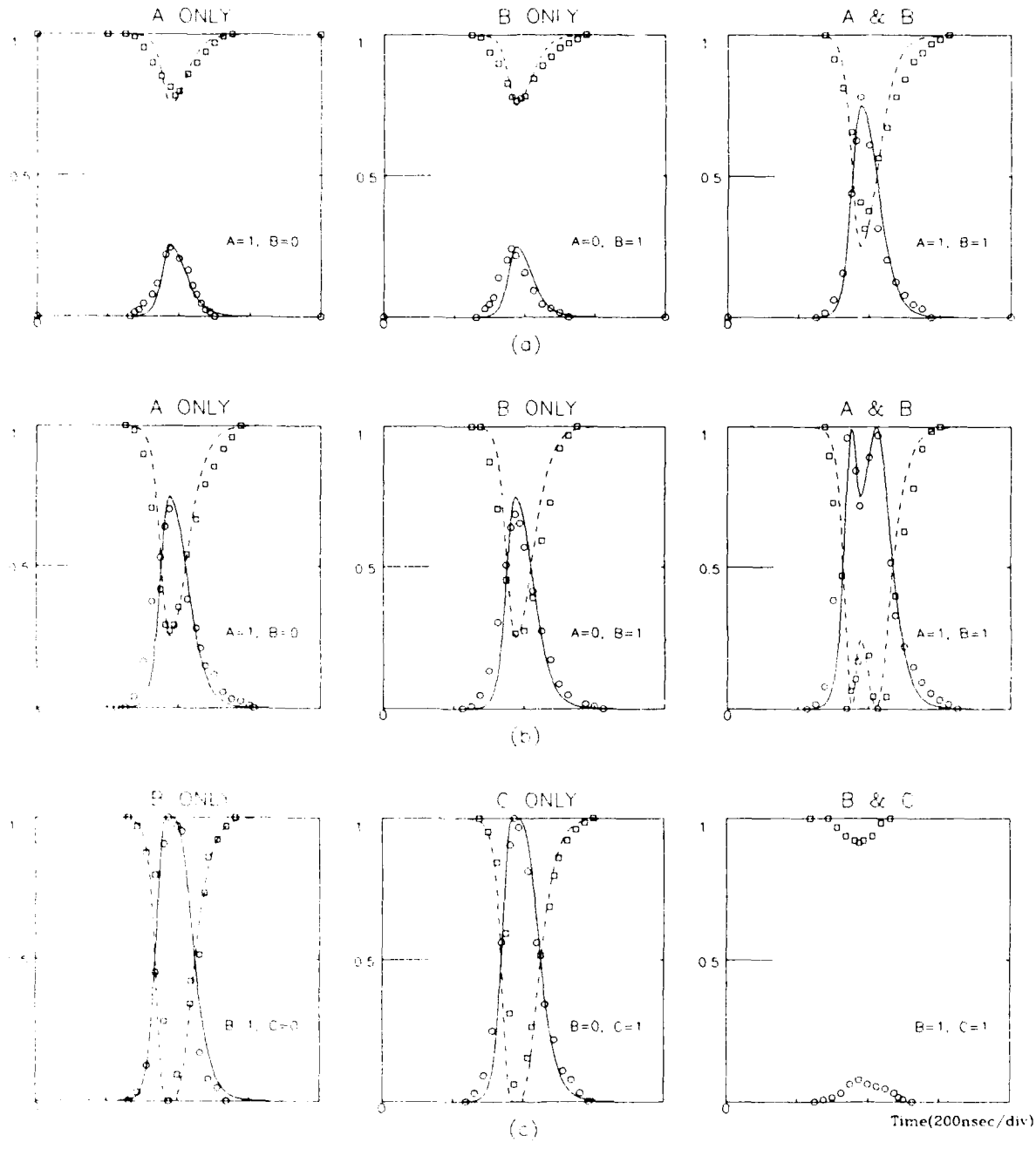

Figure 2: Experimental data: (a) AND (NAND), (b) OR (NOR), (c) XOR (XNOR) and ON (INV). Solid and dashed lines are theoretically predicted outputs for O and $\overline{O}$, respectively. Circles and squares are experimental data points of O and $\overline{O}$, respectively.

AN ULTRAFAST MULTIBEATLENGTH ALL-OPTICAL FIBRE SWITCH

N. Finlayson, B.K. Nayar and N.J. Doran
British Telecom Research Laboratories, Martlesham Heath, Ipswich, IP5 7RE UK

Considerable effort has been devoted to the development of all-optical switches in the last several years,[1] with a view to using these switches in ultrafast telecommunications. In spite of having a very low nonlinear refractive index coefficient ($n_2 = 3 \times 10^{-20}$ m^2/W), fused silica fibre is probably the best material medium for such switches owing to its extremely low loss (~0.2 dB/km). A severe challenge in using fused silica fibre is designing devices that can take full advantage of the low loss property, since the device length needs to be maximised in order to minimise the switching power. The nonlinear optical loop mirror (NOLM) has proved to be very effective in this respect, and devices as long as 9km have been successfully tested by our group. The NOLM operates on the principle of nonlinear interference between counterpropagating modes of a single fibre. In this letter we report successful all-optical switching with a device which also allows long lengths of fibre to be utilised.

Most all-optical experiments have been conducted with devices intended to operate in the limit where the nonlinear phase shift is of order π whilst the phase difference between the linear eigenmodes is either of order π or much less. The limit where the linear phase difference is much *larger* than the nonlinear phase shift (the multibeatlength limit) has been neglected, perhaps due to a notion that the behaviour would be degraded owing to random variations of the device parameters. Telecommunications fibre, however, is an environment in which two nondegenerate polarisation modes evolve in very stable fashion, even over many beat lengths.[2] Winful has predicted that complete switching is possible in a multibeatlength fibre.[3] In this paper we present experimental evidence that a multibeatlength fibre can indeed be used for all-optical switching.

Our experimental apparatus is shown in Fig. 1. A 1.32 μm mode-locked Nd:YAG laser generating 120 ps pulses (FWHM) at a repetition rate of 76 MHz is used as the source. The power is modulated by a standard half-wave plate/polarizer combination. A second half-wave plate allows us to select the azimuth angle of the incident beam relative to the fibre axes. A standard telecommunications fibre having a length of 1.1 km is the active

switching element. The polarisation beat length of standard fibers is usually estimated to be on the order of a few metres, so that we are well into the multibeatlength regime. A fibre fractional wave compensator is inserted at the end of the fibre in order to compensate for the fibre birefringence. No stabilisation measures are employed in the experiment. A rotatable analyser situated at the output performs the polarisation selection function, and photodiodes are used to measure the device response.

Time-averaged results are shown in Figure 2. Substantial switching occurs at peak powers of the order of 15W. After the curves have crossed over, flattening of the response occurs, indicative of the onset of Raman scattering. The switching was observed to be repeatable and stable on time-scales of an hour or more. The time-averaged observations are confirmed by time-resolved measurements, shown in Figure 3. At a peak input power of 6W, the perpendicular polarisation pulse is narrowed slightly with respect to the input pulse, whilst the parallel polarisation pulse is broadened. At 13 W the perpendicular pulse is narrowed further and the parallel pulse exhibits a pronounced dip. The noisy structure appearing in the pulse tails has its origins in modulational instabilty seeded by spontaneous emission. At a higher power of 16 W, the additional influence of Raman scattering becomes important and strong distortion becomes evident in the pulse tails. The influence of modulational instabilty and Raman effects was confirmed by removing the analyser and looking at the output pulse spectra.

These results demonstrate clearly that all-optical self-switching at peak power levels as low as 15W is possible in a simple device comprised of a half-wave plate, a single weakly-birefringent telecommunications fibre, a fibre compensator and a polariser. The major attraction of the device is that long lengths of 'off-the-shelf' fibre and components can be used.

References

1. Stegeman, G.I., Wright, E.M., Finlayson, N., Zanoni, R., and Seaton, C.T.: 'Third order nonlinear optics', J. Lightwave Technol., 1988, **6**, pp. 953-970.

2. Harmon, R.A.: 'Polarisation stability in long lengths of monomode fibre', Electron. Lett., 1982, **18**, pp. 1058-1060.

3. Winful H.G., 'Self-induced polarisation changes in birefringent optical fibers', Appl. Phys. Lett., 1985, **47**, pp. 213-215.

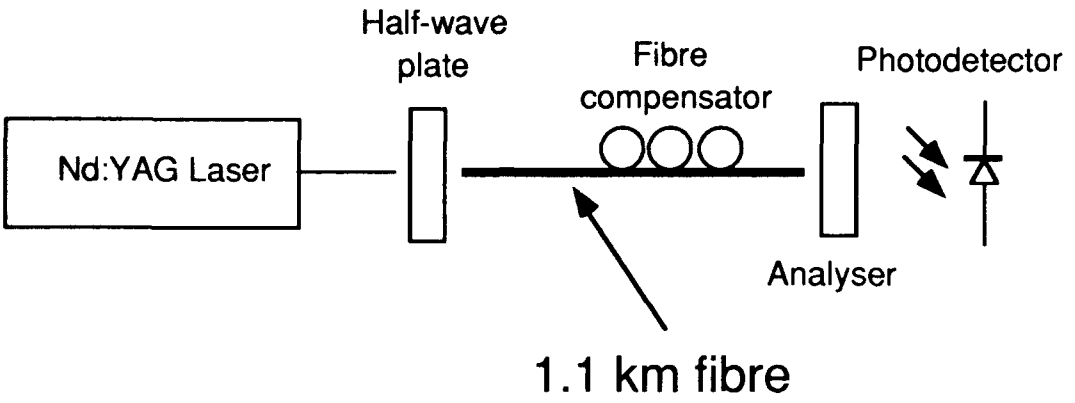

Figure 1. Schematic of experimental setup.

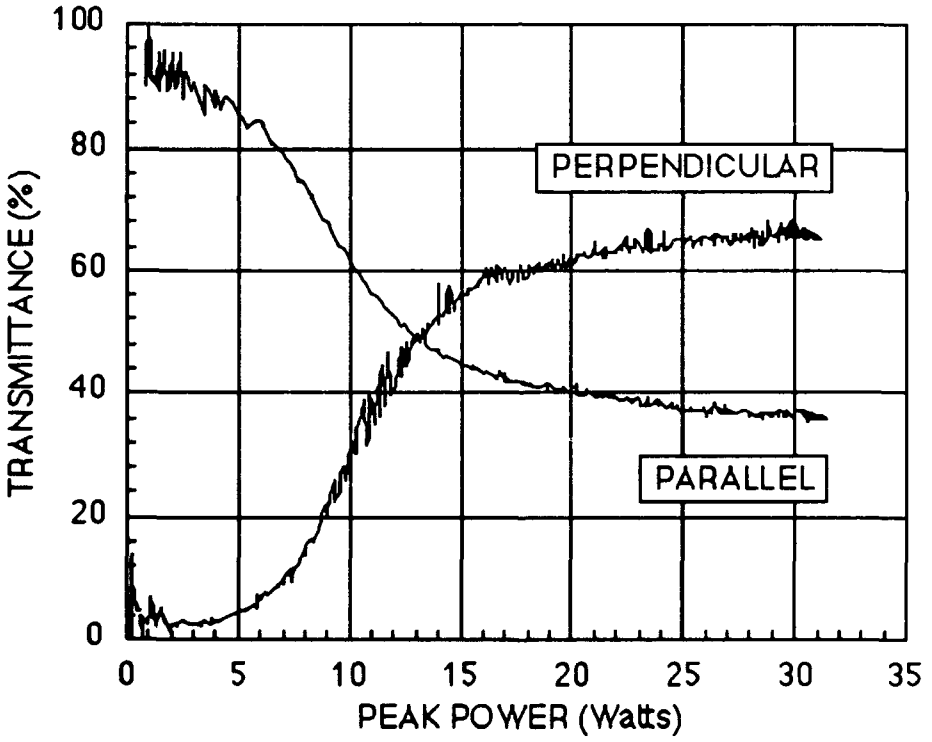

Figure 2. Time-averaged transmittance of device with analyser oriented to pass light polarised perpendicular and parallel to linear output polarisation.

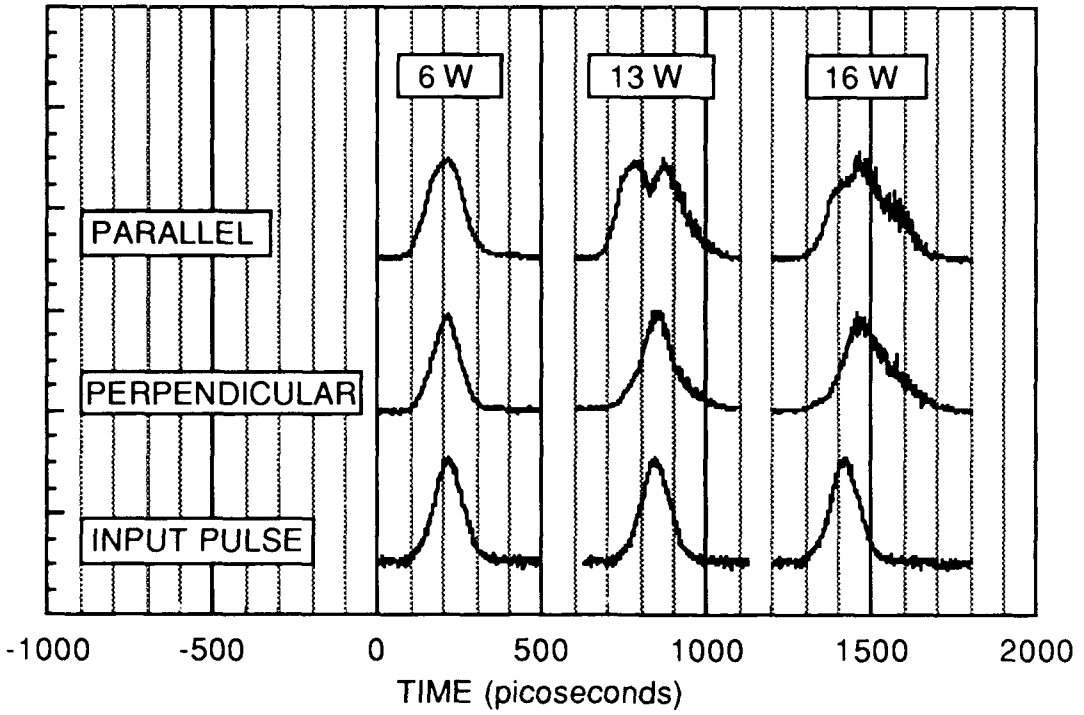

Figure 3. Pulse shaping observed for perpendicular and parallel polarisations at different power levels.

Observation of Polarization Switching and Pulse Break-Up in Spun Fiber

P. Ferro, M. Haelterman, S. Trillo, S. Wabnitz, and B. Daino

Fondazione Ugo Bordoni, Via B. Castiglione 59, 00142 Rome, Italy

1. INTRODUCTION

The nonlinear directional coupler (NLDC) [1] is a promising element for ultrafast all-optical signal processing. The experiments have demonstrated self-switching of light in fiber-optic NLDC's, such as dual-core fibers [2-3], birefringent nbers [4], and periodically twisted birefringent filters [5]. Fiber-optic nonlinear couplers exhibit an instantaneous Kerr-law response, which permits femtosecond pulse switching [3]. Whereas with fiber optic switches the switching power is relatively high, owing to the weakness of the fused quartz nonlinearity.

Earlier experiments with NLDC's have employed couplers with lengths equal to one or two linear coupling distances. In this case, the nonlinear transmission exhibits a single well-defined switching power, that is inversely proportional to the coupling distance L_c [1-5]. In this experiment, we demonstrate that complete switching of light in fibers is obtainable with a birefringent fiber coupler of any length. In addition, with a several beat lengths long birefringent fiber NLDC, the switching power is inversely proportional to the square root of the product of L_c and the total length of the fiber, and the switching behavior is similar to a nonlinear Mach-Zehnder interferometer [6]. Therefore polarization switching may be observed in long birefringent fibers at very low powers. We anticipate that he present results may also have relevant implications for the degradation of the polarization state of pulse-coded signals in fiber transmission systems.

2.EXPERIMENT

In the experiment, we have used 205 meters of York ultra low-birefringence spun fiber, that was wound on a drum. The fiber had a measured attenuation of 1.5 dB/km at $1\mu m$, a cutoff for sigle mode operation at 880 nm, and a nominal overall retardance of less than 1 degree. Spun fibers are produced by rapidly spinning the preform while drawing the birefringent fiber [7]. As a result, in the fiber the local fast and slow axes rapidly rotate and the net resulting birefringence averages to zero. Winding the fiber around a coil introduces a bending-induced linear birefringence. A resulting beat length of about 20m was estimated. Therefore the present polarization NLDC encloses about twenty linear coupling periods.

The mode-locked 100 picosecond input pulse train from a Nd-YAG laser operating at 1.06 μ m was circularly polarized at the fiber input. At the fiber output, we set as the two output ports of the present NLDC the two counterrotating circular polarization components of the emerging pulses. These were separated by means of a calibrated Babinet-Soleil compensator, followed by a Wollaston prism.

Figure (1) shows the measured circular polarization transmissions at the fiber output, versus the total average power into the fiber. Owing to the slow response time of the photodetectors, the transmission shows the energy in the two output polarizations. At low powers, the input circular polarization emerges from the fiber almost unchanged, which indicates that the total length of the fiber encloses an even number of coupling distances. The first peak of the transmission occurs for an input average power of about 200 mW. The corresponding pulse peak power is of about 26W. By interchanging from

right to left handed polarization at the fiber input, a nonreciprocal nonlinear transmission was found. This indicates of the presence of some twist-induced optical activity in the fiber [8].

Figure (2) shows the streak camera pictures of pulse profiles of both the input and the crossed circular polarization components at the fiber output. Here the input average power was 320 mW. This corresponds to the second peak in the transmission of fig.(1). As can bee seen, the center and the wings of the pulse have opposite ellipticities, which leads to a clear symmetric pulse break-up. We believe that this is the first direct picture of pulse break-up in a birefringent fiber NLDC.

3. THEORY

The output power P_o emerging from the same circular polarization as the input is [1,4,9]

$$P_o = \frac{P_i}{2}[1 + cn(\pi L/L_c|p)] \tag{1}$$

where P_i is the input power, L is the total fiber length, and $p = P_i/P_c$ is the input power, normalized to the critical power $P_c = 3\Delta\beta/R$. Here $\Delta\beta$ is the fiber birefringence, whereas $R = \omega n_2/cA_{eff}$, n_2 is the nonlinear coefficient and A_{eff} is the effective area of the fiber. For couplers of length L_c or $2L_c = L_b$, the switching power $p_s = 1$ [1-5,8]

Figure (3a,b) shows examples of the continuous wave nonlinear transmissions of eq.(1) versus the input power p, for coupler lenghts equal to $L = 20L_c$ and $100L_c$, respectively. Complete switching of the output state of the coupler first comes about at a certain switching power p_s. For $L \gg L_c$, one obtains that $p_s \ll 1$. From eq.(1), the coupling period between the two circular polarizations is

$$L_{nc}(p) = \frac{2L_cK(p)}{\pi} \tag{2}$$

where $K(p)$ is the complete elliptic integral of the first kind. By using the Taylor expansion of this integral for $p \ll 1$ [9], one obtains

$$P_o = P_i cos^2(\pi L/L_{nc}). \tag{3}$$

This yields the off-on switching power in fig.(3) $p_s^2 = 4L_c/L$, or, in real units,

$$P_s = \frac{12\pi}{R\sqrt{2LL_b}}. \tag{4}$$

This estimate agrees with the observed value of 26 W, with $n_2 = 3.2 \times 10^{-20} m^2/W$, $A_{eff} = 1 \times 10^{-11} m^2$, and $L = 205m$. The physical origin of the switching is the cumulative effect of the progressive precession of the polarization ellipse in each of the many linear beat lengths. This leads to the power-induced modulation of the fiber beat length in eq.(3).

4. CONCLUSIONS

In conclusion, we have observed the relatively low power nonlinear nonreciprocal self-switching and break-up of picosecond pulses in a 200 m long birefringent fiber nonlinear directional coupler.

This work was carried out in the framework of the agreement between Fondazione Ugo Bordoni and the Istituto Superiore Poste e Telecomunicazioni.

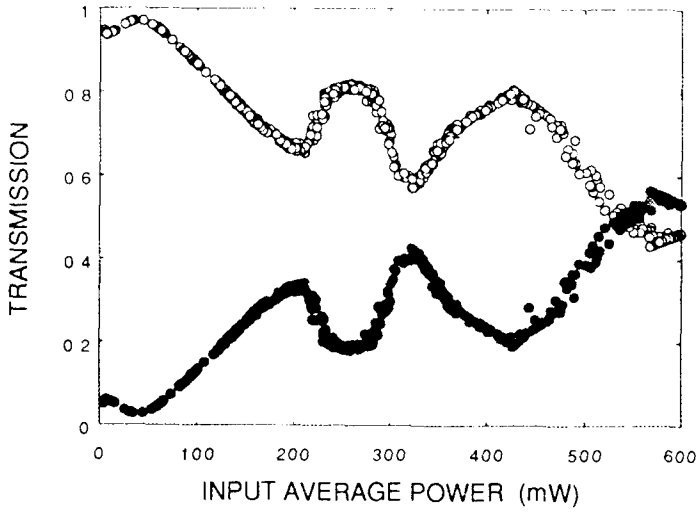

Figure [1]: Measured fraction of output energy in the two counterrotating circular polarizations versus input average power.

REFERENCES

[1] S.M. Jensen, IEEE J. Quantum *Electron.* **QE-18**,1580 (1982); A.A. Maier, Sov. J. Quantum Electron. **12**, 1190 (1982).

[2] D. D. Gusovskii, E. M. Dianov, A. A. Maier, V. B. Neustruev, V. Osiko, A. M. Prokhorov, K. Yu. Sitarkskii, and A. I. Shcherbakov, *ibidem*, **17**, 724 (1987); A.A. Maier, Yu.N. Serdyuchenko, K.Yu. Sitarskii, M.Ya. Shchelev, and I.A. Shcherbakov, *ibidem*, **17**, 735 (1987).

[3] S.R. Friberg, Y. Silberberg, M.K. Oliver, M.J. Andrejco, M.A. Saifi, and P.W. Smith, Appl. Phys. Lett. **51**, 1135 (1987); S.R. Friberg, A.M. Weiner, Y. Silberberg, B.G. Sfez, and P.W. Smith, Opt. Lett. **13**, 904 (1988).

[4] S. Trillo, S. Wabnitz, R.H. Stolen, G. Assanto, C.T. Seaton, and G.I. Stegeman, Appl. Phys. Lett. **49**, 1224 (1986).

[5] S. Trillo, S. Wabnitz, N. Finlayson, W.C. Banyai, C.T. Seaton, G.I. Stegeman, and R.H. Stolen, Appl. Phys. Lett. **53**, 837 (1988); S. Trillo, S. Wabnitz, N. Finlayson, W.C. Banyai, C.T. Seaton, G.I. Stegeman, and R.H. Stolen, IEEE J. Quantum Electron. **QE-25**, 104 (1989).

[6] B.K. Nayar, N. Finlayson, N.J. Doran, S.T. Davey, D.L. Williams, and D.J. Arkwright, Opt. Lett. **16**, 408 (1991).

[7] A.J. Barlow, J.J. Ramskov Hansen, and D.N. Payne, Appl. Opt. **20**, 2962 (1981).

[8] F. Matera, and S. Wabnitz, Opt. Lett. **11**, 467 (1986); S. Trillo, and S. Wabnitz, Appl. Phys. Lett. **49**, 752 (1986).

[9] See, e.g., *The Handbook of Mathematical Functions*, M. Abramowitz and I.A. Stegun, eds. (Dover, New York, 1965) Chapt. 17.

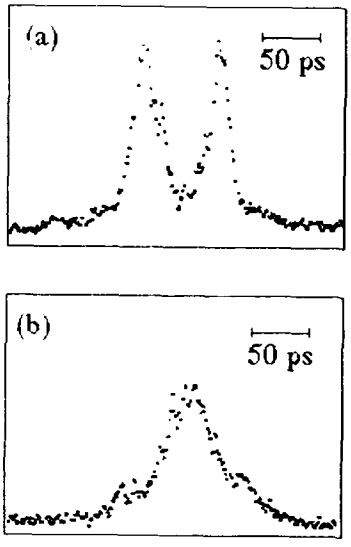

Figure [2]: Streak-camera pictures of the polarization break-up of output pulses.

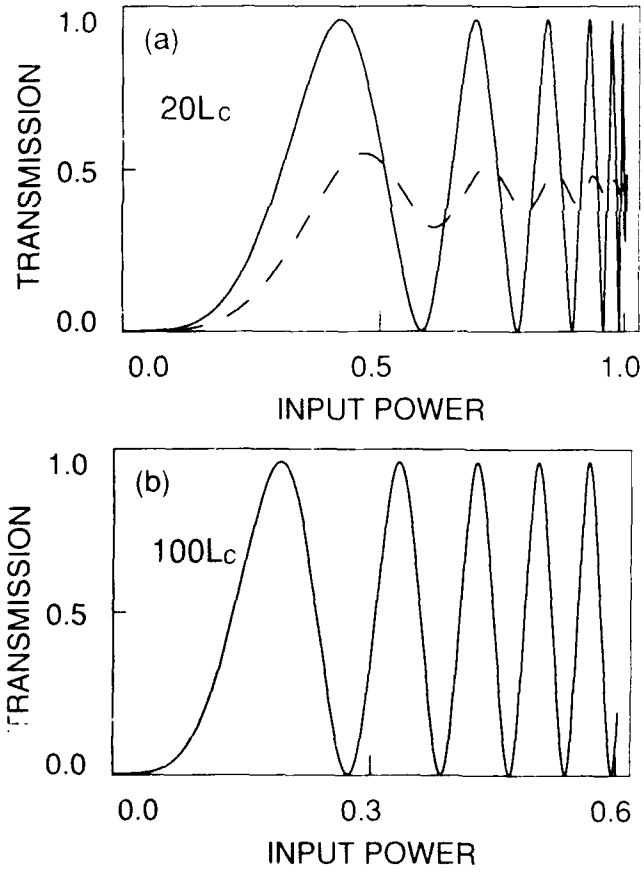

Figure [3]: Continuous wave nonlinear transmissions of long NLDC's.

NONLINEAR POLARISATION EFFECTS IN SELF-SWITCHING NONLINEAR FIBRE LOOP MIRROR DEVICES

B. K. Nayar, N. Finlayson and N. J. Doran
BT Laboratories, Martlesham Heath, Ipswich IP5 7RE, UK.

SUMMARY

The nonlinear fibre loop mirror (NOLM) has been shown to be a versatile device for all-optical switching [1], ultrafast multiplexing/demultiplexing [2], logic applications [3], pulse shaping [4] and passive mode-locking for fibre lasers [5]. Initially, the NOLM devices were fabricated using polarisation-maintaining fibres due to concerns about polarisation stability. This can be particularly significant in self switching devices due to differential *nonlinear polarisation rotation* arising from the unequal powers in the counter-propagating signals. However, the use of polarisation-maintaining fibres is not attractive as coupler fabrication is difficult and a higher loss results when splicing to standard fibres. Recently, stable operation of a dual-wavelength NOLM ultrafast multiplexer/demultiplexer has been demonstrated using 6.4 km long standard telecommunication fibre [6]. In this paper we present experimental results on nonlinear polarisation effects in a self-switching NOLM fabricated from a standard telecommunication fibre.

A schematic of the NOLM configuration used in our experiment is given in Fig. 1. The NOLM was fabricated by splicing the ends of a 2.1 km long monomode fibre to a fused fibre coupler having a power splitting ratio of 66:33. A coupler with a power splitting ratio of 94:6 was spliced to the input port of the NOLM to enable the measurement of the launch and reflected powers. A fibre polarisation controller was used in the loop to bias the device to be reflecting, transmitting or in an intermediate mode in the linear regime. The reflecting and transmitting ports are designated ports (1) and (2) respectively. A 1.32μm mode-locked Nd:YAG laser generating 120 ps pulses (FWHM) at a repetition rate of 76 MHz was used as the source. The input polarisation azimuth angle and power were varied in a controlled manner to permit investigation of their effects on the NOLM characteristic.

Initially, we biased the NOLM to be in the reflecting mode and measured the transmittance of ports (1) and (2) as a function of the peak input power. The results are plotted in Fig. 2. In the linear regime port (2) has a transmittance of about 10% which agrees with the calculated value using the coupler's power splitting ratio. This increases to 74% for an input peak power of 3.6 W and is in agreement with the calculated value using an effective fibre length of 1.92 km (fibre attenuation is 0.37 dB/km), an effective core area of 78 μm^2

and a total lumped loss of 0.7 dB. For peak input powers in excess of 7.5 W the influence of Raman scattering becomes significant and results in approximately equal transmittance from both the ports.

To investigate nonlinear polarisation effects experimentally the fibre polarisation controller was used to set different linear bias conditions. At each linear bias setting the transmittance of the reflected and transmitted ports of the NOLM were plotted as a function of the input power for 10 input polarisation azimuth angle settings at 22.5° intervals. In Figs. 3 (a) - (e) the transmittances of ports (1) and (2) are plotted as a function of the input power for linear bias conditions corresponding to (a) maximum transmittance, (b) 75% transmittance, (c) 50% transmittance, (d) 25% transmittance, and (e) minimum transmittance (i.e. optimally reflecting). It can be seen that when the device is biased in the reflecting mode (fig. 2 (e)) the nonlinear response is virtually insensitive to input polarisation azimuth angle. The device exhibits a somewhat greater sensitivity for the transmitting mode bias setting (fig. 2 (a)). For all other linear bias conditions the NOLM response is very sensitive to input polarisation azimuth angles. Thus if any external perturbations cause the linear bias conditions to drift from either the reflecting or transmitting modes the device stability will significantly deteriorate. At the meeting we will discuss the practical implications for self-switching NOLM devices fabricated using standard telecommunication fibres and provide a theoretical model for the above experimental observations.

REFERENCES

1. B.K. Nayar, K.J. Blow, and N.J. Doran, Opt. Computing & Processing, **1**, 81(1991).
2.K.J. Blow, N.J. Doran, and B.P. Nelson, Electron. Lett., **26**, 962(1990).
3. M. Jinno and T. Matsumoto, Opt. Lett., **16**, 220(1991).
4. K. Smith, N.J. Doran, and P.G.J. Wigley, Opt. Lett., **15**, 1294(1990).
5. I.N. Duling III, Electron. Lett., **27**, 544(1991).
6. B.P. Nelson, K.J. Blow, P.D. Constantine, N.J. Doran, J.K. Lucek, I.W. Marshall, and K. Smith, Accepted for publication in Electron. Letts.

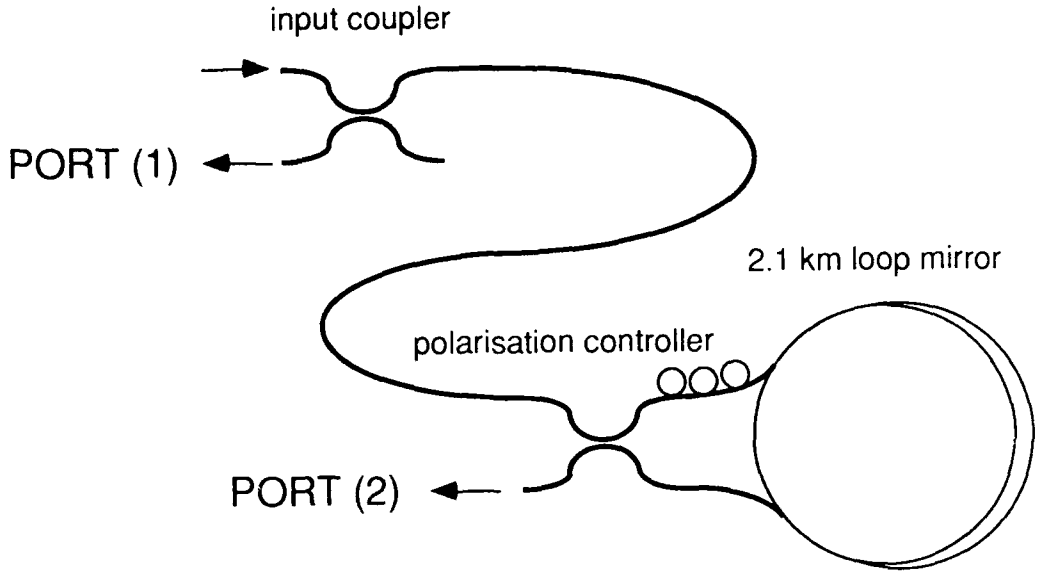

Fig. 1 Schematic of the experimental setup.

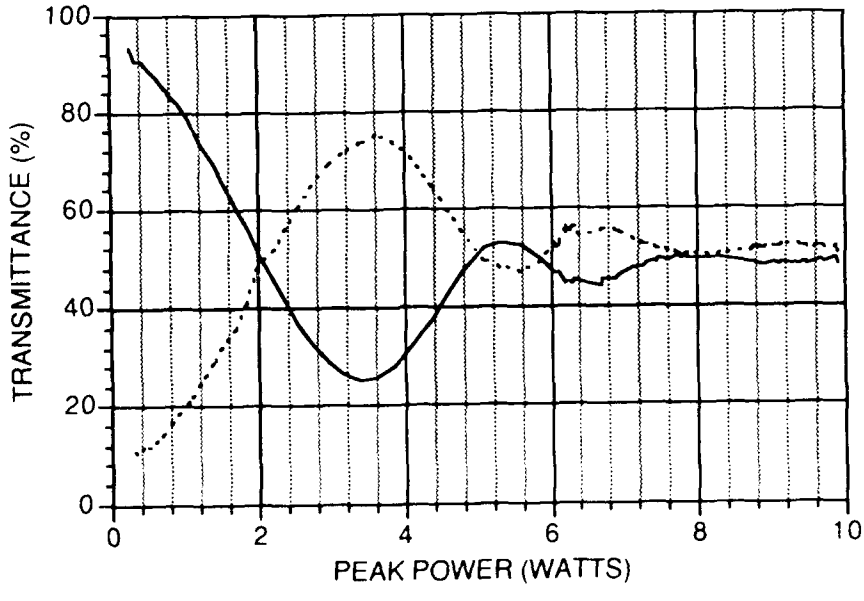

Fig. 2 Transmittance of ports (1) (solid line) and port (2) (dashed line) of the NOLM in the reflecting mode as a function of input peak power.

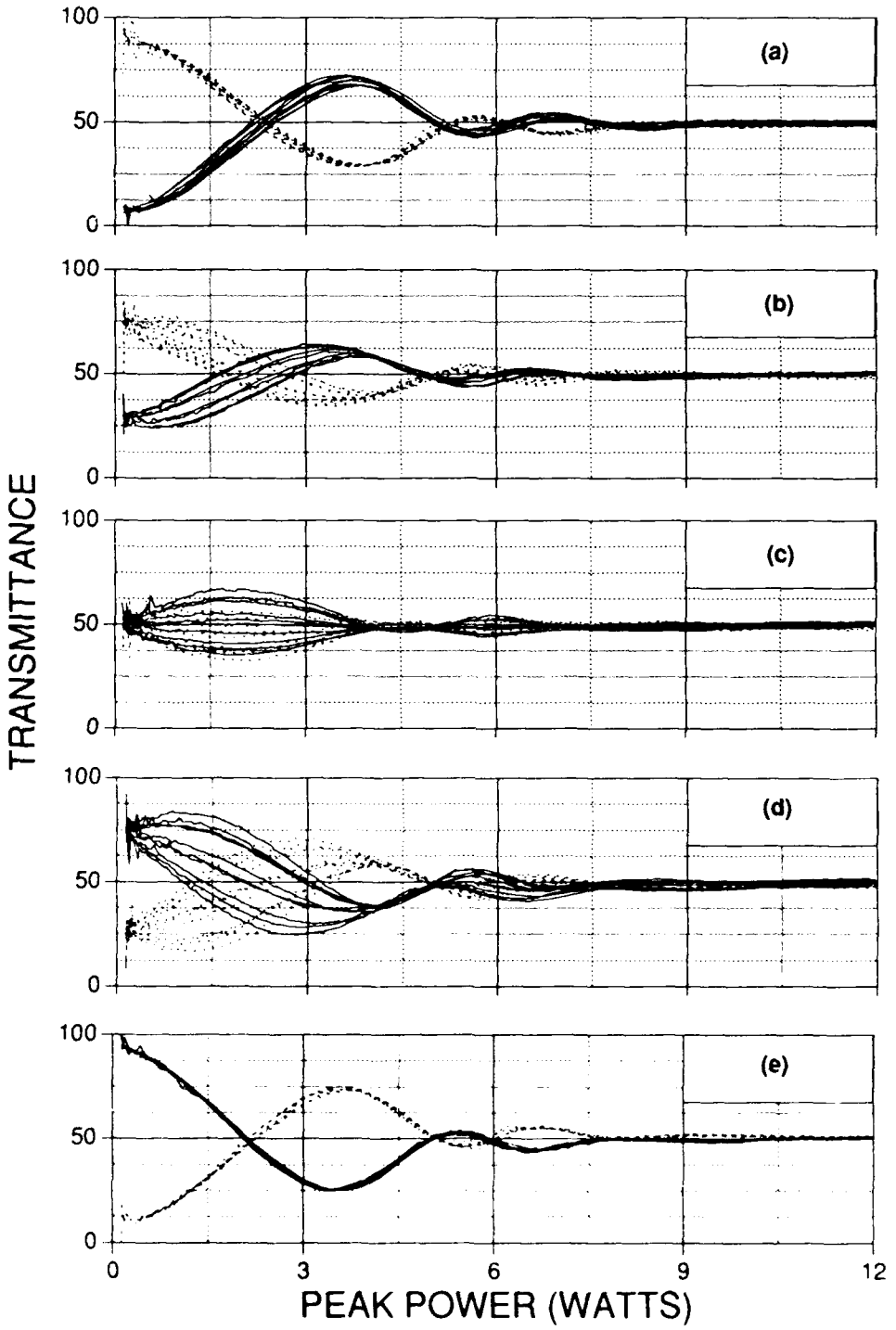

Fig. 3 Transmittance of port (1) (solid lines) and port (2) (dashed lines) of the NOLM as a function of input power and polarisation when biased for (a) maximum, (b) 75%, (c) 50%, (d) 25% and (e) minimum linear transmittance.

Fiber Switches: 2

WB 11:15am–12:30pm
Palmerston Room

Andrew C. Walker, *Presider*
Heriot-Watt University, United Kingdom

Billiard Ball Soliton Interaction Gates

M.N. Islam and C.E. Soccolich
AT&T Bell Laboratories
Holmdel, New Jersey 07733

We demonstrate a temporal, conservative-logic interaction gate that can perform AND, inversion and routing functions. The billiard-ball like logic is based on elastic collisions between temporal solitons in optical fibers. Fredkin and Toffoli [1] introduced an interaction gate (Fig. 1a) as a universal, conservative-logic primitive and discussed a spatial implementation using the collision between billiard balls where the logic operation corresponds to the locus of the balls (Fig. 1b). The fundamental interest in the interaction gate results from the reversibility of the operation; i.e. the input values can be reconstructed from the output states. However, conservative, reversible gates may have limited practical value since generally they do not have logic level restoration (such as in digital gates) and they may not have gain or fan-out.

Solitons can be used to demonstrate billiard-ball models of logic because they are internally balanced pulses that behave in many way like particles. Because of the typically weak nonlinearity of most materials, we map the spatial interaction gate of Fig. 1 into a temporal analog (i.e. different positions correspond to different time slots), which enables us then to use low energy pulses in long lengths of optical fibers. Consider two initially separated solitons that are traveling toward each other (having different group velocities or center frequencies) in a fiber. Gordon [2] has studied analytically the elastic collisions between these pulses and finds that:

— although details in the interaction region depend on the phase between the two pulses, after they separate the result is independent of the initial phase;

— the two pulses appear to pass through each other and continue with their original velocities; and

— as a result of the collision, each pulse is phase shifted and displaced so as to increase their original separation.

Some of these ideas were recently verified by two-frequency soliton experiments [3], although the temporal displacement was not explicitly studied.

Desired properties of logic gates include cascadability, phase-independent operation, low switching energy and fan-out or gain. For a cascadable gate the two inputs and the output should be at the same frequency so that the output from one gate can drive an identical gate. Yet, to observe the billiard-ball collisions we need two solitons with different group velocities. We satisfy both of the above criteria by passing one of the inputs through wavelength dependent optics so as to skew its spectrum. Our cascadable logic gate has two temporally separated, identical frequency input pulses that are combined along the same polarization using beam splitters. The logic operation depends on the time slot selected at the output, and fan-out can be obtained if one of the inputs is lower in energy than the output.

We obtain $\tau \sim 430$fsec pulses at $\lambda \sim 1.67$ μm from a passively modelocked color center laser. The input is divided into three beams, which correspond to two inputs (A and B) and one reference beam. Input A is reflected from a dichroic beam splitter with the reflectivity shown in Fig. 2. Since the reflectivity increases with increasing wavelength, the ~10 nm FWHM pulse spectrum appears to shift to longer wavelengths. The two inputs are recombined along the same polarization with input A (which travels slower) 4.5τ ahead of input B, and the timing and phase between A and B can be further varied using a delay stage and a piezo-electric transducer on one mirror. The inputs are coupled into a 1090 m length of polarization maintaining, dispersion shifted fiber. From cross-correlation measurements we find that the pulses travel $7.5\ \tau$ relative to one another in the fiber, so the walk-off length is $l_{wo} \sim 145$ m and the frequency separation is $\delta\lambda = \delta T/(D \times L) \equiv 0.61$nm.

The fiber output is combined with the orthogonally polarized reference pulse and the two are sent to a cross-correlator. In Fig. 3 we show the cross-correlation for A and B alone and with both pulses incident (A and B equal to 17 pJ in the fiber). We find that either input pulse alone arrives at the output in separate time slots, and this separation can be further increased by lengthening the fiber. When both pulses are incident, they collide in the fiber and each pulse experiences a one time displacement of 3.5 τ in the direction it originally traveled. We verified that the interaction is phase independent by varying the piezoelectric transducer and checking that the pulses still remain well separated.

The logic operation performed depends on the time slot selected at the output. In time slot # 1 we observe $A \cdot B$, which acts therefore as an AND gate. In time slot # 2 we observe $\bar{A} \cdot B$: if B is a clock pulse (B = 1) then time slot # 2 acts as an inverter. Furthermore, if A is a control beam, then time slots #1 and #2 appear as a temporal routing gate for B. We select the time slots centered around B since input B was not distored by the dichroic beam splitter in this example, and in order to cascade soliton interaction gates the desired time slot must be the only time slot seen by the next gate. For example, to cascade the AND-gate we align time slot #1 to the B-input of the next gate. Then, for a 7.5 l_{wo} fiber the next gate does not interact with the previous gate's $\bar{A} \cdot B$ or $A \cdot \bar{B}$ since they are at least 3.5τ further away.

To test if the interaction gate can exhibit gain, we varied the amplitude of input A and measured the displacement of B with and without A. In Fig. 4 the dots represent the experimentally measured displacement, and we find that to obtain at least a 2τ shift requires about 11 pJ of energy, which means that the gain is only 1.5. To compare theory and experiment, we calculate the predicted displacement from Gordon's analytic formulas. However, Ref. 2 assumes that both pulses are solitons of the form $u_i = A_i sech(A_i t)$, whereas the inputs to our fiber are of the form $u_i = A_i sech(t)$. Nonetheless, for a lowest order approximation we can employ Gordon's formulas by replacing the amplitudes A_i by the normalized energies E_i/E_s, where E_s is the fundamental soliton energy. Using experimental values for the soliton parameters (Z_o = 13.14 m, E_1 = 17 pJ, ΔV= 0.1) we generate the solid curve in Fig. 4 for E_b=E_s=17pJ. When E_a=E_b=E_s the agreement between theory and experiment is excellent since both pulses are launched as fundamental solitons. For E_a < 5 pJ (A_a < 0.5) the pulse is no longer a soliton and it disperses even before the pulses meet: the experiment diverges from the theory since we cannot obtain complete walk-through with the dispersive wave. Between 5pJ < E_a < 15 pJ the experiment oscillates around the theory probably because of the radiation field (an input A_i sech (t) will radiate for $A_i \neq 1$ to form into a soliton of lesser energy). Additionally, there may be some non-soliton component since the laser pulses are Gaussian rather than hyperbolic secant.

In summary, we have shown that the elastic collision properties of solitons can be used to implement an interaction gate. For our experimental parameters an AND-gate requires 17pJ pulses, and an inverter with a gain of 1.5 is possible with a switching energy of 11pJ. Although such a conservative logic gate may not be "practical," it is of fundamental interest to verify that particle-like properties of solitons can be used to implement a billiard ball model of logic. If materials with sufficient nonlinear index without excessive absorption become available, it should also be possible to implement an interaction gate using spatial solitons in slab waveguides.

[1] E. Fredkin and T. Toffoli, Int. J. Theor. Phys. **21**, 219 (1982).

[2] J.P. Gordon, Opt. Lett. **12**, 1038 (1987).

[3] S.R. Friberg, W. Jiang, Y. Sakai and R.J. Hawkins, in **Ultrafast Phenomena VII**, C.B. Harris, E.P. Ippen, G.A. Mourou, A.H. Zewail, eds., (Springer-Verlag, Berlin, 1990), p. 184.

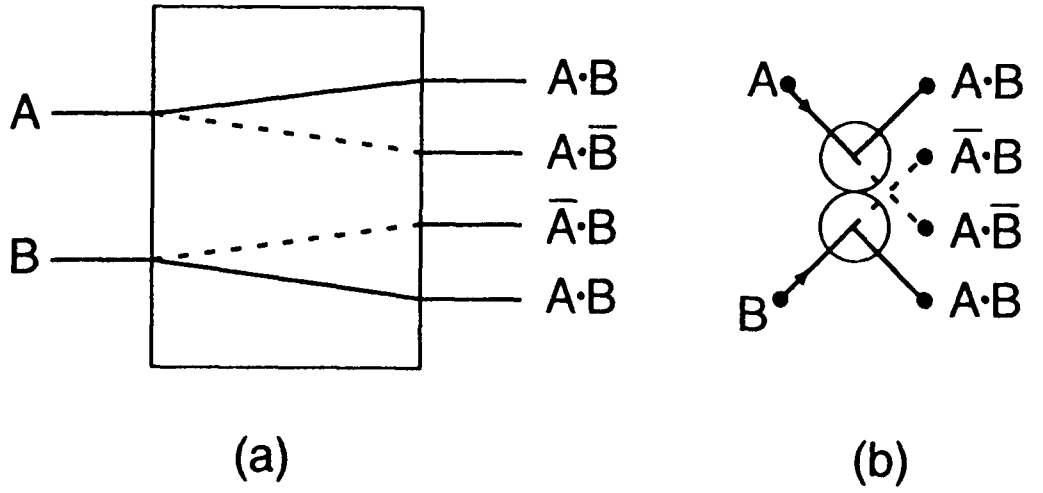

Fig. 1. (a) Schematic of an interaction gate and (b) a simple implementation using billiard balls.

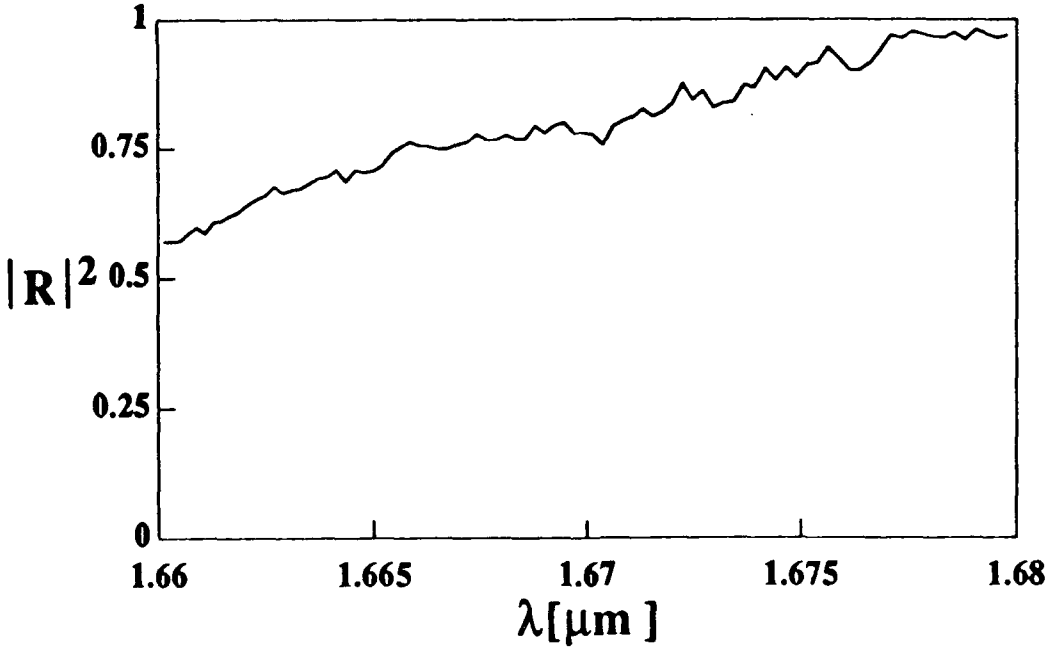

Fig. 2. Reflection coefficient of the dichroic beam splitter that is used to skew the spectrum to longer wavelengths of one input.

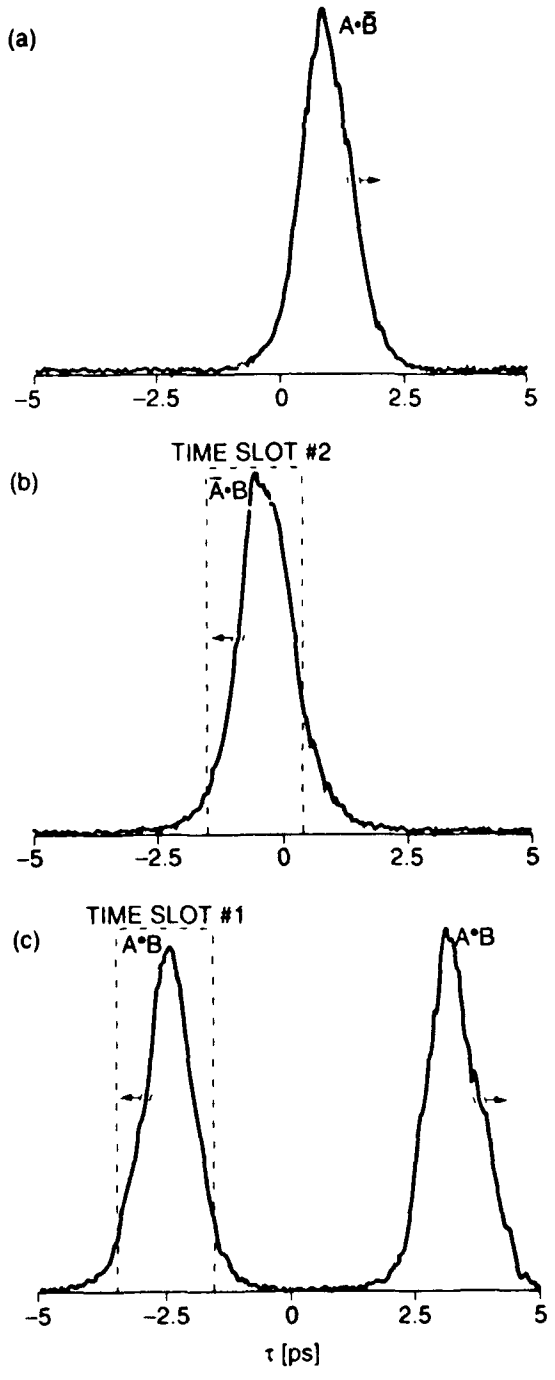

Fig. 3. Cross-correlation of soliton interaction gate output with a reference pulse for: (a) A alone; (b) B alone; and (c) A and B incident.

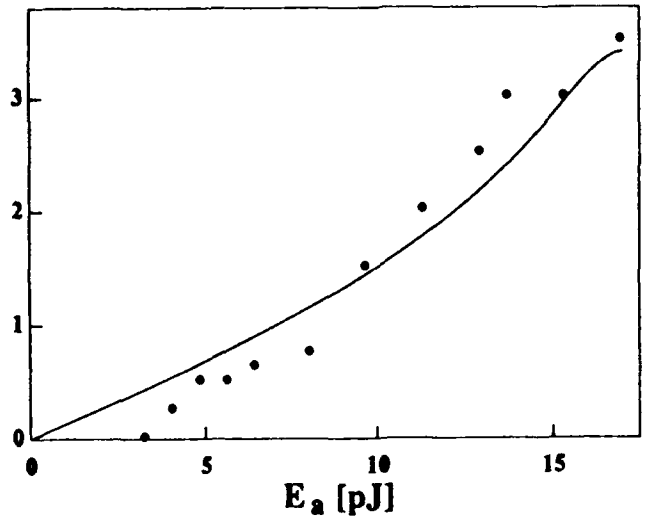

Fig. 4. Normalized displacement of input B versus energy of input A. The dots correspond to the experimental data, and the solid line is calculated from Gordon's theory [2].

Application of Ultrafast Gates to a Soliton Ring Network

C.E. Soccolich, M.N. Islam, B.J. Hong [1], M. Chbat [2] and J.R. Sauer [3]
AT&T Bell Laboratories, Room 4C-436
Holmdel, N.J. 07733-1988

We describe the application of ultrafast, all-optical logic gates to a soliton-based local or metropolitan area network. The slotted ring network discussed here serves a few hundred users and uses self routing packet switching with a 100 Gbps peak data rate and a 1.25 GHz packet rate. This is a "light-pipe" system where the data remains in optical format throughout the network, converting to electronics only at the host and destination nodes. The packet header (or address) is selected and decoded using recently demonstrated soliton dragging and trapping logic gates [1,2], which are long latency, ultrafast fiber devices that satisfy all cascadability and logic requirements for a digital optical processor. A ring network is one potential application of these logic devices that requires only a handful of gates per node.

Our purpose here is to provide an example of a complete system design that uses the features provided by ultrafast gates in order to discover and address the relevant issues regarding their use in systems. The design criterion is to exploit the bandwidth of these fast gates while minimizing their number, and to use them only in the required pipelined, feed-forward architecture. Although the following design may not be "practical" when compared to existing or contemplated wide-area networks, it is intended to stimulate consideration of utilizing the bandwidth available from optical fibers by using ultrafast gates.

The hierarchical network is a slotted ring with up to 254 user access nodes, each node spaced by several gate latencies. In this straw man example we select a trivial protocol: 1) if *ForMe* then remove packet and replace with empty packet; or, 2) if *Empty* and packet queued in buffer, then replace the empty packet with the new packet. The design focuses on the network access nodes (Fig. 1), where ultrafast gates are used to decode the header, which has the same physical format as the data. The code matching logic module operates at the bit-rate and checks if the header matches the local address or corresponds to an empty packet, and then provides electronic signal outputs that control a network of routing switches. The delay in the upper arm compensates for the latency in the logic module. The exchange/bypass network routes the incoming packet or a new packet, operates at the packet rate, and can be reconfigured in the time guard band between packets. When the packet reaches its destination, it is demultiplexed or bit-rate down-converted to speeds accessible by electronic shift registers. An optical phase-lock loop is used to synchronize the local clock to the ring data, and erbium-doped fiber amplifiers are used to compensate for the insertion and splitter losses.

Block diagrams of the code-matching logic modules and the exchange/bypass network are shown in Fig. 2. The first gate of the code-matching logic module removes the 8-bit header from the packet and performs logic level and timing restoration. The resulting signal is duplicated and forwarded to two separate selection circuits. The upper AND-gate detects if the packet is empty: an empty packet is assigned an all one header to maintain clock synchronization. The lower circuit, which consists of an XCR-gate and another AND-gate, detects if the packet should be read. We select the logic functionality for both circuits so that the desired output signal occurs only when all eight output bits are zero, making it simpler to set the threshold.

The exchange/bypass network routes the packet depending on the signals from the code-matching logic module. If READ is true, then the optical exchange/bypass network routes the incoming packet to the bit-rate down converter and switches an empty packet on-line. If the EMPTY and QUEUE bits are both on, the empty packet is replaced with the new packet. Only one input to each routing switch is used to avoid cross-talk.

Once the optical packet reaches its destination, fast gates must demultiplex the packet information to bit rates accessible by electronic shift registers. Note that bit-rate down conversion only requires devices that can operate at the repetition rate of the bits. Although ultrafast soliton trapping or dragging logic gates can be used for this function, it may be simpler and cheaper to use 2x2 narrow band devices such as

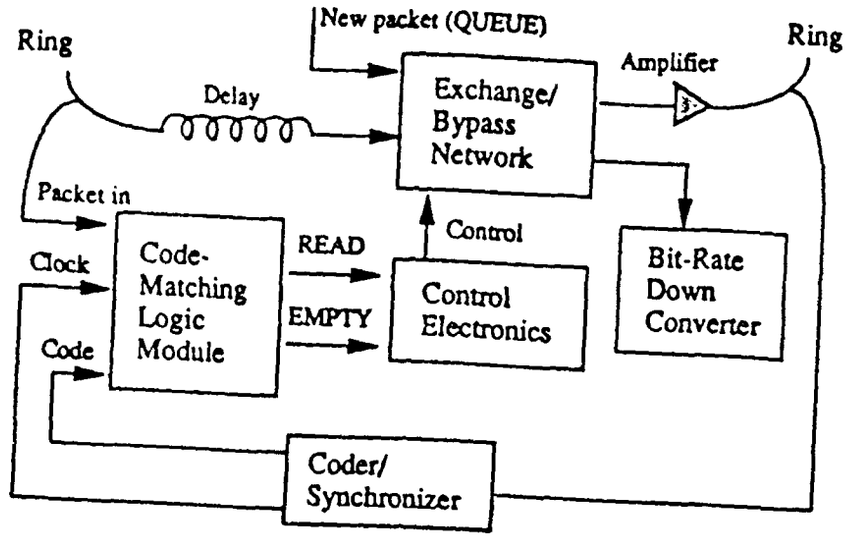

Figure 1. Schematic of a network access node in a soliton ring network.

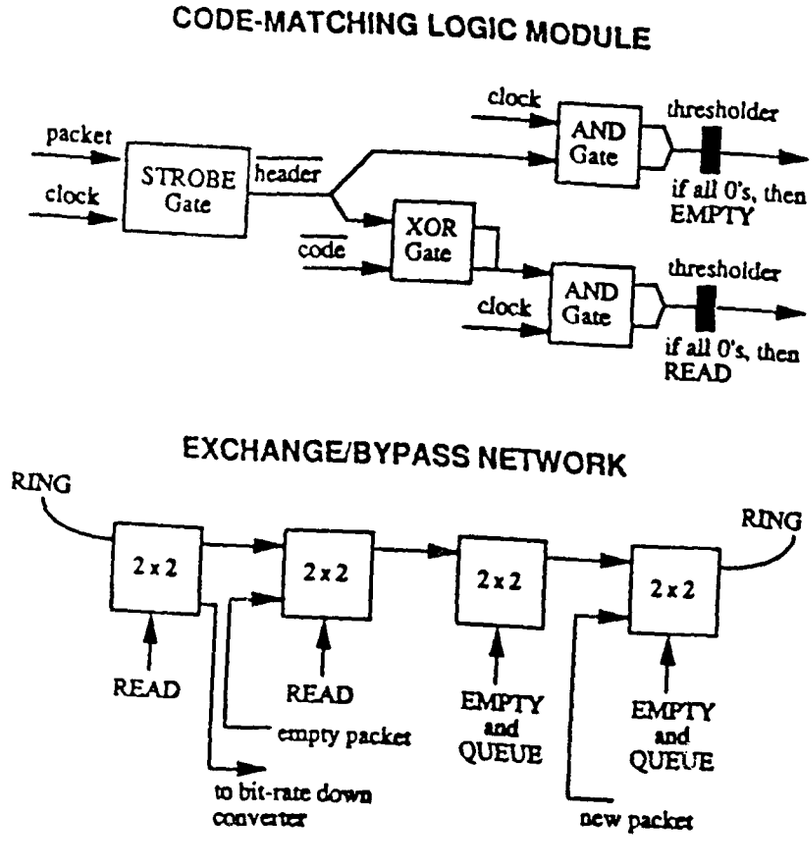

Figure 2. Block diagrams of the code-matching logic module and the exchange bypass network. The code matching logic contains the ultrafast soliton gates, while the exchange/bypass network consists of slower electro-optic switches.

$LiNBO_3$ waveguide switches. Further details on the various modules as well as failure safeguards and the scavenger network node are described in Ref. [3].

The configuration for the various soliton fiber gates used in the code-matching logic module are detailed in Fig.3. The soliton dragging strobe gate with gain and timing restoration is shown in Fig. 3a. It consists of two moderately birefringent fibers (MBF) with an erbium-doped fiber amplifier spliced in the middle, and the output is coupled to a polarization maintaining fiber (PMF). The clock and incoming packet input are combined using a polarizing beam splitter (PBS), and the inverted *Header* output is selected using a polarizer (POL). Note that *Clock* is on only during the *Header* portion of the packet and must be carefully synchronized with the incoming data using an optical phase-locked loop.

A soliton dragging XOR-gate for comparing the *Header* with the local *Code* or address is shown in Fig. 3b. The inverted *Code* and *Header* are combined using PBS, and coupled into a length of MBF spliced to a PMF. At the output the two polarizations are separated, delayed to compensate for the linear birefringence, and then recombined with a PBS followed by a POL placed at 45°. The outputs for both the strobe gate and XOR-gate are in time shift keyed (TSK) format in which a logical "1" corresponds to a properly timed pulse and a logical "0" to an improperly timed pulse.

The final stage of ultrafast gates are soliton trapping AND-gates that convert TSK outputs to amplitude modulated outputs. The two inputs are combined using a PBS, propagate in a MBF, and then pass through a narrow band frequency filter (Fig. 3c). Figure 4 shows the frequency spectrum at the MBF output with a single input pulse and both input pulses present. By placing the filter bandpass on the tail of the single pulse spectrum, we obtain a large amplitude output only when both pulses are present and temporally coincident.

By using bit-rate switches and guaranteeing bit-level synchronization, we can implement a "logic tuner" rather than a physical tuner (as in wavelength division multiplexing). For example, the frequency filter in a wavelength system is replaced by the local node address, and we transmit to different users by different codings of the header. In this time division multiplexed system each node shares the same physical representation, which makes tasks such as broadcast simpler. Also, for the time domain case the hardware in each node can be identical and the architecture is easily adapted to a packet switching environment.

In summary, we describe the access node in a 100Gbps soliton, slotted ring network that exploits the high speeds available from soliton logic gates. The ultrafast gates are used to select and decode the header and, hence, permit us to implement a "logic tuner." From this study we find several issues that arise when trying to implement the soliton ring network:

1. in the 100 Gb/s régime, the logic gates must have a switching energy at or below 1 pJ in order to maintain the optical power requirements at reasonable levels;
2. even for a system with just a few ultrafast gates, the logic gates must be cascadable, restoring both timing and amplitude, for a robust implementation;
3. optical amplifiers with high saturation power, in the range of 0.3 W, are needed for ultrafast, all-optical transport systems; and
4. clock extraction and packet injection synchronization at the bit-level are major issues for an ultrafast network.

[1] B.J. Hong is with Penn State University, [2] M. Chbat is with Princeton University, and [3] J.R. Sauer is with the Optoelectronic Computing Systems Center at the University of Colorado.

[1] M.N. Islam, C.E. Soccolich and D.A.B. Miller, "Low-energy ultrafast fiber soliton logic gates," Opt. Lett. **15**, 909 (1990).

[2] M.N. Islam, C.J. Chen and C.E. Soccolich, "All-optical Time Domain Chirp Switches," Opt. Lett. **16**, 484 (1991).

[3] J.R. Sauer, M.N. Islam, and S.P. Dijali, "A Soliton Ring Network," (submitted to J. Lightwave Tech.).

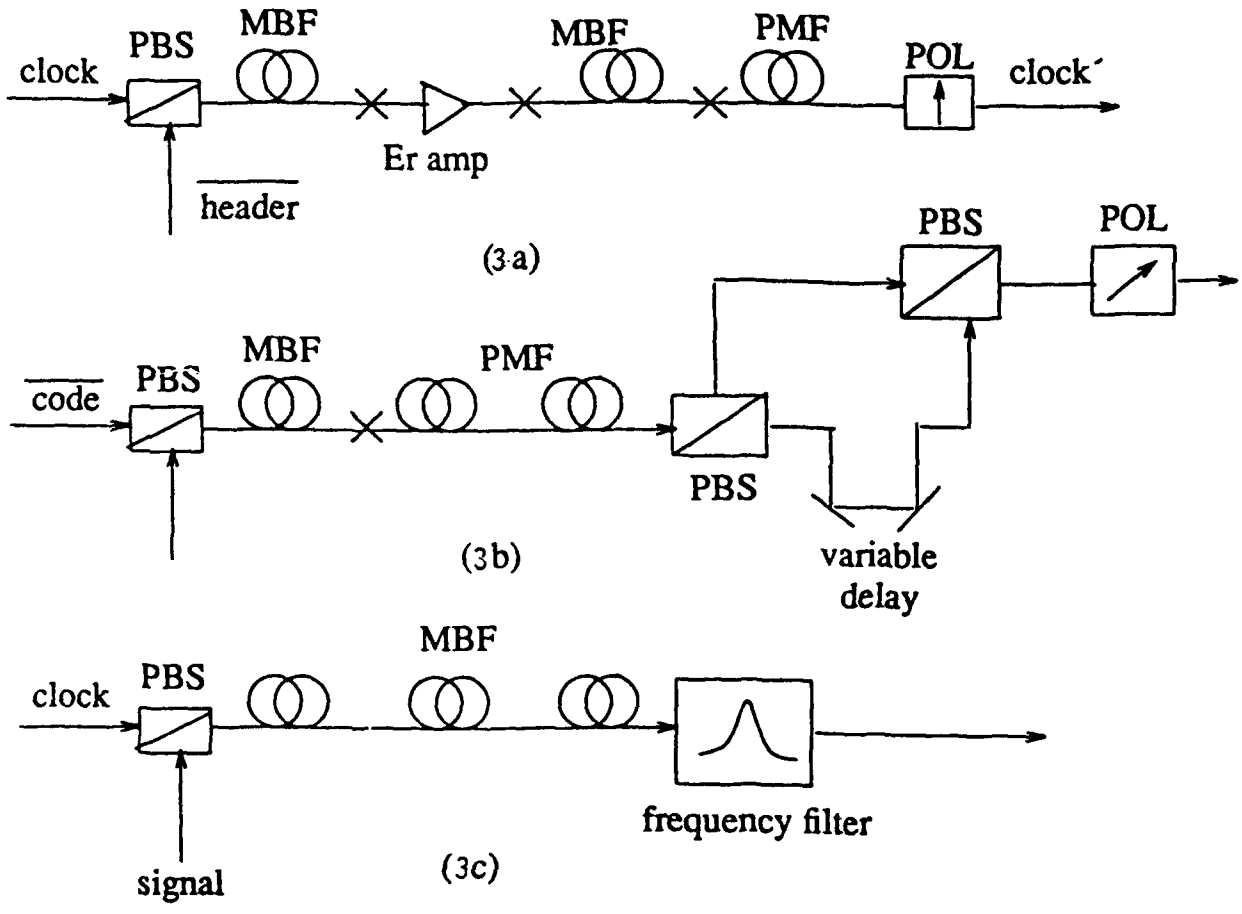

Figure 3. Schematic representation of soliton logic gates: a) Strobe gate; b) XOR gate; c) AND gate

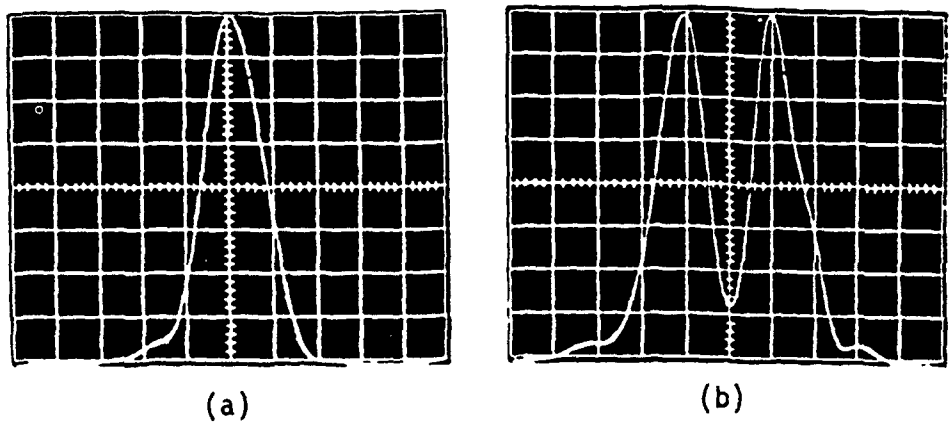

Figure 4. Spectral output of a moderately birefringent fiber before the frequency filter in the AND gate: a) only clock present at input; b) both clock and signal present at input.

All-optical routing switch with tolerance to timing jitter at 2.5 Gb/s

P. M. W. French*, M. C. Gabriel, H. Avramopoulos, D. J. Di Giovanni, R. E. LaMarche, H. M. Presby and N. A. Whitaker, Jr.

*P. M. W. French is a Royal Society University Research Fellow on leave from the Physics Department, Imperial College

AT&T Bell Laboratories, Crawfords Corner Road, Holmdel, NJ. 07733.
Tel: 908-949-1478

All-optical demultiplexing and routing are necessary for the implementation of ultra-high bit rate time-division multiplexed communications systems. While existing electro-optic demultiplexers can be operated at extremely high speeds with sinusoidal drive signals [1], there is much interest in developing systems which can switch out arbitrary patterns of pulses from a data stream. If the pulses can be completely switched out, these systems could be used in signal routing applications. The wide bandwidth of all-optical devices based on the nonlinear Kerr effect in fibers should support this mode of switching at Gb/s rates and beyond. This experiment is a demonstration of such an arbitrary, all-optical demultiplexer/router which does not require a special pulse format (e.g. solitons), which is tolerant of environmental changes and which is insensitive to timing errors between the signal and control pulses. The approach used is not wavelength-dependent and can be made insensitive to the input polarization states.

The device described here is based on a nonlinear fiber Sagnac interferometer . This has previously been used in one and two beam switching experiments and specifically as a demultiplexer [e.g. 2,3]. These earlier approaches typically used signal and control pulses at different wavelengths with WDM couplers/beam splitters to combine and separate them in the switch. In this experiment, birefringent fiber and polarization-preserving couplers were employed in a continuous fiber circuit, shown schematically in Figure 1. Employing polarization to discriminate between the signal and control channels permits the construction of a switch which is cascadable and which does not place constraints on the wavelengths of the incident signals. Also, the use of birefringent fiber, rather than non-polarization-maintaining fiber, makes the interferometer stable against temperature changes which otherwise modify the polarization of the signal pulses, and spoil the operation of the device. A further advantage of this approach is that the "slip" or walk-off between the signal and control pulses may be readily adjusted by "cross-splicing" appropriate lengths of fiber such that the pulses propagate alternately along the fast and slow axes.

Walk-off between the signal and control pulses results in complete switching of the signal pulses since they acquire a uniform phase change proportional to the integrated intensity of the control pulses [4]. In the absence of walk-off, special pulse shapes (e.g. rectangular pulses or solitons) are necessary to achieve complete switching. Since it is only the integrated intensity that matters, the control pulses may arrive at any time during a given time window which is determined by the fiber length and birefringence. Thus the switching is insensitive to timing errors in the control stream provided that this time window is longer than the pulse duration. The required control pulse energy for switching scales with the nonlinear interaction length. This need not be

limited to one walk-off length since cross-splices in the birefringent fiber can facilitate multiple interactions [5]. In the work presented here, a 500 m length of birefringent fiber was used with three cross-splices, resulting in a slip window of 380 ps. Walk-off can also be exploited in WDM-based Sagnac switches [e.g. 6] by taking advantage of group velocity dispersion. This approach, however, requires a specific matching between the fiber characteristics and the signal and control wavelengths [3].

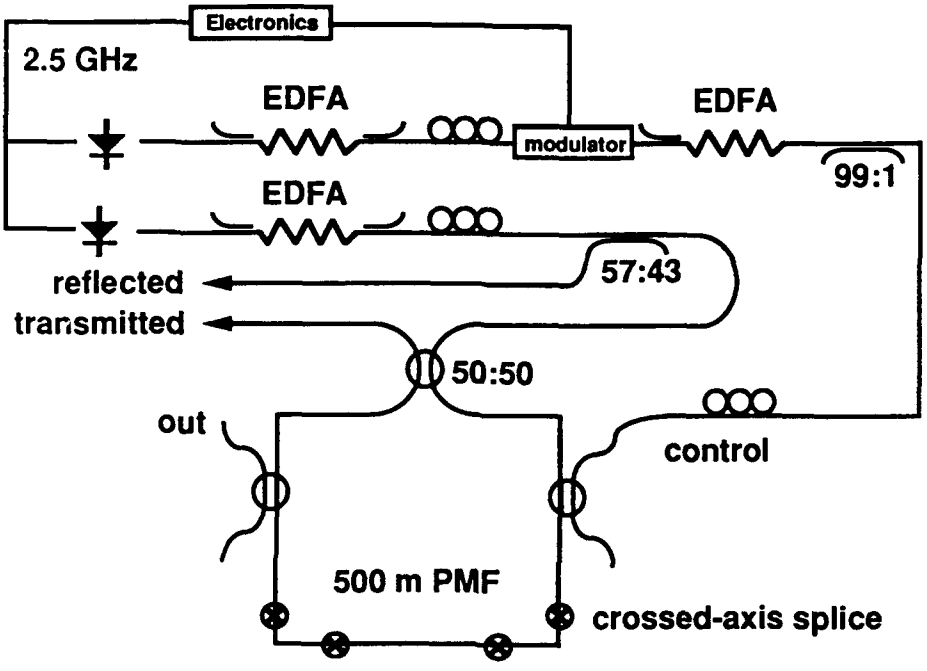

Figure 1. Experimental configuration.

In the experiment described here, both the signal and control pulses were of 80 ps duration and were derived from gain switched diode lasers which were amplified in Erbium-doped fiber amplifiers (EDFA). The signal pulses were amplified to an average power of 10 mW and sent through the Sagnac loop on one axis of the birefringent fiber. It was possible to make the cross-splices in the polarization-preserving fiber with a measured average loss of less than 0.03 dB and the polarization extinction was held at better than 15 dB. The transmitted and reflected signals were analyzed using a streak camera. The control pulses were amplified to an average power of 80 mW and injected onto the other fiber axis and then removed from the Sagnac loop using fiber polarizing beam-splitters. Complete switching was observed with a contrast ratio of 75:1 in transmission.

In order to test the sensitivity of the switch to timing jitter between the signal and control pulses, the arrival time of the signal and control pulses at the Sagnac loop was varied. Figure 2 shows how the reflectivity of the Sagnac interferometer varied as the relative delay between the pulses was adjusted. Switching was observed over a time window of 380 ps. The uniformity of switching observed over nearly the entire bit period is an attractive feature of this device. Figure 3

shows examples of streak camera traces of reflected signals from which arbitrary patterns of one or more pulses were switched out of the 2.5 Gb/s pulse stream. Complementary traces observed in transmission are also shown. The excellent stability of this system was demonstrated by directing a heat gun onto the 500 m Sagnac loop. No degradation in switching was observed.

The pulses used in this experiment were strongly chirped and their duration was approximately ten times the bandwidth-limit. In spite of this, excellent switching contrast was observed - demonstrating that the device does not require soliton or other special pulse profiles though, of course, these would also switch well. Using shorter pulses or a longer fiber in the Sagnac loop would reduce the power necessary to switch the device - the scaling being like all other interferometer switches with the control pulse required to induce a π phase change. A simple scheme has been developed which permits the device to function independently of input polarization states. Experiments are underway to demonstrate this principle and the results will be presented.

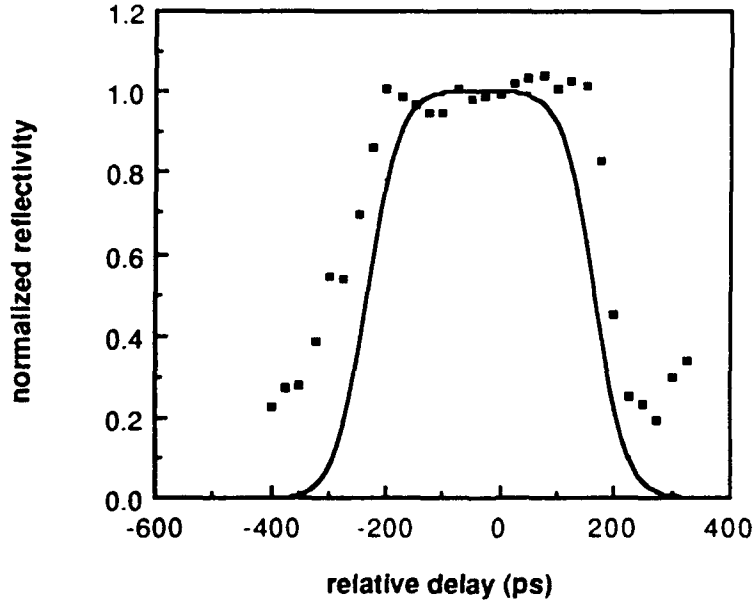

Figure 2. Plot of signal reflection against relative delay of signal and control pulses. Solid curve is theoretical prediction.

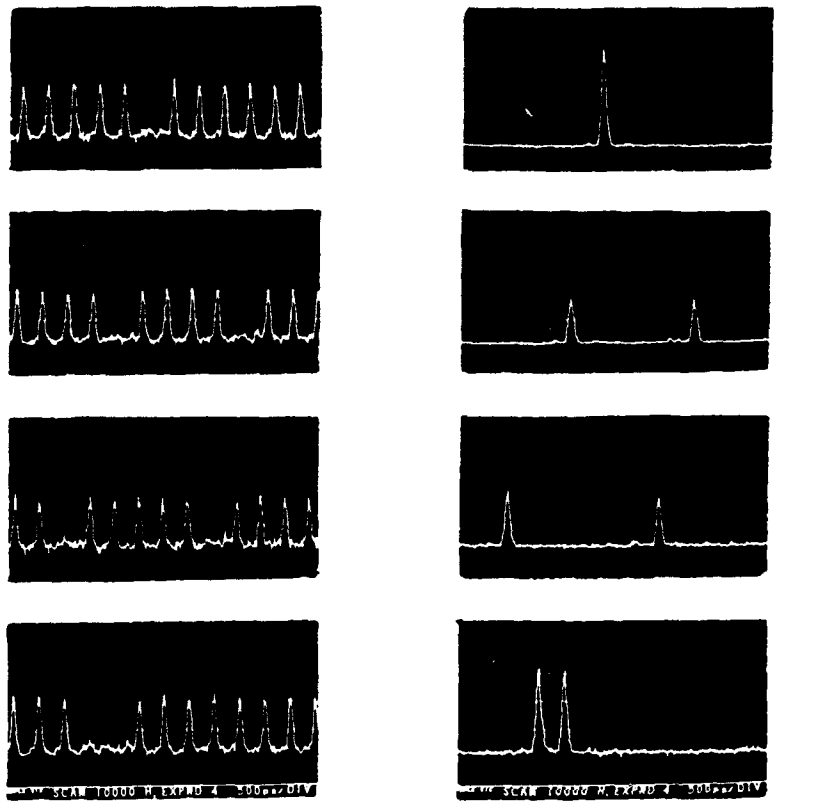

Figure 3. Reflected signal pulse trains from which selected pulses have been switched out, together with the corresponding pulse trains in transmission.

References

1) S. K. Korotky and J. J. Veselka, Proc. *OFC* 1990, Paper TuH2.
2) K. J. Blow, N. J. Doran and B. P. Nelson, *Electron. Lett.* **26** (1990) 962.
3) A. Takada, K. Aida and M. Jinno, Proc. *OFC* 1991, Paper TuN3.
4) A. Lattes, H. A. Haus, F. L. Leonberger and E. P. Ippen, *IEEE J. Quantum Electron.* **QE-19**, (1983) 1718.
5) J. D. Moores, K. Bergman, H. A. Haus and E. P. Ippen, *JOSA* **B8**, (1991) 594.
6) B. K. Nayar and H. Vanherzeele, *IEEE Photon. Lett.*, **2** (1990) 603.

Ultrafast, Dual-Path Optical Kerr Demultiplxer Utilizing a Polarization Rotating Mirror

T. Morioka, H. Takara and M. Saruwatari

NTT Transmission Systems Laboratories
1-2356 Take, Yokosuka, Kanagawa 238-03 Japan
Phone:81-468-59-3571

1. Introduction

All-optical signal processing attracts much attention to overcome the speed limitations imposed by the electrical circuits. An all-optical switching scheme using intensity-dependent refractive index in Kerr media, especially optical fibers, is one of the promising candidates for processing incoming densely time-multiplexed signals, namely optical demultiplexing, optical routing, and logic operations. To date, many excellent works on polarization switching[1], Mach-Zehnder[2] or Sagnac interferometer switching[3],[4],[5] have been presented for realizing the above functions.

In polarization switching, one of the problems associated with ultrafast switching is, however, how to avoid pulse broadening and switching instability due to birefringence in the Kerr media. Morioka *et al* utilized cross-splicing of two identical polarization-maintaning fibers to compensate for the fiber birefringence[1],[6].

This paper describes another birefringence compensation technique in which both pump and signal pulses are reflected at the exit of the switch with their polarizations flipped to a crossed state, passed through the Kerr medium again so that the signal polarization that comes out takes exactly the same form as at the input. Utilizing this technique, stable 50 Gb/s switching has been demonstrated using a 1 km PANDA fiber as a Kerr medium.

2. Polarization Rotating Mirror

Figure 1 illustrates some techniques of polarization rotation for flipping polarizations upon reflection. The most straightforward way would be using a quarter-wave plate and a 100% mirror or using only 2×2 Faraday rotator(Fig. 1(a)). A more convenient way is, however, to use a polarization-maintaining fiber pigtailed polarization beam splitter(PBS)with its two output ports connected to each other so that the polarization of the returning pulse is flipped to a crossed state. This is done experimentally by minimizing the output power coming out of the last remaining port. It should be noted that only Faraday rotator can rotate arbitrary

polarizations by 90 degrees. We employed the PBS scheme as a polarization rotating mirror to construct an ultrafast dual-path reflective optical Kerr switch.

3. Experiment

The experimental set-up is illustrated in Fig.2. A 50 Gb/s, 10 ps burst signal was generated from a 1.307 μm gain-switched LD at 8.7 GHz combined with an optical pulse multiplexer that consists of PANDA fibers and a polarizer. A pump source was a 1.313 μm CW mode-locked Nd:YLF laser that outputs a 70 ps pulse at 82 MHz which was compressed to a 10-15 ps short pulse by a fiber-grating compressor. Pump and signal pulses were combined and coupled into a 1km polarization-maintaining Kerr fiber(PANDA) by a WDM coupler with a pump polarization along one of the principal axes of the PANDA fiber and a signal polarization at 45 degrees relative to the pump. The group delay difference between the pump and the signal was calculated to be 10 ps, making the round-trip delay 20 ps.

Polarization flipping was conducted using a fiber pigtailed polarization beam splitter(PBS) with its two output ports connected to each other so that no lights comes out of the remaining port. The round-trip insertion loss of the PBS was about 1 dB. Figure 3 shows how birefringence in the Kerr medium is compensated, eliminating phase perturbations. Another advantage of this reflective configuration is that one can double the nonlinear interaction length in the Kerr medium. The outcoming pulses were extracted by a 3dB coupler placed in front of the WDM coupler and were observed with a synchroscan streak camera of a 6 ps temporal resolution. The pump pulse is filtered by the WDM coupler.

The switching results are shown in Fig. 4. Figs. 4(a)-(b) correspond to switched and unswitched parts, respectively. The required switching power was 1.5 W. The switching crosstalks come from the fact that the crosstalk of the PANDA fiber at the signal wavelength was rather poor: -16 dB on the average and -13 dB at worst. Optical Kerr modulation profiles were also observed using a CW signal as shown in Figs. 4(c)-(d). One can clearly see that the switching width of 20 ps is in good agreement with the round-trip relative delay between the pump and the signal. A more sophisticated scheme where the Kerr fiber is connected to the PBS loop is also promising as shown in Fig. 5. Here an optical circulator is used to eliminate the round-trip intrinsic 6dB loss of the 3 dB coupler. All laser-diode operation at 1.5 μm is quite possible employing the same configuration.

4. Conclusion

All-optical Kerr switching in the reflective mode is proposed and its stable 50 Gb/s operation has been demonstrated. The scheme utilizes polarization flipping at reflection that

compensates for birefringence in the Kerr media and upgrades temperature stability. This reflective scheme could be used for many other nonlinear switching applications to eliminate phase turbulence incurred in nonlinear media.

5. Acknowledgment: The authors would like to thank Drs.K. Nakagawa, and H. Ishio for their continuous encouragement.

References

(1)T. Morioka, and M. Saruwatari, "Ultrafast all-optical switching utilizing the optical Kerr effect in polarization-maintaining single-mode fibers," IEEE J. of Selected Areas in Commu. 6, 1186-1198(1988)

(2)I. H. White, R. V. Penty and R. E. Epsworth,"Demonstration of the optical Kerr effect in all-fibre Mach-Zehnder interferomter at laser diode powers," Elect. Lett. 24, 340(1988)

(3)N.J. Doran and D. Wood, "Nonlinear-optical loop mirror," Opt. Lett., 13(1), 56-58(1988)

(4)K. J. Blow, N. j, Doran, and B. P. Nelson, "Demonstration of the nonlinear fiber loop mirror as an ultrafast all-optical demultiplexer," Elect. Lett. Vol. 26, No. 4, 962-964(1990)

(5)M. Jinno and T. Mtsumoto, " Ultrafast low power and highly stable fiber Sagnac Interferometer," IEEE Photonics Tech. Lett. Vol. 2, No. 5(1990)

(6)T. Morioka, M. Tsukada, and M. Saruwatari, "Demonstration of 50 Gb/s all-optical Kerr demultiplexing utilizing pump-probe pulse walk-off in optical fibers," PS'90 PD 14D-9, Springer-Verlag Photonic Switching 2(1990)

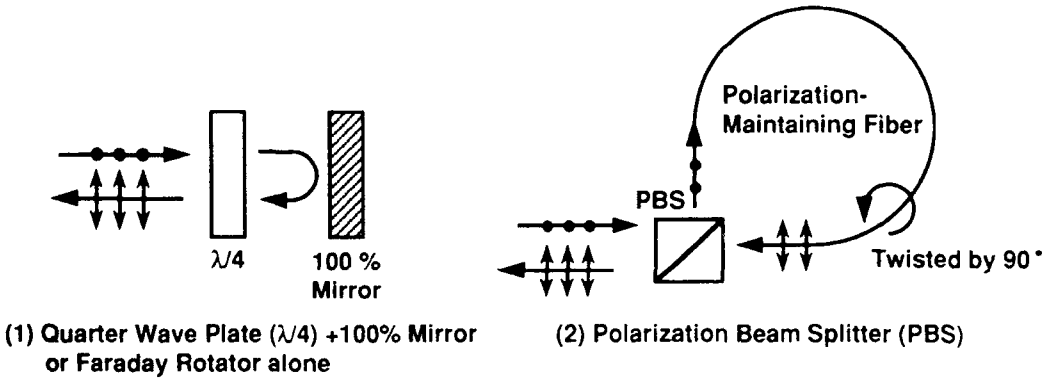

Fig. 1 Schematic drawing of polarization rotation

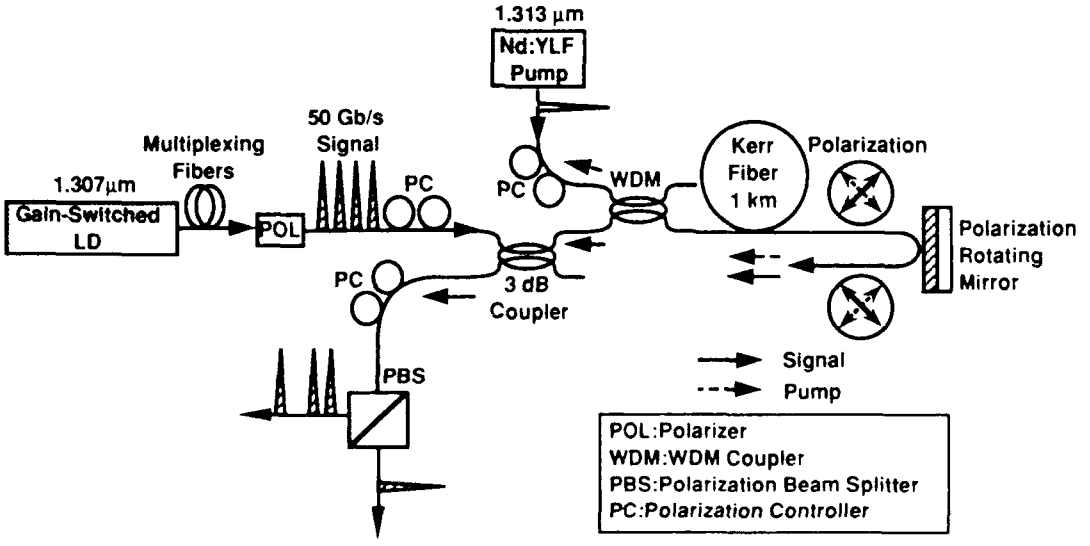

Fig. 2 Experimental set up of dual-path optical Kerr demultiplexer

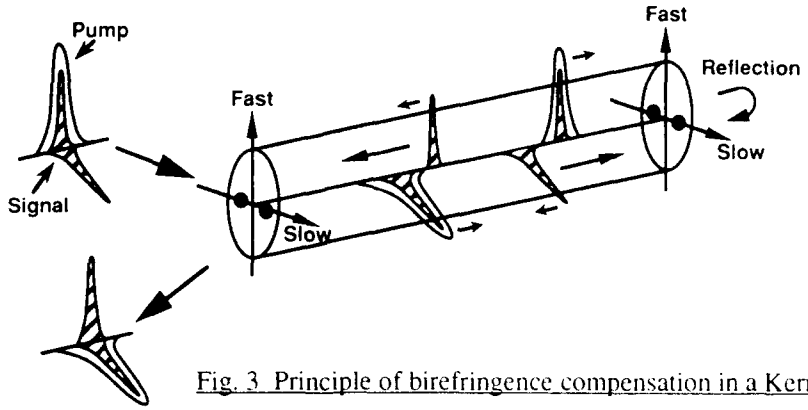

Fig. 3 Principle of birefringence compensation in a Kerr medium

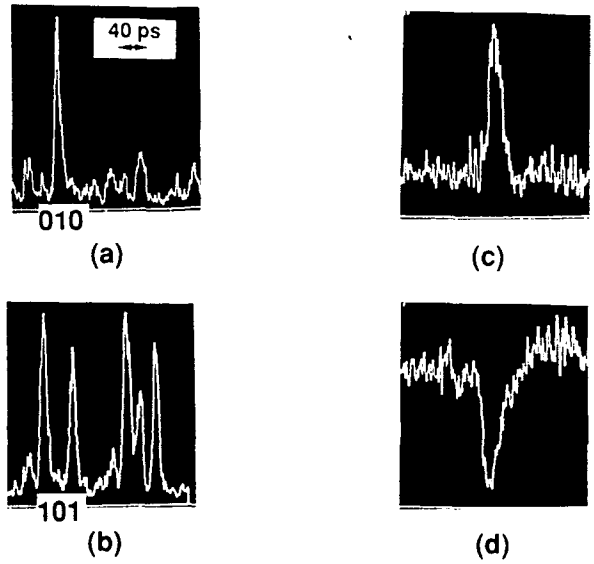

Fig.4 Experimental results: (a), (b) 50 Gb/s pulse operation (c), (d) optical Kerr modulation profiles(CW operation)

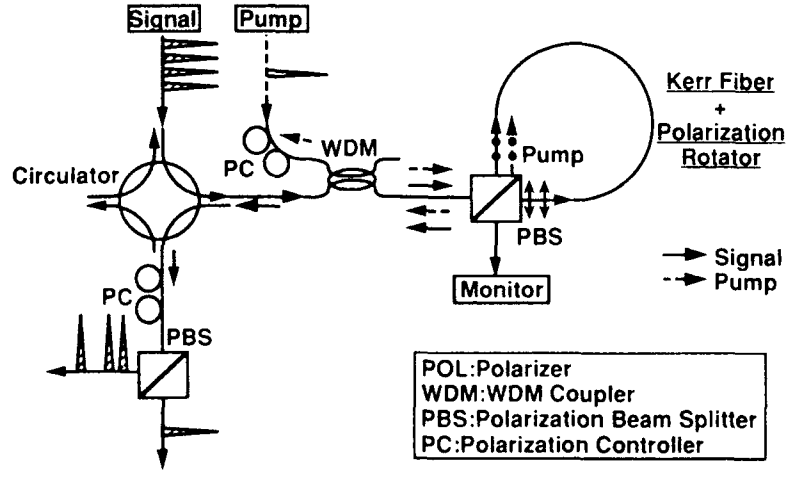

Fig. 5 Modified dual-path optical Kerr demultiplexer

Wednesday, September 4, 1991

Spatial Solitons

WC 2:00pm–4:00pm
Palmerston Room

Frank P. Payne, *Presider*
University of Cambridge, United Kingdom

SOLITON SELF-TRAPPING OF LIGHT BEAMS

A. BARTHELEMY, R. de la FUENTE (*), C. FROEHLY, O. GUY, M. SHALABY, F. REYNAUD
IRCOM (URA CNRS n° 356), Fac. Sciences, 123 rue A. Thomas, F. 87060 LIMOGES CEDEX, FRANCE
(*) Laboratorio de Optica, Facultad de Fisicas, Univ. Santiago de Compostela E - 15706 ESPANA

Abstract
"Spatial Solitons" are monochromatic patterns exhibiting stable self-trapping above their self-focusing threshold. Self-trapping stability requires the two-dimensionality of the propagating fields. We describe the generation and properties of such beams in two and three dimensions.

1 - INTRODUCTION

Free propagation of monochromatic single mode light beams through transparent bulk materials, the refractive index of which varies linearly with the optical field intensity (KERR optical nonlinearity) is *usually unstable*. For instance (figure 1) and initially smooth beam of Gaussian cross section carrying a high power P "breaks up" into a random pattern of small cells, each of them containing about an elementary "critical power $Po \equiv \lambda^2/\gamma$ 'after a propagation length $L \equiv (a^2/\lambda)(Po/P)$,

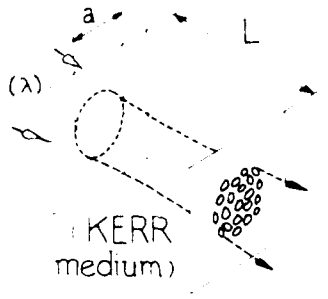

Figure 1 : unstable break-up ('Small-Scale self-focusing) of single mode laser beam well above the elementary "critical self-focusing power".

where λ : laser wavelength in the material ; a : beam waist size; γ : nonlinear coefficient of the refractive index variation ($n(I) \equiv no + \gamma I$, I being the laser illumination intensity).
On the contrary *"Spatial solitons"* are monochromatic patterns giving high power laser fields a quite *stable self-trapping*. Such a stability was both theoretically(1) and experimentally (2,3) demonstrated requiring the two-dimensionality of the field distributions.

Here will be presented
- ways of achieving two-dimensional "soliton" self-trapping of intense Laser beams either in planar waveguides or even in bulk materials,
- interactions of two neighbouring soliton beams,
- light-by-light guiding through a soliton channel, and discussion of *possible applications to all-optical fast* switching an deflection.

2 - PLANAR SOLITON BEAMS

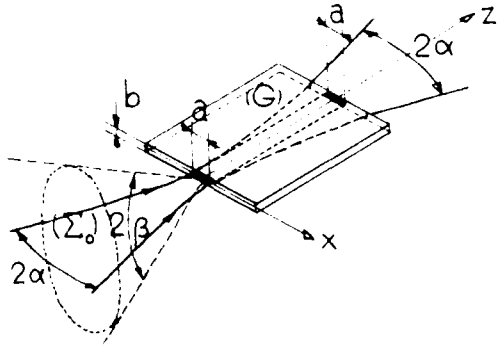

Figure 2 : two-dimensional self-trapping of a single mode "fundamental" soliton beam.

A straightforward way to fulfill the above two-dimensionality requirement is to confine light inside a planar waveguide, as shown on figure 2. An astigmatic lens focuses a single mode laser beam (Σo) with horizontal divergence α , vertical divergence β, wavelength λ , as an elliptical spot of horizontal width $a \equiv \lambda/\alpha$, vertical width $b \equiv \lambda/\beta$, on the input end of a planar waveguide (G) of thickness b. Due to the optical KERR nonlinearity of (G) a "fundamental soliton intensity" Io may be found, where the horizontal divergence falls down to zero inside (G). This intensity corresponds to exact compensation of the horizontal diffraction divergence by the intensity-induced self-convergence. It will be seen from figure 3 that this intensity is $Io \equiv \lambda^2/2a^2\gamma$), corresponding to a total "fundamental soliton power" $Po = Io \times a \times b = (\lambda^2/2\gamma)(b/a)$. The effect of the beam confinement inside a thin layer of thickness b is clearly to reduce the soliton power, but not its intensity.

Exact theory found this stable solution to exist for hyperbolic secant distributions of the field amplitude along the transverse coordinate x. Real experiments and numerical simulations show that any other smooth single mode amplitude distribution also gives rise to stable soliton self-trapping, as well as the theoretically ideal shapes. Slight deviations of the effective beam profiles with respect to their closer hyperbolic secant approximation modulate the soliton beam by noisy patterns of more and more vanishing weight with increasing propagation length : in the far field, the clean soliton shape will be recovered.

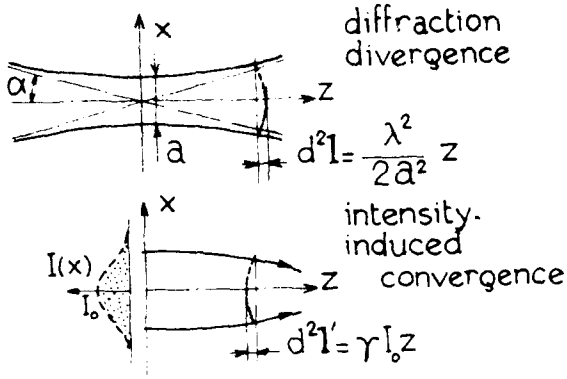

Figure 3 : at "fundamental soliton intensity", optical delays d^2I and d^2I' are equal to each other and of opposite signs

Higher order soliton beams : at twice, three times, four times ... the "fundamental" soliton amplitude Ao = $(Io)^{1/2}$ other stable beams may also be observed, in agreement with numerical simulations (4) (figure 4a). These "higher order" solitons were sequentially generated under picosecond excitation and analysed with picosecond temporal resolution (5)(6) using the experimental set-up represented on figure 4 b. The waveguide length L was taken equal to one half of the soliton periodicity (a^2/λ). Then the streak image I(x,t) showed that each pattern was stable over a wide intensity range around its average energy, jumps between two successive stable states occuring suddenly, without smooth transition through intermediate configurations.

Recent developments : these experiments were performed in a nonlinear waveguide consisting of a thin single mode layer of liquid CS_2 (refractive index 1.6) filling the space between two parallel silica plates of lower refractive index (≡ 1.5). Such liquid waveguides are of little pradical interest and of difficult use. Recently AITCHINSON and coworders (7), at Bell Laboratories (U.S.A.), demonstrated spatial soliton propagation through a solid-state planar glass waveguide. The low nonlinearity of glass was compensated by the high peak power (tens of Megawatts) of the amplified femtosecond pulses used in this experiment.

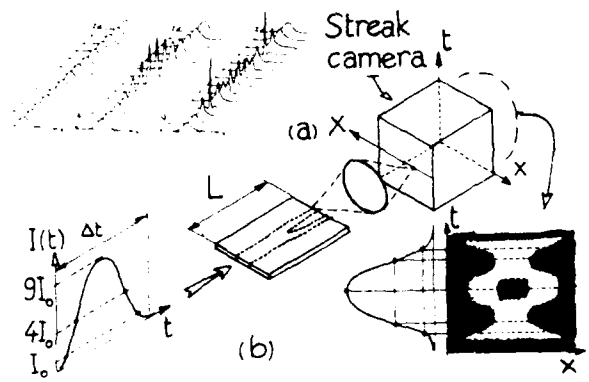

Figure 4 : (4a) : computed higher order solitons at the first three multiples of the fundamental soliton amplitude; (4b) : picosecond streak camera observation of transitions between successive order soliton beams.

"dark" soliton beams : in case of negative intensity dependence of the refractive index ("defocusing nonlinearity", where refractive index decreases while illumination increases), the stable self-trapped intensity distributions now taking the place of the previously described soliton beams are "dark solitons". Their theoretical transverse amplitude distribution is of hyperbolic tangent shape, in the place of the previous hyperbolic secant, giving them a zero intensity along the beam axis.

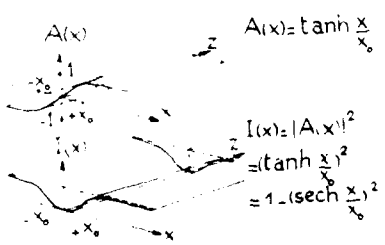

Figure 5 : "dark soliton" amplitude and intensity distributions.

Dark solitons were successively demonstrated by JEROMINEK and coworkers in Ti : $LINbO_3$planar waveguides (8) and discussed more generally by BOULANGER and MATHIEU (9). Of course the flat wings of these solitons, of nearly constant intensity up to infinity, thus containing an infinite energy, cannot be generated physically ; their approximation by finite width steps disturbs the quality of soliton propagation more and more as the observation distance z increases.

3 - SOLITON WAVEGUIDES IN HOMOGENEOUS BULK MATERIALS

The two-dimensionality of light fields required for the self-trapping stabilization may be found as well in some anisotropic intensity distributions as in the above planar waveguides. For instance a field of periodic interference fringes modulating the cross-section of a Gaussian beam (figure 6) exhibits much more regular and reproductible distortions through a three-dimensional nonlinear cell (liquid CS2 in the presented experiment) than the same Gaussian beam, if unmodulated : light concentrates along narrow lines, of average direction orthoganal to the interference fringes, of average width (a) very close to the width of a soliton beam carrying the average intensity (Io) of the laser field : $a \equiv \lambda (2\gamma Io)^{-1/2}$. This is a self-decomposition of a strongly anisotropic pattern into multiple soliton beams (10). The soliton behaviour of the cells of width (a)was

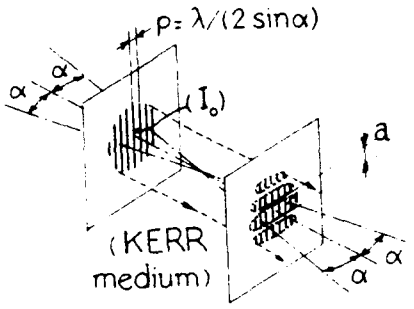

confirmed in another simpler experiment reported by BARTHELEMY and coworkers (2), where energy was concentrated into one single of the above cells (figure 7). The only care to be taken here was to keep the fringe spacing (p) smaller than the "soliton sheet" thickness (a); if not, unstable self-focusing develops chaotic structures.

- The oral presentation will also introduce other, yet unpublished soliton geometries in bulk materials.

Figure 6 : regular break-up of a periodic interference field into multiple "soliton sheets".

4 - GUIDING A LIGHT PROBE THROUGH A SOLITON CHANNEL

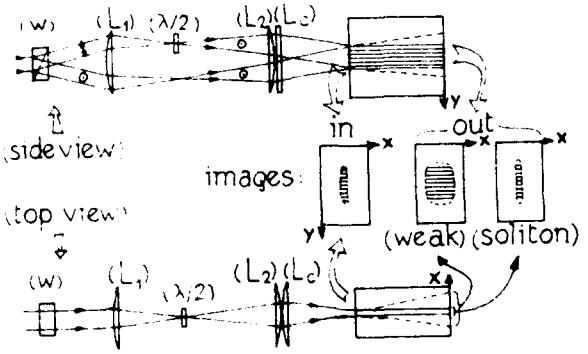

Light-induced refractive index gradients generated by the propagation of soliton beams behave like graded-index channels inside which other radiations of weak intensity may be guided as shown on figure 8. The light-induced waveguide may efficiently perform an all optical interconnection between optical fiber ends inserted on each side (A) and (B) of the planar nonlinear waveguide.

Figure 7 : self-confinement along axis x of a periodically modulated thin line into a single soliton pattern ; at the soliton intensity $I_0 \equiv (\lambda^2/a^2)\,(1/2\gamma)$ self-trapping guides light inside a refractive index thin sheet of thickness (a).

5 - INTERACTION OF TWO NEIGHBOURING SOLITON BEAMS

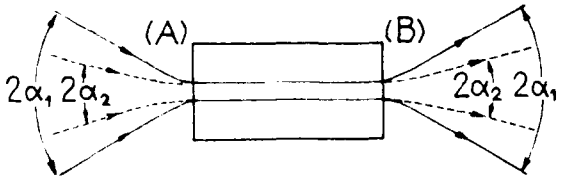

Figure 8 : single mode guided propagation of a weak green "probe" of free space divergence α_2 through a soliton waveguide induced by a strong infrared "soliton pump" of free space divergence α_1.

The interest of the above mentioned interconnections will be greatly extended by the possibility of deviating the soliton axes from their rectilinear trajectories thanks to mutual interactions between parallel soliton beams (11, 12) like on figure 9. Clearly this effect could be directly applied to fast (picosecond) opto-optical switching between fibers inserted at ports A, B, C, and also to optical logic operations (13) by just modulating the phase difference of the two interactig beams.

6 - LIMITS TO SOLITON BEAM PROPAGATION LENGTH

Along the soliton beam path other nonlinear phenomena come in competition with the KERR susceptibility. They are essentially the two-photon absorption, in the case of sub-picosecond excitation, and various types of stimulated scattering under slower excitation (nano or sub-nanosecond). These disturbances generate strong losses drastically limiting the propagation length of soliton beams. To our knowledge the maximum lengths yet achieved were always

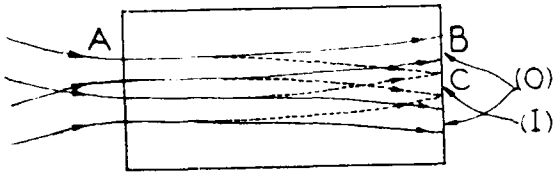

smaller than ten times the soliton periodicity in the only case of the *fundamental* soliton beam. *Higher order* solitons could never been observed over more than one single soliton period.

Figure 9 : two-soliton interaction ; (I) in-phase solitons attract each other ; when out-of-phase (O), they repell each other.

REFERENCES

(1) V.E. ZAKHAROV, A.B. SHABAT, "Exact theory of two-dimensional self-focusing and one-dimensional self-modulation of waves in nonlinear media", Sov. Phys. JETP, 1972, 34, p. 62-69.

(2) A. BARTHELEMY, S. MANEUF, C. FROEHLY, "Propagations soliton et auto-confinement de faisceaux Lasers par non-linéarité optique de KERR", Opt. Comm., 1985, 55, p. 193-206.

(3) S. MANEUF, R. DESAILLY, C. FROEHLY, "Stable self-trapping of Laser beams : observation in a nonlinear planar waveguide", Opt. Comm., 1988, 65, p. 193-198.

(4) A. HASEGAWA, F. TAPPERT, "Transmission of stationary nonlinear optical pulse in dispersive dielectric fibers I. anomalous dispersion"; Appl. Phys. Lett.; 1973, 23, 3, p. 142-144.

(5) S. MANEUF, F. REYNAUD, "First observation of higher order planar soliton beams", Proc. 14 th Congress of the International Commission for Optics, Aug. 1987, Québec, Canada ; Proceedings of the SPIE, vol. 813, p. 385-386.

(6) S. MANEUF, F. REYNAUD, "Quasi-steady state self-trapping of first, second an third order subnanosecond soliton beams" ; Opt. Comm. 1988, 66, p. 325-328.

(7) J.S. AITCHINSON, A.M. WEINER, Y. SILBERBERG, M.K. OLIVER, J.L. JACKEL, D.E. LEAIRD, E.M. VOGEL, P. W. SMITH, "Observation of spatial optical solitons in a nonlinear glass waveguide" ; Opt. Lett. 1990, 15, P. 471-473.

(8) H. JEROMINEK, C. DELISLE, R. TREMBLAY, "Optical branching effect in Ti : $LINbO_3$ waveguides", Appl. Opt. 1986, 25, p. 732.

(9) P.A. BOULANGER, P. MATHIEU, "Dark soliton in a KERR defocusing medium", Appl. Opt. 1987, 26, 1.

(10) S. MANEUF, A. BARTHELEMY, B. COLOMBEAU, C; FROEHLY, M. VAMPOUILLE, "Stable propagation of non-soliton picosecond beams through three-dimensional KERR materials"; Proc. 15 th. Congress of the International Commission for Optics, Aug. 1990, Garmisch-Partenkirchen, Germany ; Proceedings of SPIE vol. 1319, p. 99.

(11) A. BARTHELEMY, F. REYNAUD, B; COLOMBEAU ; "Single mode soliton beam waveguides", Proceedings of SPIE meeting, Cannes, France, 1987, vol. 862, P. 27.

(12) F. REYNAUD, A. BARTHELEMY ; "Optically controlled Interaction between two fundamental soliton beams", Europhysics Letters, 1990, 12, 5 p. 401-405.

(13) F. REYNAUD, A. BARTHELEMY; "AND Optical gate using soliton beams interaction" ; Proc. 15 th. Congress of I.C.O., Aug. 1990, Garmisch-Partenkirchen, Germany ; Proceedings of SPIE vol. 1319, p. 105.

Spatial dark solitons

G. A. Swartzlander Jr.[1]*, *D. R. Andersen*[2], and *A. E. Kaplan*[1]

[1] Department of Electrical and Computer Engineering
The Johns Hopkins University, Baltimore, MD 21218

[2] Department of Electrical and Computer Engineering
The University of Iowa, Iowa City, IA 52242

Dark solitons [1] have provoked much interest [2-7] since they were first shown to be particular solutions of the two-dimensional (1+1)-D nonlinear Schrödinger equation (NSE) with a negative (self-defocusing type) nonlinear coefficient n_2 (see Eq. (1) below). So far, only (1+1)-D temporal dark solitons (i.e. intensity minimums propagating along a nonlinear fiber on a quasi-cw bright background) have been observed experimentally [4-7]. Here we report the first observations [8] of stable spatial structures (e. g., stripes, crosses and grids) in the transverse cross-section of a cw optical beam propagating in a material with a self-defocusing nonlinearity, with these structures having a strongly pronounced soliton nature -- namely that of spatial dark solitons (SDS's). Although no (2+1)-D analytical solution for dark solitons in the NSE is known to date, our experimental and numerical data with various 2-D amplitude and phase masks provide strong evidence that the phenomenon observed by us is indeed due to spatial dark solitons. Furthermore, our results here on quasi-(1+1)-D propagation (see also [8,9]) have shown excellent agreement with the well known analytical results for (1+1)-D dark solitons [1]. In comparison to temporal dark solitons SDS's are easy to create and observe experimentally, requiring as little as a HeNe laser and some slightly absorbing fluid. Most recently, one of the authors (D.R.A.) with his coworkers have observed SDS's in pulse radiation in ZnSe crystals [10]. Various applications of SDS's can be envisioned, such as optical encoding, limiting, switching and computing, and nonlinear filtering.

Our exploration into SDS's formation [8a] was motivated by the observation of intriguing nonlinear transformations of far-field (Fraunhofer) diffraction patterns of a wire mesh placed at the input face of a sodium vapor cell when the laser was tuned at the self-focusing side of D_2 atomic resonance. In all the cases studied so far with rectilinear diffraction screens, the linear Fraunhofer diffraction pattern evolves into various arrays of square spots as the laser intensity increases. Subsequent measurements at the output face of the nonlinear medium (in the Fresnel or "near-field" regime) revealed the formation of very distinct dark stripes which had caused those novel nonlinear far-field patterns.

The geometric beauty of the far-field patterns and their stability over a relatively large range of intensities and driving field frequencies led us to believe that this phenomenon is not attributed to the specific physics of the nonlinearity in sodium vapor, but rather to the simple fact that the nonlinear component of refractive index is negative, i.e. $n_2 < 0$. To verify this, we tried an experiment using another phenomenon resulting in large values of $n_2 < 0$: the so-called thermal nonlinearity, which can readily be induced using low power radiation in many slightly absorptive liquids. The results of these experiments showed nonlinear far-field patterns amazingly similar to each other and to those of the sodium vapor experiment. Although the nonlinearity due to the thermal effect exhibits some spatial nonlocality, this has not appreciably affected the observed phenomenon, presumably because the characteristic scale of the nonlocality was smaller than the soliton size.

The simplest and probably most fundamental wire mesh configuration is a single opaque "cross". In this case the Fraunhofer pattern experiences a nonlinear

transformation into a grid pattern that has essentially the same characteristics as the 3×3 mesh case used by us for sodium vapor experiment (except that there are fewer spots), indicating similar nonlinear transformations in both cases. To understand the observed phenomenon, we modeled the experiment using the (2+1)-D NSE for laser beam propagation in a nonlinear medium, which was solved by us using numerical methods. The agreement between the experimental and numerical results is remarkable [8,9].

To identify the physical phenomenon which gave rise to the observed far-field patterns, we studied the specific features of wave propagation inside the nonlinear material. This was accomplished by examining the near-field patterns at the output face of the nonlinear material for different lengths of the material, and for various boundary conditions, including a single wire, two parallel wires, two orthogonal sets of parallel wires, a wire mesh, a single phase jump, multiple phase jumps intersecting at a point, and two parallel phase jumps [8]. The formation of pronounced dark stripes or grids was a universal phenomenon for all the cases studied. In general, the width of each stripe remained almost constant as the thickness of the nonlinear material increased, but decreased as the laser field strength increased. The number of these dark stripes also remained constant with propagation distance, even after collisions. These observations, together with the fact that $n_2 < 0$ suggest that the dark stripes are spatial dark solitons. Our investigation also shows that, notwithstanding orthogonal interactions, (2+1)-D dark soliton stripes behave amazingly similar to the analytical (1+1)-D dark solitons [1], i. e., it appears that soliton stripes orthogonal to each other in a cross-sectional plane, propagate almost independently of each other.

To verify that the observed phenomenon was indeed attributed to (2+1)-D dark solitons, we investigated [8] the two most fundamental cases: (*i*) an opaque cross ("amplitude mask", AM) composed of two orthogonal wires, and (*ii*) crossed phase steps ("phase mask", PM) constructed with two microscope cover slips (see Fig. 1 *(1)* and *(2)*). The corresponding near-field images are shown in Fig. 1 for a thermal nonlinear material. In the AM case, the linear Fresnel diffraction pattern (Fig. 1(1,a)) exhibits a gray shadow of the cross flanked by bright stripes. In contrast, the shadow is completely missing in the experimental nonlinear profile (Fig. 1(b)); instead, two high contrast dark stripes, that are separated by a distinct bright region, are formed parallel to both axes of the cross. In spite of the magnification in size with increasing beam power due to self-defocusing, the width of the dark stripes actually decreases, as expected for dark solitons. In the PM case, the linear Fresnel diffraction pattern displays a broad dark cross aligned with the axes of the phase steps, flanked by diffractive ringing. As the laser power is increased (see Fig. 1(2,b)), the width of the central cross decreases (even at the intersection) and does not split into two (as did the shadow of the dark opaque cross in Fig. 1(b)). This also occurs in a (1+1)-D nonlinear system when the boundary condition is a π phase step, with the central dark stripe referred to as a "fundamental dark soliton"; similarly, the pattern in Fig. 1(2b) can be regarded as a "fundamental dark soliton cross." Our numerical solutions for both nonlinear cases, shown in Fig. 1(c), again reaffirm that NSE correctly predicts the observed phenomena.

A strong verification of the soliton nature of the the observed phenomenon was achieved by comparing [9] experimentally measured parameters with the theory. We measured the soliton divergence angle, θ, with respect to the optical axis (see inset of Fig. 2), to determine the soliton characteristic parameter, $\lambda_{nl} = \theta \eta_{nl}^{-1/2}$ (the soliton amplitude and width also depend on λ_{nl}), where $\eta_{nl} \equiv |n_2| |E|^2/2n_0$. When a single wire of diameter, x_A, is small compared to the beam size, then λ_{nl} is determined by the equation $\lambda_{nl} \simeq \cos(2\lambda_{nl}A)$ [1], where $A = x_A \eta_{nl}^{1/2} k/2$. The excellent agreement between the data and theory is shown in Fig. 2. The inset (Fig. 2) illustrates the formation of a pair of diverging dark solitons for the case of a single wire.

The far-field transformation of a linear Fraunhofer pattern into a tightly organized and ordered nonlinear pattern can now be explained in terms of the formation of spatial dark soliton stripes and grids. This effect occurs, in general, because some spatial-frequency components of the incident beam are channeled into the formation of solitons, and thus are not allowed to "radiate" away from the optical axis as in the linear case.

The work at Johns Hopkins was supported by AFOSR, at Iowa by NSF. Computation was performed at the National Center for Supercomputing Applications and the Pittsburgh Supercomputing Center.

*Presently an O. N. T. Postdoctoral Fellow at the Naval Research Laboratory, Code 6546, Washington, D. C., 20375-5000.

[1] V. E. Zakharov and A. B. Shabat, Zh. Eksp. Teor. Fiz. 64, 1627 (1973) [Sov. Phys.-JETP 37, 823 (1973)].

[2] A. Hasegawa and F. Tappert, Appl. Phys. Lett., 23, 171 (1973).

[3] K. J. Blow and N. J. Doran, Phys. Lett. 107A, 55 (1985).

[4] P. Emplit, J. P. Hamaide, F. Reynaud, C. Froehly, and A. Barthelemy, Opt. Comm., 62, 374 (1987)

[5] D. Krökel, N. J. Halas, G. Giuliani, and D. Grischkowsky, Phys. Rev. Lett. 60, 29 (1988).

[6] A. M. Weiner, J. P. Heritage, R. J. Hawkins, R. N. Thurston, E. M. Kirschner, D. E. Leaird, and W. J. Tomlinson, Phys. Rev. Lett. 61, 2445 (1988).

[7] W. J. Tomlinson, R. J. Hawkins, A. M. Weiner, J. P. Heritage, and R. N. Thurston, JOSA B 6, 329 (1989).

[8] G. A. Swartzlander Jr., D. R. Andersen, J. J. Regan, H. Yin, and A. E. Kaplan, Phys. Rev. Lett. 66, 1583 (1991). Some of these results were first reported in (a) G. A. Swartzlander, Jr. and A. E. Kaplan, *Nonlinear beam propagation through a grating*, CLEO, 1989, Technical Digest Series 11, (Opt. Soc. of Am., Washington, D.C. 1989); and in (b) G. A. Swartzlander, Jr., D. R. Andersen, J. J. Regan, and A. E. Kaplan, *Observation of Spatial Dark Waves and Solitons*, Proc. OSA Annual Meeting, Post Deadline Paper, PD-7, Orlando, FL October 15-29, 1989.

[9] D. R. Andersen, D. E. Hooton, G. A. Swartzlander, Jr., and A. E. Kaplan, Opt. Lett., 15, 783 (1990).

[10] G. R. Allan, S. R. Skinner, D. R. Andersen, and A. L. Smirl, Opt. Lett. 16, 156 (1991); also S. R. Skinner, G. R. Allan, D. R. Andersen, and A. L. Smirl, "*Dark spatial soliton propagation in bulk ZnSe*," accepted for publication in IEEE JQE (1991).

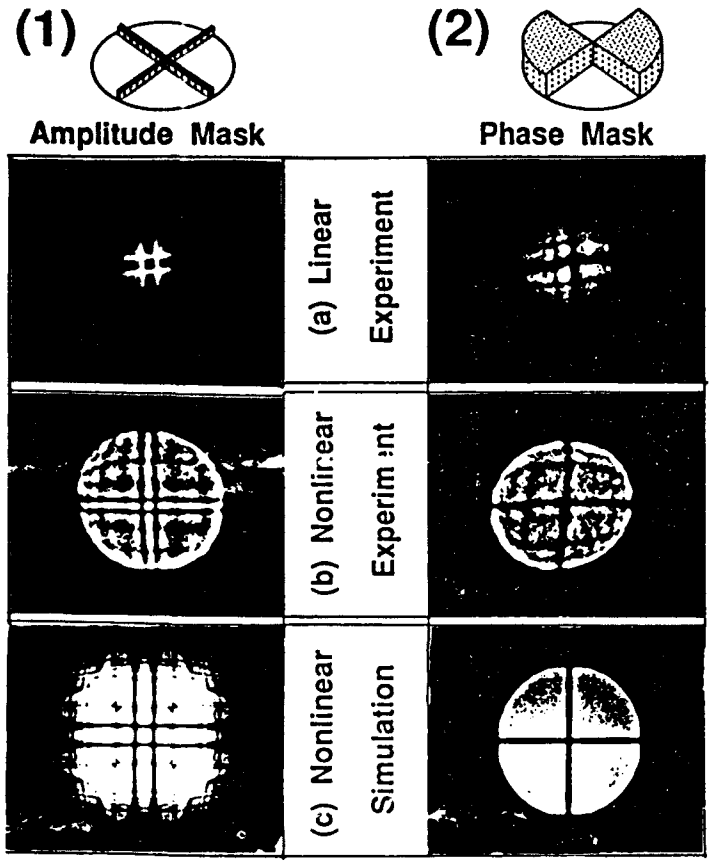

Fig.1Near-field cross-sectional images of the output sample face for propagation through an absorbing liquid with an amplitude cross (column *1*), and a phase cross (column *2*) in the incident plane.

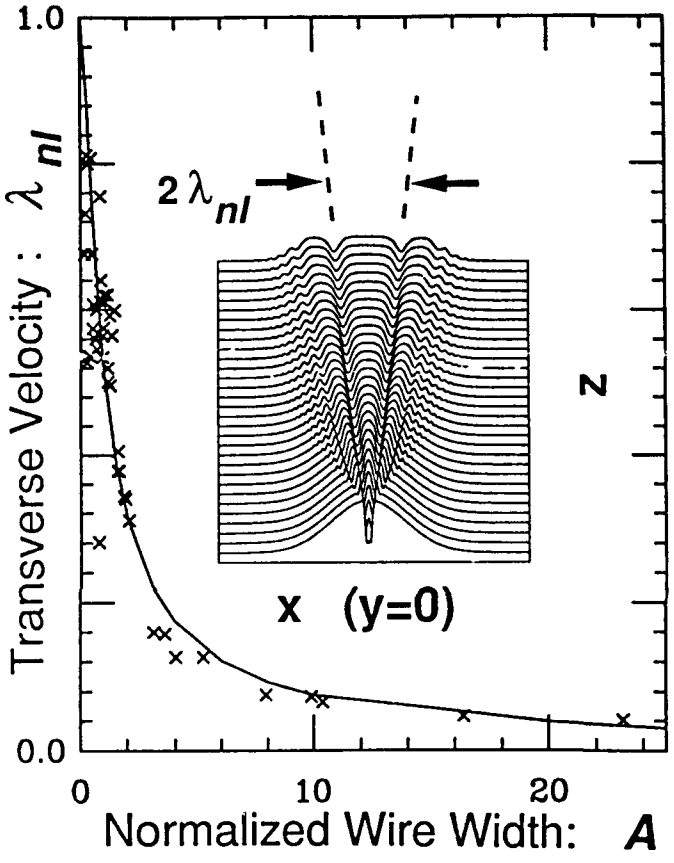

Fig.2Experimental (*X*-marks) and theoretical values (solid) of the soliton parameter λ_{nl} as a function of the normalized wire width, A when the boundary condition is a wire that bisects a Gaussian beam. Inset: Corresponding numerical solution of the (2+1)-D NSE, showing intensity profiles in the plane, y=0, and a pair of diverging dark solitons.

SPATIAL SOLITONS : MUTUAL INTERACTIONS AND MAGNETO-OPTIC SURFACES

A.D.Boardman and K.Xie

Applied Optics Group,University of Salford
Salford,M5 4WT,UK
Tel: 061-745-5253

1. Introduction

There has been a lot of recent activity on spatial solitons[1-10], including some very interesting work on soliton interactions[10]. The latter work relies entirely upon the linear theory of rays in a graded index medium. This is a valuable viewpoint but since spatial solitons are solutions of the nonlinear Schrödinger equation (NLSE) they appear to lend themselves particularly well to a particle-like description. Indeed, quite a number of authors[2-7] have adopted this fairly useful analogy with classical mechanics. It is an approach, however, that embodies a strong simplification arising from the use of the parabolic form of the Schrödinger equation. Namely, a paraxial approximation. The implication for the particle/ray approach is that, for a given direction, only a narrow cone of rays around it lie within the approximation zone. This is exactly what is required to consider the strong interaction case. If the chosen direction axis is along a real interface, for example, then only angles close to grazing instance can be permitted. This feature of the theory was anticipated a long time ago in a now famous paper by Kaplan[11].

2. Calculation details

In this paper two problems are considered using soliton theory in the representation discussed above, and hence within the usual restrictions. One problem concerns the mutual interaction of variously polarised spatial solitons with each other and the other concerns their interaction with magneto-optic surfaces.

The parabolic envelope equation for the complex amplitude, A_s, of TE polarised waves is well-known and is very easily proved to be the NLSE. TM polarised waves are more problematical and it is much less clear that, under a paraxial approximation, an envelope can also be derived that satisfies the NLSE. In fact, for a thermal type of nonlinearity, if the magnetic field component of the TM wave is $H_y = A_1\exp(i\beta z)$, where β is a dimensionless wavenumber of propagation along the z-axis, then A_1 is related to an intermediate amplitude A_2 which, in turn, is related to an envelope A_p. Both A_s and A_p now satisfy the NLSE and the forces F_p, and F_s exerted in a mutual interaction between a TE and TM soliton are

$$F_s = 4\int_{-\infty}^{\infty} |A_s|^2 \frac{d}{dx}|A_p|^2 dx \qquad (1)$$

$$F_p = 4\int_{-\infty}^{\infty} |A_p|^2 \frac{d}{dx}|A_s|^2 dx \qquad (2)$$

where all quantities are dimensionless, x is the coordinate transverse to the propagation direction z and $F_s = -F_p$, assuming that the beams are sufficiently well localised. For a pair of mutually interacting solitons with equal peak amplitude $\mathcal{A}$, and separated by a distance $L = L(z)$ (dimensionless), the force due to the TE soliton acting upon the TM soliton is

$$F_p = -8\mathcal{A}^4 \frac{\mathrm{sech}^2(\mathcal{A}L)}{\tanh^4(\mathcal{A}L)}\left[(2+\mathrm{sech}^2(\mathcal{A}L))\ln\left[\frac{1+\tanh(\mathcal{A}L)}{1-\tanh(\mathcal{A}L)}\right]-6\tanh(\mathcal{A}L)\right] \qquad (2)$$

from which it can easily be seen that $F_p \to 0$, as $L \to 0$ and $L \to \infty$. F_p has a minimum at $L = L_p$ where L_p is a solution of $\tanh(\mathcal{A}L) = 0.79018$.

TE and TM solitons always attract each other because they have orthogonal polarisations and make positive contributions to the nonlinear refractive index. If the solitons move apart then the attractive force rapidly decreases with L. In general, as the solitons move apart from L_1 to L_2, the force F_p will do work $W(L_1, L_2)$ where, using the definitions $\mathcal{T}_1 = \tanh(\mathcal{A}L_1)$, $\mathcal{T}_2 = \tanh(\mathcal{A}L_2)$

$$W(L_1,L_2)=+8\mathcal{A}^3\left[\left(\frac{1}{\mathcal{T}_1}-\frac{1}{\mathcal{T}_1^3}\right)\ln\left[\frac{1+\mathcal{T}_1}{1-\mathcal{T}_1}\right]+\frac{2}{\mathcal{T}_1^2}\right]$$

$$-8\mathcal{A}^3\left[\left(\frac{1}{\mathcal{T}_2}-\frac{1}{\mathcal{T}_2^3}\right)\ln\left[\frac{1+\mathcal{T}_2}{1-\mathcal{T}_2}\right]+\frac{2}{\mathcal{T}_2^2}\right] \qquad (3)$$

The equivalent potential created by the TE soliton for the TM soliton to move in is obtained in the limit $L_2 \to \infty$ and the limit of this potential as $L_1 \to 0$ is simply $U(0) = -\frac{8}{3}\mathcal{A}^2$.

A soliton with a trajectory that begins with a velocity v_1 at position L_1 must satisfy the classical mechanics condition that the kinetic energy plus the potential energy is constant in a conservative field. Hence, just as in the gravitational field an "escape" velocity can be defined. In this case it is $v_0 = [-2U(0)]^{\frac{1}{2}} = \frac{4\mathcal{A}}{\sqrt{3}}$. The significance of this result is that if the TM and TE beam intersect at an angle $\theta_0 > \cot^{-1}\left[\frac{v_0}{2\beta_0}\right]$ they will separate completely and leave the interaction region. If they intersect at a smaller angle they will move together with periodic bunching. These conclusions substantiate the Snyder et al results but from a solito theory point of view.

The analytical work discussed above will be confirmed by extensive numerical calculations that also support the figures attached here. Several types of interactions, TE-TE, TM-TE, TM-TM, will be reported in which the phase difference between the solitons will be varied and the *influence of diffusion* will be shown. The interaction region, in which cross-phase modulation occurs, will be critically examined and some discussion about relaxing the parabolic approximation will be presented.

A real interface to a soliton is also like a potential to a particle and within this model the Goos-Hanchen shift can be interpreted as light penetration from one medium to another. If an incident medium is nonlinear and delivers a soliton, to an interface with a second, magnetised, medium, then a small Kerr rotation of the polarisation occurs. The advantage of the particle approach to the nonlinear medium is that the Kerr radiation can be adopted by the expedient of assuming that the polarisation rotation is proportional to the path length of the beam in the magneto-optic medium and that there is a contribution form the soliton tail. The results of this calculation on comparison with and exact plane wave theory agree rather well, which is a further justification of the particle approach.

References

1. A.Barthelemey, S.Maneuf, C.Froehly, Opt.Comm., 55, 201 (1985).
2. D.Anderson, Phys.Rev.A., 27, 3135 (1983).
3. L.A.Nestrov, Opt.Spectrosc., 64, 694 (1988).
4. A.B.Aceves, J.V.Moloney, A.C.Newell, Phys.Rev.A, 39, 1828 (1989).
5. Yu.S.Kishvar, A.M.Kosevich, O.A.Chubykalo, Phys.Rev.A, 41, 1677 (1990).
6. C.Pare, M.Florjanczyk, Phys.Rev.A, 41, 6287 (1990).
7. D.R.Anderson, D.E.Hooton, G.A.Swartzlander, A.E.Kaplan, Opt.Lett., 15, 783 (1990).
8. S.R.Skinner, D.R.Anderson, JOSA B [to appear].
9. A.W.Snyder, D.J.Mitchell, L.Poladian, Opt.Lett., 16, 21 (1991).
10. A.W.Snyder, L.Poladian, D.J.Mitchell, 7th Optical Fibre Sensor Conference/15th Australian Conference on Optical Fibre Technology, Sydney, Australia, December 1990.
11. A.E.Kaplan, Sov.Phys.JETP, 45, 896 (1977).

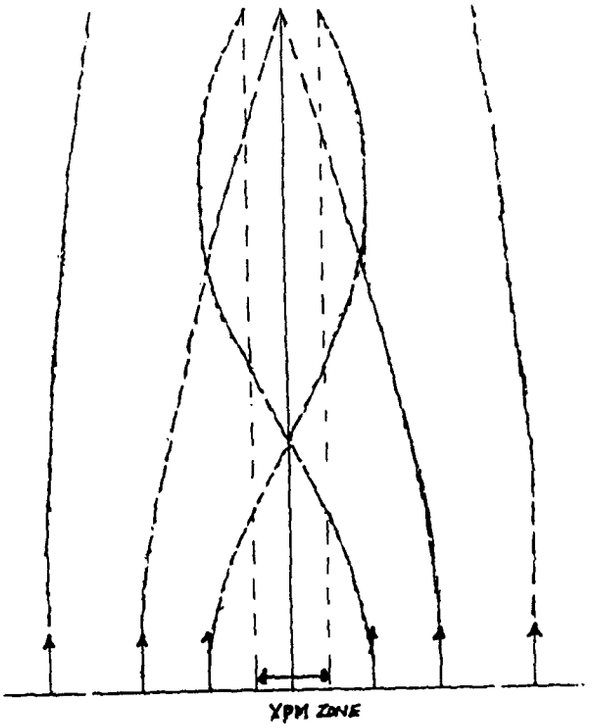

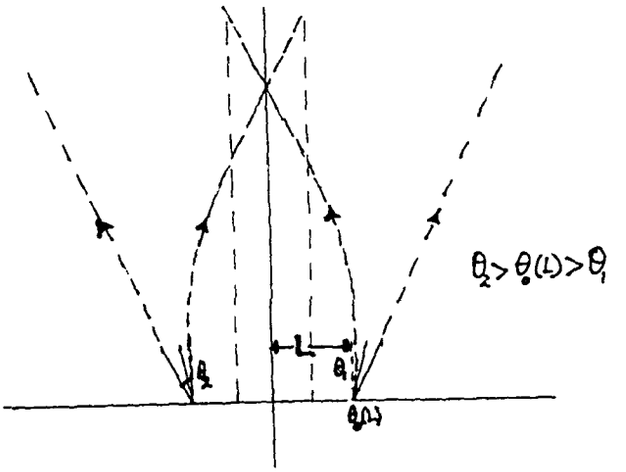

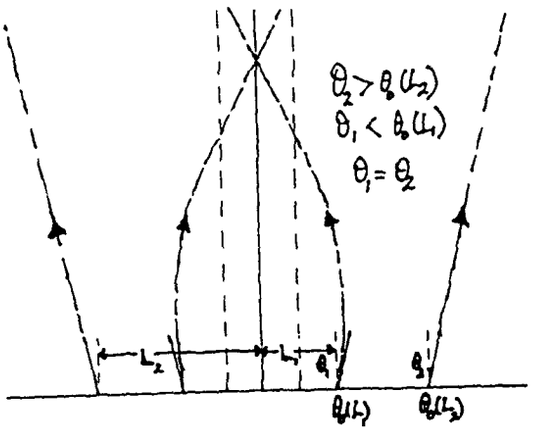

Transverse Solitary Waves: Observation and Computation

G. Khitrova, J.W. Grantham, Xu Jiajin, H.M. Gibbs
Optical Sciences Center, University of Arizona, Tucson, AZ 85721, (602) 621-2941
and
J.F. Valley
Lockheed Palo Alto Research Laboratories, 3251 Hanover St., Palo Alto, CA 94304-1187, (415) 424-2000

We present here a spatial instability, free from longitudinal feedback, in which a beam propagating in one direction in a self-focusing medium breaks up into more and more filaments as the input power is increased.[1] *These cell-exit patterns (solitary waves) are stable and highly reproducible, showing that they are seeded by fixed phase variations across the input profile and not by random fluctuations.* The physics of the formation of the solitary waves is the competition between self-focusing and diffraction leading to the eigenmodes of propagation, i.e., to the solitary-wave solutions of nonlinear Schrödinger-type equations. Our cell-exit spatial patterns are stable, even though they may jitter a little, and are highly reproducible as the input power is scanned up and down. By including the small inherent fixed-phase variations, we reproduced the experimental patterns and bifurcation routes. Consequently, even larger *aberrations were intentionally introduced.* The instability nature of this phenomenon is emphasized by the slowness (on the order of one second) with which the reproducible pattern is regained after the beam is momentarily interrupted.

The vertically linearly polarized single-mode output of a dye laser is collimated and brought to a waist at the cell entrance with a maximum of 500 mW reaching the sodium in a 10-cm-long evacuated quartz cell. Great care was taken to spatially filter the beam, to carefully clean and align the input optics, and to choose a spot on the cell window with minimal aberration.

The propagation and pattern formation of the input laser beam E_1 is computed in the paraxial and slowly-varying-envelope approximations:

$$\nabla_T^2 A_1 + 2ik_1 \partial A_1/\partial z = -\alpha_1 A_1, \qquad (1)$$

where

$$E_1(x,y,z,\omega_1) = A_1(x,y,z,\omega_1)\exp[i(k_1 z - \omega_1 t)],$$
$$k_1 = 2\pi\omega_1/c, \text{ and}$$
$$\nabla_T^2 = \partial^2/\partial x^2 + \partial^2/\partial y^2.$$

The coefficient $\alpha_1(x,y,z)$, a function of A_1 and ω_1, has been integrated over the Doppler velocity distribution; it includes both nonlinear absorption (gain) and refraction, leading to the pattern formation. Equation (1) is solved in 3 CPU minutes on a CRAY computer using fast Fourier transform techniques.

The first intentionally introduced aberration was *astigmatism induced by using two cylindrical lenses* of focal length 21 cm. The y waist was at the input cell window, while the position of the x waist (in the absence of sodium) was 8 cm inside the sodium cell. Figure 1 shows the bifurcation sequence as the laser pump detuning is increased from -0.7 to 7 GHz with laser power of 200 mW. When the detuning is larger than 4 GHz, the bifurcation process begins what we call the kaleidoscope sequence where the patterns become quite complicated, perhaps approaching spatial chaos.

The other perturbation was an *input-beam convergence* (phase $\sim r^2$), introduced onto the wavefront by changing the collimation of the light reaching a 30-cm focusing lens. We attribute the slightly non-circular symmetry of the data in Fig. 2 to small aberrations persisting through the spatial filter, namely astigmatism and coma, modeled by two asymmetric phase terms and a focus phase term.

In conclusion, we have observed spatial bifurcation sequences as interesting and complicated as temporal bifurcation sequences observed in other optical systems. They are explained as spatial

instabilities seeded by intentionally introduced aberrations. In temporal instabilities, the ω gain curve determines which frequencies in the fluctuations will be amplified; selective feedback or an injected signal is used to encourage particular directions or frequencies. In spatial instabilities, the k gain curve determines which wave vectors in the fluctuations will be amplified; input-wavefront-phase encoding is used to accentuate particular wave vectors, resulting in complicated bifurcations as a function of intensity or detuning. In self-induced transparency, the solitons of pulse propagation have areas of 2π, 4π, . . . in order that no energy be left in the highly absorbing medium. The solitary waves here permit a cw beam to propagate through a highly absorbing medium by forming transparent waveguides in which the absorption is bleached in the center of each filament. The input-phase encoding breaks the symmetry, stabilizes the spatial pattern, and makes it possible to study spatial-pattern bifurcations free of time dynamics.

The authors are grateful for support from the U.S. Air Force Office of Scientific Research and the Army Research Office, for use of the CRAY computer at Kirtland Air Force Base, and for helpful discussions with E. Wright and G. Benza.

References

1. For more detail see J.W. Grantham, H.M. Gibbs, G. Khitrova, J.F. Valley, and Xu Jiajin, Phys. Rev. Lett. **66**, 1422 (1991).

2. J.F. Valley, G. Khitrova, H.M. Gibbs, J.W. Grantham, and Xu Jiajin, Phys. Rev. Lett. **64**, 2362 (1990).

3. G. Khitrova, J.F. Valley, and H.M. Gibbs, Phys. Rev. Lett. **60**, 1126 (1988).

Figure 1. Cell-exit profiles for a pump detuning bifurcation sequence with astigmatism applied to the input laser beam. Computational patterns (a - d): $\alpha_o = 24000\ cm^{-1}$; 2X = 540; Δ ranging from +190 (a) to +1500 (d); $T_2 = 2T_1$; ku = 105, with parameters defined in Refs. 2 and 3. Corresponding experimental patterns (a' - d').

Figure 2. Cell-exit profiles for a power bifurcation sequence with focus added to the input laser beam. computational patterns (a - d): $\alpha_o L = 24000\ cm^{-1}$; Δ = +290; 2X ranging from 200 (a) to 580 (c); $T_2 = 2T_1$; ku = 105. Corresponding experimental patterns (a' - d'): $\delta\nu$ = 2 GHz; P ranging from 30 mW (a') to 220 mW (d'); radius of curvature = -3.5 cm and input waist = 76.3 μm for both the experimental and computational patterns.

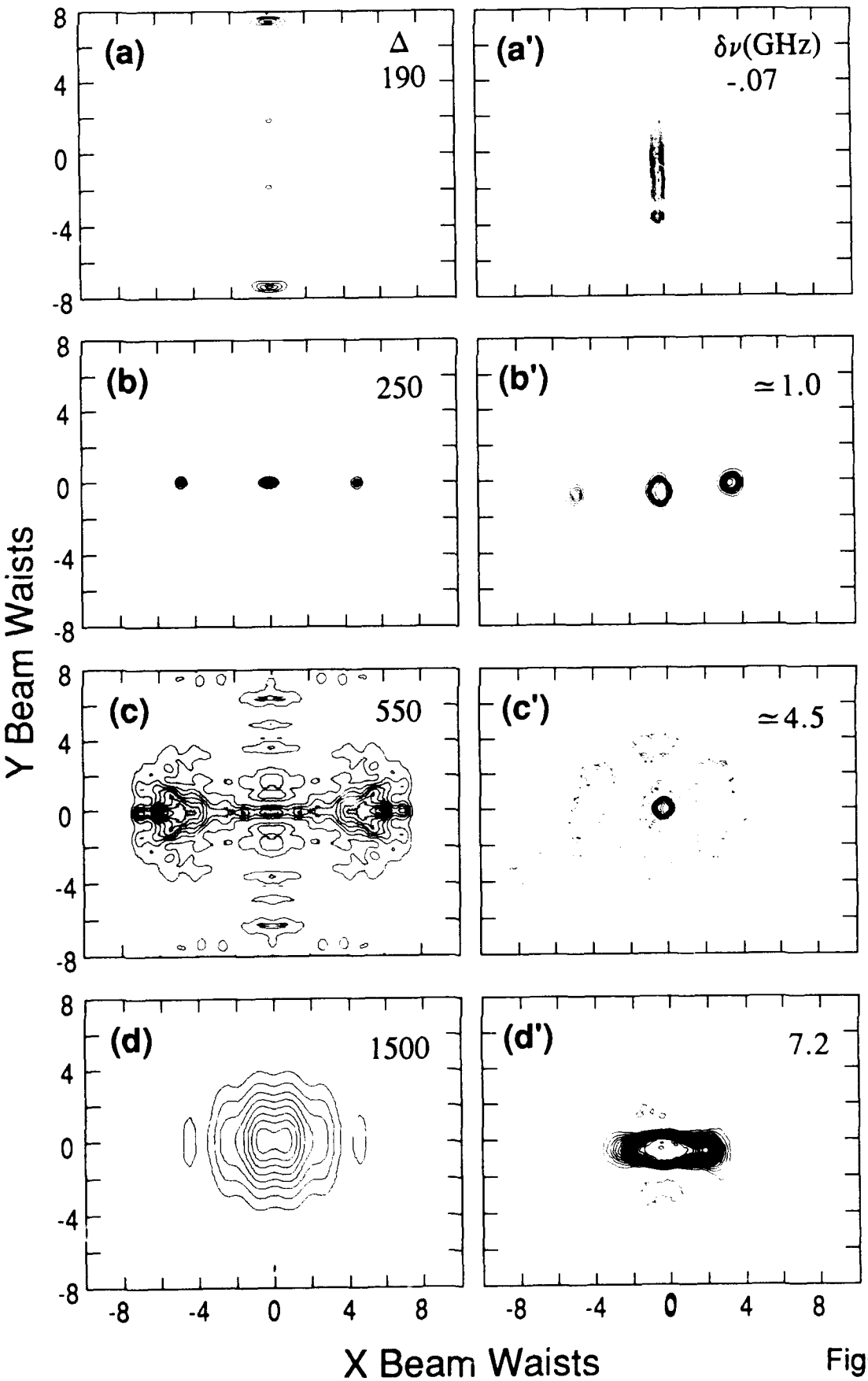
(a)
Δ
190
(a')
δν(GHz)
-.07
(b)
250
(b')
≃1.0
(c)
550
(c')
≃4.5
(d)
1500
(d')
7.2
Y Beam Waists
X Beam Waists
8
4
0
-4
-8

Figure 1

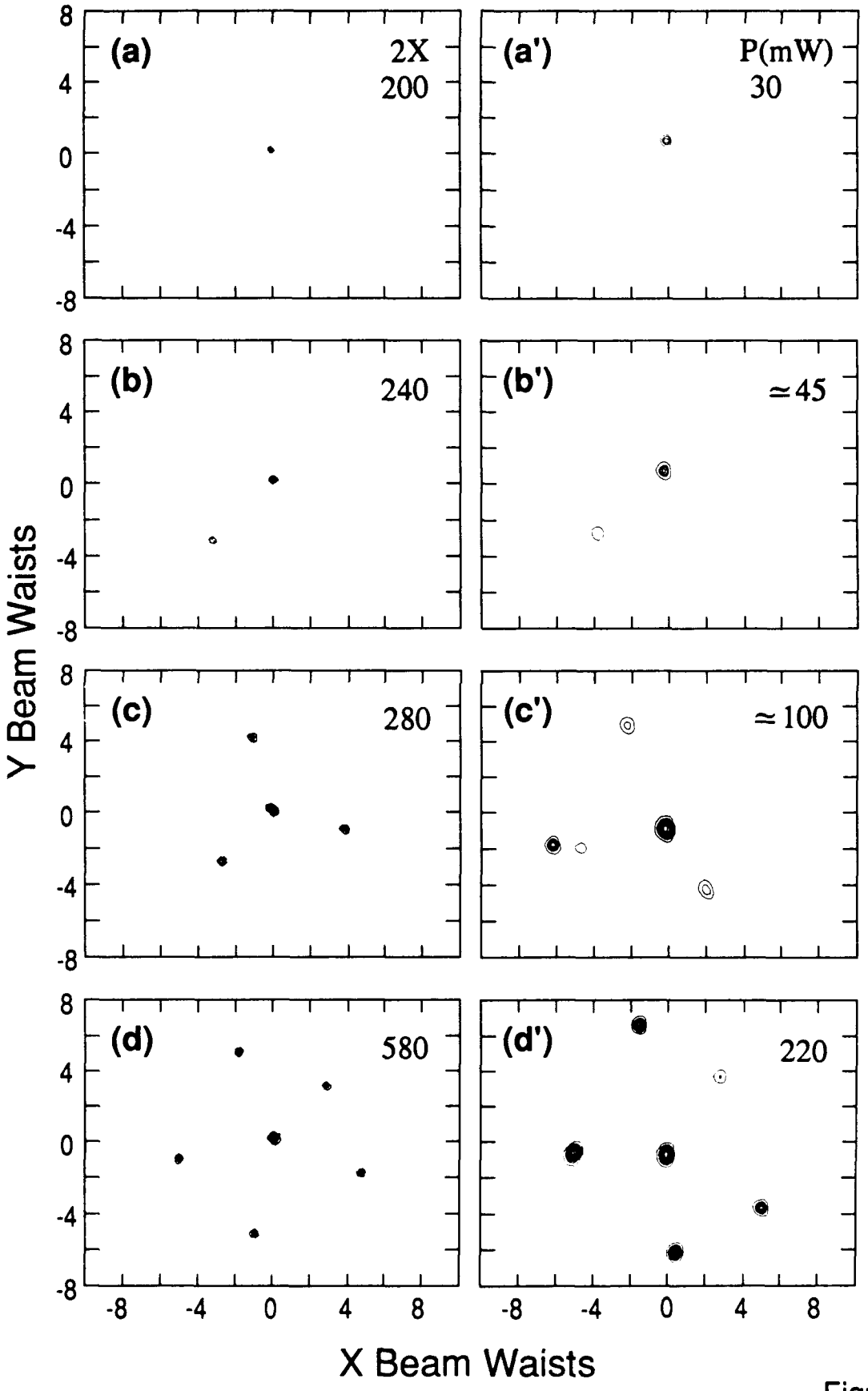
(a)
2X
200
(a')
P(mW)
30
(b)
240
(b')
≃45
(c)
280
(c')
≃100
(d)
580
(d')
220
Y Beam Waists
X Beam Waists
8
4
0
-4
-8

Figure 2

Steering One Spatial Solitary Beam by Another

A.W. Snyder
Optical Sciences Centre
Australian National University
Canberra ACT 2600
Australia
Tel: (61) (6) 249 2626

L.Poladian
Optical Sciences Centre
Australian National University
Canberra ACT 2600
Australia
Tel: (61) (6) 249 4061

D J Mitchell
Optical Sciences Centre
Australian National University
Canberra ACT 2600
Australia
Tel: (61) (6) 249 4690

Introduction: A beam of sufficient intensity can be made self guiding in a bulk medium[1,2,3,4]. It is intriguing to speculate that such solitary waves could be the building block for cellmate all optical devices and computing. Here we are concerned with directing one solitary wave by another. In particular, we show that two solitary waves, depending on various factors, can attract, repel, remain unchanged in their initial direction or spiral about each other in a double helical trajectory. Our discussion concerns both bright and dark solitary waves in Kerr and saturating material.

Theoretical foundation: An isolated soliton of field $\psi_1(x,y)$ propagates unchanged along its initial direction, inducing an (axial uniform) refractive index profile $n_1(\psi_1^2)$. Now consider an identical solitary wave at a large distance from the first. In isolation, this second solitary wave is characterized by field $\psi_2(x,y)$ and induced refractive index

profile $n_2(\psi_2^2)$. When two distant solitary wave propagate together, the field near each is in general slightly modified because of the tail of the other soliton. This interaction between the two beams will in general make them move together or apart.

Equivalent refractive index: By several theoretical approaches, e.g. the Lorentz force of electromagnetic theory or an invariant method, we have shown that the beam trajectories are identical to those of rays in an effective graded index (axially uniform) fiber. For beams of circular cross section the effective fibre also has a circular cross section. The refractive index profile $n(r)$ of this fiber depends exponentially on radial distance r, decreasing from the axis for in phase beams and increasing from the axis for beams π out of phase. In particular, $n(r)$ has the form

$$n(r) = n_0 + \int\{n_1(\psi_1^2) - n_0\}\psi_1\psi_2 dA \Big/ \int \psi_1^2 dA \qquad (1)$$

where n_0 is the refractive index at zero intensity and the integrals are taken over the infinite cross section. The radial position r coincides with the beam position. It enters into eq.(1) through ψ_2 as the center to center beam separation $2r$. The analytical results of this paper are found by substituting $n(r)$ of eq.(1) into the eikonal equation (eqs 1-28 and 2-20 of ref. [5]).

The trajectories of rays propagating in an (axially uniform) graded index profile given by eq.(1) have been discussed exhaustively in the literature, e.g. review chapters 1 and 2 of ref [5]. We can thus borrow directly from this literature to explain the interaction of solitary waves.

Solitary waves of planar symmetry: In nonlinear material consider first identical, in phase, solitary waves of planar cross section and launched at some angle 2θ to each other. These solitary waves act like rays propagating in a graded profile slab waveguide. The profile $n^2(r)$ has an exponential fall off for large r. A similar waveguide has been previously studied [chapter 1 of ref. 5]. If θ is less than some critical angle θ_c which depends on $n(r)$, then the solitary waves are 'bound' i.e. they undergo a periodic

trajectory. In other words, the solitary waves initially move together and then apart in a periodic fashion. If θ exceeds the critical angle θ_c then the solitary waves move apart. Since the profile $n(r)$ has an exponential shape, we know that the period of solitary waves with $\theta < \theta_c$ depends exponentially on beam separation. The further apart the solitary waves, the longer the period. Given the initial separation and initial inclination angle, it is clear that solitary waves interaction is characterized by the critical inclination angle θ_c, by the period and by the maximum separation of any given trajectory in analogy to rays in a graded profile guide (p13-18 of ref. [5]). The classical equations of geometric optics, together with eq(1), are used to find simple expressions for these quantities.

We have been discussing identical solitary waves excited in phase. Solitons excited 180° out of phase must always repel each other, the effect decreasing the further apart the solitons. The above results for planar solitons can be shown to be the same as those from the inverse scattering technique in a Kerr law material provided the initial separation is sufficiently large[6].

Solitary waves of circular symmetry (threshold nonlinearity): Consider next solitary waves of circular cross section e.g. those in an idealized saturating medium [7]. Such waves are known to be stable to symmetrical perturbations [7]. Again we appeal to the analogy of rays propagating in a graded profile fiber defined by eq.(1), but now the profile has a circular cross section. The properties of rays in such fibers is well known, e.g. review ch. 2 of reference [5]. Accordingly, beams are characterized by an angle θ_z inclined to the axial direction z-axis as in planar guides as well as an azimuthal (or skewness) angle θ_ϕ. If the initial directions of the two solitons are in these same plane (i.e. $\theta_\phi = 0$) the trajectories are like meridional rays and behave exactly like the planar solitons described above. However, when the solitons are launched initially skew to each other, they undergo a helical trajectory. Planar solitons with $\theta_z > \theta_c$ diverge but solitons of circular cross section, launched sufficiently skew to each other, remain bound to each other in their characteristic double helical orbit.

Non-identical solitary waves: Finally, we emphasize that the two solitary waves must be identical to realise the above effects. Well separated beams will propagate virtually unchanged from their initial direction if they differ slightly from each other. To see this we invoke the analogy of coupling between parallel guides.

Dark solitary waves: We have been discussing bright spatial solitary waves which here have a localized region of 'high' intensity with an exponential fall-off beyond. Now we consider dark spatial solitons which have a localized region of low intensity surrounded by a bright region[3,4,8,9]. Such beams have been studied in a Kerr medium where they always repel each other with planar symmetry but we have shown that they have zero interaction in an idealized (step) nonlinearity. We have also shown the existance of dark solitary waves in 3-D for both Kerr and saturating nonlinearity.

References

1. A. Barthelemy, S. Maneuf and C. Froehly, Opt. Commun. **55**, 201 (1985); S. Maneuf, R. Desailly and C. Froehly, Opt. Commun. **65**, 193 (1988); S. Manuef and F. Reynaud, Opt. Commun. **66,** 325 (1988).

2. J.S. Aitchison, A.M. Weiner, Y. Silberberg, M.K. Oliver, J.L. Jackel, D.E. Leaird, E.M. Vogel and P.W.E. Smith, Opt. Lett. **15**, 471 (1990).

3. O.R. Anderson, D.E. Hoolon, G.A. Swartzlander, A.E. Kaplan, Optics Lett., **15**, 783 (1990).

4. G.R. Allan, S.R. Skinner, D.R. Anderson and A.L. Smerl, Optics Lett., **16** 156 (1991).

5. A.W. Snyder and J.D. Love, 'Optical Waveguide Theory', London, England: Chapman and Hall (1983).

6. V.E. Zakharov and A.B. Shabat, Sov. Phys. JETP **34**, 62 (1972).

7. A.W. Snyder, D.J. Mitchell and L. Poladian, Optics Letters **16**, 21-23 (1991).

8. R.Y. Chiao, E. Garmire and C.H. Towner, Phys. Rev. Lett. **13**, 479 (1964).

9. A. Hasegawa and F. Tappert, Appl. Phys. Lett., **23**, 171 (1973).

Spatial Solitons in Planar Waveguides

R.A. Sammut, C. Pask and Q.Y. Li
Department of Mathematics, University College, University of New South Wales
Canberra, Australia
Telephone: +61 6 268 8686

Recent papers[1,2] claim to have observed spatial solitons in planar waveguides where confinement is provided in one transverse (y) dimension by a linear refractive-index difference and in the orthogonal (x) dimension by self-trapping due to an intensity-dependent refractive-index variation. If these experiments really do allow nonlinear effects to be observed independently in the x dimension, then the transverse field should take a separable form as used implicitly in Ref. 2. We explore the nature and accuracy of this assumption beginning with the stable, isolated soliton and returning at the end to the general propagation problem.

The steady-state form of the isolated soliton can be found directly using a straightforward variational technique[3,4]. We will describe this technique and apply it to planar waveguides with both Kerr-law and saturable nonlinearities. We also compare our results with the experimental observations of Aitchison et al[2] and with more detailed numerical calculations using the finite element method.

Basic Formulation for the Steady State

We consider propagation in a step-index, planar waveguide of thickness $2a$ with a nonlinearity initially of Kerr type, so that the intensity-dependent refractive index is given by

$$n^2(x,y) = n_0^2(y) + \alpha\, v^2(x,y) \tag{1}$$

where n_0 is the linear refractive index profile, v is the magnitude of the electric field, $\alpha = n_c^2 n_2 c\epsilon_0$, n_c is the core index and n_2 is the nonlinear coefficient (measured in m^2/W). In the steady state, the function v satisfies the scalar equation

$$\nabla_t^2 v + k^2(n_0^2 v + \alpha v^3) = \beta^2 v \tag{2}$$

where k is the free-space wavenumber and we have assumed that the scalar field is written in the form $E = v(x,y)\exp[i(\beta z - \omega t)]$.

Eqn (2) is equivalent to the following problem[3]: find v so that a maximum value is obtained for

$$J = \int_{-\infty}^{\infty}\int_{-\infty}^{\infty}\left[-|\nabla_t v|^2 + k^2 n_0^2 v^2 + \frac{1}{2}k^2\alpha v^4\right] dx\, dy \tag{3}$$

subject to the constraint

$$\int_{-\infty}^{\infty}\int_{-\infty}^{\infty} v^2\, dx\, dy = C = \frac{2kP}{\beta c\epsilon_0} \tag{4}$$

where P is the power in the wave.

General Results for Separable Fields

Choosing suitable trial functions and adjusting their parameters to maximize J produces good approximations to the exact solution of eqn (2)[3]. If we choose a trial function of the separable form

$$v(x,y) = A\,X(x/\omega_x)\,Y(y/\omega_y) \tag{5}$$

eqn (4) relates amplitude A and the field widths ω_x and ω_y, which then follow by solving $\partial J/\partial\omega_x = 0$ and $\partial J/\partial\omega_y = 0$. These equations yield a very simple relationship between ω_y and ω_x which shows that, although we have assumed a solution in separable form, nonlinearity connects the two dimensions. We also obtain a second equation which can be solved very easily to find ω_y and hence ω_x and A.

These equations provide some interesting qualitative information. We find that the product of the amplitude and beam-width in the unbounded direction is independent of power and is given by

$$A\,\omega_x = \frac{B}{k}\left(\frac{2}{\alpha}\right)^{1/2} \tag{6}$$

where B is a number depending on the explicit forms chosen for X and Y (e.g. $B = \sqrt{2}$ for Gaussians). For an isolated soliton in two dimensions, eqn (6) holds exactly with $B = 1$. Generally, we find that the presence of the waveguide leads to values of $B > 1$. As a result, the waveguide beam *in the x direction* is slightly broader than the soliton, with the degree of broadening depending on the shape of the beam in the y direction. These observations provide support for the soliton model used by Aitchison et al[2]

Assuming Linear Guiding in One Dimension

When the linear term $n_0^2(y)$ is much greater than the nonlinear contribution to the refractive index, it seems reasonable to approximate Y by v_L, the solution to the linear waveguiding problem $d^2v_L/dy^2 + k^2n_0^2v_L = \beta_L^2 v_L$. This fixes both Y and ω_y. We can then show that the best possible trial function of the form $v_L(y)\,X(x/\omega_x)$ for maximizing J leads to

$$E = A\,\mathrm{sech}(x/\omega_x)\,v_L(y)\exp\left[i\left(\beta_L^2 + \omega_x^{-2}\right)^{1/2} z - \omega t\right] \tag{7a}$$

$$\simeq A\,\mathrm{sech}(x/\omega_x)\exp(iz/2\beta_L\omega_x^2)v_L(y)\exp\left[i\left(\beta_L z - \omega t\right)\right] \tag{7b}$$

where $\omega_x = 4N_2^2/\alpha(k^2N_4$ and A is given by eqn (6) with $B = (N_2/N_4)^{1/2}$. (Notation: $N_m = \int_{-\infty}^{\infty} v_L^m\,dy$.) **Thus, if we assume that the field in the y-direction is unaffected by the nonlinearity, the optimum solution provided by the variational principle is indeed of the soliton form with parameters modified by the linear waveguiding.**

Strong Nonlinearity and Saturation Effects

In the case of large nonlinearity or high power, the beam will also experience some self-focussing in the y direction so the approximation of Y by v_L is too restrictive. In this case, we use a Gaussian approximation of the form $v = A\exp(-x^2/2\omega_x^2 - y^2/2\omega_y^2)$ to generate some numerical results. Figure 1 illustrates the behaviour of the self-trapped fields as a function of power, calculated using this approximation. The diagrams show the refractive index and the field distributions for three different power levels in the case where $n_f = 1.57$, $n_c = 1.55$, $a = 1\,\mu$m, $n_2 = 10^{-9}\,\mathrm{m}^2/\mathrm{W}$ (liquid crystal MBBA) and wavelength is $0.515\,\mu$m. As we would expect, with increasing power, the field becomes more closely confined to the centre of the waveguide and the presence of the cladding has a decreasing influence. The field then becomes increasingly circular.

To illustrate the effect of saturation on the self-trapped beams, we have repeated the previous calculations assuming that the refractive index in the core has an exponential saturation. This requires a change in the nonlinear term of eqn (3), but the calculation proceeds in a similar way to our previous example[3]. Figure 2 gives the results for a range of power levels and shows the behaviour we would *expect* — at low power levels, the results are very similar to those of Figure 1, but as power increases to very high levels, the refractive index approximates that of a rectangular waveguide and the beam once again becomes elliptical.

Comparisons between these approximate results and numerical solutions using the finite element method show that, provided that the power is not very close to the critical power for self-focussing in

the unsaturated case, the error in effective index is less than 0.1%. However, we can also check on the usefulness of the Gaussian approximation, by comparing our calculated results with those measured by Aitchison et al[2]. The waveguide used in their experiment has approximate parameters $n_f = 1.537$, $n_s = 1.53$, $n_2 = 3.4 \times 10^{-20}$ m^2/W and $2a \simeq 3 - 4\mu$m and their source produces 75-fsec pulses at 620 nm. They find that at a peak input power of 400 kW, the input beam propagates almost undistorted across the waveguide with a beam width (FWHM) in the x-direction of approximately 15μm. Our theoretical results show that we obtain the same beam width at an *average* power of approximately 190 kW. It is difficult to relate theory and experiment precisely here, as the waveguide parameters are only given approximately and we do not have details of the refractive index profile or of the average power launched into the waveguide. However, given all these uncertainties, the two results seem to be in quite good agreement.

The General Propagation Problem

Finally, we return to the full beam propagation problem with $E = \Psi(x, y, z)e^{-i\omega t}$. If we again assume that linear guiding dominates in the y direction and substitute $\Psi = v_1(y)\exp(i\beta_1 z)\Phi(x, z)$ into the exact field equation $\nabla^2\Psi + k^2(n_0^2(y)\Psi + \alpha|\Psi|^2\Psi) = 0$ we can obtain an (approximate) equation for Φ as follows: multiply by $v_1(y)$ and integrate over y. This produces

$$\frac{\partial^2\Phi}{\partial z^2} + 2i\beta_1\frac{\partial\Phi}{\partial z} + \frac{\partial^2\Phi}{\partial x^2} + k^2\alpha\left(\frac{N_4}{N_2}\right)|\Phi|^2\Phi = 0 . \tag{8a}$$

Making the slowly-varying approximation, $\partial^2\Phi/\partial z^2 \ll \beta_1\,\partial\Phi/\partial z$ gives

$$2i\beta_1\frac{\partial\Phi}{\partial z} + \frac{\partial^2\Phi}{\partial x^2} + k^2\alpha\left(\frac{N_4}{N_2}\right)|\Phi|^2\Phi = 0 , \tag{8b}$$

which is just the nonlinear Schrödinger equation with coefficients modified by the linear modal parameters β_1, N_2 and N_4. Eqn (4) requires $\int_{-\infty}^{\infty}|\Phi|^2\,dx = C/N_2$. The steady state solutions of eqns (8a) and (8b) are exactly those obtained in eqns (6a) and (6b), respectively.

Thus eqn (8a) has a solution which agrees with the best solution given by the variational principle for the steady state. This provides some justification for believing that eqn (8) accurately describes the nonlinear propagation of a beam.

Conclusion

In conclusion, we have begun to explore the theoretical notions underlying the observation of spatial solitons and give support for the approach of Refs 1 and 2 using variational arguments. When the beam is confined in the y–direction principally by the action of a linear refractive index profile, then our equations show that the nonlinear behaviour of the beam in the x–direction is governed by the usual nonlinear Schrödinger equation with parameters modified by the linear waveguide modal properties. When the product n_2P is large (high powers or highly nonlinear materials) nonlinearity affects both dimensions and a form of three-dimensional self-trapping occurs.

References

1. S Maneuf, R Desailly and C Froehly, *Opt. Commun.* **65**, 193 (1988)
2. J S Aitchison, A M Weiner, Y Silberberg, M K Oliver, J L Jackel, D E Leaird, E M Vogel and P W E Smith, *Opt. Lett.* **15**, 471 (1990)
3. R A Sammut and C Pask, *J Opt Soc Am B* **8**, 395 (1991)
4. A W Snyder, Y Chen, L Poladian and D J Mitchell, *Electron. Lett.* **26**, 643 (1990)

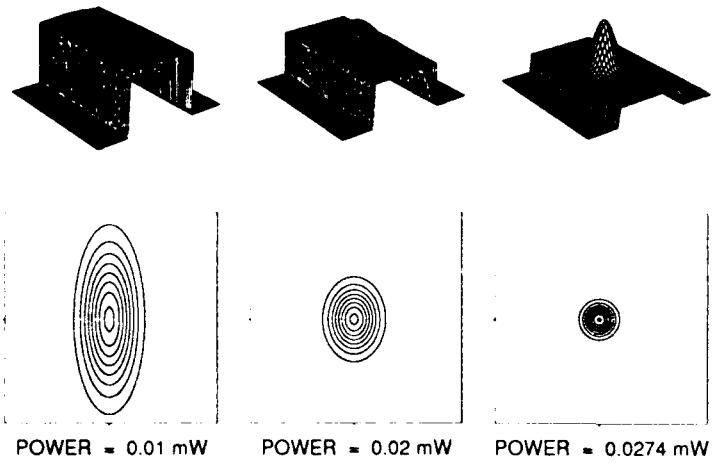

Figure 1 Nonlinear refractive index and field intensity at three different power levels in a planar waveguide with $n_f = 1.57$, $n_c = 1.55$, $a = 1\,\mu$m, $n_2 = 10^{-9}\,\mathrm{m}^2/\mathrm{W}$ and wavelength $0.515\,\mu$m. The first row shows the refractive index profile and the second row shows contour plots of the field to illustrate its increasing circularity.

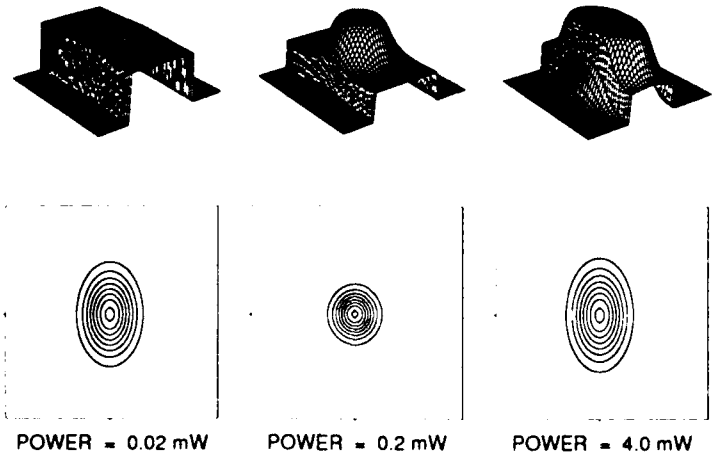

Figure 2 Nonlinear refractive index and field intensity at three diffferent power levels in a planar waveguide with exponentially saturating nonlinearity. $\Delta n_{sat} = 0.03$ and other parameters are as for Figure 1

DYNAMIC EFFECTS OF KERR NONLINEARITY AND SPATIAL DIFFRACTION ON SELF PHASE MODULATION OF OPTICAL PULSES

M. Karlsson, D. Anderson, M. Desaix, and M. Lisak

Institute for Electromagnetic Field Theory
Chalmers University of Technology
S-412 96 Göteborg, Sweden
Telephone: 031-72 15 67

It is well known, cf [1] that the optical Kerr effect can give rise to self - focusing and is responsible for self phase modulation of optical pulses. The formal analogy between the phenomena of spatial diffraction and temporal dispersion of optical pulses was pointed out very early [2]. However, only recently the two aspects have come together in the strong interest which has focussed on optical pulses propagating under the combined influence of nonlinearity, temporal dispersion and spatial diffraction [3-7]. Of particular interest is the possibility of generating optical pulses which collapse simultaneously in space and time due to the inherent instability of solitons in higher dimensions.

The dynamic interplay between spatial diffraction and temporal dispersion takes place primarily through the nonlinear self induced phase modulation. It has been suggested [3, 7] that spatial diffraction leads to spectral features, which are quantitatively and qualitatively different from those of the conventional self phase modulation results. In particular it has been claimed that , under certain circumstances, the blue might lead the red in the super continuum, thus opening the possibility for pulse compression without external gratings. However, the analysis used in Refs. [3, 7] is based on the aberrationless paraxial ray approximation; the standard analytical tool for investigating spatial self focusing phenomena. This approach which relies on an expansion of the nonlinearity around the radial center of the pulse,usually gives qualitatively correct results although the quantitative accuracy is not always very good, cf. [1]. However, the paraxial approximation tends to exaggerate the wave guide correction to the nonlinear phase shift; under certain conditions even to the point of giving the wrong sign of the nonlinear phase. For stationary propagation we have already investigated this short coming of the paraxial ray approximation and it has been found that very good agreement with numerical results, qualitative as well as quantitative, can be obtained using a variational approach [8, 9]. In the present work we analyze the dynamic interplay between nonlinearity and spatial diffraction through self phase modulation using a variational approach. We find that the paraxial result indicating the possibility of a change of sign in the regularized longitudinal phase of the pulse and the subsequent conclusion that the blue may lead the red is erroneous and only an artifact of the paraxial approximation.

The starting point of our analysis is the conventional equation for the envelope of the circularly symmetric scalar electric field, E:

$$\frac{1}{r}\frac{\partial}{\partial r}\left(r\frac{\partial E}{\partial r}\right) - 2ik\frac{\partial E}{\partial z} + \frac{2n_2k^2}{n_o}|E|^2E = 0 \qquad (1)$$

where r is the radial coordinate, z is the longitudinal coordinate, k is the linear wave number and the refractive index, n, is assumed to be of the form $n = n_o + n_2|E|^2$. For comparison with the results obtained in Refs. 6, 10 we will investigate Gaussian pulses assuming aberrationless propagation, i.e.

$$E(u,z,r) = A(u,z)\exp\left[-\frac{1}{2}\frac{r^2}{a^2(z)} + ib(z)r^2\right] \qquad (2)$$

where $u = z/v_g - t$. Since dispersion is neglected in Eq. (1), time only appears as a parameter. The time dependence of the diffraction-induced self-phase modulation is however important for the compression/decompression characteristics which appear when dispersive effects are introduced.

In the variational approach, as used in applications on optical pulse propagation problems [8, 9], Eq. (1) is reformulated as a variational problem corresponding to the Lagrangian, L :

$$L = r\left|\frac{\partial E}{\partial r}\right|^2 - ikr\left(E\frac{\partial E^*}{\partial z} - E^*\frac{\partial E}{\partial z}\right) - \frac{n_2}{n_o}k^2r|E|^4 \qquad (3)$$

Using the ansatz, Eq. (2), as trial function in the variational formulation of Eq. (1), we can integrate the r-dependence explicitly. The variational equations with respect to A, A^*, a and b of the reduced variational problem yields a system of coupled ordinary differential equations. In particular, equations for the beam width parameter, a, and the phase ϕ of the wave ($A = |A| \exp i\phi$) read:

$$\frac{d^2a}{dz^2} + \frac{1}{k^2a^3}(p-1) = 0 \qquad (4a)$$

$$k\frac{d\phi}{dz} = \frac{1}{a^2}\left(1 - \frac{3}{2}p\right) \qquad (4b)$$

where

$p \equiv n_2k^2a_o^2A_o^2/2n_o \equiv A_o^2/E_c^2$, $a_o = a(0)$, and $A_o = A(0,u) = E_o\exp(-u^2/2T^2)$ where T is the pulse duration. Other pulse characteristics are easily obtained from the solution of Eq. (4a). We emphasize that the corresponding critical field for self focusing, E_c, is twice as large as the field obtained from the paraxial result and in fact in good agreement with numerical results, cf. Ref. 9. Under the initial condition $\phi(0) = 0$, $da(0)/dz = 0$ the solution of Eq. (5) becomes

$$a(z) = a_o \sqrt{1 + (1-p)\, y^2}$$

$$\phi(z) = \begin{cases} \left(1 - \frac{3p}{2}\right)\left[\frac{1}{\sqrt{1-p}} \arctan(y\sqrt{1-p})\right], & 0 < p < 1 \\ \left(1 - \frac{3p}{2}\right)\left[\frac{1}{2\sqrt{p-1}} \ln\left(\frac{1 + y\sqrt{p-1}}{1 - y\sqrt{p-1}}\right)\right], & p > 1 \end{cases} \qquad (5)$$

where $y=z/ka_o^2$. The solutions given for the functions a(z) and b(z) are identical to those obtained from the paraxial approximation except for the definition of p which is a factor of 4 larger in the paraxial case. The solutions for the phase is also analogous to the paraxial result, but in addition to the new definition of p, the factor (1-3p/2) corresponds to the factor (1-p'/2) in the paraxial case, where p' (p'=4p) is the critical paraxial p-parameter. In particular, this implies that at the critical field ($p \rightarrow 1$ and $p' \rightarrow 1$ respectively) the variational result is $\phi = -y/2$, in good agreement with numerical results, cf Ref. [8, 9], whereas the paraxial result reduces to $\phi=+y/2$, i.e. has the wrong sign.

When the paraxial result for the phase was analyzed in the parameter range $0 < p' < 2$, [3, 7], it was found that the regularized phase, ϕ_{reg}, defined as $\phi_{reg} = \phi(u,z;p) - \phi(u,z;0)$ under certain conditions could change sign with distance of propagation. This would imply that the blue may lead the red in the super continuum and that e.g. pulse compression *without external gratings* would be possible. However, this change of sign does not persist in the more accurate variational result and must be due to the inherent short coming of the paraxial approximation. In the variational result the regularized phase always remains monotonously decreasing and negative, compare Fig 1.

In conclusion, using a variational approach we have derived expressions for the width, phase and critical self focusing field of optical pulses propagating in a homogeneous Kerr medium. It is found that the regularized longitudinal phase does not, as claimed previously, change sign but remains monotonously decreasing and negative for all values of p, thus invalidating the possibility of pulse compression without external gratings.

This work was partially supported by the Swedish Board for Technical Development.

References

[1] J. H. Marburger, Prog. Quant. Electr., 4, 35 (1975)
[2] V. E. Zakharov and A. B. Shabat, Sov. Phys. JETP 34, 62 (1972)
[3] J. T. Manassah, P. L. Baldeck and R. R. Alfano, Opt. Lett. 13, 1090 (1988)
[4] Y. Silberberg, Opt. Lett. 15, 1282 (1990)
[5] K. Okamoto and E. A. J. Marcatili, J. Lightwave Technol. 7, 1988 (1989)
[6] R. A. Sammut and C. Pask, Opt. Lett. 16, 70 (1991)
[7] J. T. Manassah, P. L. Baldeck and R. R. Alfano, Opt. Lett. 13, 589 (1988)
[8] D. Anderson, M. Bonnedal and M. Lisak, Phys. Fluids 22, 1838 (1979)
[9] M. Desaix, D. Anderson and M. Lisak, Variational approach to collapse of optical pulses, submitted to J. Opt. Soc. Am. B.
[10] D. Anderson, Phys. Rev. A 27, 3135 (1983)

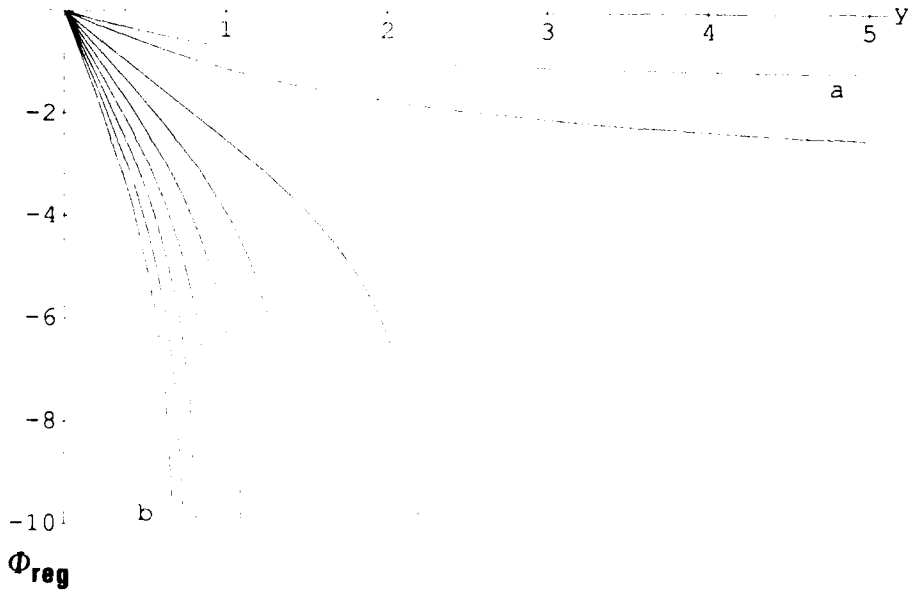

Fig. 1.The regularized phase ϕ_{reg} for u=0 as a function of normalized propagation distance $y=z/ka_0^2$ for different valves of the parameter p ranging from 0.6 (a) to 3.0 (b) with spacing 0.3.

TECHNICAL PROGRAM COMMITTEE

Allan D. Boardman, Cochair
University of Salford, UK

Nick J. Doran, Cochair
British Telecom Research Laboratories, UK

William J. Stewart, Cochair
Plessey, UK

Fatkhulla Abdulaev
Uzbek Academy of Sciences, USSR

Gunnar Arvidsson
Royal Institute of Technology, Sweden

Keith J. Blow
British Telecom Research Laboratories, UK

E. M. Dianov
USSR Academy of Sciences, USSR

Brian Henderson
University of Strathclyde, UK

A. Hadjifotiou
S. T. L., UK

Erich P. Ippen
Massachusetts Institute of Technology, USA

Mohammad Islam
AT&T Bell Laboratories, USA

Alexander E. Kaplan
The Johns Hopkins University, USA

Falk Lederer
Friedrich-Schiller-Universitat Jena, Germany

Guus Mohlmann
AKZO, The Netherlands

T. Morioka
NTT Transmission Systems Laboratories, Japan

Masataka Nakazawa
NTT Transmission Systems Laboratories, Japan

Hiroshi Nishihara
Osaka University, Japan

Daniel B. Ostrowsky
University of Nice, France

Colin Pask
Australian Defense Force Academy, Australia

Frank P. Payne
University of Cambridge, UK

Raymond Reinisch
LEMO, France

Philip Russell
University of Kent, UK

Yaron Silberberg
Bellcore, USA

John Sipe
University of Toronto, Canada

Allan W. Snyder
The Australian National University, Australia

W. Sohler
Universitat of Paderborn,
Federal Republic of Germany

George Stegeman
University of Central Florida, USA

Roger H. Stolen
AT&T Bell Laboratories, USA

Roy Taylor
Imperial College, UK

W. Jack Tomlinson
Bellcore, USA

Stefano Trillo
Fondazione Ugo Bordoni, Italy

Andrew C. Walker
Heriot-Watt University, Scotland, UK

Eva Weinert-Raczka
Technical University of Szczecin, Poland

Herbert G. Winful
University of Michigan, USA